PHYS

VOLUME

THE PHYSICAL REVIEW

A journal of experimental and theoretical physics established by E. L. Nichols in 1893

Published by the American Institute of Physics
for the
AMERICAN PHYSICAL SOCIETY

Officers

President

C. C. LAURITSEN
California Institute of Technology
Pasadena, California

Vice-President

J. H. VAN VLECK
Harvard University
Cambridge, Massachusetts

Secretary

K. K. DARROW
Bell Telephone Laboratories
Office:
Columbia University
New York 27, New York

Treasurer

C. B. PEGRAM
Columbia University
New York 27, New York

Local Secretary
for the Pacific Coast

J. KAPLAN
University of California at Los Angeles
Los Angeles, California

Managing Editor

S. A. GOUDSMIT
Brookhaven National Laboratory
Upton, Long Island
New York

BOARD OF EDITORS

Editor

S. A. GOUDSMIT

Assistant Editor

S. FRANKEL

Associate Editors

J. BARDEEN	HARVEY BROOKS	M. GOLDHABER
T. BONNER	R. F. CHRISTY	R. HOFSTADTER
R. G. HERB	C. L. CRITCHFIELD	A. W. LAWSON
W. E. LAMB, JR.	M. DEUTSCH	A. PAIS
A. J. F. SIEGERT	T. H. JOHNSON	R. SERBER
W. E. STEPHENS	BRUNO ROSSI	C. H. TOWNES

Manuscripts for publication should be submitted to S. A. Goudsmit, Brookhaven National Laboratory, Upton, Long Island, New York. The authors' institutions are requested to pay a publication charge of $10 per page which, if honored, entitles them to 100 free reprints. Instructions will be sent with galley proofs.

Proof and all correspondence concerning papers in the process of publication should be addressed to the Publication Manager, American Institute of Physics, 57 East 55 Street, New York 22, New York.

Subscription Price

United States and Canada.....$25.00
Elsewhere.....$27.00

Back Numbers[1]

Yearly bound number rate when complete year is available:
Prior to 1949: $20.00
Thereafter: $27.00
Single copies: $2.00 each, prior to July, 1929;
$1.00 each, July, 1929–December, 1941;
$3.00 each, January, 1942–December, 1946;
$1.00 each, January, 1947–December, 1948;
$1.25 each, thereafter.
General index, 1893–1920: $4.00.

Subscriptions, renewals, and orders for back numbers should be addressed to the American Institute of Physics, 57 East 55 Street, New York 22, New York.

Changes of address in the case of members of the American Physical Society should be addressed to the Treasurer; in the case of other subscribers to the American Institute of Physics.

[1] For Series I [Index of Physics Department, Cornell University, Ithaca, New York].

The Physical Review is published semi-monthly at Prince and Lemon Streets, Lancaster, Pennsylvania.

Entered as second-class matter March 6, 1917, at the Post Office at Lancaster, Pennsylvania, under the Act of March 3, 1879.

Acceptance for mailing at special rate of postage provided for in paragraph 34.40, section 34.40, P. L. & R. of 1948, authorized January 20, 1949.

THE
PHYSICAL REVIEW

A journal of experimental and theoretical physics established by E. L. Nichols in 1893

SECOND SERIES, VOL. 84, NO. 3 NOVEMBER 1, 1951

Photoneutron Thresholds*†

R. SHER, J. HALPERN, AND A. K. MANN
University of Pennsylvania, Philadelphia, Pennsylvania
(Received July 12, 1951)

A 25-Mev betatron is used to measure the photoneutron thresholds of 77 isotopes by direct detection of neutron yields as a function of maximum bremsstrahlung energy. The neutrons, moderated in paraffin, are observed with a BF_3 proportional counter and time delay circuits. Threshold energies for 31 isotopes are repetitions of previously reported values from other laboratories and those for 46 isotopes are either new or more precise determinations.

INTRODUCTION

MEASUREMENT of neutron binding energies is one method of establishing mass differences with great accuracy. In conjunction with other data, this permits mass assignments to intermediate and heavy nuclei. Such measurements also provide information about current models of nuclear structure.

The reactions from which neutron binding energies can be obtained are: (1) (p,d), (d,t), and (γ,n), in which a neutron is removed from a target nucleus; and (2) (d,p) and (n,γ), in which a neutron is added. In general, those reactions in which the incident particles are charged yield either upper or lower limits to the neutron binding energies, because it is difficult to be sure that direct transitions to the ground state of the product nucleus are involved. The reactions (1) furnish neutron binding data on the target isotope, while reactions (2) give similar data for the residual nucleus. Harvey[1] has summarized the experimental data for some 80 isotopes. Of these, 38 have been investigated by the measurement of (γ,n) threshold energies in which betatrons were used as sources of excitation.[2] Yields of the (γ,n) reactions are measured as a function of maximum bremsstrahlung energy and the threshold determined by some suitable extrapolation to zero yield. In most cases, the yield of the reaction was obtained by measurement of the radioactivity of the product nucleus. In a few cases, rhodium and iodine detectors were used to observe the neutrons from the reaction. The primary advantage of detecting neutrons rather than residual radioactivity is the possibility of measuring (γ,n) processes whose products are either stable or have very long or very short half-lives. On the other hand, a disadvantage is that identification of isotopes becomes more difficult when elements of natural isotopic composition are bombarded.

This paper will report on the measurement of (γ,n) threshold energies of 77 isotopes by a new method[3] in which neutrons are directly detected in a boron-trifluoride proportional counter. This method preserves the advantages of direct neutron detection and also permits rapid measurements which are independent of the conditions of bombardment.

DESCRIPTION OF APPARATUS

An enriched BF_3 proportional counter was imbedded in the center of a paraffin block $9''\times9''\times20''$, as shown in Fig. 1. The collimated bremsstrahlung beam from the betatron, which was $\frac{1}{2}$ inch in diameter at the collimator exit, passed through a $\frac{3}{4}$-inch-diameter hole running the length of the block and containing at its center the sample to be irradiated. Without a sample in position, the beam passed through the block undisturbed. Shielding against background neutrons was

* Part of a dissertation submitted by R. Sher in fulfillment of the requirements for the Ph.D. degree from the Graduate School of the University of Pennsylvania.

† Supported in part by the joint program of the AEC and ONR.

[1] J. A. Harvey, Phys. Rev. **81**, 353 (1951).

[2] a. G. C. Baldwin and H. W. Koch, Phys. Rev. **67**, 1 (1945); b. McElhinney, Hanson, Becker, Duffield, and Diven, Phys. Rev. **75**, 542 (1949); c. Hanson, Duffield, Knight, Diven, and Palevsky, Phys. Rev. **76**, 578 (1949); d. H. Palevsky and A. O. Hanson, Phys. Rev. **79**, 242 (1950); e. W. E. Ogle and R. E. England, Phys. Rev. **78**, 63 (1950); f. Ogle, Brown and Carson, Phys. Rev. **78**, 63 (1950); g. R. W. Parsons and C. H. Collie, Proc. Phys. Soc. (London), **A63**, 839 (1950); h. Parsons, Lees, and Collie, Proc. Phys. Soc. (London), **A63**, 915 (1950).

[3] Sher, Halpern, and Stephens, Phys. Rev. **81**, 154 (1951).

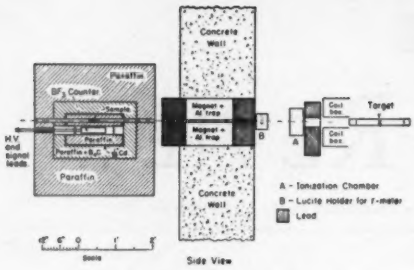

FIG. 1. Arrangement of apparatus.

obtained by surrounding the apparatus with a $\frac{1}{32}$ inch cadmium sheet, then with 4 inches of paraffin mixed with B_4C (30 percent by weight of B_4C), and finally with 12 inches of additional paraffin. Samples, from 5 to 50 grams of high purity material of natural isotopic abundance, and in powder or lump form, were placed in $\frac{3}{4}$ inch diameter thin-walled aluminum cylinders and irradiated axially. The axis of the counter (2 in. diameter, 12 in. active length, filled to a pressure of 40 cm with BF_3 enriched to 96 percent B^{10}) was parallel to and one inch from the center of the x-ray beam. The distance from the sample to the betatron target was 8.5 feet.

The x-ray beam consists of a series of sharp pulses, 0.5μsec in half-width, which on striking the sample produce a neutron intensity of similar time duration. This is repeated every 5550μsec. The BF_3 counter, which essentially detects only slow neutrons falling within its sensitive volume, will then record neutrons from the sample during a time interval dependent on the velocity distribution of neutrons leaving the sample and on the geometry of the apparatus and its effect on the diffusion time. Counts from neutrons produced outside the paraffin housing arise mainly from (γ,n) reactions in the betatron target and in the lead collimator. Those that leak through to the counter have a time distribution principally determined by the geometry of the betatron room because, in general, they have suffered collisions in the concrete shielding shown in Fig. 1 and in the walls of the room.

During the 0.5μsec time that the x-ray beam is on, the counter experiences a large pile-up of secondary electrons. The effect of pile-up was eliminated by means of a gated counting circuit, the parameters of which were determined from a study of the time distributions mentioned above. The counting circuit is represented schematically in Fig. 2. Pulses from the counter, which was operated at 2600 volts, are amplified in Atomic Instrument Company Mod. 205 and Mod. 204B preamplifier and amplifier, and after pulse-height discrimination are fed to one channel of a coincidence circuit of conventional design. The other channel of the coincidence circuit receives a gate which is triggered by the same pulse that fires the betatron expander circuit. This gate is of variable delay and time duration. The output of the coincidence circuit enters a scaler which records counts from the counter only during the gate duration.

A lower limit to the delay time of the gate was required by amplifier overloading which resulted from the pile-up. For maximum betatron intensity and a high Z sample, the amplifier fully recovered in about 15μsec. It was necessary for the gate to be of sufficient duration to allow most of the delayed neutrons to be counted. The diffusion time of the neutrons in our geometry was measured by varying the position of the gate in the interval between betatron pulses. It was found that neutrons from a sample arrived at the counter with an exponentially decreasing time distribution of half-width 100μsec. Similar measurements of the background neutrons gave a value of about 600μsec, for the half-width. For all further measurements, the time delay and duration of the gate were fixed at 30 and 300μsec, respectively.

The maximum bremsstrahlung energy was varied by expanding the electron beam of the betatron at a given value of the magnetic field using circuits similar to those previously developed.[4] The desired value of the magnetic field was measured by the voltage across a condenser in series with a large resistance both of which were across one of the magnet coils. This is indicated as "integrator stack" in the block diagram of Fig. 3. The voltage across the condenser at any time is proportional to the voltage applied to the magnet coil and hence to the magnetic field at the electron orbit. The condenser voltage was used to fire a trigger circuit whose bias was

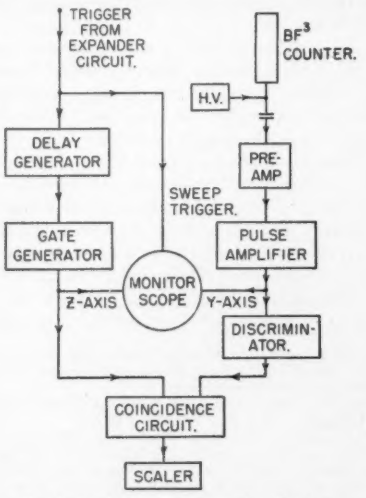

FIG. 2. Block diagram of counting circuits.

[4] McElhinney, Hanson, Becker, Duffield, and Diven, Phys. Rev. 75, 542 (1949); Katz, McNamara, Forsyth, Haslam, and Johns, Can. J. Research A28, 113 (1950).

fixed by the setting of the energy control potentiometer, hereafter called helipot. The trigger so generated, activated both the expander coils and the counter gate as mentioned above. The helipot reading was then a direct measure of the maximum x-ray energy.

PROCEDURE

In the measurement of thresholds, the neutron yields per roentgen of radiation corresponding to various maximum energies of the x-ray beam (helipot settings) were measured. The total number of roentgens striking the sample at a given helipot setting was determined with a 250 r Victoreen thimble meter imbedded in a Lucite cylinder of 8 cm diameter and located 3 feet from the betatron target. The cylinder and r-meter remained in the beam throughout the experiment. The absolute measurement of r was not required. For low Z elements, where the neutron yields are small, the samples were irradiated with about 100 r at each energy point, while for the high Z elements 50 r was sufficient. A complete run on a sample required about four hours. Two independent and complete sets of data, separated in time by at least several days, were obtained for most of the samples. At the beginning and end of each day, the yield curves for two elements selected as standards were measured. This served both as an over-all performance check of the apparatus and to determine the stability of the energy scale. Manganese and bismuth were chosen as standards because of their single isotopic constitutions, adequate neutron yields, and convenient thresholds.

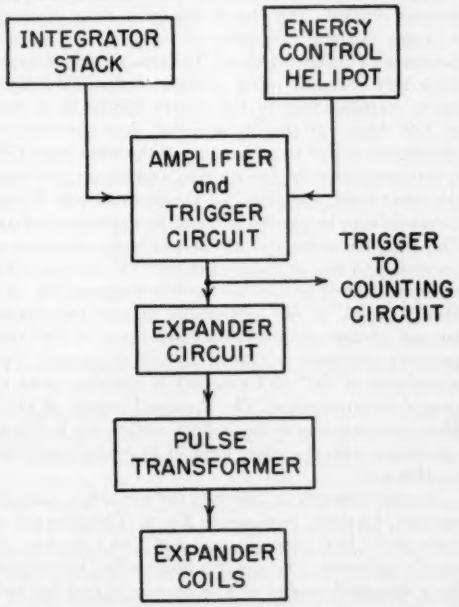

FIG. 3. Block diagram of energy control circuits.

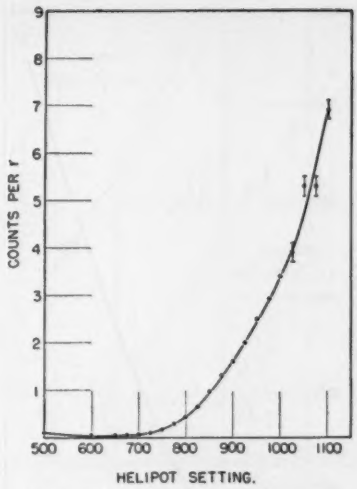

FIG. 4. Background dependence on energy.

The counting rate occurring without a sample in the target position, but with the aluminum sample holder in place, was measured over the entire energy range covered in the experiment, and with about 1000 r total irradiation at each energy point. Background measurements at various times in the course of the experiment were in agreement within statistical errors.

In order to obtain threshold values it is necessary to extrapolate the yield data from a given sample to zero yield. If the shape of the yield curve around threshold were known, it would be possible to make an unambiguous extrapolation providing no distortions of this shape were produced by counting losses and x-ray absorption in the sample. The effect of counting losses was found experimentally by observing the counting rate from a sample bombarded with bremsstrahlung of fixed high maximum energy but varying intensity. This counting loss curve was in agreement with the curve calculated on the basis of the neutron time distribution. The counting loss corrections to the yield data were seldom greater than two percent and never greater than five percent. Data taken with lead samples of several thicknesses indicated that x-ray absorption did not affect the shapes of the yield curves.

The relationship between the yield and energy is determined by the energy dependence of the cross section of the reaction, the bremsstrahlung and the detection efficiency of the apparatus. These factors are too complex for individual determination. We find, as do Parsons and Collie,[12] that all of our data can be represented by the relation $Y \sim (E-E_0)^m$, where Y is the yield, E is the maximum x-ray energy, m is a constant for a given isotope, and E_0 is taken to be the

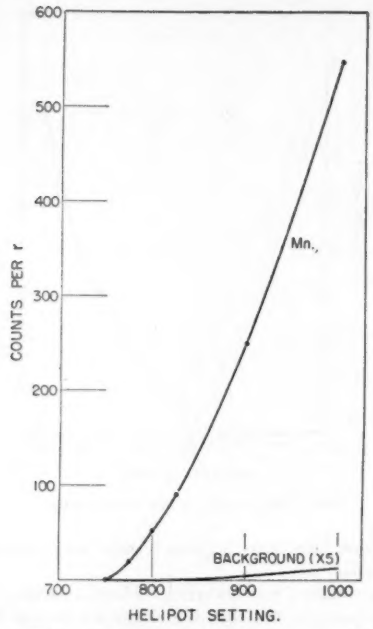

FIG. 5. Yield curve for manganese. The background is shown expanded five times.

threshold energy. In practice, E_0 and m are determined graphically by trial. It is probable that other representations would be equally satisfactory. The justification of the method used here lies in its convenience in treating the data and in the agreement of the results with known thresholds.

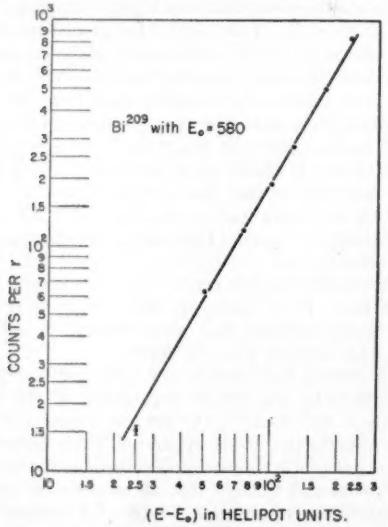

FIG. 6. Illustration of the graphical method of obtaining a threshold energy from the yield data for bismuth.

RESULTS

A curve showing the background as a function of helipot setting is presented in Fig. 4. Below 600, the background is primarily due to cosmic rays and Ra—Be sources in the laboratory. This is evidenced by the fact that the background is independent of the betatron beam in this helipot region. Consequently, while the background counts per minute are independent of the helipot setting in this region, the counts per r will rise with decreasing helipot setting because of the decreasing r per minute output of the betatron. Above 600, the background rises sharply because of the onset of (γ,n) reactions in the platinum betatron target and lead collimator. Figure 5 shows the yield curve for manganese, which has a moderate neutron yield, and the background curve magnified fivefold.

The graphical method of obtaining a threshold energy from the yield data are illustrated in the log-log plot of Fig. 6. The data are for bismuth, a singly isotopic element, for which the threshold value is known to be 7.44 Mev.[5] For an $E_0=580$ helipot units, corresponding to the known threshold energy, the data form a straight line over an energy interval of about 3.5 Mev, which is the entire region covered. If a value of E_0 differing from 580 by ± 10 units (approximately 0.15 Mev) is chosen the plot deviates strongly from a straight line.

Figure 7 shows a similar plot for iron, a multiply isotopic element. The abrupt change in slope of curve A is due to the contribution to the yield of a second isotope with higher threshold. The straight line of lesser slope was obtained using a value of $E_0=600$ helipot units, corresponding to the known threshold of Fe^{57} at 7.65 Mev.[1] It should be noted that the relative abundance of Fe^{57} is 2.1 percent. If the yield from Fe^{57} is extrapolated to higher energies and subtracted from the total yield, the data for the isotope with higher threshold may be plotted in the same manner as before. This plot, for which $E_0=810$ helipot units, is shown as curve B, and can be assigned to Fe^{56}. Of the remaining isotopes, Fe^{54} is known to have a threshold of 13.8 Mev,[3b] which is not observable in our experiment because of the small relative abundance of Fe^{54} (6.0 percent) compared to that of Fe^{56} (91.6 percent). The abundance of Fe^{58} (0.3 percent) is also too small to permit its observation. The threshold energy of 11.15 Mev corresponding to the helipot reading for Fe^{56} is in agreement with the lower limit of 11.3 Mev predicted by Harvey.[1]

Another example of the data for a multiply isotopic element, bromine, is shown in Fig. 8. The presence of both Br^{79} (50.6 percent) and Br^{81} (49.4 percent) is clearly indicated. The straight line for Br^{81} is obtained for a threshold energy of 9.95 Mev, and that for Br^{79}

[5] J. A. Harvey, Phys. Rev. 79, 241 (1950).

is for 10.60 Mev. These values are in agreement with those obtained by McElhinney *et al.*[2b] who find 10.2 and 10.7 Mev respectively, using the radioactivity method of observing (γ,n) reactions. Our bromine data were obtained from a sample of NaBr. The threshold for Na^{23} (100 percent) occurs at about 12.0 Mev, and consequently the yield from sodium does not interfere with the bromine measurements.

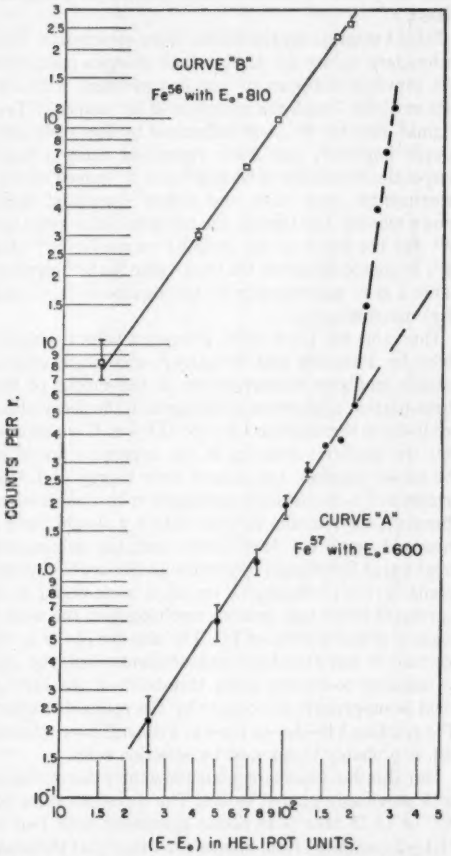

FIG. 7. Illustration of the graphical method for two isotopes of iron.

As a final illustration, the data for zinc, which are somewhat unusual, are presented in Fig. 9. Because of a fortuitous arrangement of yields, abundances, and thresholds, four of the five stable isotopes are clearly delineated; Zn^{70} with an abundance of 0.5 percent and a threshold energy of 9.2 Mev[2e] cannot be seen. The first threshold, which occurs at 6.95 Mev in Fig. 9, is assigned to Zn^{67}, which according to the mass formula should have a threshold at least 2 Mev below the threshold for any other isotope. Furthermore, the

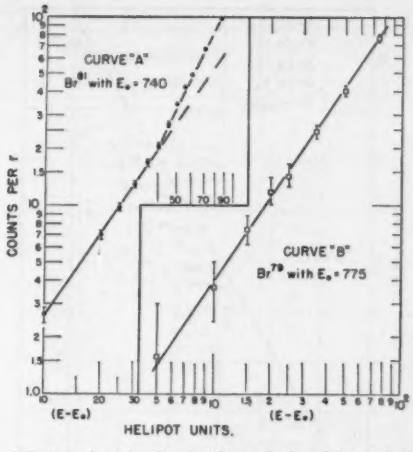

FIG. 8. Data for bromine showing the resolution of the two isotopes.

relative abundance of Zn^{67} (3.9 percent) is small compared to that of the other four isotopes and unless it had the lowest threshold it would not be detected. The assignments of 10.15 Mev to Zn^{68} and of 11.15 Mev to Zn^{66} are also based on the mass formula and relative abundance data, but are subject to more uncertainty. We find the threshold for Zn^{64} at 11.6 Mev which is in agreement with the value obtained by Hanson *et al.*[2e] (11.8 Mev) using the radioactivity method.

The procedure illustrated above has been applied to the data for 77 isotopes of 48 elements. The threshold

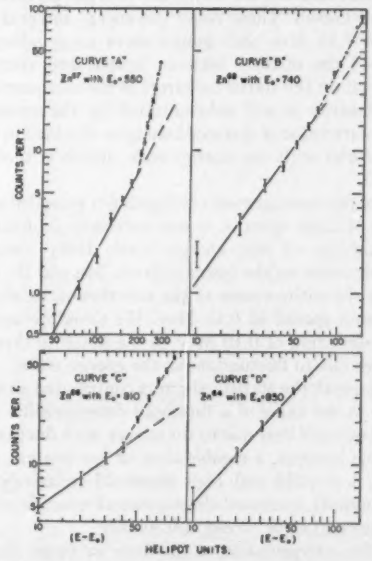

FIG. 9. Data for zinc showing resolution of four isotopes.

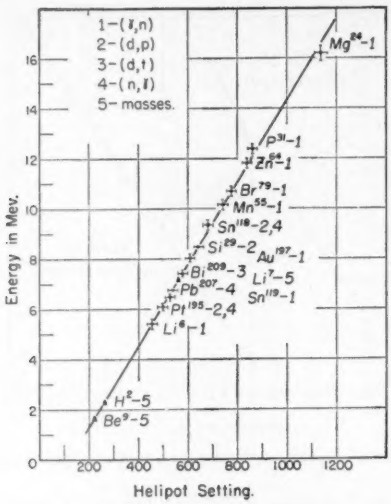

FIG. 10. Betatron energy scale.

energies of 40 isotopes represent new determinations and those of 6 isotopes are improvements in previous precision.

There are two primary factors which limit the precision of the measured thresholds, namely, the energy scale and the statistical uncertainties of the data. To calibrate the energy scale, we have obtained helipot settings corresponding to the thresholds of beryllium, deuterium and Li^7, for which the energies at threshold are well known. These cover the energy interval from 1.67 to 7.15 Mev and should serve as a calibration provided the relation between helipot and energy is linear within the statistical errors of the measurements. This linearity is well substantiated by the agreement in absolute value of threshold energies obtained in other laboratories with our energy scale, which is shown in Fig. 10.

Since the measurements of thresholds extended over a period of three months, it was necessary to determine the stability of the energy scale. Daily threshold measurements on the two standards, Mn and Bi, taken during the entire course of the experiment, exhibited a maximum spread of 0.15 Mev. We therefore assign a mean deviation of 0.10 Mev to the absolute threshold energies due to fluctuations in the energy scale.

In general, the statistical errors contributed an uncertainty in the value of a threshold determination which was about half that due to the energy scale fluctuations. In some isotopes, a combination of low isotopic abundance, low yield and high threshold (relatively high background), increased the statistical error. In no case did the total error exceed ± 0.30 Mev.

In the interpretation of the data for those elements with many isotopes of approximately equal abundances it was sometimes not possible to be certain that two or more isotopes did not contribute to the measured yield curve from which a single threshold was obtained. The threshold values for elements in which this lack of resolution might have influenced the measurements are appropriately indicated in the summary of results. We have also indicated the degree of certainty of isotopic assignment by classifying the assignments as certain (class *A*), probable (class *B*), and doubtful or unknown (class *C*).

Table I summarizes the results of the experiment. The preliminary values for 31 threshold energies contained in a previous publication,[3] are in agreement with the data in Table I with the exception of B^{10} and Sr^{87}. The original data for B^{10} were influenced by low yield and sample impurity, and upon repetition using a pure sample the thresholds of both B^{10} and B^{11} agreed within experimental error with the values computed from known masses. The error in the previous value given for Sr^{87} was the result of our inability to resolve Sr^{86} and Sr^{87}. It should be noted that the value for Sr^{87} given in Table I is in agreement with the results of (n,γ) and (d,p) measurements.

The value for Li^6 is to be compared with the result given by Titterton and Brinkley,[6] who made photographic emulsion measurements of the ranges of the alpha-particle and proton resulting from the decay of Li^8 produced in the reaction $Li^6+h\nu \rightarrow Li^5+n$. If we assume that the neutrons detected in our apparatus are from the above reaction, the ground-state energy of Li^5 so determined is in excellent agreement with their results. However, the reaction $Li^6+h\nu \rightarrow He^5+p$ should have a threshold some 0.8 Mev lower, and the subsequent break-up of He^5 should contribute to the neutron yield. Similarly, the photographic emulsion work would show a group of long-range protons resulting from the second mode of disintegration of Li^6. The absence of the latter reaction in our threshold measurements could be due to inability to resolve these thresholds if the He^5+p yield is suppressed sufficiently by the coulomb barrier. The reaction $Li^6+h\nu \rightarrow \alpha+p+n$, with still lower threshold, is probably suppressed by selection rules.

Our threshold measurements show three discrepancies with previously quoted values. The threshold value for Al^{27} of 12.75 Mev is in better agreement with that of 11.1 ± 2 computed from masses than the (γ,n) threshold of 14.0 ± 0.4 previously quoted.[2b] The 14-Mev value was obtained from observation of the 7 sec radioactivity in Al^{26}.

Although we find a value for Cu^{63} in good agreement with values obtained from radioactivity measurements, our value for Cu^{65} is outside the combined errors of the two measurements.[2b]

Harvey[1] computed a lower limit to the threshold of La^{139} from the $Ba^{138}(d,p)$ reaction and the disintegration schemes of Ba^{139} and La^{138}. The value he used for the

[6] E. W. Titterton and T. A. Brinkley, Proc. Phys. Soc. (London) **64A**, 212 (1951).

TABLE I. Summary of results.

Isotope	Percent abundance	Present measurements: Threshold (Mev)	Error (Mev)	m	Class	Previous measurements: Threshold (Mev)	Method	Reference	Threshold from mass formulas†
H^3		2.23	Calib.	1.8	*A*	2.23	masses		
Li^6	7.5	5.35	0.20	1.0	*A*	5.4±0.2	(γ,n)	‡	4.38
Li^7	92.5	7.15	Calib.	1.0	*A*	7.15±0.07	masses		15.47
Be^9	100	1.67	Calib.	0.9	*A*	1.67±0.08	masses		0.73
B^{10}	18.4	8.55	0.25	2.1	*A*	8.33±0.10	masses		6.33
B^{11}	81.6	11.50	0.25	1.0	*A*	11.32±0.10	masses		14.44
Na^{23}	100	12.05	0.20	2.5	*A*	11.7±0.5	masses		13.75
Mg^{24}	77.4	16.55	0.25	1.9	*A*	16.2±0.3	(γ,n)	2b	15.31
Mg^{25}	11.5	7.25	0.20	1.4	*A*	7.1±1.0	masses		7.54
Mg^{26}	11.1	11.15	0.20	1.1	*A*	12.0±0.9	masses		12.13
Al^{27}	100	12.75	0.20	2.0	*A*	11.1±2.0	masses		13.70
						14.0±0.4	(γ,n)	2b	
Si^{29}	6.2	8.45	0.20	1.0	*A*	8.48±0.01	(d,p)	‡	8.17
P^{31}	100	12.05	0.20	3.1	*A*	12.35±0.2	(γ,n)	2b	13.67
S^{34}	4.2	10.85	0.20	1.3	*A*	11.0±0.7	masses		12.48
Cl^{35}	75.4					9.6±1.4	masses		13.67
		9.95	0.20	1.6	*C*				
Cl^{37}	24.6					9.5±0.2	masses		11.58
V^{51}	100	11.15	0.20	1.4	*A*				10.70
Cr^{52}	83.8	11.80	0.25	2.3	*B*				11.45
Cr^{53}	9.4	7.75	0.20	1.6	*B*				7.35
Mn^{55}	100	10.00	0.20	1.4	*A*	10.15±0.2	(γ,n)	2c	10.92
Fe^{56}	91.6	11.15	0.25	1.4	*A*	≥11.3	(d,p)	1	11.62
Fe^{57}	2.1	7.75	0.20	1.5	*A*	7.65±0.10	(d,p)	1	7.76
						7.63	(n,γ)	§	
Co^{59}	100	10.25	0.20	1.5	*A*				11.13
Cu^{63}	70.1	10.85	0.20	1.5	*A*	10.9±0.2	(γ,n)	2b	11.31
Cu^{65}	29.9	9.75	0.20	1.4	*A*	10.2±0.2	(γ,n)	2a, 2b	10.26
Zn^{64}	50.9	11.65	0.20	1.1	*A*	11.8±0.2	(γ,n)	2a, 2c	11.93
Zn^{66}	27.3	11.15	0.20	0.7	*B*				10.85
Zn^{67}	3.9	7.00	0.20	2.0	*A*				7.48
Zn^{68}	17.4	10.15	0.20	1.4	*B*				9.86
Ga^{69}	61.2	10.10	0.20	1.8	*B*				10.46
Ga^{71}	38.8	9.05	0.20	1.6	*B*				9.55
As^{75}	100	10.10	0.20	1.6	*A*	10.3±0.2	(γ,n)	2f	9.78
$Se^{(?)}$		7.30	0.20	1.6	*C*				
$Se^{(?)}$		9.35	0.20	2.4	*C*				
Br^{79}	50.6	10.60	0.20	1.5	*A*	10.7±0.2	(γ,n)	2a, 2b	10.00
Br^{81}	49.4	9.95	0.20	1.4	*A*	10.2±0.2	(γ,n)	2a, 2b	9.22
Sr^{86}	9.9	9.50	0.20	1.9	*B*				9.92
Sr^{87}	7.0	8.40	0.20	1.4	*A*	8.42	(n,γ)	§	7.18
						8.52±0.2	(d,p)	1	
Sr^{88}	82.6	11.15	0.20	1.6	B				9.19
Cb^{93}	100	8.70	0.20	1.6	*A*				9.86
$Mo^{(?)}$		6.75	0.25	2.0	*C*				
$Mo^{(?)}$		7.95	0.25	2.0	*C*				
$Ru^{(?)}$		7.05	0.20	1.9	*C*				
$Ru^{(?)}$		9.50	0.20	1.6	*C*				
Rh^{103}	100	9.35	0.20	1.6	*A*				9.58
$Pd^{(?)}$		7.05	0.20	2.1	*C*				
$Pd^{(?)}$		9.35	0.20	1.6	*C*				
Ag^{109}	48.1	9.05*	0.20	2.5	*B*	9.3±0.5	(γ,n)	2a	9.20
Cd^{113}	12.3	6.55	0.20	2.0	*A*	6.44±0.15	(γ,n)	2c	6.80
In^{115}	95.5	9.05*	0.20	1.9	*B*	9.5±0.5	(γ,n)	see 1	8.85
Sn^{118}	22.5	9.10	0.20	1.8	*B*	9.33	(n,γ)	§	8.68
						9.37±0.2	(d,p)	1	
Sn^{119}	9.8	6.60	0.20	1.5	*B*	6.51±0.15	(γ,n)	2c	6.57
Sb^{121}	56					9.25±0.2	(γ,n)	2a, 2b	8.54
		8.95	0.25	2.3	*C*				
Sb^{123}	44								8.07
$Te^{(?)}$		6.50	0.20	1.9	*C*				
$Te^{(?)}$		8.55	0.20	1.7	*C*				
I^{127}	100	9.10	0.20	1.5	*A*	9.3±0.2	(γ,n)	2b	
						9.45±0.2	(γ,n)	2f	8.27
Cs^{133}	100	9.05	0.20	1.7	*A*				8.03
$Ba^{(?)}$		6.80	0.20	2.0	*C*				
$Ba^{(?)}$		8.55	0.25	1.7	*C*				
La^{139}	100	8.80	0.20	1.6	*A*	≥8.60	Calc.	See text	7.78

* These values could be influenced by the presence of a second unresolved isotope.
† C. F. v. Weizsäcker, Z. Physik **96**, 431 (1935); N. Bohr and J. A. Wheeler, Phys. Rev. **56**, 426 (1939); E. Fermi, *Nuclear Physics* (University of Chicago Press, Chicago, 1950), p. 7.
‡ Endt, Van Patter, and Bueckner, Phys. Rev. **81**, 317 (1951).
§ Kinsey, Bartholomew, and Walker, Phys. Rev. **78**, 77 (1950); **78**, 481 (1950); Bartholomew, Kinsey, and Walker, Phys. Rev. **79**, 218 (1950).

TABLE I.—*Continued.*

Isotope	Percent abundance	Present measurements: Threshold (Mev)	Error (Mev)	m	Class	Previous measurements: Threshold (Mev)	Method	Reference	Threshold from mass formulas†
Ce^{140}	89	9.05	0.20	1.4	*B*				8.09
Ce^{142}	11	7.15	0.20	1.5	*B*				7.70
Ta^{181}	100	7.55	0.20	1.8	*A*	7.7±0.2	(γ,n)	2b	7.49
$W^{(?)}$		6.25	0.30	1.0	*C*				
$W^{(?)}$		7.15	0.30	1.6	*C*				
Re^{187}	61.8	7.30*	0.30	1.5	*B*				7.35
Ir^{193}	61.5	7.80*	0.20	1.7	*B*				7.23
Pt^{194}	30.2	9.50	0.20	1.3	*B*				7.44
Pt^{196}	35.3	6.10	0.20	1.6	*A*	6.1±0.1	(γ,n)	2g	
						6.14±0.2	(d,p)	1	6.02
Pt^{198}	26.6	8.20	0.20	1.6	*B*	8.0±0.2	(d,p)	1	7.17
Au^{197}	100	7.90	0.20	1.7	*A*	8.00±0.15	(γ,n)	2c	
						8.10±0.10	(γ,n)	2g	7.38
Tl^{203}	21.9	8.80	0.20	1.6	*A*				7.26
Tl^{205}	70.9	7.55	0.20	1.1	*A*	7.48±0.15	(γ,n)	2c	
						7.7±0.2	(d,t)	5	7.02
Pb^{207}	22.6	6.75	0.20	1.3	*A*	6.737±0.01	(n,γ)	§	5.85
Pb^{208}	52.3	7.30	0.20	1.0	*A*	7.38±0.01	(n,γ)	§	6.96
Bi^{209}	100	7.40	0.20	1.7	*A*	7.44±0.05	(d,t)	5	7.16

disintegration energy of Ba^{139} is, however, higher than the present accepted value.[7] We computed from the above cycle a lower limit of 8.6 Mev for the threshold of La^{139}, which is then in agreement with our (γ,n) threshold of 8.8 Mev.

Lanthanum is a nucleus with 82 neutrons. The value of 8.8 Mev reduces the magnitude of the discontinuity in neutron binding occurring at this closed shell. However, the data for Cs^{133}, Ce^{140}, and Ce^{142} in Table I provide additional evidence for a closed shell in this region.

The values of the exponent m in the relation $Y\sim(E-E_0)^m$ have been included in Table I to completely define the data for each of the isotopes. The yield may also be expressed by the relation

$$Y=\int_{E_0}^{E_{\max}}\sigma(E)P(E,E_{\max})\eta(E)dE,$$

where $\sigma(E)$ is the cross section for the reaction at the energy E, $P(E,E_{\max})$ represents the bremsstrahlung distribution, and $\eta(E)$ is the detection efficiency of the apparatus. It should be possible, then, from measurements of m and E_0, to obtain experimental information regarding the behavior of σ in the vicinity of threshold, provided P and η are sufficiently well known. Our present information does not permit such computations.

[7] Nuclear Data, National Bureau of Standards Circular 499, September 1950.

PHYSICAL REVIEW VOLUME 84, NUMBER 3 NOVEMBER 1, 1951

Some Notes on Multiple-Boson Processes

ROY J. GLAUBER
Institute for Advanced Study, Princeton, New Jersey
(Received July 11, 1951)

Methods of calculation with nonlinear functions of quantized boson fields are developed during the discussion of two problems involving multiple boson processes. In the first of these a simple treatment is given of the multiple radiation of photons by classical current distributions, a special case of which, in effect, is the infrared catastrophe.

In the second illustration, generalizations of the scalar and pseudoscalar meson theories are considered in which the interaction hamiltonian depends exponentially on the meson field. In the pseudoscalar case such hamiltonians are closely related to the familiar form of pseudovector coupling. Assuming the over-all coupling of the nucleon and meson fields to be weak, calculations are made of the nuclear forces, and of the multiple production of mesons in meson-nucleon and in nucleon-nucleon collisions. In the latter events statistical independence of meson emissions is found to prevail.

I. INTRODUCTION

DEFICIENCIES in the mathematical techniques for handling quantized field theories obscure many questions of critical importance, such as the extent to which difficulties of the theory arise from a questionable expansion in powers of a coupling constant, and the importance of higher order corrections. An attempt has, therefore, been made, based on the developments due to Schwinger and others,[1,2] to find improved methods of computing the various matrix elements and expectation values of interest. Ideally these methods should be capable of handling rather general functions of quantized field variables, wherever possible without resorting to power series expansions. Simple rules accomplishing these ends have been found for dealing with functions of fields whose commutators with themselves are c-numbers, i.e., boson fields. While the problem of treating spinor fields remains, these methods make possible the simplification of some parts of the theory, and the generalization of others.

To illustrate both aspects of the work, the mathematical methods are developed during a discussion of two problems involving multiple-boson processes. In part II we discuss the radiation of quanta by a classical current distribution and in particular the well-known "infrared catastrophe" (the emission of an infinite number of soft photons when a charged particle is suddenly accelerated). The familiar results of Bloch and Nordsieck[3] are obtained in a rather direct way. In part III we discuss generalizations of the usual neutral scalar and pseudoscalar meson theories in which the interaction hamiltonian is allowed to depend exponentially on the meson field. A particular case of such an exponential hamiltonian involving the pseudoscalar field has been shown by Dyson[4] to result from a contact transformation performed on the familiar hamiltonian for pseudovector coupling of the pseudoscalar field. Couplings of the type introduced bring many high order aspects of the usually treated couplings much closer to the surface of the theory. Among these are higher order corrections to nuclear forces and the multiple production of mesons. We may hope, by treating these processes to gain some insight which the usual theory has not granted us.

II. RADIATION OF PHOTONS BY CLASSICAL CURRENTS

The infrared catastrophe causes low frequency divergences in the calculation of the radiative corrections to any process involving the sudden acceleration of charge, e.g., scattering in a potential field, Compton effect, pair production, etc. Bloch and Nordsieck treated the scattering of an electron by a potential by introducing several approximations, principally the neglect of pair effects and of the electron's recoil in photon emission. These approximations, which are justified by the very low energy of the photons involved, may be epitomized by saying that only the classical properties of the electron current are important. The general class of problems for which this property holds may be treated by considering the interaction of the quantized electromagnetic vector potential $A_\mu(x)$ ($\mu=1\cdots4$, $x_\mu=\mathbf{r}$, ict) with a classical current distribution $j_\mu(x)$, prescribed as a function of space and time.[5] The state vector $\Psi(\sigma)$ of the system on a space-like surface σ in the interaction representation obeys the Schrödinger equation[6]

$$i\delta/\delta\sigma(x)\Psi=H(x)\Psi, \tag{1}$$

where $H(x)$ is the interaction hamiltonian,

$$H(x)=-j_\mu(x)A_\mu(x). \tag{2}$$

The quantities we shall be interested in calculating are the probability amplitudes for the real emission of any specified number of photons. We may assume that the interaction began in the remote past when the system was in a state with no real photons present. The

[1] J. Schwinger, Phys. Rev. **74**, 1439 (1948).
[2] J. Schwinger, Phys. Rev. **75**, 651 (1949).
[3] F. Bloch and A. Nordsieck, Phys. Rev. **52**, 54 (1937).
[4] F. J. Dyson, Phys. Rev. **73**, 929 (1948).
[5] A treatment of the infrared catastrophe using classical currents has just been published by W. Thirring and B. Touschek, Phil. Mag. **42**, 244 (1951).
[6] We use units in which $\hbar=1$, $c=1$.

specification of the functions $j_\mu(x)$ may remain to the last step of the calculation.

Equations (1) and (2) are readily solved in two steps. The first is the familiar contact transformation due to Schwinger.[2] We define a new state vector $\Psi'(\sigma)$ by the relation,

$$\Psi(\sigma)=\exp\left(i\int_{-\infty}^{\sigma} j_\mu A_\mu dx\right)\Psi'(\sigma) \tag{3}$$

(in which $dx=dx_0dx_1dx_2dx_3$). Substituting into (1) and using the multiple commutator expansion to evaluate the transformed operators we find the equation of motion for Ψ'

$$\begin{aligned}&i\frac{\delta}{\delta\sigma(x)}\Psi'(\sigma)\\&=-\frac{i}{2}\int_{-\infty}^{\sigma} j_\mu(x)[A_\mu(x),A_\nu(x')]j_\nu(x')dx'\Psi'(\sigma)\\&=\frac{1}{2}\int_{-\infty}^{\sigma} j_\mu(x)D(x-x')j_\mu(x')dx'\Psi'(\sigma).\end{aligned} \tag{4}$$

This simple equation is exact since j_μ is a c-number. No quantized quantities are present in the transformed interaction, and the time dependence of $\Psi'(\sigma)$ therefore contains no real transitions. The information sought is already implicit in the part of the S-matrix given by (3). While the S-matrix is usually defined by the equation $\Psi(\infty)=S\Psi(-\infty)$, we shall find it briefer to work with an effective S-matrix defined from (3) as

$$S=\exp\left(i\int_{-\infty}^{\infty} j_\mu A_\mu dx\right). \tag{5}$$

This lacks merely the phase factor

$$\exp\left\{\tfrac{1}{2}i\int j_\mu(x)\bar{D}(x-x')j_\mu(x')dxdx'\right\}$$

which is due to the current's energy of self-interaction. A phase factor does not affect proton emission probabilities, since the latter are expressed as the absolute value squared of certain matrix elements of S. The calculation of these matrix elements occupies us next.

The operator S defined by (5) has matrix elements for the creation of any number of photons. A term which creates n photons is evidently given by the nth order term in the power series expansion of the exponential. However, n real photons may also be created by any term of order $n+2p$, where p is a positive integer. Such terms correspond to the creation of n real photons together with the virtual emissions and reabsorptions of p additional photons. Rather than consider the expansion term by term it will be convenient to develop general methods for separating real effects from their corrections due to virtual effects. We may do this in fact for functions of boson fields more general than the exponential of (5).

Let $\mathfrak{A}$ be a hermitian operator which, like $A_\mu(x)$ contains a sum of matrix elements for the creation and destruction of all possible photons. Such an operator may be a linear combination of the A_μ's evaluated at different places, or in particular the integral in the exponent of (5). Consider a power of $\mathfrak{A}$, say $\mathfrak{A}^m$. We ask now for the matrix element of $\mathfrak{A}^m$ for the creation of n real photons, where $n\leqq m$. The n factors of $\mathfrak{A}$ which are allowed to create the real photons may be chosen from the product in the binomial coefficient $\binom{m}{n}$ different ways, the remaining $m-n$ operators in each case being allowed to carry out virtual transitions. The desired matrix element, which we shall write as $\langle\mathfrak{A}^m\rangle_n$ must of course vanish unless $m-n$ is even. Setting aside for the moment some questions of commutation, if the real operators are separated from the virtual ones without changing the order of the latter, each of the partitions of the $\mathfrak{A}$'s should give the same matrix element. Their sum is

$$\langle\mathfrak{A}^m\rangle_n=\binom{m}{n}\mathfrak{A}^n\langle\mathfrak{A}^{m-n}\rangle_0, \tag{6}$$

in which the bracket $\langle\ \rangle_0$ retains its usual significance as the vacuum expectation value. The noncommutation of operators in the different factors of $\mathfrak{A}$ might be thought to add further terms to (6). Such terms though would only have the effect of correcting (6) for the cases in which some of the virtual photons are identical to the real ones. Since the density of photon states is enormous the contribution of such exact coincidences to the summations over all virtual photons implicit in the vacuum expectation is vanishingly small.[7] Equation (6) is in effect exactly correct in a quantized field theory. We may rewrite it in the symbolic form,

$$\langle\mathfrak{A}^m\rangle_n=\frac{1}{n!}\mathfrak{A}^n\left\langle\frac{d^n}{d\mathfrak{A}^n}\mathfrak{A}^m\right\rangle_0. \tag{7}$$

It is now evident that for any function $f(\mathfrak{A})$ expansible in a power series

$$\langle f(\mathfrak{A})\rangle_n=(1/n!)\mathfrak{A}^n\langle f^{(n)}(\mathfrak{A})\rangle_0, \tag{8}$$

where $f^{(n)}(\mathfrak{A})$ signifies the nth derivative.

Returning to (5) and identifying $\mathfrak{A}$ with $\int j_\mu A_\mu dx$; the effective matrix element for the creation of n photons becomes

$$\langle S\rangle_n=(1/n!)\left(i\int j_\mu A_\mu dx\right)^n\left\langle\exp\left(i\int j_\mu A_\mu dx\right)\right\rangle_0. \tag{9}$$

[7] If the quantization is carried out in a region of finite volume the corrections are easily seen to vanish as the reciprocal of the volume. Equation (6) also holds when the free factors of $\mathfrak{A}$ are used to absorb real photons. However, since we must assume that the ordering of these factors is immaterial they may not be used to emit and reabsorb the same photon. Such processes are already correctly accounted for among the vacuum fluctuations.

We require still an evaluation of the vacuum expectation of the S-matrix. To find this, we consider the quantity $\langle\exp(\lambda\mathfrak{A})\rangle_0$ as a function of the variable λ. Its derivative is

$$d/d\lambda\langle\exp(\lambda\mathfrak{A})\rangle_0=\langle\mathfrak{A}\exp(\lambda\mathfrak{A})\rangle_0$$
$$=(\Psi_{\text{vac}},\ \mathfrak{A}\exp(\lambda\mathfrak{A})\Psi_{\text{vac}}),\quad(10)$$

where the state vector for the vacuum has been written in explicitly. The only part of the operator $\exp(\lambda\mathfrak{A})$ which can contribute to the expectation value a term which does not vanish because of orthogonality is the part which creates a single photon, aside from virtual effects. This photon may then be annihilated by the remaining factor of $\mathfrak{A}$ in order to secure again the original vacuum state. Hence we may substitute $\langle\exp(\lambda\mathfrak{A})\rangle_1=\lambda\mathfrak{A}\langle\exp(\lambda\mathfrak{A})\rangle_0$ for the exponential on the right side of (10). We obtain thus a differential equation for the original expectation value

$$d/d\lambda\langle\exp(\lambda\mathfrak{A})\rangle_0=\lambda\langle\mathfrak{A}^2\rangle_0\langle\exp(\lambda\mathfrak{A})\rangle_0.\quad(11)$$

The solution, which must reduce to unity for $\lambda=0$ is evidently

$$\langle\exp(\lambda\mathfrak{A})\rangle_0=\exp(\tfrac{1}{2}\lambda^2\langle\mathfrak{A}^2\rangle_0).\quad(12)$$

Vacuum expectations of more general functions of $\mathfrak{A}$ may be found by expanding them as fourier or laplace integrals and applying (12) to the integrands.

By employing (12) the expression (9) for $\langle S\rangle_n$ may be evaluated explicitly,

$$\langle S\rangle_n=(1/n!)\left(i\int j_\mu A_\mu dx\right)^n e^{-\frac{1}{2}W},\quad(13)$$

where W is the integral

$$W=\int j_\mu(x)\langle A_\mu(x)A_\nu(x')\rangle_0 j_\nu(x')dxdx'\quad(14)$$

$$=\tfrac{1}{2}\int j_\mu(x)\langle A_\mu(x)A_\nu(x')+A_\nu(x')A_\mu(x)\rangle_0 j_\nu(x')dxdx'\quad(15)$$

$$=\tfrac{1}{2}\int j_\mu(x)D^{(1)}(x-x')j_\mu(x')dxdx'.\quad(16)$$

Use has been made, in going from (15) to (16), of Schwinger's evaluation[2] of the vacuum expectation of the symmetrized product of two A's. The function $D^{(1)}(x)$ is defined by the integral

$$D^{(1)}(x)=(2\pi)^{-3}\int e^{ik\cdot x}\delta(k^2)(dk).\quad(17)$$

Having evaluated the required matrix elements we are in a position to find the emission probabilities. The final state vector of the system $\Psi(\infty)$ is a sum of mutually orthogonal components $\Psi_n(\infty)$, each of which corresponds to a different number of photons present. Apart from a phase factor,

$$\Psi_n(\infty)=\langle S\rangle_n\Psi(-\infty)\quad(18)$$
$$=\langle S\rangle_n\Psi_{\text{vac}}.\quad(19)$$

The probability w_n for the emission of n photons is just the absolute magnitude squared of $\Psi_n(\infty)$.

$$w_n=(\Psi_n(\infty),\ \Psi_n(\infty))\quad(20)$$
$$=\langle\langle S\rangle_n\langle S\rangle_n\rangle_0.\quad(21)$$

The latter expression for w_n allows the summation over real final states of the system by employing the same formalism as is used for vacuum fluctuations. Employing the expression (13) for $\langle S\rangle_n$ we have

$$w_n=(n!)^{-2}\left\langle\left(\int j_\mu A_\mu dx\right)^n;\left(\int j_\mu A_\mu dx\right)^n\right\rangle_0 e^{-W}.\quad(22)$$

A semicolon has been used to separate the two factors in the expectation bracket in order to indicate that n photons must be created by the factor on the right and annihilated by the one on the left. No A's may be paired within a single factor since this would amount to using real photon operators to carry out vacuum fluctuations. These are already accounted for correctly in the factor e^{-W}. There are $n!$ ways of pairing the A's on either side of the semicolon and each contributes a factor W^n to the expectation value. Hence the emission probabilities form a poisson distribution,

$$w_n=W^ne^{-W}/n!.\quad(23)$$

The probability distribution assumes this simple form for the radiation from all classical systems since the successive photon emissions are statistically independent. This independence is destroyed, for example, when recoil effects are not negligible. Had a first-order perturbation calculation been made of w_1 the result would have been $w_1=W$. Evidently, the perturbation theory calculates in general in this approximation not the single photon emission probability, but the expectation value of the number emitted.

For most purposes $j_\mu(x)$ may be taken as simply the current due to a moving point charge. When the charged particle suffers a sudden change of velocity W is easily shown to be the infrared divergent integral familiar from the work of Bloch and Nordsieck, and of Pauli and Fierz.[8] The foregoing methods are also applicable to the discussion of Čerenkov radiation, for which purpose the D-functions may be generalized in a way appropriate to dispersive media.

III. MULTIPLE MESON EFFECTS

Hamiltonians for the interaction of nucleon and meson fields are usually taken, by analogy with quantum electrodynamics, to be linear in the meson field. More general types of interactions depending

[8] W. Pauli and M. Fierz, Nuovo cimento 15, 167 (1938).

nonlinearly on the meson field may, however, arise either as new assumptions, or as transformed versions of the familiar linear couplings. Calculations with such hamiltonians may be greatly simplified by some of the rules established in the previous section. As an exploratory example which, it develops, has particularly simple mathematical properties, we shall consider interactions of the form,

$$H(x)=\lambda\bar{\psi}(x)e^{\beta\varphi(x)}\psi(x), \tag{24}$$

between the spinor nucleon field $\psi(x)$ and the neutral scalar meson field $\varphi(x)$. The interaction is characterized by two coupling parameters, λ and β. The constant λ gives the over-all strength of the nucleon-meson coupling, while β determines the average number of mesons taking part in an elementary process. A corresponding pseudoscalar theory may be considered without changing notations by letting $\varphi(x)$ be a pseudoscalar field and letting β represent the matrix $i\eta\gamma_5$, where η is again a new coupling constant.

An interesting feature of interactions like (24) is that elementary events may involve high multiplicities of mesons (real and virtual) even when the coupling is weak (i.e., λ is small). Many effects of a type characteristic of the high orders of perturbation theory for the usual couplings are already present in the earliest terms of an expansion in powers of λ. We shall investigate some of the properties of such an expansion performed without specializing the parameter β.

The exponential hamiltonian (24) is of particular interest in the pseudoscalar case because of its coincidence with the result of a contact transformation performed on the familiar (linear) pseudovector coupling of the pseudoscalar field. The latter coupling is

$$H(x)=(1/\mu)j_\nu'(x)\partial\varphi(x)/\partial x_\nu+1/2\mu^2(\eta_\nu j_\nu)^2, \tag{25}$$

where

$$j_\mu'(x)=ig\bar{\psi}(x)\gamma_5\gamma_\mu\psi(x). \tag{26}$$

η_ν is the unit normal vector to the space-like surface, and μ and M are the meson and nucleon masses, respectively. Dyson has shown[4] that the hamiltonian (25) may be brought to a form containing no derivatives of the meson field by a contact transformation which suitably redefines the state vector $\Psi(\sigma)$. The new state vector $\Psi'(\sigma)$ is defined by the relation,

$$\Psi(\sigma)=e^{-iS(\sigma)}\Psi'(\sigma), \tag{27}$$

where

$$S(\sigma)=(1/\mu)\int_\sigma j_\mu'(x')\varphi(x')d\sigma_\nu', \tag{28}$$

the integration being carried out over the contemporary surface σ. ($d\sigma_\nu$ is a directed surface element parallel to η_ν.) It is not difficult to show that the Schrödinger equation satisfied by $\Psi'(\sigma)$ has the interaction hamiltonian given exactly by

$$H'(x)=M\bar{\psi}(x)\{\exp[(2ig/\mu)\gamma_5\varphi(x)]-1\}\psi(x). \tag{29}$$

The similarity of (29) to the pseudoscalar form of (24) is obvious when we note that the subtraction of a term $\lambda\bar{\psi}\psi$ from (24) would affect only the nucleon self-energy. The results to be derived from (24), therefore, include many of the higher order effects of the pseudovector coupling (25), but the approximation used, treating λ as small, is rigorously applicable to (25) only when M is small, i.e., $\mu\gg M$. Although such a limitation on the masses might be of use in treating a conjectured coupling between electrons and mesons, its effect for nucleon-meson systems is naturally quite unrealistic. The exact correspondence of (25) or (29) with the pseudoscalar form of (24) is, therefore, mainly of interest as a limiting case.

The simplest of the physical effects contained in the hamiltonian (24) is the nucleon self-energy. This is found by taking the vacuum expectation of the exponential factor.

$$\delta M=\lambda\langle e^{\beta\varphi(x)}\rangle_0, \tag{30}$$

which is evaluated, according to (11), as

$$\delta M=\lambda\exp[\tfrac{1}{2}\beta^2\langle\varphi^2(x)\rangle_0]. \tag{31}$$

To evaluate vacuum expectations of quantities quadratic in the meson field, we recall the relation,

$$\langle\varphi(x)\varphi(x')+\varphi(x')\varphi(x)\rangle_0=\Delta^{(1)}(x-x'). \tag{32}$$

The quantity $\beta^2\Delta^{(1)}(0)$ is quadratically divergent, and positive in the scalar case, negative in the pseudoscalar case. In either instance, however, its infinite effects may be removed by a redefinition, in effect a renormalization, of the constant λ. This is most directly illustrated by considering the matrix element for the collision of a meson with a nucleon, leading to the production of n mesons (including the original one). The desired matrix element is given, according to (8) by

$$\begin{aligned}\langle H\rangle_{n+1}&=\lambda\bar{\psi}(x)\psi(x)\frac{(\beta\varphi(x))^{n+1}}{(n+1)!}\langle e^{\beta\varphi(x)}\rangle_0\\&=\lambda'\bar{\psi}(x)\psi(x)\frac{(\beta\varphi(x))^{n+1}}{(n+1)!},\end{aligned} \tag{33}$$

where

$$\lambda'=\lambda\exp[\tfrac{1}{4}\beta^2\Delta^{(1)}(0)]. \tag{34}$$

Evidently if we consider the product $\lambda\exp[\frac{1}{4}\beta^2\Delta^{(1)}(0)]$ as a renormalized coupling constant λ', and regard the latter quantity as finite, the remaining effects are finite as well. This type of renormalization may be shown, by a somewhat simpler example (see Appendix) to be of use throughout the theory. It will be the only renormalization needed in order to obtain, in the lowest powers of λ, the physical effects of immediate interest.

The probabilities of the multiple production of mesons in meson-nucleon encounters[5] are readily cal-

[5] Meson-nucleon collisions, with exponential pseudoscalar coupling are also considered in a note by K. Sawada and K. Takagi, Prog. Theor. Phys. 4, 239 (1949).

culated by using the matrix element (33). Recursion relations for increasing numbers of mesons provide a convenient way of finding the required multiple integrals over the momentum spaces of the emergent particles. The results are most compactly stated for extremely energetic collisions, i.e., letting $P\dot{p}$ be the scalar product, $\mathbf{P}\cdot\mathbf{p}-P_0\dot{p}_0$, of the nucleon and meson momentum-energy vectors, we assume $-P\dot{p}\gg M^2$. In this limit, the total cross section, expressed as a sum over the possible numbers of emerging mesons is

$$\sigma=\frac{\lambda'^2\beta^4}{16\pi}\sum_{n=1}^{n_{\max}}\frac{1}{(n+1)!n!(n-1)!}\left(\frac{-\beta^2P\dot{p}}{8\pi^2}\right)^{n-1}. \quad (35)$$

The upper limit of summation is given by $n_{\max}\sim -P\dot{p}/M\mu$. The most probable multiplicity (and asymptotically the average) is

$$n\sim(-\beta^2P\dot{p}/8\pi^2)^{\frac{1}{2}}. \quad (36)$$

The meson emission is spherically symmetrical in the center-of-gravity system. Nucleon-anti-nucleon annihilation with the production of mesons is also contained in the matrix elements (33). The average multiplicity is again given by (36), expressed in terms of the scalar product of nucleon momenta.

To investigate two-nucleon processes more generally we must consider effects quadratic in λ. The two-nucleon part of the second-order hamiltonian, found by contact transformation, is an expression analogous to the hamiltonian in (4)

$$H^{(2)}(x)=\tfrac{1}{2}\int_{-\infty}^{\infty}\bar{\psi}(x)\psi(x)\mathfrak{W}(x,x')\bar{\psi}(x')\psi(x')dx', \quad (37)$$

where

$$\mathfrak{W}(x,x')=-\tfrac{1}{2}i\lambda^2[e^{\beta\varphi(x)},e^{\beta'\varphi(x')}]\epsilon(x-x'), \quad (38)$$

in which $\epsilon(x)$ is the familiar time-reversal function $x_0/|x_0|$. A distinction has been drawn between the two occurrences of β by priming the second since, in the pseudoscalar case, these are γ_5 matrices operating between different pairs of wave functions. In the scalar case they are of course identical constants. A simple theorem concerning exponential functions of operators enables us to evaluate the commutator in (38). Let a and b be any two operators whose commutator commutes with both of them. Then

$$e^ae^b=e^{a+b+\frac{1}{2}[a,b]}. \quad (39)$$

This is proved by considering the expression $e^{\zeta a}e^{\zeta b}e^{-\zeta(a+b)}$ as a function of the parameter ζ, and differentiating

$$\frac{d}{d\zeta}e^{\zeta a}e^{\zeta b}e^{-\zeta(a+b)}=e^{\zeta a}[a,e^{\zeta b}]e^{-\zeta(a+b)}=\zeta[a,b]e^{\zeta a}e^{\zeta b}e^{-\zeta(a+b)}.$$

The solution of this differential equation leads immediately to (39).

Using (39) to evaluate the commutator in (38) the interaction $\mathfrak{W}(x,x')$ is seen to be the operator,

$$\mathfrak{W}(x,x')=i\lambda^2e^{\beta\varphi(x)+\beta'\varphi(x')}\times\sinh\{\tfrac{1}{2}\beta\beta'[\varphi(x),\varphi(x')]\epsilon(x-x')\}$$
$$=-\lambda^2e^{\beta\varphi(x)+\beta'\varphi(x')}\sin\{\beta\beta'\bar{\Delta}(x-x')\}. \quad (40)$$

In the limit of very small β, which corresponds to the usual treatment of linear couplings, the interaction has the form $-\lambda^2\beta\beta'\bar{\Delta}(x-x')$, which is responsible for the familiar form of nuclear forces. For unrestricted values of β, $\mathfrak{W}(x,x')$ contains not only a rather different force between nucleons, but matrix elements as well for the creation of arbitrarily many mesons in a nucleon-nucleon collision. We consider first the nuclear forces.

The analogue of the Møller interaction between nucleons is the part of $\mathfrak{W}(x,x')$ which emits no real mesons, i.e., its vacuum expectation,

$$V(x-x')=-\lambda^2\langle e^{\beta\varphi(x)+\beta'\varphi(x')}\rangle_0\sin\{\beta\beta'\bar{\Delta}(x-x')\}$$

which, by using (11) and (32), is found to have the value

$$V(x-x')=-\lambda^2\exp[\tfrac{1}{2}\langle(\beta\varphi(x)+\beta'\varphi(x'))^2\rangle_0]\times\sin\{\beta\beta'\bar{\Delta}(x-x')\}$$
$$=-\lambda^2\exp[\tfrac{1}{2}\{\beta^2\Delta^{(1)}(0)+\beta\beta'\Delta^{(1)}(x-x')\}]\times\sin\beta\beta'\bar{\Delta}(x-x').$$

Once again the renormalization (34) may be used to remove the ambiguous factor. The result is more compactly expressed in terms of the Feynman function $\Delta_F=\Delta^{(1)}-2i\bar{\Delta}$,

$$V(x-x')=\lambda'^2\mathfrak{I}\exp[\tfrac{1}{2}\beta\beta'\Delta_F(x-x')], \quad (41)$$

where $\mathfrak{I}$ means the imaginary part.

The applicability of (41) to bound state problems may be decided, in the scalar case, by considering, in the nonrelativistic limit, the static potential between two nucleons. Recoil and retardation effects are neglected by assuming that the nucleon wave packets in (37) are slowly varying and may be evaluated at the same time. The time integration in (37) is then carried out approximately by just integrating $\mathfrak{W}(x,x')$, or in the present case $V(x-x')$. In effect, the time integral of $V(x)$ is just the nuclear potential. (For linear couplings it is easily verified that $\int_{-\infty}^{\infty}\bar{\Delta}(x)dx_0$ is the Yukawa potential.) The integration may be carried out by first expanding V in series, and gives for the first terms of the potential[10]

$$U(r)=\frac{-\lambda'^2\beta\beta'}{4\pi}\left\{\frac{e^{-\mu r}}{r}+\frac{\beta\beta'\mu}{(2\pi)^2r^2}K_1(2\mu r)+\cdots\right\}. \quad (42)$$

Near the origin the second term diverges as r^{-3}. The

[10] The bessel function $K_1(x)$ is defined by Watson, *A Treatise on the Theory of Bessel Functions* (Macmillan Company, New York, 1948).

further terms have the same signs and diverge successively as r^{-5}, r^{-7}, etc. The potential is therefore, much too strongly singular at the origin to permit a bound state.[11] In the pseudoscalar case, relativistic effects are not negligible, and the applicability of (41) can be decided rigorously only by much more detailed considerations. It appears, however, very unlikely that the interaction has bound states.

When two nucleons collide, mesons may be emitted by either one. The matrix element for the production of n mesons, in all, is given according to (8) and (40), by

$$\langle \mathfrak{W}(x,x')\rangle_n = \frac{\{\beta\varphi(x)+\beta'\varphi(x')\}^n}{n!}\langle \mathfrak{W}(x,x')\rangle_0 = \frac{\{\beta\varphi(x)+\beta'\varphi(x')\}^n}{n!}V(x-x'). \quad (43)$$

the special case of which, $n=0$, has already been considered. The form of the matrix element is a particularly simple one. Mesons of the group created by each nucleon are emitted at the same point in space-time and therefore independently of one another in momentum-space. A correlation between the momenta of the two groups is introduced, however, by the nuclear potential, and by the over-all conservation conditions for momentum and energy. In effect, the operator (43) preserves, in so far as possible, the statistical independence of the type mentioned in part II. Similar operators have already been treated in this connection by Lewis, Oppenheimer, and Wouthuysen.[12] An approximation they make to simplify their calculations, neglect of the momentum dependence in the fourier transform of the nuclear interaction, amounts to the replacement of $V(x-x')$ by a four-dimensional delta-function.[13] With this assumption, substitution of (43) into (37) gives a very simple matrix element, similar in its dependence on the meson field to (33), which was used for meson-nucleon collisions. The resulting meson production is once again spherically symmetric in the center-of-gravity system, and has an energy-dependent multiplicity proportional to (36). Experimentally observed angular distributions of mesons show a tendency to cluster around the axis of the collision. To investigate such effects with the operator (43) it will be necessary to consider interactions less singular than delta-functions.

The author is deeply indebted to Professor J. R. Oppenheimer for numerous discussions of the foregoing material. This work was begun under an AEC Postdoctoral Fellowship, and continued under the Frank B. Jewett Fellowship.

APPENDIX

It may be of interest to note that for the coupling

$$H(x)=\lambda\rho(x)e^{\beta\varphi(x)}, \quad (A.1)$$

where $\rho(x)$ is a classical scalar nucleon density, the S-matrix may be found exactly, and contains no infinities after the renormalization (34). The nth term of the S-matrix is given by

$$S^{(n)}=\frac{(-i\lambda)^n}{n!}\int P\{e^{\beta\varphi_1},e^{\beta\varphi_2}\cdots e^{\beta\varphi_n}\}\prod_{j=1}^{n}\rho_j dx_j, \quad (A.2)$$

where P is Dyson's time-ordering symbol, and φ_j and ρ_j are these functions evaluated at x_j. The reduction (39) of the product of two exponentials to a single one may be used to reduce the entire P-bracket.

$$P\{e^{\beta\varphi_1}\cdots e^{\beta\varphi_n}\}=\exp[\beta\Sigma\varphi_j-i\beta^2\sum_{j<k}\bar{\Delta}(x_j-x_k)]. \quad (A.3)$$

The matrix elements of $S^{(n)}$, because of (8), all involve the vacuum expectation of this expression, which may be written in renormalized form as

$$\lambda^n\langle P\{e^{\beta\varphi_1}\cdots e^{\beta\varphi_n}\}\rangle_0=\lambda'^n\exp[\tfrac{1}{2}\beta^2\sum_{j<k}\Delta_F(x_j-x_k)]. \quad (A.4)$$

[11] Ironically, however, for $\beta=-\beta'$ (dissimilar nucleons oppositely charged), the potential (42), although repulsive, is quite well-behaved. The series, summed over all terms, is less singular than $1/r$ near the origin (along the real axis) and may be shown to approach a finite value there for $\mu=0$.

[12] Lewis, Oppenheimer, and Wouthuysen, Phys. Rev. **73**, 127 (1948); H. Fukuda and G. Takeda, Prog. Theor. Phys. **5**, 957 (1950).

[13] Treatments to-date of multiple production by two nucleons have overlooked the interference between amplitudes for the creation of different numbers of mesons by each nucleon (the total number of mesons remaining fixed). For $V(x)\sim\delta^{(4)}(x)$ the interference effects are as important as the direct ones. Their inclusion increases the n-fold emission probability by a factor 2^n and the average multiplicity by 2!.

Classification of N^{13} Levels by Partial Wave Analysis of Proton Scattering from C^{12}*

HERBERT L. JACKSON† AND AARON I. GALONSKY
University of Wisconsin, Madison, Wisconsin

(Received July 19, 1951)

The nature of the excited levels in N^{13} between 2.24 and 5.64 Mev was investigated by analyzing the $C^{12}(p,p)C^{12}$ data of Goldhaber and Williamson. To carry out the analysis, the partial wave phase shifts were related to the level parameters by means of one level dispersion theory. Then by successive approximations of the level parameters, the partial wave expansion of the differential cross section for elastic scattering was fitted to the experimental curve. The analysis leads to the conclusion that the lower scattering anomaly is due to an $S_{\frac{1}{2}}$ level at 2.379 Mev above the ground state, and that the higher scattering anomaly results from a $P_{\frac{3}{2}}$ level at 3.501 Mev and a $D_{\frac{3}{2}}$ level at 3.549 Mev. Neither experiment nor analysis indicates any other levels in the range considered. It is shown that no other simple level assignment can account for the observed scattering cross section. The appearance of levels with $j=l+\frac{1}{2}$ instead of $j=l-\frac{1}{2}$ supports Mayer's hypothesis of level inversion in nuclei. The widths and energies of the levels obtained from the present analysis are in partial agreement with the values obtained from the (p,γ) reaction.

I. INTRODUCTION

THE low-lying energy levels of the N^{13} nucleus are currently of particular interest. For one reason, N^{13} is the mirror of C^{13}, whose levels have been observed. If the pp and nn forces are equal, the energy levels of mirror pairs such as C^{13} and N^{13} should have the same quantum numbers and similar reduced widths and characteristic energies. Thus knowledge of the energy level schemes of such nuclei will contribute toward an understanding of nuclear forces. Moreover, the level scheme of N^{13} should be fairly simple to interpret because, according to the closed shell model, this nucleus consists of a core of closed neutron and proton shells plus one outer proton. Finally, N^{13} is especially suitable for study by elastic proton scattering because: (1) its ground state is only 1.945 ± 0.004 Mev below the dissociation energy,[1] (2) the scattering nucleus C^{12} has zero spin, and (3) no other process competes seriously below 5.6 Mev. Thus, an unusually low-energy range is available for this kind of experiment, and the results are relatively easy to analyze since j can have only the values $l\pm\frac{1}{2}$.

Goldhaber and Williamson[2] obtained the $C^{12}(p,p)C^{12}$ differential cross section at a laboratory angle of 164° for bombarding energies extending from 0.32 to 4.00 Mev. Their results show two prominent scattering anomalies with maxima at 0.484 and 1.73 Mev. For convenience these anomalies are hereafter called resonances as distinct from the energy levels causing them. In order to determine the nature of the levels giving rise to these resonances, the partial wave expansion of the differential cross section for elastic proton scattering was fitted to Goldhaber's and Williamson's data. For spinless nuclei this expansion assumes the form:[3]

$$\frac{d\sigma}{d\omega}=\frac{1}{k^2}\left|-\frac{1}{2}\eta\csc^2\frac{\theta}{2}\exp i\eta\ln\csc^2\frac{\theta}{2}+\sum_{l=0}^{\infty}[(l+1)\sin\delta_l^{+}\exp i\delta_l^{+}+l\sin\delta_l^{-}\exp i\delta_l^{-}]\times P_l(\cos\theta)\exp i\alpha_l\right|^2+\frac{\sin^2\theta}{k^2}\left|\sum_{l=1}^{\infty}(\sin\delta_l^{+}\exp i\delta_l^{+}-\sin\delta_l^{-}\exp i\delta_l^{-})P_l'(\cos\theta)\exp i\alpha_l\right|^2,$$

where $d\sigma/d\omega$ is the differential cross section in the center-of-mass coordinate system; $k=1/\lambda=\mu v/\hbar$, μ being the reduced mass of the proton and v, its initial velocity; $\eta=ZZ'e^2/\hbar v$; $\delta_l^{\pm}$ is the noncoulomb phase shift of the partial wave of orbital angular momentum l and total angular momentum $j=l\pm\frac{1}{2}$;

$$e^{i\alpha_l}=\prod_{s=1}^{l}\left(\frac{s+i\eta}{s-i\eta}\right)\text{ for }l>0,\text{ and }e^{i\alpha_0}=1;$$

θ is the scattering angle in the center-of-mass coordinate system; $P_l(\cos\theta)$ is the lth Legendre polynomial; and $P_l'(\cos\theta)$ is the first derivative of $P_l(\cos\theta)$ with respect to its argument, $\cos\theta$. The first squared expression of the expansion represents those protons whose spins do not change direction in the scattering process, while the second squared expression represents those protons whose spins have been reversed.[3] Thus, the first expression gives the coherent part of the scattering and the second, the incoherent part.

The expansion of $d\sigma/d\omega$ is useful only if the phase shifts can be related to parameters characteristic of the levels involved. To connect $\delta_l^{\pm}$ with the desired level parameters we adopt the two following assumptions: (1) Elastic scattering is by far the most probable

* Supported by the Wisconsin Alumni Research Foundation and the AEC.

† Kimberly-Clark Fellow.

[1] Calculated from the Q value of the $C^{13}(d,n)N^{13}$ reaction of Bonner, Evans, and Hill, Phys. Rev. **75**, 1398 (1949), and the deuteron binding energy of R. C. Mobley and R. A. Laubenstein, Phys. Rev. **80**, 309 (1950).

[2] Gerson Goldhaber and R. M. Williamson, Phys. Rev. **82**, 495 (1951).

[3] This result follows immediately from Eqs. (4) and (5), C. L. Critchfield and D. C. Dodder, Phys. Rev. **76**, 602 (1949).

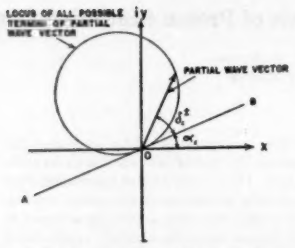

FIG. 1. Graphical representation of the dependence of the scattering amplitude of the (l, j)th partial wave on the phase shift $\delta_l^{\pm}$. Since the scattering amplitude is a complex number, it may be treated as a two-dimensional vector. As $\delta_l^{\pm}$ increases from 0° to 180°, the head of the vector traces out a circle in the complex plane. This circle is of diameter $j+\frac{1}{2}$ units, touches the origin, and is inclined at an angle α_l (see text) to the real axis. The superscript $\pm$ signifies that $j=l\pm\frac{1}{2}$.

process for each of the levels to be investigated. (2) Each of the observed scattering anomalies appreciably involves only one level of given angular momentum and parity. This assumption is, of course, the one-level approximation.

In the case of N^{13} these conditions are reasonably fulfilled. The only process present other than the elastic scattering is the (p,γ) reaction, and both the (p,p) and the (p,γ) data indicate a very simple level scheme up to 5.64 Mev. On the basis of the above assumptions the formalism of Wigner and Eisenbud[4] leads to the following simple expression for the partial wave phase shifts:[5]

$$\delta_l^{\pm}=-\text{arc tan}(F_l/G_l)_a+\text{arc tan}[\tfrac{1}{2}\Gamma_\lambda/(E_\lambda+\Delta_\lambda-E)]_a.$$

The first term on the right-hand side is usually called the potential phase shift, and the second, the resonant phase shift. The quantities F_l and G_l are the regular and irregular radial coulomb wave functions, respectively.[6] These quantities are functions of $\rho=kr$ and η, and must be evaluated for a chosen interaction radius, $r=a$. The second term depends on the interaction radius a, the incident proton energy E, and two parameters characteristic of the level. These parameters are the reduced width γ_λ^2, and the characteristic energy E_λ, which is closely related to the resonant energy E_r. Both E_λ and γ_λ^2 are independent of the momentum of the incident particle. By definition, the resonant energy E_r is that value of E for which $\delta_l^{\pm}=90°$. For low energies or high angular momenta E_r is also very nearly that value of E for which $E_\lambda+\Delta_\lambda-E=0$. The subscript λ signifies the various quantum numbers of the level. The relation between the experimental and reduced width[4] is

$$\tfrac{1}{2}\Gamma_\lambda=(k\gamma_\lambda^2/A_l^2)_a$$

where $A_l^2=F_l^2+G_l^2$, and

$$\Delta_\lambda=-\left[\frac{k\gamma_\lambda^2}{\rho}\left(\frac{\rho}{A_l}\frac{dA_l}{d\rho}+l\right)\right]_{\rho=ka}.$$

Since the arguments of the arctangents are dimensionless, and since all the quantities entering the argument of the resonance term have the dimension of energy, each quantity may be calculated either in the center-of-mass or laboratory system of coordinates, and E_λ and E may be measured from any convenient zero point. Throughout this paper E_λ, E, E_r, and γ_λ^2 are given their center-of-mass values, with the ground state of N^{13} as the energy zero, while E_p signifies the initial kinetic energy of the incident proton in the laboratory system.

II. METHOD

The analysis must begin with a choice of the parameter a because it determines the values of the coulomb wave functions and the quantities derived from them. In the formalism of Wigner and Eisenbud[4] the quantity a is completely arbitrary, except for a lower limit such that for all $r>a$, the interaction of the proton and target nucleus can be represented by a potential. However, in the one level approximation, it is advantageous to choose a as small as possible; that is, equal to the range of the noncoulomb interaction. Although the most suitable choice of a is somewhat indefinite, the value

$$a=1.45((A)^{\frac{1}{3}}+(1)^{\frac{1}{3}})\times10^{-13}\text{ cm}$$

suggested by Ehrman,[7] which is the sum of the radii of the proton and the target nucleus, was used throughout this analysis and seems satisfactory. Once a has been chosen, the analysis consists essentially of choosing those values of j, l, E_λ, and γ_λ^2 which best fit the experimental data. l and j are found by trial and error and E_λ and γ_λ^2 by successive approximation. The simplest technique is the graphical treatment worked out by Laubenstein.[8] Momentarily ignoring the factor $1/k$, one can write the amplitude of the coherent scattering thus:

$$-\tfrac{1}{2}\eta\csc^2\tfrac{1}{2}\theta\exp(i\eta\ln\csc^2\tfrac{1}{2}\theta)+\sin\delta_0\exp(i\delta_0)$$
$$+P_1(\cos\theta)\sin\delta_1^-\exp(i\delta_1^-+i\alpha_1)$$
$$+2P_1(\cos\theta)\sin\delta_1^+\exp(i\delta_1^++i\alpha_1)+\cdots.$$

This is a sum of complex numbers, each specified by its modulus and phase. The first term represents the Rutherford scattering; the second, that due to the $S_{\frac{1}{2}}$ phase shift, and so on. It is most informative to treat the terms as two-dimensional vectors in the complex plane, adding them by the closed polygon method. The coherent scattering cross section is then simply the absolute square of the resultant times $1/k^2$. For simplicity, the successive terms are called the Rutherford or R vector, the $S_{\frac{1}{2}}$ vector, the $P_{\frac{1}{2}}$ vector, and so on.

[4] E. P. Wigner and L. Eisenbud, Phys. Rev. **72**, 29 (1947).
[5] R. K. Adair, private communication.
[6] Bloch, Hull, Jr., Broyles, Bouricius, Freeman, and Breit, Revs. Modern Phys. **23**, 147 (1951).
[7] J. B. Ehrman, Phys. Rev. **81**, 412 (1951).
[8] R. A. Laubenstein, Ph.D. thesis, University of Wisconsin, 1950.

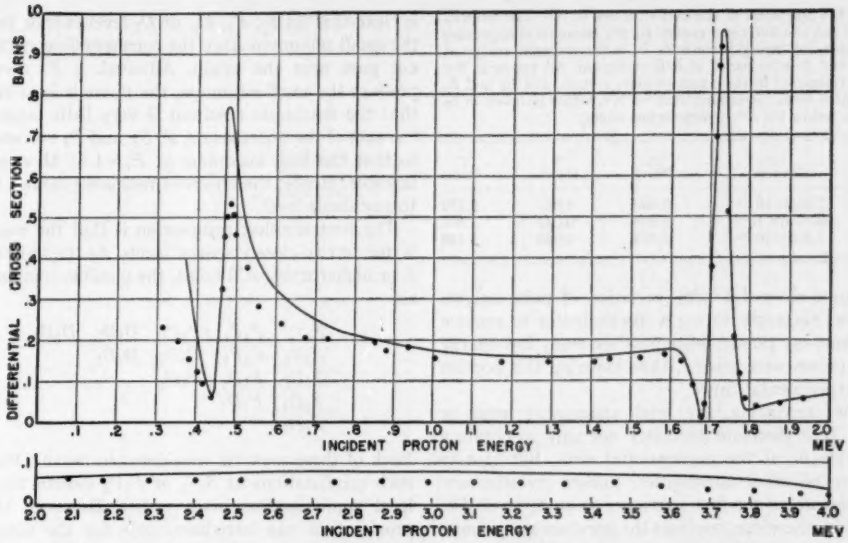

FIG. 2. Comparison of the experimental and calculated $C^{12}(p,p)C^{12}$ cross section from 0.32 to 4.0 Mev. The curve was calculated from the parameters given in Table I. The points are from Goldhaber's and Williamson's experimental data.

The partial wave vectors have other useful properties. As $\delta_l^{\pm}$ goes from 0° to 180°, the head of the associated vector describes a circle of diameter $(j+\frac{1}{2})P_l$ in the complex plane (see Fig. 1). This circle touches the origin (the point of contact corresponding to $\delta_l^{\pm}=0°$ or 180°), and is tangent to a line AB which passes through the origin and makes an angle α_l with the real axis. As $\delta_l^{\pm}$ increases, the head of the vector travels counterclockwise. The various circles, which are the loci of all possible end points of their corresponding vectors will henceforth be called the $S_{\frac{1}{2}}$ circle, the $P_{\frac{1}{2}}$ circle, and so on. Similar considerations apply to the incoherent scattering. Since this part of the scattering is proportional to $\sin^2\theta$, it is usually unimportant for scattering angles near 180°. In the present case, calculation shows that it is negligible except near the maximum of the upper resonance. Since the expansion of $d\sigma/d\omega$ depends only upon the kinematics of the scattering process, these properties of the partial wave vectors are independent of the simplifying assumptions introduced to get an analytic expression for $\delta_l^{\pm}$. From the above-discussed behavior of the scattering terms it is easy to predict the shape of any single narrow resonance if it is assumed that the other vectors contributing to the scattering change but little in the region of interest. Such is the case in the one-level approximation. Broad or overlapping levels are more difficult to analyze and require special effort to establish the uniqueness of the fit.

III. RESULTS

To fit the experimental cross section it is necessary to assign the lower resonance to an $S_{\frac{1}{2}}$ level and the higher resonance to a $P_{\frac{1}{2}}$ and $D_{\frac{1}{2}}$ level closely spaced. The letters S, P, and D designate the orbital angular momentum of the incident proton exciting the level, and hence specify the parity of the level itself. Insofar as the nucleus is accurately described by the single particle model, these letters also give the orbital momentum of the outermost proton. The numerical values of the level parameters which yield the best fit of the data thus far obtained are given in Table I. The widths Γ' were determined from plots of the (p,γ) cross section which were calculated for the values of E_λ and γ_λ^2 given in the table. Figure 2 shows the cross section curve calculated from the values in Table I together with a number of experimental points to show the agreement. The incoherent contribution to the scattering has been included and amounts to about 10 percent of the total at the peak of the upper resonance. In Fig. 2 the experimental points fall considerably below the calculated curve for energies less than 0.8 Mev. At the lower resonance the potential phase shifts are approximately zero for all l, so that the calculated maximum and minimum of that resonance depend only on the R vector and the diameter of the $S_{\frac{1}{2}}$ circle, both of which are independent of the interaction radius and hence unambiguous. It is therefore suspected that the disagreement results from poor experimental counting efficiency in this range.

The scattered protons were detected with a zinc sulfide scintillation counter which compared favorably with a proportional counter above one Mev. It was not feasible to check its performance at lower energies.[2] However, examination of the counter output with an

TABLE I. Parameters of the excited levels in N^{13}. The reduced width γ_λ^2 and characteristic energy E_λ are parameters appearing in the dispersion theory formalism. E_r is the resonant energy of the level and Γ is its width at half-maximum. All values in the table are computed in the center-of-mass system, and E_λ and E_r are measured from the ground state of N^{13}, which is taken to be 1.945 Mev below the C^{12}, p dissociation energy.

Level	γ_λ^2 (Mev cm)	E_λ (Mev)	Γ (Mev)	E_r (Mev)
$S_{\frac{1}{2}}$	7.565×10^{-13}	0.980	0.033	2.379
$P_{\frac{1}{2}}$	0.3766×10^{-13}	3.508	0.042	3.501
$D_{\frac{1}{2}}$	2.356×10^{-13}	3.593	0.040	3.549

oscilloscope showed a wide variation of pulse height. As it was necessary to use a discriminator to remove the gamma-ray pulses, quite possibly many low-energy proton pulses were missed, thus lowering this portion of the experimental curve.

To be convincing, the level assignment must be unique. It is therefore necessary not only to obtain a reasonable fit of the experimental data, but also to eliminate all other possibilities. Earlier investigators[9] have interpreted the first resonance as an $S_{\frac{1}{2}}$ level. The present fit, therefore, confirms the previous assignment. The upper resonance requires more thorough discussion. It is evident from Fig. 2 that the most informative part of the resonance lies between $E_p=1.65$ and 1.85 Mev. The crucial features of the curve are: (a) the slight rise of the curve below 1.68 Mev, (b) the very small magnitude of the minimum at 1.68 Mev, (c) the high maximum at 1.73 Mev, and (d) the shallow minimum at 1.83 Mev. Any believable level assignment must explain all these properties. In this range the R vector and the potential phase shifts are nearly constant. In addition, the potential phase shifts, $-\arctan F_l/G_l$, are nearly zero for $l>1$, so all D and higher terms not containing a resonance vanish. Wigner's criterion[4] rules out the possibility of any resonance with $l\geqslant3$. For $a=4.77\times10^{-13}$ cm,

$$\gamma_\lambda^2\leqslant3\hbar^2/2\mu a\doteq14\times10^{-13}\text{ Mev cm},$$

but for an experimental width of 40 kev and $l=3$,

$$\gamma_\lambda^2=\Gamma_\lambda A_3^2/2k\doteq32\times10^{-13}\text{ Mev cm}$$

which is over two times too large. Since for a given ρ and η, A_l increases with l, all resonances of higher orbital angular momentum are also excluded. A smaller value of a yields a larger limit, but also a much larger value for A_l^2, so the argument remains valid.

It is easy to show that no single S, P, or D level will account for the experimental shape. This is most simply done by drawing suitable vector diagrams, giving all nonresonance vectors their values at $E_p\sim1.7$ Mev and replacing the assumed resonant vector with its corresponding circle. The incoherent scattering is ignored since its only effect is to increase the maximum slightly. Figure 3 shows each possibility. From these diagrams it is clear that an $S_{\frac{1}{2}}$, $P_{\frac{1}{2}}$, $D_{\frac{1}{2}}$, or $D_{\frac{1}{2}}$ level cannot produce the small minimum since the corresponding circle does not pass near the origin. Although a $P_{\frac{1}{2}}$ level will produce the small minimum, the $P_{\frac{1}{2}}$ circle is so situated that the maximum resultant is very little larger than the sum of the nonresonant R, $S_{\frac{1}{2}}$, and $P_{\frac{1}{2}}$ vectors alone so that the high maximum at $E_p=1.73$ Mev is unattainable. Hence, the observed resonance cannot be due to any single level.

The next simplest assumption is that the resonance is due to two closely spaced levels. As the objection to F or higher levels still holds, the possible combinations are

$$\begin{array}{lllll} S_{\frac{1}{2}}S_{\frac{1}{2}} & P_{\frac{1}{2}}P_{\frac{1}{2}} & P_{\frac{1}{2}}P_{\frac{3}{2}} & D_{\frac{3}{2}}D_{\frac{3}{2}} & D_{\frac{3}{2}}D_{\frac{5}{2}} \\ S_{\frac{1}{2}}P_{\frac{1}{2}} & P_{\frac{1}{2}}P_{\frac{3}{2}} & P_{\frac{3}{2}}D_{\frac{3}{2}} & D_{\frac{3}{2}}D_{\frac{5}{2}} & \\ S_{\frac{1}{2}}P_{\frac{3}{2}} & P_{\frac{1}{2}}D_{\frac{3}{2}} & P_{\frac{3}{2}}D_{\frac{5}{2}} & & \\ S_{\frac{1}{2}}D_{\frac{3}{2}} & P_{\frac{1}{2}}D_{\frac{5}{2}} & & & \\ S_{\frac{1}{2}}D_{\frac{5}{2}}. & & & & \end{array}$$

Each of these must be considered in detail. Obviously such combinations as $S_{\frac{1}{2}}S_{\frac{1}{2}}$ or $P_{\frac{1}{2}}P_{\frac{1}{2}}$ violate the single level approximation made earlier. However, this approximation was introduced only for the purpose of obtaining an expression for $\delta_l^\pm$ in terms of the level parameters and incident proton energy. Therefore, when dealing with combinations involving two levels with the same l and j, the discussion must be independent of the analytic form of $\delta_l^\pm$. Fortunately, the properties of the locus circles are unchanged and are sufficient to eliminate all such combinations requiring consideration.

$S_{\frac{1}{2}}S_{\frac{1}{2}}$

The maximum cross section obtainable from this combination is

$$\begin{aligned}(d\sigma/d\omega)_{\max}&=k^{-2}|\mathbf{R}+\mathbf{P}_{\frac{1}{2}}+\mathbf{P}_{\frac{1}{2}}+\mathbf{S}_{\frac{1}{2}}|^2_{\max}\\&\leqslant k^{-2}(|\mathbf{R}|+|\mathbf{P}_{\frac{1}{2}}|+|\mathbf{P}_{\frac{1}{2}}|+|\mathbf{S}_{\frac{1}{2}}|_{\max})^2<0.4\text{ barn}.\end{aligned}$$

This disagrees with experiment, which gives a maximum at $E_p=1.73$ Mev of almost one barn.

$S_{\frac{1}{2}}P_{\frac{1}{2}}$ and $S_{\frac{1}{2}}P_{\frac{3}{2}}$

Figure 4 applies to the $S_{\frac{1}{2}}P_{\frac{1}{2}}$ case. The R and $P_{\frac{1}{2}}$ vectors as well as the $S_{\frac{1}{2}}$ circle are the same as in Fig. 3(a). Every point on the $S_{\frac{1}{2}}$ circle is a possible end point of the $S_{\frac{1}{2}}$ vector from which a $P_{\frac{1}{2}}$ circle may be drawn. It is easily seen that the locus of centers of all possible $P_{\frac{1}{2}}$ circles is another circle having the same radius as the $S_{\frac{1}{2}}$ circle. This is circle No. 2 in the figure. Circle No. 3 is the outer envelope of all possible $P_{\frac{1}{2}}$ circles. As no $P_{\frac{1}{2}}$ circle touches any point outside the outer envelope, the largest cross section obtainable under any circumstance is that calculated from the resultant drawn in the figure. Together with the incoherent part, which does not exceed 0.009 barn, this gives

$$(d\sigma/d\omega)_{\max}=0.54\text{ barn}$$

which is too small. The same argument is much stronger for the $S_{\frac{1}{2}}P_{\frac{3}{2}}$ case, because the diameter of the $P_{\frac{3}{2}}$ circle

[9] For bibliography see Hornyak, Lauritsen, Morrison, and Fowler, Revs. Modern Phys. **22**, 291 (1950).

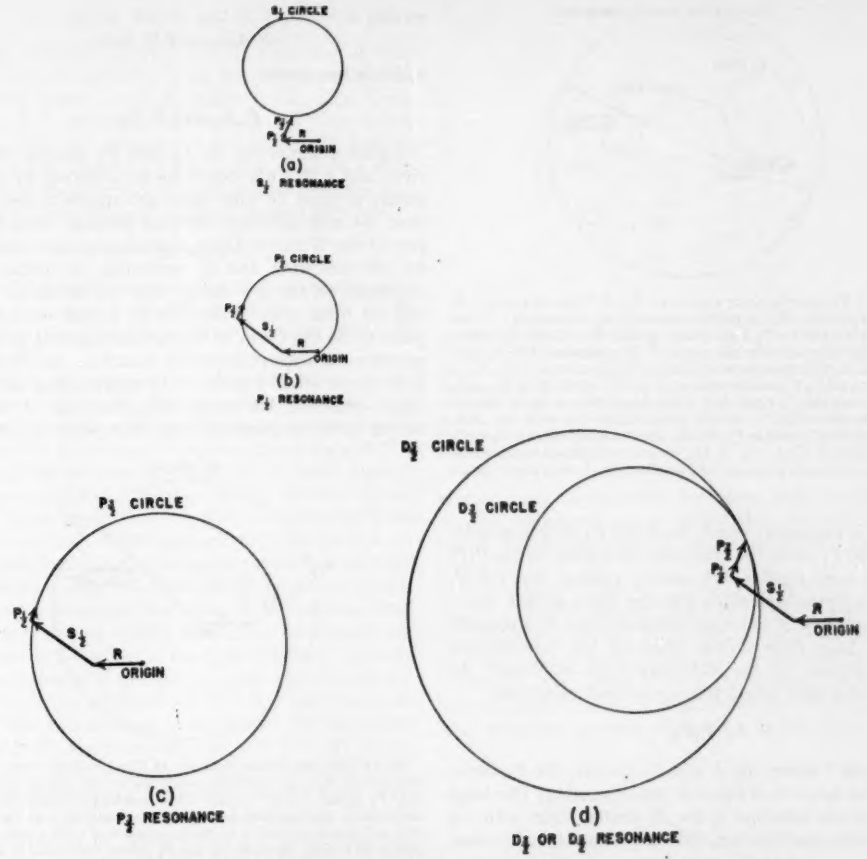

FIG. 3. The partial wave vectors at $E_p \sim 1.7$ Mev drawn on the assumption that the scattering anomaly at this energy is due to (a) an $S_{\frac{1}{2}}$ level, (b) a $P_{\frac{3}{2}}$ level, (c) a $P_{\frac{1}{2}}$ level, (d) a $D_{\frac{5}{2}}$ or $D_{\frac{3}{2}}$ level. The resonant vector is not drawn, but is represented by a circle which is the locus of all possible end points of that vector. The resultant scattering amplitude is the vector drawn from the origin to the head of the resonant vector, that is, to some point on the circle. For bombarding energies considerably below the resonant energy, the head of the resonant vector is near the head of the nonresonant vector through which the circle is drawn. As the energy increases, the head of the resonant vector moves counterclockwise around the circle. The journey is about half completed when the bombarding energy is equal to the resonant energy.

is only one-half the diameter of the $P_{\frac{3}{2}}$ circle so that the greatest possible maximum is much smaller.

$S_{\frac{1}{2}}D_{\frac{3}{2}}$ and $S_{\frac{1}{2}}D_{\frac{5}{2}}$

Figure 5 shows the general behavior of the resonance for the $S_{\frac{1}{2}}D_{\frac{3}{2}}$ combination. For definiteness, an arbitrary $S_{\frac{1}{2}}$ vector is shown, but the argument holds for any possible $S_{\frac{1}{2}}$ vector. As the potential phase shift of the $D_{\frac{3}{2}}$ wave is negligible, δ_2^- is approximately zero below the resonance. When passing through the resonance in the direction of increasing energy, δ_2^- increases from about 0° to some value near 180°. The $D_{\frac{3}{2}}$ vector consequently moves about the circle, successively passing points 1, 2, and 3. No matter how the $S_{\frac{1}{2}}$ vector misbehaves meanwhile, the minimum on the low-energy side of the maximum cannot be produced. The same argument also holds for the $S_{\frac{1}{2}}D_{\frac{5}{2}}$ case, since the only difference is an increase in the diameter of the D circle.

$P_{\frac{1}{2}}P_{\frac{3}{2}}$ and $P_{\frac{3}{2}}P_{\frac{3}{2}}$

Figure 6 applies to the $P_{\frac{1}{2}}P_{\frac{3}{2}}$ case. The R, $S_{\frac{1}{2}}$, and $P_{\frac{3}{2}}$ vectors and the $P_{\frac{1}{2}}$ circle are drawn together with the largest possible resultant. Including the incoherent part, the corresponding cross section is

$$(d\sigma/d\omega)_{\max} = 0.16 \text{ barn}$$

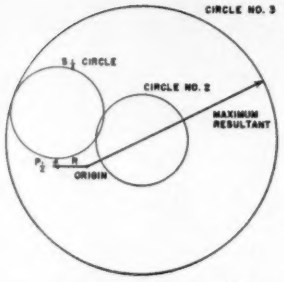

FIG. 4. The partial wave vectors at $E_p \sim 1.7$ Mev drawn on the assumption that the scattering anomaly at this energy is due to an $S_{\frac{1}{2}}$ level and a $P_{\frac{3}{2}}$ level closely spaced. The R and $P_{\frac{3}{2}}$ vectors are nearly constant over the region of the resonance. The $S_{\frac{1}{2}}$ circle is the locus of all possible end points of the $S_{\frac{1}{2}}$ vector. Circle No. 2 is the locus of all possible centers of the $P_{\frac{3}{2}}$ circle. It is the same diameter as the $S_{\frac{1}{2}}$ circle and is displaced from it by a distance equal to the radius of the $P_{\frac{3}{2}}$ circle. Circle No. 3 is the outer envelope of all possible $P_{\frac{3}{2}}$ circles. Since no part of any $P_{\frac{3}{2}}$ circle lies outside of Circle No. 3, the greatest possible scattering amplitude obtainable from an $S_{\frac{1}{2}}P_{\frac{3}{2}}$ combination is that shown in the figure.

which is impossibly small. Since the $P_{\frac{3}{2}}$ circle is smaller than the $P_{\frac{1}{2}}$ circle, the attainable maximum for the $P_{\frac{1}{2}}P_{\frac{3}{2}}$ case is even smaller. We note in passing that the $P_{\frac{1}{2}}$ circle is almost concentric with the origin so that, under the conditions of the experiment, a single $P_{\frac{1}{2}}$ resonance would have little visible effect on the experimental cross section. At the scattering angle employed, the incoherent part would produce a small maximum.

$P_{\frac{1}{2}}P_{\frac{1}{2}}$

Figure 7 shows the R and $S_{\frac{1}{2}}$ vectors, the $P_{\frac{1}{2}}$ circle, and the locus of centers of the $P_{\frac{1}{2}}$ circles. The large circle is the envelope of the $P_{\frac{1}{2}}$ circles. Even with the incoherent contribution, the maximum attainable cross section is

$$(d\sigma/d\omega)_{\max} = 0.50 \text{ barn}$$

which is too small.

$P_{\frac{1}{2}}D_{\frac{3}{2}}$ and $P_{\frac{3}{2}}D_{\frac{5}{2}}$

Figure 8 shows the R, $S_{\frac{1}{2}}$, and $P_{\frac{3}{2}}$ vectors, the $P_{\frac{3}{2}}$ circle and a $D_{\frac{3}{2}}$ circle drawn for an arbitrary $P_{\frac{3}{2}}$ vector ending at point D. This figure also applies to the $P_{\frac{3}{2}}D_{\frac{5}{2}}$ case, the only difference being an increase in the diameter of the D circle. These combinations are ruled out by the following line of reasoning. To obtain the minimum on the low-energy side, the D vector must still be quite small when the $P_{\frac{3}{2}}$ vector reaches the point C. So the D vector is practically zero at all lower energies. Somewhere below the resonance, the $P_{\frac{3}{2}}$ vector is in the vicinity of point A. In approaching the resonance from the low-energy side, the head of the $P_{\frac{3}{2}}$ vector moves counterclockwise from point A, through point B, toward point C. In so moving, the resultant becomes monotonically smaller since the D vector cannot make an appreciable contribution in this range. The experimental curve, on the contrary, shows a small but unmistakable increase in the cross section just before the minimum, so these combinations are not satisfactory.

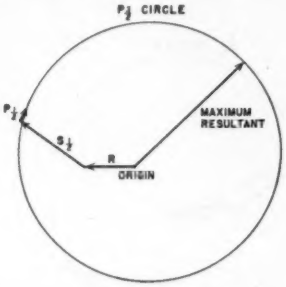

FIG. 6. The partial wave vectors at $E_p \sim 1.7$ Mev drawn on the assumption that the scattering anomaly at this energy is due to two $P_{\frac{3}{2}}$ levels closely spaced. This possibility differs from the assumption of a single $P_{\frac{3}{2}}$ level [Fig. 4(c)] only in that the phase shift δ_1^+ is now a function of the parameters of both levels. As the energy is varied, the head of the $P_{\frac{3}{2}}$ vector will move in a complicated manner about the circle. The maximum scattering amplitude attainable is that shown in the figure.

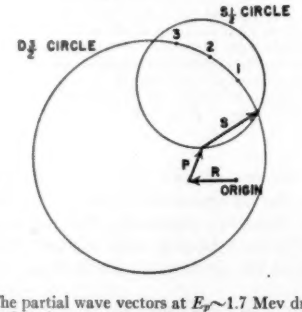

FIG. 5. The partial wave vectors at $E_p \sim 1.7$ Mev drawn on the assumption that the scattering anomaly at this energy is due to an $S_{\frac{1}{2}}$ and a $D_{\frac{3}{2}}$ resonance closely spaced. The P vector is the sum of the $P_{\frac{1}{2}}$ and $P_{\frac{3}{2}}$ vectors. The R and P vectors are nearly constant over the region of the resonance. The $S_{\frac{1}{2}}$ circle together with an arbitrary $S_{\frac{1}{2}}$ vector are shown. The position of the $D_{\frac{3}{2}}$ circle is determined by the vector S. The head of the $D_{\frac{3}{2}}$ vector lies on this circle, and as the energy increases, successively passes points 1, 2, and 3. The resultant scattering amplitude is the vector drawn from the origin to the head of the $D_{\frac{3}{2}}$ vector.

$P_{\frac{1}{2}}D_{\frac{3}{2}}$

This case differs from the $P_{\frac{1}{2}}D_{\frac{3}{2}}$ case only in that the diameter of the $D_{\frac{3}{2}}$ circle is one-third less than that of the $D_{\frac{3}{2}}$ circle. In fitting the $P_{\frac{1}{2}}D_{\frac{3}{2}}$ case, it was just possible to attain the experimental cross section and also reproduce the shape of the resonance. Efforts to attain substantially higher maxima cause unreasonable distortion of the curve. Because of the decreased size of the $D_{\frac{3}{2}}$ circle, the $P_{\frac{1}{2}}D_{\frac{3}{2}}$ combination cannot fit the experimental curve.

$D_{\frac{1}{2}}D_{\frac{1}{2}}$, $D_{\frac{1}{2}}D_{\frac{3}{2}}$, and $D_{\frac{3}{2}}D_{\frac{3}{2}}$

These combinations can be easily discarded. At this energy both D circles lie to the left of the head of the previously drawn vector as shown in Fig. 3(d). Thus, the smallest resultant obtainable is not very much smaller than the resultant of the R, $S_{\frac{1}{2}}$, $P_{\frac{3}{2}}$, and $P_{\frac{1}{2}}$ vectors alone. Since the cross section calculated from the sum of these vectors is much greater than the first minimum, none of these combinations is acceptable.‡

IV. DISCUSSION

The $C^{12}(p,\gamma)N^{13}$ reaction has two observed resonances. One is at $E_p=0.456\pm0.002$ Mev with $\Gamma=35$ kev,[10] and the other is at $E_p=1.697\pm0.012$ Mev with $\Gamma=74$ kev.[11]

These values apply in the laboratory frame of reference, and E_p is the kinetic energy of the incident proton. The corresponding values in the center-of-mass system, with E_r measured from the ground state of N^{13}, are $E_r=2.366$ Mev and $\Gamma=32$ kev for the lower capture resonance, and $E_r=3.510$ Mev and $\Gamma=68$ kev for the other. The energy of the lower level as determined from the (p,γ) reaction differs from our value for the $S_{\frac{1}{2}}$ level by 13 kev. Part of the difference is probably due to the fact that Δ_λ is large ($\sim$1.4 Mev) and varies rapidly with k and a, thus making our value of E_r uncertain, but it is impossible to explain the entire discrepancy on this basis. Our analysis of the $S_{\frac{1}{2}}$ level gives a width at half maximum of 33 kev, which agrees with the capture data. Our value of $E_r=3.501$ Mev for the $P_{\frac{3}{2}}$ level is within the experimental error quoted for the upper capture level, while our value of 3.549 Mev for the $D_{\frac{3}{2}}$ level is somewhat too high, indicating that most of the observed gamma-rays come from the $P_{\frac{3}{2}}$ level. This behavior is consistent with the assumption of a $P_{\frac{3}{2}}$ ground state for N^{13} since the $(P_{\frac{3}{2}}, P_{\frac{3}{2}})$ transition can occur by magnetic dipole or electric quadrupole radiation, and so should be much more probable than the $(D_{\frac{3}{2}}, P_{\frac{3}{2}})$ transition to the ground state which requires magnetic quadrupole or electric octopole radiation. However, the calculated widths of the $P_{\frac{3}{2}}$ and $D_{\frac{3}{2}}$ levels are only 42 and 40 kev, respectively, so that the large total width of 74 kev observed by Van Patter[11] possibly indicates that both levels participate in the capture process. One may also expect some 1.1-Mev gamma-radiation from the $(P_{\frac{3}{2}}, S_{\frac{1}{2}})$ electric dipole and the $(D_{\frac{3}{2}}, S_{\frac{1}{2}})$ electric quadrupole transitions. If such gamma-rays exist, their observation would lend support to the present level classification. However, their intensities may be quite weak on account of the relatively small energy differences between the $S_{\frac{1}{2}}$ and the $P_{\frac{3}{2}}$ and $D_{\frac{3}{2}}$ levels.

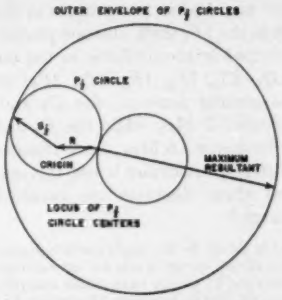

FIG. 7. The partial wave vectors at $E_p\sim1.7$ Mev drawn on the assumption that the scattering anomaly at this energy is due to a $P_{\frac{3}{2}}$ and a $P_{\frac{1}{2}}$ level closely spaced. The R and $S_{\frac{1}{2}}$ vectors are nearly constant over the region of the resonance. The $P_{\frac{3}{2}}$ vector is replaced by its circle. The small circle to the right of the origin is the locus of centers of all possible $P_{\frac{1}{2}}$ circles and the large circle is their outer envelope. Since no part of any $P_{\frac{1}{2}}$ circle lies outside the outer envelope, the greatest possible scattering amplitude is that shown in the figure.

In addition to the C^{13} levels at 3.083 and 3.677 Mev,[12] Rotblat[13] reports a level at 3.9 Mev. Assuming the equality of nn and pp forces, the existence of this level is consistent with the results of the present analysis.

Finally, the present level assignment supports Mayer's hypotheses[14] of large spin-orbit coupling and level inversion in nuclei. According to her model, the

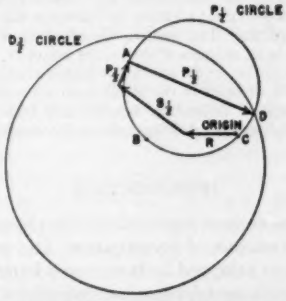

FIG. 8. The partial wave vectors at $E_p\sim1.7$ Mev drawn on the assumption that the scattering anomaly at this energy is due to a $P_{\frac{3}{2}}$ and a $D_{\frac{3}{2}}$ level closely spaced. The R, $S_{\frac{1}{2}}$, and $P_{\frac{1}{2}}$ vectors are nearly constant over the region of the resonance. The $P_{\frac{3}{2}}$ circle together with an arbitrary $P_{\frac{1}{2}}$ vector is shown. When E_p is much less than the resonant energy for the $P_{\frac{3}{2}}$ level, the head of the $P_{\frac{3}{2}}$ vector is near point A. As the energy increases, the head of the $P_{\frac{3}{2}}$ vector successively passes points B, C, and D. The $D_{\frac{3}{2}}$ circle is drawn for the $P_{\frac{3}{2}}$ vector at point D. The head of the $D_{\frac{3}{2}}$ vector is somewhere on this circle and the resultant scattering amplitude is the vector drawn from the origin to the head of the $D_{\frac{3}{2}}$ vector.

‡ *Note added in proof:* In a private communication Dr. E. P. Wigner has recently informed us that the upper limit for γ_λ^2 should be twice the value given above. This increased value does not absolutely exclude the possibility of an F level at the upper scattering anomaly. However application of the techniques used above shows that neither a single F level nor an F level in combination with another can account for the observed cross section. Since a detailed consideration of these possibilities would necessarily be quite long, it is omitted.

[10] W. A. Fowler and C. C. Lauritsen, Phys. Rev. **76**, 314 (1949).
[11] D. M. Van Patter, Phys. Rev. **76**, 1264 (1949).
[12] R. Malm and W. W. Buechner, Phys. Rev. **81**, 519 (1951).
[13] J. Rotblat, Proc. Harwell Nuclear Physics Conference, September, 1950.
[14] M. G. Mayer, Phys. Rev. **78**, 16 (1950).

unexcited N^{13} nucleus has two protons in the $1S_{\frac{1}{2}}$ shell, four protons in the $1P_{\frac{3}{2}}$ shell, and one proton in the $1P_{\frac{1}{2}}$ shell. The excited levels available to the outer proton are: $1D_{\frac{3}{2}}$, $1D_{\frac{5}{2}}$, $2S_{\frac{1}{2}}$, $1F_{\frac{5}{2}}$, $1F_{\frac{7}{2}}$, $2P_{\frac{3}{2}}$, $2P_{\frac{1}{2}}$; etc. On the basis of the present analysis, the $D_{\frac{3}{2}}$ and $P_{\frac{3}{2}}$ levels appear at about 3.5 Mev while the $D_{\frac{5}{2}}$ and $P_{\frac{1}{2}}$ levels presumably lie above 5.6 Mev, since experiment shows no other scattering anomalies below this energy. So, it appears that these doublets are inverted and the splitting is large.§

It is possible that one or more levels of high angular momentum or very small reduced width lie below 5.64 Mev, even though none was observed.[2] In the single-level approximation, the width of any level is inversely proportional to A_l^2 which increases rapidly with l. As the elastic scattering cross section was measured at 30-kev intervals away from the observed anomalies, such a level could have escaped detection.

We are most grateful to Dr. H. T. Richards for his interest, encouragement, and counsel throughout this undertaking, and to Dr. R. K. Adair and Dr. and Mrs. R. A. Laubenstein for information and advice.

§ *Note added in proof:* In the single particle approximation the reduced widths of the energy levels are approximately equal to $\hbar^2/\mu a$. (See reference 4.) On the basis of this analysis, the reduced widths of the $S_{\frac{1}{2}}$, $P_{\frac{3}{2}}$, and $D_{\frac{3}{2}}$ levels are 82 percent, 4.1 percent, and 24 percent of this value, respectively. The relatively small width of the $P_{\frac{3}{2}}$ level indicates that it is not a single particle level but rather arises from the excitation of two or more nucleons. If such is the case, the above argument does not apply so far as the $P_{\frac{3}{2}}$ level is concerned.

PHYSICAL REVIEW VOLUME 84, NUMBER 3 NOVEMBER 1, 1951

The Molecular Structure of Methyl Alcohol

DONALD G. BURKHARD* AND DAVID M. DENNISON
Harrison M. Randall Laboratory of Physics, University of Michigan, Ann Arbor, Michigan
(Received May 28, 1951)

A qualitative discussion of the near and far infrared spectrum of methyl alcohol shows that the rotational states, including the hindered rotation, may be well represented by a model consisting of a rigid hydroxyl and a rigid methyl group. These groups may perform a mutual rotation with respect to each other about the symmetry axis of the methyl group subject to a hindering potential which is assumed to have the form $V=\frac{1}{2}H(1-\cos 3x)$ where x is the angle of mutual rotation. A series of lines in the microwave spectrum, discovered by Hershberger and Turkevich, have recently been measured with great accuracy by Coles who also determined their Stark splitting. The positive identification of these lines leads at once to an estimate of the barrier height H.

The wave equation for the rotation of methyl alcohol is obtained and the matrix elements of the hamiltonian are evaluated using the wave functions derived by Koehler and Dennison on the basis of a simplified model. Diagonalizing the hamiltonian yields the energy levels which are found to predict correctly the principal features of the microwave spectrum. A quantitative comparison serves to fix the moments and product of inertia to have the values, $A=34.28$, $C_1=1.236$ and $D=-0.107$ all times 10^{-40} g cm^2. The two components of the electric moment are determined, $\mu_{\parallel}=0.893$ and $\mu_{\perp}=1.435\times10^{-18}$ esu. A relation is obtained between the barrier height H and the moment of inertia C_2 of the methyl group about its symmetry axis. Assuming C_2 to be equal to the methane moment of inertia, then $H=380$ cm^{-1}. If, in addition to taking a methane-like structure for the methyl group, it is assumed that the OH distance is the same as in water, namely 0.958A, one finds that (1) the CO distance is 1.421A, (2) the symmetry axis of the methyl group lies between the O and H atoms with the O displaced 0.084A from it and (3) the COH bond angle is 110° 15′. This latter angle is 5° 44′ greater than the apex angle in water vapor.

INTRODUCTION

THE spectrum of methyl alcohol has been examined by a number of investigators. The region from 2.5μ to 26μ was mapped by Borden and Barker[1] and the principal fundamental vibration frequencies were identified. The spectrum from 20μ to 57μ was measured by Lawson and Randall[2] who found it to consist of an intense series of irregularly but closely spaced lines. These are undoubtedly connected with the torsional vibration or hindered rotation of the molecule. More recently the microwave spectrum has been explored. A series of lines around 25,000 Mc which, from the regularity of their spacing, must clearly have a common origin, were discovered by Hershberger and Turkevich.[3] These lines were also observed by Dailey[4] and later were remeasured with high precison by Coles.[5] Coles not only found many more members of the series but also determined the number and spacing of the Stark components. Edwards, Gilliam, and Gordy[6] have measured a number of lines between 50,000 Mc and 35,000 Mc.

The general structure of methyl alcohol is fairly well known from chemical and spectroscopic evidence and is shown in Fig. 1. The methyl group is presumably very similar to the methyl group in methane or in the methyl

* Now at the Department of Physics, University of Colorado, Boulder, Colorado.
[1] A. Borden and E. F. Barker, J. Chem. Phys. **6**, 553 (1938).
[2] J. R. Lawson, thesis, University of Michigan (1938).
[3] W. D. Hershberger and J. Turkevich, Phys. Rev. **71**, 554 (1947).
[4] B. P. Dailey, Phys. Rev. **72**, 84 (1947).
[5] D. K. Coles, Phys. Rev. **74**, 1194 (1948).
[6] Edwards, Gilliam, and Gordy (to be published). We are very much indebted to Professor Gordy for sending us a preliminary account of their work.

halides where it is known that the CH distance is about 1.10A and the HCH angle is closely equal to the tetrahedral angle of 109° 28′. The distance between the carbon and oxygen has been estimated from electron diffraction measurements on similar molecules to be about 1.44A. There is little doubt but that the oxygen atom must lie close to the symmetry axis of the methyl group although not necessarily directly upon it. The symmetry axis may be defined as the line passing through the carbon atom and the center of gravity of the three hydrogen atoms. The OH distance is most probably of the same order as it is in the water molecule, namely, 0.958A and as a first approximation it is expected that the COH angle will be about equal to 105°, the apex angle in water.

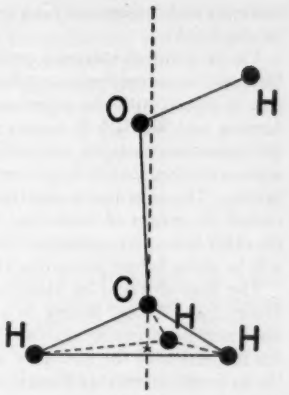

FIG. 1. The general structure of methyl alcohol.

The fundamental vibrations of methyl alcohol are 12 in number, of which one is to be associated with a torsional motion of the hydroxyl group with respect to the methyl group. This torsional motion has often been called a hindered rotation. Clearly, as the hydrogen of the hydroxyl group moves in a circle whose axis is the symmetry axis of the methyl group, it will encounter a potential with three identical minima. If the potential barriers separating the minima are sufficiently high, the hydrogen will oscillate with the torsional frequency. If the equal barriers are sufficiently low, the motion will approximate a free rotation of the hydroxyl group relative to the methyl group.

It was found by Borden and Barker[1] that, excluding the torsional frequency, the remaining fundamental frequencies are relatively high, the lowest being approximately 1000 cm^{-1}. The torsional frequency, as will appear from the present analysis, is only around 250 cm^{-1} and, consequently, the forces giving rise to the torsional oscillation are of the order of 16 times weaker than those producing the other fundamental vibrations. Thus, to a high degree of approximation in treating the problem of hindered rotation in methyl alcohol, one may consider that both the hydroxyl group and the methyl group are individually rigid and that their mutual motion consists only of a rotation of the one group relative to the other where the angle between the symmetry axis of the methyl group and the line of the hydroxyl group remains constant. The potential energy associated with this motion must be periodic and repeat itself upon a rotation through 120°. Since little is known concerning the detailed nature of such hindering potentials it is natural at the outset to assume the simple sinusoidal form, namely $V=\frac{1}{2}H(1-\cos 3x)$ where x is the angle of mutual rotation. This form will be used throughout the present work and, while it is undoubtedly only approximately correct, it appears evident that the most important features of the spectrum can be well represented by it. A similar situation is encountered with the ammonia molecule, where the inversion levels are relatively independent of the precise form of the double minimum potential.

Among the early discussions of the theory of hindered rotation are those by Nielsen,[7] and by Koehler and Dennison.[8] In the work of Koehler and Dennison the molecule was assumed for simplicity to consist of two symmetrical rotators having a common axis joining them. These rotators represented the hydroxyl and the methyl groups, and their moments of inertia along the symmetry axis were designated C_1 and C_2, respectively. In the present paper this simplifying assumption with regard to the hydroxyl group will not be employed but for a general understanding of the nature of the energy levels and for a qualitative estimate of the height of the barrier the Koehler-Dennison discussion will be sufficiently exact. They found that the rotational energy —including the hindered rotation—could be written as the sum of two terms $E=E_\alpha+E_\beta$, where

$$E_\beta=h^2[(J^2+J-K^2)/2A+K^2/2C],$$

and is thus equal to the usual rotational energy of a symmetrical top. A is defined as the moment of inertia about an axis which is perpendicular to the symmetry axis and which passes through the center of gravity of the molecule and $C=C_1+C_2$. E_α represents the internal or hindered rotation contribution and consists of successive groups of levels, each group containing three levels identified by the quantum number $\tau=1$, 2 or 3. The groups were denoted by the number $n=0, 1, 2, \cdots$. The qualitative interpretation is that, when the barrier is relatively high, each group represents a vibrational energy level of the torsional oscillation. Thus their positions (for high barrier) are approximately given by $h\nu_t(n+\frac{1}{2})$, where ν_t is the torsional frequency. The fact that each group contains 3 levels is of course due to the threefold nature of the potential. The splitting of the levels in any group is a periodic function of the rotational quantum number, K, times the ratio of moments of inertia $C_1/(C_1+C_2)$ but in order of magnitude it is equal to the exchange frequency between two minima. It is thus the analog of the inversion frequency in

[7] H. H. Nielsen, Phys. Rev. **40**, 445 (1932).
[8] J. S. Koehler and D. M. Dennison, Phys. Rev. **57**, 1006 (1940).

ammonia and consequently is a sensitive function of the barrier height.

The far infrared spectrum predicted by Koehler and Dennison was exceedingly complicated and to this extent only it agreed with the experimental results found by Lawson and Randall. It was so complex a function of the molecular constants, and the individual calculations were so tedious, that it did not seem practical to proceed further. The microwave spectrum has, however, furnished the means of evaluating the barrier height and the other molecular constants. The qualitative reasoning will be given before presenting the exact theory.

The lines observed by Hershberger and Turkevich,[3] Dailey,[4] and Coles,[5] belong to a series and their positions may be expressed as an analytic function of J^2+J. An inspection of the structure of the energy levels of the molecule shows that there is only one type of transition which can give rise to a series of lines in this region. It is (expressed as an emission rather than as an absorption line) $J\rightarrow J$, $K\rightarrow K-1$, $\tau\rightarrow\tau'$, $n=0\rightarrow 0$ and the series members correspond to $J=K$, $K+1$, $K+2$, etc. The Stark effect measurements of Coles show that the first line which lies at 24,934 Mc or 0.831 cm^{-1} has $J=2$ and the series has been traced as high as $J=30$. Since the series is analytic the position of a possible line with $J=1$ can be predicted with great accuracy. No line is found at this point and one must conclude that the first member of the series corresponds to $J=2\rightarrow 2$. The K transition must therefore be $K=2\rightarrow 1$.

The frequency of the transition can be expressed as the sum of two terms $\nu=\nu_a+\nu_\beta$, where ν_β is the contribution due to the usual rotational energy of a symmetrical top; namely, since $K=2\rightarrow 1$, $\nu_\beta=(3h/8\pi^2c)\times(1/C-1/A)$. The values of A and C, the moments of inertia for the entire molecule, may be estimated from the approximate dimensions given earlier and a substitution yields $\nu_\beta=9.9$ cm^{-1} and therefore $\nu_a=-9.1$ cm^{-1}. The situation is thus one in which the microwave lines result from a large positive term due to the usual rotation and on almost equally large negative term arising from the hindered rotation. An examination of the form of the hindered rotation levels shows that the selection rules (see reference 8) permit only one transition which results in a negative term. This is $\tau=1\rightarrow 2$.

The energy E_a, as is shown in reference 8, depends upon the quantum number K, upon the moments of inertia C_1 and C_2 and upon the barrier height, H. A rather crude initial estimate gives $C_1=1.43\times 10^{-40}$ and $C_2=5.33\times 10^{-40}$ and these lead to a barrier height $H=325$ cm^{-1}. The value for barrier height just obtained is not an accurate one since a simplified theory and approximate moments of inertia have been used but it must be of the right order of magnitude. The crucial point in its derivation was the identification of the microwave lines. About this the Stark effect measurements leave little doubt. Further progress requires the development of a more exact theory. It will be shown that this theory predicts (1) the magnitude of the Stark effect coefficients and (2) the spacing of the lines in the microwave series. Using the approximate values for C_1, C_2, and H it is found that both of these quantities agree qualitatively with the experimental results. It may be remarked that no agreement is obtained if the microwave lines are assumed to be due to a transition $K=1\rightarrow 2$ and $\tau=2\rightarrow 1$ with $\nu_\beta=-9.9$ and $\nu_a=+10.7$ cm^{-1}; a possibility which up to now could not be excluded.

The following procedure will be adopted:

1. The methyl alcohol will be represented by a model consisting of a rigid hydroxyl and a rigid methyl group. It is assumed that the hydroxyl group can rotate about the symmetry axis of the methyl group subject to the potential $V=\frac{1}{2}H(1-\cos 3x)$, where x is the angle of mutual rotation.

2. The kinetic energy will be derived and from this the Schroedinger wave equation obtained.

3. Matrix elements of the hamiltonian will be found using the wave functions of the simplified model employed by Koehler and Dennison. The matrix elements are all diagonal in the quantum number J but, in addition to the elements diagonal in K, possess elements where $K\rightarrow K\pm 1$ and $K\rightarrow K\pm 2$. Diagonalizing the hamiltonian yields the energy levels.

4. The predicted microwave spectrum will be compared with the observed spectrum for the purpose of obtaining values for the molecular constants.

KINETIC AND POTENTIAL ENERGIES

The kinetic energy of the model which has been chosen to represent the methyl alcohol molecule—namely, a rigid methyl group and a rigid hydroxyl group which may rotate with respect to each other—may be derived in the following manner. Consider two vectors $\boldsymbol{\varrho}_1$ and $\boldsymbol{\varrho}_2$ drawn from the center of gravity of the molecule (which for simplicity is assumed to be stationary) to the respective centers of gravity of the hydroxyl and methyl groups. Let $\mathbf{r}_i$ be a vector drawn from the center of gravity of the hydroxyl group to the mass m_i of that group. Let $\mathbf{R}_i$ be the corresponding vector from the center of gravity of the methyl group to the mass M_i. Let x, y, z and X, Y, Z be two sets of axes moving rigidly with the hydroxyl and methyl groups respectively and with origins at the centers of gravity of those groups. The Z axis is taken to be the symmetry axis of the methyl group and z is chosen to be parallel to Z. The oxygen and hydrogen atoms comprising the hydroxyl group are assumed to lie in the yz plane.

The angular velocities of the hydroxyl and methyl groups will be denoted by the vectors $\boldsymbol{\omega}$ and $\boldsymbol{\Omega}$, respectively, and their components along the moving axes will be ω_x, ω_y, ω_z and Ω_X, Ω_Y, Ω_Z.

With these definitions the vector velocities of the individual particles in each group are, respectively,

$$\mathbf{v}_i=d\boldsymbol{\varrho}_1/dt+\boldsymbol{\omega}\times\mathbf{r}_i, \quad \mathbf{V}_i=d\boldsymbol{\varrho}_2/dt+\boldsymbol{\Omega}\times\mathbf{R}_i.$$

Since, from their definitions $\Sigma m_i\mathbf{r}_i=\Sigma M_i\mathbf{R}_i=0$, twice the kinetic energy becomes

$$2T=\Sigma m_i(d\boldsymbol{\varrho}_1/dt)^2+\Sigma M_i(d\boldsymbol{\varrho}_2/dt)^2 +\Sigma m_i(\boldsymbol{\omega}\times\mathbf{r}_i)^2+\Sigma M_i(\boldsymbol{\Omega}\times\mathbf{R}_i)^2.$$

The vector $\boldsymbol{\varrho}_1$ has a constant length and lies in the zy plane. The angle which it makes with the OH line is a constant. Thus, $\boldsymbol{\varrho}_1$ moves as though it were rigidly connected to the hydroxyl group. The velocity of the center of gravity of the entire molecule as seen from the moving x, y, z coordinate system is $(\boldsymbol{\omega}\times\boldsymbol{\varrho}_1)$. This is, however, the negative of the velocity of the x, y, z origin as viewed from the center of gravity of the molecule. Therefore,

$$d\boldsymbol{\varrho}_1/dt=-(\boldsymbol{\omega}\times\boldsymbol{\varrho}_1).$$

From the definitions of $\boldsymbol{\varrho}_1$ and $\boldsymbol{\varrho}_2$ one has

$$\Sigma m_i\boldsymbol{\varrho}_1+\Sigma M_i\boldsymbol{\varrho}_2=0,$$

and a substitution yields

$$2T=\Sigma m_i(\boldsymbol{\omega}\times\boldsymbol{\varrho}_1)^2+\Sigma M_i(\boldsymbol{\omega}\times\boldsymbol{\varrho}_2)^2 +\Sigma m_i(\boldsymbol{\omega}\times\mathbf{r}_i)^2+\Sigma M_i(\boldsymbol{\Omega}\times\mathbf{R}_i)^2.$$

Since the z and Z axes are always parallel, $\omega_z^2+\omega_y^2$ is necessarily equal to $\Omega_X^2+\Omega_Y^2$. Expanding the above expression one obtains

$$2T=A(\Omega_X^2+\Omega_Y^2)-(A-B)\omega_y^2 -2D\omega_y\omega_z+C_1\omega_z^2+C_2\Omega_Z^2.$$

The meaning of these moments and products of inertia are most easily seen by constructing a coordinate system ξ, η, ζ whose origin lies at the center of gravity of the entire molecule and whose axes are parallel to the axes xyz. If μ_i denotes a mass of either of the two groups, $A=\Sigma\mu_i(\eta_i^2+\zeta_i^2)$ and is the moment of inertia of the molecule about the ξ axis. $B=\Sigma\mu_i(\xi_i^2+\zeta_i^2)$ is the moment of inertia about the η axis. One may define $C=\Sigma\mu_i(\xi_i^2+\eta_i^2)$ as the moment about the ζ axis. $D=\Sigma\mu_i\eta_i\zeta_i$ is the product of inertia with respect to the $\eta\zeta$ axes. $C_2=\Sigma M_i(X_i^2+Y_i^2)$ and is the moment of inertia of the methyl group along the Z or symmetry axis and $C_1=C-C_2=A-B$.

The orientation of the x, y, z axes which determine the position of the hydroxyl group may be expressed by means of the eulerian angles θ, ϕ_1, ψ and, as usual, one one obtains

$$\omega_x=\dot\theta\cos\phi_1+\dot\psi\sin\theta\sin\phi_1,$$
$$\omega_y=-\dot\theta\sin\phi_1+\dot\psi\sin\theta\cos\phi_1,$$
$$\omega_z=\dot\phi_1+\dot\psi\cos\theta.$$

The eulerian angles which fix the orientation of the methyl group are θ, ϕ_2, ψ and, since the z and Z axes are always parallel, only differ from the earlier ones in the angle ϕ_2 which measures the rotation of the methyl group about its symmetry axis. The expressions for Ω_X, Ω_Y, and Ω_Z may be obtained from ω_x, ω_y, ω_z by merely introducing ϕ_2 instead of ϕ_1. A substitution now yields the kinetic energy as a function of θ, ψ, ϕ_1, ϕ_2, and their time derivatives.

The potential energy must be a periodic function of the relative rotation of the methyl and hydroxyl groups, that is, of $\phi_1-\phi_2$ and must have a period of $2\pi/3$. As explained earlier, it is expected that the principal features of the spectrum will depend upon the periodic nature of the potential function and upon its general properties (such as the height of the barrier) but will be largely independent of any finer details. For this reason it is natural to choose the simple sinusoidal form,

$$V=\tfrac{1}{2}H[1-\cos3(\phi_1-\phi_2)].$$

The wave equation may be obtained in the usual manner by expressing the laplacian in the curvilinear coordinates for which the metric is given by $2T$. After writing out the laplacian, making the substitutions,

$$\phi=(C_1/C)\phi_1+(C_2/C)\phi_2,\quad x=\phi_1-\phi_2$$

and inserting the hindering potential, the wave equation takes the following form:

$$\mathrm{I}\left\{\frac{(A+B)C_1-D^2}{2A(BC_1-D^2)}\left[\frac{1}{\sin\theta}\frac{\partial}{\partial\theta}\left(\sin\theta\frac{\partial u}{\partial\theta}\right)+\cot^2\theta\frac{\partial^2u}{\partial\phi^2} -\frac{2\cot\theta}{\sin\theta}\frac{\partial^2u}{\partial\phi\partial\psi}+\frac{1}{\sin^2\theta}\frac{\partial^2u}{\partial\psi^2}\right]+\frac{1}{C}\frac{\partial^2u}{\partial\phi^2}+\frac{C}{C_1C_2}\frac{\partial^2u}{\partial x^2} +\frac{2}{\hbar^2}\left[E-\frac{H}{2}(1-\cos3x)\right]u,\right.$$

$$\mathrm{II}\left\{+\frac{D^2}{C_1(BC_1-D^2)}\left[\frac{C_1^2}{C^2}\frac{\partial^2u}{\partial\phi^2}+\frac{2C_1}{C}\frac{\partial^2u}{\partial\phi\partial x}+\frac{\partial^2u}{\partial x^2}\right],\right.$$

$$\mathrm{III}\left\{+\frac{2D}{BC_1-D^2}\left[\left(\frac{\partial^2u}{\partial\psi\partial x}+\frac{C_1}{C}\frac{\partial^2u}{\partial\phi\partial\psi}-\cos\theta\frac{\partial^2u}{\partial\phi\partial x} -\frac{C_1}{C}\cos\theta\frac{\partial^2u}{\partial\phi^2}-\frac{1}{2}\sin\theta\frac{\partial u}{\partial\theta}\right)\frac{\cos(\phi+(C_2/C)x)}{\sin\theta} -\left(\frac{\partial^2u}{\partial\theta\partial x}+\frac{C_1}{C}\frac{\partial^2u}{\partial\theta\partial\phi}+\frac{1}{2\sin\theta}\frac{\partial u}{\partial\psi}-\frac{\cos\theta}{2\sin\theta}\frac{\partial u}{\partial\phi}\right) \times\sin\left(\phi+\frac{C_2}{C}x\right)\right],\right.$$

$$\mathrm{IV}\left\{+\frac{(A-B)C_1+D^2}{2A(BC_1-D^2)}\left[\left(\frac{1}{\sin^2\theta}\frac{\partial^2u}{\partial\psi^2}-\frac{\partial^2u}{\partial\theta^2}+\cot^2\theta\frac{\partial^2u}{\partial\phi^2} -\frac{2\cot\theta}{\sin\theta}\frac{\partial^2u}{\partial\phi\partial\psi}+\cot\theta\frac{\partial u}{\partial\theta}\right)\cos2\left(\phi+\frac{C_2}{C}x\right) +\left(2\cot\theta\frac{\partial^2u}{\partial\theta\partial\phi}-\frac{2}{\sin\theta}\frac{\partial^2u}{\partial\theta\partial\psi}+\frac{2\cot\theta}{\sin\theta}\frac{\partial u}{\partial\psi} -(1+2\cot^2\theta)\frac{\partial u}{\partial\phi}\right)\sin2\left(\phi+\frac{C_2}{C}x\right)\right]=0.\right.$$

The boundary conditions governing the solutions of the wave equation are the same as those which were applicable to the simpler model studied by Koehler and Dennison[8] and are that the functions must remain finite at the poles $\theta=0$ or π and that they must be periodic with period 2π in the angles ψ, ϕ_1, and ϕ_2.

It will be noted that the wave equation has been divided into four groups of terms. Group I when set equal to zero is identical with the wave equation discussed by Koehler and Dennison providing their moment of inertia A is replaced by

$$2A(BC_1-D^2)/(AC_1+BC_1-D^2).$$

Its solutions, subject to the above boundary conditions, may be written,

$$u=\frac{1}{2\pi}e^{iK\phi}e^{iM\psi}\Theta_{JKM}\exp(-iC_1Kx/C)P_{(x)}{}^{K\tau n}.$$

The quantity $e^{iK\phi}e^{iM\psi}\Theta_{JKM}$ is the usual symmetric top wave function. $M_{(x)}=\exp(-iC_1Kx/C)P_{(x)}{}^{K\tau n}$ satisfies the equation

$$d^2M/dx^2+(R+S\cos 3x)M=0,$$

where

$$R=(2C_1C_2/C\hbar^2)(E^{K\tau n}-H/2),\quad S=C_1C_2H/C\hbar^2.$$

The total energy is equal to the sum of $E^{K\tau n}$ and E^{JK} where the latter is the symmetrical top energy,

$$E^{JK}=[\hbar^2(AC_1+BC_1-D^2)/4A(BC_1-D^2)]\times(J^2+J-K^2)+\hbar^2K^2/2C.$$

The boundary conditions require $P_{(x)}{}^{K\tau n}$ to be periodic in x with period 2π and it is customary to express it as

$$P_{(x)}{}^{K\tau n}=\sum_{-\infty}^{+\infty}a_me^{imx},$$

where m is an integer that may be shown to increase in steps of 3. The first kind where $\tau=1$ has a series where m takes on the values $\cdots-6, -3, 0, 3, 6, \cdots$. When $\tau=2$, m may be $\cdots-4, -1, 2, 5, \cdots$ and when $\tau=3$, $m=\cdots-5, -2, 1, 4, \cdots$. Both $E^{K\tau n}$ and the a_m are determined through finding the roots of continued fractions.[9]

The matrix elements of the hamiltonian corresponding to the complete wave equation will now be evaluated using the wave functions which are the solutions of the Group I terms. Since we shall be interested in the Stark effect it will be convenient to add these terms to the hamiltonian. They are

$$\mu_{11}\mathcal{E}\cos\theta+\mu_{\perp}\mathcal{E}\sin\theta\cos\phi_1,$$

where

$$\phi_1=\phi+C_2x/C.$$

$\mathcal{E}$ is the electric field intensity and μ_{11} and $\mu_{\perp}$ are the respective components of the permanent electric moment of the molecule, parallel and perpendicular to the symmetry axis of the methyl group. $\mu_{11}\mathcal{E}\cos\theta$ belongs with the Group I terms and $\mu_{\perp}\mathcal{E}\sin\theta\cos\phi_1$ with Group III.

The Group I terms yield elements of the hamiltonian which are diagonal in all four quantum numbers. Since the Group II terms do not contain θ, ϕ or x, explicitly, they are diagonal in JK and τ but need not be diagonal in n. Each term of Group III contains either the sine or cosine of $\phi+C_2x/C$ and will therefore connect states where $K\rightarrow K\pm1$. Similarly Group IV terms connect states where $K\rightarrow K\pm2$. The actual evaluation of the matrix elements may be performed through the known properties of the symmetric top wave functions (see for example Reiche and Rademaker).[10] Assembling these results one obtains

$$H_{JK\tau n}^{JK\tau n}=\hbar^2\Big[\{(AC_1+BC_1-D^2)(J^2+J-K^2)/4A(BC_1-D^2)\}+K^2/2C-(D^2/2C_1(BC_1-D^2))\int_0^{2\pi}(P^{K\tau n})^*\frac{d^2}{dx^2}P^{K\tau n}dx\Big]+E^{K\tau n}+\mu_{11}\mathcal{E}KM/(J^2+J),$$

$$H_{JK\tau n'}^{JK\tau n}=-[\hbar^2D^2/2C_1(BC_1-D^2)]\int_0^{2\pi}(P^{K\tau n})^*\frac{d^2}{dx^2}P^{K\tau n'}dx,$$

where $n'\neq n$

$$H_{JK+1\tau'n'}^{JK\tau n}=\Big\{[\hbar^2D/2(BC_1-D^2)]\int_0^{2\pi}\Big[\frac{e^{-iz}}{i}(P^{K\tau n})^*\frac{d}{dx}P^{K+1\tau'n'}-\frac{1}{2}e^{-iz}(P^{K\tau n})^*P^{K+1\tau'n'}\Big]dx+[\mu_{\perp}\mathcal{E}M/2(J^2+J)]\int_0^{2\pi}e^{-iz}(P^{K\tau n})^*P^{K+1\tau'n'}dx\Big\}[(J+K+1)(J-K)]^{\frac{1}{2}},$$

$$H_{JK+2\tau'n'}^{JK\tau n}=[\hbar^2(AC_1-BC_1+D^2)/8A(BC_1-D^2)][(J-K)(J-K-1)(J+K+1)(J+K+2)]^{\frac{1}{2}}\times\int_0^{2\pi}(P^{K\tau n})^*e^{-2iz}P^{K+2\tau'n'}dx.$$

[9] In the formulas (16), (17), and (18) given by Koehler and Dennison (see reference 8), the right-hand side of the equations should have a positive and not a negative sign.

[10] F. Reiche and H. Rademaker, Z. Physik. 41, 453 (1927).

In these formulas there is no restriction on the values of n' but the only nonvanishing elements will be those for which τ' obeys the following rules. For the elements where $K \rightarrow K+1$ the possible τ connections are $1 \rightarrow 3$, $3 \rightarrow 2$ and $2 \rightarrow 1$. For the elements where $K \rightarrow K+2$ the nonvanishing elements are those where τ goes from $1 \rightarrow 2$, $2 \rightarrow 3$, or $3 \rightarrow 1$.

The energy levels of the system are found as usual by calculating the roots of the determinant

$$|H^{JK\tau n}_{JK'\tau'n'} - E\delta_{K'}{}^{K}\delta_{\tau'}{}^{\tau}\delta_{n'}{}^{n}| = 0.$$

The τ connections given above have as their consequence that the energy determinant factors into three determinants. These may be designated by listing the possible K and τ values which characterize their diagonal terms.

	$K=\cdots$	-4	-3	-2	-1	0	1	2	3	$4\cdots$,
Determinant 1:	$\tau=\cdots$	1	3	2	1	3	2	1	3	$2\cdots$,
Determinant 2:	$\tau=\cdots$	3	2	1	3	2	1	3	2	$1\cdots$,
Determinant 3:	$\tau=\cdots$	2	1	3	2	1	3	2	1	$3\cdots$.

From the definition of the quantum number τ (see reference 8) the states K, $\tau=1, 2, 3$, are, respectively, identical with the states $-K$, $\tau=1, 3, 2$. For this reason the roots of determinant 1 are identical with those of determinant 2 and the levels so found are therefore all doubly degenerate. An examination of the symmetry properties of the molecule shows that they belong to the class E and that consequently their degeneracy cannot be removed by any perturbation having threefold symmetry.

The roots of determinant 3, with the exception of the root corresponding to $K=0$, $\tau=1$ which is single, all occur in pairs the members of which may be shown to belong to the symmetry classes A_1 and A_2. If the asymmetry of the molecule is small, the separation of the levels belonging to a pair becomes very small and decreases rapidly as K increases.

The solution which has been obtained for the model consisting of a rigid hydroxyl and a rigid methyl group which are coupled through a hindered rotation may be compared with the results found by Koehler and Dennison for the model in which both groups were rigid symmetric rotators. There are five principal differences all of which, in the case of methyl alcohol, where $(A-B)$ and D are small compared with A, have only minor effects upon the infrared spectrum but which assume importance in considering the details of the microwave spectrum. They are:

1. In that part of the energy which was described as the rotational energy of a symmetrical top $1/A$ has been replaced by

$$\frac{AC_1+BC_1-D^2}{2A(BC_1-D^2)} = \frac{1}{A} + \frac{C_1{}^2+D^2}{A(BC_1-D^2)}.$$

2. The diagonal element has been augmented by the term

$$-[h^2D^2/2C_1(BC_1-D^2)]\int_0^{2\pi} (P^{K\tau n})^* \frac{d^2}{dx^2} P^{K\tau n} dx.$$

For methyl alcohol the coefficient, when divided by hc, is of the order of 0.01 cm^{-1}. The integral for the state $K=0$, $\tau=1$, $n=0$ is of the order of -1.5 and its absolute value increases with K so that at $K=10$ it is approximately -7.

3. There now exists an off-diagonal term connecting the states K and $K\pm1$. For moderate values of J (10 or less) the numerical value of this term is much less than the difference between the diagonal elements of the states it connects. The usual approximation methods show that these off-diagonal elements contribute a term to the energy which is mainly proportional to J^2+J and which depends upon the quantum numbers K, τ and n.

4. The off-diagonal elements connecting the states K and $K\pm2$ have much the same properties as those just discussed and they will yield a term in the energy that is mainly proportional to $(J^2+J)^2$.

Qualitatively, effects 3 and 4 are just what are necessary to explain the series of lines observed by Coles[5] since their members may be expressed as a power series in which the terms involving (J^2+J) and $(J^2+J)^2$ are of dominant importance.

5. The energy levels $K=1$, $\tau=3$; $K=2$, $\tau=2$; $K=3$, $\tau=1$; $K=4$, $\tau=3$; etc., have become doublets with a spacing which decreases rapidly for large K values but which increases with J. This particular effect is the exact analog of the fact that the energy levels of the symmetrical top with the exception of $K=0$, become double if the top becomes asymmetric. Since neither of the levels $K=2$, $\tau=1$ or $K=1$, $\tau=2$ belong to the above class, the lines of the microwave series measured by Coles would not be expected to be double and are not observed to be.

It should be remarked that the matrix elements of the hamiltonian do degenerate properly to the elements of the hamiltonian for a rigid rotator when the barrier height goes to infinity. This degeneration is not immediately self-evident since the former elements contain C_1 while the latter contain only the total moment of inertia C. The point is that the diagonal elements (as the barrier becomes very high) contain the large term $h\nu_t(n+\frac{1}{2})$, where ν_t is the torsional frequency. The integrals occurring in the off-diagonal elements connecting n to $n\pm1$ are proportional to $\nu_t{}^{\frac{1}{2}}$. The diagonalization process involves dividing the squares of the off diagonal elements by the difference of the diagonal elements they connect and thereby a number of finite terms are introduced which bring about the desired degeneration.

INTERPRETATION OF THE MICROWAVE SPECTRUM AND EVALUATION OF MOLECULAR CONSTANTS

It is expected that the first line of the normal rotation series, namely $J=1\rightarrow0$, $K=0\rightarrow0$, $\tau=1\rightarrow1$, $2\rightarrow2$ or $3\rightarrow3$, should fall in the region of 48,000 to 50,000 Mc. Edwards, Gilliam, and Gordy[6] have measured several lines in this neighborhood. A study of the corresponding lines due to isotopic molecules of methyl alcohol (to be reported later) appears to show that the strong line found at 49,867.2 Mc can be uniquely assigned to this transition. The only off-diagonal terms which might contribute to this transition are small and to a high order of approximation,

$$(h/8\pi^2)[(AC_1+BC_1-D^2)/A(BC_1-D^2)]=49{,}867.2\times10^6.$$

The small off-diagonal terms referred to predict that this line should be a doublet corresponding to the transitions $\tau=1\rightarrow1$ and to the two coincident transitions $\tau=2\rightarrow2$ and $3\rightarrow3$. An estimate of the doublet separation yields a value of only a fraction of a megacycle and consequently it might well have escaped observation.

It is convenient to consider next the Stark effect to which the diagonal elements furnish the term $\mu_{11}\mathcal{E}KM/(J^2+J)$. The process of diagonalizing the hamiltonian will involve squaring the off-diagonal elements and the cross product from $|H^{J\ K\ \tau\ n}_{JK\pm1\tau'n'}|^2$, gives rise to a first-order Stark energy which may be shown to have the form

$$[\tfrac{1}{2}h^2D/(BC_1-D^2)][\mu_\perp\mathcal{E}M/(J^2+J)][f_1+(J^2+J)f_2].$$

The coefficients f_1 and f_2 are functions of K, τ and n and depend upon the indicated integrals containing $P_{(x)}{}^{K\tau n}$ and upon the resonance denominators.

The problem of evaluating the molecular constants for methyl alcohol is one of successive approximation and after one or two attempts the following trial values were selected,[11] $C_1=1.24\times10^{-40}$, $C_2=5.34\times10^{-40}$ and $H=368$ cm^{-1}. The integrals entering f_1 and f_2 are found to be quite insensitive to small changes in the constants and the most important of the resonance denominators is determined by the microwave lines themselves and, consequently, is independent of C_1, C_2 and H.

The microwave lines in question correspond to the transitions $J\rightarrow J$, $M\rightarrow M$ and K, τ, $n=2$, 1, 0$\rightarrow$1, 2, 0. The first-order Stark frequencies for these transitions have been calculated using the trial values of the constants and are given by the formula,

$$\mu_{11}\mathcal{E}M/h(J^2+J)+[D/\{8\pi^2c(BC_1-D^2)\}]\times[\mu_\perp\mathcal{E}M/(J^2+J)][0.105(J^2+J)-0.152].$$

The Stark frequencies measured by Coles may be expressed in cycles per second and are well represented by,[12]

$$[0.0111+0.877/(J^2+J)]M\mathcal{E}\times10^{-18}/h.$$

Identifying the corresponding terms one obtains,

$$\mu_{11}=0.893\times10^{-18}\text{ esu},$$

$$\mu_\perp hD/8\pi^2c\mu_{11}(BC_1-D^2)=0.1184\text{ cm}^{-1}.$$

The total electric moment of methyl alcohol has been meaxured by Kubo[13] and found to have the value 1.69 $\times10^{-18}$ esu and consequently, the absolute value of $\mu_\perp$ should be 1.435×10^{-18}. Further,

$$hD/8\pi^2c(BC_1-D^2)=-0.07368\text{ cm}^{-1}.$$

The table of atomic electronegativities shows that the component of the electric moment perpendicular to the axis lies along the positive y axis while the parallel component lies along the negative z axis and therefore $\mu_\perp/\mu_{11}$ in our notation, is negative. For this reason the Stark effect measurements demand that the product of inertia D must be negative.

It is interesting to calculate the components of the electric moment from the table of bond moments given by Pauling.[14] Assuming that the bond angle COH is 105° as in water vapor these yield $\mu_\perp=1.46$, and $\mu_{11}=-0.81\times10^{-18}$ esu. The total moment would then be 1.67×10^{-18} esu. The agreement between these approximate values and the Stark effects results is remarkably good.

The positions of the lines observed by Coles may be expressed by means of a power series in (J^2+J). The lines up through $J=8$ are accurately represented by

$$\nu=\nu_0+a(J^2+J)+b(J^2+J)^2+c(J^2+J)^3+d(J^2+J)^4$$

where, in megacycles, $\nu_0=24{,}948.13$, $c=-0.4094\times10^{-4}$, $a=-2.9656$, $d=-0.3168\times10^{-6}$, and $b=0.11258$.

The diagonalization of the hamiltonian gives rise, as mentioned earlier to two sets of terms, one proportional to J^2+J and the other to $(J^2+J)^2$. These results are correct for values of J where the magnitude of the off-diagonal elements is much smaller than the difference between the diagonal terms they connect. This condition obtains for J less than 10, and the dominant terms expressing the positions of the lines are indeed seen to be those proportional to (J^2+J) and to $(J^2+J)^2$.

It will prove convenient to examine first the contribution from the off diagonal terms for which $K\rightarrow K\pm2$. Their evaluation requires the calculation of the various integrals

$$\int_0^{2\pi}(P^{K\tau n})^*e^{-2iz}P^{K+2\tau'n'}dx$$

[11] The values $h=6.624\times10^{-27}$ and $C=2.99776\times10^{10}$ were used in the calculations.

[12] The figures shown here differ by about 2 percent from those given in reference 5 and represent Coles' latest values. We wish to thank Dr. Coles and his associates for many helpful discussions and for keeping us fully informed on the progress of their work.

[13] M. Kubo, Sci. Papers, Inst. Phys. Chem. Research Tokyo **26**, 242 (1935).

[14] L. Pauling, *Nature of the Chemical Bond* (Cornell University Press, Ithaca, New York 1939), p. 68.

as well as the diagonal elements in order to obtain the resonance denominators. All of these quantities depend upon the molecular constants C_1, C_2, and H but fortunately again they are not sensitively dependent. Using the trial values given earlier the energy levels and fourier coefficients of $P^{K\tau n}$ were calculated and the contribution from the off-diagonal elements $K\rightarrow K\pm 2$ were obtained. The final result for the transition in question, namely $K\tau n=210\rightarrow 120$ was, in cm^{-1},

$$\Delta\nu=\left[\frac{h(C_1^2+D^2)}{32\pi^2cA(BC_1-D^2)}\right]^2[0.0635(J^2+J)^2 -0.241(J^2+J)-0.662].$$

The coefficient b may be expressed in cm^{-1} and upon equating this to the first term in the above formula, one finds

$$\frac{h(C_1^2+D^2)}{32\pi^2cA(BC_1-D^2)}=7.691\times 10^{-3}\text{ cm}^{-1}.$$

The experimental data have now been made to yield three relations involving the three constants A, $C_1=A-B$ and D. The numerical solution for these quantities gives,

$$A=34.281\times 10^{-40},\quad C_1=1.236\times 10^{-40},$$
$$D=-0.107\times 10^{-40}\text{ g cm}^2.$$

The accuracy of the determination will be discussed later.

The coefficient of the J^2+J term in the series observed by Coles cannot be utilized directly for the evaluation of the moments of inertia. The reason for this is that it depends upon three effects, only two of which can be calculated with any exactness. These are (1) the J^2+J contribution coming from the off-diagonal elements $K\rightarrow K\pm 2$. From the above formula, this has the numerical value -0.43 Mc, (2) The off-diagonal elements of the hamiltonian $K\rightarrow K\pm 1$ can be calculated using the trial values of C_1C_2 and H. These result in an addition to the frequency of (in cm^{-1}),

$$[hD/8\pi^2c(BC_1-D^2)]^2[-0.0052(J^2+J)+0.055].$$

Using the values for the moments of inertia this becomes, in megacycles,

$$-0.85(J^2+J)+8.9.$$

The sum of these two contributions falls short of the experimental constant a by 1.70 Mc and is due to (3) the centrifugal stretching. This effect is best understood by considering a rotation of the molecule essentially about the A or B axes, that is $K\ll J$. A centrifugal force proportional to J^2+J will attempt, among other things, to increase the HOC angle. An increase of this angle will presumably lower the potential barrier slightly since for values of the angle around 180° the barrier goes to zero. A decrease in the barrier height increases the distance between the hindered rotation levels E^{210} and E^{120}. Since this is a negative contribution to the microwave lines in question the effect will be to displace the lines towards smaller frequencies and since the change in the angle and hence in the barrier height is very small it will be proportional to J^2+J. An order of magnitude estimate can be made in the following manner. From the frequency of the vibration resulting from the change in the HOC bond angle the bond angle force constant may be obtained. Balancing this against the centrifugal force the distortion of the angle $\delta\alpha$ is found. Making the rather crude assumption that the proportional change in the hindered rotation levels is equal to the proportional change in the angle, that is, to $\delta\alpha/(180°-\alpha_0)$ one obtains that the lines will be displaced by the amount $-2(J^2+J)$ Mc; a result which is consistent with the $-1.70(J^2+J)$ Mc cited above.

The last and most important step in the cycle of calculations will be to use the origin of the microwave series, ν_0 to provide a relation between the moments of inertia and the barrier height. The difference between the diagonal elements for which $JK\tau n=J210$ and $J120$ is equal to ν_0 minus the small constant terms 8.93 and -1.18 Mc arising from the respective off-diagonal elements $K\rightarrow K\pm 1$ and $K\rightarrow K\pm 2$. This quantity is 24,940.38 Mc which, for uniformity with the previous expressions, will be expressed in cm^{-1}:

$$0.83197=(h/8\pi^2c)\left[3/C-\frac{3(AC_1+BC_1-D^2)}{2A(BC_1-D^2)} -(D^2/(BC_1-D^2)C_1)\left(\int_0^{2\pi}(P^{210})^*\frac{d^2}{dx^2}P^{210}dx -\int_0^{2\pi}(P^{120})^*\frac{d^2}{dx^2}P^{120}dx\right)\right]+(E^{210}-E^{120})/hc.$$

The two integrals in the above expression have been calculated using the trial values for C_1, C_2, and H mentioned earlier and are equal to -1.662 and -2.444, respectively. They are not critically dependent upon the constants and in any case the magnitude of the whole term is small being only -0.00501 cm^{-1}. Substituting for the moments of inertia A, C_1, and D one obtains

$$3h/8\pi^2cC+(E^{210}-E^{120})/hc=3.33220\text{ cm}^{-1}.$$

There are still two unknown constants, the barrier height H and the moment of inertia of the methyl group about its symmetry axis, C_2. The latter quantity has the value 5.328×10^{-40} g cm^2 in methane and this has been chosen as the point about which to make an expansion. The energy difference $E^{120}-E^{210}$ was calculated for a number of values of its variables, namely C_1/C and $\alpha=2\pi^2cC_1C_2H/hC$ and in the region of interest,

$$(E^{120}-E^{210})/hc=9.7386\text{ cm}^{-1}-(0.671)(\alpha^2-11.2) +4.12(C_1/C-0.19).$$

TABLE I. Barrier height H for several values of moment of inertia C_2.

$C_2\times10^{40}$	H, cm^{-1}
5.428	383.3
5.328	380.2
5.228	377.0

Using now the relation imposed by the origin of the microwave series, Table I has been constructed.

There is no reason to suppose that C_2 is precisely equal to the methane moment of inertia, and in fact measurements on other molecules containing methyl groups (such as the methyl halides) have revealed variations in C_2 of as much as 0.17×10^{-40}. It is however evident that H is not unduly sensitive to C_2, and in the remainder of this paper for purposes of discussion C_2 will be arbitrarily taken to be 5.328×10^{-40}.

DISCUSSION OF THE MOLECULAR CONSTANTS

The methyl alcohol constants as determined from the microwave spectrum are $A=34.28\times10^{-40}$, $H=380$ cm^{-1}, $C_1=1.236$, $\mu_{11}=0.893\times10^{-18}$ esu, $D=-0.107$, $\mu_\perp=1.435\times10^{-18}$, $C_2=5.328$ (assumed).

Since the microwave line at 49,867.2 Mc is, in the main, determined by A only, it is estimated that the value given above is probably not in error by more than a few tenths of a percent, provided of course that the microwave line has been properly identified. C_1 and D, on the other hand, depend more intimately upon the hindered rotation energies and matrix elements which are less well known since among other things the use of a sinusoidal potential function is only an assumption, although a plausible one. It is probable that C_1 and D are correct to within a few percent. It should be remarked that the moments and products of inertia given here are the effective ones for the normal vibrational state and not the equilibrium moments and products which would require many additional data for their determination.

The three quantities A, C_1, and D are, of course, quite insufficient for a determination of the six structural parameters of the molecule. If, however, the dimensions of the methyl group and of the hydroxyl group are assumed to be known, it is possible from the moments and product of inertia to fix the relative position of one group with respect to the other. In conformity with the somewhat arbitrary choice that has been made for C_2, the methyl group will be taken to have a methane like structure, that is, the CH distance will be set equal to 1.093A and the HCH angle will be 109° 28′.

Some information on the hydroxyl dimension may be obtained from a consideration of the vibration frequencies. The OH stretching frequency in methyl alcohol has been identified by Borden and Barker[1] and observed to lie at 3683 cm^{-1}. From the known force constants of the water molecule[15] one may calculate the vibration frequency to be associated with OH. After making an appropriate compensation for the effect of the anharmonic terms in the potential one obtains 3660 cm^{-1}. From Badger's rule this close equality of the frequencies would indicate that the OH equilibrium distance in methyl alcohol should not differ appreciably from its value in water, namely 0.958A. Assuming this to be the case, the quantities A, C_1, and D lead to the following results.

1. The symmetry axis of the methyl group, which was defined as the line determined by the carbon atom and the center of gravity of the three hydrogens, falls between the oxygen and the hydrogen of the hydroxyl group. The distance of the oxygen from the symmetry axis is 0.084A. This result depends principally upon the product of inertia D and in fact to a large extent upon the fact that D is small and negative. It is therefore considered to be quite reliable.

2. The COH angle has the value 110° 15′ and is, in the main determined by C_1, D, and the assumption regarding the OH distance. It is appreciably, but perhaps not unreasonably, larger than the apex angle in water vapor[15] of 104° 31′. One might speculate that the large COH angle may be connected with the fact that the hindering potential barrier is somewhat lower than was originally anticipated.

3. The CO distance is found to be 1.421A. This figure depends upon the moments and products of inertia, upon the OH distance and the dimensions of the methyl group, and consequently is not as certain as one would wish.

The machinery that has been developed for obtaining the rotational energy levels of the methyl alcohol molecule is unfortunately very cumbersome. In an effort to gain an over-all picture of the levels it may be pointed out that by far the largest part of the energy comes from the diagonal terms of the hamiltonian and, of these, the expression

$$-[\hbar^2D^2/2C_1(BC_1-D^2)]\int_0^{2\pi}(P^{K\tau n})^*\frac{d^2}{dx^2}P^{K\tau n}dx$$

is very small and may often be neglected. The remaining terms may be divided into the rotational energy of a symmetrical top and an internal rotation $E^{K\tau n}$. Using the numerical constants for the moments and products of inertia, the former may be expressed in wave numbers and becomes

$$0.83174(J^2+J-K^2)+4.2638K^2.$$

The internal rotation energy is a periodic function of $2\pi C_1K/3C$ and hence may be expanded as a fourier series in the angle γ which has here the numerical value $\gamma=(22.589)°$K. For the levels where $\tau=1$ and $n=0$, the internal energy in wave numbers has been calculated

[15] B. T. Darling and D. M. Dennison, Phys. Rev. **57**, 128 (1940).

to be

$$E^{K10}=136.3958-6.2785\cos\gamma$$
$$+0.2507\cos2\gamma-0.0190\cos3\gamma.$$

The remaining levels of this group, namely those for which $\tau=2$ and 3 and $n=0$, may be found by increasing γ by 120° and by 240°, respectively.

The higher internal energy levels cannot be determined with great accuracy at present, since these levels are near or above the top of the potential barrier and will depend to a larger extent upon the exact form of the hindering potential. The following formulas, which have been calculated for a sinusoidal potential, can only be considered as a guide to the true positions of the levels.

$$E^{K11}=368.9+48.6\cos\gamma+9.1\cos2\gamma+2.7\cos3\gamma,$$

$$E^{K12}=608-124\cos\gamma+17\cos2\gamma-12\cos3\gamma.$$

It must be emphasized that the values just given for the symmetrical top and the hindered rotation energies, as well as the figures for the molecular dimensions and barrier height, are dependent upon the moment of inertia C_2 and therefore must be viewed as provisional. Since it is unlikely that C_2 could differ from the methane moment of inertia by more than a few percent, it is believed that they are, at any rate, qualitatively correct.

The theory of the rotation of the methyl alcohol molecule as developed in the present paper appears to be successful in that it correctly predicts the principal features of the microwave spectrum and of the Stark splitting of the lines. The structural constants which have been derived from the experimental data are all reasonable. It would, however, be desirable to make further comparisons of the predictions of the theory with experimental observations in the hope of obtaining better values for the constants, of investigating the exact form of the hindering potential, and of finding a number of self-consistency checks. Two series of researches are being currently pursued with these purposes in mind. (1) The far infrared spectrum of methyl alcohol has been mapped from 22μ to 200μ. The entire region is found to be filled with intense lines whose spacing, while irregular, is of the order of from 1 to 1.5 cm^{-1}. It is believed that, by making use of the theory, most of these lines can be identified and the energy levels determined. Since the energy levels for $n=0$, 1, 2, and probably 3 are well populated at room temperature, the complete rotation spectrum must involve many transitions and is understandably complex. (2) Recently the microwave spectra of the isotopic methyl alcohol molecules with C^{13}, O^{18}, and deuterium have been measured. These data together with the correct identification of some of the other microwave lines which have been observed and which do not belong to the series considered hitherto, should provide many checks on the validity of the theory.

Microwave Spectrum of Methyl Alcohol

RICHARD H. HUGHES, WILLIAM E. GOOD,* AND DONALD K. COLES
Westinghouse Research Laboratories, East Pittsburgh, Pennsylvania

(Received June 4, 1951)

A series of absorption lines of $C^{13}H_3O^{16}H$ which was studied from $J=2$ to $J=10$ by Coles has now been followed up to $J=30$. The corresponding series for $C^{13}H_3O^{16}H$ and $C^{13}H_3O^{18}H$ have been found. The lines of the $C^{13}H_3O^{16}H$ series have been identified and measured from $J=2$ to $J=31$ and the lines of the $C^{13}H_3O^{18}H$ series from $J=2$ to $J=26$. Accurate Stark-effect measurements have been made of several low J lines of each of the above series and the coefficients tabulated. The frequencies of many other $C^{13}H_3O^{16}H$ lines between 20,000 and 40,000 Mc have been measured and tabulated. The order of the Stark effect, quantitative Stark-effect information, and J values of these lines are listed when known. The frequencies of several $C^{13}H_3O^{16}H$ lines which are not members of the above series are listed.

METHYL alcohol is one of the lightest and simplest molecules which is capable of internal rotation. In this molecule (Fig. 1), the OH group rotates around the axis of the CH_3 group. Since many of the alcohol absorption lines in the microwave region involve changes in both the internal and external rotations of the molecule, considerable information on both types of rotation is obtainable from the microwave spectrum. Because of the excellent resolution in the microwave region, it appears that microwave data are eminently suited for investigating the phenomenon of internal rotation in molecules.

Hershberger and Turkevich[1] and Dailey[2] have reported about twenty-five microwave absorption lines for ordinary methyl alcohol. Dailey discovered that some of the lines possess a linear Stark effect, and divided the lines between 20,000 and 26,000 Mc into those with symmetric Stark-effect patterns and those with asymmetric patterns. Five of the lines appeared to form a converging series. Coles[3] resolved the first "line" in this series into three separate lines and, by counting Stark components, was able to establish the J values of the lines from $J=2$ up to $J=10$. He measured the frequencies of these lines accurately and determined the coefficients of the first-order Stark effects. Dennison and Burkhard[4] have identified this series with the (absorptive) transitions $K=1\rightarrow2$; $\tau=2\rightarrow1$ and $J\rightarrow J$.

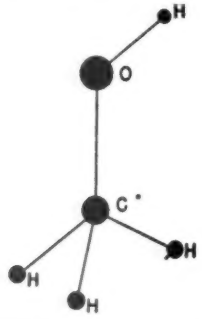

FIG. 1. Methyl alcohol molecule.

This paper describes a much more extensive study of ordinary methyl alcohol. Two other isotopic methyl alcohols have been prepared and studied. For their preparation see the Appendix. In particular, the aforementioned series has been found and traced in the spectra of $C^{13}H_3OH$ and $CH_3O^{18}H$. No attempt has been made to locate all the lines detectable on our spectrograph for these latter two isotopic molecules. Stark-effect studies of many of the lines are reported below.

Most of the methyl alcohol lines that we have observed exhibit a first-order Stark effect, similar to that exhibited by symmetric-top molecules. This appeared somewhat surprising to us, since the reported levels of rigid asymmetric rotors do not possess a linear Stark effect. In the case of very slightly asymmetric rigid rotors, the K-type doubling may be too small to resolve, so that they appear to have a first-order Stark effect, or a very close degeneracy may occur accidentally. But in any event, a necessary condition for a first-order Stark effect is a degeneracy of two rigid rotor levels of different symmetry species. In their theoretical treatment of the symmetrical rotator with hindered rotation (an approximation to the methyl alcohol molecule) Koehler and Dennison[5] pointed out that the internally rotating CH_3 group triples the number of energy levels, but at the same time brings about certain essential (and some nonessential) double degeneracies. The later theoretical discussion of methyl alcohol by Burkhard and Dennison (previous paper) deals with the modification in the levels and wave functions when an asymmetry is introduced. It is found that, in addition to a shift in the position of the levels, one-third of them are split into doublets and that this splitting is the exact analog of the splitting of the

* Now at Electronics Park, General Electric Company, Syracuse, New York.

[1] W. D. Hershberger and J. Turkevich, Phys. Rev. **71**, 554 (1947).

[2] B. P. Dailey, Phys. Rev. **72**, 84 (1947).

[3] D. K. Coles, Phys. Rev. **74**, 1194 (1948).

[4] See the preceding paper. Their preliminary results were presented in 1948 and 1949 at the Ohio State Symposia on Molecular Structure.

[5] J. S. Koehler and D. M. Dennison, Phys. Rev. **57**, 1106 (1937).

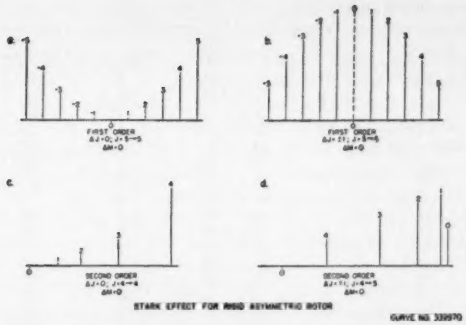

FIG. 2. Typical Stark effect patterns for asymmetric rotors. Methyl alcohol exhibits all types except c. This figure was drawn using the formulas given by S. Golden and E. B. Wilson, Jr., J. Chem. Phys. **16**, 669 (1948). The first-order Stark effect shown above is caused by a very close degeneracy of two asymmetric rotor levels of the same J. Dr. Kenneth Hurd has kindly pointed out to us that Fig. 2 does not include patterns due to a very close degeneracy of two levels of different J. An exact degeneracy of the type referred to by Dr. Hurd appears to be rather rare, however, in high resolution spectroscopy. It may be referred to as an "accidental" degeneracy. The type of degeneracy indicated in Figs. 2a and 2b may be called a "K-type" degeneracy—since it is due to a close coincidence of two levels with the same value of J and K. For many rigid molecules K-type degeneracy occurs for the higher values of K. For example, if the methyl alcohol were rigid, the two levels with $J=4$ and the same value of $K=4$ would be separated by about 0.0001 Mc. Higher values of $K=J<40$ would have a still smaller splitting. Such a very close K-type doublet would be observed as a single level possessing a first-order Stark effect.

levels of a rigid symmetric rotor when an asymmetry is introduced. They state that the lines of our series $K=1\rightarrow2$, $\tau=2\rightarrow1$, $J\rightarrow J$ arise from transitions between levels which are not split into doublets and they predict that these lines should show a first-order Stark effect in agreement with our observations.

Since the symmetric rotor possesses a first-order Stark effect while an asymmetric rotor with its K-type doubling does not, it seems very plausible that the doublet levels of the methyl alcohol molecule will not possess a first-order Stark energy. Burkhard and Dennison inform us that this appears to be the case although all of the details have not been worked out yet. Experimentally, about twelve lines have been found which do not possess a first-order Stark effect. In such lines only a small second- (or higher) order Stark effect is observed.

APPARATUS

A microwave spectrograph employing Stark-effect modulation[6] was used for all of these measurements. Sine-wave modulation at 85 kc was employed during most of the work although square wave modulation at 85 kc was used occasionally. The accurate frequency measurements were accomplished with a frequency standard very similar to that previously described.[6,7] A Collins 51-J receiver was used to interpolate between the 50-Mc reference frequencies obtained on the addition of a small 50-Mc voltage to the standard 500-Mc signal fed into the harmonic generator. It is believed that most of the frequencies quoted in the tables are within ±0.1 Mc and that many are closer than that.

THE SPECTRUM OF $C^{13}H_3O^{16}H$

A survey has been made of the spectrum of a sample of chemically pure methyl alcohol between 20,000 and 40,000 Mc. The spectrum is rich in strong lines and contains over one hundred lines with intensities greater than 10^{-8} cm^{-1}. Table I lists eighty-five lines, most of which are associated with $C^{12}H_3O^{16}H$. Lines known to be due to $C^{13}H_3O^{16}H$ and $C^{12}H_3O^{18}H$ are listed in Tables IV and V. Some of the weaker lines of Table I may be strong lines of the isotopic molecules, but all lines for which the J value has been specified are known to arise from the most abundant isotopic molecule. From the appearance of the lines on the Stark-effect microwave spectrograph, the lines are readily separated into those giving a first-order Stark effect and those giving a second-order Stark effect.

The existence of a series of several lines was first indicated by Hershberger and Turkevich[1] and later by Dailey[2] and Coles.[3] These lines exhibit first-order Stark patterns such as that shown in Fig. 2a, splitting up into $2J$ components symmetrically placed about the original line frequency. As the outer components are most intense and the intensities seem to be proportional to M^2, it appears that $\Delta J=0$ for these transitions. Dennison and Burkhard,[4] have suggested an interpretation for this series of lines. From the fact that the first line is $J=2$, they concluded that K changes from 1 to 2. From energy considerations they have identified this series as arising from transitions in which the external quantum number K changes from 1 to 2, the internal quantum number τ changes from 2 to 1, and

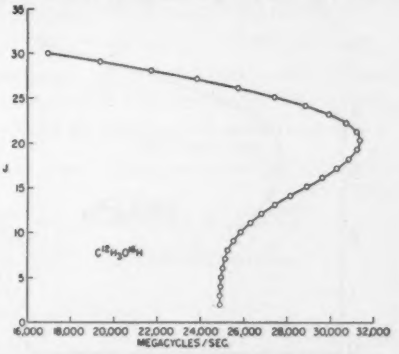

FIG. 3. Series of first-order Stark-effect lines in $C^{13}H_3O^{16}H$, arranged according to their rotational quantum number, J.

[6] McAfee, Jr., Hughes, and Wilson, Jr., Rev. Sci. Instr. **20**, 821 (1949). A. H. Sharbaugh, Rev. Sci. Instr. **21**, 120 (1950).

[7] W. E. Good and D. K. Coles, Phys. Rev. **71**, 383 (1947).

TABLE I. Methyl alcohol spectrum (mainly $C^{12}H_3O^{16}H$).

Lower J	$\pm\Delta J$[a]	Frequency	Stark order	Intensity	Lower J	$\pm\Delta J$[a]	Frequency	Stark order	Intensity
30	0	16,941.6	1	*W*	14	0	28,169.31	1	*M*
...	...	17,911.1	...	...	3	1	28,316.03	1	*M*
29	0	19,390.18	1	*W*	24	0	28,874.45	1	*W*
...	...	20,171.07	...	*M*	15	0	28,905.70	1	*M*
...	...	20,346.83	1	...	8, 9, or 10	1	28,969.9	2	*M*
high	...	20,908.87	1	...	...	...	29,113.76	1	*M*
10 or 11	1	20,970.65	2	*M*	16	0	29,636.91	1	*M*
...	...	21,244.2	...	*W*	...	...	29,889.33	1	
10 or 11	1	21,550.31	2	*M*	23	0	29,973.06	1	*W*
28	0	21,708.68	1	*W*	17	0	30,308.00	1	*M*
8 or more	1	23,121.20	2	*M*	...	...	30,678.66	1	*W*
...	...	23,347.53	2	*W*	...	...	30,693.42	...	*W*
8 or 9	1	23,444.82	2	*M*	22	0	30,752.26	1	*M*
27	0	23,854.25	1	*W*	18	0	30,858.40	1	*M*
...	...	24,533.7	2	*W*	21	0	31,209.75	1	*M*
3	0	24,928.70	1	*M*	19	0	31,226.70	1	*M*
4	0	24,933.47	1	*M*	20	0	31,358.31	1	*M*
2	0	24,934.38	1	*M*	...	...	31,673.05±0.2	...	*W*
5	0	24,959.08	1	*S*	high J	...	31,757.42	1	*M*
6	0	25,018.14	1	*S*	...	...	31,977.82	1	*M*
...	...	25,056.31	2	*W*	...	...	32,379.37	1	*M*
7	0	25,124.88	1	*S*	...	...	32,398.44	...	*W*
8	0	25,294.41	1	*S*	...	...	33,089.91	1	*M*
		25,322.98	1	*W*	...	...	33,414.1±0.2	...	*W*
9	0	25,541.43	1	*S*	...	...	33,566.20	...	*W*
26	0	25,787.12	1	*W*	...	...	33,568.2±2	...	*W*
10	0	25,878.18	1	*S*	18 to 22	1	33,691.63	2	*M*
9 or 10	1	26,120.50	2	*M*	18 to 22	1	33,693.74	2	Forbidden
11	0	26,313.11	1	*M*	18 to 22	1	34,001.35	2	Forbidden
...	...	26,550.15	...	*W*	18 to 22	1	34,003.69	2	*M*
...	...	26,778.9	...	*W*	14 or greater	1	34,236.91	1	*S*
...	...	26,783.18	...	*W*	...	...	34,417.86	1	*M*
12	0	26,847.27	1	*M*	...	...	35,161.6	2	
...	...	27,227.02	...	*W*	...	...	35,478.55	...	*W*
12 or more	1	27,283.29	1	*S*	...	...	35,738.32	...	*W*
25	0	27,470.99	1	*W*	3	1	36,169.24	1	*M*
13	0	27,472.54	1	*M*	high	...	36,248.14	1	*M*
...	...	27,700.1	2	*M*	...	...	37,044.68	1	*M*
...	...	27,817.50	...	*W*	7	1	37,703.72	1	*M*
...	...	27,820.87	...	*M*	5	1	38,293.5	1	*M*
...	...	28,119.5	...	*W*	5	1	38,452.69	1	*M*

[a] All of the $\Delta J=0$ lines belong to a series identified by Burkhard and Dennison as $K=1\rightarrow2$, $r=2\rightarrow1$, and $J\rightarrow J$.

the over-all rotational quantum number J remains constant.

We have now extended this series from $J=10$ to $J=30$ (see Fig. 3). The $J=11$ and 12 lines were definitely identified by splitting the lines into components and counting them. This procedure becomes more and more difficult for larger J's because of the large number of weak components. As there are quite a few other first-order lines in the region of this series which do not belong to it, a method is needed for identifying the high J's. The high J's were identified by constructing a table of differences up to the seventh difference, by which means it was possible to predict the frequency of a line within a few megacycles. The series was not taken beyond $J=30$ because the equipment required to go below 16,000 Mc was not readily available.

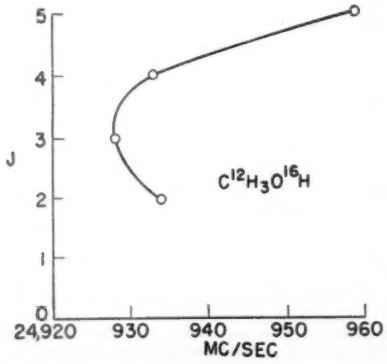

FIG. 4. Start of series of Fig. 3.

The plot of the series in Fig. 3 shows that the line spacing is very small for the lower members of the series, but tends to get larger with increasing J. The series changes direction at $J=20$. Figure 4 shows the start of the series. It will be noted the $J=2$ is at a higher frequency than $J=3$ and $J=4$. There is a possibility that some very weak lines in Table I are caused by J's around 40 for which values the (reversed) transition frequency may be back in this microwave region.

The intensities of these lines have not been measured. The lines appeared to become stronger from $J=2$ up to about $J=15$ and then to get weaker again. From the facts that the $J=5$ and 6 lines of $C^{13}H_3O^{18}H$ were several times noise in a naturally occurring methyl alcohol sample and that the sensitivity of the spectrograph is close to 10^{-8} cm^{-1}, the intensities of the $J=5$ and 6 lines are estimated to be between 1 and 5×10^{-8} cm^{-1}. The most intense lines are probably somewhat more intense than 5×10^{-8} cm^{-1}. The following ranges are assumed for the estimated intensities in Tables I, IV, and V: $S>10^{-8}$ cm^{-1}; $10^{-8}>M>5\times10^{-7}$ cm^{-1}; 5×10^{-7} cm$^{-1}>W$. The Stark effect of the first members of this series is discussed in detail in the section, "Quantitative Stark-Effect Measurements."

There are several other first-order Stark-effect lines in this spectrum. They show Stark-effect patterns such as that displayed in Fig. 2b for which the following formula applies:[8]

$$\Delta\nu_M(\text{Mc})=BME(\text{esu}), \qquad (1)$$

where $\Delta\nu_M$ is the frequency deviation of the Mth component from the original line frequency, and E is the field intensity in electrostatic units. All components except $M=0$ have a first-order Stark effect while the latter, shown dotted, has a second-order Stark effect. As the inner components on either side of the original line frequency are most intense, we assume that $\Delta J=\pm1$ for these transitions. The coefficients of ME for the components of these are listed in Table II. Twelve components were counted on each side for the line listed as $J=12$ or more, although it was difficult to determine the exact number of components because the outer ones became very weak. Despite the fact that the J value was not determined unambiguously, the coefficient B can be determined with certainty.

There is a set of four lines in the ordinary methyl alcohol spectrum which gives rise to a much more complicated Stark pattern than do any of the lines mentioned previously. These lines form a set very similar to that shown in Fig. 5 for $C^{13}H_3O^{16}H$, which we call a mirror image pattern. Two of the lines, those which occur at 33,691.63 and 34,003.69 Mc, are second order at low voltages with the components of one line moving in opposite directions from those of the other on the application of a weak field. At 33,693.74 and 34,001.35 there are forbidden lines which begin to appear only when a Stark field is applied. At a field of a few volts per cm a second-order line and its neighboring forbidden line seem to merge and the mixture gives a Stark effect which appears to be approximately first order. The coefficient of ME for the mixture of the two lines near 34,000 Mc has been determined to be 1.25 Mc/esu. From the fact that the first-order Stark effect pattern is similar to that of Fig. 2b, it is concluded that $\Delta J=\pm1$ during these transitions. Eighteen components were counted on one side of the Stark pattern, but the outer ones were so weak that the end of the pattern could not be determined. There were indications that there were more components and that the J value was probably somewhere between 18 and 22. A more complete description of a mirror image set of this type is given in the section on $C^{13}H_3O^{16}H$, since the $C^{13}H_3O^{16}H$ set was easier to study.

[8] S. Golden and E. Bright Wilson, Jr., J. Chem. Phys. **16**, 669 (1948).

TABLE II. Linear Stark-effect coefficients for $C^{12}H_3O^{16}H$ lines with $\Delta J=\pm1$.

Lower J	Frequency (Mc)	B, coefficient of ME (Mc/esu)
12 or more	27,283.29	0.93
3	28,316.03	3.40
14	34,236.91	0.82
3	36,169.24	6.52
7	37,703.72	3.09
5	38,293.32	13.0
5	38,452.69	13.0

The two $J=5$ lines listed in Table II appear to be related. The lines are unsymmetrical at low voltages. They both appear to be first order at low voltages, but with stronger components on the low frequency side of the low frequency line and on the high frequency side of the high frequency line, giving the lines a mirror image appearance. On the application of increasing voltage the components on the sides of the same line become more equal in intensity, and there is some possibility that there is even an interchange in intensities with the weaker components becoming the stronger at the higher voltages. These lines may be the same type as those discussed in the previous paragraph, but with the separation between a line and its neighboring forbidden transition smaller than the resolution of the spectrograph.

Eleven lines with a second-order Stark effect have been observed in the methyl alcohol spectrum in addition to the two in the mirror image pattern discussed previously. For a typical Stark pattern refer to Fig. 2d. These lines appear to have Stark effects in fair agreement with the rigid rotor formula:[8]

$$\Delta\nu_M(\text{Mc})=(C+DM^2)E^2(\text{esu}), \qquad (2)$$

where $\Delta\nu_M$ is the deviation in Mc of the frequency of the component M from the original line frequency, and

TABLE III. Approximate Stark-effect coefficients of second-order lines.

Frequency	C[a] (Mc/(esu)^2)	D[a] (Mc/(esu)^2)	Lowest possible value of the smaller J
20,970.65	+	+	10
21,550.31	see following discussion		10
23,121.20	+	+	8
23,347.53	+	+	...
23,444.82	+0.16	+0.011	8
26,120.50	0.32	−0.038	9
27,700.1	+	−	...
28,969.0	+0.16	−0.034	8
35,161.6	+	+	...

[a] Refer to Eq. (2).

TABLE IV. Spectrum of $C^{13}H_3OH$.

Lower J	$\pm\Delta J$[a]	Frequency	Stark order	Intensity
31	0	17,870.5	1	*W*
30	0	20,329.32	1	*W*
29	0	22,672.90	1	*W*
28	0	24,860.62	1	*W*
27	0	26,855.01	1	*W*
12	1	26,979.03	2	*M*
12	1	26,980.40	2	forbidden
3	0	27,047.19	1	*M*
4	0	27,050.45	1	*M*
2	0	27,052.97	1	*M*
5	0	27,072.17	1	*M*
12	1	27,104.80	2	forbidden
12	1	27,105.93	2	*M*
6	0	27,122.76	1	*M*
7	0	27,215.60	1	*M*
8	0	27,364.12	1	*M*
9	0	27,581.65	1	*M*
10	0	27,880.04	1	*M*
11	0	28,267.71	1	*M*
26	0	28,621.04	1	*W*
12	0	28,747.67	1	*M*
...	...	28,869.59	1	...
13	0	29,315.20	1	*M*
14	0	29,955.72	1	*M*
25	0	30,127.80	1	*W*
15	0	30,643.69	1	*M*
16	0	31,342.31	1	*M*
24	0	31,350.19	1	*W*
17	0	32,004.43	1	*M*
23	0	32,271.10	1	*W*
18	0	32,575.53	1	*M*
22	0	32,883.47	1	*M*
19	0	32,998.94	1	*M*
21	0	33,192.97	1	*M*
20	0	33,220.05	1	*M*

[a] See footnote to Table I.

E is the electrostatic field strength in electrostatic units. C and D are roughly constant. It is believed that these lines are $J\rightarrow J\pm1$, as the components of low M are strongest. Table III lists information about the second-order Stark-effect lines which have been studied in detail. Because of the experimental difficulties of observing the outer weak components and of the difficulty of resolving the inner components, the Stark coefficients and J values are only approximate. The line at 21,550.31 Mc has been studied in more detail and at least eleven components were seen. The pattern is best described by the following equation containing a fourth-order term:

$$\Delta\nu_M=0.33E^2+1.74\times10^{-2}M^2E^2-1.18\times10^{-6}M^4E^4. \quad (3)$$

The E^4 dependence of the last term has not been definitely established.

Bak, Knudsen, and Madsen[9] have reported eighteen lines of methyl alcohol. Our results are in agreement with theirs if we assume that certain of their lines between 24,901 and 25,449 Mc are actually smeared-out Stark components produced by the high electric fields they employed.

Miss Girdwood has reported on the microwave spectrum of methyl alcohol in the *Canadian Journal of Research*.[10] She lists a large number of lines between 23,500 and 24,900 Mc which are not to be found in Table I. We have not been able to detect others than those listed in the table even on searching through the spectral region several times. Dr. A. L. Schawlow of Columbia University[11] has not been able to find the new lines nor does he detect the shifts in the line frequencies of methyl alcohol when water vapor is admitted to the wave guide, as reported by Miss Girdwood. We suspect that most of the lines in her tabulation (which are spaced regularly about sixty Mc apart) are due to standing waves in the apparatus, rather than to absorption by methyl alcohol.

The large number of accurately measured lines should make this substance useful for the rough calibration of wave meters throughout the region of from 20,000 to 40,000 Mc. Since many of these strong lines have a linear Stark effect, they should be useful as standards for the calibration of a Stark-effect wave guide at low voltages. A line especially recommended for this use is the $J=3\rightarrow4$ at 36,169 Mc which is rather intense.

THE SPECTRUM OF $C^{13}H_3O^{16}H$

Table IV contains the lines which have been definitely proven to be given by $C^{13}H_3O^{16}H$. These are lines which are much stronger in a concentrated sample than they are in an ordinary methyl alcohol sample.

A series of first-order Stark-effect lines very similar to that for $C^{12}H_3O^{16}H$ shown in Fig. 3 corresponding to the transitions $K=1\rightarrow2$, $\tau=2\rightarrow1$, and $\Delta J=0$ has been found for this molecule. It starts just above 27,000 Mc instead of at 24,928 Mc as in the ordinary alcohol and reaches a maximum frequency at the same J value of 20. The members have been identified from $J=2$ up to $J=31$. The beginning of the series is very similar to that in Fig. 4, except that $J=4$ is midway between $J=3$ and $J=2$.

There is a set of four lines plotted in Fig. 5 which give rise to a complicated Stark pattern. The lines at 26,979.03 and 27,105.93 are second order at low voltages. As the components of the lower line move towards lower frequencies and the components of the high frequency line move toward higher frequencies, the lines appear to be mirror images. Near each of these lines there is a forbidden line which appears only when

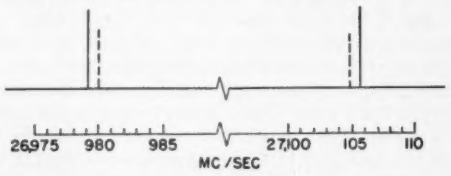

FIG. 5. Mirror image pattern in $C^{13}H_3O^{16}H$. The solid lines are allowed transitions, the dotted ones are forbidden transitions (in the absence of an electric field).

[9] Bak, Knudsen, and Madsen, Phys. Rev. **75**, 1622 (1949).

[10] B. Girdwood, Can. J. Research **28**, 180 (1950).

[11] A. L. Schawlow, private correspondence.

a voltage is applied. With increasing voltage the "forbidden" line becomes stronger and stronger. At a field of a few volts per cm, each allowed line and its neighboring "forbidden" line seem to merge. At a slightly higher voltage the mixture gives a Stark effect which is approximately first order. A plot of the position of the components from the mixed lines near 26,980 Mc is shown in Fig. 6 for two voltages. As the lines at these voltages appear to be first order, the coefficient of ME is roughly determined to be 3.5 Mc/esu. The patterns are unsymmetrical, with frequency displacements on the low frequency side being ten percent greater than those on the high frequency side. The pair at 27,106 Mc, show the same Stark pattern with approximately the same coefficient. From the fact that the inner components are most intense, we conclude that $\Delta J=\pm 1$.

It appears that the observations on the "mirror image" lines can be brought into accord with the theory proposed by Burkhard and Dennison. These lines may correspond to transitions between doublet levels. (See Fig. 7.) Between two doublet levels four transitions are in principle possible but the selection rules, in the absence of external perturbations, exclude two of these. The Stark electric field does, however, perturb the system and hence these extra or forbidden lines may appear. From our experimental data it is impossible to tell whether the larger splitting belongs to the upper level, as shown in Fig. 7, or to the lower level.

The second-order Stark coefficient should be large because of the near degeneracy of the two lower levels. At rather low field strengths the two levels originally separated by 1.2 Mc merge and the Stark effect becomes first order. A theoretical discussion of the Stark effect of slightly asymmetric rigid rotors by Penney[12] seems to apply qualitatively to this particular group of levels, even though the over-all energy level scheme is greatly changed in methyl alcohol by the phenomenon of internal rotation.

One other line was found for the C^{13} concentrated sample. An extensive search for other lines was not made, because our primary objective was to provide information on the isotope effect of the long series of first order lines. Undoubtedly, there are other first-order lines and some second-order lines in this spectral region.

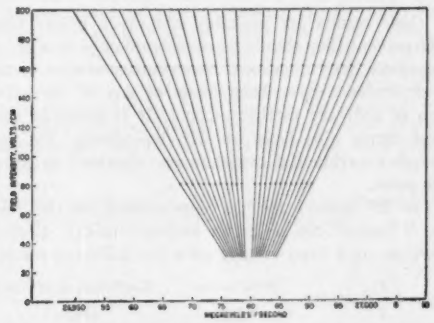

FIG. 6. Stark effect of lower frequency pair of lines in Fig. 5.

[12] W. G. Penney, Phil. Mag. 11, 602 (1931).

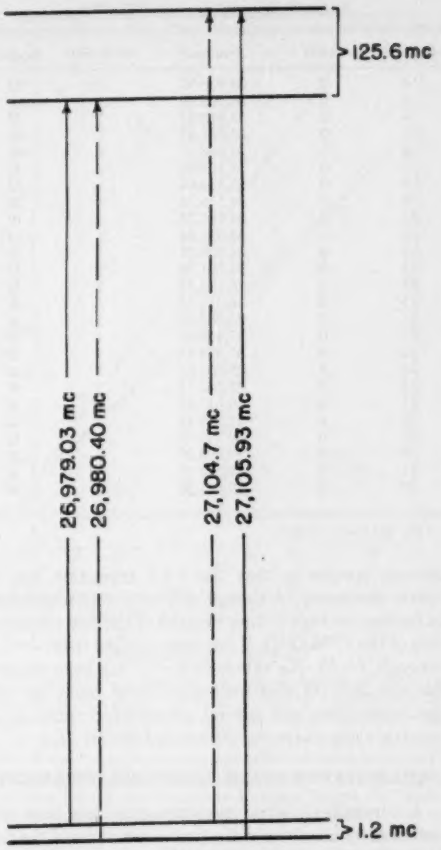

FIG. 7. A possible energy level diagram to explain the mirror image pattern of Fig. 5.

THE SPECTRUM OF $C^{13}H_3O^{18}H$

The spectrum of a sample containing twenty percent $C^{13}H_3O^{18}H$ and eighty percent $C^{12}H_3O^{16}H$ has been observed between 33,900 and 39,700 Mc. Table V lists the lines known definitely to come from $C^{13}H_3O^{18}H$. This list contains only lines belonging to the series $K=1\rightarrow 2$, $\tau=2\rightarrow 1$, and $J\rightarrow J$ which corresponds to that seen for the other isotopic molecules. This series, which starts at 33,918 Mc instead of at 24,928 for the ordinary molecule, has much the same appearance as that for the ordinary methyl alcohol shown in Fig. 3. Its beginning is different from that of the other two

TABLE V. Spectral lines of $C^{12}H_3O^{18}H$.

Lower J	$\pm\Delta J$*	Frequency	Stark order	Intensity
2	0	33,918.97	1	M
3	0	33,925.49	1	M
4	0	33,943.63	1	M
5	0	33,981.35	1	M
6	0	34,048.42	1	M
7	0	34,155.63	1	M
8	0	34,314.64	1	M
9	0	34,536.74	1	M
26	0	34,761.75	1	W
10	0	34,831.64	1	M
11	0	35,206.11	1	M
12	0	35,661.78	1	M
13	0	36,193.55	1	M
25	0	36,312.57	1	W
14	0	36,787.33	1	M
15	0	37,418.97	1	M
24	0	37,579.85	1	W
16	0	38,053.87	1	M
23	0	38,547.73	1	W
17	0	38,647.87	1	M
18	0	39,149.41	1	M
22	0	39,210.48	1	M
19	0	39,505.01	1	M
21	0	39,574.97	1	M
20	0	39,661.80	1	M

* See footnote of Table I.

isotopic species in that the $J=2$ transition has the lowest frequency. Although difficulty was experienced in finding the high J lines because of the low concentration of the $C^{12}H_3O^{18}H$, it has been studied from $J=2$ up through $J=26$. No extensive study has been made of the spectrum of this molecule. There must be other first-order lines and several second-order lines in the spectral region between 20,000 and 40,000 Mc.

QUANTITATIVE STARK-EFFECT MEASUREMENTS

Accurate Stark-effect measurements have been made on the early members of the first-order series of the three isotopic molecules. Less accurate measurements made of several of the other first-order lines as well as on some of the second-order lines in ordinary methyl alcohol have been discussed earlier.

A Stark-effect microwave spectrograph incorporating an X-band wave guide with a center electrode was used for these measurements. To determine the coefficients the line was split into components with dc fields of from ten volts/cm up to several hundred volts/cm. The dc voltage applied to the electrode was measured by a type K potentiometer after reduction by a voltage dividing network, giving voltage measurements better than 0.1 percent. A low 85-kc modulating voltage was used to make the components visible on the spectrograph. Frequencies were measured with the same standard used in making line frequency measurements. The wave guide was calibrated by measuring the Stark effect for methyl fluoroform, taking the measurements of Shulman and others[13] as standard. The dimension of the wave guide was also measured and found to correspond with that calculated from the above calibration with methyl fluoroform.

Coles[3] found that the frequency shift for a Stark component of a line of the $C^{12}H_3O^{16}H$ series is rather accurately described by the following formula:

$$\Delta\nu_{MJ}(\text{Mc})=[A(J^2+J)^{-1}+B]ME(\text{esu}), \quad (4)$$

where $\Delta\nu_{MJ}$ is the shift of the Mth Stark component from the line center frequency in Mc, and A, B are constants.

A plot of the results of our measurements for the three series is shown in Fig. 8. Here a small contribution from a term proportional to M^2 was eliminated by taking the average shift of the components M and $-M$. An interesting point to note is that the three lines extrapolate to the same point at $J(J+1)=0$. A more surprising result is the pronounced increase in the slope, by 50 percent, on substituting O^{18} for O^{16}. From the above plot, the following equations have been derived for the Stark effects of the three series:

$C^{12}H_3O^{16}H$:

$$\Delta\nu_{MJ}(\text{Mc})=[131.1/(J^2+J)+1.710]ME(\text{esu}) \quad (5)$$

$C^{13}H_3O^{16}H$: $\Delta\nu(\text{Mc})=[131.3/(J^2+J)+1.751]ME$ (6)

$C^{12}H_3O^{18}H$: $\Delta\nu(\text{Mc})=[131.0/(J^2+J)+2.646]ME$. (7)

The coefficients obtained by Coles[3] for $C^{13}H_3OH$ differ from these values by about 2 percent, because he made no correction for the wave guide being different from its nominal size. In Eq. (2) of the same article, the factor $M/(J^2+J)^{\frac{1}{2}}$ should have been placed outside of the square bracket.

As mentioned previously, the displacement of each component has a small contribution from terms higher in order than the first. The coefficients of E^2 for some of the components of lines of $C^{12}H_3O^{16}H$ are given as follows:

J	M	Coefficient of E^2 (Mc/(esu)^2)
2	Av. of 2 and -2	0.37
3	-3	0.38

As these results are probably not much better than ± 15 percent they should be considered only as order of magnitude determinations. No extensive studies of the E^2 dependence have been made of any of the other lines of ordinary methyl alcohol. It is probable that these terms also have an M^2 dependence, but not enough experimental evidence was obtained to prove this point.

The M^2 dependence has been studied for the $J=7$ and 9 lines of the series for ordinary methyl alcohol, however, at a fixed voltage with the following results:

J	Field in esu	Coefficient of M^2 (Mc)
7	1.345	0.024
9	1.345	0.0165

These figures are believed to be accurate within ± 10

[13] Shulman, Dailey, and Townes, *Stark Effects in Microwave Spectroscopy*, Columbia Radiation Laboratory (1949).

percent. As no measurements were taken at different voltages, it is not known if this contribution comes from a M^2E^2 term.

CONCLUSION

Because of the additional complexity introduced into this spectrum by the internal rotation, a detailed analysis of the spectrum is a difficult problem. Interpretation of the main features of the spectrum has already been achieved by D. M. Dennison and associates.[4,5,14] For a complete solution it is desirable to have supplemental microwave information at higher frequencies, and some measurements on the deuterated compounds. Fortunately, considerable progress in these two directions has already been achieved at Duke University.[15] It appears that an analysis of these microwave data will provide a rather exact determination of the structure and hindering potential barrier in this molecule, the lightest and simplest representative of a large and important class of molecules capable of internal rotation.

APPENDIX

Preparation of $C^{13}H_3O^{16}H$

This material was prepared by the hydrolysis of methyl iodide containing C^{13}. At 80°C or higher water hydrolyzes methyl iodide, replacing the iodine by a hydroxyl group. Approximately 1 gram of Eastman Kodak concentrated C^{13} methyl iodide (roughly 50 percent $C^{13}H_3I$ and 50 percent $C^{12}H_3I$), 0.6 g of sodium hydroxide, and 1 g of water were put into a 500 ml flask cooled with dry ice to prevent loss of the volatile methyl iodide. The sodium hydroxide neutralizes the hydroidic acid formed during the reaction and may help increase the velocity of the reaction by increasing the hydroxyl ion concentration. After cooling the flask with liquid air, the air was pumped out and the flask sealed to prevent loss of the very volatile reactant and product during the prolonged heating. The flask was heated for several days at 90°C. Testing for methyl iodide by cooling the flask with liquid air and then observing the amount of dense oily methyl iodide present in warming the flask showed it to be present until the fifth day. After the mixture was cooled with liquid air, the noncondensible gases were pumped off. One-half hour of pumping on the sample at dry ice temperature was necessary to remove the small amount of methyl iodide still remaining.

Because of the small amount of product, excessive losses would occur during an ordinary distillation. The vapor pressure of alcohol is between 0.01 and 0.1 mm of mercury at dry ice temperature which is adequate for microwave spectroscopy. The pressure of water at dry ice temperature is not sufficient to dilute the alcohol vapor appreciably. After the sample had been cooled by a dry ice bath, its vapor was used to fill the absorption cell. Although this sample has been used to fill the guide many times, there is no apparent reduction in its delivery.

[14] D. M. Dennison and E. Ivash (private communication).
[15] Edwards, Gilliam, and Gordy (to be published).

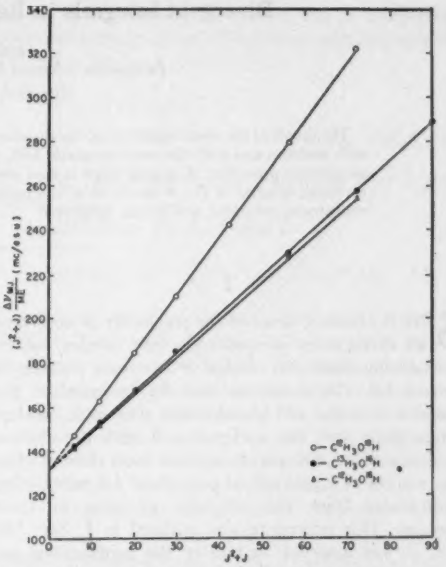

FIG. 8. Stark-effect coefficients for the series of first-order Stark-effect lines $K=1\rightarrow2$, $\tau=2\rightarrow1$, $J\rightarrow J$.

Preparation of $C^{13}H_3O^{18}H$

The compound was prepared by the hydrolysis of ordinary methyl iodide with H_2O^{18}. Dr. A. O. C. Nier of the University of Minnesota generously donated this heavy oxygen isotope in the form of oxygen gas, in which the ratio of $O^{16}O^{18}$ to O_2^{16} was 0.52.[16] The H_2O^{18} was formed as a by-product in the oxidation of ammonia to produce N_2O^{18}. As the addition of ordinary sodium hydroxide would have diluted the concentrated oxygen isotope too much, sodium hydroxide was formed by adding enough sodium to react with about half of the water and pumping off the generated hydrogen. As an excess of water with heavy oxygen remained, the solution was essentially the same as that in the preparation of $C^{13}H_3OH$. The hydrolysis treatment was the same as that in the preparation of C^{13} methyl alcohol, except that several more days were required for the completion of the reaction. Apparently the rate of reaction was slower because the amount of excess water was considerably less. As the oxygen gas had originally contained only 20 percent O^{18} atoms, the resultant alcohol was 80 percent ordinary methyl alcohol and only 20 percent $C^{13}H_3O^{18}H$. The filling of the microwave cell was the same as that for the C^{13} methyl alcohol.

We are grateful to Dr. G. R. Sprengling and Mr. David Lide of the Chemical Department of the Westinghouse Research Laboratories, who assisted in the preparation of the $C^{13}H_3O^{16}H$ and $C^{13}H_3O^{18}$ samples.

[16] A partially enriched O^{18} sample furnished by the AEC to Dr. A. O. C. Nier was further enriched by thermal diffusion in his plant at the University of Minnesota which was financed by the Committee on Growth of the National Research Council acting for the American Cancer Society.

PHYSICAL REVIEW VOLUME 84, NUMBER 3 NOVEMBER 1, 1951

Divergent Integrals in Renormalizable Field Theories

ABDUS SALAM*
Institute for Advanced Study, Princeton, New Jersey
(Received June 22, 1951)

The proofs of the renormalization of the theories of scalar and pseudoscalar mesons in scalar interaction with nucleons and with the electromagnetic field, given previously by the author, depended on a certain subtraction procedure. A general proof is here given that this subtraction procedure, when applied to a divergent integral in the S matrix of a renormalizable field theory, does, in fact, lead to an absolutely convergent, covariant, and unique remainder.

I

SINCE Dyson's[1] proof of the possibility of absorbing all divergences in spinor electrodynamics, by renormalizing mass and charge, it has been possible to extend his considerations and to renormalize the theories of scalar and pseudoscalar mesons in (scalar) interactions with the nucleons, and with the electromagnetic field.[2] The proofs in these cases depend upon the success of a generalized procedure[3] for subtracting divergences from the integrals occurring in these theories. This procedure was outlined in I, Sec. III, and it was asserted that after the subtractions are carried out in a prescribed manner, the remainder is an absolutely convergent integral in a strict mathematical sense. A proof of this statement is given in this note. The conditions under which such a procedure succeeds brings out clearly the difference between theories which can be renormalized and those for which the concept of renormalization of constants has proved inadequate.

Regarding the general structure of the graphs and the corresponding integrals occurring in the matrix elements of Dyson's S matrix, we note the following:

(i) In a connected Feynman-Dyson graph consisting of N vertices and F internal lines, $n=F-N+1$ lines can be chosen such that the momenta corresponding to the remaining $(N-1)$ lines can be expressed as linear sums of the momentum variables $l_1, l_2, \cdots l_n$ which can be assigned to these n lines. Thus, the graph gives rise to an n-fold integral $I(n)$ over these basic variables.[4]

(ii) For all "renormalizable" theories (i.e., the theories for which the number of primitive divergent graphs is governed by conditions of the type $E<a$, E being a linear sum of the number of external lines and a being a fixed constant), not only is the number of primitive divergent graphs limited, but further, perhaps more important, the degree of divergence of the integrals[5] corresponding to these graphs does not depend on the order of the graphs.

(iii) We are interested in the absolute and not the conditional convergence of our final expressions; that is to say, their convergence must be independent of the choice of basic variables. Irrespective of the choice of basic variables, all the possible divergent subintegrations can be detected graphically by seeing which parts of the graph satisfy the condition $E<a$, where E is the number of external lines of the part in question. By a "wrong" choice of basic variables, it is possible to make some of the integrals corresponding to these parts conditionally convergent; for example, a subintegration[6] which conditionally converges for l_1 and l_2 integrations may diverge if $l_1'=l_1+l_2$ is chosen as a basic variable. The proof the effectiveness of the subtraction procedure given in Sec. II depends on the following lemma

Lemma 1:—There exists at least one "correct" choice of basic variables, such that every possible genuinely divergent part of the graph has associated with it a divergent subintegration over one or more of the basic variables.

This lemma is proved in Sec. III. In any graph there may be more than one set of "correct" variables. It is also shown in Sec. III that the finite remainder after the proposed subtractions is the same for any "correct" set. It will be seen in Sec. III that the lemma is true under extremely restrictive conditions. These happen to be precisely the conditions which renormalizable field theories satisfy.

II

The detailed prescription for subtracting divergences from overlapping graphs has been given in I, Sec. III. We write the given integral $I(n)$ as

$$\begin{aligned} I(n)=&D(l_1)R(l_2l_3\cdots l_n)+D(l_2)R(l_1l_3\cdots l_n)+\cdots \\ &+D(l_1l_2)R(l_3l_4\cdots l_n)+\cdots \\ &+D(l_1l_2l_3)R(l_4l_5\cdots l_n)+\cdots+\cdots \\ &+D(l_1l_2\cdots l_n)+I_a(l_1l_2\cdots l_n). \quad (1) \end{aligned}$$

* Now at Government College, Lahore, Pakistan.

[1] F. J. Dyson, Phys. Rev. **75**, 1736 (1949).

[2] Abdus Salam, Phys. Rev. **82**, 217 (1951), referred to as I; and "Renormalized S matrix for scalar electrodynamics," to be published.

[3] This procedure was suggested by F. J. Dyson, to whom the author is deeply indebted for kind help and discussion.

[4] The domain of integration is in fact a $4n$-dimensional space; but the treatment being wholly relativistic, the 4 components of any vector are never separately considered. We, therefore, speak of n-fold rather than $4n$-fold integrations.

[5] The degree of divergence of an integral is estimated by employing the basic considerations given in Sec. V of Dyson's paper and merely counting the powers of relevant l in the numerator and denominator of the integrand.

[6] If a set of variables $l_al_b\cdots l_m$ is held fixed, the integration over the remaining variables is called a subintegration.

Here $D(i_i i_j \cdots)$ is the true divergence from the part of the graph corresponding to the $i_i i_j \cdots$ subintegration and R's represent the reduced integrals. It is to be shown that I_e, the remainder left after all terms $D \times R$ have been subtracted from $I(n)$ is absolutely convergent.

In general, the integrand of $I(n)$ is a product of "simple" factors F, H, J, etc., each "simple" factor F being a function of one single variable i_i and external momenta (p), and of overlap factors G, K, etc., which are functions of more than one variable.

In any term like $D(i_1)R(i_2 i_3 \cdots i_n)$, $D(i_1)$ is a divergent constant; analytically, $D(i_1)$ is a divergent constant obtained by an operation $T(i_1)$ on the i_1 subintegration, the integrand of this subintegration consisting of all those factors F, G, etc., in the integrand of $I(n)$ which contain i_1. All momenta other than i_1 in these factors are treated as "external." There is one operator $T(i_1)$ for each type of divergence in the theory; this operator may correspond, for example, to giving all the "external" momenta special "free-particle" values or may also involve differentiations with respect to "external" momenta before such "free" values are substituted if the divergence over i_1 subintegration is more than logarithmic. In practice, the operation T may be even more complicated, but in all cases (so far developed) T acts by changing the values of "external" momenta. In actual fact, the result of operation $T(i_1)$ is not merely $D(i_1)$ but $D(i_1)\gamma_\mu$, $D(i_1)\delta_{\mu\nu}$, or $D(i_1)\Delta_F^{-1}$, etc., where γ_μ, $\delta_{\mu\nu}$, etc., will be called "vertex factors." These "vertex factors" are absorbed in the reduced integrals. $R(i_2 i_3 \cdots i_n)$, for example, is an integral with the integrand consisting of all factors G, H, etc., in the original integrand which do not contain i_1, multiplied by the "vertex factor" from the i_1 integration. $R(i_2 i_3 \cdots i_n)$ corresponds to a graph, called the reduced graph, which has exactly the same number of external lines as I, but is of lower order in ϵ.

We notice at this stage that the operation

$$[1-T(i_1)]I(n)=[I(n)-D(i_1)R(i_2 i_3 \cdots i_n)]$$

can be thought of graphically as the insertion of the convergent part of the i_1 integration at the appropriate place in the reduced graph $R(i_2 i_3 \cdots i_n)$.

The general procedure for obtaining a true divergence, $D(i_1 i_2)$, for example, has been formulated in **1**, Sec. III. Consider the integral

$$[1-T(i_1)-T(i_2)]I=[I-D(i_1)R(i_2 i_3 \cdots i_n) - D(i_2)R(i_1 i_3 \cdots i_n)]. \quad (2)$$

An operation $T(i_1 i_2)$ on this new integral gives $D(i_1 i_2)$. For this operation all momenta other than i_1, i_2 are "external" and explicitly the operation is only designed to make the double integration over $i_1 i_2$ in

$$[1-T(i_1 i_2)][1-T(i_1)-T(i_2)]I(n) \quad (3)$$

convergent. It was shown in **1**, Sec. II, that (3) in fact proves to be convergent over i_1 and i_2 integrations considered singly as well. The proof may be repeated. Holding i_2 fixed, we rewrite (3) as

$$=[1-T(i_1)]I-T(i_1 i_2)[1-T(i_1)]I - [1-T(i_1 i_2)]T(i_2)I. \quad (4)$$

The first two terms obviously converge over i_1 integration.

We can rewrite the third term as

$$[1-T(i_1 i_2)]T(i_2)I=[1-T(i_1 i_2)]D(i_2)R(i_1 i_3 \cdots i_n).$$

$T(i_1 i_2)$ operates only on the $i_1 i_2$ integration, giving all variables "external" to the $i_1 i_2$ integration certain special values. Here, since $D(i_2)$ is a constant and does not contain any external momenta, $T(i_1 i_2)$ operates, in effect, only on that part of the integrand which contains i_1. The convergence of $[1-T(i_1 i_2)]D(i_2) \times R(i_1 i_3 \cdots i_n)$ over i_1 is clear dimensionally, since $D(i_2)$ being divergent, the degree of divergence of $R(i_1 i_3 \cdots i_n)$ in i_1 cannot exceed that of the $i_1 i_2$ divergence, which $[1-T(i_1 i_2)]$ is explicitly designed to remove. In the example considered in **I**, Sec. II, $T(i_1)$ and $T(i_2)$ represent extraction of (logarithmic) vertex part divergences, while $T(i_1 i_2)$ is designed, in the first place, to extract (linear) self-energy divergences. $D(i_2)$ thus being a logarithmic divergence, the i_1 integration in $R(i_1 i_2 \cdots i_n)$ can at most be linearly divergent. The operation $[1-T(i_1 i_2)]$ therefore suffices to produce convergence over i_1 in $[1-T(i_1 i_2)]T(i_2)I$. This is an important point for the subsequent proof.

In the general case I_e is convergent for the over-all n-fold integration by its very construction, since it is obtained from Φ defined in Eq. (5) below by an operation $[1-T(i_1 i_2 \cdots i_n)]$, which operation subtracts from Φ the true divergence $D(i_1 i_2 \cdots i_n)$:

$$\Phi=I-D(i_1)R(i_2 \cdots i_n)\cdots-D(i_1 i_2)R(i_3 \cdots i_n)\cdots \\ \vdots \quad \cdots \quad \vdots \\ -D(i_1 i_2 \cdots i_{n-1})R(i_n)\cdots. \quad (5)$$

We now want to show that I_e is also convergent over all subintegrations $i_1, \cdots, i_1 i_2, \cdots, i_1 i_2 \cdots i_{n-1}, \cdots$ as well. Combining this with the discussion given in Sec. III, this will establish that I_e is absolutely convergent in a strict mathematical sense and all mathematical operations are valid for it.

By rearranging the terms in $I_e(n)$, we shall first exhibit that $I_e(n)$ is convergent over the $(i_2 i_3 \cdots i_n)$ subintegration, explicitly. The proof proceeds inductively. Suppose that $I_e(n-1)$ obtained from any $(n-1)$ fold integral $I(n-1)$ by subtracting true divergences $\times$reduced integrals converges over all its possible subintegrations as well as over the $(n-1)$ fold inte-

gration. We rewrite Eq. (5) as follows:

$$\Phi=[I-D(t_2)R(t_1t_3\cdots t_n)-D(t_3)R(t_1t_2\cdots t_n)$$
$$-\cdots-D(t_n)R(t_1\cdots t_{n-1})-D(t_2t_3)R(t_1t_4\cdots t_n)$$
$$-\cdots-D(t_2t_3\cdots t_n)R(t_1)]$$
$$-[D(t_1)R(t_2t_3\cdots t_n)-D(t_1t_2)R(t_3t_4\cdots t_n)\cdots$$
$$-D(t_1t_n)R(t_2\cdots t_{n-1})\cdots-D(t_1t_2t_3)R(t_4t_5\cdots t_n)\cdots$$
$$\cdots\cdots\cdots\cdots\cdots\cdots$$
$$-D(t_1t_3\cdots t_n)R(t_2)-D(t_1t_2\cdots t_n)R(t_3)\cdots$$
$$-D(t_1t_2\cdots t_{n-1})R(t_n)]. \quad (6)$$

Then we have

$$I_c(n)=[1-T(t_1\cdots t_n)]\Phi. \quad (7)$$

If t_1 is held fixed, it acts as an "external" momentum vector for the terms in the first bracket. The integrand in $R(t_1)$ contains (apart from the "vertex factor") those factors in the integrand of $I(n)$ which do not contain any other basic variable except t_1, and these factors are therefore common to all the terms in the first bracket in Eq. (6). Apart from these, the first bracket is precisely $I_c(n-1)$ and, consequently, convergent over $t_2t_3\cdots t_n$ integration, by assumption.

To exhibit the explicit convergence of the second bracket, we derive an alternative expression for the true divergences.

Consider $D(t_1t_2)$. We write

$$D(t_1t_2)R(t_3t_4\cdots t_n)=T(t_1t_2)[I-D(t_2)R(t_1t_3\cdots t_n)$$
$$-D(t_1)R(t_2t_3\cdots t_n)]$$
$$=T(t_1t_2)[I-D(t_2)R(t_1t_3\cdots t_n)]$$
$$-D(t_1)D_R(t_2)\times R(t_3t_4\cdots t_n). \quad (8)$$

Here $D_R(t_2)R(t_3t_4\cdots t_n)$ is the result of the operation $T(t_1t_2)$ (which, $D(t_1)$ being a constant, is effectively now an operation on t_2 integration alone) on $R(t_2t_3\cdots t_n)$. The reduced integral $R(t_3t_4\cdots t_n)$ from this operation, obtained by omitting all factors containing t_2 in the integrand of $R(t_2t_3\cdots t_n)$ is the same as that obtained by omitting all factors containing t_1t_2 from the integrand of I. As noted before $[I-D(t_2)R(t_1t_3\cdots t_n)]$ can be thought of as the graph obtained from $R(t_1t_3\cdots t_n)$ by inserting in the appropriate place the convergent remainder $G_c(t_2)$ of the t_2 integration in I. The operation $T(t_1t_2)$ now implies that from the resulting expression another divergent constant is evaluated. For our purposes, however, the essential point is that $T(t_1t_2)[I-D(t_2)R(t_1t_3\cdots t_n)]$ is convergent over t_2. To emphasize this we write $T(t_1t_2)[I-D(t_2)R(t_1t_3\cdots t_n)]$ as $(G_c(t_2)\rightarrow\int dt_1dt_2)_0R(t_3t_4\cdots t_n)$. Here, $(G_c(t_2)\rightarrow\int dt_1dt_2)_0$ is the divergent constant mentioned above and is such that in its integral representation the t_2 integration is convergent. Its multiplier $R(t_3t_4\cdots t_n)$ is an integral with the integrand consisting of those factors in the integrand of I which contain neither t_1 nor t_2 and is thus the correct reduced integral. Hence, finally we have

$$D(t_1t_2)R(t_3\cdots t_n)=[(G_c(t_2)\rightarrow\int dt_1dt_2)_0$$
$$-D(t_1)D_R(t_2)]\times R(t_3\cdots t_n). \quad (9)$$

It may be noted here that if we take two variables t_1 and t_i such that the parts corresponding to t_1 and t_i integrations do not overlap, then we have $D_R(t_i)=D(t_i)$. (The true divergence for the t_i subintegration of the reduced integral $R(t_2\cdots t_n)$ is the same as that of the original integral $I(t_1t_2\cdots t_n)$.) It was shown in Sec. 3, 1, that for such a case we have $D(t_1t_i)=-D(t_1)D(t_i)$. Hence, it follows that $(G_c(t_i)\rightarrow\int dt_1dt_i)_0=0$, which is compatible with its graphical interpretation.

We shall prove a similar result for $D(t_1t_2t_3)$. By definition we have

$$D(t_1t_2t_3)R(t_4\cdots t_n)=T(t_1t_2t_3)[I-D(t_2)R(t_1t_3\cdots t_n)$$
$$-D(t_3)R(t_1t_2t_4\cdots t_n)-D(t_2t_3)R(t_1t_4\cdots t_n)]$$
$$+T(t_1t_2t_3)\begin{bmatrix}-D(t_1)R(t_2t_3\cdots t_n)\\-D(t_1t_2)R(t_3t_4\cdots t_n)\\-D(t_1t_3)R(t_2t_4\cdots t_n)\end{bmatrix}. \quad (10)$$

The expression in the first square bracket is convergent on account of our inductive assumption for the t_2t_3 integration. Precisely as above, we can write the result of operating $T(t_1t_2t_3)$ on the first bracket as

$$(G_c(t_2t_3)\rightarrow\int dt_1dt_2dt_3)_0R(t_4\cdots t_n).$$

By a repeated use of Eq. (9), the remaining terms in Eq. (10) can be written as

$$=-T(t_1t_2t_3)[D(t_1)\{R(t_2t_3\cdots t_n)-D_R(t_2)R(t_3t_4\cdots t_n)$$
$$-D_R(t_3)R(t_2t_4\cdots t_n)\}$$
$$+(G_c(t_3)\rightarrow\int dt_1dt_3)_0R(t_2t_4\cdots t_n)$$
$$+(G_c(t_2)\rightarrow\int dt_1dt_2)_0R(t_3t_4\cdots t_n)]$$
$$=-[D(t_1)D_R(t_2t_3)+(G_c(t_2)\rightarrow\int dt_1dt_2)_0D_R(t_3)$$
$$+(G_c(t_3)\rightarrow\int dt_1dt_3)_0D_R(t_2)]\times R(t_4\cdots t_n). \quad (11)$$

So that, finally we have

$$D(t_1t_2t_3)R(t_4\cdots t_n)=[(G_c(t_2t_3)\rightarrow\int dt_1dt_2dt_3)_0$$
$$-(G_c(t_2)\rightarrow\int dt_1dt_2)_0D_R(t_3)$$
$$-(G_c(t_3)\rightarrow\int dt_1dt_3)_0D_R(t_2)$$
$$-D(t_1)D_R(t_2t_3)]R(t_4\cdots t_n). \quad (12)$$

This can be generalized immediately by an inductive proof as follows:

$$D(t_1t_2\cdots t_r)R(t_{r+1}\cdots t_n)$$
$$=[(G_c(t_2\cdots t_r)\rightarrow\int dt_1dt_2\cdots dt_r)_0$$
$$-(G_c(t_3\cdots t_r)\rightarrow\int dt_1dt_3\cdots dt_r)_0D_R(t_2)$$
$$\cdots\cdots\cdots\cdots\cdots\cdots$$
$$-(G_c(t_2\cdots t_{r-1})\rightarrow\int dt_1dt_2\cdots dt_{r-1})_0D_R(t_r)$$
$$-(G_c(t_4\cdots t_r)\rightarrow\int dt_1dt_4\cdots dt_r)_0D_R(t_2t_3)$$
$$\cdots\cdots\cdots\cdots\cdots\cdots$$
$$-(G_c(t_5\cdots t_r)\rightarrow\int dt_1dt_5\cdots dt_r)_0D_R(t_2t_3t_4)$$
$$\cdots\cdots\cdots\cdots\cdots\cdots$$
$$-(G_c(t_r)\rightarrow\int dt_1dt_r)_0D_R(t_2t_3\cdots t_{r-1})$$
$$\cdots\cdots\cdots\cdots\cdots\cdots$$
$$-D(t_1)D_R(t_2t_3\cdots t_r)]\times R(t_{r+1}\cdots t_n). \quad (13)$$

All that remains now is to substitute from Eq. (13) in the expression obtained after operating $[1-T(t_1t_2\cdots t_n)]$ on the second bracket of Eq. (6). We obtain

$$
\begin{aligned}
&-D(t_1)[R(t_2t_3\cdots t_n)-D_R(t_2)R(t_3\cdots t_n)-\cdots\\
&\qquad -D_R(t_2t_3)R(t_4\cdots t_n)-\cdots\\
&\qquad \cdots\cdots\cdots\cdots\\
&\qquad -D_R(t_2t_3\cdots t_n)]\\
&-[(G_c(t_2)\rightarrow \int dt_1dt_2)_0\{R(t_3\cdots t_n)-D_R(t_3)R(t_4\cdots t_n)\\
&\qquad -D_R(t_3t_4)R(t_5\cdots t_n)-\cdots-D_R(t_3\cdots t_n)\}]\\
&-[(G_c(t_3)\rightarrow \int dt_1dt_3)_0\{R(t_2t_4\cdots t_n)\\
&\qquad -D_R(t_2)R(t_4\cdots t_n)\cdots\\
&\qquad -D_R(t_2t_4)R(t_5\cdots t_n)\cdots-D_R(t_2t_4\cdots t_n)\}]\\
&\qquad \cdots\cdots\cdots\cdots\\
&-[(G_c(t_2t_3)\rightarrow \int dt_1dt_2dt_3)_0\{R(t_4\cdots t_n)\\
&\qquad -D_R(t_4)R(t_5\cdots t_n)\cdots\\
&\qquad -D_R(t_4t_5)R(t_6t_7\cdots t_n)-D_R(t_4t_5\cdots t_n)\}]\\
&\qquad \cdots\cdots\cdots\cdots\\
&-(G_c(t_2\cdots t_n)\rightarrow \int dt_1dt_2\cdots dt_n)_0. \qquad (14)
\end{aligned}
$$

By our inductive hypothesis each expression in square brackets in the above converges for the $t_2t_3\cdots t_n$ integration if t_1 is held fixed. This proves the result. Since the inductive hypothesis assumes the convergence of $I_c(n-1)$ for all its possible subintegrations, we have succeeded in establishing the convergence of $I_c(n)$ over all subintegrations t_2, t_2t_3, $\cdots$, $t_2t_3\cdots t_{n-1}\cdots$ as well.

By different rearrangements we could prove the convergence of $I_c(n)$ over any other subintegration over $(n-1)$ variables. This shows that $I_c(n)$ is absolutely convergent, provided we can give a proof of the lemma stated in Sec. I. This is done in the next section.

III

In this section we give a proof of the lemma stated towards the end of Sec. I, on which the discussion in Sec. II depends. The proof is long, and only an outline will be given. We first investigate the condition for primitive divergents for the most general mixture of fields. Consider a graph with E_b as the total number of external boson and E_f as the total number of external fermion lines. Let N_i stand for the number of such vertices in the graph as have i lines incident; thus, i may be any integer equal or greater than two. The number of boson lines at each vertex of the type i is b_i and the number of fermion lines f_i.

If F stands for internal lines, then we have the relations,

$$E_b+2F_b=\sum b_iN_i, \quad E_f+2F_f=\sum f_iN_i.$$

We restrict ourselves to theories[7] in which the integrals for matrix-elements can be written in momentum space by setting in the integrand $\Delta_F(l)$ for each boson line, $S_F(l)$ for each fermion line, and a vertex factor of the general form t^{α_i} for each vertex of the type i. The condition for convergence of a graph, following Dyson, is derived as

$$2F_b+F_f-[4(F-N+1)+\sum\alpha_iN_i]>1.$$

Since $N=\sum N_i$, this reduces to

$$\tfrac{1}{2}E_f+E_b+\sum N_i(4-\alpha_i-b_i-\tfrac{1}{2}f_i)-4>1.$$

The upper limit to the number of primitive divergent graphs is therefore given by the following condition:[8]

$$\tfrac{1}{2}E_f+E_b<5+\sum(\alpha_i+b_i+\tfrac{1}{2}f_i-4)N_i.$$

This result shows that if for a mixture of fields the number of primitive divergent graphs does not depend on the order of the graphs considered, then this number is governed by a condition of the type $E<a$ with $a=5$. Any graph in these theories, with four or more external fermion lines or five or more external boson lines must be (at least "superficially"[9]) convergent. This implies that if we open one single line of any graph with at least two external fermion lines, and if the resulting graph is a "connected" graph (i.e., the resulting graph does not split into pieces each joined to the other by a single line), it must converge superficially. The same result holds *a fortiori* if two or more lines which leave the graph connected are opened simultaneously. It is also seen to be valid for all graphs with boson lines external except for boson self-energy graphs. In this case, opening one boson line may produce a connected graph with 4 external boson lines which may diverge logarithmically. However, precisely this was the case treated in 1(B), where it was shown that such divergences affect only the mass-renormalization constant. These divergences were called "final"[10] and it was proved quite generally that one could effectively proceed as if these divergences did not exist. We can therefore state the following as a general rule: *If in any graph one or more lines are opened such that the graph still remains "connected," the resulting graph is either superficially convergent or such that its divergence is "final" and we can effectively proceed as if the divergence doesn't exist.* Using the above result we proceed to the direct proof of Lemma 1. By "exhibiting" a part of a graph we mean opening enough lines so that the momenta

[7] This excludes β-formalism of meson theory, for which the propagation function is

$$T_F(l)=\{i\beta l-K+(1/K)[(\beta l)^2-\beta^2]\}/(\beta^2+K^2).$$

[8] For a theory to have a finite number of primitive divergents, it is clear that $\sum(\alpha+b+\frac{1}{2}f-4)N$ must equal zero. This therefore excludes all vector couplings for meson-nucleon interactions ($b=1$, $f=2$, $\alpha=1$), meson-pair theories ($b=2$, $f=2$) and Fermi types of interaction between four spinor particles ($f=4$).

[9] An integral is "superficially" convergent, if by counting the powers of l in the integrand, the integral itself is found to be convergent, while any one of its subintegrations diverges.

[10] One further instance of a "final" divergence [not noted in 1(B)] is provided by vertex parts with 2 meson and 1 external photon line. If the external photon line belongs to a 3-vertex, opening one of the internal meson lines at this vertex may produce a connected M-part. This M-divergence can be treated as "final." The reduced integral in this case is a vertex part which can be shown to be a function of the external photon momentum $(p-p')$ only. The reduced integral would therefore vanish from the familiar arguments of gauge-invariance.

associated with the external lines of the part become fixed. It is clear that any part (convergent or divergent) may be exhibited by opening all its external lines. If we can show that the number of lines, some or all of which need to be opened, to exhibit every divergent part contained in a graph, is never greater than n (the number of independent momenta at our disposal), we will have proved the lemma. For we can then associate basic momenta with these lines, and thus have a "correct" choice of basic variables.

All internal lines belonging to any graph can be divided into two mutually exclusive sets. Lines in set (a) have the property that if any one of them is opened the graph splits into two or more parts each joined to the other by a single line (called a "bridge"). All lines not belonging to set (a) fall in set (b) which thus includes lines which if opened singly leave the graph connected.

The lines in set (a) can further be divided into distinct classes; If opening a line l_a^1 splits the graph into separate pieces joined by single lines (bridges) l_a^2, l_a^3, $\cdots$, it is obvious that the result of opening l_a^2 would be to split the graph into pieces joined by bridges $l_a^1, l_a^3, \cdots$. If a basic momentum variable t is assigned to l_a^1, the lines l_a^2, l_a^3, etc., acquire momenta $t+p$, where p are linear sums of momenta of external lines. All these lines will belong by definition to class R_a. We can assign all lines in set (a) uniquely to various classes $R_1, R_2, \cdots R_s$. No line (a) can belong to more than one class at a time, and each class must contain at least two lines. If those vertices of the graph at which external lines are incident are 3-vertices, each internal line at such a vertex certainly belongs to some one of these classes. For distinction we shall label such classes as R^{ext}. If R^{ext} consists of just the two internal lines incident at the external vertex defining R^{ext}, then the effective result of opening one of these external lines is one single connected graph with external lines one more than the original graph. We further distinguish such R^{ext} by writing these as $\mathbf{R}^{\text{ext}}$.

The connection of these sets and classes with divergences in a graph is obvious. On account of the rule stated above, opening a line (b) leaves the graph connected and therefore at least superficially convergent, while a line (a) may split the graph into pieces at least one of which has external lines satisfying $E<a$. To "exhibit" these divergences, it is therefore essential that a basic momentum variable be associated with this line (a). If (a) belongs to a class R_a, an assignment of the basic variable to any other line in R_a is, from the definition of a class, clearly an equivalent and a "correct" procedure. As a first step towards the proof of Lemma 1 we show that s, the number of effective classes, which can split the graph into pieces all or some of which satisfy $E<5$ is always $\leqslant n$.

For graphs consisting entirely of 4-vertices the result is trivial. For this case, we have $n=F-N+1$, while $2F+E=4N$. Each of the s classes must contain at least two lines; since the minimum number of lines in the classes, $2s$, must not exceed the total number of internal lines F, we have $2s\leqslant F=2n+\frac{1}{2}E-2$. For the case of divergent graphs with $E\leqslant 4$, this shows that $s\leqslant n$.

To prove the result for graphs with 3-vertices we establish Lemma 2.

Lemma 2:—The maximum number of classes s for a proper graph with n basic vectors and no external lines is $n-2$.

For the proof it is unnecessary to distinguish between boson and fermion lines. We can always obtain any graph with n basic vectors from a graph with $(n-1)$ basic vectors by adding a new line with its terminating vertices on two existing lines of the graph with $(n-1)$ basic vectors. In general, the addition of a new line does not add to the number of the existing classes except for two cases: (i) when the terminating vertices of the new line both belong to the same line of the original graph and (ii) when these vertices belong to two lines already belonging to a class. In both these cases the number of classes is increased at most by one. The proof of the lemma follows by induction, since the result is obviously true for $n=2$. We also notice that at the new terminating vertices there are at most two lines belonging to set (a), while the newly added line itself must belong to set (b). Generalizing from this, we have the result that at no vertex can there be more than two (a) lines incident. We shall have occasion to use this result.

We now consider the effect of adding external lines to such graphs. Each external line may produce at most one new class $\mathbf{R}^{\text{ext}}$, so that the general result is that for a graph with n independent vectors and E external lines

$$\max s\leqslant n+E-2.$$

We can now show that for $E=3$, at least one of classes $\mathbf{R}^{\text{ext}}$ either produces a convergent connected graph when one of its 2 lines is opened, or a "final" divergence. The former is true for $\mathbf{R}^{\text{ext}}$ formed by the external photon or meson line in vertex parts in all theories except scalar electrodynamics where this $\mathbf{R}^{\text{ext}}$ introduces, as noted before, merely a "final" divergence. Excluding this from the classes of interest we have $s\leqslant n$ for $E=3$. For the case $E=4$, opening one of the lines of an $\mathbf{R}^{\text{ext}}$ must produce a connected graph with five external lines, i.e., a subintegration which is superficially convergent. This is not true, however, if two of the R^{ext} coincide (i.e., when two external lines are adjacent), in which case the graph produced has just four external lines. Thus, in this case too the effective number of classes which exhibit divergent parts is governed by $s\leqslant n$.

With these preliminary results we now prove that we can choose a set of n lines which if opened singly or in pairs, etc., would exhibit all the divergences of the graph. Consider the case $s=n$. We assign s basic

momenta to the s lines, selected one each from the s classes R. The assignment of all momenta is complete and it remains to prove that we only need open some or all of these n lines to exhibit every possible divergence. We notice now that for this case the lines (b) acquire an additional property. By counting the lines and vertices we can show that at each vertex there are precisely two lines (a) and not more than one line (b). (We are here dealing with graphs with 3-vertices only), and also there are in all just $(n-1)$ lines (b). If we open one of these lines (b), the graph still remains "connected." Lines (a) defined for the original graph retain their property of splitting graphs even for the new graph; therefore, there are already two (a) lines at each vertex of the new graph. We have seen that at any vertex there cannot be more than two (a) lines. This shows that the (b) lines of the original graph remain the (b) lines of the new graph. The "connectedness" of the graph no longer depends on the lines (b); in other words, lines (b), which were defined in the first place on account of their property of leaving the graph connected if opened one at a time, acquire the further property that they still leave the graph connected if more than one of them are opened simultaneously.[11] The result of opening any set of these lines will therefore never be a divergent part. All divergent parts of the graphs are thus exhibited by opening one or more of lines (a); analytically, this assignment of basic momenta will insure that the entire number of divergences in the graph never exceeds the possible subintegrations at our disposal, and therefore the lemma is proved.

The uniqueness of $I_c(l_1 l_2 \cdots l_n)$ for a different "correct" choice of basic momenta follows immediately from the concept of classes. For the case dealt with above, the choice is correct only if the basic lines are selected one each from a class R. Since all other lines in a class acquire momenta $p+l$, if l is the basic line which belongs to R, all "correct" choices are completely equivalent, and obtainable one from the other by trivial transformations involving only linear sums of external momenta (p). This proves the result.

We will not deal in detail here with the proof of Lemma 1 for the case of $s<n$ where some at least of the $(n-1)$ fold integrations are "superficially" convergent. The proof requires formulation of rules for assignment of the remaining $(n-s)$ moments which is not difficult.

The proofs in this section, though tedious, are essential because it is important to realize that a subtraction procedure is worthless unless it can be shown that it leads to unique absolutely convergent results.

The author is indebted to Dr. P. T. Matthews and Dr. Res Jost for help in Sec. III and to Professor J. R. Oppenheimer for the very kind hospitality of the Institute for Advanced Study.

[11] This result is of course not true for $s<n$.

PHYSICAL REVIEW VOLUME 84, NUMBER 3 NOVEMBER 1, 1951

The Absorption Spectrum of GaCl

FRANKLYN K. LEVIN* AND J. G. WINANS
University of Wisconsin, Madison, Wisconsin
(Received April 23, 1951)

The absorption spectrum of GaCl has been measured and analyzed to provide values for molecular constants. The energy of dissociation for the ground state has been determined from a predissociation limit as less than 5.00 volts and probably greater than 4.98 volts.

INTRODUCTION

WHILE studies of the vibrational spectra of molecules formed by the elements from a single column of the periodic table are not uncommon, investigations of the rotational spectra from various elements in one column have been rare. Such a study has been started for the chlorides formed by the elements of column III. An analysis of the rotational structure of the InCl molecule was made by Froslie and Winans;[1] the rotational spectrum of AlCl was analyzed by Holst.[2]

Two previous investigations of the spectrum of GaCl have been made. Petrikalm and Hochberg[3] obtained the vibrational spectrum in absorption in the region from 3220A to 3470A. The dispersion was sufficient to check the isotope shift due to Cl^{35} and Cl^{37}, but not enough to make a vibrational analysis of the bands. Miescher and Wehrli[4] working with somewhat larger spectrographs confirmed the assignment of the spectrum to GaCl and showed that the heads around 3300A belonged to two overlapping systems. Although Miescher and Wehrli made a thorough and accurate vibrational analysis of the three systems obtained in absorption, the dispersion of their instruments was not sufficient to analyze the rotational structure or determine the position of the null lines.

In the present investigation, the spectrum was

* Now with Carter Oil Company, Tulsa, Oklahoma.
[1] H. M. Froslie and J. G. Winans, Phys. Rev. **72**, 481 (1947).
[2] W. Holst, Z. Physik **93**, 55 (1935).
[3] A. Petrikalm and J. Hochberg, Z. Physik **86**, 214 (1933).
[4] E. Miescher and M. Wehrli, Helv. Phys. Acta **7**, 331 (1934).

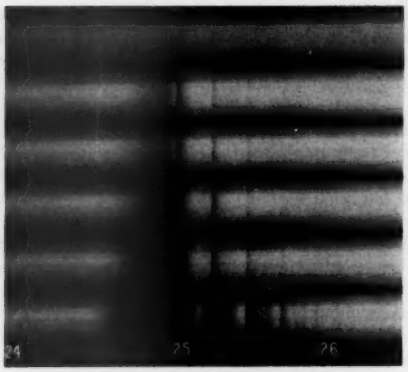

FIG. 1. Spectrum of system *C* of GaCl.

photographed in the third and fourth orders of the 21-foot Wisconsin grating spectrograph. This instrument has a resolving power 90,000 and a dispersion of 0.88A per millimeter in the third order. The grating is one ruled by R. W. Wood on an aluminum surface to give maximum intensity at 11,000A in the first order.

EXPERIMENTAL PROCEDURE

In this study, two fused quartz absorption cells 10 centimeters long and 2.5 centimeters in diameter were used. For preparing these cells a short Pyrex capsule containing commercial quality anhydrous $GaCl_3$ was placed in a vertical tube attached to the pumping system between the cell and liquid air trap. The cell was evacuated and heated at a temperature of 1100°C for forty-eight hours after a "sticking-vacuum" was obtained.

When the cell had cooled, a hole was blown in a quartz side tube and a small ball of oxide-free gallium quickly dropped in. The hole was sealed and pumping resumed until a "sticking-vacuum" reappeared. After the heating and evacuation the small capsule containing $GaCl_3$ was broken with a magnetic hammer and some of its contents distilled into the absorption cell by the use of a hand torch. When the cell was sealed off, it contained a small amount of $GaCl_3$ and a piece of gallium metal. At the temperatures used in this experiment, the trichloride was converted to monochloride and the chlorine released reacted with Ga to form more GaCl.

While photographing spectra, the absorption cell occupied the center of a large furnace. A side arm projected into a small second furnace to control the pressure.

In the preliminary absorption experiments, a hydrogen discharge tube was used as a source of continuous radiation. This source was satisfactory for obtaining survey plates with a medium quartz spectrograph. It was, however, not sufficiently intense for use with the grating spectrograph.

The intense continuum between 2570A and 5000A from an H-3 mercury arc was found to be satisfactory. With this source it was possible to photograph two of the band systems of GaCl in either the third or fourth order of the grating spectrograph with an exposure time of three to ten hours. For wavelengths below 2537A, a water-cooled H-6 mercury lamp gave a continuum with intensity such that a fifteen-minute exposure showed the absorption bands between 2480A and 2537A. For the spectral region between 2537A and 2570A where there are many band heads of one of the systems of GaCl, no completely satisfactory light source was available. A Cooper-Hewitt mercury arc operated slightly above the rated power gives a weak continuous background between broadened atomic lines. With exposure times up to eighteen hours, it was possible to obtain about half of the band heads known to exist in the 2537A to 2570A region.

To eliminate the overlapping of orders of the grating spectrograph, the spectral region of interest was separated with a quartz prism between the source and slit.

One of the two quartz absorption cells was also used to obtain the emission spectrum of GaCl. A long wire attached to the tip of a low voltage Tesla coil was inserted into the furnace so that it just cleared the side of the cell.

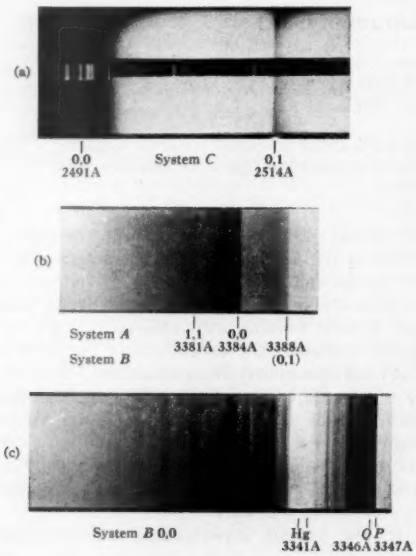

FIG. 2. Bands of GaCl.

DESCRIPTION OF SPECTRUM

The emission spectrum after one-hour exposure with the medium quartz spectrograph showed not only the GaCl emission bands but also lines of atomic gallium.

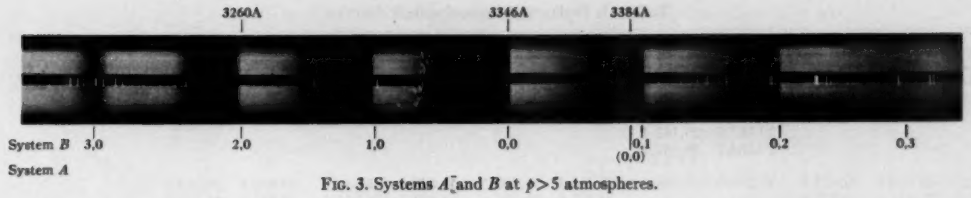

FIG. 3. Systems A and B at $p>5$ atmospheres.

The atomic gallium presumably arose from dissociation of $GaCl_3$ in the discharge.

The general characteristics of the absorption spectrum of gallium chloride are the same as those of indium chloride (reference 1, Fig. 2). The spectrum of system C at pressures corresponding to saturation of $GaCl_3$ from 120°C to 250°C taken with the medium quartz spectrograph is shown in Fig. 1.

A narrow absorption region appears first near 2500A. With increasing temperature and pressure this system broadens toward the red and slightly toward the shorter wavelengths until at a pressure of one atmosphere and at a temperature of 500°C it extends from 2440 to 2760A. The bands in this system are all degraded toward longer wavelengths and alternate bands have sharp double heads. At higher pressures another system of absorption bands appears near 3350A. This consists of six groups of overlapping bands with sharp heads on the long wavelength sides. These bands, extending from 3220 to 3440A, may be arranged as indicated by the isotope shift into two systems.

Two regions of continuous absorption are observed at the higher pressures. The one near 2100A broadens toward longer wavelengths with increasing pressure and the other at 2430A increases in intensity with comparatively little broadening as the pressure is increased. At a pressure of one atmosphere these two continuous regions and the band system from 2440 to 2760 overlap to give continuous absorption from below 2100 to 2610A.

The (0,0) and (1,0) bands of the 2440 to 2760 system in the fourth order are shown in Fig. 2(a) and the (0,0) bands of the two systems near 3300A, in the third order, are shown in Fig. 2(b) and 2(c). The system between 2440 and 2740A consists of a progression of bands with sharp heads alternating with a progression of diffuse bands. Miescher and Wehrli have shown that this system denoted as system C consists of $(0,v'')$ and $(1,v'')$ progressions with (0,0) head at 2490A. The bands with sharp heads form a $(0,v'')$ progression and show no detectable rotational structure other than the sharp heads. The diffuse bands form a $(1,v'')$ progression. In the corresponding system for indium chloride the $(0,v'')$ bands showed rotational structure, the $(1,v'')$ bands showed sharp heads but no other rotational structure, and the $(2,v'')$ bands were diffuse. A few of the strong bands of indium chloride were observed as an impurity spectrum in the absorption spectra of gallium chloride.

The absorption bands between 3220A and 3440A consisting of two overlapping systems were denoted by Miescher and Wehrli as systems A and B. The (0,0) head for the system A is at 3384 and for the system B at 3347A. These are shown in Figs. 2(b) and 2(c). In the present investigation, all of the bands in both systems A and B were found to have rotational structure and several of the bands in system B showed "Q" branches. To ascertain the extent of these systems, some absorption spectra were photographed with a $GaCl_3$ pressure exceeding five atmospheres as determined from the temperature. An example is shown in Fig. 3.

In the emission spectrum, systems A and B appear with high intensity but there is no evidence of any bands of system C. The emission spectrum showed also three sequences of bands degraded toward the red lying between 2370 and 2450, and several additional sequences, also degraded toward longer wavelengths between 2910 and 3210A. It was not possible to obtain enough dispersion or intensity to identify with certainty the molecules responsible for these bands.

ANALYSIS

Vibrational Analysis

The vibrational analysis of the band systems of GaCl made by Miescher and Wehrli[4] was found to be correct both as to the position of the band heads and assignment of quantum numbers. However, since the spectrographs used in the present investigation had higher dispersion, the data are probably more accurate.

A fundamental difficulty in analyzing systems A and B lies in the overlapping of a band of one system by bands belonging to the other system or by the rotational structure of other bands of the same system. Consequently, it was possible to fix the position of the band

TABLE I. Q heads for system B $Ga^{69}Cl^{35}$.

v' \ v''	0		1		2
0	29,873.9 (390.4)	(363.2)	29,510.6 29,512.5[a]	(360.6)	29,150.0 29,153.2[a]
1	30,264.3 30,256.9[b] (379.1)				
2	30,636.0[b]		30,286.6		

[a] $Ga^{71}Cl^{35}$.
[b] $Ga^{69}Cl^{37}$.

TABLE II. Deslandres' table of system A of GaCl.

v'' / v'	0 Obs.	0 Calc.	1 Obs.	1 Calc.	2 Obs.	2 Calc.	3 Obs.	3 Calc.	4 Obs.	4 Calc.	5 Obs.	5 Calc.
0	29,539.0	29,539.0	29,176.1 29,177.8 29,182.6 29,184.2	29,176.2 29,177.8 29,182.4 29,184.1	28,815.5 28,818.9	28,815.7 28,819.0						
1	29,929.5 29,927.6 29,922.3 29,920.5	29,929.5 29,927.6 29,922.3 29,920.3	29,566.6	29,566.6	29,206.1 29,207.8 29,211.9 29,213.3	29,206.2 29,207.6 29,211.9 29,213.4	28,848.1 28,851.4 28,860.6 28,863.4	28,848.2 28,851.3 28,860.4 28,863.5	28,492.4 28,497.2 28,510.5	28,492.6 28,497.4 28,511.0		
2	30,315.3 30,311.7	30,315.3 30,311.5	29,952.5 29,950.4 29,944.8 29,942.8	29,952.4 29,950.4 29,944.8 29,942.8			29,234.1 29,235.3 29,239.8	29,233.9 29,235.3 29,239.2	28,878.0 28,881.5 28,890.0	28,878.3 28,881.3 28,889.9	28,524.6 28,529.3	28,525.2 28,529.8
3			30,333.3 30,329.8 30,319.2	30,333.2 30,329.5 30,319.0	29,972.9 29,970.4 29,965.2 29,963.0	29,972.8 29,970.6 29,965.0 29,963.0					28,906.5 28,909.1 28,917.1	28,906.1 28,909.0 28,917.2
4			30,709.1 30,703.2	30,709.1 30,703.6	30,348.8 30,344.3	30,348.7 30,344.9	29,991.5 29,988.6	29,990.7 29,988.5				
5			31,080.3	31,080.0	30,719.7 30,714.2	30,719.5 30,714.0	30,361.9 30,358.1 30,347.2	30,361.5 30,357.7 30,347.4				
6					31,084.8 31,078.8 31,058.1	31,085.2 31,078.0 31,058.6	30,727.0 30,722.5 30,707.1	30,727.2 30,721.7 30,707.0	30,371.7 30,368.1	30,371.6 30,367.8		
7							31,087.1	31,087.6	30,732.2 30,712.3	30,732.0 30,712.2	30,379.0	30,378.9

head precisely in only a few cases. In general, errors of ± 0.1 cm^{-1} were possible. System A arising from a $^3\Pi_0 \leftarrow {}^1\Sigma_0^+$ transition (see next section) has only P and R branches while system B representing a $^3\Pi_1 \leftarrow {}^1\Sigma_0^+$ transition has P, Q, and R branches. None of the bands was resolved in the neighborhood of the null line, but a few Q heads, which effectively coincide with the null line, could be measured for system B. These are listed in Table I.

Tables II and III are Deslandres' schemes[5] of wave numbers for the band heads of systems A and B. In many cases, heads corresponding to the four isotopic components $Ga^{69}Cl^{35}$, $Ga^{71}Cl^{35}$, $Ga^{69}Cl^{37}$, and $Ga^{71}Cl^{37}$ were detected and are given in that order. Also listed are values calculated from the formulas:

$$\nu = 29{,}524.3 + \begin{matrix}395.3\\393.4\\388.1\\386.2\end{matrix}(v'+\tfrac{1}{2}) - \begin{matrix}2.3\\2.3\\2.2\end{matrix}(v'+\tfrac{1}{2})^2 + \begin{matrix}0.015\\0.015\\0.014\\0.014\end{matrix}(v'+\tfrac{1}{2})^3$$

$$- \begin{matrix}365.3\\363.6\\358.7\\357.0\end{matrix}(v''+\tfrac{1}{2}) + \begin{matrix}1.2\\1.2\\1.2\\1.2\end{matrix}(v''+\tfrac{1}{2})^2$$

for system A and

$$\nu = 29{,}856.3 + \begin{matrix}395.3\\393.4\\388.1\\386.2\end{matrix}(v'+\tfrac{1}{2}) - \begin{matrix}2.5\\2.5\\2.4\\2.4\end{matrix}(v'+\tfrac{1}{2})^2$$

$$- \begin{matrix}365.3\\363.6\\358.7\\357.0\end{matrix}(v''+\tfrac{1}{2}) + \begin{matrix}1.2\\1.2\\1.2\\1.2\end{matrix}(v''+\tfrac{1}{2})^2$$

for system B.

The differences between the experimental and calculated values are less than one wave number. Because of the uncertainty in the position of the heads and because band heads rather than origins were measured, the agreement is satisfactory. Several bands not found by Miescher and Wehrli[4] are included here. In one case [the (1,1) band of system B] a head reported by them proved to be due to a chance coincidence of rotational lines of the (0,0) band.

The coefficients in the formulas for the heads due to $Ga^{71}Cl^{35}$, $Ga^{69}Cl^{37}$, and $Ga^{71}Cl^{37}$ were calculated theoretically from the coefficients found empirically for $Ga^{69}Cl^{35}$. The agreement between the measured and calculated values shows that there can be little doubt that the bands are due to GaCl.

The band heads measured for system C are listed in Table IV. The heads for the $(0,v'')$ progression could

[5] The formulas quoted can be found in Gerhard Herzberg, *Molecular Spectra and Molecular Structure* (D. Van Nostrand, Inc., New York, 1950). All theory necessary for the interpretation can also be found there.

TABLE III. Deslandres' table of system *B* of GaCl.

v'' / v'	0		1		2		3		4		5		6	
	Obs.	Calc.	Obs.	Calc.	Obs.	Calc.	Obs.	Calc.	Obs.	Calc.	Obs.	Calc.	Obs.	Calc.
0	29,870.9	29,870.9	29,508.1 29,509.8 29,514.5 29,516.2	29,508.0 29,509.7	29,147.5	29,147.5								
1	30,261.1 30,259.3 30,254.0 30,252.1	30,261.1 30,259.2 30,253.9 30,251.9					29,179.7	29,179.7	28,824.1 28,829.0 28,842.8 28,847.3	28,824.2				
2	30,646.1 30,642.6 30,632.2 30,628.5	30,646.3 30,642.6 30,632.3 30,628.5	30,283.5 30,281.7 30,276.5	30,283.4 30,281.4 30,275.9					29,209.2	29,209.4	28,856.2 28,860.8	28,856.2 28,860.9		
3	31,026.3 31,020.7 31,005.8 30,999.8	31,026.6 31,021.0 31,005.3 31,000.3	30,663.8 30,660.0 30,649.8	30,663.7 30,659.9 30,649.5					29,589.4	29,589.6			28,886.3 28,890.0	28,885.7 28,890.3
4			31,038.8 31,033.4	31,038.8 31,033.3	30,678.8 30,675.1	30,678.4 30,674.6								
5			31,408.5	31,409.0	31,048.7 31,043.4 31,028.6 31,023.0	31,048.6 31,043.0 31,028.2 31,022.6	30,691.7 30,687.2	30,690.5 30,686.7						
6							31,055.8 31,050.6 31,036.0 31,030.7	31,055.7 31,050.2 31,035.6 31,030.0						
7							31,414.6	31,415.8	31,059.9 31,050.6 31,040.9 31,034.8	31,060.2 31,054.8 31,040.6 31,034.9	30,707.1	30,707.1		
8											31,061.3	31,062.2		

be measured accurately. The separations between vibrational states of the ground state may therefore be accurately determined. The wave numbers listed for the $(1,v'')$ progression are those of the centers of the diffuse bands.

Even though the heads of only the $(0,v'')$ progression of system *C* were known, a method for getting the vibrational constants of the upper electronic state was devised. The wave numbers of the $(0,v'')$ progression can be represented by

$$\nu = \nu_e + \tfrac{1}{2}\omega_e' - \tfrac{1}{4}\omega_e' x_e' - \omega_e''(v''+\tfrac{1}{2}) + \omega_e'' x_e''(v''+\tfrac{1}{2})^2$$

for $Ga^{69}Cl^{35}$ and

$$\nu^i = \nu_e + \tfrac{1}{2}\rho\omega_e' - \tfrac{1}{4}\rho^2\omega_e' x_e' - \rho\omega_e''(v''+\tfrac{1}{2}) + \rho^2\omega_e'' x_e''(v''+\tfrac{1}{2})^2$$

for each of the other isotopic combinations. Since system *C* has the same lower electronic state as systems *A* and *B*, ω_e'' and $\omega_e'' x_e''$ are known. Thus average values of $\nu_e + \frac{1}{2}\omega_e' - \frac{1}{4}\omega_e' x_e'$ and $\nu_e + \frac{1}{2}\rho\omega_e' - \frac{1}{4}\rho^2\omega_e' x_e'$ can be calculated for the progression. The values so obtained for the three most abundant isotopic combinations give three linear equations to be solved for the unknowns ν_e, ω_e' and $\omega_e' x_e'$. Because the isotopic shift is small and the heads of the less abundant isotopic components weak, the values of $\nu_e + \frac{1}{2}\rho\omega_e' - \frac{1}{4}\rho^2\omega_e' x_e'$ for system *C* of GaCl showed too much scatter to apply the method successfully.

The values for the separation of the vibrational levels of the lower states as determined from the measurements of heads in systems *A*, *B*, and *C* are listed in Table V. Also listed are the separations calculated from

$$G(v+\tfrac{1}{2}) = \begin{matrix} 365.3 \\ 363.6 \\ 358.7 \\ 357.0 \end{matrix} (v''+\tfrac{1}{2}) - \begin{matrix} 1.2 \\ 1.2 \\ 1.2 \\ 1.2 \end{matrix} (v''+\tfrac{1}{2})^2.$$

The agreement among the values leaves little doubt

TABLE IV. Deslandres' table for system *C* of GaCl.

v' \ v''	0	1	2	3	4	5	6	7	8	9
		39,775.8	39,414.1			38,348.0	37,996.7	37,648.8	37,302.7	36,958.9
0	40139[a]			39,061[a]	38,703[a]					
		39,778.1				38,356.7	38,007.3	37,660.7	37,316.7	36,974.5
		39,783.1		39,078.3	38,728.8	38,381.6	38,036.2	37,694.9		
		39,786.6		39,083.8	38,735.6	38,390.4	38,046.9	37,707.4		
1	40260[a]				38,820[a]	38,469	38,114	37,760	37,400[a]	37,030[a]

[a] Measured by Mlescher and Wehrli. (See reference 4.)

TABLE V. $\Delta G(v+\frac{1}{2})$ for the ground state of GaCl.

v''	System *A*	System *B*	System *C*	Calculated
0	362.8	362.9		362.8
1	360.6	360.5	361.7	360.5
	358.9	359.4		358.8
	353.8	354.0		354.0
	352.4			352.3
2	357.0	358.0		358.0
	356.2	356.4		356.3
		351.3		351.7
		349.9		350.0
3	355.6	355.7		355.6
		354.2		353.9
		350.1	349.5	349.3
			348.2	347.8
4	353.0	353.4		353.1
		352.2		351.5
			347.2	346.9
			345.2	345.4
5			351.3	350.7
			349.4	349.1
			345.4	344.6
			343.5	343.0
6			347.9	348.3
			346.6	346.7
			341.3	341.2
			339.5	340.7
7			346.1	345.8
			344.0	344.2
8			343.8	343.4
			342.2	341.8

that all three systems have the same lower electronic state. The lack of any absorption bands with a ground state different from that for these systems shows that there are no low-lying excited electronic states.

Rotational Analysis

Of the bands shown in Fig. 3, three are sufficiently clear of overlapping structure for rotational analysis. These are the (0,0) and (0,1) bands of system *B* and the (0,0) band of system *A*. All are shaded toward shorter wavelengths; hence, all form heads in the *P* branch.[5] In addition to *P* and *R* branches, the bands of system *B* have *Q* branches.

System B (0,0) Band

The (0,0) band of system *B* was the first band analyzed. The *Q* branch, spreading toward the violet from the *Q* head, intersects both the *R* branch and that part of the *P* branch returning from the head. Alternately, the lines are in phase and not resolved and out of phase and resolved as shown in Fig. 2(c). Beyond this region of poorly defined, broad lines are a series of pairs of lines approximately equally spaced. The stronger member of each pair was found to be a member of the *R* branch; the weaker, a member of the *P* branch.

TABLE VI. Calculated values of $\nu_0-\nu_h$.

m (assumed)	$\nu_0-\nu_h$, cm^{-1}
35	4.95
36	3.97
37	3.09
38	2.55

A preliminary numbering of the *P* and *R* branches was found by the following procedure. The *Q* branch can be represented in the first approximation[6] by

$$\nu=\nu_0+eJ(J+1) \tag{1}$$

where $e=B_{v'}-B_{v''}$. It is found experimentally that e is small so ν_0 can be taken to be at the *Q* head.

The corresponding equation for the *P* and *R* branches is

$$\nu=\nu_0+dm+em^2 \tag{2}$$

where $d=B_{v'}+B_{v''}$. $m=J+1$ for the *R* branch, and $-J$ for the *P* branch, and J is the rotational number for the lower electronic state. The separation between the missing line and head is

$$\nu_0-\nu_h=d^2/4e. \tag{3}$$

The quantity $\nu_0-\nu_h$ was found by measurement under the assumption that $\nu_0=\nu_{Q\text{ head}}$.

The absolute values of m for the resolved lines in the *R* branch were not known but the difference of m values for any two *R* lines could be found by counting. Two equations were formed:

$$\nu_m=\nu_0+dm+em^2 \quad \nu_{m+\Delta m}=\nu_0+d(m+\Delta m)+e(m+\Delta m)^2.$$

A value was assumed for m and then d and e were calculated with $\nu_0=\nu_{Q\text{ head}}$. These values of d and e were next substituted into (3) to calculate $\nu_0-\nu_h$. The assumed value of m was then changed systematically until near agreement with the measured value of $\nu_0-\nu_h$ was attained. The test was very sensitive as shown in Table VI.

The observed value of $\nu_0-\nu_h$ was 2.95 ± 0.10 cm^{-1}. This fixes the correct m as 37. Then considering 3.09 to be the correct value of $\nu_0-\nu_h$, the value of ν_0 was determined. With the numbering known, small changes could be made in the values of the coefficients of (2) to get the best possible fit to all the resolved *R* branch lines. The semi-empirical formula, with a small cubic correction, is

$$\nu=29{,}873.88+0.3053m+0.00768m^2+0.7\times10^{-6}m^3. \tag{4}$$

The corresponding values of the molecular constants are

$$B_0'=0.1565\text{ cm}^{-1} \quad \text{and} \quad B_0''=0.1488\text{ cm}^{-1}.$$

With the use of Eq. (4), it was found that a few sharp lines near the *Q* head belonged to a portion of the *P* branch with J the same as that in a resolved section of the *R* branch. Combination differences $\Delta_2F'(J)=R(J)-P(J)$ and $\Delta_2F''(J)=R(J-1)-P(J+1)$ obtained are listed in Table VII.

TABLE VII. Fine structure of some bands of the intercombination systems of GaCl.

Wave numbers of the lines of the bands and the combination differences for these bands.

(0,0) Band of System *A*

J	*R*(*J*)	*P*(*J*)	$\Delta_2F'(J)$	$\Delta_2F''(J)$	$\frac{\Delta_2F'(J)}{(J+\frac{1}{2})}$	$\frac{\Delta_2F''(J)}{(J+\frac{1}{2})}$
20	29,552.11					
21	29,552.83					
22	29,553.54					
23	29,554.24					
24	29,554.91					
25	29,555.66					
26	29,556.42					
27	29,557.14					
28	29,557.96					
29	29,558.78					
30	29,559.59					
31	29,560.42			18.77		0.5959
32	29,561.21	29,540.82	20.39	19.35	0.6274	0.5954
33	29,562.17	29,541.07	21.10	19.92	0.6299	0.5946
34	29,563.04	29,541.29	21.75	20.59	0.6304	0.5968
35	29,563.94	29,541.58	22.36	21.15	0.6299	0.5958
36	29,564.88	29,541.89	22.99	21.75	0.6299	0.5959
37	29,565.77	29,542.19	23.58	22.36	0.6288	0.5961
38	29,566.73	29,542.52	24.21	22.95	0.6288	0.5961
39	29,567.72	29,542.82	24.90	23.58	0.6304	0.5970
40	29,568.71	29,543.15	25.56	24.14	0.6311	0.5960
41	29,569.72	29,543.58	26.14	24.67	0.6299	0.5945
42	29,570.72	29,544.04	26.68	25.36	0.6278	0.5967
43	29,571.76	29,544.36	27.40	25.91	0.6299	0.5956
44	29,572.85	29,544.81	28.04	26.47	0.6301	0.5948
45	29,573.91	29,545.29	28.62	27.20	0.6290	0.5978
46	29,575.00	29,545.65	29.35	27.71	0.6312	0.5959
47	29,576.12	29,546.20	29.92	28.24	0.6299	0.5945
48	29,577.20	29,546.76	30.44	28.90	0.6276	0.5959
49	29,578.29	29,547.22	31.07	29.52	0.6277	0.5964
50	29,579.46	29,547.68	31.78	30.02	0.6293	0.5945
51	29,580.67	29,548.27	32.40	30.70	0.6291	0.5961
52	29,581.82	29,548.76	33.06	31.18	0.6297	0.5939
53	29,583.07	29,549.49	33.58	31.78	0.6277	0.5940
54	29,584.29	29,550.04	34.25	32.41	0.6284	0.5947
55	29,585.54	29,550.66	34.88	33.00	0.6285	0.5946
56	29,586.78	29,551.29	35.49	33.58	0.6281	0.5943
57	29,588.04	29,551.96	36.08	34.26	0.6275	0.5958
58	29,589.33	29,552.52	36.81	34.83	0.6292	0.5954
59	29,590.60	29,533.21	27.29	35.39	0.6284	0.5948
60	29,591.97	29,553.94	38.03	35.94	0.6286	0.5940
61	29,593.26	29,554.66	38.60	36.56	0.6276	0.5945
62	29,594.59	29,555.41	39.18	37.11	0.6269	0.5938
63	29,595.98	29,556.15	39.83	37.64	0.6272	0.5928
64	29,597.35	29,556.95	40.40	38.31	0.6264	0.5940
65	29,598.76	29,557.67	41.09	38.94	0.6273	0.5945
66	29,600.18	29,558.41	41.77	39.44	0.6281	0.5931
67	29,601.65	29,559.32	42.33	40.08	0.6271	0.5938
68	29,603.09	29,560.10	42.99	40.70	0.6276	0.5942
69	29,604.61	29,560.95	43.66	41.28	0.6282	0.5940
70	29,606.08	29,561.81	44.27	41.92	0.6279	0.5946
71	29,607.56	29,562.69	44.87	42.50	0.6276	0.5944
72	29,609.06	29,563.58	45.48	43.06	0.6273	0.5939
73	29,610.57	29,564.50	46.07	43.64	0.6268	0.5937
74	29,612.15	29,565.42	46.73	44.19	0.6272	0.5932
75	29,613.71	29,566.38	47.33	44.76	0.6269	0.5928
76	29,615.27	29,567.39	47.88	45.32	0.6259	0.5924
77	29,616.84	29,568.39	48.45	45.88	0.6252	0.5920
78	29,618.46	29,569.39	49.07	46.43	0.6251	0.5915
79	29,620.12	29,570.41	49.72	47.02	0.6254	0.5914
80	29,621.83	29,571.44	50.39	47.66	0.6260	0.5920
81	29,623.47	29,572.47	51.00	48.29	0.6258	0.5925
82	29,625.19	29,573.54	51.65	48.81	0.6261	0.5916
83	29,626.88	29,574.66	52.22	49.47	0.6254	0.5925
84	29,628.60	29,575.72	52.88	50.07	0.6258	0.5925
85	29,630.32	29,576.81	53.51	50.66	0.6258	0.5925
86	29,632.05	29,577.94	54.11	51.21	0.6255	0.5920
87	29,633.83	29,579.11	54.72	51.82	0.6254	0.5922
88	29,635.62	29,580.23	55.39	52.41	0.6259	0.5922
89	29,637.41	29,581.42	55.99	53.01	0.6256	0.5923
90	29,639.24	29,582.61	56.63	53.64	0.6257	0.5927
91	29,641.06	29,583.77	57.29	54.18	0.6261	0.5921
92	29,642.97	29,585.06	57.91	54.82	0.6261	0.5926
93	29,644.77	29,586.24	58.53	55.37	0.6260	0.5922
94	29,646.63	29,587.60	59.03	55.90	0.6247	0.5915
95	29,648.57	29,588.87	59.70	56.50	0.6251	0.5916
96	29,650.49	29,590.13	60.36	57.17	0.6255	0.5924
97	29,652.38	29,591.40	60.98		0.6254	
98	29,654.39			58.37		0.5926
99	29,656.39	29,594.01	62.38		0.6269	
100	29,658.32			59.51		0.5921
101	29,660.22	29,596.88	63.34	60.07	0.6240	0.5918
102	29,662.27	29,598.25	64.02	60.57	0.6246	0.5909
103	29,664.35	29,599.65	64.70	61.28	0.6251	0.5921
104	29,666.35	29,600.99	65.36	61.84	0.6255	0.5918
105	29,668.52	29,602.51	66.01	62.42	0.6237	0.5917
106	29,670.50	29,603.93	66.57	63.08	0.6251	0.5923
107	29,672.51	29,605.44	67.07	63.57	0.6239	0.5913
108	29,674.70	29,606.93	67.77	64.11	0.6246	0.5909
109	29,676.80	29,608.40	68.40	64.81	0.6247	0.5919
110	29,678.93	29,609.89	69.04	65.36	0.6248	0.5915
111	29,681.12	29,611.44	69.68	65.90	0.6249	0.5910
112	29,683.27	29,613.03	70.24	66.55	0.6244	0.5916

Wave numbers of the lines of the bands and the combination differences for these bands.

(0,0) Band of System *A*

J	*R*(*J*)	*P*(*J*)	$\Delta_2F'(J)$	$\Delta_2F''(J)$	$\frac{\Delta_2F'(J)}{(J+\frac{1}{2})}$	$\frac{\Delta_2F''(J)}{(J+\frac{1}{2})}$
113	29,685.52	29,614.57	70.95	67.15	0.6251	0.5916
114	29,687.67	29,616.12	71.55	67.75	0.6249	0.5917
115	29,690.72	29,617.77	72.15	68.32	0.6247	0.5915
116	29,692.16	29,619.35	72.81	68.90	0.6250	0.5914
117	29,694.44	29,621.02	73.42	69.54	0.6249	0.5918
118	29,696.45	29,622.62	73.83	70.08	0.6230	0.5913
119	29,698.99	29,624.36	74.63	70.42	0.6245	0.5892
120	29,701.24	29,626.03	75.21	71.22	0.6241	0.5910
121	29,703.60	29,627.77	75.83	71.77	0.6241	0.5907
122	29,705.98	29,629.47	76.51	72.38	0.6246	0.5909
123	29,708.27	29,631.22	77.05	73.08	0.6239	0.5917
124	29,710.61	29,632.90	77.71	73.58	0.6242	0.5910
125	29,713.01	29,634.68	78.33	74.14	0.6241	0.5908
126	29,715.43	29,636.47	78.96	74.79	0.6242	0.5912
127	29,717.83	29,638.22	79.61	75.46	0.6244	0.5918
128	29,720.32	29,639.97	80.35	75.91	0.6253	0.5907
129	29,722.74	29,641.92	80.82	76.59	0.6241	0.5914
130	29,725.21	29,643.73	81.48	77.13	0.6244	0.5910
131	29,727.67	29,645.61	82.06	77.71	0.6240	0.5910
132	29,730.14	29,647.50	82.64	78.26	0.6237	0.5906
133	29,732.66	29,649.41	83.25	78.80	0.6235	0.5903
134	29,735.18	29,651.34	83.84	79.34	0.6233	0.5899
135	29,737.77	29,653.32	84.45	79.87	0.6232	0.5894
136	29,740.28	29,655.31	84.97	80.63	0.6225	0.5907
137	29,742.87	29,657.14	85.73	81.17	0.6235	0.5903
138	29,745.48	29,659.11	86.37	81.80	0.6236	0.5906
139	29,748.06	29,661.07	86.99	82.37	0.6236	0.5905
140	29,750.70	29,663.11	87.59	82.90	0.6234	0.5900
141	29,753.36	29,665.16	88.20	83.49	0.6233	0.5900
142	29,755.97	29,667.21	88.76	84.09	0.6229	0.5901
143	29,758.58	29,669.27	89.31	84.76	0.6224	0.5907
144	29,761.33	29,671.21	90.12	85.17	0.6237	0.5894
145	29,763.96	29,673.41	90.55	85.79	0.6223	0.5896
146	29,766.67	29,675.54	91.13	86.37	0.6220	0.5896
147	29,769.40	29,677.59	91.81	86.90	0.6224	0.5892
148	29,772.22	29,679.77	92.45	87.47	0.6226	0.5890
149	29,775.00	29,681.93	93.07	88.11	0.6225	0.5894
150	29,777.73	29,684.11	93.62		0.6221	
151	29,780.51			89.31		0.5895
152	29,783.22	29,688.42	94.80	89.79	0.6216	0.5888
153		29,670.72		90.33		0.5885
154		29,692.89				
155		29,695.16				
156		29,697.41				
157		29,699.85				
158		29,702.03				
159		29,704.47				
160		29,706.76				
161		29,709.06				
162		29,711.38				
163		29,713.83				
164		29,716.16				
165		29,718.55				
166		29,720.98				
167		29,723.43				
168		29,725.86				
169		29,728.29				
170		29,730.81				
171		29,733.40				
172		29,735.81				
173		29,738.46				
174		29,740.99				
175		29,743.52				
176		29,746.28				
177		29,748.70				
178		29,751.37				
179		29,753.99				
180		29,756.63				
181		29,759.28				
182		29,761.96				
183		29,764.61				
184		29,767.40				
185		29,770.22				
186		29,772.75				
187		29,775.81				
188		29,778.40				
189		29,781.04				
190		29,783.81				

(0,0) Band of System *B*

J	*R*(*J*)	*P*(*J*)	*Q*(*J*)	$\Delta_2F'(J)$	$\Delta_2F''(J)$	$\frac{\Delta_2F'(J)}{(J+\frac{1}{2})}$	$\frac{\Delta_2F''(J)}{(J+\frac{1}{2})}$
32	29,892.44						
33	29,893.25						
34	29,894.07				21.26		0.5989
35	29,894.88				21.84	0.6277	0.5984
36	29,895.72	29,872.81	29,884.05	22.91	22.39	0.6283	0.5971
37	29,896.60	29,873.04	29,884.64	23.56	23.01	0.6275	0.5977
38	29,897.49	29,873.33	29,885.24	24.16	23.58	0.6268	0.5970
39	29,898.35	29,873.59	29,885.92	24.76	24.14	0.6274	0.5960
40	29,899.32	29,873.91	29,886.40	25.41			

TABLE VII.—*Continued.*

Wave numbers of the lines of the bands and the combination differences for these bands.

(0,0) Band of System *B*

J	$R(J)$	$P(J)$	$Q(J)$	$\Delta_2F'(J)$	$\Delta_2F''(J)$	$\frac{\Delta_2F'(J)}{(J+1)}$	$\frac{\Delta_2F''(J)}{(J+1)}$
41	29,900.23	29,874.21	29,887.07	26.02	24.75	0.6270	0.5964
42	29,901.19	29,874.57		26.62	25.36	0.6264	0.5967
43	29,902.17	29,874.87		27.30	25.94	0.6276	0.5963
44	29,903.18	29,875.25		27.93	26.55	0.6276	0.5966
45	29,904.21	29,875.62		28.59		0.6284	
46	29,905.25				27.78		0.5974
47	29,906.11	29,876.43		29.68		0.6248	
48	29,907.25						
49	29,908.33						
50	29,909.45						
51	29,910.60						
52	29,911.73				31.25		0.5952
53	29,912.91	29,879.35		33.56		0.6273	
54	29,914.09						
55	29,915.31						
56	29,916.53				33.61		0.5949
57	29,917.76	29,881.70		36.06	34.28	0.6271	0.5962
58	29,918.86	29,882.25		36.61	34.93	0.6258	0.5971
59	29,920.12	29,882.83		37.29	35.43	0.6267	0.5955
60	29,921.39	29,883.43		37.96	36.07	0.6274	0.5962
61	29,922.65	29,884.05		38.60		0.6276	
62	29,923.96						
63	29,925.26						
64	29,926.54						

(0,1) Band of System *B*

15			29,512.64				
16			29,512.86				
18			29,513.46				
19			29,513.79				
21			29,514.52				
22			29,514.85				
23			29,515.16				
27			29,516.78				
28			29,517.28				
29			29,517.81				
30			29,518.27				
31			29,518.74				
32			29,519.33				
33			29,519.92				
34			29,520.42				
36	29,533.14		29,521.43				
37	29,534.01		29,522.03		22.37		
38	29,535.01	29,510.77	29,522.63	24.24	22.90		
39	29,535.90	29,511.11	29,523.36	24.79	23.62		
40	29,536.80	29,511.39		25.41	24.19		
41	29,537.79	29,511.71	29,524.51	26.08	24.71		
42		29,512.09	29,525.22		25.38		
43		29,512.41	29,525.93				
44			29,526.47				
45		29,513.46	29,527.43				
46			29,528.24				
47			29,529.03				
48			29,529.91				
49			29,530.62				
50			29,531.47				
54			29,534.74				
55			29,535.48				
56			29,536.35				
58			29,538.39				

Combination differences for System *B*

(0,0) Band of System *B*

J	$\Delta_1F'(J)=R(J)-Q(J)$	$\Delta_1F'(J)=Q(J+1)-P(J+1)$	$\Delta_1F''(J)=R(J)-Q(J+1)$	$\Delta_1F''(J)=Q(J)-P(J+1)$
35		11.24	10.85	
36	11.67	11.60	11.08	11.01
37	11.96	11.91	11.36	11.31
38	12.25	12.33	11.57	11.65
39	12.43	12.49	11.95	12.01
40	12.92	12.86	12.25	12.19
41	13.16			12.50

(0,1) Band of System *B*

36	11.71			
37	11.98		11.38	
38	12.38	12.25	11.65	11.52
39	12.54			11.97
40		12.80	12.29	
41	13.16	13.13	12.57	12.42

For small values of J,

$$\Delta_2F(J)=4B_v(J+\tfrac{1}{2}).$$

Hence, $4B_v$ is the slope of the straight line resulting when $\Delta_2F(J)$ is plotted against J. The values of molecular constants determined from the slopes are

$$B_0'=0.1568\ \text{cm}^{-1},\quad B_0''=0.1490\ \text{cm}^{-1}.$$

The combination differences for the Q branch lines are

$$\Delta_1F'(J)=R(J)-Q(J)=Q(J+1)-P(J+1),$$

$$\Delta_1F''(J)=R(J)-Q(J+1)=Q(J)-P(J+1),$$

listed in Table VII. The agreement between the two sets of values for $\Delta_1F(J)$ confirms the absolute numbering of the band. The values of $\Delta_1F(J)$ are likely to be less reliable than those of $\Delta_2F(J)$ because the Q "lines" are broad combinations of not quite coincident Q and R or Q and P lines. Using these relations, it was possible to choose from the region of intersecting P, R, and Q branches those lines belonging to the Q branch. The Q branch lines are listed in Table VII.

System B (0,1) Band

The (0,1) band of system B shows only two very small regions clear of the intersecting Q branch. Since the (0,0) and (0,1) bands have a common upper vibrational state, the combination differences $\Delta_2F'(J)$ must be the same for both bands. Some resolved lines near the Q heads were assumed to be P lines and the corresponding R lines calculated from the relation $R(J)=P(J)+\Delta_2F'(J)$, $\Delta_2F'(J)$ being taken from the (0,0) band data. The assumed J was varied systematically until wave numbers calculated agreed with those measured. The numbering was thus established. The values of $\Delta_2F'(J)$ are listed in Table VII. Since there are only four of them, the molecular constants cannot be found by plotting $\Delta_2F(J)$ *vs* J. Since the values of $\Delta_1F'(J)$ were known, from the (0,0) band measurements, the lines belonging to the Q branch of the (0,1) band could be identified. The wave numbers of these lines were plotted against $J(J+1)$, to obtain a line of slope $e=B_0'-B_1''$. The measured value of the slope gave $e=0.0081$. The analysis of the (0,0) band gave $B_0'=0.1568\ \text{cm}^{-1}$. Hence, $B_1''=0.1487\ \text{cm}^{-1}$.

To a good approximation, the variation of the rotational constant B_v with vibrational energy is expressible as

$$B_v=B_e-\alpha_e(v+\tfrac{1}{2}),$$

where B_e is the rotational constant in the theoretical vibrationless state and α_e is a constant much less than B_e and characteristic of the electronic state. From values of B_0'' and B_1'' there is obtained $\alpha_e=0.0003\ \text{cm}^{-1}$.

System A (0,0) Band

The (0,0) band of system A has extensive P and R branches but no Q branch. Near the head, the lines are not resolved and at great distances from the head, the P branch lines become diffuse. Between these regions are a great number of pairs of fairly sharp lines, the weaker of each pair belonging to the head producing P branch. Since there was no Q head, the method of analysis followed for system B could not be used.

Using three among several resolved R branch lines so that the relative rotational quantum numbers were

known, the constants for Eq. (2) were calculated for arbitrary values of m. The values of m were then changed until the coefficient $d=(B_0'+B_0'')$ was nearly the same as that found for the (0,0) band of system B. This assumption of nearly equal molecular constants for the two $^3\Pi$ states gave an m numbering good to ± 2. An absolute numbering was then obtained from the requirement that the $\Delta_2F''(J)$ must be the same for this band and the (0,0) band of system B, the lower vibrational state being a common state. The wave numbers and values of $\Delta_2F''(J)$ are listed in Table VII. At $J=77$ an extra line was found both in the P and R branches. This indicates a perturbation in the lower rotational state. The fact that this perturbation was observed for the same value of J in both P and R branches shows that the relative numbering of the P and R branches is correct.

From the plot of $\Delta_2F(J)$ against J, $B_0'=0.1568$ cm^{-1} and $B_0''=0.1485$ cm^{-1}.

The branches extend to sufficiently large values of J to warrant the use of a term in $(J+\frac{1}{2})^3$ in the equations for $F(J)$ and $\Delta_2F(J)$. This term is the correction for the effect of the centrifugal force on the internuclear distance. With this addition

$$\Delta_2F(J)=4B(J+\tfrac{1}{2})-8D(J+\tfrac{1}{2})^3.$$

When $\Delta_2F(J)/(J+\frac{1}{2})$ is plotted against $(J+\frac{1}{2})^2$, there should result a straight line with an intercept $4B$ and a slope $(-8D)$. The values of $\Delta_2F(J)/(J+\frac{1}{2})$ taken from Table VI are plotted against $(J+\frac{1}{2})^2$ in Fig. 4. The values of B obtained from the intercepts and D determined from the slopes are

$$B_0'=0.1568 \text{ cm}^{-1} \qquad B_0''=0.1484 \text{ cm}^{-1}$$

$$D_0'=2.4\times10^{-6} \text{ cm}^{-1} \quad D_0''=2.4\times10^{-6} \text{ cm}^{-1}.$$

The experimental points in Fig. 4 deviate markedly from a straight line at low values of $(J+\frac{1}{2})^2$. This same effect appears in the corresponding curves published by Froslie and Winans[1] for InCl. No explanation for this deviation was offered by them nor has one been found in the literature. The function $\Delta_2F(J)/(J+\frac{1}{2})$ is very sensitive at low J values to small changes in wavelength measurements, so that the whole phenomenon may well represent a systematic measuring error.

A determination of the position of the null line was made using the relation

$$R(J-1)+P(J)=2\nu_0+2eJ^2.$$

Let e' be an approximate value so that the true value is $e=e'+\Delta e$. Then $R(J-1)+P(J)=2\nu_0+2e'J^2+2\Delta eJ^2$.

When $R(J-1)+P(J)-2e'J^2$ is plotted against J^2 a straight line results whose intercept gives $2\nu_0$ and slope gives $2\Delta e$. In this way using $e'=0.008$, it was determined that $\nu_0=29{,}542.0$ cm^{-1} and $e=B'-B''=0.00843$ cm^{-1}. The values obtained from combination differences were $e=0.0083$ and 0.0084 cm^{-1}.

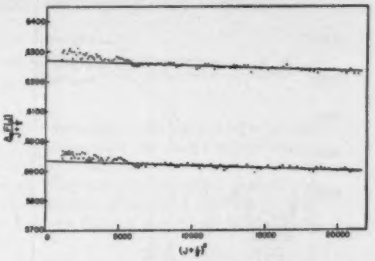

FIG. 4. Plot of $\Delta_2F(J)$ *versus* $(J+\frac{1}{2})^2$ for the (0,0) band of system A of GaCl.

This rotational analysis appears to be satisfactory. The constants found by different procedures agree surprisingly well considering the fact that many of the lines are somewhat diffuse.

ELECTRONIC CONFIGURATION FOR GaCl AND DISSOCIATION ENERGY

The ground state of Ga is $^2P_{\frac{1}{2}}$ and that of Cl is $^2P_{\frac{3}{2}}$. As a chlorine atom in the ground state approaches a gallium atom in the ground state, the molecular states singlet and triplet Σ, Π, and Δ are formed.

If we consider the molecular states to result from the configuration of the $5p$ electrons of the Cl atom and the $1p$ electron of the gallium atom, a closed shell of six electrons $\sigma^2\pi^4$ forms the ground state and this state can be only $^1\Sigma_0^+$. The state of next higher energy has electrons $\pi^3\sigma$ giving states $^3\Pi_{2,1,0}$ and $^1\Pi_1$. Of the three band systems observed, system C at 2500A is the most intense in absorption and appears at the lowest pressure. A singlet-singlet transition should be more intense than a singlet-triplet intercombination transition. Hence the system C is considered to be $^1\Pi\leftarrow{}^1\Sigma_0^+$ and systems A and B $^3\Pi-{}^1\Sigma_0^+$.

Of the three possible systems resulting from $^3\Pi-{}^1\Sigma_0^+$, $^3\Pi_2-{}^1\Sigma_0^+$ is forbidden by the strict selection rule $\Delta\Omega=0, \pm1$. Theory further shows that when $\Omega=0$ in both electronic states, the allowed transitions have $\Delta J=\pm1$ only, giving bands with P and R branches but no Q branch. System A has only P and R branches and therefore must arise from a $^3\Pi_0-{}^1\Sigma_0^+$ transition whereas system B which has P, Q, and R branches represents a $^3\Pi_1-{}^1\Sigma_0^+$ transition.

The predissociation that occurs in system C makes it possible to fix the energy of dissociation of GaCl within narrow limits. System C is a $^1\Pi_1\leftarrow{}^1\Sigma_0^+$ transition, and Kronig's selection rules for predissociation ($\Delta J=0$, $\Delta S=0$, $\Delta\Lambda=0, \pm1$, $+\leftrightarrow-$, $s\leftrightarrow a$) require that the perturbing state be a $^1\Sigma$, $^1\Pi$, or $^1\Delta$ state. The $^1\Sigma$ state can be eliminated immediately, for it could perturb only one component of the $^1\Pi_1$ state in accordance with the selection rules

$$\Delta J=0 \quad \text{and} \quad +\leftrightarrow-.$$

In such a case, only the P and R branches or the Q

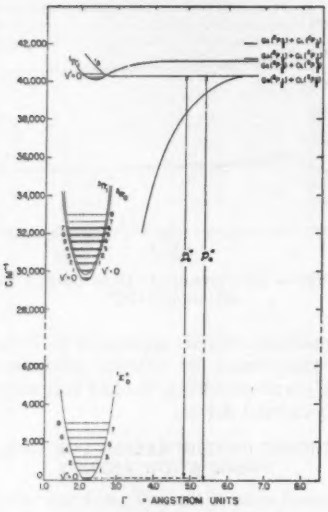

FIG. 5. The potential curves for the low-lying states of GaCl.

branch would be affected. Experimentally, it is found that all branches are missing. A choice between the two remaining possible states $^1\Pi$ and $^1\Delta$ may be made since the narrow continuous absorption band observed at 2430A, appears to represent an absorption from the $^1\Sigma_0^+$ ground state into the state causing the predissociation. The selection rule $\Delta\Lambda=0, \pm1$ forbids an absorption to a $^1\Delta$ state but permits an absorption to a $^1\Pi$ state. The intensity of this continuous absorption is much less than that of the absorption system C ($^1\Pi\leftarrow{}^1\Sigma_0^+$) and corresponds more nearly to that of the forbidden systems A and B ($^3\Pi_{1,0}-{}^1\Sigma_0^+$). The state causing predissociation could be $^1\Delta$ or $^3\Pi$ depending upon whether the selection rule $\Delta\Lambda=0, \pm1$ for absorption is stronger or weaker than the rule $\Delta S=0$ for predissociation, but it is probably $^1\Pi$. It is shown as $^1\Delta$ in Fig. 5.

Since the state $v'=0$ for the $^1\Pi$ state of system C shows no rotational structure but the bands have sharp heads, the rotational levels are probably not perturbed at small values of J. Consequently, it is likely that the state $v'=0$ is stable for low values of J and unstable for higher values of J. The state $v'=1$ is unstable for all values of J since the bands of this state are diffuse. Potential energy curves are shown in Fig. 5.

The absorption spectrum of GaCl is very similar to that of InCl. For InCl the state $v'=0$ for system C is stable and rotational structure is observed to values of $J>100$. The bands with $v'=1$ for InCl show sharp heads but no other rotational structure and the bands with $v'=2$ are diffuse. For GaCl, the bands in system C with $v'=0$ show sharp heads but no other rotational structure and the bands with $v'=1$ are diffuse. The predissociating limit must therefore either lie between the energies of states $v'=1$ and $v'=2$ for InCl and between the energies of $v'=0$ and $v'=1$ for GaCl or at an energy not much less than this. This fixes an upper limit to the energy of dissociation as

$$D_0''=4.68 \text{ volts for InCl}$$

$$D_0''=5.00 \text{ volts for GaCl}$$

with a lower limit not fixed but probably not over about 0.01 volt below 4.66 volts for InCl and 4.98 volts for GaCl. If the predissociation, as is likely, is of the type which sets in rapidly as the energy of the molecule exceeds the energy of the predissociation limit, the values for the dissociation energies are

$$\text{For InCl} \quad D_0''=4.655\pm0.005 \text{ volts.}$$

$$\text{For GaCl} \quad D_0''=4.99 \pm0.01 \text{ volts.}$$

The very pronounced differences between bands for $v'=0$, 1, and 2 show that the character of the predissociation changes rapidly with energy.

The possibility that the state causing predissociation has dissociation products different from normal Cl and normal Ga cannot be ruled out. If the dissociation products for this limit are Ga $^2P_{\frac{1}{2}}$ and Cl $^2P_{\frac{1}{2}}$ or Ga $^2P_{\frac{1}{2}}$ and Cl $^2P_{\frac{3}{2}}$, the predissociation should have been more complete since there would be three possible dissociation limits, one at energy about 0.1 volt below the energy of state $v'=0$.

It is considered unlikely that a stable state such as that of InCl capable of sustaining a rotation of $J>100$ without dissociating could exist at an energy as much as 0.1 volt above a dissociation limit. The dissociation energies are therefore considered to be most likely those listed above.

On the Relativistic Pseudoscalar Meson Theory of the Deuteron

MAURICE M. LÉVY*
Institute for Advanced Study, Princeton, New Jersey
(Received June 29, 1951)

The existence of stationary states of the neutron-proton system is discussed on the basis of a two-particle Dirac equation, including a retarded pseudoscalar interaction. This interaction (in which the possibility of creation of nucleons pairs is disregarded) is treated according to two different models: in the first one, the negative energy states of each nucleon are supposed to be filled, and the interaction is limited to transitions between positive energy states only; in the second model, which is the generalization of the "one-particle" theory, the negative energy states are considered as empty. It is shown that, in both cases, no stable stationary state exists with such an interaction.

I. INTRODUCTION

THE calculation of the interaction between two nucleons in the pseudoscalar meson theory leads, as is well known, to a static approximation which is too strongly singular at small distances to allow for the existence of stationary states of the system. It has long been hoped that a relativistic calculation of this interaction might lower its singularity at the origin, and a tentative approach to this problem will be made in this paper. Within the limits of the approximations which will be made below, the answer is, however, negative.

There are, in general, two different ways to treat relativistically a bound system of two particles interacting through a field. In the first method, which has been mostly used in the past, the interaction is calculated independently of the equations of motion of the two particles ("adiabatic" approximation); this interaction is then introduced into a wave equation, and the motion of the particles is worked out as a second step. In the second method, the calculation of the interaction to a certain order in the coupling constant is not separated from the derivation of the equations of motion, valid to the same order. A "non-adiabatic" treatment of this form has been used by Tamm[1] and Dancoff[2] for the study of the scalar interaction between two nucleons. Only the first method will be discussed in this paper (see, however, our concluding remarks).

The relativistic energy density of interaction of a system of two nucleons, calculated by means of the method of Møller[3] to the second order in the coupling constant, can be written, in the pseudoscalar case, as:

$$W(1,2)=-\bar{\psi}(2)\gamma_5^{(2)}\psi(2)\bar{\Delta}(x_1-x_2)\bar{\psi}(1)\gamma_5^{(1)}\psi(1), \quad (1),$$

where the indices 1, 2 refer to the two particles. $\psi(1)$ $\psi(2)$ are the wave functions of the nucleons, $\bar{\Delta}$ is the well-known four dimensional Green function as defined by Schwinger.[4] The interaction (1) includes nondiagonal elements which connect two particle states with others, in which pairs of nucleons are present.[5] Following Van Hove,[6] we shall make, in the following, two essential approximations:

(a) The nondiagonal elements of $W(1,2)$ will be neglected.

(b) In the momentum representation of the function $\bar{\Delta}$, the fourth component of the momentum of each nucleon will be identified with its corresponding free energy (a system of units in which $\hbar=c=1$ is used throughout this paper). This will enable us to express the energy of interaction in a three-dimensional form and, therefore, to use the conventional definition of stationary states, in which the times of the two-particles are set equal.

With these two assumptions, the matrix elements of the energy of interaction between a neutron and a proton, corresponding to a pseudoscalar meson field (with pseudoscalar and pseudovector couplings), can be written, in the momentum representation, as

$$V^{(2)}_{m_1,m_2}=-\tfrac{1}{2}f_3^2\sum_{m_1,m_2}\chi^{(1)*}_{m_1}\rho_2^{(1)}\chi^{(1)}_{m_1}\mathbf{T}\chi^{(2)*}_{m_2}\rho_2^{(2)}\chi^{(2)}_{m_2}$$
$$\times\left[\frac{1}{\epsilon_K^2-(E_{n_1}-E_{m_1})^2}+\frac{1}{\epsilon_K^2-(E_{n_2}-E_{m_2})^2}\right] \quad (2)$$

with $f_3=f_1+(2M/\mu)f_2$, $\epsilon_K^2=K^2+\mu^2$; $\mathbf{T}$ is an arbitrary isotopic spin operator. In the interaction $V^{(2)}$, a second term has been neglected [Eq. (20)] of Van Hove's paper), which can be removed from the second-order interaction by means of a canonical transformation given by Dyson.[7] This term gives no contribution to real processes which occur with conservation of the energy. However, for virtual processes, in which the energy is not conserved in the intermediate states, this term can contribute to the interaction. We note, however, that this term vanishes for a pure pseudoscalar coupling ($f_2=0$, $f_3=f_1$); in order to avoid any am-

* On leave of absence from the Centre National de la Recherche Scientifique, Paris, France.

[1] I. Tamm, J. Phys. (U.S.S.R.) **9**, 449 (1945).

[2] S. M. Dancoff, Phys. Rev. **78**, 382 (1950).

[3] C. Møller, Z. Physik **70**, 786 (1931); Ann. Physik **14**, 531 (1932).

[4] J. Schwinger, Phys. Rev. **75**, 651 (1949) (Eq. A.21).

[5] Equation (1) can be generalized as to include higher order effects, by introducing a more general function $\bar{\Delta}'(x_1-x_2)$, satisfying an inhomogeneous linear integral equation.

[6] L. Van Hove, Phys. Rev. **75**, 1519 (1949).

[7] F. J. Dyson, Phys. Rev. **72**, 929 (1948).

TABLE I. Classification of the 16 components of the fourier coefficient $\varphi(p)$ of the wave function according to the spin direction and the sign of the corresponding free energy of particles (1) and (2).

		$E^{(1)}=+E_p$ $\sigma_3^{(1)}=+1$	$E^{(1)}=+E_p$ $\sigma_3^{(1)}=-1$	$E^{(1)}=-E_p$ $\sigma_3^{(1)}=+1$	$E^{(1)}=-E_p$ $\sigma_3^{(1)}=-1$
$E^{(II)}=+E_p$	$\sigma_3^{(II)}=+1$	$\varphi_{11}^{(1)}$	$\varphi_{11}^{(2)}$	$\varphi_{12}^{(1)}$	$\varphi_{12}^{(2)}$
	$\sigma_3^{(II)}=-1$	$\varphi_{11}^{(3)}$	$\varphi_{11}^{(4)}$	$\varphi_{12}^{(3)}$	$\varphi_{12}^{(4)}$
$E^{(II)}=-E_p$	$\sigma_3^{(II)}=+1$	$\varphi_{21}^{(1)}$	$\varphi_{21}^{(2)}$	$\varphi_{22}^{(1)}$	$\varphi_{22}^{(2)}$
	$\sigma_3^{(II)}=-1$	$\varphi_{21}^{(3)}$	$\varphi_{21}^{(4)}$	$\varphi_{22}^{(3)}$	$\varphi_{22}^{(4)}$

biguity, we shall therefore restrict ourselves to this case.[8]

Now, in order to calculate the energy levels of the system, our next step is to insert the interaction (2) into a wave equation. In the framework of the "adiabatic" approximation, the only possibility we have is to introduce $V^{(2)}$ into a two-particle Dirac equation,

$$(H_1+H_2-E)\psi(\mathbf{x}_1,\mathbf{x}_2)+V^{(2)}\psi(\mathbf{x}_1,\mathbf{x}_2)=0, \qquad (3)$$

where $H_i=\boldsymbol{\gamma}^{(i)}\cdot\mathbf{grad}^{(i)}+M$, and E is the total energy of the system. We consider, here, the equation as given in a phenomenological way, and resulting more or less from an intuitive generalization of the ordinary notion of potential. There exists, however, field-theoretical arguments which justify, within the approximations (a) and (b), the inclusion of $V^{(2)}$ into Eq. (3) (see footnote 16).

With an equation like (3), a delicate question arises, as to the way to treat the transitions to negative energy states of the nucleons, which are included in interaction (2). In this connection we note that the very use of Eq. (3), and also the approximations (a) and (b) which have been made for $V^{(2)}$, exclude the possibility of taking into account the creation of virtual nucleon pairs. There are, therefore, only two ways to use Eq. (3): model (A)—to consider all negative energy states as filled, and, consequently, to limit the interaction to transitions between positive energy states only; and model (B)—to consider all negative energy states as empty, and, therefore, allow the interaction to connect free states of all energies: this is the generalization to two particles of the "one-particle" theory.

This last model, which is only possible because pair creation is excluded, is rather unattractive. The slightest departue from the assumptions (a) and (b) would invalidate the discussion of this model, whereas it will still be possible to use model (A) as a basis of comparison with more elaborate calculations (to ascertain, for example, the importance of pair creation, etc. . . .).

In the following, the existence and the stability of stationary states of the neutron-proton system will be discussed separately in the framework of models (A) and (B). For this purpose, Eq. (3) will be expressed in the momentum representation, and the behavior at high momenta of the fourier coefficients of the wave function will be investigated. It will be shown, however, that both models do not allow for stationary states of the system. There are two essential reasons for this negative result. First, the part of the interaction which behaves as r^{-3} in the nonrelativistic limit (and which, in the relativistic domain, is less singular), is, however, still too strongly singular for small separations of the nucleons to allow for the existence of stationary states. The second reason is that there also occurs, in the interaction, terms which tend to a δ-function in the nonrelativistic approximation, but which cannot be eliminated covariantly, because they depend on momenta in the relativistic domain (see Sec. III). These terms dominate in the whole range of momentum transfers, and reverse the sign of the interaction. However, even if the isotopic factor is chosen in such a way as to make the complete interaction attractive, the singularity of these pseudo-"contact" terms is too strong to allow for stationary states of the system. In contrast with the nonrelativistic calculations, the singlet states are not favored with respect to the triplet states.

[8] Since the special contribution of the pseudovector coupling is more singular than $V^{(2)}$, and negative conclusion relating to the latter will also probably be valid for the former.

II. GENERAL EQUATIONS

In the barycentric system, the sixteen-components wave function $\psi(\mathbf{x})$ ($\mathbf{x}=\mathbf{x}_1-\mathbf{x}_2$) is expanded by means of its fourier coefficients:

$$\psi(\mathbf{x})=\sum\varphi(\mathbf{p})u_I(\mathbf{p})u_{II}(-\mathbf{p})e^{i\mathbf{p}\cdot\mathbf{x}}, \qquad (4)$$

where u_I and u_{II} are the amplitudes of the Dirac spinors corresponding to particles (1) and (2). The amplitude $\varphi(\mathbf{p})$ has 16-components which are classified in four sets of four-component amplitudes φ_{ij} $(i,j=1,2)$ according to the sign of the corresponding free energy of each nucleon. The "even" components correspond to $i=j$, the "odd" components, to $i\neq j$. In model (A), only the first set φ_{11} will be different from zero; in model (B), the four sets will give contributions. The four components of each partial amplitude φ_{ij} are numbered according to the different spin orientations of the two nucleons. The complete classification of the components of $\varphi(\mathbf{p})$ is summarized in Table I.

With these notations, the amplitude φ_{ij} obeys the following equation:

$$[E-E_i(p)-E_j(p)]\varphi_{ij}(\mathbf{p})=\lambda\sum_{k,l}\int_{(\mathbf{p}')}(\mathbf{p}',k|\rho_2^{(I)}|\mathbf{p},i)\mathbf{T}(\mathbf{p}',l|\rho_2^{(II)}|\mathbf{p},j)\times\Delta_{kl}{}^{i,j}(\mathbf{p},\mathbf{p}')\varphi_{kl}(\mathbf{p}')d\mathbf{p}' \qquad (5)$$

where

$$\Delta_{k,l}{}^{ij}(\mathbf{p},\mathbf{p}')=\tfrac{1}{2}\left[\frac{1}{\omega^2-[E_i(p)-E_k(p')]^2}+\frac{1}{\omega^2-[E_j(p)-E_l(p')]^2}\right], \qquad (6)$$

and $\omega=[(\mathbf{p}-\mathbf{p}')^2+\mu^2]^{\frac{1}{2}}$, $E_1(p)=+E_p$, $E_2(p)=-E_p$, $E_p=(p^2+M^2)^{\frac{1}{2}}$, and $\lambda=(2\pi)^{-3}f_1^2$. The matrix elements of ρ_2 are easily calculated. One has, for example,

$$(\mathbf{p}', k|\rho_2^{(1)}|\mathbf{p}, i)=u_k^*(\mathbf{p}')\rho_2^{\mathrm{I}}u_i(\mathbf{p})$$
$$=\left[\frac{[M+E_i(p)][M+E_k(p')]}{4E_i(p)E_k(p')}\right]^{\frac{1}{2}}\boldsymbol{\sigma}_{\mathrm{I}}\cdot(\mathbf{P}_i-\mathbf{P}_k'), \quad (7)$$

where $\mathbf{P}_i=\{1/[M+E_i(p)]\}\mathbf{p}$, and where $\boldsymbol{\sigma}_{\mathrm{I}}$ (and $\boldsymbol{\sigma}_{\mathrm{II}}$) are two commuting Pauli spin vector-matrices, relating to particles (1) and (2).

III. DISCUSSION OF MODEL (A)

We shall consider separately the singlet and the triplet states of our system, the corresponding eigenvalues of the isotopic spin operator being $T^{(1)}$ and $T^{(3)}$.

Case (1) Singlet States

We have $\varphi_{11}^{(1)}=\varphi_{11}^{(4)}=0$, $\varphi_{11}^{(3)}=-\varphi_{11}^{(3)}=B(\mathbf{p})$. The equation for B can easily be brought to the following form:

$$(E-2E_p)B(\mathbf{p})$$
$$=\lambda T^{(1)}\int\frac{1}{4E_pE_{p'}}\left[1-\frac{\mu^2}{\omega^2-(E_p-E_{p'})^2}\right]B(\mathbf{p}')d\mathbf{p}'. \quad (8)$$

The first term of the kernel goes over, in the nonrelativistic limit, to $1/4M^2$, that is, in coordinate space, to $(1/4M^2)\delta(\mathbf{x})$. It corresponds, therefore, to the "contact-term" of the static pseudoscalar interaction, the existence of which was first emphasized by Belinfante.[9] Its contribution vanishes for states of angular momentum different from zero. The second term of the kernel tends, in the nonrelativistic limit, to the ordinary Yukawa potential.

For the ^1S state, which is the only one to be physically interesting, we first look at the analytical behavior of the kernel of Eq. (8) for high values of the momenta. The first term is actually preponderent in the whole range of variation of p and p'. The second one is of the order of μ^2/M^2 and tends rapidly to zero for high momenta. Neglecting it, we get, apart from a normalization coefficient: $B(\mathbf{p})=[E_p(E-2E_p)]^{-1}$, and the value of E is determined by the equation,

$$\frac{1}{\lambda T^{(1)}}=\int\frac{d\mathbf{p}'}{4E_{p'}^2[E-2E_{p'}]}. \quad (9)$$

The integral of the right-hand side diverges logarithmically for high momenta (a nonrelativistic treatment of the "contact" term would have led to a linear divergence). The system, therefore, does not have any stable ^1S state.

We have to note, however, that, in momentum space, such an analytical examination as has just been made can be misleading. If the isotopic factor $T^{(1)}$ is chosen in such a way as to make the ordinary Yukawa potential attractive, the first term of the kernel of Eq. (8) represents a singular repulsive interaction, less singular, however, in the relativistic region, than a δ-function.[10] On the other hand, it can be shown, by means of the standard coordinate space method, that an interaction consisting of an ordinary attractive potential $V(r)$ plus a repulsive δ-function will allow for the existence of bound states. In this case, however, we shall show in the Appendix that a straightforward transformation of the problem into the momentum representation [which would lead to an equation analogous to (8)], is entirely misleading: this difficulty is due to the fact that the fourier transformation implies regularity conditions for the wave function which are too restrictive from the physical point of view.

However, in the case of a repulsive δ-function, a limiting process can be defined, by which the contribution of the singular potential is removed from the momentum space wave equation. The physical justification to this procedure is that, in fact, a genuine contact interaction can always be eliminated covariantly at the outset, by addition of a direct coupling term in the initial hamiltonian.[11] This is not the case in our problem, because the singular term of the kernel of Eq. (8) depends on momenta, and goes over to a δ-function only in the nonrelativistic limit. We have reached, therefore, the following conclusions:

(a) If Eq. (8) is considered as given, in the momentum representation, we can rightly say that it has no solution corresponding to a finite value of the coupling constant.

(b) Every limiting process which can be defined for suppressing the singular part of the kernel of Eq. (8) will have the aspect of an arbitrary cutoff at large momenta, with no physical justification whatever.

(c) This limiting process would, moreover, be misleading, because it could also be used in order to remove an attractive singular interaction, whereas, in this case, we know that no stable stationary states are possible. As will be seen in the study of the triplet states, an

[9] F. Belinfante, *Theory of Heavy Quanta* (Leiden thesis, 1939), p. 88.

[10] In order to have an idea of the singularity of this interaction, the passage to the "velocity dependent" operators of Wheeler [Phys. Rev. **50**, 643 (1936)] can be made, with the following result:

$$\int\frac{1}{4E_pE_p}B(\mathbf{p}')d\mathbf{p}'\sim\int\frac{1}{rr'}K_1(Mr)K_1(Mr')b(\mathbf{x}')d\mathbf{x}',$$

where $b(\mathbf{x})$ is the fourier transform of $B(\mathbf{p})$. The right-hand side behaves like $1/r^2$ for small distances, provided that the integral on $\mathbf{x}'$ converges.

[11] An interaction of the form $(f_1/2M)^2\boldsymbol{\sigma}^{(1)}\cdot\boldsymbol{\sigma}^{(2)}\delta(r)$ can be eliminated covariantly by writing the hamiltonian of the interacting nucleon and pseudoscalar meson fields in the following way:

$$H=H(\text{free nucleon})+H(\text{free meson})+H(\text{interaction})+H_{\text{dir}},$$

where H_{dir} is given by

$$H_{\text{dir}}=-(f_1^2/4M^2)\int\psi^*(1)\psi^*(2)\boldsymbol{\sigma}^{(1)}\cdot\boldsymbol{\sigma}^{(2)}\psi(1)\psi(2)d\mathbf{x}_1d\mathbf{x}_2$$

where $\psi(1)$ and $\psi(2)$ are the spinor-wave functions of the nucleons. In the calculations of Van Hove (see reference 6), there occurred other real "contact" terms which were cancelled in this way.

attractive singular interaction does occur, which we have no right to suppress.

These conclusions will be illustrated more precisely in the Appendix, where the superposition of a repulsive δ-function and a regular attractive potential is examined in momentum space.[12]

As a concluding remark, we note that the logarithmic divergence of the right-hand side of (9) is not due, as in the problem investigated by Ma,[13] to the cancellation of the quadratic terms in the denominators of the interaction (2), which become bilinear functions of p and p'. If this were true, the occurence of the divergence would be independent of the value of the angular momentum; furthermore, it would occur as well for the scalar case, and in Eq. (8), for the second term of the kernel. It is true that we lose two powers of p at high momenta, one on the left-hand side of the equation, which becomes linear in p, the other in the denominator of the interaction term. But, on the other hand, we gain two other powers of p, from the introduction of the factor $(4E_pE_{p'})^{-1}$. It can be seen that the divergence actually comes from the peculiar angular dependence of the matrix elements of ρ_2.

Case (2) Triplet States

To simplify the discussion, we are obliged, in this case, to separate the angular variables. Using the same notations as Kemmer,[14] we introduce the three symbolic vectors

$$\begin{aligned}(2j+1)^{\frac{1}{2}}\mathbf{X}_j{}^m &= \{[(j+m)_2]^{\frac{1}{2}}Y_j{}^{m-1};\\ &\quad -[(j+m+1)(j-m+1)]^{\frac{1}{2}}Y_j{}^m;\\ &\quad [(j-m)_2]^{\frac{1}{2}}Y_j{}^{m+1}\},\\ \mathbf{Y}_j{}^m &= \{-[(j+m)(j-m+1)]^{\frac{1}{2}}Y_j{}^{m-1};\\ &\quad -2mY_j{}^m;\ [(j+m+1)(j-m)]^{\frac{1}{2}}Y_j{}^{m+1}\},\\ (2j+1)^{\frac{1}{2}}\mathbf{Z}_j{}^m &= \{[(j-m)_2]^{\frac{1}{2}}Y_j{}^{m-1};\\ &\quad [(j+m)(j-m)]^{\frac{1}{2}}Y_j{}^m;\\ &\quad [(j+m)_2]^{\frac{1}{2}}Y_j{}^{m+1}\},\end{aligned} \tag{10}$$

where the notation $(n)_2$ means $n(n+1)$. The amplitude $\varphi_{11}(\mathbf{p})$ can now be considered also as a vector, the components of which are $\varphi_{11}{}^{(1)}$, $\varphi_{11}{}^{(2)}=\varphi_{11}{}^{(3)}$, $\varphi_{11}{}^{(4)}$. In polar coordinates, it is expressed as

$$\phi_{11}=\mathbf{X}_{j-1}{}^m A^{(1)}(p)+\mathbf{Z}_{j+1}{}^m A^{(2)}(p). \tag{11}$$

We use a reduced system of units: $\epsilon=E/2M$, $\rho=p/M$, $k^2=\mu^2/2M^2$, $\chi=1-k^2$, and, moreover, we put

$$A^{(1)}+A^{(2)}=R,\quad jA^{(1)}-(j+1)A^{(2)}=S. \tag{12}$$

The radial equations are then simply

$$\begin{aligned}&[\epsilon-(1+\rho^2)^{\frac{1}{2}}]R(\rho)\\ &=2\pi\lambda T^{(3)}\int_0^\infty\{[\mathcal{K}_j(\rho,\rho')-j\mathcal{L}_j{}^{(1)}(\rho,\rho')]R(\rho')\\ &\qquad+\mathcal{L}_j{}^{(2)}(\rho,\rho')S(\rho')\}\rho'^2d\rho',\end{aligned} \tag{13a}$$

$$\begin{aligned}&[\epsilon-(1+\rho^2)^{\frac{1}{2}}]S(\rho)\\ &=-2\pi\lambda T^{(3)}\int_0^\infty\{[\mathcal{K}_j(\rho,\rho')-(j+1)\mathcal{L}_j{}^{(1)}(\rho,\rho')]S(\rho')\\ &\qquad+j(j+1)\mathcal{L}_j{}^{(2)}(\rho,\rho')R(\rho')\}\rho'^2d\rho',\end{aligned} \tag{13b}$$

with

$$\begin{aligned}\mathcal{K}_j&=(P^2+P'^2)\Delta_{j-1}-2PP'\Delta_j,\\ \mathcal{L}_j{}^{(1)}&=(P^2+P'^2)(\Delta_{j-1}-\Delta_{j+1})/(2j+1),\\ \mathcal{L}_j{}^{(2)}&=(P^2-P'^2)(\Delta_{j-1}-\Delta_{j+1})/(2j+1),\end{aligned} \tag{14}$$

where we have put $P=|\mathbf{P}_1|$ and

$$\Delta_j(\rho,\rho')=\frac{[1+(1+\rho^2)^{\frac{1}{2}}][1+(1+\rho'^2)^{\frac{1}{2}}]}{4[(1+\rho^2)(1+\rho'^2)]^{\frac{1}{2}}}\frac{1}{\rho\rho'}Q_j(U_1). \tag{15}$$

Here, $U_1=(1/\rho\rho')[(1+\rho^2)^{\frac{1}{2}}(1+\rho'^2)^{\frac{1}{2}}-\chi]$, and Q_j is the Legendre function of the second kind. In particular, one has:

$$Q_0(U_1)=\tfrac{1}{2}\,\mathrm{Log}[(U_1+1)/(U_1-1)]. \tag{16}$$

For $j=1$ (ground state of the deuteron), we can write explicitly:

$$\mathcal{K}_1=\frac{1}{4[(1+\rho^2)(1+\rho'^2)]^{\frac{1}{2}}}\left[1-\frac{k^2}{\rho\rho'}Q_0(U_1)\right],$$

$$\mathcal{L}_1{}^{(1)}=\frac{1}{4[(1+\rho^2)(1+\rho'^2)]^{\frac{1}{2}}}\cdot\frac{[(1+\rho^2)(1+\rho'^2)]^{\frac{1}{2}}-1}{2\rho\rho'}\times[U_1-(U_1{}^2-1)Q_0(U_1)], \tag{17}$$

$$\mathcal{L}_1{}^{(2)}=\frac{1}{4[(1+\rho^2)(1+\rho'^2)]^{\frac{1}{2}}}\cdot\frac{1}{2\rho\rho'}\left[\frac{\rho^2}{1+(1+\rho^2)^{\frac{1}{2}}}-\frac{\rho'^2}{1+(1+\rho'^2)^{\frac{1}{2}}}\right][U_1-(U_1{}^2-1)Q_0(U_1)].$$

U_1 tends to $k^2/\rho\rho'$ for small values of ρ and ρ', and to 1 for high momenta. $\mathcal{K}_1$ includes, in the nonrelativistic limit, the contact interaction and the Yukawa potential. $\mathcal{L}_1{}^{(1)}$ and $\mathcal{L}_1{}^{(2)}$ include terms which have, for low momenta, the characteristic r^{-3} and r^{-2} behavior.[15] For

[12] We gratefully acknowledge interesting discussions with Dr. Oppenheimer, in connection with this point.

[13] S. T. Ma, Phys. Rev. **82**, 275 (1951).

[14] N. Kemmer, Helv. Phys. Acta **10**, 47 (1937).

[15] It should be noted that it is rather ambiguous to speak, in the momentum representation, of a singularity equivalent to r^{-3}. The r^{-3} interaction, being too strongly singular at the origin, cannot be fourier transformed, unless an appropriate convergence factor is used. In this case, the "fourier transform" of r^{-3} is defined as a constant, and, therefore, cannot be distinguished from the fourier transform of a three-dimensional δ-function.

high momenta, the expression corresponding to the first term in the bracket of $\mathfrak{L}_1^{(1)}$ has the same structure as the first term in $\mathfrak{K}_1$, but differs by a factor of one-half. Therefore, these two singular terms cancel each other in the kernel of Eq. (13b), but not in (13a). More precisely, we can neglect the terms in $(k^2/\rho\rho')Q_0(U_1)$ and $(U_1^2-1)Q_0(U_1)$, which are very small compared to unity, and write:

$$R(\rho)\sim a/\rho^2+\mathcal{O}(1/\rho^3), \quad S(\rho)\sim b/\rho^2+\mathcal{O}(1/\rho^3). \tag{18}$$

Defining also:

$$c_n\sim T^{(1)}\int^{\infty} d\rho'/\rho'^n, \tag{19}$$

(c_1 is logarithmically divergent, c_2 and c_3 are convergent), we obtain the following set of equations:

$$\begin{aligned}(1+\tfrac{1}{4}\pi\lambda c_1)a+\tfrac{1}{4}\pi\lambda c_2 b=0,\\ (1+\tfrac{1}{2}\pi\lambda c_3)b-\tfrac{1}{2}\pi\lambda c_2 a=0,\end{aligned} \tag{20}$$

together with the condition $a\neq 0$. The Eq. (20) imply therefore that $\lambda\sim 1/c_1$, which means that the system tends to collapse for small separations of the nucleons. The logarithmic divergence represented by c_1 is not removed if the "contact" term is dropped, because of a term in $\mathfrak{L}_1^{(1)}$, which has the same structure for high momenta, and which, in the nonrelativistic limit, includes the $1/r^3$ interaction. (This term would lead to a linear divergence, if treated nonrelativistically.) As was noted before, this term, being attractive, cannot be removed by means of a limiting process analogous to the one which is defined in the Appendix.

IV. DISCUSSION OF MODEL (B)

In this model, the whole set of amplitudes φ_{ij} has to be considered. The kernel of Eq. (5), defined by (6), takes three distinct values according to the possibilities: $i=k$, $j=l$; $i\neq k$, $j\neq l$; and $i=k$, $j\neq l$ (which is equivalent to $i\neq k$, $j=l$). The consequence is that the triplet and the singlet states cannot, in general, be treated separately. However, we are only interested, for the moment, in the behavior of the equations for $p\gg M$. In this extreme relativistic case, the triplet and singlet systems can be separated; furthermore, inside each of these corresponding reduced sets of equations, the contributions of the "even" and "odd" parts of the amplitude φ can also be studied separately, which is very convenient for the discussion of the results.

Case (1) Singlet States

The amplitude $\varphi(\mathbf{p})$ can be considered, in this case as an antisymmetrical tensor. The non-vanishing components can be written as: $\varphi_{11}^{(2)}=-\varphi_{11}^{(3)}=\frac{1}{2}(A+B)$, $\varphi_{22}^{(2)}=-\varphi_{22}^{(3)}=\frac{1}{2}(A-B)$; $\varphi_{12}^{(1)}=-\varphi_{21}^{(1)}=C_1$, $\varphi_{12}^{(2)}=-\varphi_{21}^{(2)}=\varphi_{12}^{(2)}=-\varphi_{21}^{(3)}=C_2$, $\varphi_{12}^{(4)}=-\varphi_{21}^{(4)}=C_3$.

(a) Equations for the "Even" Components

These equations are very similar to (8). We set the following definition:

$$D_{\pm}(\mathbf{p},\mathbf{p}')=\frac{M^2}{2}\left[\frac{1}{\omega^2-(E_p-E_{p'})^2}\pm\frac{1}{\omega^2-(E_p+E_{p'})^2}\right], \tag{21}$$

and we have the equations:

$$\begin{aligned}EA-2E_pB&=\lambda T^{(1)}\int\frac{\mu^2}{M^2}\cdot\frac{1}{2E_pE_{p'}}D_-(\mathbf{p},\mathbf{p}')A(\mathbf{p}')d\mathbf{p}',\\ EB-2E_pA&=-\lambda T^{(1)}\int\frac{1}{2E_pE_{p'}}\\ &\quad\times\left[1-\frac{\mu^2}{M^2}D_+(\mathbf{p},\mathbf{p}')\right]B(\mathbf{p}')d\mathbf{p}'.\end{aligned} \tag{22}$$

In the nonrelativistic limit, D_+ goes over to the ordinary Yukawa potential and D_- goes to zero. Neglecting terms of the order of μ^2/M^2, we have, therefore, the approximate solutions: (apart from a normalization coefficient): $A=[(E^2-4E_p^2)]^{-1}$, $B=(E/2E_p)A$. For large momenta, B is very small compared to A, and we see that, for the latter, the "contact" terms arising from the contributions of the two even parts φ_{11} and φ_{22} have cancelled each other. There exist a finite eigenvalue for the energy-level which is roughly given by:

$$\frac{1}{\lambda T^{(1)}}=-\frac{E}{2}\int\frac{d\mathbf{p}'}{E_{p'}^2[E^2-4E_{p'}^2]}. \tag{23}$$

(b) Equations for the "Odd" Components

In this group of equations, there appear component of angular moment $j-1$ and $j+1$. Denoting the three functions C_1, C_2, C_3 by a single symbolic vector $\mathbf{C}$, we can write, in polar coordinates, the angular dependence of these functions as:

$$\mathbf{C}=\mathbf{X}_{j-1}{}^{m}H_1(\hat{p})+\mathbf{Z}_{j+1}{}^{m}H_2(\hat{p}). \tag{24}$$

For $j=0$ (^1S state), only the second term of the right-hand side is different from zero, and the corresponding equation, with the reduced units of Sec. III, case (2), is the following:

$$\epsilon H_2=2\pi\lambda T^{(1)}\int_0^{\infty}[1-(U_1-1)Q_0(U_1)-(U_2-1)Q_0(U_2)]\times\frac{H_2(\rho')\rho'^2d\rho'}{4[(1+\rho^2)(1+\rho'^2)]^{\frac{1}{2}}}, \tag{25}$$

where we have put: $U_2=(1/\rho\rho')\{[(1+\rho^2)(1+\rho'^2)]^{\frac{1}{2}}+\chi\}$. It is found that, in this case, the contribution to the "contact" terms arising from the odd components of the amplitude add together, and the integral of the right-hand side is linearly divergent. The reason for this

even stronger singularity is that the left-hand side of Eq. (25) is independent of the momentum, instead of being linear in p as in the case of the even components.

Case (2) Triplet States

We shall in this case, only summarize the results, which are entirely analogous to what we have seen before.

(a) There appear, in the equations, two kinds of singular terms which, in the nonrelativistic limit, include the contact interaction and the r^{-3} potential. In the extremely relativistic limit ($p \gg M$), these interaction terms produce logarithmic divergences for the even components and linear divergences for the odd components.

(b) The preceding singularities cancel each other completely in the contributions from the even components and, on the contrary, add together in the contributions from the odd ones.

At first sight, it seems, therefore, that there exists a possibility to allow for the existence of stationary states of the system: the odd components φ_{12} and φ_{21} of the amplitude $\varphi(\mathbf{p})$ must be set equal to zero. However, in the formalism of the "one-particle" model, this possibility is only apparent. Indeed, we have seen that the separation of the equations into separate systems for the odd and even components can only be made in the extreme relativistic limit. If one sets, therefore, $\varphi_{12}=\varphi_{21}=0$, the equations corresponding to intermediate values of the momenta will imply that the whole amplitude $\varphi(\mathbf{p})$ has to be equated to zero.[16] Consequently, there does not exist, in model (B), any stable stationary states of the neutron-proton system.

V. SUMMARY AND CONCLUSION

The results of the preceding investigation can be summarized as follows: In the pseudoscalar meson theory, a retarded interaction between two nucleons, valid to the second order in the coupling constant, has been considered. In this interaction, two essential approximations have been made: (a) The creation of virtual nucleons pairs is excluded; (b) in the momentum representation of the interaction, the fourth component of the momenta is identified with the free energy of the corresponding nucleon.

This interaction has been introduced into a two-particle Dirac equation, and the transitions between free states of the nucleous have been treated in two ways, according to whether the negative energy states are supposed to be filled or empty. In both cases, it has been shown that the interaction, although less singular than the static pseudoscalar potential, does still not allow for stable stationary states of the deuteron. On the other hand, it is well known that this interaction leads, in the Born approximation, to an unacceptable description of the neutron-proton scattering at high energies. The evidence obtained so far seems, therefore, to indicate that this interaction [with approximations (a) and (b)] is completely unsuited to the relativistic treatment of the neutron-proton system.

This conclusion can be substantially modified if a different approach to the problem, with less restrictive approximations than (a) and (b), is used. This can be done, for example, by means of the method which has been used by Tamm[1] and Dancoff[2] for the scalar meson interaction, or by means of the covariant equation which has recently been proposed by Bethe and Salpeter.[17] In the Tamm-Dancoff method, it has been found by Dancoff himself (unpublished) and by the author, that, in the pseudoscalar theory, the second-order interaction will probably allow for stationary states of the deuteron. However, one does not know whether such states will be acceptable (especially in view of the scattering experiments) or whether the corresponding value of the coupling constant (fitted to give the correct value of the ground-state binding energy) is sufficiently small to make a second order calculation consistent. These problems are being investigated, and the results will be reported later.

The author would like to express his gratitude to Professor Oppenheimer, for the hospitality extended to him at the Institute for Advanced Study, and for his continued encouragement. He is also very indebted to Professor Rosenfeld, Dr. Pais, and Dr. Brueckner for many discussions and helpful suggestions at various stages of this work.

APPENDIX. THE DEFINITION OF A REPULSIVE CONTACT INTERACTION IN THE MOMENTUM REPRESENTATION

We consider, in coordinate space, the Schrödinger equation for a system of two particles interacting through a potential represented, as a function of the relative distance, in Fig. 1. This potential consists of an ordinary attractive interaction $V(r)$, plus a singular repulsive potential $G_a(r)$, with a very short-range a and

[16] This conclusion would be different if, instead of Eqs. (5), we had a system of eight equations only, with an amplitude including only the eight "even" components. Such a system of equations can be justified, to some extent, in the following way:

Starting from the covariant integral equation for two particles which has been proposed by Bethe and Salpeter (see reference 17), one makes the approximation (*b*) of Sec. I, in the interaction. With this approximation, it is possible to derive an equation for an amplitude corresponding to equal times for the two particles (that is, the amplitude for the two-particle part of the state which is considered). This equation is apparently identical in form to Eq. (5), but is only equivalent to a system of eight equations, the amplitude itself including only the "even" components. Therefore, this special equation would allow for the existence of stationary states of the system. However, the approximation (*b*) of Sec. I appears, in the equation of Bethe and Salpeter, as artificial and superfluous. It seems more promising, in this case, to have the equation for the amplitude corresponding to different times of the particles solved as it stands, the times being set equal only afterwards, in the solution itself. Such an investigation is being carried on, and the results will be reported later.

[17] H. A. Bethe and E. Salpeter, Phys. Rev. 82, 309 (1951), and private communication. See also, Y. Nambu, Prog. Theor. Phys. 5, 614 (1950), and M. Gell-Mann and F. Low, Phys. Rev. 84, 350 (1951).

a strength proportional to a^{-3}. One has therefore:

$$\lim_{a\to 0} G_a(r) \sim \delta(\mathbf{r}). \tag{A1}$$

The fourier transform of $V(r)$ will be denoted by $W(p)$; we list below some fourier transforms of $G_a(r)$ for different shapes of the coordinate potential:

$$\text{Well:} \quad U_a^w(p) = (3U_0/a^3p^3)(\sin ap - ap\cos ap),$$

$$\text{Gaussian:} \quad U_a^g(p) = U_0 \exp(-a^2p^2), \tag{A2}$$

$$\text{Exponential:} \quad U_a^e(p) = U_0/(1+a^2p^2)^2.$$

All these functions tend to U_0 for $a\to 0$, which we take as the fourier transform of $U_0\delta(r)$.

In coordinate space, we denote by $\bar{\psi}(r)$ the wave function of the system, in the absence of the singular interaction $G_a(r)$. We suppose that it has been normalized in such a way as $\bar{\psi}(0)=1$. In the presence of $G_a(r)$, the corresponding wave function $\psi_a(r)$ has, when $a\to 0$, the following limit:

$$\psi_0(r) = \lim_{a\to 0}\psi_a(r) = \begin{cases} \bar{\psi}(r) & \text{for } r>0, \\ 0 & \text{for } r=0. \end{cases} \tag{A3}$$

$\psi_0(r)$ has therefore a singularity at the origin.

In momentum space, we denote by $\bar{\Phi}$, Φ_a and $\Phi_0=\lim_{a\to 0}\Phi_a$, the fourier transforms of $\bar{\psi}$, ψ_a and ψ_0 respectively. A completely "naive" translation of (A3) could be written:

$$\Phi_0 = \bar{\Phi}(p), \quad \int \Phi_0(\mathbf{p})d\mathbf{p} = 0, \tag{A4}$$

because these conditions would be fulfilled only for very unusual forms of $V(r)$. Instead, we write, in momentum space, the Schrödinger equations satisfied by $\bar{\Phi}$ and Φ_a:

$$(p^2 - Mw)\bar{\Phi}(\mathbf{p}) + (2\pi)^{-3}M\int W(\mathbf{p}-\mathbf{p}') \times \bar{\Phi}(\mathbf{p}')d\mathbf{p}' = 0, \tag{A5}$$

$$(p^2 - Mw)\Phi_a(\mathbf{p}) + (2\pi)^{-3}M\int [U_a(\mathbf{p}-\mathbf{p}') + W(\mathbf{p}-\mathbf{p}')]\Phi_a(\mathbf{p}')d\mathbf{p}' = 0, \tag{A6}$$

(w being the binding energy), and take the limit of the last equation as follows:

$$(p^2 - Mw)\Phi_0(\mathbf{p}) + (2\pi)^{-3}M\int W(\mathbf{p}-\mathbf{p}')\Phi_0(\mathbf{p}')d\mathbf{p}' = -\lim_{a\to 0}(2\pi)^{-3}M\int U_a(\mathbf{p}-\mathbf{p}')\Phi_a(\mathbf{p}')d\mathbf{p}' = 0. \tag{A7}$$

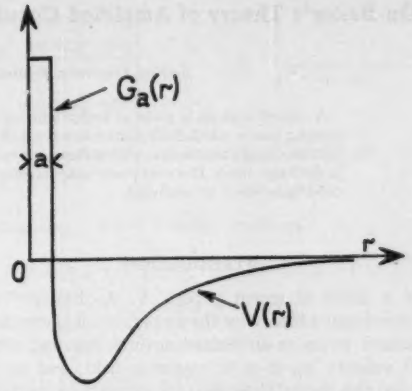

FIG. 1. Coordinate space potential as a function of the relative distance.

This shows that the first condition (A4) is correct, but that the second one must be replaced by the second part of (A7). We see also that the effect of the singular interaction is completely eliminated from the momentum representation by the limiting process of (A7). This limiting process, if we look at the analytical form of the functions given in (A2), appears merely as a more or less strong cutoff which makes to vanish otherwise divergent integrals.

In order to understand what the situation is, with respect to Eq. (8) of the text, we assume for a while that the limit of the second term of (A6) can be taken as the product of the limits of its constituents. We obtain an equation:

$$(p^2 - Mw)\Phi_0(\mathbf{p}) + (2\pi)^{-3}M\int [U_0 + W(\mathbf{p}-\mathbf{p}')]\Phi_0(\mathbf{p}')d\mathbf{p}' = 0 \tag{A8}$$

which is analogous to Eq. (8) of the text. (It coincides with it in the nonrelativistic limit, if $U_3 = p^2/4M^2$, and if $V(r)$ is the ordinary Yukawa potential.) An analytical examination of this equation analogous to our procedure of Sec. III, shows, as it must be, that it has no solution for a value of U_0 different from zero. The momentum representation is therefore, in this case, misleading, because (A8) is the equation which we would have written if we had started directly with $\delta(\mathbf{r})$, instead of defining it at the limit of $G_a(r)$. On the other hand, the limiting process of (A7) is also, in a sense, misleading, because, if $G_a(r)$ were attractive, Eq. (A7) would still have a solution, because the limit of the right-hand side is independent of the sign of $U_a(p)$.

On Bailey's Theory of Amplified Circularly Polarized Waves in an Ionized Medium*

R. Q. Twiss
Services Electronics Research Laboratory, Baldock, Herts, England

A critical analysis is given of Bailey's theory of propagation in an ionized medium. It is shown that the growing waves, which Bailey interprets as amplified waves, can only be excited by reflection and it is argued that this theory can explain neither the excess radiation observed from sunspots nor the excess noise observed in discharge tubes. However power amplification is possible in a drifting ionized medium under certain ideal conditions which are analyzed.

1. INTRODUCTION

IN a series of recent papers, V. A. Bailey[1–3] has developed a theory for the amplification of circularly polarized waves in an ionized medium moving, with a drift velocity u_0, in a dc magnetic field; and he has applied this theory to explain the excess noise radiation observed in sunspots.[4]

In this paper we shall discuss in some detail the criticisms of this theory, which we have outlined elsewhere.[5] In particular, we shall show that the growing[6] electromagnetic wave which is interpreted as an amplified wave by Bailey is, in fact, a reflected wave which can be excited only at a surface of discontinuity in the medium.

Despite this it is ideally possible to find physically realizable boundary conditions such that the medium provides a definite power amplification over those frequency bands where this growing wave exists, and we have analyzed the physical mechanism by which the energy associated with this amplification is transferred to the electromagnetic field from the dc kinetic energy of the electron drift velocity. It is extremely improbable, however, that these conditions could be encountered in a sunspot, and we conclude that the explanation of the excess noise radiation must lie elsewhere.

In order to prove that a particular wave can be excited only by reflection, it is necessary to obtain a transient solution for the electromagnetic propagation in a moving ionized medium, which specifically takes into account the boundary conditions. Instead of attempting to do this by modifying Bailey's analysis, it seemed simpler to develop a direct solution with the aid of the Fourier-Laplace transform theory and then to compare the conclusions drawn from the steady-state and transient analysis with those obtained by Bailey.

The analysis in this paper has been developed under rather special limiting assumptions. However some of the conclusions are of more general application and, in order to develop these, we have discussed the physical nature of the propagation in some detail.

2. THE BOUNDARY AND INITIAL CONDITIONS

In his original paper,[2] Bailey considers the complex case of electromagnetic propagation at an arbitrary angle to the direction of motion of a two-beam plasma acted on by an external magnetic field. However, when applying this theory to the sunspot radiation, he deals only with the unidimensional case where the direction of propagation, of drift velocity and of magnetic field are all parallel, and we shall make the same restriction here.

It is customary, in the theory of propagation in a plasma or electron gas, to separate the disturbance in the medium into longitudinal and transverse oscillations, a procedure which is rigorously justifiable in the unidimensional case if, as we assume, the disturbance is so small that nonlinear effects are negligible. In this paper we consider only the transverse fields and ignore the longitudinal oscillations altogether.

The boundary conditions we shall use are illustrated graphically in Fig. 1. We assume that a plane electromagnetic wave of angular frequency Ω_0 is normally incident, at time $t=0$, upon the interface at $z=0$ between media I and II. Medium II contains a uniform electron stream, or plasma with infinitely massive positive ions, moving with velocity $\mathbf{u}_0=(0, 0, u_0)$ under the action of an external magnetic field of flux density $\mathbf{B}=(0, 0, \mathcal{B}_0)$, which is bounded by surfaces of discontinuity at $z=0$ and $z=d$. In order to simplify the algebra we shall assume that any free charges in medium I are stationary. This restriction will not materially affect the nature of the solution, and does not apply to medium III which can contain free moving charge.

It is further necessary to make some assumptions about the initial transverse velocity modulation. A number of alternatives exist, but a complete discussion of these is beyond the scope of this paper. Instead we shall make the simplest choice that is physically plausible, and assume that this modulation is independent of the incident electromagnetic field over the surface at which the electrons enter medium II that is at $z=0$ for $u_0>0$ and at $z=d$ for $u_0<0$.

The boundary conditions described above are reasonably close to those characteristic of an idealized unidi-

* Acknowledgment is made to the Admiralty for permission to submit this paper for publication.

[1] V. A. Bailey, Nature **161**, 599 (1948).
[2] V. A. Bailey, J. Roy. Soc. N.S.W. **82**, 107 (1948).
[3] V. A. Bailey, Aust. S. Sci. Res. (A) **1**, 351 (1948).
[4] V. A. Bailey, Phys. Rev. **78**, 428 (1950).
[5] R. Q. Twiss, Phys. Rev. **80**, 767 (1950).
[6] By a growing wave we mean any wave the amplitude of which increases exponentially in the positive direction whether it be an amplified wave or a reflected wave attenuated in the negative direction.

mensional electron tube, where medium I might be a thermonic cathode emitting a stream of electrons with velocity u_0 while medium III might be an anode structure. They would also be applicable to the case where medium I was formed by a uniform stream of neutral gas molecules, which was partially ionized at the surface $z=0$, and in which partial recombination or further ionization took place at $z=d$. However they give at best a very idealized approximation to what we might expect to prevail in a gas discharge tube where the drift velocity u_0 is likely to be small compared with the root-mean-square thermal velocity, or in a sunspot where well-defined surfaces of discontinuity would hardly exist.

3. MATHEMATICAL THEORY

It is well known from the theory of the ionosphere that an arbitrary plane wave is split into two independent circularly polarized waves by an axial magnetic field. Accordingly we look for the transient response of the medium of Fig. 1 when a circularly polarized electromagnetic wave, with

$$\mathbf{E}=(E(\Omega_0)\cos\Omega_0 t, E(\Omega_0)\sin\Omega_0 t, 0) \tag{1}$$

is normally incident, at time $t=0$, upon the interface between media I and II at $z=0$.

When Ω_0 is negative we have a left-hand or counter-clockwise wave, when Ω_0 is positive a right-hand or clockwise wave.

In the unidimensional case, which we are considering, the field variables $\mathbf{E}$, $\mathbf{H}$ and the ac transverse velocity $\mathbf{v}(z,t)$ are independent of the transverse co-ordinates while, since the longitudinal oscillations are not excited, we have for the time dependent fields

$$E_z(z,t)=H_z(z,t)=u_z(z,t)=\rho(z,t)=0. \tag{2}$$

In medium II where the dc magnetic flux density is $\mathbf{B}_0=(0,0,B_0)$ and the dc electron velocity is $\mathbf{u}_0=(0,0,u_0)$ the transverse fields satisfy the Lorentz force equation

$$\left(\frac{\partial}{\partial t}+u_0\frac{\partial}{\partial z}+\nu\right)m\mathbf{v}(z,t) = -e\mathbf{E}(z,t)-e\mu_0\mathbf{u}_0\times\mathbf{H}(z,t)-e\mathbf{v}(z,t)\times\mathbf{B}_0 \tag{3}$$

and the maxwell equations

$$\begin{aligned}\nabla\times\mathbf{E}(z,t)&=-\partial\mathbf{B}(z,t)/\partial t;\\ \nabla\times\mathbf{H}&=\rho_0\mathbf{v}(z,t)+\partial\mathbf{D}(z,t)/\partial t,\end{aligned} \tag{4}$$

where ρ_0 is the dc space charge density, ν is the collision frequency, μ_0 is the magnetic permeability of free space, $-e$ is the electron charge, and $m=m_0/(1-u_0^2/c^2)^{\frac{1}{2}}$ is the relativistic electron mass. The other maxwell equations and the charge conservation equation are automatically satisfied for the transverse unidimensional case.

The solution of Eqs. (3), (4) is much simplified if, following Stratton,[7] we use a complex algebra and write

[7] J. A. Stratton, *Electromagnetic Theory* (McGraw-Hill Book Company, Inc., New York, 1941), Sec. 5.16.

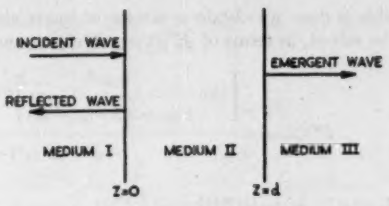

FIG. 1. Boundary conditions.

$$E(z,t)=E_x(z,t)+iE_y(z,t);\quad H(z,t)=H_x(z,t)+iH_y(z,t);\quad V(z,t)=v_x(z,t)+iv_y(z,t) \tag{5}$$

so that the incident wave at $z=0$ is

$$E_{\text{in}}(0,t)=E(\Omega_0)\cos\Omega_0 t+iE(\Omega_0)\sin\Omega_0 t = E(\Omega_0)\exp(i\Omega_0 t). \tag{6}$$

Equations (3), (4) may then be written

$$\begin{aligned}&\left(\frac{\partial}{\partial t}+u_0\frac{\partial}{\partial z}+\nu\right)mV(z,t)\\ &\quad=-eE(z,t)+ieB_0V(z,t)-ieu_0\mu_0H(z,t),\\ &\frac{\partial E(z,t)}{\partial z}-i\mu_0\frac{\partial}{\partial t}H(z,t)=0;\\ &i\frac{\partial}{\partial z}H(z,t)=\rho_0V(z,t)+\epsilon_0\frac{\partial}{\partial t}E(z,t).\end{aligned} \tag{7}$$

To solve these equations under the given initial conditions we take the fourier-laplace transforms first with respect to t, and then with respect to z, where

$$\begin{aligned}&L_t\{f(z,t)\}=f^*(z,\omega)=\int_0^\infty f(z,t)\exp(-i\omega t)dt,\\ &L_t^{-1}\{f^*(z,\omega)\}=f(z,t)\\ &\quad=(2\pi)^{-1}\int_{-\infty-i\gamma}^{+\infty-i\gamma}f^*(z,\omega)\exp(i\omega t)d\omega\end{aligned} \tag{8}$$

and

$$\begin{aligned}&L_z\{f^*(z,\omega)\}=f^{*\dagger}(k,\omega)\\ &\quad=\int_0^\infty f^*(z,\omega)\exp(-ikz)dz,\\ &L_z^{-1}\{f^{*\dagger}(k,\omega)\}=f^*(z,\omega)\\ &\quad=(2\pi)^{-1}\int_{-\infty-i\gamma}^{+\infty-i\gamma}f^{*\dagger}(k,\omega)\exp(ikz)dk.\end{aligned} \tag{9}$$

γ is a positive real number such that all the singularities of $f^{*\dagger}(k,\omega)$ lie above the line $\text{Im}(k)+\gamma=0$ and all the singularities of $f^*(z,\omega)$ lie above the line $\text{Im}(\omega)+\gamma=0$.

If this is done we obtain a system of linear algebraic equations for $E^{*\dagger}(k,\omega)$, $H^{*\dagger}(k,\omega)$, and $V^{*\dagger}(k,\omega)$ which may be solved, in terms of $E^*(0,\omega)$, $H^*(0,\omega)$, and $V^*(0,\omega)$ to give

$$E^{*\dagger}(k,\omega)=\frac{\left[ik+\frac{u_0\omega_0^2}{c^2(\omega+u_0k-\omega_H-i\nu)}\right]E^*(0,\omega)-\omega\mu_0H^*(0,\omega)-\left[\frac{\omega\mu_0u_0\rho_0}{\omega+u_0k-\omega_u-i\nu}\right]V^*(0,\omega)}{-k^2+(\omega^2/c^2)-(\omega_0^2/c^2)(\omega+u_0k)/(\omega+u_0k-\omega_H-i\nu)}, \tag{10}$$

$$H^{*\dagger}(k,\omega)=(-k/\omega\mu_0)iE^{*\dagger}(k,\omega)+[E^*(0,\omega)/\omega\mu_0], \tag{11}$$

$$V^{*\dagger}(k,\omega)=\frac{\omega+u_0k}{\omega+u_0k-\omega_H-i\nu}\frac{e}{\omega m}iE^{*\dagger}(k,\omega)+\frac{u_0V^*(0,\omega)-(u_0/\omega)H^*(0,\omega)}{\omega+u_0k-\omega_H-i\nu}, \tag{12}$$

where

$$\omega_0=(-e\rho_0/\epsilon_0m)^{\frac{1}{2}} \tag{13}$$

is the plasma angular frequency, and

$$\omega_H=eB_0/m \tag{14}$$

is the cyclotron angular frequency.

The initial constants $E^*(0,\omega)$, $H^*(0,\omega)$, and $V^*(0,\omega)$ are to be determined by the boundary conditions which can be applied after inversion from the complex k-plane onto the real z-axis. In the present case, where $E^{*\dagger}(k,\omega)$ is an algebraic function of k which is $O(k^{-1})$ as $k\to\infty$, the inversion can be carried out immediately from Eq. (9) by aid of the theory of residues. We have

$$\left.\begin{aligned}E^*(z,\omega)&=\sum_{n=1}^{3}\exp(ik_nz)[a_n(\omega)E^*(0,\omega)\\&\quad+b_n(\omega)iH^*(0,\omega)+c_n(\omega)V^*(0,\omega)],\\-iH^*(z,\omega)&=\sum_{n=1}^{3}\frac{1}{Z_n(\omega)}\exp(ik_nz)[a_n(\omega)E^*(0,\omega)\\&\quad+b_n(\omega)iH^*(0,\omega)+c_n(\omega)V^*(0,\omega)],\end{aligned}\right\} \tag{15}$$

where

$$\left.\begin{aligned}a_n(\omega)&=\left[k_n\left(k_n+\frac{\omega-\omega_H-i\nu}{u_0}\right)+\frac{\omega_0^2}{c^2}\right]\Big/\prod_{m\neq n=1}^{3}(k_n-k_m),\\b_n(\omega)&=\omega\mu_0\left(k_n+\frac{\omega-\omega_H-i\nu}{u_0}\right)\Big/\prod_{m\neq n=1}^{3}(k_n-k_m),\\c_n(\omega)&=\omega\mu_0\rho_0\Big/\prod_{m\neq n=1}^{3}(k_n-k_m),\end{aligned}\right\} \tag{16}$$

where k_n is one of the three roots of the characteristic equation

$$\left(k+\frac{\omega-\omega_H-i\nu}{u_0}\right)\left(k^2-\frac{\omega^2}{c^2}\right)+\frac{\omega_0^2}{c^2}\left(k+\frac{\omega}{u_0}\right)\equiv\prod_{n=1}^{3}(k-k_n)=0 \tag{17}$$

and where

$$Z_n(\omega)=-\omega\mu_0/k_n \tag{18}$$

is the characteristic impedance of the wave with propagation constant k_n.

In the complex algebra of our present treatment, the impedance of a medium looking in the positive direction across a transverse plane may be written[8]

$$Z(\omega)=E^*(z,\omega)/-iH^*(z,\omega) \tag{19}$$

and the boundary condition on the electromagnetic field components is satisfied at a surface of discontinuity if there is an impedance match there.

Now from Eqs. (6) and (8) the fourier-laplace transform with respect to time of the incident electromagnetic wave is

$$E_{\text{in}}^*(\omega)=E(\Omega_0)/i(\omega-\Omega_0). \tag{20}$$

If in medium I there is just one wave reflected from the surface of discontinuity at $z=0$, then the condition for an impedance match at this surface is

$$-Z_{\text{I}}=\frac{E_{\text{in}}^*(\omega)-E^*(0,\omega)}{E_{\text{in}}^*(\omega)/Z_{\text{I}}+iH^*(0,\omega)}, \tag{21}$$

where Z_{I} is the impedance of medium I, and $E_{\text{in}}^*(\omega)$ is given by Eq. (21). Similarly the boundary condition at $z=d$ gives the equation

$$Z_{\text{II}}=\frac{E^*(d,\omega)}{-iH^*(d,\omega)}=\frac{\sum_{n=1}^{3}\exp(ik_nd)[a_nE^*(0,\omega)+b_niH^*(0,\omega)+c_nV^*(0,\omega)]}{\sum_{n=1}^{3}\exp(ik_nd)[a_nE^*(0,\omega)+b_niH^*(0,\omega)+c_nV^*(0,\omega)]/Z_n(\omega)}. \tag{22}$$

[8] This definition is the natural one to use in the present case where we wish to utilize the connection of the impedance concept with the Poynting vector. Under other circumstances it would be useless, as the impedance so defined is dependent on the relative magnitude of the amplitudes of the electromagnetic and space charge velocity fields.

When $u_0>0$ we assume that $V^*(0,\omega)$ is independent of $E^*(0,\omega)$. It would be permissible to take it as zero, but in order to see what happens when the medium is excited by an initial velocity modulation rather than by an incident electromagnetic wave we shall take

$$V(0,t)=V(\Omega_0)\exp(i\Omega_0 t) \tag{23}$$

so that

$$V^*(0,\omega)=V(\Omega_0)/[i(\omega-\Omega_0)]. \tag{24}$$

When $u_0<0$ we assume that $V^*(d,\omega)=V(\Omega_0)/[i(\omega-\Omega_0)]$ is independent of $E(\Omega_0)$.

If we solve Eqs. (21), (22) for the unknowns $E^*(0,\omega)H^*(0,\omega)$ we find that

$$\left.\begin{aligned} E^*(z,\omega)&=\sum_{n=1}^{3}\frac{A_n(\omega)}{i(\omega-\Omega_0)}\exp(ik_n z),\\ -iH^*(z,\omega)&=\sum_{n=1}^{3}\frac{1}{Z_n(\omega)}\frac{A_n(\omega)}{i(\omega-\Omega_0)}\exp(ik_n z),\end{aligned}\right\} \tag{25}$$

where

$$A_n(\omega)=\frac{\sum_{m=1}^{3}(1-Z_{II}/Z_m)[2(a_nb_m-a_mb_n)E(\Omega_0)+i\{c_n(b_m+Z_1a_m)-c_m(b_n+Z_1a_n)\}V(\Omega_0)]\exp(ik_md)}{\sum_{l=1}^{3}(1-Z_{II}/Z_l)(b_l+Z_1a_l)\exp(ik_ld)} \tag{26}$$

for $u_0>0$.

The solution for the reverse beam, where $u_0<0$, is of a similar although not identical form.

The steady-state solution, assuming that this exists, can immediately be written down from Eq. (25), and we have

$$\left.\begin{aligned} E(z,t)&\to\sum_{n=1}^{3}A_n(\Omega_0)\exp[i(k_n(\Omega_0)z+\Omega_0 t)]\\ &\qquad\qquad\text{as } t\to\infty,\\ -iH(z,t)&\to\sum_{n=1}^{3}[A_n(\Omega_0)/Z_n(\Omega_0)]\\ &\quad\times\exp[i(k_n(\Omega_0)z+\Omega_0 t)]\text{ as } t\to\infty,\end{aligned}\right\} \tag{27}$$

where $k_n(\Omega_0)$ are the roots of the characteristic Eq. (17) which may be written in the more familiar form

$$-k^2+\frac{\Omega_0^2}{c^2}-\frac{\omega_0^2}{c^2}\frac{\Omega_0+u_0k}{\Omega_0+u_0k-\omega_H-i\nu}=0. \tag{28}$$

Of course, the limiting expression of Eq. (27) is only valid if the moving plasma flow is stable. For the moment let us consider that this is so and analyze the steady state solution and Bailey's interpretation of it, before returning to the transient analysis.

4. THE STEADY-STATE ANALYSIS AND BAILEY'S THEORY

(i) The Propagation Constants

When $u_0=0$, the familiar ionosphere case, the characteristic equation, Eq. (28), reduces to

$$-k^2+\frac{\Omega_0^2}{c^2}-\frac{\omega_0^2}{c^2}\frac{\Omega_0}{\Omega_0-\omega_H}=0, \tag{29}$$

where we have also neglected the effects of scattering by taking $\nu=0$.

In this case there are but two partial waves with the same polarization, one of which is interpreted as a wave reflected from the far side of the ionosphere, the plane $z=d$ of Fig. 1. Since there are two possible directions of polarization there are four partial waves in all. When there is no external magnetic field, so that $\omega_H=0$, the propagation constant is independent of the direction of polarization. However, when $\omega_H\neq0$ one distinguishes between the ordinary waves, the polarization of which rotates in the opposite sense to that of an electron moving in the external magnetic field, and the extraordinary waves, the polarization of which rotates in the same sense as an electron; the waves are extraordinary if $\Omega_0\omega_H>0$ and ordinary if $\Omega_0\omega_H<0$. From Eq. (1), the right-hand waves are ordinary if $\omega_H<0$, extraordinary if $\omega_H>0$ and the left-hand waves are extraordinary if $\omega_H<0$ ordinary if $\omega_H>0$.

From Eq. (29) the propagation constants may be written

$$k=\pm i\alpha=\pm i\{[\Omega_0/(\Omega_0-\omega_H)][\omega_0^2-\Omega_0(\Omega_0-\omega_H)]\}^{\frac{1}{2}}/c \tag{30}$$

hence, for the ordinary waves, where $\Omega_0\omega_H<0$, there is an attenuation band, where k is pure imaginary, in the range

$$0\leqslant|\Omega_0|<\tfrac{1}{2}[(\omega_H^2+4\omega_0^2)^{\frac{1}{2}}-|\omega_H|], \tag{31}$$

and a pass band, where k is real, in the range

$$\tfrac{1}{2}[(\omega_H^2+4\omega_0^2)^{\frac{1}{2}}-|\omega_H|]\leqslant|\Omega_0|<\infty; \tag{32}$$

while for the extraordinary waves, where $\Omega_0\omega_H>0$, there is an attenuation band

$$|\omega_H|<|\Omega_0|<\tfrac{1}{2}[(\omega_H^2+4\omega_0^2)^{\frac{1}{2}}+|\omega_H|], \tag{33}$$

and two pass bands

$$0<|\Omega_0|<|\omega_H|$$

and

$$\tfrac{1}{2}[(\omega_H^2+4\omega_0^2)^{\frac{1}{2}}+|\omega_H|]<|\Omega_0|<\infty. \tag{34}$$

When the electrons possess a drift velocity $u_0 \ll c$ the critical frequencies which define the edges of the pass and attenuation bands are slightly altered, as are the propagation constants of these fields waves. In addition there is now a third wave present with a propagation constant that is real for all frequencies. Except in the immediate neighborhood of the critical frequencies the propagation constant $k_2(\Omega_0)$, of this wave is given by

$$k_2(\Omega_0) = -(\Omega_0 - \omega_H)/u_0 \tag{35}$$

to the first order in u_0/c.

It is thus a space charge wave that propagates with a velocity very nearly equal to that of the electron stream. Its analog, in the ionosphere case, is a fixed spatial distribution of transverse velocity modulation, which would not appear as a solution.

Except near the critical frequencies, the propagation constants of the field waves can be found from Eq. (28) by a perturbation method such as Newton's rule, and if

$$k_1 = -i\alpha + \beta; \quad k_3 = i\alpha + \beta, \tag{36}$$

where $i\alpha$ is given by Eq. (30), then for $(u_0/c)^2 \ll 1$

$$\beta = u_0\omega_H\omega_0^2/[2c^2(\Omega_0 - \omega_H)^2]. \tag{37}$$

It will be noted that the characteristic roots are numbered in such a way that k_1 and k_3 are the propagation constants of the growing and decaying waves respectively, so that

$$\mathrm{Re}(ik_1) \geqslant \mathrm{Re}(ik_2) \geqslant \mathrm{Re}(ik_3).$$

From Eq. (37), we see that β is always real so that the effect of a small drift velocity of the medium is to turn the field waves in the attenuation band from pure evanescent into growing and decaying waves that propagate at a very high phase velocity $O(c^2/u_0)$. Except near the critical frequencies, the imaginary part of the propagation constant is unaltered to the first order in (u_0/c).

When we allow for the presence of scattering, so that ν in Eq. (28) is not zero, we have that

$$\left.\begin{aligned} k_2(\Omega_0) &= (i\nu/u_0) - (\Omega_0 - \omega_H)/u_0, \\ k_1(\Omega_0) &= -i\alpha + \frac{\omega_0^2}{2c^2(\Omega_0 - \omega_H)^2}\frac{\Omega_0\nu}{\alpha} + \frac{u_0\omega_H\omega_0^2}{2c^2(\Omega_0 - \omega_H)^2}, \\ k_3(\Omega_0) &= +i\alpha - \frac{\omega_0^2}{2c^2(\Omega_0 - \omega_H)^2}\frac{\Omega_0\nu}{\alpha} + \frac{u_0\omega_H\omega_0^2}{2c^2(\Omega_0 - \omega_H)^2}, \end{aligned}\right\} \tag{38}$$

so that the space charge wave is attenuated as $\exp(-\nu z/u_0)$, while, in the pass band, the forward traveling field wave becomes a decaying wave and the backward traveling wave becomes a growing wave; on the other hand, in the attenuation band, the velocity of propagation of the growing wave is made more negative and that of the decaying wave more positive.

(ii) Bailey's Interpretation

All this is in accord with the conclusion that the growing wave is a reflected wave, but is opposed to Bailey's interpretation, based entirely upon the direction of propagation, that it is a directly excited amplified wave. From Eq. (38) we see that if

$$\nu < |u_0\alpha\omega_H/\Omega_0| \tag{39}$$

and if

$$u_0\omega_H/\Omega_0 < 0 \tag{40}$$

then the growing wave propagates in the positive direction. It is shown by Bailey that the direction of real energy flow associated with any individual wave is the same as its direction of propagation. Hence, when the inequalities (39) and (40) are satisfied, the energy flow associated with the growing wave is out of the medium at the surface of discontinuity at $z = d$; and Bailey concludes that the growing wave is not reflected but excited directly at the incident surface $z = 0$, and that the energy can escape if the medium beyond $z = d$ is either amplifying or transparent at this frequency. Since $\omega_H\Omega_0 < 0$ for the ordinary waves, we see that, on this theory, they are amplified if

$$u_0 > 0$$

and that the extraordinary waves are amplified if

$$u_0 < 0.$$

It must be admitted that this argument from the direction of energy flow has been widely regarded as conclusive in determining whether a given partial wave is amplified or no; nevertheless it is insufficient. The proof of this, given in the next section, is based upon the transient analysis; but the importance of the question and its relevance to cases other than that considered by Bailey, may justify its consideration from the more familiar steady-state analysis as well.

(iii) Criticisms of Bailey's Theory

The most striking conclusion from Bailey's theory is that the presence of even the smallest axial magnetic field in a drifting electron gas is sufficient to transform it from an attenuating into an amplifying medium where the rate of growth of a disturbance is nearly equal to the rate of decay in the absence of the magnetic field. It is true that, when scattering is taken into account, the magnetic field has to attain a finite value before the medium becomes amplifying, given, from inequality (39), by the inequality

$$|\omega_H| > |\Omega_0\nu/\alpha u_0|. \tag{41}$$

But even so, an infinitesimal change in magnetic field transforms a reflected wave into an amplified wave.

A second criticism is suggested by relativity considerations: the dependence of the wave propagation on the uniform motion of the medium implies a special frame of reference. This can only be provided by the

surfaces of discontinuity in the medium. For were these to move with the medium the propagation would be the same, except for a Lorentz transformation, as in the stationary ionosphere.

Accordingly the surfaces of discontinuity play a fundamental role in the excitation of these growing waves, which is in direct contrast to the familiar amplification process in a traveling wave tube or space charge wave amplifier where the nature of the initial and terminal impedance is comparatively unimportant.[9]

Finally we see from Eqs. (23)–(25) that the amplitudes of the three partial waves at the initial plane $z=0$ depend upon the boundary conditions at $z=d$, which strongly implies that one of the partial waves is reflected, while if

$$Z_{II} \neq Z_I(\Omega_0) \quad \text{and} \quad Z_I \neq -(b_1/a_1) \tag{42}$$

then the amplitude $A_1(\Omega_0)$ of the growing wave is proportional to $\exp[-i(k_1-k_2)d]$, which is hardly compatible with the assumption that this wave is directly excited.

However, when the inequalities (42) are not satisfied, an electromagnetic wave incident at $z=0$ will be amplified as it crosses the medium; to show that this result is consistent with the claim that the growing wave is reflected it seems essential to use the transient analysis.

5. THE TRANSIENT ANALYSIS

There is no need to obtain a full transient solution to decide whether a given partial wave is reflected or not. Instead let us consider the term

$$[A_1(\omega)/i(\omega-\Omega_0)]\exp(ik_1z)$$

of $E^*(z,\omega)$ in Eq. (22), which corresponds to the growing wave, and ask how large t must be before this term contributes to $E(z,t)$. Now $E(z,t)$ is identically zero for $t<z/c$, since this is the minimum time taken by a signal, applied at $z=0$, $t=0$, to reach z. By the same token the necessary and sufficient condition that a given term of $E^*(z,\omega)$ should correspond to a reflected wave is that its contribution to $E(z,t)$ be identically zero, at least until a time $t\geqslant(2d-z)/c$ where d is the distance of the first reflecting surface from the initial plane $z=0$.

From the theory of the fourier-laplace transform, it is known that the inverse transform $f(t)$ of a meromorphic function $f^*(\omega)$ such that

$$f(\omega)\sim\exp\left(\frac{-i\omega\xi}{v}\right)\left[\frac{a_1}{\omega}+\frac{a_2}{\omega^2}+\cdots\right] \tag{43}$$

as $\omega\to\infty$, is identically zero for all $t<\xi/v$. Hence the question as to whether or not a particular partial wave is reflected is determined by its asymptotic behavior for large enough ω.

[9] In the traveling wave tube, a frame of reference is provided by the external helical structure, while in the space charge wave amplifier there is relative motion between the various electron beams.

TABLE I. Asymptotic approximations for the parameters of Eq. (26) as $\omega\to\infty$.

	$n=1$	$n=2$	$n=3$
k_n	$(\omega/c)(1-\omega_0^2/\omega^2)$	$-(\omega-\omega_H)/u_0$	$-(\omega/c)(1-\omega_0^2/\omega^2)$
Z_n	$-Z_0(1+\omega_0^2/\omega^2)$	u_0Z_0/c	$Z_0(1+\omega_0^2/\omega^2)$
A_n	$1/2$	$\omega_H\omega_0^2/\omega^3$	$1/2$
b_n	$Z_0/2$	$Z_0(u_0^2\omega_0^2\omega_H/c^2\omega^2)$	$-Z_0/2$

From Eqs. (6), (17) one can build up Table I, where $Z_0=(\mu_0/\epsilon_0)^{\frac{1}{2}}$ is the characteristic impedance of free space, and where we have ignored terms of $O(u_0/c)$ and taken $\nu=0$.

With these approximations the denominator of $A_n(\omega)$ in Eq. (26) is given for large enough ω by

$$\left\{\frac{Z_0}{2}\left(1+\frac{Z_I}{Z_0}\right)\left(1+\frac{Z_{II}}{Z_0}\right)\exp\left(\frac{i\omega d}{c}\right)\right.$$
$$-Z_{II}\frac{u_0^2\omega_0^2\omega_H}{c^2\omega^3}\exp\left[\frac{-i(\omega-\omega_0)d}{u_0}\right]$$
$$\left.-\frac{Z_0}{2}\left(1-\frac{Z_I}{Z_0}\right)\left(1-\frac{Z_{II}}{Z_0}\right)\exp\left(\frac{-i\omega d}{c}\right)\right\}^{-1}. \tag{44}$$

If Z_I and Z_{II} are physically realizable, they must have positive real parts, and therefore

$$\left|\frac{Z_0}{2}\left(1+\frac{Z_I}{Z_0}\right)\left(1+\frac{Z_{II}}{Z_0}\right)\right|>0.$$

If $\mathrm{Im}(\omega)$ is sufficiently negative, so that

$$\mathrm{Re}[\exp(i\omega d/c)]$$

is sufficiently large, one can expand this expression as a convergent binomial series of the form

$$\left[\frac{Z_0}{2}\left(1+\frac{Z_I}{Z_0}\right)\left(1+\frac{Z_{II}}{Z_0}\right)\right]^{-1}\exp\left(\frac{-i\omega d}{c}\right)$$
$$+\text{terms of order }\exp\left[-i\left(\frac{n'\omega d}{c}+\frac{m'\omega d}{u_0}\right)\right],$$

where $n'+m'\geqslant 2$. Now the γ, in Eq. (9) which defines the contour for the inverse transforms, may assume any finite value; in particular it may be chosen so large that the above expansion is justified on and within the closed contour formed by the line $\mathrm{Im}(\omega)+\gamma=0$ and the lower infinite half-circle.

Hence we can express

$$[A_1(\omega)/i(\omega-\Omega_0)]\exp(ik_1z)$$

by an asymptotic series of the form

$$\sum_{n,m}a_{n,m}(\omega)\exp(i\omega/c)[z-(nd+mcd/u_0)], \tag{45}$$

where $a_{n,m}(\omega)$ is a power series in ω^{-1} and where

$n+m \geqslant 2$. A given term of this series contributes to $E(z, t)$ only if

$$t > (n/c+m/u_0)d-z/c, \text{ where } n+m \geqslant 2,$$

and therefore no term contributes until

$$t > (2d-z)/c,$$

which shows that the growing wave is indeed reflected.

A similar analysis can be carried through for the other two partial waves to show that the amplitude of the space charge wave is identically zero until a time $t > z/u_0$, while the decaying field wave is identically zero until a time $t > z/c$; this is what we would expect if these two waves were directly excited at the initial surface.

6. POWER AMPLIFICATION IN AN IONIZED MEDIUM

(i) The Ideal Termination

For the case of the forward waves, where $u_0 > 0$, we showed from Eqs. (24) and (27) that the steady-state amplitude of the growing wave was proportional, for large enough d, to

$$\exp(ik_1 z) \cdot \exp[i(k_2-k_1)d] \sim \exp[-(\alpha+\nu/u_0)d] \cdot \exp(\alpha z)$$

if both the inequalities (42) are satisfied. Even at $z=d$ the amplitude of this wave is $\sim\exp(-\nu d/\mu_0)$ so appreciable amplification cannot be taking place. This is no longer the case however either if

$$Z_{II} = Z_I(\Omega_0) \tag{46}$$

or if

$$Z_I = -b_1(\Omega_0)/a_1(\Omega_0) \tag{47}$$

when, from Eqs. (24) and (27), the amplitude of the growing wave is proportional, for large enough d, to

$$A_1 \exp(ik_1 z) \approx \exp(ik_1 z) \exp(-ik_2 d) \sim \exp(-\nu d/u_0 + \alpha z). \tag{48}$$

If $\alpha > \nu/u_0$, which is normally the case, then the amplitude of this wave increases indefinitely with z, and power amplification is possible as we shall show.

Let us consider the first of these two alternatives that given by Eq. (46). The necessary and sufficient condition that this is physically realizable is that $Z_I(\Omega_0)$ have a positive real part, so that the ideal termination absorbs power from the medium.

From Eq. (18),

$$Z_I(\Omega_0) = -\Omega_0\mu_0/k_1(\Omega_0)$$

and since $k_1(\Omega_0) = \beta - i\alpha$ where β, α are given by Eq. (38), this condition requires that

$$\Omega_0\beta = \frac{\Omega_0^2\omega_0^2}{2c^2(\Omega_0-\omega_H)^2}\left(\frac{u_0\omega_H}{\Omega_0} + \frac{\nu}{\alpha\Omega_0^2}\right) < 0,$$

or that

$$\nu < |\Omega_0\omega_H/\alpha| \quad \text{and} \quad u_0\omega_H/\Omega_0 < 0,$$

which are just the conditions that the growing wave be amplified on Bailey's theory.[10]

That power amplification is indeed possible when the medium is thus ideally terminated follows from the fact that the rate at which real electromagnetic energy flows out of the medium at $z=d$ is given by

$$\mathrm{Re}[E(d, \Omega_0) \cdot -i\bar{H}(d, \Omega_0)] \sim \mathrm{Re}[Z_{II}(\Omega_0)] \exp 2(\alpha - \nu/u_0)d, \tag{49}$$

where $\bar{H}(d, \Omega_0)$ is the complex conjugate of $H(d, \Omega_0)$. If $\alpha > \nu/u_0$ and $\mathrm{Re}[Z_{II}(\Omega_0)] > 0$, this output power can be made arbitrarily large by choosing d large enough. However this is only possible when the terminating impedance possesses its ideal value, and no power amplification is possible unless the medium has nearly the right impedance. To show that this is so we will consider the normal case where the terminating impedance is non-ideal, which will throw additional light on the physical nature of the propagation.

(ii) Non-Ideal Termination

When the termination is so far from the ideal that the first term in the denominator of $A_n(\omega)$ is much larger than the others, that is when

$$|(1-Z_{II}/Z_1)(b_1+Z_1a_1)| \exp(\alpha d) \gg \left|\sum_{l=2}^{3}(1-Z_{II}/Z_l)(b_l+Z_1a_l)\exp(ik_l d)\right|. \tag{50}$$

We have that

$$\left.\begin{aligned} A_1(\Omega_0) &\approx E(\Omega_0)\frac{u_0}{c}\frac{\omega_0^2}{(\Omega_0-\omega_H)^2} \times \frac{(Z_{II}/Z_0)\exp[-(\alpha+\nu/u_0)d]}{(1-i\alpha Z_{II}/\Omega_0\mu_0)(1-i\alpha Z_1/\Omega_0\mu_0)}, \\ A_2(\Omega_0) &\approx E(\Omega_0)\frac{u_0^2}{c^2}\frac{2\Omega_0\omega_0^2}{(\Omega_0-\omega_H)^3}\frac{1}{(1-i\alpha Z_1/\Omega_0\mu_0)}, \\ A_3(\Omega_0) &\approx E(\Omega_0)\frac{2}{1-i\alpha Z_1/\Omega_0\mu_0}, \end{aligned}\right\} \tag{51}$$

where we have used the approximate values for a_n, b_n given in Table II, and have taken $V^*(0, \omega)$, the initial velocity modulation, equal to zero.

These results can be interpreted as follows. Let us suppose that medium I is transparent to the incident wave, frequency Ω_0 which carries a real power $P(\Omega_0)$. If $u_0 = 0$ all of this power is reflected if medium II is sufficiently wide; but if $u_0 \neq 0$ a fraction $\sim(u_0/c)P(\Omega_0)$ is transmitted by medium II. Of this transmitted power, the greater part is carried by the decaying wave

[10] The coincidence is trivial. The condition that $\mathrm{Re}[Z(\Omega^0)] > 0$ is identical with the requirement that the energy flow associated with the growing wave be in the positive direction.

TABLE II. Approximate values of the coefficients of Eq. (26) for $u_0/c \ll 1$ and $\nu/u_0 < \alpha$.

	$n=1$	$n=2$	$n=3$
k_n	$-i\alpha+(u_0/c^2)\omega_H\omega_p^2/[2(\Omega_0-\omega_H)^2]$	$-[(\Omega_0-\omega_H)/u_0]+i\nu/u_0$	$i\alpha+(u_0/c^2)\omega_H\omega_p^2/[2(\Omega_0-\omega_H)^2]$
a_n	$1/2$	$(u_0/c)^2\cdot\Omega_0\omega_p^2/(\Omega_0-\omega_H)^3$	$1/2$
b_n	$-\Omega_0\mu_0/2i\alpha$	$-Z_0(u_0/c)^2\Omega_0\omega_p^2\omega_H/(\Omega_0-\omega_H)^4$	$\Omega_0\mu_0/2i\alpha$
Z_n	$\Omega_0\mu_0/i\alpha$	$Z_0(u_0/c)\Omega_0/(\Omega_0-\omega_H)$	$-\Omega_0\mu_0/i\alpha$

of amplitude $A_3(\Omega_0)$, but a fraction $(u_0^3/c^3)(u_0/c)P(\Omega_0)$ is carried by the space charge wave. If the medium is sufficiently wide and $\alpha > \nu/u_0$ the space charge wave is much larger in amplitude than the decaying wave[11] at $z=d$, and the power in the reflected wave is therefore of the same order of magnitude at $z=d$ as the power in the space charge wave. This power is very much smaller than the incident power so that under these circumstances power amplification is out of the question.

The conditions for power amplification are thus extremely critical, as they rely on what is essentially resonant reflection; moreover when these conditions are met they are more likely to lead to instability around the feedback path formed by the space charge wave and the reflected field wave than to amplification. It may be noted, however, that once the reflected wave has been resonantly excited, there exists a physical mechanism by which it can be maintained.

(iii) The Physical Mechanism of Power Amplification

We shall now show how the ac kinetic and electromagnetic energy associated with the growing wave is obtained from the dc kinetic energy of the electron beam once the wave has been established.

The work done by the electromagnetic field on the moving charge in unit time and unit volume is

$$W = -e\mathbf{E}\cdot\rho\mathbf{v}.$$

In the present case, where $\mathbf{E}$ has no longitudinal component and where ρ is time-independent

$$W = -e\mathbf{E}_\tau\cdot\rho_0\mathbf{v}_\tau$$

where the subscript τ refers to the transverse components.

If we use the complex algebra of Sec. 3 we may write this as

$$W = -e\rho_0\,\mathrm{Re}[E(z,\Omega_0)\cdot\bar{V}(z,\Omega_0)],$$

where

$$\bar{V}(z,\Omega_0) = v_x(z,\Omega_0) - iv_y(z,\Omega_0).$$

Hence, if the electromagnetic field is to gain energy at the expense of the moving charge, we must have

$$W = -e\rho_0\,\mathrm{Re}[E\cdot\bar{V}] < 0.$$

Now this energy is gained at the expense of the space charge ac kinetic energy which is itself continually increasing. The common source for both these increasing ac energies is the dc kinetic energy of the electrons, and it is made available by the interaction of the electron drift velocity with the ac magnetic field. The effect of this interaction is continually to turn the electrons at right angles both to the ac transverse magnetic vector and to the dc longitudinal drift velocity, in just the right sense to supply the required transverse ac energy.

We can derive the mathematical conditions for this energy transfer from the transverse force Eq. (12) which may be written

$$\left(\frac{\partial}{\partial t}+u_0\frac{\partial}{\partial z}\right)mV = -eE - ieu_0\mu_0 H + iem\omega_H V.$$

If we multiply through by $\bar{V}$, the complex conjugate of V, and equate the real parts of both sides we get

$$\mathrm{Re}\left[\frac{d}{dt}\frac{1}{2}mV\bar{V}\right] = \mathrm{Re}[-eE\cdot\bar{V} - ieu_0\mu_0 H\cdot\bar{V}]$$

and if the ac velocity field is to increase exponentially we must have

$$\mathrm{Re}[E\cdot\bar{V} + iu_0\mu_0 H\cdot\bar{V}] < 0.$$

From Eqs. (10)–(12) it can be shown that these conditions will be met, in the steady state, for the growing wave if

$$\nu < |\Omega_0\omega_H/\alpha| \quad \text{and} \quad u_0\omega_H/\Omega_0 < 0$$

which are just the conditions, given by Bailey, of Eqs. (39), (40).

From some points of view this is rather surprising. We have an electron stream moving at a very slow speed interacting with an electromagnetic field propagating with a very high phase velocity; just the condition that normally justifies neglect of the interaction between the space charge and the magnetic components of the field. However, when the field waves have almost pure imaginary propagation constants, $\mathbf{H}$ is nearly parallel to $\mathbf{E}$. Hence, although $\mathbf{H}\times\mathbf{u}_0$ is small it is nearly parallel to $\mathbf{v}$, while $\mathbf{E}\cdot\mathbf{v}$ is small since $\mathbf{E}$ is nearly perpendicular to $\mathbf{v}$. The effect of the magnetic field components on the moving charge is thus comparable with, and indeed greater than the effect of the electric field components, in an attenuating medium.

[11] The power in the space charge wave is dissipated by scattering and decays at a rate $\sim\exp(-2\nu z/u_0)$, while the power in the decaying wave is transferred by radiation pressure to increase the dc kinetic energy of the moving electrons and decays at a rate $\exp(-2\alpha z)$.

(iv) Conditions in Sunspots and Discharge Tubes

What we have said above applies directly only to the forward waves when terminated ideally at the surface $z=d$; other special cases arise when Eq. (47) is satisfied, and for the reverse waves when $u_0<0$. Furthermore the medium might be excited by an initial velocity modulation rather than by an external electromagnetic wave. In all of these, however, amplification is only possible, if at all, under very critical conditions, which would hardly be encountered in a sunspot or indeed anywhere in a star. If the parameters of the medium such as the magnetic field or space charge density do not change rapidly with wavelength, then the impedance looking in any direction in a region where the field waves have a complex propagation constant is nearly equal to the characteristic impedance of the decaying wave and not, as is essential for amplification, to that of the growing wave. Even with the most generous allowance for the effects of turbulence, it seems incredible that the impedance discontinuity could be so large as to involve a complete reversal of sign. Furthermore this critical impedance would have to be just right for an appreciable time since the steady state in which power amplification is possible has to be built up by a resonant reflection which, in the language of the electronics engineer, has a very high Q. Finally it may be noted that even if the electromagnetic energy could be generated by freak conditions it could not escape, since it would occur at a level where the characteristic impedance of the medium was largely reactive and therefore attenuating.

In a discharge tube definite surfaces of discontinuity exist at cathode and anode, and it is conceivable that at certain frequencies the right conditions might exist for power amplification. Even granting this, however, it seems hardly possible to explain the experimental results of Bailey and Landecker[12] on this theory, because this amplification is too small. Using glass discharge tubes and a longitudinal magnetic field of a few hundred gauss, these workers measured, at low frequencies, noise power outputs corresponding to a blackbody temperature of 10^7 to 10^{13} degrees Kelvin. At low frequencies for which $\Omega_0<\omega_H$ it is only the ordinary waves that are amplified. From Eq. (30) it follows that the maximum power amplification attainable with the ordinary waves is $\exp(2\omega_0 z/c)$ which works out at 20 db/meter when, as in the experiments of Bailey and Landecker the plasma frequency is about 100 Mc/sec. The observed noise power corresponded to a blackbody temperature which at some frequencies was as high as 10^{13} degrees Kelvin. As the electron temperature is only 3×10^4 degrees an amplification of 85 decibels would be needed if the observed phenomena were thus to be explained. The discrepancy is even more serious when the effects of magnetic field are taken into account. At a frequency of 1 Mc/sec the amplification of the ordinary waves with an axial magnetic field of 200 gauss is only 2 db/meter while the observed noise power corresponded to blackbody temperature of 10^{12} degrees Kelvin.

[12] V. A. Bailey and K. Landecker, Nature **166**, 259 (1950).

7. CONCLUSIONS

We have shown that the growing waves which Bailey interpreted as amplified waves can be excited only by reflection. If the medium is ideally terminated in the characteristic impedance of this growing wave, the wave amplitude can be built up to a large amplitude by a process of resonant reflection. But this termination is very critical and it is most unlikely that the required conditions would be found in a sunspot. Even so if amplification did take place the radiation would be generated at a level from which it could not escape. The explanation of the excess noise radiation from sunspots must be sought elsewhere.

Under special circumstances, it is conceivable that amplification of the transverse waves could take place in a discharge tube. However the maximum amplification attainable seems too small to account for the experimental results of Bailey and Landecker,[12] even under the most favorable circumstances.

From relativity considerations, we argued that any amplification in an infinite ionized medium drifting with a monochromatic velocity parallel to a magnetic field must depend entirely on conditions at the transverse surfaces of discontinuity, since these alone provide a frame of reference with respect to which the medium is moving.

The same argument would also apply to a cylindrical beam of finite cross section moving in empty space, or bounded by a perfect conductor, or with any transverse boundary condition the qualitative form of which was unaltered by a longitudinal Lorentz transformation.

A general criterion as to the conditions that a growing wave be a true amplified wave cannot be obtained from a unidimensional analysis. From the transient analysis for this special cases however, it appears that a growing field[13] wave is probably a reflected and not an amplified wave though this is not the case for the traveling wave tube. On the other hand, if the associated energy flow is in the positive direction, a growing space charge wave is almost certainly a true amplified wave, at least as long as all the electrons are moving in the same direction.

Whether or not a given wave is excited by reflection cannot be decided from its direction of propagation and energy flow at a finite frequency. We have shown that only the behavior at arbitrarily large frequencies is relevant.

[13] By a field wave we mean a wave which propagates, if at all, at a speed comparable to c and which exists even when the space charge density is zero. By a space charge wave we mean a wave which propagates at a speed comparable to that of the moving space charge and which vanishes when the space charge density goes to zero.

It has usually been assumed in the past that one can neglect the interaction between an electron beam, moving at a speed small compared with c, and the magnetic components of an electromagnetic wave propagating with a phase velocity near to or greater than c. We have shown that this is not always justified and that in some circumstances such as propagation in an attenuating medium, the interaction with the magnetic components is more important than the interaction with the electric components in some particulars at least.

This analysis has served once again to stress the importance of taking initial and boundary conditions into account in a discussion of propagation in an active medium.

PHYSICAL REVIEW VOLUME 84, NUMBER 3 NOVEMBER 1, 1951

A High Energy Proton-Proton Collision with Associated Events

V. D. Hopper, S. Biswas, and J. F. Darby
Physics Department, University of Melbourne, Melbourne, Australia
(Received July 16, 1951)

An event observed in a nuclear emulsion is interpreted as an incident proton of energy 1000 Bev colliding with a hydrogen nucleus and producing a cone of six charged mesons. The presence of three neutral mesons is deduced from two electron pairs and one triplet in the region of the cone. The triplet is due to an electron pair produced by a gamma-ray of energy 24 Bev in the field of an electron. An additional electron pair is produced by bremsstrahlung. The kinetic energies of several particles are deduced from scattering measurements and these range from 800 Mev to 17 Bev. The total energy of the shower is estimated as 100 Bev. In the center-of-mass system the mesons have energies of the order of 400 Mev and an almost isotropic distribution. It is concluded that most of the energy is carried by two neutrons, and only one-tenth of the energy of the primary particle goes to meson production. The results are compared with the theories of multiple meson production.

I. INTRODUCTION

MOST of the data published on very high energy collisions with nuclei deal with the interaction of protons, neutrons, or heavier nuclei with the light (C, N, O) and heavy (Ag, Br) groups of nuclei present in photographic emulsions, and in these cases as many as thirty minimum ionization tracks have been produced, which have been shown[1] to be mainly mesons. Some of these mesons arise from the interaction of the primary particle with a single nucleon (multiple production), but if the energy of the primary particle is distributed over a part of the nucleus plural production of mesons by interactions between many pairs of nucleons is possible. It is clear that it is of fundamental importance to the theory of meson production to study collisions of protons or neutrons with hydrogen nuclei—events which are likely to be missed in nuclear emulsions as all tracks are at minimum ionization. Very few examples of these collisions have been published. An event described by Camerini *et al.*[2] occurred near the edge of the plate, so no detailed measurements could be made. Pickup and Voyvodic[3] have found four such events, but the energies of only a few particles could be measured because the lengths of tracks in the emulsion were short. A collision of a very energetic singly charged particle with a nucleus heavier than hydrogen has been observed by Lord, Fainberg, and Schein,[4] in which, however, the mesons are most probably produced by a single nucleon-nucleon encounter.

This paper describes an event in which a singly-charged particle with an estimated energy of the order of 1000 Bev collides with a nucleus to produce a shower of seven particles at minimum ionization one of which, however, is an electron. The event was observed in an Ilford G-5 emulsion, 400μ thick, which was exposed to cosmic radiation at 70,000 ft. Since no tracks of ionization above the minimum were observed, it is most likely that the atom struck was hydrogen. The event fortunately occurred near the center of the plate, and the primary particle was traveling almost parallel to the emulsion surface, so very long tracks of most of the secondary particles are visible, allowing detailed study. The region around the event was carefully scanned, and three electron pairs and one triplet associated with the event were found. The triplet is due to production of an electron pair in the field of an electron by a photon of energy about 24 Bev.

II. DESCRIPTION OF THE EVENT

The primary collision consists of a singly-charged particle at minimum ionization producing seven secondary particles, also at minimum ionization, within a cone of half-angle about 11°. One of the secondaries is an electron of energy 60 Mev, and is probably a knock-on

[1] P. H. Fowler, Phil. Mag. 41, 169 (1950).
[2] Camerini, Fowler, Lock, and Muirhead, Phil. Mag. 41, 413 (1950).
[3] E. Pickup and L. Voyvodic, Phys. Rev. 82, 265 (1951).
[4] Lord, Fainberg, and Schein, Phys. Rev. 80, 970 (1950).

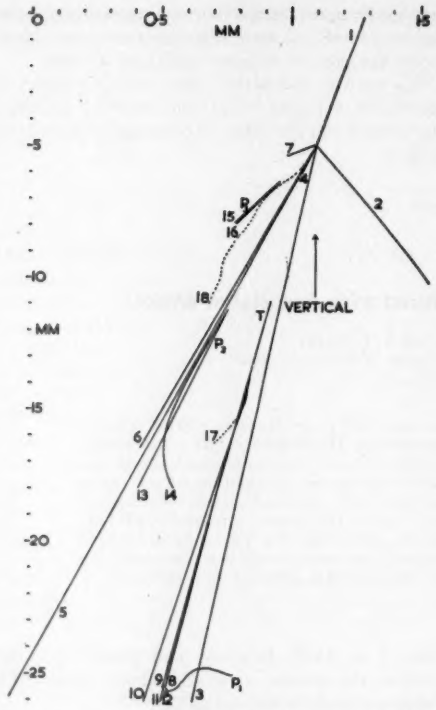

FIG. 1. Diagram of the tracks of the high energy collision including the triplet T_1 and three electron pairs, P_1, P_2, and P_3. The lateral scale is ten times the vertical so as to separate the close tracks. High energy knock-on electron tracks are shown as dotted lines.

electron produced near the point of collision; the others are protons or mesons.

The distribution of the secondary charged particles is shown in Fig. 1, and a mosaic of the primary collision in Fig. 2. Track 1 is the primary which has a length in the emulsion of 8 mm. Tracks 2, 3, and 5 are about 20 mm and track 6 about 10 mm long, so detailed scattering measurements of these could be made.

The energies of the particles were obtained from scattering measurements by the method given by Fowler.[1] For these particles the small angle scattering is of the order of 0.003° per 100μ and to obtain an accurate value of the scattering, cell lengths from 1000 to 4000μ were used; then the "noise-level" is less than the mean deviation of the chord per 100μ, and a correction is made for it in the following way.

Let D_n' represent the measured mean deviation for cell length n, where the unit of cell length is 100μ, and D_n the true deviation due to scattering alone.

Assume $D_n'^2 = D_n^2 + D_0^2$, where D_0 is the noise-level The angular deviation per unit cell length, $\alpha(100)$, is

$$\alpha(100) = D_n/n^{\frac{1}{2}},$$

and

$$D_n'^2 = n^3\alpha^2(100) + D_0^2.$$

A plot of $D_n'^2$ against n^3 should give a straight line of slope $\alpha^2(100)$ and of intercept D_0^2 at $n=0$. The value of $\alpha'(100) = D_n'/n^{\frac{1}{2}}$ tends to the limit $\alpha(100)$ as n is increased. This procedure was followed for the more energetic tracks of length greater than 12 mm. Results for tracks 3 and 5 are given in Table I.

From the value of $\alpha(100)$, the momentum p of a fast particle was obtained from[5]

$$p\beta \simeq 40/\alpha(100) \text{ Mev}/c.$$

and of a slow particle from Fig. 3 of reference 1.

The values of $\alpha(100)$, kinetic energies and other relevant data for all tracks are listed in Table II.

For track 2 the value of $\alpha(100)$ is large and the noise-level unimportant. Track 6 is not long enough to treat in the same way as Nos. 3 and 5, so the mean value of the noise found for them was combined with the measured mean deviation in a cell 2000μ long to give the energy of the particle. For particles 4 and 7 the lengths in the emulsion are too short to allow any scattering measurements to be made. Track 18 has a length of 6.2 mm in the emulsion at minimum grain density which, combined with the large value of $\alpha(100)$, 0.5°, shows that it is an electron.

Associated with the star are one triplet and three electron pairs; their positions and orientations are shown in Fig. 1. A mosaic of the triplet is given in Fig. 3 and a drawing in Fig. 4. The grain density at the start is nearly three times minimum, indicating that the three tracks start at one point. Track 10 separates from the other two after 1300μ and tracks 8 and 9 can be separated after 4000μ.

Track 9 shows a marked difference of mean deviation between the two portions of its length from 4 to 8 mm and from 8 to 13 mm, indicating a large energy loss near 8 mm. The first part (4–8 mm) is too short to give a corrected value of $\alpha(100)$, but the comparison of the measured values of $\alpha'(100)$ for cell length 1000μ for this part of track 9 with that for track 8 indicates that probably both were initially of about the same order of energy, namely, 12 Bev. The second part of track 9 (8–13 mm) has a mean scattering of 0.031° per 100μ, corresponding to an electron energy of about 1 Bev. The angle between tracks 8 and 9 is very small, being of order 0.004°.

At a distance of 13.3 mm from the origin of the triplet there is an electron pair (P_1, tracks 11 and 12, Figs. 3 and 4) between tracks 8 and 9. The pair tracks pass through the edge of the emulsion after 600μ, so their energies cannot be estimated. Track 17, also at minimum ionization, begins 4 mm from the origin of the triplet; scattering measurements give $\alpha(100) = 1.24°$, corresponding to a knock-on electron of energy 24 Mev.

[5] Dilworth, Goldsack, Goldschmidt-Clermont, and Levy, Phil. Mag. 41, 1032 (1950).

An electron pair P_2 (tracks 13 and 14) begins 6.2 mm from the center of the star, the angle between the tracks being 0.43°. Mean scattering angle for track 13 is 0.02° and its energy is 2 Bev, the corresponding figures for the first 3.5 mm of track 14 being 0.093° and 300 Mev. For the remaining 3.5 mm of track 14, $\alpha(100)$ is 0.385° and the energy is 85 Mev, indicating that a large energy loss has occurred at about 3.5 mm from its origin. The electron pair P_3, originating 1.5 mm from the star, consists of tracks 15 and 16 at 0.05° to one another. As the track lengths are short only the lower limits of energy can be given as 1.25 Bev and 800 Mev, respectively.

The grain densities of all the long tracks were measured and it was found that the grain density of a track increased gradually from the surface to a depth of 40μ, after which it reached a constant value. The grain densities of tracks which are more than 40μ below the surface are given in Table II. It may be noted that the grain densities of the electron tracks over a range of energies from 60 Mev to 12 Bev do not show any significant increase with energy, although ionization loss is expected to increase over this energy range.

III. DISCUSSION OF THE TRIPLET AND PAIRS

It has been assumed in the preceding description that the three particles forming the triplet are electrons. From the measurements of scattering and grain density it is not possible to distinguish electrons, mesons and protons at these high energies. However, the fact that there is a knock-on electron (track 17) of energy 24 Mev produced by one of the particles, 8 or 9 indicates that one at least of these is not a proton, as the maximum energy of an electron knocked on by a 12-Bev proton is 6 Mev. Further, if the event were a neutron-proton collision the incident neutron producing the event T_1 must originate from the main star. Thus, it should have only a fraction of the energy of the incident proton (track 1), and consequently, the angular spread of the secondary particles in T_1 should be several times larger than that of the main star. But the observed angular spread of the particles in T_1 is extremely small ($\sim$0.004°) compared with the half-angle of the cone of the main star of 11°.

The result is consistent with the assumption of the production of an electron pair by a gamma-quantum in the field of an electron. This type of event has been observed by Gaerttner and Yeater[6] in a cloud chamber with γ-rays of energies between 5 and 100 Mev. They found a triplet-pair ratio of 1 to 12 and a maximum energy for the recoil of 3 Mev. The γ-ray energy required to produce the triplet which we observe is of the order of 24 Bev and a recoil electron energy of 400 Mev (track 10) is reasonable.

The average angle ϕ between a pair electron and the γ-ray is approximately given by[7]

$$\phi = m_0c^2/E,$$

FIG. 2. Mosaic showing the primary particle and the charged secondary particles resulting from the nucleon-nucleon collision.

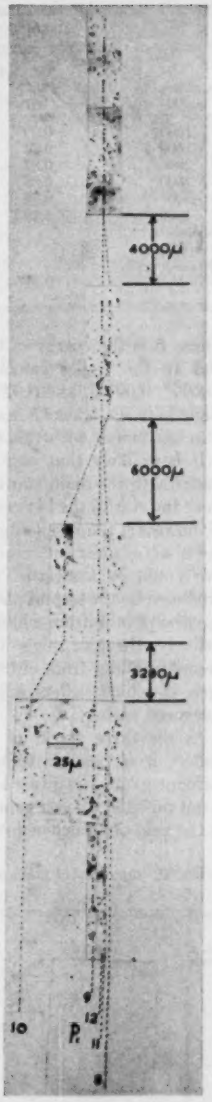

FIG. 3. Mosaic showing sections of the three electron tracks 8, 9, and 10 forming the triplet produced by the photon of energy 24 Bev. The beginning of the electron pair P_1 (tracks 11 and 12) is shown between tracks 8 and 9.

[6] E. R. Gaerttner and M. L. Yeater, Phys. Rev. 78, 621 (1950).

[7] B. Rossi and K. Greisen, Revs. Modern Phys. 13, 258 (1941).

TABLE I. Scattering measurements for two long tracks using various cell lengths.

Cell lengths (μ)	Track 3 D_s' (μ)	Track 3 $\alpha'(100\mu)$ (degrees)	Track 5 D_s' (μ)	Track 5 $\alpha'(100\mu)$ (degrees)
1000	0.49	0.0084	0.51	0.0092
1600	0.74	0.0066	0.64	0.0058
2000	0.87	0.0056	0.78	0.0050
2600	0.88	0.0038	0.88	0.0038
3000	0.94	0.0032	0.93	0.0022
4000	1.19	0.0027	1.31	0.0030
Corrected $\alpha(100\mu)$ "Noise-level"		0.0022		0.0025
D_0	0.71		0.63	

where E is the energy of the electron. For tracks 8, 9, and 10 the angles calculated from this relation are 0.0017°, 0.0017°, and 0.07°, respectively. The observed angle between tracks 8 and 9 is less than 0.004° which is in agreement with this result.

It is unlikely that pair P_1 (Fig. 1) is directly associated with the main star as the perpendicular distance from the star to the bisector of the pair of tracks is 40μ. If, however, the recoil track is in such a direction that the bisector does not coincide with the γ-ray then this pair could be associated with the main star, and be produced by the second photon from the neutral meson, the first photon from which produced the triplet. Alternatively, the pair might be produced by a photon of bremsstrahlung from either of the electrons 9 or 10, each of which suffers a large energy loss along its measured path.

As the three tracks of the triplet are highly collimated, it is possible to obtain the direction of the incident gamma-ray to a high degree of accuracy. This is not possible when a gamma-ray produces an electron in the field of a nucleus owing to the uncertainty in the direction of recoil of the nucleus. In the present case the direction of the γ-ray passes within 1μ of the star and it has an energy of 24 Bev. Comparing the values of the energies of the charged mesons and their angular distribution (see Fig. 5), it seems unlikely that the neutral meson N_1, producing this γ-ray had an energy much higher than 30 Bev. If we assume that the neutral meson had this energy and gave rise to one photon of 24 Bev and a second photon of 6 Bev, then the rest lifetime T_0 of the neutral meson is less than 10^{-14} sec. This estimated limit T_0 does not vary greatly with the energy assumed for the second photon. For example, for a neutral meson of energy 50 Bev the value of T_0 is less than 3.6×10^{-15} sec. From a study of pair production, Carlson, Hooper, and King[8] obtained a value of T_0 less than 5×10^{-14} sec and Lord, Fainberg, and Schein,[4] from a single pair, a value less than 2×10^{-15} sec.

The ratio of the energies of the electrons in pair P_2 is 6:1 and a line drawn dividing the angle subtended by the electrons in the ratio 1:6 passes within 5μ of the star center. For pair P_3 where the angle between the electrons is only 0.05° the bisector of this angle passes within 0.25μ of the center of the star. It is clear that both these pairs are associated with this event. The energy of the γ-ray producing the pair P_2 is 2.3 Bev and that producing P_3 is greater than 2 Bev. From Fig. 5, assuming that the direction of the neutral meson is approximately coincident with the γ-ray, the energies of the neutral mesons, N_2 and N_3, producing pairs P_2 and P_3 are estimated to be 18 Bev and 3.0 Bev, respectively.

IV. DISCUSSION OF THE HIGH ENERGY STAR

The energies of four of the secondary particles 2, 6, 5, and 3 are plotted in Fig. 5 against the angles between the directions of the secondary and primary particles.

TABLE II. Summary of grain densities, mean scattering angles, directions, and energies of all tracks. Estimated energies of neutral mesons are also given.

No. of track	Length (mm)	Grain density /50μ	$\alpha(100)$ degrees	Assumed nature of particle	Kinetic energy (Bev)	Angle with primary in l-system	Kinetic energy of neutral mesons (Bev)
1	8	min		proton	1000		
2	20	min	0.045	meson	0.80	6.80°	
3	20	min	0.0022	meson	17	0.88°	
4	1	min		meson	(~4)	2.9°	
5	20	min	0.0025	meson	15	1.0°	
6	11	12.24±0.20	0.0062	meson	6	2.1°	
7	0.45	min		meson	(~0.2)	11.5°	
T_1 8	14	12.65±0.20	0.0029	electron	12		
T_1 9	14	12.16±0.20	<0.008	electron	~12	0.51°	(30)
T_1 10	14	12.65±0.20	0.076	electron	0.40		
P_1 11	0.6	min		electron			
P_1 12	0.6	min		electron			
P_2 13	6.8	12.84±0.30	0.02	electron	2.0	0.94°	(18)
P_2 14	13.0	12.23±0.20	0.093	electron	0.3		
P_3 15	1.4	min	<0.026	electron	>1.25	3.42°	(3)
P_3 16	1.4	min	<0.041	electron	>0.80		
17	1.4	min	1.24	electron	0.024		
18	6.2	12.70±0.4	0.496	electron	0.060	3.0°	

[8] Carlson, Hooper, and King, Phil. Mag. 41, 701 (1950).

Assuming that a smooth curve connects energy and angle, the energies for particles 4 and 7 are estimated (see Table II). The energies and angles of the two pairs P_2 and P_3 and triplet T_1 are also shown on the figure. The energies given in Table II for the neutral mesons producing them are estimated from the curve, assuming the same distribution in energy with angle for neutral mesons as for charged mesons.

Camerini *et al.*,[2] and Pickup and Voyvodic[3] found similar events some of which contained odd numbers of shower particles, and the latter authors suggested that to conserve charge a collision with a heavy nucleus must be assumed. In the present event, although it first appeared that there were seven charged shower particles, one of these was later identified as an electron of much lower energy than any of the others. This is most probably a knock-on electron. The event can, therefore, be explained as a proton-proton collision producing six charged and three or more neutral mesons and this satisfies the conservation of charge. If a heavy nucleus were involved one would expect some evaporation particles of low energy to be emitted.

If it is assumed that the six charged and three neutral particles represent all the mesons produced in the event, then the energy of the meson shower is about 100 Bev. For these nine particles the value of β and the resolved component $\beta_z=\beta\cos\theta$ in the direction of the incident particle are tabulated in Table III.

If we convert the velocities of the particles from the laboratory system (l-system) to a system where the center of mass of these particles is at rest (c-system), the resultant momentum will be zero. The momentum p_z' of a particle in the c-system is given by

$$cp_z'=B_c w(\beta_z-\beta_c),$$

where $c\beta_c$ is the velocity of the c-system, $B_c=1/(1-\beta_c^2)^{\frac{1}{2}}$, and w is the total energy of the particle in the l-system. Since $\Sigma p_z'$ for all particles is zero in the c-system, then

$$\beta_c=\Sigma w\beta_z/\Sigma w.$$

The energy w' and angle θ' of a particle in the c-system are calculated from the relations:

$$w'=B_c w(1-\beta_c\beta_z),$$
$$\tan\theta'=\tan\theta\beta_z/B_c(\beta_z-\beta_c)$$

and are given in Table III.

In this system the particles have about the same order of energy and the sum of the energies is 4.04 Bev. The particles are not confined to a forward and backward cone.

If the process is assumed to be a proton-proton collision, where the velocity of the incident proton before collision in the c-system is $c\beta_c$, the total energy W' of the two protons in the c-system is

$$W'=2M_0c^2B_c=44.2 \text{ Bev},$$

where M_0 is the rest mass of a proton.

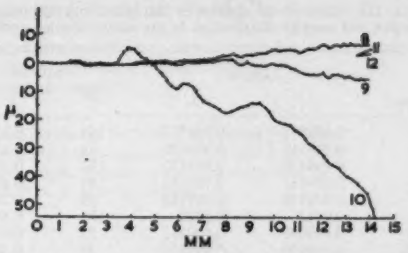

FIG. 4. Enlarged drawing of the electron tracks forming the triplet showing multiple scattering and the position of the electron pair.

Thus only one-tenth of the available energy is taken by the meson shower. In this case the excess must be ascribed to additional neutral particles. If we assume two neutrons are produced, each of these must have energies of 20 Bev in the c-system and about equal and opposite momenta.

In the l-system the energy of the primary proton is given by the relation

$$W=M_0c^2B\simeq 2M_0c^2B_c^2$$

which gives $W=1000$ Bev. The total energy of the neutrons is of the order of 900 Bev and the sum of the energies of the observed particles is 100 Bev. If this

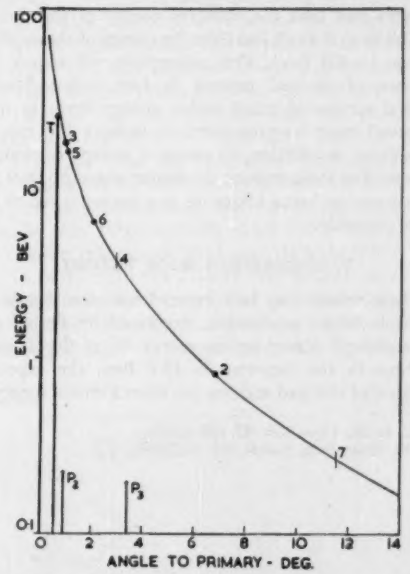

FIG. 5. Energies of four secondary particles, 3, 5, 6, and 2 plotted against their angles relative to the primary particle direction in the laboratory system. Energies of photons producing triplet T_1 and pairs P_2 and P_3 are represented on the diagram at their corresponding angles. Estimated values for tracks 4 and 7 are indicated.

TABLE III. Velocities of mesons in the laboratory system, and energies and angular distribution in the center-of-mass system.

Meson	l-system β	l-system β_x	c-system Angle θ'	c-system Energy (Bev) ϵ'
2	0.988895	0.981973	164	0.42
3	0.999967	0.999839	42	0.43
4	0.999429	0.998130	114	0.27
5	0.999957	0.999757	49	0.41
6	0.999740	0.999140	88	0.25
7	0.9112	0.8929	176	0.86
N_1	0.999989	0.999952	23	0.67
N_2	0.999970	0.999825	39	0.46
N_3	0.999007	0.99721	127	0.27

excess energy of 900 Bev is carried instead by two unobserved neutral mesons, these will have a total energy of 40 Bev in the c-system which is ten times as great as the sum of the energies of the other nine mesons, which is unlikely.

Another alternative that might be considered is that two of the charged particles in the shower are protons. The grain densities of protons having kinetic energies less than 1 Bev are significantly above the minimum value and so track 2 cannot be a proton. Track 7, which is at minimum ionization, would correspond to a proton of total energy >1.94 Bev, a value much higher than was estimated from Fig. 5. If, however, we assume that track 7 is due to a proton of energy 1.94 Bev and that one of the other fast tracks is also due to a proton, we still find that the observed energy of the shower ($\sim$100 Bev) is much less than the energy of the incident proton ($\sim$400 Bev). This assumption will reduce the number of charged mesons to four and additional neutral mesons of much higher energy than the ones observed must be postulated to balance the energy. This gives, in addition, an excess of neutral to charged mesons. For these reasons the former assumption of the excess energy being taken by two neutrons seems the more plausible.

V. COMPARISON WITH THEORY

These results may be compared with the theories of multiple meson production, developed by Fermi[9] and Heisenberg.[10] Assuming the energy W' of the incident protons in the c-system is 44.2 Bev, the expected number of charged mesons (n) from Fermi's theory is given by the following relation for the intermediate range of energy.

$$n=1.34(\epsilon'-2)^{\frac{1}{4}}/\epsilon'$$

where $\epsilon'=W'/M_0c^2$ and M_0 is the mass of the proton. This gives the number of charged mesons produced as 8 or 9. Alternatively, if the formula for the extremely high energy case

$$n=1.2(W/M_0c^2)^{\frac{1}{4}}$$

is considered where W is the energy of the incident proton in the l-system we get a value of n of 7. Our observed number is 6.

On the Heisenberg theory the average number N of charged and uncharged mesons produced is given by

$$N=W'/m_0c^2\ln(W'/m_0c^2),$$

where m_0c^2 is the meson rest mass. This gives a value of n of 55 against an observed number of approximately 9.

Both of these results have been obtained on the assumption that practically all the energy in the c-system goes to the meson production. In the present event only one-tenth of the energy has been used in this way. Assuming $W'=4$ Bev, Fermi's formula for the intermediate energy ranges gives $n=1$ and the Heisenberg formula $N=8.5$.

In the theory of meson production by Fujimoto *et al.*,[11] it has been assumed that a fraction of the incident energy may go to meson production and the angular distribution should be isotropic in the c-system. Also Freir and Ney[12] observed a collision of a carbon nucleus with a proton and estimated that one-third of the energy of one of the protons of the carbon nucleus went to meson production. In the present event it is concluded that one-tenth of the energy of the primary proton is used in meson production and the mesons are isotropically distributed in the c-system.

The authors wish to thank Professor L. H. Martin for his support and encouragement. The cooperation of the Commonwealth Meteorological Service in exposing the plates at high altitudes is gratefully acknowledged. We wish to thank Mr. H. N. Brann for his help in this matter. One of the authors (S.B.) is indebted to the Commonwealth Government of Australia for a UNESCO Fellowship.

[9] E. Fermi, Phys. Rev. **82**, 683 (1951).
[10] W. Heisenberg, Nature **164**, 65 (1949).
[11] Fujimoto, Fukuda, Hayakawa, and Yamaguchi, Prog. Theor. Phys. **5**, 669 (1950).
[12] P. Freir and E. P. Ney, Phys. Rev. **77**, 337 (1950).

Excitation Functions for Deuterons and Protons on Mg*

F. O. Bartell and Sheldon Softky
Radiation Laboratory, Department of Physics, University of California, Berkeley, California
(Received July 23, 1951)

Yields of F^{18}, Na^{22}, and Na^{24} have been measured as a function of energy for both deuterons and protons on Mg. In some cases the yield of a single isotope can be attributed to a single nuclear reaction over a certain energy interval, this being done by a consideration of thresholds. These excitation curves are given over the ranges 0 to 20 Mev and 0 to 190 Mev for deuterons and from 0 to 31 Mev for protons.

INTRODUCTION

PREVIOUS work[1] with the 190-Mev deuterons from the 184-inch Berkeley cyclotron has pointed to interesting nuclear reactions which might be investigated with both this machine and the 60-inch Crocker cyclotron, and the Berkeley proton linear accelerator. It has been noticed in particular that at high energy, nuclear reactions which result in a product nucleus of much lower atomic number tend to go more probably by boiling off two or more α-particles plus additional neutrons from the excited nucleus than by evaporation of charged particles of lower binding energy. This process fitted into the picture of the incident high energy particle exciting the target nucleus by inelastic collision,[2] the excited nucleus then decaying by boiling off fragments ranging in size from individual nucleons to "fission fragments."[2] In this picture the nucleus which plays the role of the compound nucleus is simply the target nucleus itself with a large amount of excitation energy. Since several reactions had been found at high energy in which the excitation seemed to be carried away preferentially by two or more α-particles,[1] it was interesting to ask if there were any reactions going by the usual mechanism of formation of a compound nucleus, in which it could be shown that the excitation was lost by boiling off more than one α-particle. At the threshold for such a reaction, when defined to include the height of the coulomb barrier of the compound nucleus to the α's inside it, there is ample energy for neutron evaporation to compete with the process in question, and so one might conclude that if the boiling off of α's does occur, it must compete with neutron evaporation; otherwise the excitation would first be lost by neutron evaporation while the energy is being distributed among the nucleons in the compound nucleus.

Table I. Reaction thresholds.

Reaction	Threshold (from masses) (Mev)	Threshold + barrier (Mev)
$Mg^{24}(p,\alpha He^3)F^{18}$	25.0	31.4
$Mg^{24}(n,\alpha H^2)F^{18}$	24.2	29.0
$Mg^{24}(d,2\alpha)F^{18}$	6.6	12.9
$Mg^{25}(p,2\alpha)F^{18}$	11.5	17.7
$Mg^{25}(n,\alpha H^2n)F^{18}$	31.3	35.4
$Mg^{25}(d,2\alpha n)F^{18}$	13.7	19.0
$Mg^{26}(p,2\alpha n)F^{18}$	23.6	28.9
$Mg^{26}(n,\alpha H^2 2n)F^{18}$	43.4	46.9
$Mg^{26}(d,2\alpha 2n)F^{18}$	25.8	30.4
$Mg^{24}(p,He^3)Na^{22}$	15.3	20.4
$Mg^{24}(d,\alpha)Na^{22}$	−3.1	+1.9
$Mg^{25}(p,\alpha)Na^{22}$	1.7	6.7
$Mg^{25}(d,\alpha n)Na^{22}$	3.9	8.0
$Mg^{25}(p,\alpha n)Na^{22}$	13.8	17.9
$Mg^{26}(d,\alpha 2n)Na^{22}$	11.4	14.9

The reaction studied first was $Mg^{24}(d,2\alpha)F^{18}$, whose energetic threshold (threshold not including coulomb barrier height) is 6.6 Mev. With the 20-Mev deuterons from the 60-inch cyclotron, one could be reasonably sure of getting a yield of F^{18} even for cross sections as low as 10^{-29} cm^2 because of the high beam strengths available. This excitation curve was also investigated with the 190-Mev deuterons from the 184-inch cyclotron, and in the course of this work the excitation curves for $Mg^{24}(d,2p)Na^{24}$ and $Mg^{24}(d,\alpha)Na^{22}$ plus $Mg^{25}(d,\alpha n)Na^{22}$ plus $Mg^{26}(d,\alpha 2n)Na^{22}$ were also found from theshold to 190 Mev, since Na^{24} and Na^{22} activities occurred as a background that had to be subtracted from the total target activity to get the F^{18} activity.

The other reaction of this type that was studied was $Mg^{25}(p,2\alpha)F^{18}$ with the 32-Mev proton beam from the Berkeley linear accelerator. The excitation curve for $Mg^{25}(p,\alpha)Na^{22}$ was also obtained below 18 Mev in this same work, and a composite yield of this and

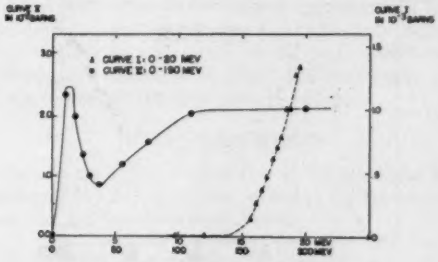

FIG. 1. Deuteron excitation of F^{18} from Mg^{24}.

* This work was performed under the auspices of the Atomic Energy Commission.

[1] Bartell, Helmholz, Softky, and Stewart, Phys. Rev. **80**, 1006 (1950).

[2] R. Seber, Phys. Rev. **72**, 1114 (1947).

[3] R. Batzel and G. T. Seaborg, Phys. Rev. **79**, 528 (1950).

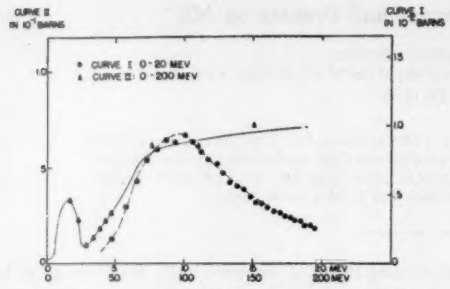

FIG. 2. Deuteron excitation of Na^{22} from Mg^{24}, Mg^{25}, Mg^{26}.

$Mg^{24}(p,He^3)Na^{22}$ and $Mg^{26}(p,\alpha n)Na^{22}$ from 18 Mev to 31 Mev. We notice that we have here a set of four nuclear reactions which represent the formation and decay of the same compound nucleus, Al^{26}, formed by $Mg^{24}+d$ and $Mg^{25}+p$.

METHOD

The excitation curves were measured by the usual method of bombarding stacks of foils and measuring the induced activities in the foils as a function of time in order to identify the radioactive products by their half-lives. The absorber thickness that the incident particles passed through in order to reach a given foil in the stack is then an indication of the particle energy for that foil as found from a range-energy curve. The activity observed, F^{18}, is a 110-min β^+ emitter of about 0.7-Mev maximum energy and with no γ. After a target of Mg or Al had been bombarded by deuterons or protons of sufficient energy and allowed to cool for about an hour, the only activities easily measurable with the thin mica window Geiger counter used were F^{18}, Na^{24}, the well-known β^- emitter of 15-hour half-life, and Na^{22}, a β^+ emitter of about 3-year half-life. These very different half-lives were ideal to measure in the automatic sample-changing and recording counter which is available for this work, and since no chemistry was necessary, many foils could be run at once for greater accuracy in the curves. The 24-sample automatic counter, constructed at this laboratory by H. Robinson and A. Hartzell of the chemistry electronics group, has performed without breakdown for many weeks of operating time, and made it possible to get at least four points per half-life on the composite decay curves, so that resolution of the activities was easy and positive.

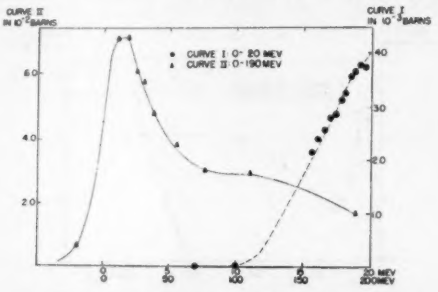

FIG. 3. Deuteron excitation of Na^{24} from Mg^{24}.

The bombardments on the 60-inch cyclotron were carried out with a beam of 20-Mev deuterons collimated to $\frac{1}{8}$ in. by $\frac{1}{2}$ in. and and the energy was measured by an absorber foil wheel and Faraday cup described by E. L. Kelly.[4] Two types of target were bombarded: a stack of 22 Mg metal foils each 9 mg/cm² thick, and a stack of "foils" prepared by pressing the oxide of separated Mg^{24} isotope into 0.015-in. thick beryllium masks. These powder "foils" turned out to be exceptionally uniform in thickness and were about 40 mg/cm² thick. Stacks of each type were bombarded and current-monitored after measuring the beam energy; then the targets were put on the sample-changing counter and their activity was followed down to the long-lived Na^{22}. The possible contaminants in the Mg targets which could also give F^{18} as a product from deuterons of this energy are O^{17}, F^{19}, and Na^{22}. Since the abundance of O^{17} is only 0.039 percent and the Mg metal foil targets gave the same yield of F^{18} as the MgO targets which were 50 percent O, it seems safe to discount $O^{17}(d,n)F^{18}$ as causing the activity. A very sensitive spot test for F in the Mg showed less than 1 part F in 5000, and for $F^{19}(d,dn)F^{18}$ to account for the activity its cross section would have to be the geometrical cross section of F^{19}, 0.5×10^{-24} cm², and it would have to be present in greater than ten times this amount. Finally, spectrographic analysis of the Mg showed less than 0.01 percent Na, so this eliminates $Na^{23}(d,d\alpha n)F^{18}$.

The bombardments on the 184-inch cyclotron also were on both types of Mg target and took place in the internal electrostatically deflected beam of 190-Mev deuterons. It was not possible to measure the incident energy of these deuterons, and so 190 Mev is the figure used as the most probable energy. In these bombardments Cu absorbers of accurately known thickness were inserted between the target foils in order to degrade the beam energy, the beam was collimated by a $\frac{3}{4}$-in. diameter hole in a $1\frac{1}{2}$-in. thick Cu block, and current to the target stack was maximized by adjusting the position of the entire target assembly in the deflected beam. Al metal foils, 0.002 in. thick, were placed coincident with the Mg foils and the excitation curves from Mg monitored by comparing them with the known excitation curve for $Al^{27}(d,\alpha p)Na^{24}$ as measured by Hubbard[5] and by Meinke.[6] The excitation curve for $Al^{27}(d,d2\alpha n)$-F^{18} was incidentally measured, since the F^{18} activity also showed up quite strongly in these Al monitor foils. The entire apparatus used in these 184-inch cyclotron runs is described in great detail by Meinke.[6]

The bombardments on the linear accelerator were

[4] E. L. Kelly and E. Segrè, Phys. Rev. **75**, 999 (1949).
[5] H. Hubbard, Phys. Rev. **75**, 1470 (1949).
[6] W. W. Meinke, Ph.D. thesis, University of California.

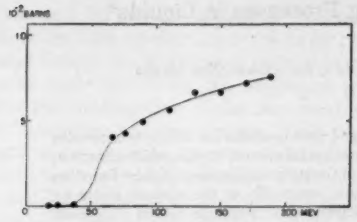

FIG. 4. Deuteron excitation of F^{18} from Al^{27}.

simply on a stack of 24-Mg metal foils, each about 36 mg/cm² thick. The 32-Mev proton beam was monitored by the standard beam monitor which measures current to the stack.

RESULTS

Deuterons

Figure 1 shows the excitation function $Mg^{24}(d,2\alpha)F^{18}$ from 0–20 Mev and from 0–190 Mev. The ordinates for Curves I and II are different. Comparison of the yields from the targets of separated $Mg^{24}O$ and from the metal foils showed conclusively that the reaction is indeed due to Mg^{24}, and the much thinner foils of the metal gave higher energy definition than could ever be obtained with powder pellets. The observed threshold corresponds to that calculated from nuclear masses plus the height of the coulomb barrier of the compound nucleus to the two α-particles inside it. Reference to Table I shows that below 19 Mev $(d,2\alpha)$ is the only energetically possible way to make F^{18} from any of the Mg isotopes. This is therefore a nuclear reaction in which it has been proved that the entire deuteron enters the nucleus, as contrasted to one of the stripping processes such as (d,p), because none of the reactions making F^{18} by neutrons or protons on Mg^{24} are energetically possible in this region. Undoubtedly the curve for the F^{18} yield from Mg^{24} at high energy represents several other reactions as well, such as $(p,\alpha He^3)$, $(n,\alpha H^3)$, $(d,2d\alpha)$, etc. In fact, one might attribute the second rise in the curve to the setting-in of the aforementioned inelastic processes at high energy after the usual compound nucleus process has become less probable.

The composite yield curve for $Mg^{24}(d,\alpha)Na^{22}$, $Mg^{25}(d,\alpha n)Na^{22}$, and $Mg^{26}(d,\alpha 2n)Na^{22}$ is given in Fig. 2 for both 0–20 Mev and 0–190 Mev and those for Na^{24} from Mg^{24}, which might be either $Mg^{24}(d,2p)Na^{24}$ or $Mg^{24}(n,p)Na^{24}$, and for $Al^{27}(d,d2\alpha n)F^{18}$ are given in Figs. 3 and 4. As before, the ordinates for Curves I and II are different.

The deuterons giving Curve II of these excitation functions have a distribution in energy between 190 Mev and 196 Mev when they enter the absorber stack. The 22 g/cm² of Cu absorber broadens this distribution so that deuterons which passed through the stack are

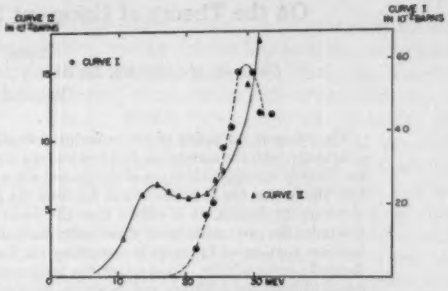

FIG. 5. Curve I: Excitation of F^{18} from Mg^{25} by protons. Curve II: Excitation of Na^{22} from Mg^{24}, Mg^{25}, and Mg^{26} by protons.

distributed between 0 Mev and about 30 Mev, hence the abscissa is badly distorted at energies below 50 Mev and some curves show a yield apparently below zero energy. Neutrons also cause a yield apparently below zero energy.

Protons

Figure 5, Curve I, shows the excitation function $Mg^{25}(p,2\alpha)F^{18}$ from 0–31 Mev. Reference to Table I will show that this is the only energetically possible reaction to produce F^{18} from any of the Mg isotopes below 29 Mev. In this case, the protons available were of high enough energy so that some of the back side of the characteristic compound nucleus peak was obtained. Figure 5, Curve II, shows the yield of Na^{22} from the natural isotopic mixture of Mg, which is 78.6 percent Mg^{24}, 10.1 percent Mg^{25}, and 11.3 percent Mg^{26}. The part of the curve below 18 Mev must represent only $Mg^{25}(p,\alpha)Na^{22}$, as reference to Table I will show.

CONCLUSIONS

Although the absolute yields are probably not accurate to better than a factor of two due to self-absorption and scattering of the low-energy β-particles counted, it appears that the peak yield of $(d,2\alpha)$ is about 0.020 barn and of $(p,2\alpha)$ about 0.060 barn. We can compare these with a $Na^{23}(d,p)Na^{24}$ peak of about 0.400 barn[7] and with an $Al^{27}(d,\alpha p)Na^{24}$ peak of greater than 0.050 barn[5,6] to get an idea of how these reactions compare with other known ones on nearby nuclei; and while it is obvious that $(d,2\alpha)$ and $(p,2\alpha)$ do not compete very successfully with reactions like (d,p), their cross sections are comparable to $(d,\alpha p)$ and their peaks are at approximately the same particle energy.

ACKNOWLEDGMENTS

Thanks are due to Professor A. C. Helmholz for his continued advice and assistance, and to the accelerator crews for making the bombardments.

[7] D. C. Peaslee, Phys. Rev. 74, 1001 (1948).

On the Theory of Coherent Scattering Processes in Liquids*

LOUIS GOLDSTEIN
University of California, Los Alamos Scientific Laboratory, Los Alamos, New Mexico
(Received May 29, 1951)

The coherent scattering structure factor of liquids for x-rays and slow neutrons are shown to determine completely both the correlation function and the direct local interaction function of liquids, which quantities are the only operating elements of the general static liquid model of Ornstein and Zernike. Of these functions only the former has been derived so far from the data accumulated essentially on the coherent scattering of x-rays by liquids. It is shown that the directly available experimental structure factors completely determine the even moments of these molecular distribution functions. The zeroth moment of the correlation function augmented by unity is essentially the liquid concentration fluctuation which determines its isothermal compressibility. These quantities become thus directly derivable from the structure factor measurements without any arbitrary and uncertain manipulations. In terms of the model, a straightforward method leads, with the empirically obtainable total cross section, to the total incoherent slow neutron scattering cross sections in liquids. These should yield information on their energy spectrum not available through other types of scattering processes, such as x-rays, for instance.

I. INTRODUCTION

THE knowledge of the distribution of the atoms or molecules, around one chosen arbitrarily, in a liquid in statistical equilibrium enables one to evaluate rigorously the intensity of coherently scattered waves of any type by this liquid. According to statistical mechanics, the knowledge of the intermolecular forces leads formally to the spatial distribution function of the liquid molecules which determines completely its coherent scattering properties. In practice such a procedure founded on first principles has not as yet led to definite results of a general character because of its analytical complexity.[1] In view of this complexity it was natural that a number of attempts should have been made in order to derive semi-empirical liquid models.[2] Among these the one suggested by Ornstein and Zernike[3] in connection with a possible solution of the critical opalescence problem of visible radiation appears to be quite general. As a matter of fact, one of the two operating elements of this liquid model, the two-atom or two-molecule spatial distribution function was shown to be directly accessible to experiment through the coherent scattering structure factor of x-rays and recently also of slow neutrons.[4] Since the derivation of this result, practically all work on the coherent scattering of x-rays by liquids culminated in the empirical determination of the local molecular or radial distribution function.[5] The Ornstein-Zernike (O.Z.) liquid model is founded on the assumed existence of a direct intermolecular interaction function whose range would be expected to be of the same order of magnitude as that of the elementary intermolecular forces. This direct interaction function determines, in turn, an indirect interaction function which enters into the definition of the two-atom or two-molecule radial distribution function. The latter expresses the probability of finding a molecule in a volume element whose center is at some specified distance from a molecule chosen arbitrarily. As far as we are aware, the fundamental relation of the O.Z. liquid model which is actually the definition of the indirect interaction function in terms of the direct interaction function has been left partially out of account in x-ray work. It is one of the main points of this work to redirect attention to the possibility of a complete verification of the O.Z. liquid model through a fuller exploitation of the experimental data already accumulated on the coherent intensity structure factor of a number of monatomic or molecular liquids. The interest in the O.Z. static liquid model has been further widened recently through a study of the analogies existing between the molecular distributions of this model and that of ideal Bose-Einstein fluids undergoing condensation in momentum space, whose complete and rigorous formalism is based on first principles.[6] Also the possibility of using slow neutrons in the investigation of the coherent scattering by liquids in the critical region may lead to a further verification of the O.Z. theory in this region.[6,7] Furthermore, the basis of the model has been broadened somewhat through a new derivation of its central relation.[8]

The general coherent scattering properties of this model will of course be valid both for x-rays and slow

* The abstract of this paper has appeared in Phys. Rev. **83**, 225(A) (1951).

[1] J. E. Mayer and M. G. Mayer, *Statistical Mechanics* (John Wiley and Sons, Inc., New York, 1941), where the theory of the equation of state of vapors illustrates the difficulties alluded to.

[2] J. Frenkel, *Theory of Liquids* (Oxford University Press, London, 1947).

[3] L. S. Ornstein and F. Zernike, Amsterdam Proc. **17**, 793 (1914); F. Zernike, Amsterdam Proc. **19**, 1520 (1916); L. S. Ornstein and F. Zernike, Physik. Z. **19**, 134 (1918) and **26**, 761 (1926).

[4] F. Zernike and J. A. Prins, Z. Physik **41**, 184 (1927).

[5] N. S. Gingrich, Revs. Modern Phys. **15**, 90 (1943); A. H. Compton and S. K. Allison, *X-Rays in Theory and Experiment* (D. Van Nostrand Company, Inc., New York, 1935); R. W. James, *Diffraction of X-rays* (Bell and Sons, London, 1948). For the neutron experiments see O. Chamberlain, Phys. Rev. **77**, 305 (1950).

[6] L. Goldstein, Phys. Rev. **83**, 289 (1951).

[7] L. Goldstein, Phys. Rev. **81**, 326(A) (1951).

[8] M. J. Klein and L. Tisza, Phys. Rev. **76**, 1861 (1949).

neutrons and for visible radiation, in transparent liquids, in the limit appropriate to the latter case.

A second major point, although quite qualitative, of this work turns out to be the recognition that the experimental investigation of the slow neutron incoherent scattering processes might yield important information on the energy spectrum of liquids. While their coherent scattering phenomena is determined by the spatial distribution of the liquid molecules, whereby an averaging over all the possible states of liquid motion is automatically performed, the slow neutron incoherent processes associated with both energy and momentum exchange of the neutrons with the liquid as a whole appear to provide a unique set of information on the motions of the liquid as a whole in a relatively wide energy interval. This type of information is not available through x-rays.

It seems of interest to outline first the main features of the O.Z. static liquid model. We should like, in doing so, to go somewhat beyond the original presentation.[1] This will be attempted in the next section. The subsequent sections will then be devoted to the study of the general coherent scattering properties of this liquid model and to a qualitative discussion of the possible importance of the slow neutron incoherent scattering phenomena for obtaining information on the energy spectrum of a liquid as a whole.

II. THE LIQUID MODEL[1]

Let the probability of finding a liquid molecule in a volume element $dv(r)$ whose center is at a distance r from the center of a molecule situated at the origin be given by

$$P(r)dv=[1+Q(r)]dv/V, \tag{1}$$

where $P(r)$ is the probability density and V stands for the total volume of the liquid. The mean number of molecules in $dv(r)$ is

$$dn(r)=(N/V)dv+(N/V)Q(r)dv. \tag{2}$$

where N is the total number of molecules in V. The accidental deviation of the concentration from its mean is thus,

$$dn(r)/dv-N/V=\delta(r)=(N/V)Q(r). \tag{3}$$

In order to derive the average deviation from the mean concentration at a point, chosen arbitrarily within the liquid to be the origin of the coordinate system, it will be assumed that this deviation is a linear superposition of the deviations in all neighboring volume elements. Adopting a continuum representation, one has thus

$$\delta(0)=\int_V \delta(r)f(r)dv(r)=(N/V)\int_V Q(r)f(r)dv. \tag{4}$$

The direct influence function $f(r)$, depending only on the length of the radius vector $\mathbf{r}$, is determined by the intermolecular forces and its range should be about the range of these forces. Hence, the integration in (4) may be extended over the volume V or even the whole space.

Assuming throughout central forces, the function $Q(r)$ appearing in the two-particle probability density $P(r)$, Eq. (1), should depend only on the length $|\mathbf{r}|$. Furthermore, the presence of a molecule at the origin cannot very much affect the probability to find another one at a great distance from it. Hence, the function $Q(r)$ should tend to vanish for large values of its argument or the mean concentration should prevail at large distances from a molecule chosen arbitrarily within the liquid. Surface effects will be omitted throughout this paper. On the other hand, the strongly repulsive character of the intermolecular forces at small separations will prevent two molecules from approaching each other, so that the probability (1) should tend to vanish at small distances.

Consider the problem of finding the mean deviation from the average concentration at some point $\mathbf{r}$, as caused by the indirect action of a given deviation at some other point, which may be chosen to be the origin of the coordinate system. This indirect action may be seen to come about through the local or short range interactions between the molecules situated in the space surrounding the one at the origin and the other at the point $\mathbf{r}$. Through these interactions any deviation from the average concentration $\delta(0)$, at the origin, will affect the deviation $\delta(r)$ at the point $\mathbf{r}$, no matter how large r is. This indirect action is already expressed by the function $Q(r)$ defined by Eq. (3). It may be redefined more completely in the following way, as shown by Ornstein and Zernike.[3] Let

$$\delta(r, 0)=g[r, \delta(0)dv(0)]; \quad r>0, \tag{5}$$

express the assumption that the deviation at $\mathbf{r}$ is some function of r and $\delta(0)$. This is equivalent to the following more general relation

$$\delta(r, r')=g[|\mathbf{r}-\mathbf{r}'|, \delta(r')dv(r')], \quad r\neq r', \tag{5a}$$

and, hence,

$$\delta(0, r')=g[r', \delta(r')dv(r')], \quad r'>0. \tag{5b}$$

The preceding relation may now be used on the left-hand side of Eq. (4), while (5a) or $\delta(r, r')$ may be used for $\delta(r)$ in the integral on the right-hand side of Eq. (4). We thus obtain,

$$g[r', \delta(r')dv(r')]=\int g[|\mathbf{r}-\mathbf{r}'|, \delta(r')dv(r')]f(r)dv(r) + f(r')\delta(r')dv(r'). \tag{6}$$

The second term on the right-hand side originates in that Eq. (5a) is not valid at $r=r'$ and the right-hand side of Eq. (4) has to be completed by the direct action $f(r)$. Since the preceding equation cannot depend on any particular choice of $\delta(r')dv(r')$, one should have

$$g[s, \delta(f)dv(s)]=g(s)\delta(s)dv(s), \tag{7}$$

and, Eq. (6), becomes, switching primes,

$$g(r)=\int g(|\mathbf{r}-\mathbf{r}'|)f(r')dv(r')+f(r). \tag{8}$$

This states that the indirect interaction or correlation between a molecule at the origin and one at a distance r is equal to their short-range interaction $f(r)$ augmented by the sum of the correlations of all those molecules which have a direct or short-range interaction with the one at the origin. This relation has been obtained recently in a more direct way by Klein and Tisza[8] in their discontinuous transcription of the O.Z. continuum liquid model.

We may write Eq. (5) in the following form

$$\delta(r)=g(r)\delta(0)dv(0), \tag{9}$$

which, when multiplied by $\delta(0)$ and taking averages, over the liquid volume, leads to

$$\langle\delta(r)\delta(0)\rangle_{Av}=g(r)\langle\delta(0)^2\rangle_{Av}dv(0). \tag{10}$$

But this equation is evidently independent of the choice of the origin of the coordinate system, and one has to have also

$$\langle\delta(r)\delta(0)\rangle_{Av}=g(r)\langle\delta(r)^2\rangle_{Av}dv(r). \tag{11}$$

Equations (10) and (11) impose that

$$\langle\delta(0)^2\rangle_{Av}dv(0)=\langle\delta(r)^2\rangle_{Av}dv(r)=\cdots=\text{constant}. \tag{12}$$

This constant may be obtained approximately in the following way. Since (N/V) is the mean concentration of the molecules in the liquid, in a volume element dv, there are, on the average, $(N/V)dv$ molecules. If dv is small enough, then there will be either one or no molecule in dv. The deviations from the mean number of molecules, in the two eventualities, are, according to Eq. (3),

$$\delta_1 dv=1-(N/V)dv;\quad \delta_2 dv=-(N/V)dv,$$

respectively. Hence,

$$\lim_{dv\to 0}\delta_1(-\delta_2)dv\cong\langle\delta^2\rangle_{Av}dv=(N/V), \tag{13}$$

and Eq. (11) becomes, with Eqs. (3), (5), and (9),

$$\langle\delta(r)\delta(r')\rangle_{Av}=(N/V)g(r-r')=(N/V)^2Q(r-r'). \tag{14}$$

In a large volume, the accidental excess or defect in the total number of molecules may be written as

$$\Delta N=\int_V\delta(r)dv,$$

and,

$$\langle\Delta N^2\rangle_{Av}=\int\int_V\langle\delta(r)^2\rangle_{Av}dv(r)dv(r')+\int_V\int_V\langle\delta(r)\delta(r')\rangle_{Av}dv(r)dv(r')$$

$$=N\left[1+(N/V)\int_V Q(r)dv\right], \tag{15}$$

a relation which was proved rigorously in the statistical mechanics of ideal symmetric fluids where the correlation is strictly a quantum effect.[6]

While Eq. (8) cannot give the indirect interaction or correlation function $g(r)$ unless $f(r)$, the possibly short-range direct interaction function, is known, it leads to a satisfactory determination of its asymptotic expression as shown by Zernike.[3]

Let

$$F=\int f(r)dv;\quad r_f^2=\int f(r)r^2dv=\epsilon^2, \tag{16}$$

F is the space integral of the short-range direct interaction function and ϵ^2 is the mean square of its range. The quantity $(\epsilon^2)^{\frac{1}{2}}$ is of the order of magnitude of the range of the intermolecular forces. At all distances $r\gg\epsilon$ where $f(r)$ is vanishingly small and provided that $\rho>\epsilon$ one finds

$$g(r)=[3F/(2\pi\epsilon^2)]e^{-r/\rho}/r;\quad r\gg\epsilon, \tag{17}$$
$$\rho^2=\epsilon^2/6(1-F).$$

With ϵ being about the range of the intermolecular forces ϵ^3 is, approximately, the volume per molecule V/N, and

$$g(r)_{r\gg\epsilon}=(3F/2\pi\epsilon^3)e^{-r/\rho}/(r/\epsilon)=(N/V)(3F/2\pi)e^{-r/\rho}/(r/\epsilon). \tag{18}$$

The correlation function is thus, in this approximation,

$$Q(r)_{r\gg\epsilon}=(3F/2\pi)e^{-r/\rho}/(r/\epsilon), \tag{19}$$

and the two-particle probability density defined by Eq. (1) becomes, asymptotically,

$$P(r)_{r\gg\epsilon}=(1+Q(r))/V=[1+(3F/2\pi)e^{-r/\rho}/(r/\epsilon)]V^{-1}. \tag{20}$$

The latter, of course, has the required form, tending toward the constant limit V^{-1} at large separation r.

It is of interest to consider more closely the range ρ, Eq. (17), of the correlation function $Q(r)$ or the indirect interaction function $g(r)$ which is proportional to it. According to Eq. (15),

$$\langle\Delta N^2\rangle_{Av}/N=1+\int g(r)dv=1+G. \tag{21}$$

But in a large volume and as long as the state of the fluid is different from the critical state, $\langle\Delta N^2\rangle_{Av}/N$ is determined by statistical thermodynamics[9] to be

$$\langle\Delta N^2\rangle_{Av}/N=NkT\chi_T/V, \tag{22}$$

the fluid having temperature T, k denoting Boltzmann's constant and χ_T the isothermal compressibility in this state. Multiplying both sides of the integral equation (8) by $dv(r)$ and integrating over the whole volume V or the whole space, one obtains

$$G(1-F)=F,\quad 1+G=(1-F)^{-1}=NkT\chi_T/V. \tag{23}$$

[9] M. v. Smoluchowski, Ann. Physik **25**, 205 (1908).

Hence, the range ρ of the g-function, or the correlation function $Q(r)$, is, according to (17),

$$(\rho)^2=(\epsilon^2/6)(1+G)=NkT\chi_T\epsilon^2/6V. \quad (24)$$

The space integrals F, G, together with the functions f and g are, of course, temperature dependent.

In normal liquids at temperatures T small in comparison with the critical temperature T_c, $\langle\Delta N^2\rangle_{kl}/N$ or $(NkT\chi_T/V)$ may be small in comparison with unity. Hence, at these low temperatures,

$$-1\leqslant G(T\ll T_c)<0,\ F(T\ll T_c)<0,\ |F(T\ll T_c)|>1. \quad (25)$$

At such temperatures the range of the g-function is thus small compared with the range ϵ of the f-function. Under these conditions with the molecular distribution function, Eq. (1), being

$$dn(r)/dv=NP(r)=(N/V)+(N/V)Q(r)$$
$$=(N/V)+g(r), \quad (26)$$

$g(r)$ vanishing at small distances already, this function or $Q(r)$ has to be negative essentially over the interval $r\lesssim\rho\ll\epsilon$. This is of course necessary for the probability density $P(r)$ has to become small at small separations.

As the liquid temperature increases, the right-hand side of Eq. (23) increases, both G and F increase algebraically and vanish when the classical value of the fluctuation $\langle\Delta N^2\rangle_{kl}$ is reached from below. That is, when classical or ideal conditions prevail, at some temperature T_i,

$$\langle\Delta N^2\rangle_{kl}/N=NkT_i\chi_T/V=1;\quad T_i=(V/Nk\chi_{T_i}),$$
$$G(T_i)=F(T_i)=0, \quad (27)$$

and

$$(\rho)^2_{T_i}=\epsilon^2/6, \quad (28)$$

the two functions have about the same range. The fact that the space integrals increase indicates that with the g-function becoming necessarily negative at close distances, there is a distance interval r over which $g(r, T)$ becomes positive so as to compensate for the negative portion of the space integral. The oscillatory character of $g(r, T)$, and also of $f(r, T)$ may thus be safely inferred from these general results.

At temperatures $T>T_i$, both $G(T)$ and $F(T)$ become positive, with $F(T)$ tending toward unity and $G(T)$ toward large positive values as the temperature approaches the critical temperature T_c. Simultaneously the range of $g(r, T)$ becomes very large, of the order of magnitude of the linear dimensions of the vessel containing the liquid. One thus obtains

$$\underset{r\gg\epsilon,\ T\to T_c}{g(r, T)}=\frac{3}{2\pi\epsilon^2 r}, \quad (29)$$

i.e., the correlation density function becomes the long-range $(1/r)$ function. Explicitly, one has thus

$$\lim_{T\to T_c} G(T)\gg 1,\quad \lim_{T\to T_c} F(T)=1. \quad (30)$$

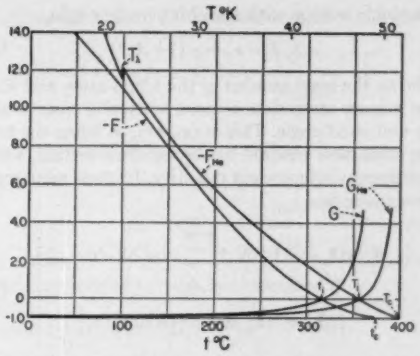

FIG. 1. The space integrals (F,G) for liquid water, and (F_{He},G_{He}) for liquid helium as a function of the temperature. The lower abscissa scale in °C (water) and the upper in °K (helium).

We have represented, in Fig. 1, $F(T)$ and $G(T)$ for water and liquid helium. The over-all similarity in the behavior of these so different liquids with respect to the space integrals of their direct and indirect interaction functions is evident. The radical change in the behavior of $g(r, T)$ at temperatures $T>T_i$ is clearly exhibited by these curves. The λ-anomaly in liquid He appears through the slight discontinuity in $F(T)$ at the λ-point. This indicates already that any experimental data which may yield $F(T)$ or some quantities closely connected with it cannot show but a small temperature effect in crossing the λ-point. This is so because the spatial arrangement of the atoms in liquid helium, associated with a complete averaging over the states of motion of the liquid as a whole will likely change only slightly in crossing the λ-point. It is to be noted that the water curves refer to the saturated liquid, while the helium curves correspond to slightly compressed helium.

III. THE COHERENT SCATTERING STRUCTURE FACTOR OF LIQUIDS

It is easy to prove that the liquid coherent scattering cross section per atom or molecule, per unit solid angle, is

$$\sigma_L(\lambda, \theta)=\sigma(\lambda, \theta)F_L^2(\lambda, \theta), \quad (31)$$

where $\sigma(\lambda, \theta)$ is the individual bound atom coherent scattering cross section and $F_L^2(\lambda, \theta)$ is the coherent intensity structure factor of the liquid. The structure factor F_L^2 is the same for all types of waves. The specificity of the liquid cross sections for the different types of waves is included into $\sigma(\lambda, \theta)$. For unpolarized incident electromagnetic waves, $\sigma(\lambda, \theta)$ is supposed to include the polarization factor $\frac{1}{2}[1+\cos^2(2\theta)]$, beside the elementary atomic cross section. In the case of molecules it is assumed to include also the elementary intramolecular structure factor. For an unpolarized beam of slow neutrons incident on a monatomic liquid

of a single isotope with vanishing nuclear spin,

$$\sigma(\lambda, \theta)=\sigma_{\infty}=\sigma_s(1+A^{-1})^2, \tag{32}$$

A being the mass number of the liquid atom and σ_s the free solitary atom slow neutron scattering cross section per unit solid angle. This is $(\sigma_i/4\pi)$, σ_i being the total free atom slow neutron scattering cross section, which is an energy-independent quantity. In these monatomic liquids, one has

$$\sigma_L(\lambda, \theta)/\sigma(\lambda, \theta)=1+N^{-1}\sum_{\substack{i}}^{N}\sum_{\substack{j\\ i\neq j}}^{N}\cos[\Delta\mathbf{k}\cdot(\mathbf{r}_i-\mathbf{r}_j)]; \tag{33}$$

$$|\Delta\mathbf{k}|=2|\mathbf{k}|\ \sin\theta=(4\pi\sin\theta)/\lambda,$$

$\mathbf{k}$ is the propagation vector and 2θ the scattering angle. In monatomic liquids, with a single isotope with spin or several isotopes, one finds, for slow neutrons, with σ_{∞} denoting the bound atom elastic cross section per unit solid angle, averaged over the different isotopes and spin configurations and σ_c the bound atom coherent scattering cross section averaged again over the different isotopes and spin configurations of the neutron and scattering nuclei,

$$\frac{\sigma_L(\lambda, \theta)}{\sigma_{\infty}}=1+\tau N^{-1}\sum_{\substack{i}}^{N}\sum_{\substack{j\\ i\neq j}}^{N}\cos[\Delta\mathbf{k}\cdot(\mathbf{r}_i-\mathbf{r}_j)], \tag{34}$$

$$\tau=\sigma_c/\sigma_{\infty}<1,$$

showing that the right-hand side contains the ratio of the cross sections τ and ceases to be a purely kinematical quantity.

In terms of the continuous two-atom distribution function, Eq. (1),

$$P(r_{nm}, T)=V^{-2}[1+Q(r_{nm}, T)];\quad r_{nm}=|\mathbf{r}_n-\mathbf{r}_m|,$$

the liquid structure factor per atom may be written as

$$F_L^2(\Delta k, T)=1+N^{-1}\sum_{\substack{n}}^{N}\sum_{\substack{m\\ n\neq m}}^{N}\int\cos[\Delta\mathbf{k}\cdot(\mathbf{r}_n-\mathbf{r}_m)]\times P(r_{nm}, T)dv_n dv_m. \tag{35}$$

Explicitly,

$$F_L^2(\Delta k, T)=1+\frac{N}{V^2}\int\cos[\Delta\mathbf{k}\cdot(\mathbf{r}_n-\mathbf{r}_m)]dv_n dv_m + \frac{N}{V}\int\cos(\mathbf{r}\cdot\Delta\mathbf{k})Q(r, T)dv. \tag{36}$$

The second term on the right-hand side yields the uncorrelated or ideal fluid structure factor, which is extremely small for all scattering angles and Δk values, with the exception of the immediate vicinity of the forward direction or almost completely vanishing Δk values, it shall be omitted henceforth. Hence, the liquid structure factor (36) becomes

$$F_L^2(\Delta k, T)=1+\int g(r, T)\cos(\mathbf{r}\cdot\Delta\mathbf{k})dv, \tag{37}$$

according to the definition of the indirect interaction function $g(r, T)$ in terms of the correlation function $Q(r, T)$, Eq. (14). Integrating over the angles, one finds

$$F_L^2(\Delta k, T)=1+4\pi\int_0^{\infty}\frac{\sin(r\Delta k)}{(r\Delta k)}g(r, T)r^2dr. \tag{38}$$

In the limit of small Δk, one obtains, at once,

$$\lim_{\Delta k\to 0}F_L^2(\Delta k, T)=1+\int_0^{\infty}g(r, T)dv=1+G(T). \tag{39}$$

But the right-hand side is, according to the properties of the liquid model, $\langle\Delta N^2\rangle_{\text{av}}/N$, Eq. (21). Hence, away from the critical state of the fluid,

$$\lim_{\Delta k\to 0}F_L^2(\Delta k, T)_{T\neq T_c}=\langle\Delta N^2\rangle_{\text{av}}/N=NkT\chi_T/V. \tag{40}$$

The very small angle coherent scattering structure factor is independent of the details of the scattering process, that is Δk or $\sin\theta/\lambda$, λ being the wavelength of the incident waves in the medium surrounding the scattering liquid. The structure facor in this limit depends only on the over-all statistical properties of the liquid, the molecular concentration (N/V), the temperature and the isothermal compressibility in the state of equilibrium under consideration. The general result (40) has been first obtained by Brillouin[10] in his investigation of x-ray scattering in fluids using the method of Einstein[11] elaborated in his theory of scattering of visible radiation arising from density fluctuations in a fluid in statistical equilibrium as suggested by Smoluchowski.[9] Again for x-rays, using a different approach, the result (40) has been given by Zernike and Prins.[4] The same result obtains in the coherent scattering of slow neutrons with vanishing momentum change and for atoms with zero spin nuclei.[6,7] One obtains at once for bound scatterers, whose elastic scattering cross section is different from their coherent scattering cross section, using Eq. (34) together with (36),

$$\lim_{\Delta k\to 0}F_L^2(\Delta k, T)_{T\neq T_c}=1+\tau G(T)=(1-\tau)+\tau\langle\Delta N^2\rangle_{\text{av}}/N =(1-\tau)+(NkT\chi_T\tau/V). \tag{41}$$

Here τ is the cross-section ratio σ_c/σ_{∞} defined in connection with Eq. (34).

We should like to investigate further the complete structure factor formula (37). If the indirect interaction or correlation interaction $g(r, T)$ or $Q(r, T)$ were known,

[10] L. Brillouin, Ann. Phys. 17, 88 (1922).
[11] A. Einstein, Ann. Phys. 33, 1275 (1910).

the structure factor would be completely determined. This is, however, not the case. We may now express the structure factor (38) in terms of the direct interaction function $f(r, T)$ of the liquid model. To do this we have to use the integral equation (8) connecting $f(r, T)$ and $g(r, T)$. Multiplying both sides of this equation by $\cos(\mathbf{r}\cdot\Delta\mathbf{k})$ and integrating over the liquid volume or the whole space, we obtain

$$G(\Delta k, T)=F(\Delta k, T)[1-F(\Delta k, T)]^{-1}, \quad (42)$$

where[12]

$$G(\Delta k, T)=\int \cos(\mathbf{r}\cdot\Delta\mathbf{k})g(r, T)d\mathbf{v}(r),$$
$$F(\Delta k, T)=\int \cos(\mathbf{r}\cdot\Delta\mathbf{k})f(r, T)d\mathbf{v}(r). \quad (43)$$

Clearly, in the limit $\Delta k\to 0$,

$$\lim_{\Delta k\to 0} G(\Delta k, T)=G(T), \quad \lim_{\Delta k\to 0} F(\Delta k, T)=F(T), \quad (44)$$

and, in this limit, Eq. (42) reduces to Eq. (23). The structure factor (37) becomes thus

$$F_L^2(\Delta k, T)=1+G(\Delta k, T)=[1-F(\Delta k, T)]^{-1}, \quad (45)$$

and for the cross-section ratio (34) different from unity, in the coherent scattering of slow neutrons,

$$\frac{F_L^2(\Delta k, T)}{\tau\neq 1}=1+\tau G(\Delta k, T)=\frac{1-(1-\tau)F(\Delta k, T)}{1-F(\Delta k, T)}. \quad (46)$$

Integrating over the angles in $F(\Delta k, T)$, one obtains

$$F(\Delta k, T)=4\pi\int\frac{\sin(\Delta kr)}{(\Delta kr)}f(r)r^2dr. \quad (47)$$

If we denote by r_F^{2n}, the $2n$-th moment of the direct interaction function $f(r, T)$, we find, expanding $\sin(\Delta kr)/\Delta kr$ and integrating term by term,

$$F(\Delta k, T)=\sum_0^\infty(-)^n\frac{(\Delta k)^{2n}r_F^{2n}}{(2n+1)!}, \quad (48)$$

$$r_F^{2n}=\int r^{2n}f(r, T)4\pi r^2dr; \quad r_F^0=F(T).$$

Writing $F(\Delta k, T)$ in the form,

$$F(\Delta k, T)=F(T)+\sum_1^\infty(-)^n\frac{(\Delta k)^{2n}r_F^{2n}}{(2n+1)!},$$

the structure factor (45) becomes, with (22) and (23),

$$F_L^2(\Delta k, T)=\left[1-F(T)+\sum_{n=1}^\infty(-)^{n+1}\frac{(\Delta k)^{2n}r_F^{2n}}{(2n+1)!}\right]^{-1}$$
$$=[\langle\Delta N^2\rangle_{\rm Av}/N]\left[1+(\langle\Delta N^2\rangle_{\rm Av}/N)\times\sum_1^\infty(-)^{n+1}\frac{(\Delta k)^{2n}r_F^{2n}}{(2n+1)!}\right]^{-1}. \quad (49)$$

Again, denoting by r_G^{2n} the $2n$-th moment of the $g(r, T)$ function, one obtains, with (43) and (45), another expression for the structure factor,

$$F_L^2(\Delta k, T)$$
$$=1+4\pi\int\frac{\sin(\Delta kr)}{\Delta kr}g(r, T)r^2dr$$
$$=1+G(T)+\sum_1^\infty(-)^n(\Delta k)^{2n}r_G^{2n}/(2n+1)!$$
$$=[\langle\Delta N^2\rangle_{\rm Av}/N]+\sum_1^\infty(-)^n(\Delta k)^{2n}r_G^{2n}/(2n+1)! \quad (50)$$

where use has been made of Eq. (23) and where

$$r_G^0=G(T); \quad r_G^{2n}=\int r^{2n}g(r, T)d\mathbf{v}. \quad n\geqslant 1. \quad (50a)$$

The structure factor formulas (49) and (50) are, of course, rigorous within the formalism of the liquid model. However, the model does not determine f and g, but operates only with these quantities. It is, however, of interest to discuss these structure factors in terms of what is known of the f- and g-functions. Assume first that Δk is quite small or that the series in the denominator of (49) or (50) may be neglected in comparison with $\langle\Delta N^2\rangle_{\rm Av}/N$. Then one sees that the very small angle coherent scattering structure factor will vary with the liquid temperature so as to increase with it. This point was discussed in detail in an earlier paper.[6]

Consider the liquid at some low temperature $T<T_i$, T_i being the characteristic temperature defined above, Eq. (27). And assume further that the first term in the infinite series appearing in (49) is large enough to be included in the structure factor, for small Δk values. At low temperatures, we have seen that the space integral of the f-function is large and negative; see Fig. 1 for the case of water and liquid He, for instance. This makes it likely that r_F^2 is also negative, so that for small but finite Δk values the structure factor will tend to increase from its minimum value at the limit $\Delta k\to 0$. Or, using (50), inasmuch as at low temperatures $G(T)$ is again negative of the order of (-1), one might

[12] The $F(\Delta k, T)$ integral should not be confused with the liquid structure factor $F_L^2(\Delta k, T)$ which we always write as a square with the subscript L.

expect r_G^2 to be also negative on account of its very short range at these temperatures. This again would tend to indicate, as in Eq. (49), an increase of the structure factor with increasing Δk-values, for small Δk.

At high temperatures, $T > T_i$, approaching the critical region, both F and G are positive. One then finds at once that for small Δk values the structure factor decreases from its limiting value for vanishing Δk, that is from $\langle \Delta N^2 \rangle_{\text{Av}}/N$ or $(NkT\chi_T/V)$. At $T > T_i$ and for Δk values where only the first term in the series appearing in (49) or (50) may be considered to be significant, these results are seen to be rigorous. For small Δk values the theory gives a good qualitative account of the observed structure factors in liquids,[13] particularly at higher temperatures.

It is of course visible in (37) or (43) that in the limit of Δk becoming large,

$$\lim_{\Delta k \to \text{large}} F_L^2(\Delta k, T) = 1.$$

The difficulty associated with this limit has been pointed out previously[6] and will not be discussed here.

In the critical region, which has been discussed in some detail,[6] in particular for small angle scattering, we see at once from (49), remembering that the space integral $F(T)$ tends toward unity as $T \to T_c$, that

$$\lim_{T \to T_c} F_L^2(\Delta k, T) = \left[\sum_1^\infty (-)^{n+1} (\Delta k)^{2n} r_F^{2n} / (2n+1)! \right]^{-1}. \quad (51)$$

For small Δk values the preceding structure reduces to the one given previously.[6] The singular character of this formula in the limit of $\Delta k \to 0$ does not seem to create any particularly great difficulties, on account of the necessarily finite solid angles at which the observations are made. However, this structure factor may become quite large for small Δk values, a result which agrees qualitatively with the experimental data available in a very few cases, such as argon, nitrogen,[13] and ether.[14]

We may add here that the oscillatory character of $F(\Delta k, T)$ or $G(\Delta k, T)$ make it evident that the liquid structure factors should exhibit the same type of behavior. Since the f- and g-functions are unknown, we close this discussion of the structure factors based on the rather meagre information available on these functions and turn rather to the problem of their determination through the experimental investigation of the coherent scattering properties of liquids for x-rays and slow neutrons.

[13] See the review article, quoted in reference 5 and the exhaustive work on argon, both liquid and vapor, by A. Eisenstein and N. S. Gingrich, Phys. Rev. **58**, 307 (1940), and **62**, 261 (1942). See also the recent work on nitrogen by R. L. Wild, J. Chem. Phys. **18**, 1627 (1950).

[14] F. H. W. Noll, Phys. Rev. **42**, 337 (1932).

IV. THE DETERMINATION OF THE DIRECT (f) AND INDIRECT (g) INTERACTION FUNCTIONS

The experimental data on the coherent scattering structure factor allow one to obtain the indirect interaction function $f(r, T)$ in addition to the correlation density $g(r, T)$ which alone was, so far, the ultimate goal of most experimental work on the coherent scattering of x-rays by liquids. The molecular distribution function

$$dn(r)/dv = (N/V)(1+Q(r, T)) = (N/V)P(r, T) = (N/V) + g(r, T), \quad (3)$$

is of course one of the important quantities characterizing a liquid, and the preceding definition may be looked upon as being quite general and independent to a large extent of any liquid model. It is thus justified to attempt to derive, from the experimentally determined coherent structure factor, the distribution function (3). One finds at once, using Eq. (38),

$$\int_0^\infty \sin(\Delta k, r) g(r, T) r dr = [F_L^2(\Delta k, T) - 1](\Delta k/4\pi), \quad (52)$$

and, by Fourier's theorem,

$$g(r, T) = (1/2\pi^2 r) \int_0^\infty [F_L^2(\Delta k, T) - 1] \times (\Delta k) \sin(\Delta k r) d(\Delta k), \quad (53)$$

a relation first obtained by Zernike and Prins.[4] By Eq. (46) and for slow neutrons in liquids with the cross-section ratio τ or (σ_c/σ_∞), assumed to be known, one has to divide the right-hand side by τ. A normalization relation[15] resulting from the definition of the distribution function may be of interest here. Since the probability density, Eq. (1)

$$P(r, T) = [1 + (V/N) g(r, T)] V^{-1},$$

has to vanish at very small separations, $g(r, T)$ has to tend toward $(-N/V)$ and (53) yields

$$\lim_{r \to 0} g(r, T) = -\frac{N}{V} = \frac{1}{2\pi^2} \int_0^\infty (\Delta k)^2 [F_L^2(\Delta k, T) - 1] d(\Delta k). \quad (54)$$

Again, for slow neutrons, the right-hand side is to be divided by τ if the latter is different from unity.

The knowledge of the correlation density $g(r, T)$ enables one to determine the f-function according to the central theorem of the liquid model expressed by the integral equation (8). While an analytical discussion of this equation would be difficult because of the fact that the g-function resulting from the measured structure factors, according to Eq. (53), becomes available

[15] See the last work quoted in reference 5.

only in tabular form, nevertheless numerical methods applied to Eq. (8) should lead to the determination of the function $f(r, T)$. This procedure may, however, be avoided. Indeed, Eq. (45) yields

$$1-F(\Delta k, T)=1-4\pi\int_0^\infty \frac{\sin(\Delta kr)}{(\Delta kr)}f(r, T)r^2dr$$

$$=F_L^{-2}(\Delta k, T), \quad (55)$$

or

$$\int_0^\infty \sin(\Delta kr)f(r, T)rdr=[1-F_L^{-2}(\Delta k, T)](\Delta k/4\pi),$$

and, using again Fourier's theorem,

$$f(r, T)=(1/2\pi^2r)\int_0^\infty [1-F_L^{-2}(\Delta k, T)]$$

$$\times(\Delta k)\sin(\Delta kr)d(\Delta k). \quad (56)$$

In the case of slow neutrons and with $\tau\neq 1$, one finds

$$f(r, T)=\frac{1}{2\pi^2r}\int_0^\infty \frac{F_L^2-1}{F_L^2-1+\tau}(\Delta k)\sin(\Delta kr)d(\Delta k). \quad (57)$$

Hence the numerical analysis which has to be applied to the experimental data in order to derive from them $g(r, T)$, leads equally well to the determination of $f(r, T)$. One has thus the following result: the coherent scattering structure factor of a liquid completely determines the molecular type of interaction functions $g(r, T)$ and $f(r, T)$ which are the basic elements of the liquid model. The theory can now be directly checked by a substitution of these functions into the integral equation (8).

Another method can, however, be followed here leading directly to the value $\langle\Delta N^2\rangle_{kT}/N$ at the temperature or temperatures at which $g(r, T)$ and $f(r, T)$ have been determined. The mean square fluctuation $\langle\Delta N^2\rangle_{kT}/N$ or $(nkT\chi_T)$ may or may not be known, depending on the knowledge of the compressibility χ_T. In general the latter quantity is unknown. A rather good check on the f- and g-function may be obtained by evaluating their space integrals, $F(T)$ and $G(T)$, respectively. Then,

$$1+G(T)=[1-F(T)]^{-1}=(nkT\chi_T) \quad (23)$$

the first equation is fully equivalent to the integral equation. While the knowledge of $G(T)$ and $F(T)$ leads to $\langle\Delta N^2\rangle_{kT}/N$ or the compressibility χ_T. It seems that the preceding method of obtaining the compressibility is of interest insofar as it should yield values whose precision is closely connected with the one reached in obtaining $G(T)$ or $F(T)$. This method does not involve any particular uncertainties such as the one associated with obtaining the extrapolated structure factor in the forward direction from the small angle coherent scattering structure factor.[16] Also, the first equality in (23), if verified with the g- and f-functions may indicate that the mean square fluctuation so obtained could yield a fair value of the compressibility.

The experimental data on the coherent structure factor of liquids may be further exploited since they give rise to a more complete determination of the direct and indirect interaction functions of the model. Equation (49) gives, indeed

$$-F(T)+\sum_1^\infty(-)^{n+1}\frac{(\Delta k)^{2n}r_F^{2n}}{(2n+1)!}=F_L^{-2}(\Delta k, T)-1. \quad (58)$$

Since $F(T)$ is the zeroth moment of the f-function, Eq. (48), the left-hand side contains all the even moments of this function. Now, in the limit of very small Δk values the moments r_F^{2n} $(n\geqslant 1)$ do not contribute at all. As the value of Δk increases the higher order moments become operative. Suppose now, that one chooses a series of Δk values, which are rather moderate so that all terms beyond the i'th in the infinite series may be neglected. Then with $(i+1)$ different Δk values and the associated structure factor values, one may set up a system of $(i+1)$ linear equations in the unknowns $F(T)$, r_F^2, r_F^4, $\cdots r_F^{2i}$. Hence, these moments of the f-function may be obtained with an accuracy depending on the choice of the Δk values beside that of the F_L^2-values. But the larger i is, the better is the accuracy of the moments. Hence both $\langle\Delta N^2\rangle_{kT}/N$ or $(nkT\chi_T)$ and the moments of the f-function are obtained directly from the structure factor, without taking its fourier transform which is a cumbersome procedure. Clearly if the f-function itself has been obtained with Eq. (57), its moments may be evaluated and compared with the ones derived with Eq. (58). This affords a further check on the degree of validity of keeping only a finite number of terms in the moment series in Eq. (58). Similarly, Eq. (50) yields, with a similar treatment, the even moments of the g-function.

It is now necessary to compare the moments of the f- and g-functions. We have multiplying both sides of Eq. (8) by r^2 and integrating over the whole space,

$$r_G^2=r_F^2\frac{1+r_G^0}{1-r_F^0}=r_F^2\frac{1+G}{1-F}=r_F^2(nkT\chi_T)^2, \quad (59)$$

where use has been made of the definitions (48) and (23). One then finds in a similar way the following general relation between the even moments of these functions,

$$r_G^{2n}-r_F^{2n}=\sum_{2\lambda=0}^{n}\sum_{\mu=0}^{n-2\lambda}\frac{2^{2\lambda}}{2\lambda+1}\binom{n}{2\lambda}\binom{n-2\lambda}{\mu}$$

$$\times r_G^{2n-2\lambda-2\mu}r_F^{2\lambda+2\mu}, \quad (60)$$

$$r_G^0=G;\quad r_F^0=F;\quad \binom{\alpha}{\beta}=\frac{\alpha!}{(\alpha-\beta)!\beta!}.$$

[16] See J. Yvon, J. phys. et radium 7, 201 (1946), and the recent work of Wild quoted in reference 14.

With the preceding relation one obtains for the fourth and sixth moments, denoting by $\nu(T)$ the quantity $(nkT\chi_T)$,

$$r_G^4=\nu^2[r_F^4+(10/3)(r_F^2)^2\nu];$$
$$r_F^4=\nu^{-2}[r_G^4-(10/3\nu)(r_G^2)^2];$$
$$r_G^6=\nu^2[r_F^6+14\nu r_F^4 r_F^2+(70/3)(r_F^2)^3\nu^2];$$
$$r_F^6=\nu^{-2}[r_G^6-(14/\nu)r_G^4 r_G^2+(70/3\nu^2)(r_G^2)^3].$$

The relations between the higher order moments increase in complexity, but can be obtained without any difficulty. The moments r_F^{2n} and r_G^{2n} $(2n=0, 2, 4, \cdots)$ obtained directly from the structure factors have to satisfy the preceding relations. A direct check on the liquid model is thus obtained again.

V. REMARKS ON THE SCATTERING OF SLOW NEUTRONS BY LIQUIDS

A rather important and difficult problem arises now in connection with slow neutron coherent scattering, namely the problem of their incoherent scattering. The incoherently scattered neutrons are, of course, observed simultaneously with those scattered coherently. While in the x-ray case the incoherently scattered radiation intensity can be evaluated and the observed scattered radiation corrected for it,[6] in the case of slow neutron scattering the incoherent process associated with the exchange of both energy and momentum between the neutrons and the liquid as a whole appears to be considerably more complicated than in x-ray scattering. In solids the slow neutron incoherent scattering may be described as a process of energy and momentum exchange described with the help of a model of $3N$ harmonic oscillators, for a solid formed of N atoms for instance. The corresponding problem in liquids has not even been set up because of a complete lack of a satisfactory molecular liquid model.

There appears to be a possibility of obtaining some information on the incoherent scattering of slow neutrons by liquids. One may indeed evaluate the total coherent scattering cross section, within the framework of the present liquid model, by the use of Eq. (45). The coherent scattering cross section per atom, in a monatomic liquid, and per unit solid angle is

$$\sigma_{Lc}(\Delta k, T)=\sigma_\infty F_L^2(\Delta k, T)=\sigma_\infty[1+G(\Delta k, T)], \quad (61)$$

with the cross-section ratio τ supposed to be unity. The total coherent cross section becomes

$$\sigma_{Lc}(k, T)=2\pi\int_0^{\pi/2}\sigma_L(\Delta k, T)\sin 2\theta d(2\theta)$$
$$=4\pi\sigma_\infty\left\{[\langle\Delta N^2\rangle_{kl}/N]+\sum_1^\infty(-)^n\frac{(2k)^{2n}r_G^{2n}}{(n+1)(2n+1)!}\right\}, \quad (62)$$

σ_∞ being independent of the scattering angle. In a molecular liquid the situation is more complicated since the angular integration involves also the coherent cross sections of the molecule per unit solid angle depending on Δk because of intramolecular and elementary intermolecular interference effects.[17]

The preceding total coherent cross-section formula is of interest insofar as it may yield the moments r_G^{2n}. Indeed, at small neutron energies where the total incoherent scattering cross section should be small in comparison with the total coherent one, or with x-rays, a series of transmission measurements as a function of the wavelength of the incident waves leads to a system of linear equations in the moments r_G^{2n}.

The moments r_G^{2n}, and also $\langle\Delta N^2\rangle_{kl}/N$, may be evaluated from the structure factor according to the procedure described above. In order to minimize the intervention of the incoherent scattering, which is unknown, it would be necessary to derive them from those structure factor values which correspond to peak values or from regions in the vicinity of peaks. It is indeed reasonable to assume that the intensity of the incoherently scattered neutrons near the coherent peaks, and particularly near the main peak, would be relatively smaller than in other regions. Then, with the moments so derived, Eq. (62) enables one to obtain a fair value of the total coherent cross section. Slow neutron transmission measurements at the same temperature yield $(\sigma_{Lc}+\sigma_{Li})$, the sum of the total coherent, σ_{Lc}, and total incoherent, σ_{Li}, cross sections per liquid atom.[18] It is hereby assumed that the pure absorption of the slow neutrons is completely absent or that the absorption cross section is quite small in comparison with the smaller of the two scattering cross sections σ_{Le} and σ_{Li}. The difference between the scattering cross section resulting from the transmission measurements and the one computed by (62) is the total incoherent cross section per liquid atom. It should be noted that (62) cannot be used in the critical region, although it should be valid close to it.

One would expect that the incoherent cross section be smaller for heavier than for lighter liquids, in a way similar to the case of solids. Here, at neutron energies small in comparison with the Debye energy $k\Theta$, Θ being the characteristic temperature of the solid, a practically rigorous evaluation of the incoherent cross section per solid atom is possible.[19] In general, however, the evaluation of the solid incoherent cross sections appears to be extremely laborious. But since the total coherent cross section may be obtained rigorously, it is seen that this result combined with transmission

[17] That the elementary molecular cross sections multiplying the diffuse coherent structure factor term, unity in Eq. (61), and the normal interference term, $G(\Delta k, T)$, were different for x-rays already has been shown by P. Debye, J. Math. Phys. 4, 153 (1925).

[18] In a detailed investigation of σ_{Li} the spin and isotope incoherence should be separated from the direct momentum-energy exchange effect.

[19] See A. Akhiezer and I. Pomeranchuk, J. Exp. Theoret. Phys. 17, 770 (1947).

measurements might again yield the unknown solid incoherent cross section. The latter of course should become identical at higher neutron energies with the free atom scattering cross section, both in solids and liquids. Here the following rather interesting problem automatically suggests itself. This is a comparative study of the solid and liquid incoherent cross sections per atom, for the same element. Because of the temperature and structure difference existing between the two phases, one would expect that the incoherent cross sections be different. The incoherent cross section of the solid or liquid is indeed a measure of the probability for the slow neutron to exchange energy and momentum with the solid and liquid as a whole. There is therefore no reason, *a priori*, that these cross sections, or their detailed behavior with the neutron energy be similar. On the contrary, one might expect to obtain from the variations of the incoherent cross section in monatomic liquids, as a function of the neutron energy and liquid temperature, some pertinent elementary information which may prove useful for the understanding of the possible states of motion of liquids.

The total slow neutron coherent scattering cross section may also be obtained directly from the experimental data. If the data are uncorrected for incoherent scattering, one may obtain by a numerical or graphical integration the total scattering cross section. Slow neutron transmission measurements should then check these results.

In the only systematic experiments on the coherent scattering of slow neutrons on liquid sulfur, lead, and bismuth by Chamberlain,[5] the incoherent cross sections of these elements have been determined by identifying the observed differential cross section at the smallest value of the parameter $\sin\theta/\lambda$ with the differential cross section per unit solid angle of the incoherent process. This appears to be justified in these cases because the limiting forward coherent scattering structure factor ($nkT\chi_T$), which we have evaluated only approximately because of lack of data, leads for these liquids to a very small forward differential coherent cross section. Even though in liquid lead and bismuth the smallest $(\sin\theta/\lambda)$ values at which observations have been made are not so small, one finds that by taking into account approximately the first term in the infinite series in the denominator of the right-hand side of Eq. (49), using for $|r_{\rho}{}^{3}|$ the value n^{-1}, n being the approximate concentration, the omission of the coherent scattering at small angles appears to be justified. The observed small angle scattering cross section may thus be ascribed to the incoherent process. Assuming further approximate angular independence of the incoherent scattering cross section per unit solid angle, a correction for this process may thus be performed. Difficulties may arise in liquids and under conditions where ($nkT\chi_T$) is large, as it certainly is above the temperature T_i, defined by Eq. (27), and also at temperatures T not too small compared with T_i. It should be noted that if the incoherent scattering has been taken into account correctly, the new coherent structure factor should lead to correct moments $r_{\rho}{}^{2n}$ and $r_{\sigma}{}^{2n}$ independently of the choice of the parameter $(\sin\theta/\lambda)$, that is, structure factor values near the coherent minima should then yield the same moments as those near peaks.

A final remark may be of interest here. We have assumed throughout this work that the coherent and elastic free or bound atom cross sections were known. It is seen that in those liquids where x-ray structure factors are available, a measurement of the slow neutron coherent cross section per liquid atom, under the same temperature and pressure conditions as the x-ray measurements, could yield the free or bound atom cross sections averaged over the different isotopes. The same remark applies to molecular liquids, although here conditions become considerably more complicated and a careful evaluation of the molecular coherent scattering structure factor is indispensable.

In conclusion we may then say that the coherent scattering data in liquids determine both the correlation density function $g(r, T)$ and the direct interaction function $f(r, T)$ of the Ornstein-Zernike static liquid model. A direct use of the experimental coherent structure factors allows one to determine with a fair degree of accuracy the mean square fluctuation of the concentration and with it the liquid compressibility in the thermodynamic state under investigation. The difficult problem of disentangling the coherent from the incoherent scattering process in the case of slow neutrons has been shown to be soluble in terms of the total cross sections associated with these processes. Simultaneously, it is shown that the experimental investigations of the slow neutron incoherent scattering in liquids may yield information on the energy spectrum of liquids, whose knowledge might be helpful for the establishment of a dynamic liquid model.

Dielectric Properties of Lead Zirconate

G. SHIRANE, E. SAWAGUCHI, AND Y. TAKAGI
Tokyo Institute of Technology, Oh-okayama, Tokyo, Japan
(Received June 6, 1951)

In order to distinguish whether it is really a ferroelectric or not, the dielectric response of $PbZrO_3$ ceramic to biasing dc field has been examined. In contrast to ordinary ferroelectrics, an effect is scarcely detected below the Curie point of 233°C even up to a field strength of 20 kv/cm, except for a slight increase of permittivity at the vicinity of the transition point. In addition, the Curie temperature decreases with increasing biasing field attaining the value $\Delta T_c = -1.7$°C for 20 kv/cm.

The hysteresis loops of this ceramic have been studied. So long as the amplitude of the applied ac field is less than a critical field of about 23 kv/cm, the *D–E* curves are almost always linear, except that a slight upward curvature becomes perceptible just at the temperature range wherein permittivity increases, and never show any hysteresis characteristics even just below the Curie point. But if the amplitude of the applied field is greater than this threshold value, anomalous hysteresis loops of very impressive form are observed in a narrow temperature range just below the Curie point.

These experimental facts all seem to suggest that $PbZrO_3$ may be, not a ferroelectric, but an antiferroelectric. A preliminary pyroelectric test also seems to show that no net polarization grows spontaneously when the sample is cooled through its Curie point.

I. INTRODUCTION

BARIUM titanate[1] has attracted much interest because of its peculiar ferroelectric properties. Lead titanate,[2] as well as several colombates and tantalates[3] of perovskite structure, were also reported to be ferroelectrics of the same type. Recently, Roberts[4] has reported that the variation of the dielectric constant of lead zirconate is also very similar to that of barium titanate, having its Curie point at 236°C. But our recent investigation[5] on $PbZrO_3$ has revealed several intrinsic differences between this material and $BaTiO_3$, not only in dielectric properties but also in dilatometric and calorimetric ones.

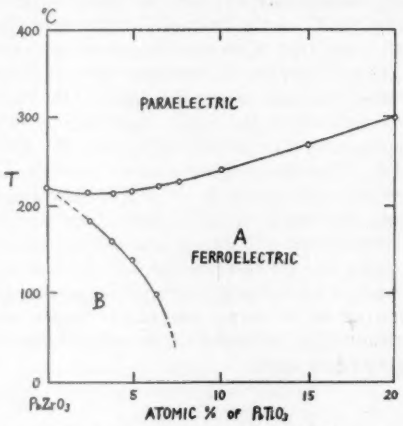

FIG. 1. Phase diagram of the $PbZrO_3$–$PbTiO_3$ system.

Moreover, our investigation[6] on the solid solutions of the $Pb(Zr-Ti)O_3$ system has shown the existence of another transition, for example at 140°C in $Pb(Zr95-Ti5)O_3$, besides the ordinary ferroelectric-paraelectric Curie point (Fig. 1). The phase denoted by *A* is surely ferroelectric, for hysteresis loops of typical form have been observed there. On the other hand, the intrinsic nature of the phase denoted by *B*, including pure $PbZrO_3$ itself, has remained open to question, because in this region neither hysteresis loop nor piezoelectric effect has been observed yet. Since this phase is merely a continuation of pure $PbZrO_3$, its nature will become clear if we investigate the pure material itself.

Two possibilities are conceivable: (1) although $PbZrO_3$ is indeed a ferroelectric, yet it is accompanied by an enormously large coercive field; or (2) it is in fact an antiferroelectric, in which spontaneous polarizations of component sublattices are antiparallel to each other producing no net polarization as a whole. Of course, a direct and decisive method of discriminating between these two hypotheses may be provided by x-ray analysis of precise atomic displacements. In addition, however, among purely phenomenological methods, a pyroelectric test and an examination of its dielectric response to the dc field may be the most helpful. The results of such investigations on pure $PbZrO_3$ will be reported here.

II. SPECIMEN

Specimens were prepared from reagent-grade PbO and ZrO_2 of high purity containing as impurities only very small amounts of Ti (0.21 percent), Fe (0.05 percent) and Si (0.03 percent). These ingredients were mixed in equimolar proportion and sintered at about 1250°C after a preliminary calcination. It is difficult to

[1] See for instance, A. von Hippel, Revs. Modern Phys. **22**, 221 (1950).
[2] Shirane, Hoshino, and Suzuki, Phys. Rev. **80**, 1105 (1950).
[3] B. Matthias, Phys. Rev. **75**, 1771 (1949).
[4] S. Roberts, J. Am. Ceram. Soc. **33**, 63 (1950).
[5] Shirane, Sawaguchi, and Takeda, Phys. Rev. **80**, 485 (1950). Sawaguchi, Shirane, and Takagi, J. Phys. Soc. Japan **6** (to be published).
[6] G. Shirane and A. Takeda, J. Phys. Soc. Japan (to be published).

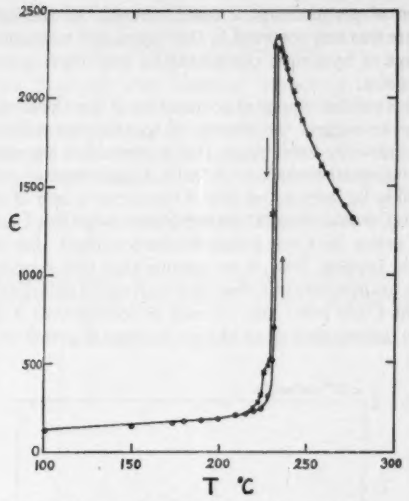

FIG. 2. Dielectric constant of lead zirconate at varying temperatures.

obtain a very tight specimen but the sintered ceramics were good enough for dielectric measurements, being free from porosity.

Dielectric test samples, 1 mm in thickness, were coated on both sides with evaporated gold film. Permittivity was measured with a heterodyne method at 1 Mc/sec and 10 v/cm. Curves for both rising and falling temperatures are shown in Fig. 2. Above the Curie point of 233°C, it was found that the Curie-Weiss law $\epsilon = C/(T - T_p)$ is valid to a good approximation with $C = 1.2 \times 10^5$ °C and $T_p = 185$°C. These results are in good agreement with those obtained by Roberts.[4] It should be pointed out here that the paraelectric Curie point T_p is somewhat lower than the transition point, in contrast to the case of $BaTiO_3$.

The small anomaly at 225°C observed in the permittivity curve on cooling is similar in its shape, though less distinct, to that previously found at 203°C on the cooling curve of our former $PbZrO_3$ of lower purity,[5] and hence it seems to be due to the same sort of origin.

III. EFFECT OF DC BIAS ON THE CURIE POINT

We have measured the permittivity of $PbZrO_3$ ceramic under a biasing dc field of 10 kv/cm as a function of temperature (Fig. 3). Measurements were carried out in a bath of liquid paraffin which was stirred vigorously, and the temperature of the specimen was measured by a potentiometer using a copper-constantan thermocouple directly attached to one of the electrodes.

As shown in Fig. 3, the permittivity below the Curie point is scarcely influenced by the dc field except that it does increase slightly just below the Curie point. On the other hand, a decrease of permittivity is observed above the Curie point. At room temperature, the permittivity is strictly invariant even up to a biasing field of 20 kv/cm. In addition, the Curie point is shifted towards lower temperature by 1.5(±0.2)°C under this biasing field, and at the same time the peak value of the permittivity increases slightly. These results are just opposite to the case of barium titanate,[7] in which a rise of the Curie temperature and a considerable decrease of permittivity even below the Curie point were observed under a biasing field.

Figure 4 shows the transition temperature of $PbZrO_3$ as a function of biasing dc field for both rising and falling temperatures. It decreases with increasing dc field and begins to show a tendency of saturation at about 20 kv/cm. Such an effect should be rather difficult to understand if this crystal belongs to a ferroelectric, because the dc field must surely compel every dipole moment to be in one direction, so that a certain amount of rise in the Curie temperature may be expected, as is actually observed in $BaTiO_3$.

IV. HYSTERESIS LOOPS

A. Hysteresis Loops at an ac Amplitude of 20 kv/cm

A circuit essentially similar to that of Sawyer and Tower[8] was used to display the polarization-electric

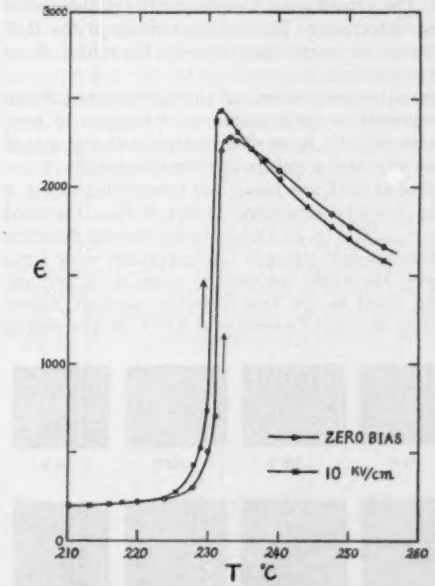

FIG. 3. Effect of a biasing dc field of 10 kv/cm on the permittivity (at 1 Mc/sec) of $PbZrO_3$ at rising temperatures.

[7] S. Roberts, Phys. Rev. **71**, 890 (1947). Cross, Dennison, Nicolson, and Widdington, Nature **163**, 635 (1949).
[8] C. Sawyer and C. Tower, Phys. Rev. **35**, 269 (1930).

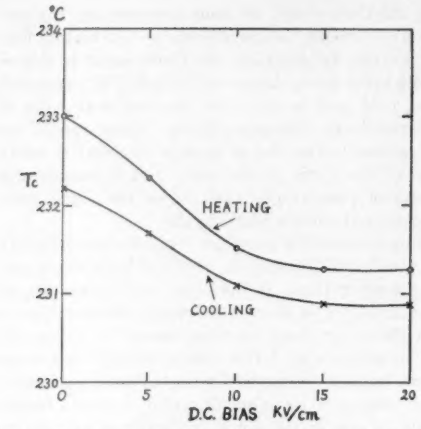

FIG. 4. Curie temperature of $PbZrO_3$ at rising and falling temperatures as a function of biasing dc field.

field curve on a cathode-ray tube. Figure 5 shows a series of results obtained by the ac field of 20 kv/cm and 50 cycles/sec at various increasing temperatures. Ordinary hysteresis loops have not been observed; the curves are always almost linear, except that a slight upward curvature is noticeable just below the Curie point. The situation is also quite similar in the case of falling temperature. These characteristics of the D–E relation are of course consistent with the results of the preceding section.

The maximum polarization at this field strength can be estimated on oscillographs as a function of temperature (Fig. 6); in marked contrast with the case of barium titanate,[9] a sudden increase of polarization was observed at the Curie point. The resemblance of Fig. 6 to Fig. 2 is very impressive. In fact, if P_{max} is reduced to $4\pi P_{max}/E$ (Fig. 7), that is, to the average dielectric constant for field strength E, the reduced value turns out over the whole temperature range to be approximately equal to the true dielectric constant. Corresponding to a small anomaly at 225°C on the cooling curve of permittivity, a small anomaly of the same nature was also observed in this figure, but no essential change of hysteresis characteristics was found around this point.

This sudden change of polarization at the Curie point seems to suggest the absence of spontaneous polarization below the Curie point. If this crystal had any spontaneous polarization at all, such a phenomenon could possibly be interpreted only if the coercive field of this crystal would remain extraordinary large even until just below the Curie point. It seems unlikely that this would happen. Now, if we assume that this substance is an antiferroelectric, then this increase of polarization at the Curie point may at once be interpreted; it is a mere consequence of an abrupt increase of permittivity

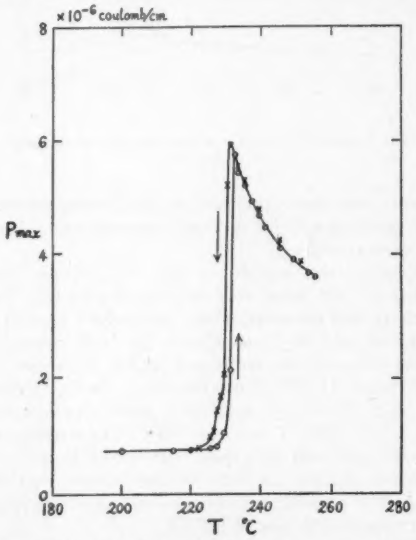

FIG. 6. Maximum polarization as a function of varying temperature at $E_{max}=20$ kv/cm.

at this point. In fact the jump of $4\pi P_{max}/E$ is about 2500, being of the same order of magnitude as the jump of permittivity which is estimated to be 2000.

Considering the dielectric, dilatometric, and calorimetric data, it seems certain that the transition in $PbZrO_3$ is of the first order; hence we can apply the Clausius-Clapeyron equation. It can be written, in the general case,

$$\frac{dT_c}{dE}=-\frac{T_c}{L}\left(\Delta P_s+\frac{\Delta\epsilon\cdot E}{4\pi}\right),$$

where E denotes the applied dc field, L the latent heat, ΔP_s the jump of spontaneous polarization if it exists, and $\Delta\epsilon$ the jump of permittivity. In the absence of ΔP_s,

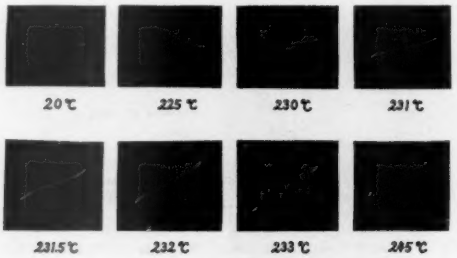

FIG. 5. Hysteresis loops of $PbZrO_3$ at rising temperatures. $E_{max}=20$ kv/cm.

[9] J. K. Hulm, Nature **160**, 127 (1947).

this equation can be written in the integrated form:

$$\Delta T_c = -(T_c/L)(\Delta\epsilon \cdot E^2/8\pi).$$

Upon inserting the observed values of $\Delta\epsilon = 2000$, $T_c = 506°K$ and $L = 300$ cal/mole, we get $\Delta T_c = -0.16°C$ for $E = 10$ kv/cm and $\Delta T_c = -0.62°C$ for $E = 20$ kv/cm. Although these values are smaller than the observed ones, at least the direction of the change is right.

B. Hysteresis Loops at an ac Amplitude of 30 kv/cm

Figure 8 shows the results of $E_{max} = 30$ kv/cm as a function of rising temperature. As seen in this figure,

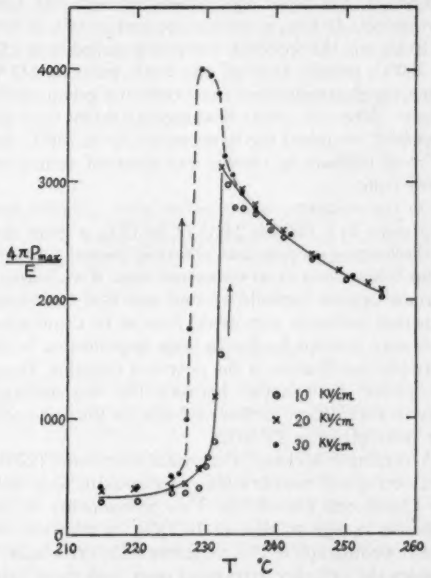

FIG. 7. $4\pi P_{max}/E$ of $PbZrO_3$ for 10 kv/cm, 20 kv/cm, and 30 kv/cm as a function of rising temperature.

anomalous hysteresis loops were observed near the Curie point, namely, at temperatures from 227° to 233°C. The temperature range becomes narrower with decreasing ac amplitude and completely disappears at a field strength of 23 kv/cm. Outside this anomalous range, D–E characteristics are almost strictly linear.

We have estimated the maximum polarization at 30 kv/cm and plotted the reduced values of $4\pi P_{max}/E$ in Fig. 7, in which for comparison the results for 20 kv/cm and 10 kv/cm are also plotted. The broken line in the figure corresponds to the region in which strange hysteresis loops, and accordingly an anomalous increase of polarization, are observed. The good agreement of these three curves with each other may be considered to be proof of the good linearity of the D–E characteristics over a sufficiently large amplitude of the ac field.

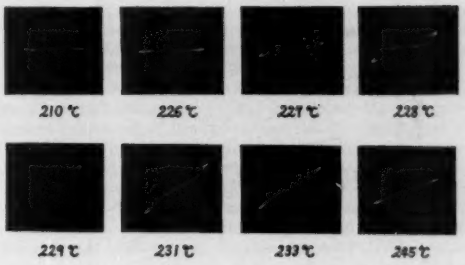

FIG. 8. Hysteresis loops of $PbZrO_3$ at rising temperatures. $E_{max} = 30$ kv/cm.

A careful study of Fig. 8 reveals that the anomalous hysteresis loops show a tendency toward saturation, as in the case of the normal hysteresis loops of barium titanate, suggesting that this substance shows ferroelectric characteristics if it is subject to this high field strength. Taking account of our assumption that $PbZrO_3$ may be antiferroelectric below its Curie point, we can at once arrive at a reasonable interpretation as schematically shown in Fig. 9. When the external field increases beyond a critical field E_c, the ferroelectric state may become more stable than the antiferroelectric one; hence typical hysteresis loops may be seen only above E_c. Such a situation should be realized if the free energy curves for this substance have characteristics as shown in Fig. 10. By the application of the external field it is certain that the free energy of the ferroelectric state, if compared with those of the antiferroelectric and paraelectric ones, must be lowered considerably.

This critical field E_c depends sensitively on the temperature and also on the amounts and species of the impurities contained in the specimen, though the reason is yet unknown. This field seems to be higher when the specimen is of higher purity. With increasing amounts of impurity or of Ti concentration in the $Pb(Zr-Ti)O_3$ series, E_c decreases until at last it becomes negative and a stable ferroelectric region appears between the para-

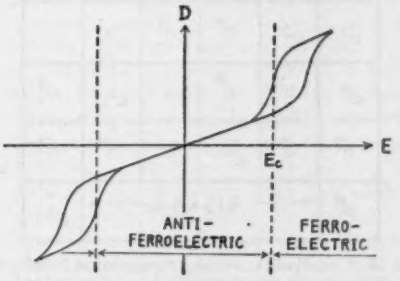

FIG. 9. Tentative explanation of the anomalous hysteresis loops of $PbZrO_3$ at 30 kv/cm.

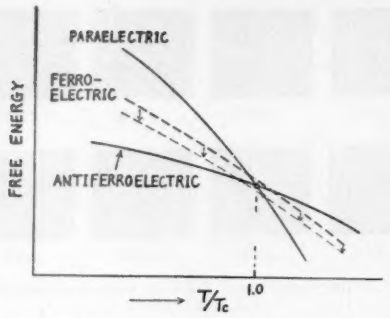

FIG. 10. Schematic curves for the free energies of the three phases of $PbZrO_3$. The free energy of the ferroelectric phase should be lowered by an electric field, as shown in this figure.

electric and antiferroelectric ones (Fig. 1). For the present specimen, E_c starts from about 23 kv/cm at 233°C and reaches about 30 kv/cm at 226°C. As already shown in Fig. 4 the Curie temperature *versus* the biasing dc field curve shows a saturation tendency at about 20 kv/cm. This effect will be understood if we take into account the fact that a ferroelectric state is forced to be realized under the very high field.

In the course of our observations we found an interesting phenomenon. If a specimen is heated or cooled several times through the Curie point, being always subject to a high ac field beyond E_c, it gradually shows large hysteresis loops of elliptic form at the vicinity of the Curie point; the loops may presumably be due to some increase in conductivity. At the same time, the specimen becomes more and more fragile, and is eventually reduced to a powder. Nevertheless, a Debye photograph of this specimen shows completely the same reflection patterns as those of the initial one.

This effect is probably due to the fact that the stresses produced in polycrystalline ceramics by the high field strength, which enforces alignment of the dipoles in one direction, are large enough to cause internal cracks. Such an effect has never been observed so long as the specimen is kept under a field not stronger than 23 kv/cm.

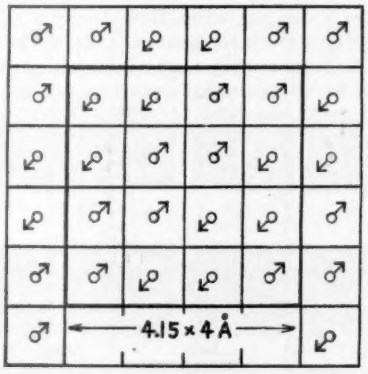

FIG. 11. A model of the atomic arrangement of $PbZrO_3$, (001) plane. Although the true symmetry may be orthorhombic, we choose here tetragonal axes. An arrow shows the displacement of a heavy ion (probably a Pb ion).

V. DISCUSSION

The close resemblance of the dielectric constant curves of $PbZrO_3$ and $BaTiO_3$ is insufficient by itself to secure the ferroelectricity of $PbZrO_3$. Rather, all the experimental facts described above seem to support unanimously our present assumption of the antiferroelectricity of $PbZrO_3$.

Further, the following pyroelectric test has been carried out. At first, under the application of a dc field of 10 kv/cm, the specimen was slowly cooled from 250° to 200°C, passing through the Curie point at 233°C. Then the electrodes were connected to a galvanometer circuit. After an initial discharging current had disappeared, we raised the temperature up to 250°C, but no more discharging current was observed around the Curie point.

On the contrary, whenever we gave a similar field treatment to a ceramic plate of $BaTiO_3$, a great deal of discharging current was observed around its Curie point.[10] Moreover, it was observed that, if we heated a barium titanate ceramic without any field treatment, a current (although very weak) flows at its Curie point. This may perhaps be due to some imperfection in the isotropic distribution of the polarized domains. Hence the above discrepancies between the two materials may be regarded as further evidence for the absence of net polarization in $PbZrO_3$.

According to Megaw,[11] the crystal structure of $PbZrO_3$ is a tetragonal modification of perovskite type with $a=4.150$A and $c/a=0.988$. This tetragonality is just opposite in sign to that of $BaTiO_3$. In addition, the Debye photograph of $PbZrO_3$ shows some extra lines[11,12] besides the ordinary tetragonal ones, and these extra lines completely disappear in the cubic region above the Curie point.[13] Attention must be paid to these extra lines, because an existence of superstructure is at least a necessary condition for antiferroelectricity.

We have synthesized minute single crystals and have examined several specimens of flake-like form under a polarization microscope. It turned out that single domain crystals show symmetry extinction and are biaxial crystals; that is to say, they do not have tetragonal symmetry but have an orthorhombic one, although the deviation from the tetragonal structure is very small. X-ray patterns[14] of this single crystal clearly show

[10] E. Sawaguchi and T. Akioka, J. Phys. Soc. Japan **4**, 117 (1949).
[11] H. D. Megaw, Proc. Phys. Soc. (London) **58**, 113 (1946).
[12] A. Hoffmann, Z. physik. Chem. **B28**, 65 (1935).
[13] R. Ueda and G. Shirane, J. Phys. Soc. Japan **6** 209 (1951).
[14] Sawaguchi, Maniwa, and Hoshino, presented at the meeting of the Phys. Soc. Japan on April 1, 1951, held at T.I.T. Tokyo, Japan.

the existence of a superstructure having a unit cell of $4a \times 4a \times c$. Our analysis, which is near completion, seems at present to give the atomic arrangement shown schematically in Fig. 11, in which an antiparallel set of dipolar orientations due to opposite shifts of heavy ions (probably Pb ions) may be noted. Details of the x-ray analysis will be published in the near future.

In conclusion, we wish to express our sincere thanks to Dr. S. Roberts for his many helpful comments on our work.

Note added in proof.—Recently, C. Kittel [Phys. Rev. **82**, 729 (1951)] discussed the possibility of realization of antiferroelectricity, showed that antiferroelectric crystals may be expected to occur in nature, and gave some criteria for identifying them. Very recently, S. Roberts [Phys. Rev. **83**, 1078 (1951)] has observed a very small but definite piezoelectric effect in polarized $PbZrO_3$ ceramic, in contrast to the negative result of our pyroelectric test. But the observed effect is very small, being approximately one-thousandth that of $BaTiO_3$, and this suggests that the spontaneous polarization of this crystal may also be so small that its detection by a pyroelectric test is beyond the limit of our apparatus. Our experiments have shown that the spontaneous polarization of $PbZrO_3$ may be, if it exists, far less than one-hundredth that of $BaTiO_3$. So it must be concluded, in reference to the recent result of x-ray analysis of $PbZrO_3$ single crystal by Sawaguchi, Maniwa, and Hoshino [Phys. Rev. **83**, 1078 (1951)], that $PbZrO_3$ is strongly antiferroelectric in the direction perpendicular to the c-axis and very weakly ferroelectric in the c-direction.

PHYSICAL REVIEW VOLUME 84, NUMBER 3 NOVEMBER 1, 1951

Bombardment of Copper with Tritons

D. N. KUNDU AND M. L. POOL
Ohio State University, Columbus, Ohio

(Received July 13, 1951)

Tritons have been accelerated to 6.5 Mev in a cyclotron and made to bombard stacks of copper foils. Among the triton induced reactions, the following have been identified: $Cu^{63}(t,d)Cu^{64}$ (12.9 hours), $Cu^{63}(t,n)$-Zn^{65} (250 days), $Cu^{63}(t,He^3)Ni^{62}$ (2.6 hours), and $Cu^{65}(t,p)Cu^{67}$ (2.44 days) with relative cross sections for the various reactions as 11:64:6:10, respectively. The Oppenheimer-Phillips process appears to be operative in case of tritons of this order of energy.

I. INTRODUCTION

TRITONS have already been used as bombarding particles for effecting nuclear reactions. In the earlier experiments,[1] the tritons had been produced by some suitable primary reaction, like Be+d, and the tritons thus obtained were then made to bombard various target nuclei. The maximum energy of the tritons was about 10.5 Mev. Later workers[2–5] used low-energy tritons and obtained reactions on tritium and lithium.

In the present investigations, tritium gas obtained in small amounts through the courtesy of the Isotopes Division of the Oak Ridge National Laboratory have been accelerated to 6.5 Mev in the cyclotron.[6] Various triton reactions with copper have been made. Relative cross sections and certain other reaction characteristics have been studied.

II. EXPERIMENTAL

A few cubic centimeters of tritium gas were sealed in glass capsules which were contained in a special housing connected to the cyclotron vacuum chamber through suitable capillary tubes and stop cocks. Arrangements were made so that from the outside the seal of a capsule could be crushed open and the gas fed between the dees in controlled amounts. The ion source was a single tungsten filament at the center of the vacuum chamber with the accelerating plates placed above and below the dee surfaces. The frequency of the oscillator was reduced from its normal 10.4 to 6.7 megacycles by the use of a bank of vacuum condensers placed in parallel both with the dee and the grid lines. The maximum current rating of the magnet could then be utilized. The natural leakage of the vacuum system was reduced to a practical minimum of 2 to 3 cc per hour. The gas from the exhaust of the backing pump was reinjected in controlled amounts through a closed recirculation system. The gaseous impurities introduced into the vacuum system through natural leakage consisted of nitrogen and oxygen. A stage of purification was incorporated in the circulation system so that the tritium could be freed from these gases, if and when necessary, with the use of a liquid hydrogen trap.

A stack of copper foils each 0.001 inch thick was mounted in a special target holder. The stack was thus shielded on all sides except for a small slot through which the triton beam bombarded the foils. The bombardment was continued, through the recirculation system, for two hours. The activities produced in

[1] D. N. Kundu and M. L. Pool, Phys. Rev. **72**, 101 (1947); **73**, 22 (1948).
[2] Sanders, Allen, Almquist, Dewan, and Pepper, Phys. Rev. **79**, 238 (1950).
[3] Los Alamos Group, Phys. Rev. **79**, 238 (1950).
[4] Allen, Almquist, Dewan, and Pepper, Phys. Rev. **81**, 315 (1951).
[5] E. Almquist, Can. J. Research **28A**, 433 (1950).
[6] Pool, Kundu, Weiler, and Donaven, **82**, 305 (1951).

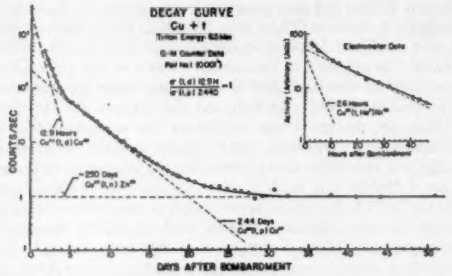

FIG. 1. Decay curve of the first copper foil after bombardment with 6.5-Mev tritons showing the half-lives 2.6 hours, 12.9 hours, 2.44 days, and 250 days.

individual foils were followed in the customary way with G-M counters and electrometers under the same geometry for each apparatus. Frequent absorption measurements were made at different stages of the decay to confirm the identification of the activities. From the extrapolated activities at the time of the termination of the bombardment, the saturation intensities corresponding to an infinite duration of bombardment for the various periods were calculated. Each saturation intensity was then converted into the number of disintegrations per second, I_∞, by taking into account the known disintegration scheme of the activity in question and also the counting characteristics of the instruments. For two activities produced from the same target isotope in the same bombardment, the relative cross section was estimated as $\sigma(1)/\sigma(2) = I_\infty(1)/I_\infty(2)$, where the numbers stand for the activities compared.

III. RESULTS

The decay curve of the first copper foil is given in Fig. 1. The insert shows the initial part of the decay made by use of an ionization chamber and electrometer. Each curve has been analyzed into its various component periods as indicated and these latter are separately examined in the following paragraphs. A similar study of the second foil is shown in Fig. 2. Here the activities are much lower in magnitude. The third and the rest of the deeper foils were also measured but no activity attributable to the triton bombardment was found. A few typical aluminum absorption measurements on the first copper foil are reproduced in Fig. 3, and are discussed below in conjunction with the corresponding periods.

2.44-Day Cu^{67}

This activity is found to be produced with considerable clearness in the first foil with an intensity at the end of the bombardment of 218 counts per second as seen in Fig. 1. The same activity was also produced in the second foil (Fig. 2) but the corresponding initial intensity was only 0.87 count per second. The absorption curve made 10 days after bombardment, shown in Fig. 3, was at a time when the activity was predominately of the 2.44-day half-life. This half-life is thus found to be associated with negatrons of maximum energy 0.54 Mev. The activity results from the reaction $Cu^{63}(t,p)Cu^{67}$ in agreement with the assignment made[7] on the basis of bombardments on enriched isotopes of Ni and on Cu and Zn.

If the relative stopping power of copper be taken as 2.56 mg/cm² as equivalent to 1 cm of air at 760 mm pressure and 15°C from the data of Mano,[8] the 6.5-Mev tritons will have a range of 2.16 mils in copper and will, therefore, penetrate into the third foil. The maximum energy of the tritons entering the first three foils are 6.5, 4.5, and 1.5 Mev, respectively. The (t,p) reactions thus proceeds with measurable yield of Cu^{67} with tritons of energy less than 4.5 Mev.

12.9-Hour Cu^{64}

This activity is produced only in the first and the second foils with initial intensities 2400 and 23 counts per second respectively as found from Figs. 1 and 2. Cu^{64} is known[9] to decay by the emission of 0.57-Mev negatrons (43 percent), 0.66-Mev positrons (21 percent) and K-capture (36 percent). The beta-end point measured at 0.61 Mev, and shown in Fig. 3, is approximately in agreement as a mean value. The reaction is $Cu^{63}(t,d)Cu^{64}$ or $Cu^{63}(t,np)Cu^{64}$.

2.6-Hour Ni^{65}

This half-life is observed only in the first foil. Part of the decay curve followed with the electrometer is shown in the insert in Fig. 1 from which it is seen that the ionization produced by this activity is comparable with that by the 12.9-hour Cu^{64}. The reaction is $Cu^{65}(t,He^3)Ni^{65}$. Here, as in the previous (t,d) case, the out-going

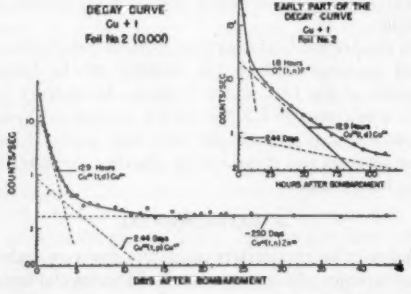

FIG. 2. Decay curve of the second copper foil after bombardment with 6.5-Mev tritons. The 1.8-hour F^{18} activity from traces of oxygen in the foil is seen in the initial part of the curve.

[7] D. N. Kundu and M. L. Pool, Phys. Rev. **78**, 488 (1950).
[8] G. Mano, Ann. phys. **1**, 407 (1934); J. phys. et radium **5**, 628 (1934).
[9] "Nuclear data," Circular of the National Bureau of Standards 499, p. 59, Sept. 1, 1950.

particle is probably a single He^3 nucleus rather than some other suitable number of separate particles. The ratio of the cross sections $\sigma^{65}(t,He^3)/\sigma^{65}(t,p)=0.6$.

250-Day Zn^{65}

An activity with a long half-life of approximately this duration was produced in the first and second foil only. The initial activity in the first foil was 1 count per second (Fig. 1) whereas in the second foil (Fig. 2), it is only 0.17 count per second. The reaction is $Cu^{63}(t,n)Zn^{65}$. The apparent low activity is understandable in the light of the disintegration characteristics[9] of Zn^{65}. This radioactive nucleus decays largely by K-capture (96.7 percent). However, the relative cross section on calculation is found to be $\sigma^{63}(t,d)/\sigma^{63}(t,n)=0.17$.

IV. DISCUSSION

The production of the 2.44-day activity definitely established that the bombarding agent had been tritons; for, this activity is not produced from copper by protons, deutrons, or alpha-particles. Also, because this activity was not produced beyond the triton range, the successive capture of two neutrons, available from spurious sources, is ruled out as a mechanism for the production of Cu^{67}.

When the isotopic abundances of Cu^{63} (69.09 percent) and Cu^{65} (39.91 percent) are taken into account along with the decay scheme of the radioactive product nuclei, the relative cross sections of the different reactions for 6.5-Mev tritons become $\sigma^{63}(t,n):\sigma^{63}(t,d):\sigma^{65}(t,p):\sigma^{65}(t,He^3)=64:11:10:6$. Therefore, it is evident that with tritons as bombarding particles, it is as easy to introduce a single neutron into a Cu^{63} nucleus and form Cu^{64} as it is to introduce two neutrons or a dineutron into Cu^{65} and form Cu^{67}.

The explanation as to how the 2.6-hour Ni^{65} activity could be formed appears to be interesting. The reaction involved is necessarily of the (t,He^3) type. The question arises, even though the tritons of 6.5 Mev could still form a compound nucleus, the out-coming He^3 will have to overcome a very steep potential barrier by virtue of its double charge. One way of explaining the phenomenon would be to suppose that the He^3 overcame the potential barrier on "borrowed energy" obtained from the building of the three added nucleons to the target Cu^{65} nucleus and returned the amount necessary to maintain energy conservation as it left the barrier. An alternative view may be to postulate that the triton never entered the target nucleus at all but thus was only a charge exchange between a neutron within the triton and a proton within the target nucleus when the triton was in the close vicinity of the nucleus. The phenomenon of charge exchange, however, is known so far only in the domain of very high energy collisions between nucleons.

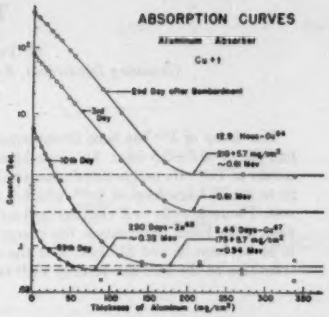

FIG. 3. Absorption curves on the first copper foil at different stages during the decay.

With regard to the (t,p) reaction, it may be asked whether a part at least of the observed yield was through a stripping process analogous to the Oppenheimer-Phillips[10] mechanism in deutron reactions. Compared to the deutron, the triton is a more tightly bound nucleus. However, the extent of the stripping in Oppenheimer-Phillips mechanism depends on the ratio of the kinetic energy of the bombarding particle to its binding energy. From the curves calculated by Bethe[11] in the case of the deutron, one finds that even when the ratio is $\frac{1}{2}$ the penetration probability by the Oppenheimer-Phillips process for copper is 10 times larger than that by the compound nucleus formation process although this ratio is hard to evaluate quantitatively due to the difficulties involved in the wave-mechanical treatment with the triton, it is still expected that for values of $\frac{1}{2}$ or even less, the Oppenheimer-Phillips process would contribute substantially to the total yield in the (t,p) and (t,d) reactions.

V. ACKNOWLEDGMENTS

It is a pleasure to acknowledge the help received from the Development Fund of the Ohio State University. Our indebtedness to Mr. F. G. Boyle and Col. E. C. Mallary for the valuable help in constructional details, and to Mr. Paul E. Wiler at the operational stage is gratefully acknowledged. Thanks are also due the Ghosh Board of the Calcultta University for providing travel facilities for one of the authors.

[10] J. R. Oppenheimer and M. Phillips, Phys. Rev. 48, 500 (1935).
[11] H. A. Bethe, Phys. Rev. 53, 39 (1938).

The Decay of I^{125}

G. Friedlander and W. C. Orr*
Chemistry Department, Brookhaven National Laboratory, Upton, New York†
(Received July 17, 1951)

The decay of I^{125} has been investigated. The nuclide decays entirely by orbital electron capture with a half-life of 60.0±0.5 days. An upper limit of 5×10^{-4} was set for the fraction of I^{125} decaying to the 58-day isomer of Te^{125}. By proportional counter and coincidence measurements it was established that all transitions go to the 35.4-kev level of Te^{125}, which is a $d_{3/2}$ state. The I^{125} ground state can be assigned a $d_{3/2}$ configuration. The ratio of L_I to K electron capture was determined to be between 0.18 and 0.45, with a most probable value 0.30. From these ratios, the energy difference between the ground states of I^{125} and Te^{125} was found to be between 95 and 215 kev, with the most probable value 115 kev. The corresponding fl values for the transition to the 35.4-kev level of Te^{125} fall in the range of allowed transitions.

A 56-day isotope of iodine was first reported by Reid and Keston[1] as a product of the deuteron bombardment of tellurium. Glendenin and Edwards[2] studied the radiations associated with this nuclide, found only K and L x-rays of tellurium, and gave convincing arguments for assignment to mass 125. Since Te^{125}, the product of the electron capture decay of I^{125}, has two well characterized low-lying levels[3–5] at 35.4 kev and at 145 kev (the latter is the 58-day isomeric state), it seemed of interest to investigate the decay scheme of I^{125} in further detail.

A sample of "I^{125}" prepared by deuteron bombardment of tellurium at the Washington University cyclotron was obtained carrier-free from the Isotopes Division of the AEC, in the form of a slightly basic iodide solution. After addition of carrier iodide, an aliquot of the sample was subjected to further radiochemical purification by means of cycles of oxidation of iodide to iodine, extraction into CCl_4, and reduction to iodide; the constant specific activity indicated the absence of non-isotopic radioactive impurities. Thin iodine samples for counting were prepared by reduction of an aqueous iodine solution with a copper foil; thin uniform films of cuprous iodide could thus be produced. Approximately 6 months were required after irradiation, before the 8-day I^{131} and 13-day I^{126} were no longer detectable. The decay curve plotted in Fig. 1 was started about 200 days after bombardment and shows a half-life of 60.0±0.5 days over a period of about 7 months.

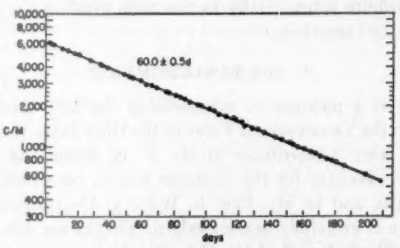

Fig. 1. Decay curve of I^{125}, started about 200 days after preparation of the source from Te+d bombardment.

To determine whether any of the I^{125} decays go through the 58-day isomeric state of Te^{125}, small amounts of tellurium and iodine carriers were added to a fraction of the iodine sample, exchange between the iodine activity and the carrier was assured by an oxidation-reduction cycle, and a tellurium fraction was carefully purified from iodine. The tellurium was found to be inactive; taking into account the chemical yield, the relative counting efficiencies of the G-M counter for the I^{125} and Te^{125} radiations, and the time since the previous purification of the iodine sample, a conservative upper limit of 5×10^{-4} can be set for the fraction of I^{125} decays going to the 58-day Te^{125m} isomer. This result supersedes the previously reported[6] indication of a growth of Te activity from an old I^{125} source.

Absorption experiments on an I^{125} sample showed the presence of K and L x-rays of the tellurium region, in agreement with the work of Glendenin and Edwards.[2] In a windowless counter, a very soft electron component, presumably Auger electrons, was also observed. With a krypton-filled proportional counter[5] and pulse-height analyzer[7] a 35-kev gamma-ray was found in the decay of I^{125}. The pulse-height distribution in the region of this gamma-ray and of the tellurium K x-rays is shown in Fig. 2. Comparison with a sample of 58-day Te^{125m} showed that the intensity ratio of 35-kev gamma-radiation to Te K x-rays in the I^{125} decay is 0.83±0.06 times that in the Te^{125m} decay. The presence of the characteristic 35.4-kev gamma-ray of Te^{125} in the iodine radiations serves as a confirmation of the assignment of the 60-day iodine to I^{125}.

From the relative intensities of the unconverted

* Permanent address: Department of Chemistry, University of Connecticut, Storrs, Connecticut.
† Research carried out under the auspices of the AEC.
[1] A. F. Reid and A. S. Keston, Phys. Rev. **70**, 987 (1946).
[2] L. E. Glendenin and R. R. Edwards, Phys. Rev. **71**, 742 (1947).
[3] R. D. Hill, Phys. Rev. **76**, 333 (1949).
[4] J. C. Bowe and G. Scharff-Goldhaber, Phys. Rev. **76**, 437 (1949).
[5] Friedlander, Perlman, and Scharff-Goldhaber, Phys. Rev. **80**, 1103 (1950).
[6] Friedlander, Goldhaber, and Scharff-Goldhaber, Phys. Rev. **74**, 981 (1948).
[7] Bernstein, Brewer, and Rubinson, Nucleonics **6**, No. 2, 39 (1950).

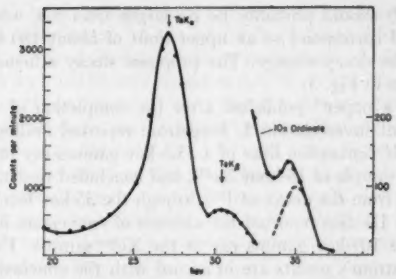

FIG. 2. Pulse-height spectrum of I^{125} taken in a krypton-filled proportional counter. The region of the 35-kev peak is shown on a magnified scale (ordinate readings on the right). The dashed curve is obtained by subtraction of the extrapolated tail of the K_β peak from the experimental curve.

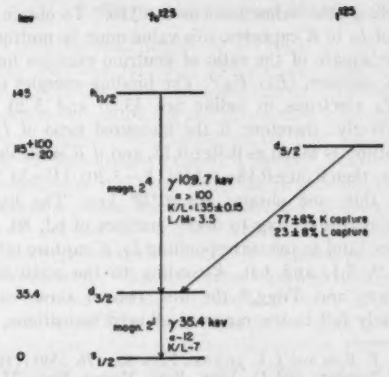

FIG. 3. Decay scheme of I^{125}, with the low-lying levels of Te^{125}. The internal conversion data are taken from references 4, 5, and 10.

35.4-kev gamma-rays and Te K x-rays in I^{125} and Te^{125m}, deductions about the fraction f_{35} of the I^{125} decays going to the 35.4-kev level and about possible L capture can be made. Let f_K be the fraction of the I^{125} atoms decaying by K electron capture (the remainder presumably decaying by L capture), y the K fluorescence yield of tellurium, c_K the fraction of 35-kev transitions converted in the K shell, and c_γ the fraction of 35-kev gamma-rays that are unconverted. The fraction of 109.7-kev transitions of Te^{125m} converted in the K shell (which contributes to the K x-ray intensity in Te^{125m}) can be deduced from the measurements[8,9] of the K/L and L/M ratios; a value of 0.51 ± 0.03 will be used for this conversion fraction. Then the number of Te K x-rays emitted per disintegration is $(f_K+f_{35}c_K)y$ for I^{125} and $(0.51+c_K)y$ for Te^{125m}. The number of 35.4-kev quanta emitted per disintegration is $f_{35}c_\gamma$ for I^{125} and c_γ for Te^{125m}. Therefore,

$$\frac{f_{35}c_\gamma}{(f_K+f_{35}c_K)y}=(0.83\pm0.06)\frac{c_\gamma}{(0.51\pm0.03+c_K)y}.$$

y and c_γ cancel, and the equation may be solved for f_K/f_{35},

$$f_K/f_{35}=(0.61\pm0.06)+(0.20\pm0.07)c_K.$$

It has been shown[5] that the fraction c_K is about 0.8 if the 35.4-kev transition is magnetic dipole, and about 0.3 if it is electric quadrupole. According to an analysis by Goldhaber and Sunyar[10] this transition is to be classified as magnetic dipole, with little or no admixture of electric quadrupole. Therefore c_K will be taken as 0.8, and f_K/f_{35} becomes 0.77 ± 0.08.

The following arguments show that essentially all the I^{125} decays go to the 35-kev level, i.e., that $f_{35}=1$. The spin of the ground state of Te^{125} has been measured[11] as 1/2. The 35.4- and 145-kev levels have been characterized[3,4] as $d_{3/2}$ and $h_{11/2}$ states, respectively, on the basis of shell theory and of the data on the Te^{125m} decay. Shell theory predicts that the ground state of I^{125}, with an even number of neutrons and 53 protons, should be $d_{5/2}$ or $g_{7/2}$, more probably $d_{5/2}$ because the spin of I^{127} is known to be 5/2, and odd numbered isotopes of an odd Z element differing by two mass numbers usually have the same spin. The $g_{7/2}$ configuration for I^{125} can actually be exluded on the following grounds. The $g_{7/2}\rightarrow d_{3/2}$ transition (to the 35.4-kev state) would be twice forbidden, and could therefore not take place with the observed lifetime unless the decay energy were very high (at least of the order of 1 Mev); on the other hand, with such a high decay energy, the first forbidden transition to the $h_{11/2}$ isomeric level in Te^{125} would then be expected to be much more prominent, in contradiction to experimental evidence. I^{125} must thus be assumed to be in a $d_{5/2}$ state. The transition to the $d_{3/2}$ 35.4-kev level then becomes allowed, that to the $s_{1/2}$ ground state twice forbidden, and a value $f_{35}=1$ is very plausible. Corroborative evidence for the fact that most if not all the I^{125} decays go to the 35-kev state was obtained from a photon-photon coincidence measurement with scintillation counters. The number of coincidences per photon was approximately the same for I^{125} as for Te^{125m}, in agreement with the proportional counter results. The statistics in the coincidence experiment were, however, poor.

If $f_{35}=1$, the fraction, f_K, of I^{125} decaying by K electron capture can now be taken as 0.77 ± 0.08, the remainder of the decays presumably occurring by L_I electron capture. The best value for the ratio of L_I to K capture is thus $0.23/0.77=0.30$, with the limits of error on f_K corresponding to ratios of 0.18 and 0.45. Although the uncertainty in the L_I to K ratio is large, some deductions about the decay energy of I^{125} are possible. The ratio of electron densities for the L_I and

[8] Hill, Scharff-Goldhaber, and Friedlander, Phys. Rev. 75, 324 (1949).
[9] Kern, Mitchell, and Zaffarano, Phys. Rev. 76, 94 (1949).
[10] M. Goldhaber and A. W. Sunyar, Phys. Rev. 83, 906 (1951).
[11] G. R. Fowles, Phys. Rev. 76, 571 (1949).

K shells at the iodine nucleus is 0.116.[12] To obtain the ratio of L_I to K captures, this value must be multiplied by the square of the ratio of neutrino energies for L_I and K capture, $(E_{L_I}/E_K)^2$. The binding energies of K and L_I electrons in iodine are 33.20 and 5.20 kev respectively; therefore, if the measured ratio of L_I to K captures is taken as 0.30 ± 0.15, and if E is the decay energy, then $0.30\pm0.15=0.116[(E-5.20)/(E-33.2)]^2$. From this, one obtains $E=80^{+\infty}_{-18}$ kev. The log(ft) values corresponding to decay energies of 62, 80, and 240 kev (and to the corresponding L_I/K capture ratios) are 4.9, 5.1, and 6.0. According to the analysis of Feenberg and Trigg,[13] the first two of these values definitely fall in the range of allowed transitions, but log(ft) should probably be no larger than 5.8, which would correspond to an upper limit of about 180 kev for the decay energy. The proposed decay scheme is shown in Fig. 3.

In a paper[14] published after the completion of the present investigation I. Bergström reported finding L and M conversion lines of a 35.5-kev gamma-ray in an aged sample of 18-hour Xe^{125}, and concluded that they arose from the decay of I^{125} through the 35-kev level of Te^{125}. He also reported the absence of conversion lines of the 109-kev gamma-ray in the Xe^{125} sample. Thus, Bergström's results are in accord with the conclusions drawn in the present paper.

Miss E. Wilson gave valuable aid in some of the measurements. The authors are indebted to Dr. M. Goldhaber for helpful discussions.

[12] M. E. Rose and J. L. Jackson, Phys. Rev. **76**, 1540 (1949).
[13] E. Feenberg and G. Trigg, Revs. Modern Phys. **22**, 399 (1950).
[14] I. Bergström, Phys. Rev. **82**, 111 (1951).

PHYSICAL REVIEW VOLUME 84, NUMBER 3 NOVEMBER 1, 1951

Configuration Interaction in the Pb III Spectrum

J. N. P. HUME AND M. F. CRAWFORD
McLennan Laboratory, University of Toronto, Toronto, Canada
(Received July 16, 1951)

The Slater and the configuration perturbation parameters were evaluated for configurations of Pb III by fitting the calculated to the observed term values. The wave functions of 52 levels were determined in terms of the (LS) functions, and for many of the levels were found to be linear combinations of the (LS) functions of two or more configurations. The g-values, hyperfine structure interval factors, and isotope shifts evaluated from the precise wave functions are in excellent agreement with the observed values. Thus the theory gives an internally consistent explanation of the spectroscopic properties. Since the isotope shifts were calculated as a field effect the agreement shows that the specific mass effect is relatively unimportant for heavy elements. The values of the shift and hyperfine structure interaction constant for the 6s electron obtained from this analysis are 0.50 cm^{-1} and 2.60 cm^{-1}, respectively.

I. INTRODUCTION

MANY calculations have been performed to test Slater's[1] theory of complex spectra for unperturbed configurations. The Slater method gives expressions for the energies of the levels arising from a given electronic configuration in terms of parameters which are integrals of the radial parts of the wave functions. The standard procedure is to evaluate these parameters from the observed energies of some of the levels and check them by calculating the energies of the other levels of the configuration. In a number of cases a more complete check has been effected by using these parameters to calculate the wave functions and from these wave functions evaluating other spectroscopic observables.[2–5] In those cases where the calculated values did not agree with the observed values the discrepancies were attributed in general to configuration interaction.

The theory of configuration interaction was formulated by Condon,[6] and Ufford and Shortley.[7] For the electrostatic interaction they have shown that, in an (LS) representation, there are off-diagonal matrix elements only between those levels of configurations of the same parity that have the same term-type L, the same multiplicity S, and the same J. In the case of perturbed configurations there are an increased number of parameters and it becomes much more important to check the theory by calculating other spectroscopic observables. Little has been done in the way of definite and detailed calculations of these effects.

Bacher[8] used numerical wave functions to calculate the off-diagonal matrix elements between the p^2 and sd configurations of Mg I and showed that the configura-

[1] J. C. Slater, Phys. Rev. **34**, 1293 (1929).
[2] D. R. Inglis and N. Ginsberg, Phys. Rev. **43**, 194 (1933).
[3] M. F. Crawford, Phys. Rev. **47**, 768 (1935).
[4] A. T. Goble, Phys. Rev. **48**, 346 (1935).
[5] J. B. Green and B. Fried, Phys. Rev. **54**, 876 (1938); and others.
[6] E. U. Condon, Phys. Rev. **36**, 1121 (1930).
[7] C. W. Ufford and G. H. Shortley, Phys. Rev. **42**, 167 (1932).
[8] R. F. Bacher, Phys. Rev. **43**, 264 (1933).

tion interaction was adequate to account for the anomalous distribution of the *sd* levels. Ufford,[9] Marvin,[10] Many,[11] and Rohrlich[12] have performed calculations and each noted that consideration of the configuration interactions improved the general agreement between their calculated and observed energies. Marvin[10] calculated wave functions for Co I and from these determined the effect of the perturbations on the Zeeman *g*-values. However, in Co I the coupling is near (*LS*) and since perturbations only occur between similar (*LS*) terms the *g*-values are not sensitive to configuration interaction.

A more critical test of the theory would be a detailed calculation for a spectrum in which there are strong configuration interactions, in which the coupling is such that the spectroscopic observables are sensitive to the interactions and finally for which the experimental values are known for comparison with the calculated values. Pb III is such a spectrum. Both its even and odd levels are highly perturbed. A fairly complete term analysis has been made for the spectrum,[13] and other spectroscopic observables are known for most of the levels. The hyperfine structure interval factors and isotope shifts have been measured by Crawford, McLay, and Crooker[13] and the *g*-values by Green and Loring.[14]

II. DETERMINATION OF THE PARAMETERS

A. Unperturbed Configurations

To evaluate the parameters appearing in the energy matrix from the observed energies of the levels of an unperturbed configuration the procedure is: (1) To set set up the energy matrices for the configuration in terms of the parameters (one matrix for each J value). (2) To equate the sum of the diagonal elements of each of these matrices to the sum of the observed energies of the levels with the corresponding value of J and obtain a set of linear equations for the parameters.

If there are more equations than parameters, a least-square method can be used to find the best values of the parameters. If the number of equations equals the number of parameters, the solution is direct. If there is one less equation than parameters, all parameters can be expressed in terms of one independent parameter. This independent parameter is then varied until the best fit between predicted and observed energies of the levels is obtained when the complete secular equations are solved. For unperturbed configurations the evaluation of the parameters is direct even for complicated configurations.

B. Perturbed Configurations

If the observed energies of the levels do not fit the energy matrices for each configuration separately a perturbation between configurations is indicated. The procedure for evaluating the parameters is the same as for unperturbed configurations except that the matrices for all configurations involved in the perturbation must be considered together, with the proper off-diagonal elements between them. The number of parameters will be the same as for the individual configurations without perturbations plus the off-diagonal parameters between levels of the same term-type and multiplicity. However, the number of diagonal sums is sharply reduced, by a factor of two or more, since all levels with the same J from all perturbing configurations must be included in one sum where before there were as many sums as configurations. In this case the number of linear equations is considerably less than the number of parameters. Thus there are an increased number of independent parameters. These independent parameters must be varied by successive approximations until the best fit of calculated and observed energies is obtained. This process of successive approximations is extremely complicated. In the Pb III spectrum there are two independent parameters for the even terms and six for the odd terms.

When it is necessary to use the method of successive approximations, often a good first approximation can be obtained by using the unperturbed values of the parameters. When this first approximation is not good, as is the case when the perturbation is appreciable, better estimates of certain of the parameters can be obtained from unperturbed levels of other configurations of the same spectrum or from data for configurations of other stages of ionization of the same element. However, these roughly estimated values of the parameters must be improved before any measure of the perturbation can be obtained.

For two perturbing configurations it was found convenient to split the diagonal sum equation for a given J value into two equations, each corresponding to the diagonal sum of an unperturbed configuration, and to correct these two parts by adding a parameter P to one equation and subtracting it from the other. In this way the diagonal sum for both configurations together is unchanged, while the sum for the individual configurations is altered due to perturbation. This "perturbation parameter" P is a measure of the off-diagonal element between configurations and replaces it as one of the independent parameters in the calculation. This can be extended to the case where more than two configurations are involved. For the odd terms there was a large amount of work in each approximation since it was necessary to expand a fifth- and a sixth-order determinant and solve the resultant secular equations for the energies of the levels. Thus it was important to gain from each calculation as much information

[9] C. W. Ufford, Phys. Rev. **44**, 732 (1933).
[10] H. H. Marvin, Phys. Rev. **47**, 521 (1935).
[11] A. Many, Phys. Rev. **70**, 511 (1946).
[12] F. Rohrlich, Phys. Rev. **74**, 1372 (1948).
[13] Crawford, McLay, and Crooker, unpublished data; Phys. Rev. **54**, 313(A) (1938). A. M. Crooker, Can. J. Research **A14**, 115 (1936).
[14] J. B. Green and R. A. Loring, Phys. Rev. **43**, 459 (1933).

TABLE I. $6snd$ configurations.

n	F_d	G_d	a_d	Energy levels $J=2$ calc.	obs.	diff.
6	155055	−3297	604	151758	151884	125
				158050	157925	
7	202512	726	259	201597	201597	0
				203302	203302	
8	221662	220	158	221301	221307	6
				221944	221938	
9	232295	123	102	232075	232097	22
				232464	232442	

as possible to permit the choice of an improved set of parameters for the next approximation. This was accomplished by leaving the off-diagonal elements between configurations as parameters in the numerical matrices even though, inherently, they were fixed by the choice of "perturbation parameters" P. The matrix then was converted to a secular determinant by introducing W into the diagonal terms and was expanded

TABLE II. $6snp$ configurations.

n	F_p	G_p	a_p	Energy levels $J=1$ calc.	obs.	diff.
6	82960	10183	12380	63965	64391	425
				75765	75340	
7	174981	664	3400	171290	171081	210
				176970	177181	
8	208400	283	1409	206968	206979	11
				209329	209318	

into several parts, namely, the unperturbed part (i.e., the determinant without contributions due to the presence of the off-diagonal elements between configurations) and parts in which the off-diagonal elements appeared as coefficients. These parts were plotted qualitatively against W to show the signs of the contributions of the various parts to the value of the determinant. The resultant of these graphs should be zero at

TABLE III. $6snf$ configurations.

n	F_f	G_f	a_f	Energy levels $J=3$ calc.	obs.	diff.
5	1353	−16	40	190279	189785	495
				190407	190901	
6	665	201	15	214455	214477	22
				214868	214846	

TABLE IV. Energies for $6p^2$.

J	calc.	obs.	diff.
2	183024	178432	4600
	160224	164818	
0	194783	188615	6170
	136382	142551	

the values of W that are observed energies of the levels. These "perturbation diagrams" are useful in determining the direction in which a parameter must be changed to improve the agreement between the calculated and observed values of the energies, and can be plotted from very approximate values of the parameters.

III. ENERGIES ON LEVELS NEGLECTING CONFIGURATION INTERACTION

The energy matrices for the configurations of Pb III are given in Condon and Shortley's *Theory of Atomic Spectra*.[15] For sl configurations the formulas are

$$
\begin{aligned}
&{}^3L_{l+1}=F_l-G_l+\tfrac{1}{2}la_l\\
&\left.\begin{matrix}{}^1L_l\\ {}^3L_l\end{matrix}\right\}=F_l-\tfrac{1}{4}a_l\pm[(G_l+\tfrac{1}{4}a_l)^2+\tfrac{1}{4}l(l+1)a_l^2]^{\frac{1}{2}} \qquad (1)\\
&{}^3L_{l-1}=F_l-G_l-\tfrac{1}{2}(l+1)a_l.
\end{aligned}
$$

The matrices for the other configurations can be obtained from the matrices in Table VII by neglecting the off-diagonal elements between configurations.

In evaluating the parameters some levels are fitted exactly while the entire error is forced into the remaining levels. For example in the sl configurations the levels with the highest and lowest J-values are fitted exactly. The energies of the levels are relative to ${}^1S_0$ of the $5d^{10}6s^2$ configuration as zero and are those given by Crawford, McLay, and Crooker.[13] Tables I to V give the parameters and the calculated and observed energies of the levels which are not fitted exactly. The units are wave numbers (cm^{-1}).

The results in Table I show good agreement between calculated and observed energies for $6s7d$, $6s8d$, and

TABLE V. Energies for $5d^96s^26p$.

J	calc.	obs.	diff.
1	197100	197319	−200
	183750	184268	−500
	175200	174600	+600
2	198800	199344	−500
	177650	177906	−250
	174600	173986	+600
	154550	154494	+ 50

[15] E. U. Condon and G. H. Shortley, *Theory of Atomic Spectra* (Cambridge University Press, London, 1935).

TABLE VI. Energy matrices for Pb III.

Even levels[a]

$J=3$		$J=1$		
Level	$^3D_3(sd)$	Level	$^3D_1(sd)$	$^3P_1(p^2)$
$^3D_3$	$F_d-G_d+a_d$	$^3D_1$	$F_d-G_d-(3/2)a_d$	
		$^3P_1$		$R_d-\frac{1}{2}R_e-\frac{1}{2}a_p$

$J=0$			
Level	$^3P_0(p^2)$	$^1S_0(p^2)$	$^1S_0(6s7s)$
$^3P_0$	$R_d-\frac{1}{2}R_e-a_p$	$-\sqrt{2}a_p$	
$^1S_0$		$R_d+(10/25)R_e$	D
$^1S_0$			F_e+G_e

$J=2$				
Level	$^3P_2(p^2)$	$^3D_2(p^2)$	$^1D_2(sd)$	$^3D_2(sd)$
$^3P_2$	$R_d-\frac{1}{2}R_e+\frac{1}{2}a_p$	$(1/\sqrt{2})a_p$		
$^1D_2$		$R_d+(1/25)R_e$	A	
$^1D_2$			F_d+G_d	$(3/2)^{\frac{1}{2}}a_d$
$^3D_2$				$F_d-G_d-\frac{1}{2}a_d$

Odd levels[b]

$J=0$			$J=4$		
Level	$^3P_0(d^9p)$	$^3P_0(sp)$	Level	$^3F_4(d^9p)$	$^3F_4(sf)$
$^3P_0$	$-F_0-7F_2$	B	$^3F_4$	$-F_0-2F_2$	C
	$+(3/2)a_d+\frac{1}{2}a_p$			$-a_d+\frac{1}{2}a_p$	
$^3P_0$		$F_p-G_p-a_{1p}$	$^3F_4$		$F_f-G_f+(3/2)a_f$

$J=1$					
Level	$^3P_1(sp)$	$^1P_1(sp)$	$^3P_1(d^9p)$	$^1P_1(d^9p)$	$^3D_1(d^9p)$
$^3P_1$	$F_p-G_p-\frac{1}{2}a_{1p}$	$\frac{1}{2}a_{1p}$	B		
$^1P_1$		F_p+G_p		B'	
$^3P_1$			$-F_0-7F_2$	$\frac{1}{2}\sqrt{2}a_d-\frac{1}{2}\sqrt{2}a_p$	$-\frac{1}{2}\sqrt{3}a_d-\frac{1}{2}\sqrt{3}a_p$
			$+\frac{1}{2}a_d+\frac{1}{2}a_p$		
$^1P_1$				$-F_0-7F_2+20G_1$	$(\frac{1}{2}\sqrt{6})a_d-(\frac{1}{2}\sqrt{6})a_p$
$^3D_1$					$-F_0+7F_2$
					$+(5/4)a_d-\frac{1}{2}a_p$

$J=3$					
Level	$^3F_3(sf)$	$^1F_3(sf)$	$^3F_3(d^9p)$	$^1F_3(d^9p)$	$^3D_3(d^9p)$
$^3F_3$	$F_f-G_f-\frac{1}{2}a_f$	$\sqrt{3}a_f$	C		
$^1F_3$		F_f+G_f		C'	
$^3F_3$			$-F_0-2F_2$	$(2/\sqrt{3})a_d+(1/\sqrt{3})a_p$	$-(\sqrt{2}/3)a_d-(\sqrt{2}/3)a_p$
			$+\frac{1}{2}a_d-\frac{1}{2}a_p$		
$^1F_3$				$-F_0-2F_2$	$-(1/\sqrt{6})a_d+(1/\sqrt{6})a_p$
				$+90G_2$	
$^3D_3$					$-F_0+7F_2$
					$-(5/6)a_d+\frac{1}{2}a_p$

$J=2$						
Level	$^3P_2(sp)$	$^3P_2(d^9p)$	$^3D_2(d^9p)$	$^1D_2(d^9p)$	$^3F_2(d^9p)$	$^3F_2(sf)$
$^3P_2$	$F_p-G_p+\frac{1}{2}a_{1p}$	B				
$^3P_2$		$-F_0-7F_2$	$9\sqrt{3}(-d'-p')$*	$9\sqrt{2}(-d'+p')$	0	
		$+(3\sqrt{5})(-3d'-p')$				
$^3D_2$			$-F_0+7F_2$	$(\sqrt{30})(5d'+p')$	$(4\sqrt{7})(-d'-p')$	
			$+(\sqrt{5})(5d'-p')$			
$^1D_2$				$-F_0+7F_2$	$-(2\sqrt{42})(-d'+p')$	
$^3F_2$					$-F_0-2F_2$	C
$^3F_2$					$-(8\sqrt{5})(-2d'+p')$	$F_f-G_f-2a_f$

[a] In the matrices for the even terms, p^2 refers to configuration $5d^{10}6p^2$, sd to configuration $6s6d$, $a_d=a_{6d}$ and $a_p=a_{6p}$.
[b] In the matrices for the odd terms sp refers to the $6s7p$ configuration, sf to the $6s5f$ configuration, and d^9p to the $5d^96s^26p$ configuration, $a_p=a_{6p}$, $a_d=a_{5d}$, and $a_f=a_{5f}$.
* Note $d'=(1/12\sqrt{5})a_{5d}$, $p'=(1/12\sqrt{5})a_{6p}$.

$6s9d$. We conclude that these levels are not perturbed. The agreement for the levels of $6s6d$ appears fairly good, but Bacher[8] has shown that a negative value of G_d is not probable. A strong perturbation is thus indicated.

Table II shows that the $6s6p$ and $6s7p$ configurations are perturbed. The $6s8p$ levels are not appreciably perturbed.

Table III shows that the $6s5f$ levels are strongly perturbed since a negative value of G_{5f} is not acceptable. The agreement for the $6s6f$ levels is fair, but from the detailed analyses of the other configurations there is

TABLE VII. $6sns$ configurations. T = term value relative to ionization. n^* = effective quantum number.

	$^3S_1$ sequence		$^1S_0$ sequence			
n	T obs.	$(n-n^*)$	T obs.	$(n-n^*)$	T calc.	diff.(T_c-T_0)
7	107438	3.967	103739	3.913	102640	−1100
8	59629	3.930	58121	3.877	58270	+ 150
9	38178	3.914	37612	3.875	37612	0
10	26568	3.903	26278	3.871	26278	0

evidence that the $J=3$ levels are displaced to higher term values by about 22 cm^{-1}. Assuming this displacement the parameters are $a_{6f}=15$ and $G_{6f}=180$. This perturbation of the $J=3$ levels has no appreciable effect on their wave functions.

The parameters calculated for the $6p^2$ configuration are $R_d=170{,}287$, $\frac{1}{2}R_e=6767$, $a_p=16{,}176$; and for the $5d^96s^26p$ configuration are $-F_0=176{,}786$, $F_2=510$, $G_1=586$, $a_{6p}=12{,}800$, $a_{5d}=8840$.

Tables IV and V show that both the $6p^2$ and $5d^96s^26p$ configurations are highly perturbed. The $J=3$ levels for $5d^96s^26p$ have not been calculated since there are insufficient experimental observations.

IV. ENERGIES CONSIDERING PERTURBATIONS

The energy levels of configurations that are shown by the calculations in the previous section to be perturbed are recalculated taking configuration interaction into account. The off-diagonal elements were calculated explicitly in terms of the integrals of the radial parts of the wave functions. However, it is not necessary to know the exact form of these elements unless they are to be evaluated absolutely, as Bacher[8] did, from central-field wave functions. Hence in the matrices of Table VI the off-diagonal elements between configurations are merely written as parameters A, B, C, etc.

A. Even Levels

The levels of $6s6d$, $6p^2$, and $6s7s$ perturb each other. If the "perturbation parameters" P are added to the diagonal sum equations for these configurations we obtain 7 linear equations in 9 unknowns. Thus we have two independent parameters which must be varied until the best fit of all calculated and observed energies is obtained. Fortunately a good estimate of one parameter can be made by examining the perturbation of the $^1S_0$ and $^3S_1$ levels of the $6sns$ series. The Rydberg-Ritz relationship $n-n^*=a+bT$ predicts that a plot of T, the term value relative to ionization, against $(n-n^*)$, the quantum defect, should be a straight line for an unperturbed sequence. A plot of the data in Table VII shows that the $^3S_1$ sequence is unperturbed, but that the $^1S_0$ sequence is perturbed by a level between the $n=7$ and $n=8$ members. Considering the $n=9$ and $n=10$ members of the $^1S_0$ sequence as unperturbed and drawing a straight line through them the unperturbed positions of the $n=7$ and $n=8$ members can be estimated. Since the displacement of the $n=8$ member from its unperturbed position is very much less than the displacement of the $n=7$ member, as seen from Table VII, the perturbation calculation was simplified by including only the $n=7$ member.

The one remaining independent parameter was then varied and the best fit was obtained with the following values of the parameters: $R_d=167{,}047$, $\frac{1}{2}R_e=6367$, $a_p=10{,}500$, $F_{6d}=159{,}555$, $G_{6d}=1201$, $a_{6d}=605$, and $F_{7s}+G_{7s}=154{,}983$. The off-diagonal elements are $A=10{,}300$ and $D=10{,}210$. The energies and wave functions calculated using these values of the parameters are shown in Table VIII. All levels which were perturbed have been brought into agreement with the observed values to within an average error of 100 cm^{-1}. For the unperturbed calculations the average error was 3600 cm^{-1}. This improvement in the agreement is a good confirmation of the theory of configuration interaction, but a more complete check will be effected by using these wave functions to compute the g-values, hfs interval factors and isotope shifts in Sec. V.

B. Odd Levels

The unperturbed calculations for the odd configurations $6s6p$, $6s7p$, $5d^96s^26p$, and $6s5f$ indicate a mutual perturbation of their levels. It would be extremely difficult to handle a calculation if all four configurations were considered at one time. Only the mutual perturbation of $5d^96s^26p$, $6s7p$, and $6s5f$ was considered. It was possible, however, to make approximate allowances in this calculation for the effect of $6s6p$ on the other three configurations. This was accomplished by examining the perturbation of the $6snp$ series using the Rydberg-Ritz relationship. From this relationship the approximate unperturbed positions of the $6snp$ levels were determined and a set of parameters fitted to these values. The Rydberg-Ritz relationship showed that for $6s6p$ the $J=0$ level is perturbed relatively more than the other levels. Accordingly only the $J=0$ level of $6s6p$ was included in the diagonal sum equations of $6s7p$, $5d^96s^26p$, and $6s5f$. The calculated energies and wave functions of the $6s6p$ levels listed in Table VIII are obtained from the parameters $F_{6p}=83{,}100$, $G_{6p}=9900$ and $a_{6p}=12{,}000$; in addition for the $J=0$ level a displacement of -700 cm^{-1} arising from the perturbation by $6s7p$ and $5d^96s^26p$ is included.

When the perturbation parameters P were included in the unperturbed diagonal sums there were 7 equations for 13 parameters (i.e., 6 independent parameters). The value of the magnetic parameter a_{7p} was estimated from a_{6p} and a_{8p} to be approximately 3100. The value of a_{6p} to be used for the $5d^96s^26p$ configuration was known from other configurations to be between 12,000 and 13,000. Liberal use was made of the perturbation diagrams described in Sec. II in arriving, after many trials, at the final set of parameters. The parameters are $-F_0=176{,}926$, $F_2=572$, $G_1=578$, $a_{6p}=12{,}900$, $a_{5d}=8780$, $G_{7p}=1100$, $F_{7p}=175{,}050$, $a_{7p}=3100$, and the

TABLE VIII. Wave functions, calculated and measured observables.

Even levels

Level[a]	Calc.	Obs.	Diff.	Wave function	g-Value calc.	g-Value obs.	hfs int. factor calc.	hfs int. factor obs.	Isotope shift calc.	Isotope shift obs.
2_0	142545	142551	+6	$+0.832(^3P_0p^2)+0.429(^1S_0p^2)-0.351(^1S_06s7s)$	···	···	0	0	−0.45	−0.4
3_1	150084	150084	0	$+1.00(^3S_16s7s)$	2.00	1.98	1.54	1.53	+0.06	+0.06
4_2	152045	151885	−160	$-0.323(^3P_2p^2)+0.605(^1D_2p^2)-0.723(^1D_26sd)+0.089(^3D_26sd)$	1.05	1.06	0.09	*	−0.24	−0.25
5_0	153785	153783	−2	$-0.433(^3P_0p^2)+0.105(^1S_0p^2)-0.895(^1S_06s7s)$	···	···	0	0	−0.10	−0.10
6_1	155432	155432	0	$+1.00(^3P_1p^2)$	1.50	···	−0.07	*	−0.50	−0.44
7_1	157444	157444	0	$+1.00(^3D_16sd)$	0.50	0.50	−0.65	−0.62	0	−0.06
8_2	158070	157925	−145	$-0.070(^3P_2p^2)+0.077(^1D_2p^2)-0.032(^1D_26sd)-0.993(^3D_26sd)$	1.16	1.15	0.18	0.29	0	0.00
9_2	158957	158957	0	$+1.00(^3D_26sd)$	1.33	1.33	0.43	0.44	0	0.00
10_3	164325	164818	+493	$-0.828(^3P_2p^2)+0.179(^1D_2p^2)+0.528(^1D_26sd)+0.063(^3D_26sd)$	1.34	1.40	−0.02	*	−0.36	−0.32
11_2	178615	178432	−183	$+0.452(^3P_2p^2)+0.772(^1D_2p^2)+0.446(^1D_26sd)+0.014(^3D_26sd)$	1.10	···	0.00	*	−0.40	−0.40
12_0	188615	188615	0	$-0.346(^3P_0p^2)+0.898(^1S_0p^2)+0.272(^1S_06s7s)$	···	···	0	0	−0.46	···
13_1	197893	197893	0	$+1.00(^3S_16s8s)$	2.00	2.00	1.44	1.43	+0.03	+0.03
14_0	199250	199401	+151	$+1.00(^1S_06s8s)$	···	···	0	0	+0.03	+0.03
15_1	201399	201399	0	$+1.00(^3D_16s7d)$	0.50	0.50	−0.65	−0.68	0	0.00
16_2	201597	201597	0	$-0.187(^1D_26s7d)+0.982(^3D_26s7d)$	1.16	1.16	0.40	0.41	0	0.00
17_2	202047	202047	0	$+1.00(^1D_26s7d)$	1.33	1.33	0.43	0.43	0.00	0.00
18_2	203302	203302	0	$+0.982(^1D_26s7d)+0.187(^3D_26s7d)$	1.00	0.98	−0.19	−0.19	0.00	0.00
25_1	221205	221205	0	$+1.00(^3D_16s8d)$	0.50	···	−0.65	···	0.00	···
26_2	221301	221307	+6	$-0.318(^1D_26s8d)+0.949(^3D_26s8d)$	1.15	···	0.52	···	0.00	···
27_2	221600	221600	0	$+1.00(^1D_26s8d)$	1.33	···	0.43	···	0.00	···
28_2	221944	221938	−6	$+0.949(^1D_26s8d)+0.318(^3D_26s8d)$	1.02	···	−0.30	···	0.00	···
35_1	232019	232019	0	$+1.00(^3D_16s9d)$	0.50	···	−0.65	···	0.00	···
36_2	232075	232097	+22	$-0.344(^1D_26s9d)+0.937(^3D_26s9d)$	1.14	···	0.53	···	0.00	···
37_2	232274	232274	0	$+1.00(^1D_26s9d)$	1.33	···	0.43	···	0.00	0.00
38_2	232464	232442	−22	$+0.937(^1D_26s9d)+0.344(^3D_26s9d)$	1.02	···	−0.31	···	0.00	···

Odd levels[b]

Level	Calc.	Obs.	Diff.	Wave function	g-Value calc.	g-Value obs.	hfs int. factor calc.	hfs int. factor obs.	Isotope shift calc.	Isotope shift obs.
1_0°	60500	60397	−100	$+0.996(^3P_06s6p)-0.083(^3P_16s7p)$						
2_1°	64650	64391	−250	$-0.282(^3P_16s6p)+0.905(^3P_16s6p)$						
3_2°	79200	78985	−200	$+1.00(^3P_26s6p)$						
4_1°	95550	95340	−200	$+0.905(^3P_16s6p)+0.282(^3P_16s6p)$						
5_2°	154480	154494	−14	$-0.063(^3P_2sp)+0.805(^3P_2d^2p)+0.501(^3D_2d^2p)$	1.36	···	0.06	···	+0.49	···
				$-0.268(^1D_2d^2p)+0.155(^3F_2d^2p)$						
6_2°	···	···		No wave function calculated						
7_0°	171022	170917	−105	$+0.080(^3P_06s6p)+0.993(^3P_06s7p)+0.080(^3P_0d^2p)$	···	···	0	0	0	0.0
8_1°	170945	171081	+136	$-0.884(^3P_1sp)+0.380(^1P_1sp)+0.239(^3P_1d^2p)$	1.42	1.38	1.19	1.23	+0.04	+0.05
				$+0.032(^1P_1d^2p)+0.127(^3D_1d^2p)$						
9_0°	173330	173329	−1	$+0.996(^3F_0d^2p)+0.083(^3F_3sf)$	1.25	···	0.08	···	+0.50	···
10_2°	174080	173986	−94	$+0.510(^3P_2sp)-0.424(^3P_2d^2p)+0.374(^3D_2d^2p)$	1.14	0.97	0.30	0.23	+0.37	+0.46
				$-0.360(^1D_2d^2p)+0.538(^3F_2d^2p)-0.020(^3F_3sf)$						
11_1°	174630	174601	−29	$-0.071(^3P_1sp)-0.564(^1P_1sp)+0.635(^3P_1d^2p)$	1.14	1.135	0.03	0.00	+0.34	+0.35
				$-0.388(^1P_1d^2p)+0.354(^3D_1d^2p)$						
12_2°	176100	176023	−77	$-0.834(^3P_2sp)-0.268(^3P_2d^2p)+0.155(^3D_2d^2p)$	1.32	1.34	0.51	0.55	+0.15	+0.12
				$-0.077(^1D_2d^2p)+0.445(^3F_2d^2p)-0.063(^3F_3sf)$						
13_1°	177130	177181	+51	$+0.460(^3P_1sp)+0.619(^1P_1sp)+0.486(^3P_1d^2p)$	1.14	1.15	−0.32	−0.38	+0.20	+0.20
				$+0.071(^1P_1d^2p)+0.412(^3D_1d^2p)$						
14_2°	177950	177906	−44	$+0.138(^3P_2sp)+0.200(^3P_2d^2p)-0.114(^3D_2d^2p)$	0.90	1.08	0.12	0.16	+0.48	+0.46
				$+0.728(^1D_2d^2p)+0.629(^3F_2d^2p)-0.022(^3F_3sf)$						
15_2°		178957		No wave function calculated, mainly (d^2p)						
16_1°	184260	184268	+8	$-0.063(^3P_1sp)-0.336(^1P_1sp)-0.032(^3P_1d^2p)$	0.92	0.96	0.10	0.10	+0.44	+0.45
				$+0.840(^1P_1d^2p)+0.421(^3D_1d^2p)$						
17_3°		189785		No wave function calculated, mainly (sf)				*		0.0
18_2°	190260	190288	+28	$-0.020(^3P_2d^2p)+0.045(^3D_2d^2p)+0.045(^1D_2d^2p)$	0.67	0.67	−0.42	−0.40	+0.01	+0.06
				$+0.077(^3F_2d^2p)+0.994(^3F_3sf)$						
19_4°	190430	190429	−1	$+0.996(^3F_3sf)-0.083(^3F_4d^2p)$	1.25	1.25	0.32	0.31	0.00	0.0
20_3°		190901		No wave function calculated, mainly (sf)				0.09		+0.04
21_0°	192675	192880	+205	$+0.996(^3P_0d^2p)-0.083(^3P_06s7p)$	···	···	0	0	+0.50	···
22_3°		196847		No wave function calculated, mainly (d^2p)						+0.50
23_1°	197470	197319	−151	$+0.100(^3P_1sp)-0.579(^3P_1d^2p)-0.362(^1P_1d^2p)$	0.91	···	0.14	···	+0.49	···
				$+0.725(^3D_1d^2p)$						
24_2°	199240	199344	+104	$+0.235(^3P_2d^2p)-0.752(^3D_2d^2p)-0.490(^1D_2d^2p)$	1.07	···	0.21	···	+0.50	···
				$+0.366(^3F_2d^2p)+0.055(^3F_3sf)$						
25_0°	206809	206809	0	$+1.00(^3P_06s8p)$						
26_1°	206968	206979	+11	$+0.877(^3P_16s8p)-0.480(^1P_16s8p)$						
27_2°	208922	208922	0	$+1.00(^3P_26s8p)$						*
28_1°	209329	209318	−11	$+0.480(^3P_16s8p)+0.877(^1P_16s8p)$						*
29_4°	214434	214434	0	$+1.00(^3F_46s6f)$						
30_3°	214455	214477	+22	$+1.00(^3F_36s6f)$						
31_2°	214486	214486	0	$+1.00(^3F_26s6f)$						
32_4°	214824	214846	+22	$+1.00(^1F_36s6f)$						

[a] The level numbers are not those given by Crooker (reference 13), but can be correlated by their term values.
* The asterisk indicates that the measurements show that the hfs interval factor is small.
[b] In the table for the odd levels sp refers to the $6s7p$ configuration, sf to the $6s5f$ configuration, and d^2p to the $5d^96s^26p$ configuration.

off-diagonal parameters $B=1700$, $B'=-3000$, $C=1400$, also $F_{5f}-G_{5f}-2a_{5f}=190{,}150$.

An approximate calculation was carried out for the $J=3$ levels, but since the 6_3^o level has not been located the calculated values of the energies are much more uncertain. On this account, the wave functions were not calculated for the $J=3$ levels. The 6_3^o level would have largely $5d^96s^26p$ character and thus the only strong transitions would be with $5d^96s^26d$ levels. These transitions would be in the ultraviolet and thus difficult to observe. The other $J=3$ levels from the d^9p configuration have more of the $6s5f$ character. It is because of this that their combinations with levels of sd character were sufficiently strong to be observed.

Although these calculations for the odd levels were extremely complicated the agreement as shown by the energy differences in Table VIII is excellent. The error for the perturbed levels has been reduced from an average of approximately 400 cm^{-1} in the unperturbed calculation (Table V) to an average error of less than 100 cm^{-1} in the perturbed calculation. This final error is well within the limit of accuracy of the numerical solution of the determinants. This does not appear to be a large correction, but since the odd configurations overlap each other this perturbation of the energies represents a large perturbation of the wave functions. Thus we have an appreciable intermingling of the character of the interacting levels. The wave functions of the levels can now be calculated from the numerical energy matrices as linear combinations of the (LS) wave functions of the mutually perturbing configurations. The coupling coefficients in the linear combinations are the elements of the transformation matrices which will convert the energy matrix in the (LS) representation to the intermediate system, that is, will diagonalize the energy matrix.[4]

V. CALCULATION OF THE OTHER SPECTROSCOPIC OBSERVABLES

The wave function of a given level is expressed as a linear combination of the (LS) wave functions by means of the (LS) coupling coefficients K or as a linear combination of the (jj) wave functions by means of the (jj) coupling coefficients C. From these coupling coefficients the other spectroscopic observables can be calculated. The values of the wave functions in (LS) representation, and the calculated spectroscopic observables (g-values, hfs interval factors and isotope shifts) appear in Table VIII. The observed values are listed in the table for comparison.

A. g-Values

The Zeeman g-values can be calculated simply from the (LS) g-values and the (LS) coupling coefficients of the levels.[16] The calculation of the g-values using the wave functions determined from the energy levels does not involve the introduction of any additional experimentally determined quantity. This is a good independent check of the wave functions because in Pb III where the coupling is not near (LS) the g-values are sensitive to the perturbation.

For the most part the calculated g-values are in excellent agreement with the observed g-values. There seems to be a slight discrepancy in the values for the 10_2^o and 14_2^o levels. The g-value for the former is too high and the latter too low by approximately the same amount. The calculation for these levels is extremely sensitive to the perturbation and it is possible that the evaluation of the intermingling of their characters is slightly in error.

B. Hyperfine Structure Interval Factors

The hyperfine structure (hfs) interval factors of the various levels of the configurations can be calculated by the method of Breit and Wills[17] as functions of the hfs interaction constants of the valence electrons and the coefficients, C's, of the (jj) wave functions. The hfs interval factor $a(J)$ of a level of a many-electron configuration is a function of the one-electron interaction constants $a(j)$. The formula for a non-s electron as given by Goudsmit[18] is

$$a(j)=\frac{\Delta\nu l(l+1)K(j,Z_i)g(I)}{Z_i j(j+1)(l+\frac{1}{2})\lambda(l,Z_i)1838}=\begin{cases}a' & \text{for } j=l+\frac{1}{2}\\ a'' & \text{for } j=l-\frac{1}{2}.\end{cases} \tag{2}$$

For an s electron the interaction constant is

$$a(s)=\frac{8Ra^2Z_iZ_0^2K(\frac{1}{2},Z_i)g(I)}{3n^{*3}1838}. \tag{3}$$

The symbols are defined by Goudsmit. If two configurations interact the wave function for each level is expressed as a linear combination of the (jj) wave functions of all levels with the same J. Thus the hfs interval factor of a given level can be written in terms of the one-electron interaction constants and the (jj) coupling coefficients for that level. The C's are calculated from the (LS) coupling coefficients K by means of the $(jj)\leftrightarrow(LS)$ transformation matrices.[15] The $a(j)$'s can be calculated from Goudsmit's formulas (2) and (3) if $g(I)$ is obtainable from an unperturbed J level.

The hfs formulas for the p^2, sf, sd, sp, and $nsn's$ configurations are given by Breit and Wills.[17] The formulas for a d^9p configuration are the same as for a dp configuration and have been calculated for this work. They are

$$A(J=4)=\tfrac{5}{8}a_d'+\tfrac{3}{8}a_p',$$

$$A(J=3)=(1/24)C_1^2(17a_d'+7a_p')+\tfrac{1}{2}C_2^2(a_d''+a_p')+\tfrac{1}{8}C_2^2(5a_d'+a_p'')+(1/3)^{\frac{1}{2}}C_1C_2a_d'''-(5/9)^{\frac{1}{2}}C_1C_3a_p''';$$

[15] J. B. Green, Phys. Rev. **64**, 151 (1943).

[17] G. Breit and L. A. Wills, Phys. Rev. **44**, 470 (1933).

[18] S. Goudsmit, Phys. Rev. **37**, 663 (1931) and **43**, 636 (1933).

where the C's are defined by the relation,

$$(3)_3 = C_1(5/2,3/2)+C_2(3/2,3/2)+C_3(5/2,1/2),$$

in which $(3)_3$ symbolizes the wave function of a state with $J=3$, $m=3$ in intermediate coupling and $(5/2,3/2)$ symbolizes the (jj) wave function of the state $J=3$, $m=3$ arising from the $(5/2,3/2)$ jj-sub group, and so on.

$$A(J=2) = (1/12)C_1^2(11a_d'+a_p')+\tfrac{1}{2}C_2^2(a_p'+a_d'') +\tfrac{1}{6}C_3^2(7a_d'-a_p'')+\tfrac{1}{4}C_4^2(3a_d''+a_p'') +(7/3)^{\frac{1}{2}}C_1C_2a_d'''-(14/9)^{\frac{1}{2}}C_1C_3a_p''' -\sqrt{2}C_3C_4a_p'''+(2/3)^{\frac{1}{2}}C_3C_4a_d''',$$

where

$$(2)_2 = C_1(5/2,3/2)+C_2(3/2,3/2) +C_3(5/2,1/2)+C_4(3/2,1/2).$$

$$A(J=1) = \tfrac{1}{4}C_1^2(7a_d'-3a_p')+\tfrac{1}{2}C_2^2(a_d''+a_p') +\tfrac{1}{4}C_3^2(5a_d''-a_p'')-(3/5)^{\frac{1}{2}}C_1C_2a_d'''-\sqrt{3}C_2C_3a_p''',$$

where $(1)_1 = C_1(5/2,3/2)+C_2(3/2,3/2)+C_3(3/2,1/2)$.

A value of $a_{6s}=2.60$ cm^{-1} is obtained from the hyperfine structure of the $^3D_1$ and $^3D_3$ levels of $6s6d$ and $6s7d$. These levels are unperturbed and independent of coupling and give the value of a_{6s} to within 4 percent. Using this value of a_{6s} and Goudsmit's formulas we can calculate the values of the interaction constants for the other electrons. From the term value of $5d^{10}6s$ of Pb IV $n^*=2.265$ for the $6s$ electron, $Z_i=78$, $Z_0=4$. Thus we obtain from Eq. (3) a value of $g(I)=0.99(4)$. Substituting this value in Eq. (2) and using for the p electron $Z_i=78$ and $\Delta\nu_{6p}=18{,}000$ we find $a_{6p}''=0.52$ and $a_{6p}'=0.05$. Using also $\Delta\nu_{7p}=4000$ we obtain $a_{7p}''=0.13$ and $a_{7p}'=0.01$. For the d electron an approximate value of $Z_i=70$ was used.[19] Thus $\Delta\nu_{5d}=22{,}000$ gives $a_{5d}''=0.21$ and $a_{5d}'=0.09$. The other interaction constants a_{6p}''', a_{7p}''', a_{5d}''', a_{6d}', a_{6d}'', and a_{6d}''' are all negligible. These values show that the contributions of the $6p$ and $5d$ electrons to the hfs interval factor of a level cannot be neglected relative to the contribution of the $6s$ electron. However, since in general they are appreciably smaller than a_{6s}, they need not be known to the same precision. Hence, the approximate values calculated here are adequate.

Even Levels

The calculated hfs of all the levels are in very good agreement with the observations. For those levels for which the hfs has been resolved the quantitative agreement is quite satisfactory. For those levels whose hyperfine structures have not been resolved the agreement is also satisfactory in that the theory predicts small interval factors.

Odd Levels

The calculated values of hfs interval factors are in good agreement with those measured by Crooker except in two respects: Firstly, the values for the $10_2°$ and $14_2°$ levels indicate that there is a slight error in the wave functions for these levels as evidenced also from the calculation of their g-values. Secondly, the interval factor given by Crooker for $16_1°$, designated $c8_1°$ in his paper, is ~ -0.2 cm^{-1} compared to the predicted value $+0.1$. Crooker inferred a negative interval for this level because no Pb^{207} component was directly observable in the patterns of 32384 cm^{-1} ($4_2-16_1°$) and 30485 cm^{-1} ($5_0-16_1°$), indicating that the stronger Pb^{207} components were merged with the Pb^{206} and Pb^{208} components. This single discrepancy suggested that possibly Crooker's conclusion was in error. Accordingly the structures of these two lines were re-examined with a Leeds and Northrup microphotometer and their density contours reduced to intensity contours. The contour of 32384 cm^{-1} showed that the two clearly resolved components had an intensity ratio equal to the relative abundance of Pb^{206} and Pb^{208}, and that between these two components there was the intensity contribution expected for the Pb^{207} components. The intensity between these two components cannot be ascribed to lack of resolution since on the same plate another two-component pattern with smaller separation showed a much deeper minimum. The hfs separation of $16_1°$ then must be normal, and smaller than the separation of the level 4_2 since a well-defined Pb^{207} component was not observed between the even isotopic components. An analysis of the intensity contour of 30485 cm^{-1} confirmed this conclusion. Thus the interval factor of $16_1°$ is $+0.10$ cm^{-1}, in agreement with the calculated value.

This comparison forms an independent check on the validity of the wave functions determined from the multiplet structure since effectively only one observable, namely $a_{6s}=2.60$,[20] has been used in addition to the wave functions determined from the energies. The values of the hfs interaction constants of the other valence electrons were calculated by the approximate formulas of Goudsmit.[18] Undoubtedly, by making a slight adjustment in these interaction constants a closer agreement between predicted and observed values could have been obtained. However, the consistency of the theory is more clearly illustrated by using the minimum number of experimentally determined quantities.

C. Isotope Shifts

The theory of isotope shifts in heavy elements was developed by Bartlett,[21] Rosenthal and Breit,[22,23] and Racah.[24] According to their theory the levels of the lighter isotope will be slightly more stable than the

[19] E. Fermi and E. Segrè, Z. Physik 82, 729 (1933).

[20] This value leads to a nuclear magnetic moment in good agreement with that obtained by the induction method. Schawlow, Hume, and Crawford, Phys. Rev. 76, 1876 (1949).

[21] J. H. Bartlett, Nature 128, 408 (1931).

[22] J. E. Rosenthal and G. Breit, Phys. Rev. 41, 459 (1932).

[23] G. Breit, Phys. Rev. 42, 348 (1932) and 44, 418 (1933).

[24] G. Racah, Nature 129, 723 (1932).

corresponding levels of the heavier and the shifts between corresponding levels will depend on the type of valence electron, decreasing in order of ns, $np_{1/2}$, $np_{3/2}$, $nd_{3/2}$, etc., with the shift due to the s electron being by far the largest, and decreasing with increasing n for all types of electrons. The shifts for all levels of an unperturbed configuration will be approximately the same since they are due principally to the $6s$ electrons.

When two or more configurations A, B, C, etc., perturb each other the isotope shift of a perturbed level can be calculated as follows.[23] Neglecting the contribution to the isotope shift (I.S.) of all except the $6s$ electrons, the I.S. of all levels of A without perturbation would be $(\text{I.S.})_A$, where $(\text{I.S.})_A$ depends on the number of $6s$ electrons in the configuration; likewise for configurations B, C, etc. Then the isotope shift of the perturbed level is given by

$$(\text{I.S.})=\sum K_A^2(\text{I.S.})_A+\sum K_B^2(\text{I.S.})_B+\cdots,$$

where K_A is the (LS) coupling coefficient of a level of configuration A in the wave function of the perturbed level, and so forth. Since the K_A's and K_B's, etc., have been determined from the energies of the levels, the isotope shifts can be calculated if the shift per $6s$ electron is known.

The datum for isotope shifts of Pb III in Table VIII is zero shift for the $5d^{10}6s$ configuration of Pb IV. Relative to this datum the configuration $5d^96s^26p$ has one extra $6s$ electron, and $5d^{10}6p^2$ is short one $6s$ electron. The configurations $6snp$, $6snd$, $6snf$, and $6sns$ have the same number of $6s$ electrons as $5d^{10}6s$. Taking the isotope shift per $6s$ electron to be 0.50 cm^{-1} the unperturbed isotope shift is $+0.50$ cm^{-1} for each level of the configuration $5d^96s^26p$, -0.50 cm^{-1} for each level of the configurations $5d^{10}6p^2$, and 0 cm^{-1} for the $6snl$ configurations. For the $6sns$ configurations there will be a small positive shift due to the ns electron.

The excellent agreement between the observed and calculated values of the isotope shifts is perhaps the most direct confirmation of configuration interaction, since without interaction all shifts would be either $+0.50$, -0.50, or 0 cm^{-1}. Errors of the order of 5 percent are introduced by neglecting the shift due to the $6p_{1/2}$ electron,[25] but in general this is smaller than the experimental errors in the measured shifts. The observed isotope shift of a level gives very directly a measure of the perturbation of the level by levels of other configurations. This calculation also shows that the isotope shifts in Pb III can be quantitatively accounted for on the basis of the field theory alone, and is the best evidence to date that the specific mass effect is relatively unimportant for the heavy elements.[25]

[25] M. F. Crawford and A. L. Schawlow, Phys. Rev. **76**, 1310 (1949).

VI. $6sng$ CONFIGURATIONS

The levels of the even isotopes for the $6sng$ configurations have anomalous distributions. Wolfe's equations,[26] which involve an additional parameter can, of course, be fitted to the levels, Using one of the two sets of parameters obtainable by fitting Wolfe's equations the hyperfine structures due to the odd isotope were consistently explained. In this calculation it was necessary to work directly with the F matrices, because the multiplet and hyperfine structures are comparable. However, the values of the parameters required to account for the observed hyperfine structures appear to be anomalous on the basis of the simple theory, since the spin-other orbit parameter is positive and appreciably larger than the spin-orbital parameter which is negative. The negative value of the latter suggested that perturbations by levels of configurations in which a core electron is excited should be considered.[27] An approximate calculation of the perturbations by levels of $5d^96s^26d$ indicated that they are not the cause of the anomalous distribution. It may be that the anomalous parameters obtained with Wolfe's equations are the result of neglecting the spin-spin magnetic interaction.[28] If the latter is included in the formulas a direct comparison cannot be made since there are more parameters than observables. A test would require the evaluation of some of the parameters from numerical wave functions.

VII. CONCLUSIONS

This calculation shows that the theory is capable of giving an internally consistent explanation of multiplet structure, hyperfine structure, isotope shifts, and g-factors; and that remarkably good agreement can be obtained if one is willing to spend sufficient time on the evaluation of the parameters. In principle the theory could be further checked by calculating relative intensities, but this was not done since relative intensities in Pb III have not been measured.

[26] H. C. Wolfe, Phys. Rev. **41**, 443 (1932).
[27] M. Phillips, Phys. Rev. **44**, 644 (1933).
[28] H. H. Marvin, Phys. Rev. **71**, 102 (1947).

Variational Scattering Theory in Momentum Space
I. Central Field Problems

WALTER KOHN*
Institute for Theoretical Physics, Copenhagen, Denmark
(Received July 23, 1951)

Variational principles for scattering problems in a central field are formulated in momentum space and studied in detail. The method allows of generalization to collisions of composite particles, including disintegrations, into more than two end products, which will be discussed in a forthcoming paper.

I. INTRODUCTION

THE variational method has for many years been a valuable tool for the solution of the Schroedinger equation in bound state problems. But only rather recently Hulthén[1] has pointed out that it may also be applied to a study of scattering phenomena. Following Hulthén's work, which dealt with one-dimensional equations, the method was slightly modified by the author and extended to more general problems.[2] These included calculation of the scattering amplitude in three-dimensional collision problems, and of the elements of the scattering matrix in elastic or inelastic collisions of composite particles, with the limitation that no disintegrations into three or more units were energetically allowed.

Such methods were applied by the author[3] and more extensively by Verde and Troesch[3] to the collisions of neutrons and deuterons, and by Huang[4] and Massey and Moiseiwitsch[5] to the scattering of electrons by a hydrogen atom.

A different approach, based on an integral equation formulation of the Schroedinger equation, has been developed by Schwinger[6] and extensively applied to collisions of two elementary particles. However, no useful generalization of this method to yield the elements of the scattering matrix in collisions of composite particles has so far been found.

Variational methods have already been so useful in collision theory that for some time it has seemed very desirable to generalize them further, so as to cover the many physically interesting processes in which two composite particles collide and break up into three or more units. Examples are the disintegration of a deuteron by a fast neutron or the ionization of a hydrogen atom by a high energy electron. The difficulty in carrying out this generalization lay in the fact that when a disintegration into three or more particles can take place, the form of the wave function in the asymptotic region is very complicated due to the involved correlation of the positions and momenta of the particles. On the other hand it was to be expected that such a generalization is in principle possible.

Meanwhile, the clue for overcoming these difficulties had been given quite a long time ago by Heisenberg[7] in his work on the S-matrix. It was shown there that the asymptotic behavior of the wave function in coordinate space is reflected in the singularities of the momentum wave function. Generalizing a result obtained by Dirac,[8] Heisenberg showed that the asymptotic behavior of several outgoing particles is described, in momentum space, quite simply by a singularity of the form $\delta_+(E-\Sigma_i p_i^2/2m_i)$, where $\delta_+(x)=(2\pi ix)^{-1}+\frac{1}{2}\delta(x)$, E is the total energy and p_i, m_i are the momenta and masses of the particles.

This suggested investigating the entire variational theory of collision processes in momentum space. Indeed it is somewhat surprising that this was not done earlier, since the momentum representation is probably the most natural one for a description of scattering.

In bound state problems, one does not find any essentially new features by going into the momentum space. In fact the coordinate and momentum wave functions have a rather similar character since they are both finite and both vanish as their arguments approach infinity.

On the other hand, in collision theory the coordinate wave function extends over infinite regions of space but is finite everywhere, while the momentum wave function vanishes at infinity but has very significant singularities. It is not surprising then that the formulation of variational principles in momentum space differs considerably from the corresponding formulation in coordinate space. In particular, the greater simplicity of the momentum wave function suggests directly a variational formulation of disintegration processes.

The present paper introduces the momentum space method in the simple case of central field problems. Such problems have been studied in great detail in coordinate space so that one has considerable familiarity with them. Just for this reason they afford a good practice ground to get acquainted with the characteristic features of

* Post-doctoral N.R.C. fellow, on leave of absence from Carnegie Institute of Technology, Pittsburgh, Pennsylvania.
[1] L. Hulthén, Arkiv Mat. Astron. Fysik, **35A**, No. 25 (1948); references to Hulthén's earlier work may be found in this paper.
[2] W. Kohn, Phys. Rev. **74**, 1763 (1948).
[3] M. Verde, Helv. Phys. Acta **22**, 339 (1949). A. Troesch and M. Verde, Helv. Phys. Acta **24**, 39 (1951).
[4] S. S. Huang, Phys. Rev. **76**, 477 (1949).
[5] H. S. W. Massey and B. L. Moiseiwitsch, Proc. Roy. Soc. (London) **205**, 483 (1951).
[6] J. Schwinger, mimeographed lecture notes (Harvard, 1947).
[7] W. Heisenberg, Z. Physik **120**, 513 (1943).
[8] P. A. M. Dirac, *Quantum Mechanics* (Clarendon Press, Oxford, 1947), third edition, Sec. 50.

variational scattering theory in the somewhat "unanschaulich" momentum space. The generalization to three-dimensional problems and to collisions of composite particles will be given in a forthcoming paper.

II. THE SINGULARITIES OF THE MOMENTUM WAVE FUNCTION

It is well known that in the case of a single particle scattered by a spherically symmetrical center of force and in the case of two particles interacting through a central potential, the Schroedinger equation can be separated and leads to a radial equation for each angular momentum, l. For S-scattering, $l=0$, one obtains the equation,

$$[-(d^2/dx^2)+V(x)-k^2]\psi(x)=0, \tag{2.1}$$

where $V(x)$ and k^2 are proportional to the potential and total energy respectively. We shall confine ourselves to the case of $l=0$ until Sec. VII, when we shall make the obvious extension to higher angular momenta.

If the potential falls off more rapidly than x^{-1}, the wave function ψ satisfies the boundary conditions,

$$\psi(0)=0, \quad \lim_{x\to\infty}\psi(x)=\sin kx+\tan\eta\cos kx, \tag{2.2}$$

where η is the phase shift whose evaluation is the object of a theoretical scattering calculation.

Passing to the momentum representation, we note that the eigenfunctions of the square of the momentum satisfying the first of the boundary conditions (2.2) are $\sin px$. Hence we expand $\psi(x)$ as

$$\psi(x)=\int_0^\infty \varphi(p)\sin px\,dp \tag{2.3}$$

with the understanding that if $\varphi(p)$ is singular, the principal value of the integral is to be taken. Substituting (2.3) into (2.1) and defining

$$V(p,p')=V(p',p)=(2/\pi)\int_0^\infty \sin p'x V(x)\sin px\,dx \tag{2.4}$$

we obtain the usual momentum space equation,

$$(p^2-k^2)\varphi(p)+\int_0^\infty V(p,p')\varphi(p')dp'=0, \tag{2.5}$$

where again the principal value of the integral is understood.

We are interested in the behavior of $\psi(x)$ for large values of x and therefore must examine how this behavior is reflected in the momentum space function $\varphi(p)$. Now it is well known that if $g(p)$ is a function free from singularities, then $\int_0^\infty g(p)\sin px\,dp\to 0$ as $x\to\infty$; for, due to the highly oscillatory character of $\sin px$, the positive and negative contributions to the integral tend to cancel. It follows that if we transform back from momentum to coordinate space by means of (2.3) only the singularities of $\varphi(p)$ will determine the asymptotic behavior of $\psi(x)$.

To examine the singular behavior of $\varphi(p)$, we replace (2.5) by the integral equation,

$$\varphi(p)=\delta(p-k)-\frac{1}{p^2-k^2}\int_0^\infty V(p,p')\varphi(p')dp'. \tag{2.6}$$

Actually the inhomogeneous term, $\delta(p-k)$ should be multiplied by an arbitrary constant; however, choosing this constant equal to 1 merely fixes a convenient normalization of the wave function. Now since $V(p,p')$ is a regular function of p and p', the integral in (2.6) is also a regular function of p, even though $\varphi(p)$ has singularities. Thus we see that the singular behavior of $\varphi(p)$ can be described by the expression,

$$\varphi(p)=\delta(p-k)-B(p)/(p^2-k^2), \tag{2.7}$$

with the understanding that $B(p)$ is free from singularities.

Our previous considerations already indicated that the phase shift η is determined by the value of B at the singular point $p=k$. To show this in detail we transform (2.7) back to coordinate space by means of (2.3), giving

$$\psi(x)=\sin kx-\int_0^\infty \frac{B(p)}{p^2-k^2}\sin px\,dp. \tag{2.8}$$

We separate out the singular part of $B(p)/(p^2-k^2)$ by writing

$$\frac{B(p)}{p^2-k^2}=\frac{B(k)}{2k}\frac{1}{p-k}+\left[\frac{B(p)}{p^2-k^2}-\frac{B(k)}{2k(p-k)}\right]. \tag{2.9}$$

For large x the term in square brackets which is regular gives no contribution, so that we only require the improper integral $\int_0^\infty (p-k)^{-1}\sin px\,dp$ whose principal value approaches $\pi\cos kx$ as $x\to\infty$. Hence

$$\lim_{x\to\infty}\psi(x)=\sin kx-\frac{B(k)\pi}{2k}\cos kx, \tag{2.10}$$

so that by definition of the phase-shift η, we find the required connection,

$$\tan\eta=-\pi B(k)/2k, \tag{2.11}$$

between η and $B(k)$.

III. FORMULATION OF THE VARIATIONAL PRINCIPLE IN MOMENTUM SPACE

In reference 2 a variational principle for the phase shift was developed in the coordinate representation. Calling now η_0 the correct phase shift, η the phase shift of a trial function satisfying the boundary conditions (2.2), and I the functional

$$I\equiv-\int_0^\infty \psi(x)[-(d^2/dx^2)+V(x)-k^2]\psi(x)dx \tag{3.1}$$

it was found that the expression,

$$k\tan\eta_0 = k\tan\eta + I, \tag{3.2}$$

was stationary relative to variations of ψ. In other words the integral I, which vanishes for the correct ψ, plays the role of a first-order correction to the tangent of the trial phase shift.

It is of course possible to express $\tan\eta$ and I in terms of the momentum wave function. However, because of the nonintegrability of ψ, such a procedure is somewhat delicate and in fact does not lead to a very desirable formulation. We prefer therefore to postpone this development (see Sec. IV) and meanwhile formulate variational principles based directly on the Schroedinger equation in momentum space.

In the case of a bound state problem one knows that the first variation of the functional

$$\int_0^\infty \varphi(p)\left[(p^2-E)\varphi(p)+\int_0^\infty V(p,p')\varphi(p')dp'\right]dp \tag{3.3}$$

vanishes for the correct wave function and one can use this fact for a determination of the energy E and the wave function φ. This is just the momentum analog of the statement that if $\psi(\infty)=0$ the first variation of I, Eq. (3.1), is zero. It is thus natural also in the case of a collision problem, to investigate the expression,

$$J\equiv\int_0^\infty \varphi(p)\left[(p^2-k^2)\varphi(p)+\int_0^\infty V(p,p')\varphi(p')dp'\right]dp. \tag{3.4}$$

We consider this J as a functional of $\varphi(p)$'s, whose singularities are described by the form (2.7). In particular this includes functions for which $B(k)=0$ and which therefore have only the δ-function singularity.

The integrand in (3.4) contains singular terms. Thus, to give a definite meaning to the integral, we must agree on how to deal with such terms. We therefore make the following conventions:

$$\int_0^\infty \delta(p-k)(p^2-k^2)\delta(p-k)dp=0, \tag{3.5}$$

$$\int_0^\infty \frac{F(p)}{p^2-k^2}dp=\lim_{\delta\to 0}\left[\int_0^{k-\delta}\frac{F(p)}{p^2-k^2}dp+\int_{k+\delta}^\infty\frac{F(p)}{p^2-k^2}dp\right]. \tag{3.5^1}$$

Equation (3.5) is obtained when $\delta(p-k)$ is approximated by a nonsingular function because of the antisymmetry about the point $p=k$. It is therefore reasonable to postulate a similar relationship for the δ-functions themselves. Integrals of the type (3.5^1) are usually evaluated either by by-passing the singularity in the complex plane, which gives a complex result, or by taking the principal value. Since our problem is entirely real we have chosen the latter alternative. We could, of course, have adopted different conventions, but it should be remarked that they all lead to the same final results.

Let us now first evaluate J for the correct wave function, $\varphi_0(p)$. Although for this function the square bracket in (3.4) is zero, we shall see that the corresponding value of J, denoted by J_0, does not vanish. For, substituting for $\varphi_0(p)$ on the left of (3.4) the form (2.7), we find

$$J_0=J_0^{(1)}+J_0^{(2)}, \tag{3.6}$$

where

$$J_0^{(1)}=\int_0^\infty \delta(p-k)\left[(p^2-k^2)\varphi_0(p)+\int_0^\infty V(p,p')\varphi_0(p')dp'\right]dp, \tag{3.7}$$

$$J_0^{(2)}=\int_0^\infty -B_0(p)\left[\varphi_0(p)+\frac{1}{p^2-k^2}\int_0^\infty V(p,p')\varphi_0(p')dp'\right]dp. \tag{3.7^1}$$

Now $J_0^{(1)}$ contains the term $\delta(p-k)(p^2-k^2)\delta(p-k)$ whose integral we equate to zero. Thus we are left with

$$J_0^{(1)}=-B_0(p)+\int_0^\infty V(k,p')\varphi_0(p')dp'=0, \tag{3.8}$$

as a comparison of (2.6) and (2.7) shows. On the other hand, by (2.6), the square bracket in (3.7^1) equals $\delta(p-k)$ so that

$$J_0=J_0^{(2)}=-B_0(k). \tag{3.9}$$

Thus the expression J_0, which vanishes in bound state problems, equals, in the present case, a constant times $\tan\eta_0$.

It is important for our later work to see clearly the origin of this nonvanishing result. It comes from the term $\varphi_0(p)(p^2-k^2)\varphi_0(p)$ in (3.4). The $\varphi_0(p)$ on the right contains a term $\delta(p-k)$ which when multiplied by (p^2-k^2) vanishes and hence gives no contribution to the square bracket in (3.4). However, when this term is further premultiplied by the factor $-B_0/(p^2-k^2)$, contained in $\varphi_0(p)$, it becomes $-B_0(p)\delta(p-k)$, resulting in $-B_0(k)$ on integration.

Next we calculate the first variation of J. Since we consider only trial functions of the form (2.7), the variation of φ may be written as $\delta\varphi(p)=-\delta B(p)/(p^2-k^2)$ and we obtain

$$\delta J=2\int_0^\infty -\frac{\delta B(p)}{p^2-k^2}\left[(p^2-k^2)\varphi_0(p)+\int_0^\infty V(p,p')\varphi_0(p')dp'\right]dp$$
$$=-2\delta B(k). \tag{3.10}$$

Hence the combination $J+2B(k)$ is stationary. This means that to the first order in $\delta\varphi$ we have the equation,

$$J+2B(k)=J_0+2B_0(k)=B_0(k) \\ =-(2k/\pi)\tan\eta_0, \quad (3.11)$$

which provides the desired stationary expression for $\tan\eta_0$.

As a simple check we can obtain the Born approximation from (3.11), by setting $\varphi(p)=\delta(p-k)$ so that $B(k)=0$. This gives, correctly,

$$V(k,k)=-(2k/\pi)\tan\eta_0. \quad (3.12)$$

When the functional J in (3.11) is written out in full using the form (2.7) of $\varphi(p)$, one obtains among other terms

$$2\int_0^\infty -\frac{B(p)}{p^2-k^2}(p^2-k^2)\delta(p-k)dp=-2B(k)$$

which precisely cancels the $2B(k)$ in (3.11). If we now for convenience replace (2.7) by

$$\varphi(p)=\delta(p-k)+\chi(p) \quad (3.13)$$

where $\chi(p)$ may have only a $(p^2-k^2)^{-1}$ singularity, (3.11) becomes in full

$$\int_0^\infty \chi(p)(p^2-k^2)\chi(p)dp+V(k,k)+2\int_0^\infty V(k,p)\chi(p)dp \\ +\int_0^\infty \chi(p)V(p,p')\chi(p')dpdp' \\ =-(2k/\pi)\tan\eta_0. \quad (3.14)$$

Remarks on Regularization

We have seen that the extra term $2B(k)$ in (3.11) just removes the contributions to J coming from the singular point of $\chi(p)$. It follows that if $\chi(p)$ is replaced by a "regularized" function, in which the singularity at $p=k$ has been smeared out, the term $2B(k)$ in (3.11) will not occur. This allows one to write (3.11) in a more compact, though entirely equivalent form.

Thus let us define, corresponding to a function $\varphi(p)$, the regularized functions,

$$\varphi_\epsilon(p)=\delta(p-k)+\chi_\epsilon(p), \quad (3.15)$$

depending on the parameter ϵ. We assume that for all nonvanishing values of ϵ, $\chi_\epsilon(p)$ is a nonsingular function; but that as $\epsilon\to 0$, $\chi_\epsilon(p)$ approaches the singular $\chi(p)$ in the sense that if $F(p)$ is any smooth function,

$$\lim_{\epsilon\to 0}\int_0^\infty F(p)\chi_\epsilon(p)dp \\ =\text{principal value of}\int_0^\infty F(p)\chi(p)dp. \quad (3.16)$$

An example of such a regularized function is

$$\chi_\epsilon(p)=-\mathrm{Re}[B(p)/(p^2-k^2-i\epsilon)].$$

Next we define

$$J'(\varphi)=\lim_{\epsilon\to 0}J(\varphi_\epsilon). \quad (3.17)$$

Then, clearly, $J'(\varphi)=J(\varphi)+2B(k)$, so that (3.11) may be put into the form,

$$J'(\varphi)=B_0(k)=-(2k/\pi)\tan\eta_0, \quad (3.18)$$

or in full

$$\lim_{\epsilon\to 0}\int_0^\infty \varphi_\epsilon(p)\Big[(p^2-k^2)\varphi_\epsilon(p) \\ +\int_0^\infty V(p,p')\varphi_\epsilon(p')dp'\Big]dp \\ =B_0(k)=-(2k/\pi)\tan\eta_0. \quad (3.19)$$

When this is written out in terms of $\chi_\epsilon(p)$ and the limit $\epsilon\to 0$ is taken, one is of course led back to (3.14). The interesting feature of (3.19) is, however, that it shows that the expectation value of $(H-E)$ evaluated by suitable regularization is stationary even in scattering problems; but in contrast to bound state problems the stationary value is not zero but a constant times $\tan\eta_0$.

IV. RELATION TO THE VARIATIONAL FORMULATION IN COORDINATE SPACE

Both forms in which we have expressed the variational principle [Eqs. (3.11) and (3.18)] are apparently not simple transcripts of the coordinate space principle (3.2). For if one formally expresses I in terms of the momentum wave function, (3.2) becomes

$$\int_0^\infty \varphi(p)\Big[(p^2-k^2)\varphi(p) \\ +\int_0^\infty V(p,p')\varphi(p')dp'\Big]dp+B(k)=B_0(k). \quad (4.1)$$

It is really not surprising that we seem to have here yet another form of the variational principle, since by handling the singularities in different ways we obtained the two different forms (3.11) and (3.18). In fact we may already guess that the coordinate space principle is equivalent, in momentum space, to regularizing just one of the two wave functions occurring in the functional J.

To clarify this point, let us re-write carefully the definition (3.1) of I as

$$I=-\lim_{a\to\infty}\int^a \psi(x)\Big[-\frac{d^2}{dx^2}+V(x)-k^2\Big]\psi(x)dx. \quad (4.2)$$

Passing into momentum space, this becomes

$$I=-\lim_{\alpha\to\infty}\int_0^\infty dx\int_0^\infty dp\int_0^\infty dp'\varphi(p)\sin px \times\left[(p'^2-k^2)\varphi(p')+\int_0^\infty V(p',p'')\varphi(p'')dp''\right]\times\sin p'x. \quad (4.3)$$

The integration over x gives

$$\int_0^\infty \sin px\sin p'xdx=\tfrac{1}{2}\left[\frac{\sin(p-p')a}{(p-p')}-\frac{\sin(p+p')a}{(p+p')}\right]=\tfrac{1}{2}\pi\Delta_a(p,p') \quad (4.4)$$

where for $p, p'>0$, $\lim_{a\to\infty}\Delta_a(p,p')=\delta(p-p')$, i.e., $\Delta_a(p,p')$ is a regularized δ-function. We now conveniently introduce the regularized function,

$$\varphi_a(p')=\int_0^\infty \Delta_a(p,p')\varphi(p)dp. \quad (4.5)$$

Then the variational principle (3.2) can be written as

$$\lim_{a\to\infty}\int_0^\infty \varphi_a(p')\left[(p'^2-k^2)\varphi(p')+\int_0^\infty V(p',p'')\varphi(p'')dp''\right]dp'+B(k)=B_0(k), \quad (4.6)$$

which confirms our expectation that one of the φ's is regularized. The stationary character of (4.6) may also be checked directly in momentum space.

V. BILINEAR FORM OF THE VARIATIONAL PRINCIPLE; SCHWINGER'S VARIATIONAL PRINCIPLE IN MOMENTUM SPACE

In our later work, we shall have occasion to use bilinear forms $J(\varphi_1,\varphi_2)$ in order to discuss transition between two asymptotic states. It is therefore convenient to introduce such forms already in the one-dimensional case. Moreover, the bilinear forms show clearly the connection with Schwinger's variational principle.

We consider then the bilinear functional,

$$J(1,2)=J(2,1)=\int_0^\infty \varphi_1(p)\left[(p^2-k^2)\varphi_2(p)+\int_0^\infty V(p,p')\varphi_2(p')dp'\right]dp, \quad (5.1)$$

for functions of the form,

$$\varphi_i(p)=\delta(p-k)-B_i(p)/(p^2-k^2), \quad i=1,2. \quad (5.2)$$

As before we find that if $\varphi_1=\varphi_2=\varphi_0$,

$$J_0(1,2)=-B_0(k) \quad (5.3)$$

and

$$\delta J(1,2)=-\delta B_1(k)-\delta B_2(k). \quad (5.4)$$

Hence we have, in analogy with (3.11), the variational principle,

$$J(1,2)+B_1(k)+B_2(k)=B_0(k), \quad (5.5)$$

and, in analogy with (3.18),

$$J'(1,2)=B_0(k). \quad (5.6)$$

We may note in passing that the corresponding expression in coordinate space has the less symmetrical form,

$$I(1,2)+k\tan\eta_2=k\tan\eta_0. \quad (5.7)$$

Already, in reference 2, Schwinger's variational principle was derived in coordinate space from a bilinear expression such as (5.7). We can also derive it in momentum space, most easily from (5.5).

For $\varphi_2(p)$ we use any trial function of the form,

$$\varphi_2(p)=\delta(p-k)-B_2(p)/(p^2-k^2). \quad (5.8)$$

The function $\varphi_1(p)$ is constructed from $\varphi_2(p)$ according to the equation,

$$\varphi_1(p)=\delta(p-k)-\frac{B_0(k)}{p^2-k^2}\frac{\int_0^\infty V(p,p')\varphi_2(p')dp'}{\int_0^\infty V(k,p')\varphi_2(p')dp'}; \quad (5.9)$$

here $B_0(k)$ is the unknown correct value of B at $p=k$, given by

$$B_0(k)=\int_0^\infty V(k,p')\varphi_0(p')dp'.$$

It may be seen, from the integral equation (2.6), that if $\varphi_2=\varphi_0$, then φ_1 as defined by (5.9) also equals φ_0. Furthermore, however, φ_1 has the correct singular behavior,

$$\varphi_1(p)=\delta(p-k)-B_0(k)/(p^2-k^2), \quad p\approx k, \quad (5.10)$$

regardless of the correctness of φ_2. Thus, in general, if φ_2 is some approximation to φ_0, φ_1 will be a better approximation, which is the reason for the practical success of this method.

Using now the fact that $B_1(k)=B_0(k)$ and substituting φ_2 and φ_1 into (5.5), one obtains after some simplification

$$B_0(k)=\left[\int_0^\infty V(k,p)\varphi_2(p)dp\right]^2\Big/\times\left[\int_0^\infty \varphi_2(p)V(p,p')\varphi_2(p')dpdp'+\int_0^\infty \varphi_2(p')V(p',p)(p^2-k^2)^{-1}\times V(p,p'')\varphi_2(p'')dpdp'dp''\right]. \quad (5.11)$$

This is just the momentum transcript of the stationary expression for $\cot\eta_0$ given by Schwinger in coordinate space.

VI. PRACTICAL APPLICATION

As usual, the stationary expressions which we have derived enable us to obtain approximate values for the stationary quantity, $\tan\eta_0$, as well as the wave function $\varphi_0(p)$. Practical procedures for accomplishing this in coordinate space have been described by Hulthén[1] and the author.[2] They may be directly taken over into momentum space and therefore will be only briefly outlined here.

Following reference 2, we use as trial function a linear combination of the type,

$$\varphi(p)=A\delta(p-k)+\chi(p), \tag{6.1}$$

where $\chi(p)$ is a superposition of a finite number of functions:

$$\chi(p)=\sum_0^n c_k\chi_k(p). \tag{6.2}$$

Because of the extra factor A in (6.1), compared to (3.13), Eq. (3.14) must be replaced by

$$\int_0^\infty \chi(p)(p^2-k^2)\chi(p)dp+A^2V(k,k)$$

$$+2A\int_0^\infty V(k,p)\chi(p)dp+\int_0^\infty \chi(p)V(p,p')$$

$$\times\chi(p')dpdp'=-(2k/\pi)A^2\tan\eta_0. \tag{6.3}$$

The stationary character of this equation may be directly verified by dividing through by A^2 and calling $\chi/A=\chi'$, which leads one back to the form (3.14).

The condition that (6.3) be stationary with respect to variations of the parameters A and c_k leads to $(n+1)$ homogeneous linear equations for the $(n+1)$ parameters. They are compatible only if the determinant of the coefficients vanishes. This determinant is a function of $\tan\eta_0$ and, as in reference 2, it may be shown that its vanishing fixes a unique value for $\tan\eta_0$, in contrast to the $(n+1)$ eigenvalues in bound state problems. The values of c_k/A may be obtained by substituting the value of $\tan\eta_0$ into n of the linear equations for A and c_k and solving.

If one wants to evaluate the integrals of (6.3) in momentum space it is important to note that, while the correct $\chi_0(p)$ has a singularity of the type $-B_0(p)/(p^2-k^2)$, it is not necessary to work with singular trial χ's. For it is clear from (6.3) that slight regularization of $\chi_0(p)$ does not materially effect the value of $\tan\eta_0$. This is a fortunate circumstance since analytical work with singular wave functions is generally very difficult.

Alternatively, one may of course go back to the coordinate space for the evaluation of the integrals. There, calling

$$\int_0^\infty \chi(p)\sin pxdp=f(x) \tag{6.4}$$

one finds, the stationary equation,

$$\int_0^\infty f(x)[-(d^2/dx^2)+V(x)-k^2]f(x)dx$$

$$+2A\int_0^\infty \sin kxV(x)f(x)dx$$

$$+A^2\int_0^\infty \sin^2kxV(x)dx=-A^2k\tan\eta_0. \tag{6.5}$$

The condition that $\chi(p)$ may only have a singularity of the type $-B(p)/(p^2-k^2)$ means that $f(x)$, if it extends to infinity, must be asymptotically proportional to $\cos kx$. Incidentally (6.5) may be considered as an alternative and perhaps useful form of the variational principle (3.2) to which it is equivalent.

VII. EXTENSION TO HIGHER ANGULAR MOMENTA

The radial Schroedinger equation, corresponding to angular momentum l, is

$$\left(-\frac{d^2}{dx^2}+V(x)+\frac{l(l+1)}{x^2}-k^2\right)\psi(x)=0. \tag{7.1}$$

There are now two types of "momentum"-representations to which one may transform. The first is the space of solutions of the equations,

$$[-(d^2/dx^2)-p^2]\psi_p(x)=0, \tag{7.2}$$

which, in view of the boundary condition $\psi(0)=0$, are just the $\sin px$ considered before. In this case $V(x)+l(l+1)/x^2$ is to be regarded as the total potential $V'(x)$, but otherwise the treatment is exactly analogous to that of S-scattering.

Alternatively, one may transform to the space of solutions of the equations,

$$\left(-\frac{d^2}{dx^2}+\frac{l(l+1)}{x^2}-p^2\right)\psi_p(x)=0, \tag{7.3}$$

namely, the functions

$$\psi_p(x)=(px)j_l(px). \tag{7.4}$$

These obey the orthonormality relations,

$$\int_0^\infty \psi_p(x)\psi_{p'}(x)dx=\tfrac{1}{2}\pi\delta(p-p'). \tag{7.5}$$

Expanding $\psi(x)$ in (7.1) as

$$\psi(x)=\int_0^\infty \varphi(p)\psi_p(x)dp, \tag{7.6}$$

one finds the equation,

$$(p^2-k^2)\varphi(p)+\int_0^\infty V(p,p')\varphi(p')dp'=0 \tag{7.7}$$

where now

$$V(p,p')=V(p',p)=(2/\pi)\int_0^\infty \chi_p(x)V(x)\psi_{p'}(x)dx. \tag{7.8}$$

It is easily verified that the function, which in coordinate space has the asymptotic behavior

$$\psi(x)\to(kx)[j_l(kx)-\tan\eta\, n_l(kx)] \tag{7.9}$$

satisfies the integral equation,

$$\varphi(p)=\delta(p-k)-(p^2-k^2)^{-1}\int_0^\infty V(p,p')\varphi(p')dp' \tag{7.10}$$

and that for the correct $\varphi_0(p)$

$$\int_0^\infty V(k,p')\varphi_0(p')dp'=-(2k/\pi)\tan\eta_0. \tag{7.11}$$

A variational principle for η_0 is now established just as before. Using functions of the form,

$$\varphi(p)=\delta(p-k)-B(p)/(p^2-k^2) \tag{7.12}$$

and defining J as in (3.4), with the new meaning (7.8) for $V(p,p')$, we find, corresponding to (3.11), the equation,

$$J+2B(k)=B_0(k)=-(2k/\pi)\tan\eta_0. \tag{7.13}$$

The rest of the development is entirely parallel to that of S-scattering.

VIII. DISCUSSION

We have seen how, in the simple case of scattering by a central field, a consideration of the basic integral,

$$J\equiv\int_0^\infty \varphi(p)\left[(p^2-k^2)\varphi(p)+\int_0^\infty V(p,p')\varphi(p')dp'\right]dp$$

leads to a stationary expression for the tangent of the phase shift. To establish this variational principle, it was essential to know beforehand the form of the singularities of the momentum wave function. This was very easy in the simple case considered. But quite generally it is clear that the form of the singularities is independent of the details of the interaction, and thus one expects that it can be established without actually solving the Schroedinger equation.

This expectation is borne out by the work of Dirac[8] and Heisenberg.[7] It enables one to cast more complicated scattering problems, particularly also those involving disintegrations, into variational form. A discussion of such problems will be given in a forthcoming paper.

ACKNOWLEDGMENTS

This work was carried out during the author's tenure of a postdoctoral fellowship from the National Research Council, whose financial assistance is gratefully acknowledged. It is a great pleasure to thank Professor N. Bohr for the privilege of working in his institute and Professor C. Møller for his kind interest in this work.

Note added in proof: Dr. G. J. Kynch of the University of Birmingham has informed me that some time ago he has done similar unpublished work on the two body problem.

Thermodynamic Properties of a Non-Ideal He^3-He^4 Solution Model

J. C. Morrow
Department of Chemistry, University of North Carolina, Chapel Hill, North Carolina
(Received May 18, 1951)

Deviations from ideality for He^3–He^4 solutions are calculated on the basis of a simple real solution model. Expressions for equilibrium total pressure are derived for situations with and without superfluid He^4. Effects of non-ideality on previously reported calculations of lambda-point dependence on He^3 concentration are examined, and an equation representing the lambda-points of concentrated as well as dilute He^3 solutions is given. The results are used in the comparison of various bases for treatment of the lambda-point shift. Assumption that the partial molal enthalpy of superfluid vanishes gives more satisfactory results than assumption of zero partial molal entropy of superfluid.

I. INTRODUCTION

THERMODYNAMIC treatment of ideal liquid solutions of He^3 and He^4 has been given recently by a number of investigators.[1–4] Previous workers have pointed out the dependence of theoretical results on assumption of solution ideality and have indicated the difficulty of obtaining any precise measure of ideality deviation from available measurements of solution properties. Systematic estimation of non-ideality corrections is, therefore, important for the understanding of real solution behavior. This paper considers the calculation of corrections for a simple real solution model and the comparison of model properties with those of the ideal and actual solutions.

II. CHEMICAL POTENTIALS

At temperatures for which there is no superfluid, solutions of He^3 and He^4 are two component mixtures. Interaction of these non-electrolytes gives rise to deviations from ideality conveniently described by the excess chemical potentials of the substances, that is, the differences between actual chemical potentials and values for ideal mixtures. A useful representation of the excess chemical potential of A in a two-component mixture, A and B, is $\mu_A^E=\sum_i k_i f_B^i$. The volume fraction of component B, f_B, is defined as

$$N_BV_B/(N_AV_A+N_BV_B) \quad \text{or} \quad x_B/(x_AV_A+x_BV_B),$$

where V_j is the molar volume of pure j and N_j is the number of moles of substance j.

Scatchard has considered[5] the results of non-electrolyte interaction and has shown that, for a simple solution model, $k_i=0$ for $i\neq 2$ and

$$k_2=V_A(a_{AA}^{\frac{1}{2}}-a_{BB}^{\frac{1}{2}})^2, \tag{1}$$

where $-a_{jj}$ is the energy of unit volume of pure liquid j minus that of the same quantity of perfect gas j at the same temperature. Using this model, one can express potentials of isotopic helium solutions as

$$\mu_3=\mu_3^0+RT\ln x_3+V_3af_4^2, \tag{2}$$

$$\mu_4=\mu_4^0+RT\ln x_4+V_4af_3^2, \tag{3}$$

where $a\equiv(a_{33}^{\frac{1}{2}}-a_{44}^{\frac{1}{2}})^2$. Detailed description of the solution model, derivation of Eq. (1), and extension of the treatment to mixtures with more than two components has been given by Scatchard.[6,7]

One of the chief recommendations for the above expression for the potentials is that it seems to combine reasonable approximation with simplicity of mathematical form. More complicated equations have been used but often the data are not precise enough to warrant the added terms.

The assumptions on which the derivation rests are listed in reference 7. The relations of these assumptions to the validity of the simple equation have been considered by many investigators. The assumption of temperature independence for the molecular distribution function and the related ideal entropy of mixing have been discussed critically for various deviations by Hildebrand and Wood,[8] Guggenheim,[9] Scatchard and Hamer,[10] and Hildebrand.[11] Kirkwood[12] has calculated the effect of sorting on the thermodynamic properties. Even when the temperature is such as to produce critical mixing, the correction for the excess free energy is only about five percent. For isotopic solutions this correction can be neglected.

In practice, use of a Flory-Huggins excess entropy of mixing instead of the zero value of the above development does not seem to be justified until the ratio of molar volumes becomes greater than 2 to 1; the ratio for He^3 and He^4 (about 1.4 to 1) makes the use of this correction inappropriate.

[1] J. W. Stout, Phys. Rev. **76**, 864 (1949).
[2] C. J. Gorter, Physica **15**, 523 (1949).
[3] O. G. Engel and O. K. Rice, Phys. Rev. **78**, 55 (1950).
[4] O. K. Rice, Phys. Rev. **79**, 1024 (1950).
[5] G. Scatchard, Chem. Revs. **8**, 323 (1931).
[6] G. Scatchard, Kemisk **13**, 77 (1932).
[7] G. Scatchard, Trans. Faraday Soc. **33**, 160 (1937).
[8] J. H. Hildebrand and S. E. Wood, J. Chem. Phys. **1**, 817 (1933).
[9] E. A. Guggenheim, Proc. Roy. Soc. (London) **A148**, 304 1935).
[10] G. Scatchard and W. J. Hamer, J. Am. Chem. Soc. **57**, 1805 (1935).
[11] J. H. Hildebrand, *Solubility* (Reinhold Publishing Corporation, New York, 1936).
[12] J. G. Kirkwood, J. Phys. Chem. **43**, 97 (1939).

Correction for nonzero volume change on mixing[7] is a multiplicative term in the excess free energy $1-\beta_0 a f_3 f_4/2$ where β_0 is the compressibility of the isolated components. Even though β for helium is very large compared with other liquids, the value to be subtracted from unity is of the order of 10^{-2}; in view of other uncertainties, the error arising from use of the zero volume change equation, that is, Eq. (1) can be neglected.

Use of the geometric mean of a_{33} and a_{44} as a rough approximation for a_{34}, which enables one to obtain the energy parameter for a mixture from the parameters of its components, has been discussed by Hildebrand and Wood[8] and by Hildebrand.[11]

On the basis of the above treatments, calculation of a gives a reasonable expression for chemical potential as a function of composition. The quantity a_{jj} is very nearly equal to the heat required to vaporize one cm^3 of liquid j minus the corresponding external work. In the following calculations the experimental heats of vaporization were used and the perfect gas law was employed to obtain the gas volume portion of the external work. Calculated in this manner, a is 0.1005 cal/cm^3. Densities and heats of vaporization used are those given by Keesom[13] for He^4 and those given by Grilly, Hammel, and Sydoriak[14] for He^3.

III. SOLUTION VAPOR PRESSURES

Conditions for liquid-vapor equilibrium include the equality of liquid and vapor chemical potentials. Equations (2) and (3) with $\mu_{il}^0(P_i^0, T)+\bar{V}_{il}(P-P_i^0)$ replacing $\mu_{il}^0(P, T)$ can be used for the liquid potentials, since the liquids can be taken as incompressible without very great error at the low pressures considered. The vapor potentials can be easily obtained if the equation of state of the gas mixture is known. One can use an expression stopping with terms in $1/V$ such as

$$PV=(N_3+N_4)RT[1+(N_3+N_4)B_y/V]$$

where $B_y=B_3y_3^2+2B_{34}y_3y_4+B_4y_4^2$; B_i is the second virial coefficient of the gas i, and y_i is the gas mole fraction.

Neither experimental nor quantum-mechanical (computed) values are available for B_{34}, but it seems reasonable that the value estimated from properties of the pure gases will be as good an approximation as the rest of the calculations. Various rules for obtaining mixture parameters have been reviewed by Beattie.[15] For the simple equation of state chosen, probably the best rule is the Lorentz approximation $B_{34}=(B_3^{\frac{1}{3}}+B_4^{\frac{1}{3}})^3/8$ which is obtained by averaging molecular diameters.

The chemical potentials of the gases i and j of a two-component system obeying the above equation of state are given by

$$\mu_{ig}(P, T)=\mu_{ig}^0(P_i^0, T)+RT\ln(py_i/P_i^0)+B_i(P-P_i^0)+r_i,$$

where $r_i=(2B_{ij}-B_i-B_j)(1-y_i)^2P$ and j refers to the other component. Equating potentials and remembering that the sum of y_3 and y_4 must be unity, one has for the total pressure

$$P=P_4^0x_4\exp\{[k_4f_3^2+(\bar{V}_{4l}-B_4)(P-P_4^0)-r_4]/RT\}+P_4^0x_3\exp\{[k_3f_4^2+(\bar{V}_{3l}-B_3)\times(P-P_3^0)-r_3]/RT\}. \quad (4)$$

The y_i values obtained from a Dalton-Raoult computation are sufficiently close for calculation of the r_i since the r terms are small corrections. By successive approximations, P can then be obtained for any given liquid mole fraction from the temperature and properties of the pure gases and liquids.

Vapor pressures of the pure liquids (as functions of T) and liquid volumes are given in references 13 and 14; B as a function of temperature is available for both isotope three[16] and isotope four.[17] Experimental pressures for testing (4) are not available, but P is known to be greater than the ideal value. The signs of terms in the exponentials insure that the deviations calculated from (4) are in the right direction. It should be noted that (4) can hold below 2.19°K for a range dependent on x_3 since He^3 depresses the lambda-point.

For temperatures less than the lambda-temperature, the treatment must be modified to include the influence of superfluid. Rice and Engel[18] have proposed corrections for the presence of superfluid. Adding these correction terms to the chemical potential expressions (2) and (3) multiplies the nonsuperfluid total pressure by corresponding corrections so that

$$\text{total pressure}=P_s(x_3+x_{4n})^{-1}\times\exp\{S_\lambda[x_{4s}+\ln(1-x_{4s})]/R(r+1)\},$$

where P_s is the right side of (4) with x_{4n} replacing x_4, S_λ is the entropy at the lambda-point, r is an empirical constant given in reference 18, n refers to normal fluid, and s refers to superfluid. It is important to note that the mole fractions used to evaluate P_s, as well as the correction factor, must be calculated from the total number of moles $N_3+N_{4n}+N_{4s}$. Rice and Engel[18] have indicated the use of the equality of normal and superfluid chemical potentials for calculation of x_{4n} and x_{4s} from the total amount of He^4 and the total amount of He^3 in a given sample. As it should, the expression for the total pressure reduces to P, the nonsuperfluid value, when $x_{4s}=0$.

IV. LAMBDA-POINTS OF THE SOLUTION MODEL

Thermodynamic investigation of the He^3 composition effect on He^3-He^4 solution lambda-points, as described by Rice,[4] has involved the assumption of solution ideality. Investigation of the lambda-point-composition relation for the non-ideal model described above can

[13] W. H. Keesom, *Helium* (Elsevier Publishing Company, Inc., New York, 1942).
[14] Grilly, Hammel, and Sydoriak, Phys. Rev. **75**, 1103 (1949).
[15] J. A. Beattie, Chem. Revs. **44**, 178 (1949).
[16] van Kranendonk, Compaan, and de Boer, Phys. Rev. **76**, 998 (1949).
[17] J. Kistemaker and W. H. Keesom, Physica **12**, 227 (1946).
[18] O. K. Rice and O. G. Engel, Phys. Rev. **78**, 183 (1950).

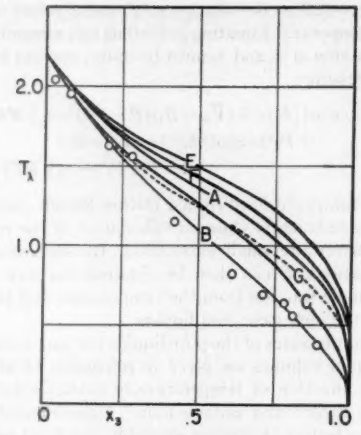

FIG. 1. Lambda-temperature *vs* He^3 mole fraction. Experimental points are circled.

point in some measure to the relative importance of the ideality assumption. The fundamental equation of Engel and Rice[3] in the two fluid lambda-point discussion is

$$-\bar{S}_{4n,\lambda}dT_\lambda=-\bar{S}_{4n,\lambda}dT_\lambda+(\partial\mu_{4n}/\partial x_3)_\lambda dx_3 \qquad (5)$$

where the notation is the same as that of reference 3. Rearrangement of (5) gives the change of T_λ with composition as

$$dT_\lambda/dx_3=(\partial\mu_{4n}/\partial x_3)_\lambda/(\bar{S}_{4n}-\bar{S}_{4s}). \qquad (6)$$

Non-ideality effects for the solution model appear in the partial derivative in (6), and these effects are introduced explicitly by calculation of this quantity from (3). Equation (3) is appropriate since the mole fraction of superfluid is taken as zero along the lambda-curve. Noting that $x_3+x_4=1$, expressing f_3 in terms of mole fractions and volumes, and taking μ_{4n}^0, V_3, V_4, and a as properties of the pure materials, one obtains by differentiation of (3)

$$\begin{aligned}(\partial\mu_{4n}/\partial x_3)_\lambda&=-RT_\lambda/(1-x_3)\\&\quad+2V_4^2V_3af_3/(x_3V_3+x_4V_4)^2\\&=-1.987T_\lambda/(1-x_3)\\&\quad+152.66x_3/(2.397+x_3)^3 \qquad (7)\end{aligned}$$

if $V_3=38.86$ cm³/mole, $V_4=27.42$ cm³/mole, and $a=0.1005$ cal/cm³.

With the information of (7) available, the problem of representing T_λ as a function of x_3 is reduced to that of representing the partial molal entropies as functions of T_λ and x_3. Since the solution model has as one of its basic features zero excess entropy, the concentration dependence is simple. The temperature dependence is more speculative, and each of the possibilities discussed by Engel and Rice[3] for the ideal solution is considered here.

There remains one further uncertainty concerning the superfluid term. Previous workers have shown that either $\bar{S}_{4s}=0$, or $\bar{H}_{4s}=0$ is a possibility. Assumption of the former and of solution ideality gives essentially the results of Gorter,[2] while the latter gives those of Rice.[4] Starting with either the Gorter or Rice case, one can distinguish subcases depending on the heat capacity behavior assumed.

Cases for which $\bar{S}_{4s}=0$

For the Gorter case, Eq. (6) yields the general result,

$$dT_\lambda/dx_3=D/\bar{S}_{4n}, \qquad (8)$$

where $D\equiv(\partial\mu_{4n}/\partial x_3)_\lambda$. If C_p is zero and, therefore, $\bar{S}_{4n}^0$ is temperature independent, $\bar{S}_{4n}=1.59-R\ln(1-x_3)$ where the experimental value at the normal lambda-point, 1.59 cal/deg/mole, has been used. Since D is known from (7), the equation can be integrated. The results appear as curve E in Fig. 1.

Assumption of a linear heat capacity will make $\bar{S}_{4n}^0$ equal to AT and $\bar{S}_{4n}=AT-R\ln(1-x_3)$. The constant A is 0.725 cal/deg²/mole since S_{4n}^0 is 1.59 cal/deg/mole when T is 2.19°K. The results of this heat capacity assumption appear as curve F.

The third heat capacity subcase appears as curve A. Here the heat capacity is assumed to remain equal to its value of 2.2 cal/deg/mole at 2.19°K for a short interval and then decrease to zero according to a T cube relationship, so that there must be a separate discussion for each part of the C_p curve. The method of determination of the range for constant C_p and for AT^3 value of C_p is that given by Engel and Rice,[3] but the entropy and enthalpy data are those used by Rice.[4] As a result

$$C_p=2.2 \text{ cal/deg/mole}, \qquad 2.19°\text{K}\geqslant T\geqslant 1.48°\text{K},$$
$$C_p=0.679T^3 \text{ cal/deg/mole}, \qquad 1.48°\text{K}\geqslant T\geqslant 0°\text{K}.$$

For the upper portion of the curve

$$\bar{S}_{4n}=2.2\ln T-0.135-R\ln(1-x_3),$$

while for the lower part $\bar{S}_{4n}=0.2263T^3-R\ln(1-x_3)$. This modified cubic behavior seems to give the closest approximation to the experimental values for any of the $\bar{S}_{4s}=0$ cases.

Cases for which $\bar{H}_{4s}=0$

Engel and Rice,[3] in examining ideal solutions, assumed that $\bar{H}_{4s}$ vanishes, rather than $\bar{S}_{4s}$, and transformed (6) to read

$$dT_\lambda/dx_3=DT_\lambda/\bar{H}_{4n,\lambda}. \qquad (9)$$

The problem of determining the lambda-temperature shift, then, is that of expressing $\bar{H}_{4n}$ as a function of x_3 and T_λ.

Scatchard has calculated[7] for the model solution the

heat of mixing, a quantity in general different from the excess free energy because of the volume change on mixing. Discarding compressibility terms, one has approximately $H^M=E_v{}^M+V^MT\alpha_0/\beta_0$ where α_0 is the coefficient of thermal expansion for the isolated components. Assuming that $\alpha_0=\alpha_4$, the value for He^4, and differentiating, one has $\bar{H}_{4n}=\bar{H}_{4n}{}^0+V_4af_3{}^2(1+\alpha_4T)$. For the very small values of T considered, α_4 is about 0.03 deg^{-1}. Thus it appears that, if one discards the thermal expansion term, $\bar{H}_{4n}=\bar{H}_{4n}{}^0+V_4af_3{}^2$, and the excess free energy and the enthalpy of mixing will, for the special circumstances considered, be alike. This treatment of the enthalpy is rather rough, and its best justification is perhaps the simplicity of the concentration dependence. Certainly the assumption of a zero heat of mixing is no bolder than the above. So both zero and nonzero heats of mixing are to be considered along with the three types of temperature behavior used in the previous section. There are, then, six subcases under the general case $\bar{H}_{4s}=0$.

For the zero heat of mixing and zero heat capacity $\bar{H}_{4n}=2.95$ cal/mole, the experimental value for $\bar{H}_{4n}{}^0$ at the normal lambda-point. Integration of the T_λ equation for this value gives results shown as curve A; the points are not identical with those of the previous section presented as curve A, but are so close that a single graph is sufficient to represent both sets of results.

A linear C_p and zero heat of mixing produce $\bar{H}_{4n}=1.21+0.3625T_\lambda{}^2$. Integration of (9) for this set of assumptions yields the results appearing as curve C.

The modified cubic C_p and zero heat of mixing give $\bar{H}_{4n}=2.2T_\lambda-1.868$ between the normal lambda-point and 1.48°K and $\bar{H}_{4n}=0.1698T_\lambda{}^4+0.5736$ below 1.48°K. Curve B represents the lambda-temperatures obtained.

In order to modify the above enthalpies in accordance with the nonzero heat of mixing described, one has only to add to each expression for $\bar{H}_{4n}$ the term $V_4af_3{}^2$, that is, $2.76f_3{}^2$. The zero heat capacity assumption then will give curve F. The linear C_p will produce curve A, and the modified cubic results in curve G. Again it should be noted that the points for $C_p=0$ and $C_p=AT$ do not fall precisely on curves F and A, but they are so close that separate curves are not desirable in the figure.

Solution of the Differential Equations

Constants of integration appearing in solutions of the lambda-point shift equations can be determined from the condition that T_λ has its normal value, 2.19°K, when there is no He^3, that is, when x_3 is zero. Each of the differential equations was solved by numerical integration, T_λ being determined for $0\leqslant x_3\leqslant 1$ in steps of 0.02 in x_3. The values for curve (B), the closest to the experimental points, are represented empirically by

$$T_\lambda=2.19/[1-3.397\log_{10}(1-x_3)]+0.04175x_3+0.2195x_3{}^2-0.471x_3{}^3$$

for $0\leqslant x_3\leqslant 0.93$; the largest deviation of this equation from the integration values is 0.005°. For solutions more concentrated than 0.93, the deviations are too large for use of the equation and integration values are quoted here as 0.276°K for $x_3=0.94$ and 0.222°K for $x_3=0.96$, respectively.

V. COMPARISON OF MODEL AND EXPERIMENTAL BEHAVIOR

Precise measurement of equilibrium total pressure considered in Sec. III offers a means of determining the degree of success of the non-ideality theory without involving any of the speculations of Sec. IV. If one could obtain such pressures and vapor compositions, the actual values of the excess potentials could be found and could then be used in the solution of problems appearing in Sec. IV. As it is, one can but check a number of assumptions at once by examining the experimental T_λ *vs* x_3 curve. The direction of deviation from Raoult's law is known and the non-ideality model considered does offer agreement. So the lambda-point properties of the model mixture can be at least a general guide to the success of some superfluid property assumptions in the T_λ treatment.

For the model considered, better results are obtained for assumption of vanishing $\bar{H}_{4s}$ than for vanishing $\bar{S}_{4s}$. The entire group of $\bar{S}_{4s}$ curves (E, F, and A) lies a considerable distance to one side of the experimental curve, while the $\bar{H}_{4s}$ group in general lies much closer and provides one member (curve B) giving an excellent representation of the experimental points. Comparison of C_p models shows that, for any given situation, the modified cubic behavior gives better agreement than the linear. The assumption of temperature invariance for entropy and enthalpy leads to the greatest departure from agreement for any basic choice. This feature would seem a considerable improvement over the ideal treatment in which at least one of the $C_p=0$ curves lies very near the experimental values.

Within the group for which $\bar{H}_{4s}$ is zero, the results for vanishing mixing enthalpy of He^4 are better than for the composition dependent value (e.g., compare curves B and G). This fact is a reminder that (2) and (3) do not provide the whole picture of non-ideality. Finally, the properties of the simple model considered here seem to support the idea that, for the actual solution, the heat of mixing of He^3 and He^4 is very small, that $\bar{H}_{4s}=0$, and that the heat capacity of normal He^4 goes to zero at $T=0$°K in a manner similar to that of Engel and Rice's modified cubic relation.

Phase Shifts in the Molecular Beam Method of Separated Oscillating Fields*

NORMAN F. RAMSEY AND HENRY B. SILSBEE
Harvard University, Cambridge, Massachusetts
(Received July 20, 1950)

The effects of phase differences between the two oscillating fields in the separated oscillating fields method for molecular beam radiofrequency spectroscopy is discussed theoretically. It is shown that measurements in which the relative phase is changed from 0° to 180° effectively double the intensity of the signal and hence increase the sensitivity of the apparatus. Phase shifts of $\pi/2$ radians give resonances in the form of dispersion curves. Consequently, measurements in which the phase is changed from $+\delta$ to $-\delta$, where δ is near 90°, give particularly sensitive means of determining the resonance frequency.

IN Ramsey's[1] original paper on the molecular beam resonance method with separated oscillating fields, the only case considered was that in which the two oscillating fields were in the same phase. However, if the second field leads the first by a phase angle δ the first part of the earlier paper[1] must be modified by the replacement of $\omega(\tau+T)$ by $\omega(\tau+T)+\delta$ in Eqs. (8e) and (8f). As a result, the λT in Eq. (12) is replaced by $\lambda T-\delta$ and the probability for transition from state p to state q is

$$ {}_aP_{p,q}=4\sin^2\theta\sin^2\tfrac{1}{2}a\tau[\cos\tfrac{1}{2}(\lambda T-\delta)\cos\tfrac{1}{2}a\tau - \cos\theta\sin\tfrac{1}{2}(\lambda T-\delta)\sin\tfrac{1}{2}a\tau]^2, \quad (1)$$

where τ is the length of time the molecule is in each of the oscillating field regions, T is the length of time in the intermediate regions, $\hbar be^{i\omega t}$ is the perturbation inducing the transition, and the remaining quantities are defined by

$$ a=[(\omega_0-\omega)^2+(2b)^2]^{\frac{1}{2}}, \qquad \omega_0=(W_q-W_p)/\hbar, $$
$$ \cos\theta=(\omega_0-\omega)/a, \qquad \sin\theta=2b/a, \quad (2) $$

and

$$ \lambda=[(\bar{W}_q-\bar{W}_p)/\hbar]-\omega. \quad (3) $$

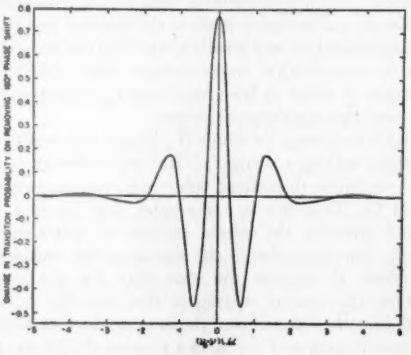

FIG. 1. Theoretical change in transition probability on removing 180° phase shift.

The interesting limit for (1) is that near resonance where $|\omega_0-\omega|$ is much less than $2b$, in which case

$$ {}_aP_{p,q}=\sin^2 2b\tau\cos^2\tfrac{1}{2}(\lambda T-\delta). \quad (4) $$

This expression may be averaged over the molecular velocities with the usual molecular beam weighting factor to yield

$$ \langle {}_aP_{p,q}\rangle_{Av}=2\int_0^\infty \exp(-y^2)\,y^3\sin^2\left(\frac{2bl}{\alpha y}\right) \times\cos^2\left(\frac{\lambda L}{2\alpha y}-\frac{\delta}{2}\right)dy, \quad (5) $$

where y is the molecular velocity divided by the most probable velocity $\alpha=(2kT/m)^{\frac{1}{2}}$ while l is the length of each oscillating field region and L is the length of the intermediate region.

The numerical work of evaluating (5) can be much simplified by the use of trigonometric expansions to reduce it to a sum of terms involving only the two integral functions,

$$ I(x)=\int_0^\infty \exp(-y^2)\,y^3\cos(x/y)dy, \quad (6) $$

and

$$ K(x)=\int_0^\infty \exp(-y^2)\,y^3\sin(x/y)dy. \quad (7) $$

With this notation, (5) becomes

$$ \langle {}_aP_{p,q}\rangle_{Av}=\tfrac{1}{4}-\tfrac{1}{2}I(4bl/\alpha)+\cos\delta[\tfrac{1}{2}I(\lambda L/\alpha) -\tfrac{1}{4}I(4bl/\alpha+\lambda L/\alpha)-\tfrac{1}{4}I(4bl/\alpha-\lambda L/\alpha)] +\sin\delta[\tfrac{1}{2}K(\lambda L/\alpha)-\tfrac{1}{4}K(4bl/\alpha+\lambda L/\alpha) +\tfrac{1}{4}K(4bl/\alpha-\lambda L/\alpha)]. \quad (8) $$

The functions $I(x)$ and $K(x)$ have been tabulated by Kruse and Ramsey[2] and may be used to evaluate the transition probability.

The value of (8) depends not only on δ and λ but also on $2bl/\alpha$. As discussed in the previous paper,[1] the most suitable value of $2bl/\alpha$ for many purposes is 0.600π;

* This work was partially supported by the joint program of the ONR and AEC.
[1] N. F. Ramsey, Phys. Rev. **78**, 695 (1950).
[2] U. E. Kruse and N. F. Ramsey, J. Math. Phys. **30**, 40 (1951).

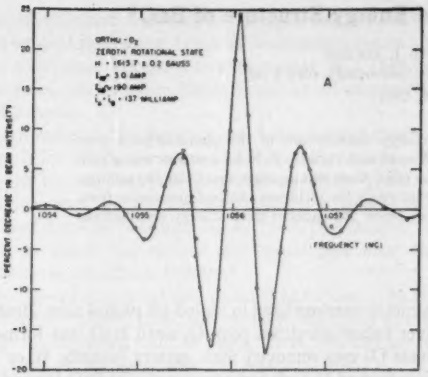

FIG. 2. Experimental change in beam intensity on removing 180° phase shift with ortho-D_2 in zeroth rotational state.

consequently all of the accompanying curves are for this value.

One of the most useful cases of the introduction of a relative phase shift δ is that in which the change in molecular beam intensity is measured as δ is changed from 0 to π-radians. Then

$$\langle {}_0P_{p,q}\rangle_{Av}-\langle {}_\pi P_{p,q}\rangle_{Av}\equiv A=I(\lambda L/\alpha)-\tfrac{1}{2}I(4bl/\alpha+\lambda L/\alpha)-\tfrac{1}{2}I(4bl/\alpha-\lambda L/\alpha). \quad (9)$$

This expression is plotted in Fig. 1 as a function of $(\nu_0-\nu)L/\alpha$, where $\nu=\omega/2\pi$, with the value of 0.600π for $2bl/\alpha$. For comparison purposes, an experimental curve of the change in beam intensity for the nuclear resonance in ortho-D_2 is shown in Fig. 2.

The change in the ordinate between maxima and minima in Fig. 1 is just double that in Fig. 2 of the earlier paper[1] in which the change in beam intensity is to be observed when the oscillator is successively turned off and on. Therefore, the phase shifting method of observation provides the equivalent of a doubling of the beam intensity which can be of great value in experiments where the beam intensity is a limiting factor.

An additional feature of the method is that the rf amplitude is constant, which is an advantage if the beam detector is sensitive to rf "pickup." Also, the slowly varying first two terms of (8) are not observed since they are independent of δ. This may be an advantage in searching for resonances, particularly if lines are close together.

An alternative case of considerable interest is that in

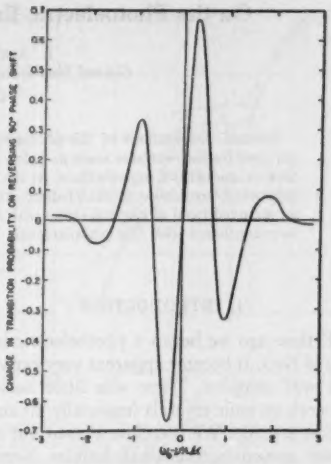

FIG. 3. Theoretical change in transition probability on reversing 90° phase shift.

which δ is changed from $\frac{1}{2}\pi$ to $-\frac{1}{2}\pi$. Then (8) becomes

$$\langle {}_{\frac{1}{2}\pi}P_{p,q}\rangle_{Av}-\langle {}_{-\frac{1}{2}\pi}P_{p,q}\rangle_{Av}\equiv B=K(\lambda L/\alpha)-\tfrac{1}{2}K(4bl/\alpha+\lambda L/\alpha)+\tfrac{1}{2}K(4bl/\alpha-\lambda L/\alpha). \quad (10)$$

The graph of this expression is plotted in Fig. 3. The curve can be seen to be of a dispersion type and to pass through zero at the resonance frequency. Since the curve is very steep as it passes through the resonance value, this technique provides a particularly sensitive means for experimentally locating the exact resonance frequency.

Theoretical curves for other phase shifts can be obtained from (8). However, the calculation can often be simplified by noting from (8), (9), and (10) that

$$\langle {}_\delta P_{p,q}\rangle_{Av}=\tfrac{1}{4}-\tfrac{1}{2}I(4bl/\alpha)+\tfrac{1}{2}A\cos\delta+\tfrac{1}{2}B\sin\delta. \quad (11)$$

For the value of $2bl/\alpha$ equal to 0.600π,

$$\langle {}_\delta P_{p,q}\rangle=0.383+\tfrac{1}{2}A\cos\delta+\tfrac{1}{2}B\sin\delta, \quad (12)$$

where A and B can be obtained from Fig. 1 and Fig. 3.

In particular, from (12) one sees that

$$\langle {}_\delta P_{p,q}\rangle_{Av}-\langle {}_{-\delta}P_{p,q}\rangle_{Av}=B\sin\delta. \quad (13)$$

Therefore, a curve passing sharply through zero at resonance can be obtained even if the phase shift departs somewhat from $\frac{1}{2}\pi$ provided only that the one phase shift is exactly the negative of the other.

On the Photoelectric Emission and Energy Structure of BaO*

L. Apker, E. Taft, and J. Dickey
General Electric Research Laboratory, Schenectady, New York
(Received July 16, 1951)

Spectral distributions of the photoelectric yield and energy distributions of the photoelectrons were obtained for BaO surfaces made in widely different ways. A small and variable yield for $h\nu < 5$ ev was attributed to unidentified imperfections. At the optical absorption edge, there was an effect much like the exciton-induced photoemission in alkali halides. At $h\nu \sim 5$ ev, an abrupt rise in the yield was ascribed to emission from an occupied band of electron states with an upper edge 5 ev below the vacuum level. Energy distributions were consistent with this interpretation.

1. INTRODUCTION

SOME time ago we began a photoelectric investigation of BaO. It became apparent very early that the problem was complex. There was little basic photoelectric work on ionic crystals (especially divalent ones) to serve as a guide. We therefore turned our attention to simpler materials, the alkali halides. Some of the subsequent results have been reported.[1] They form much of the basis for the point of view taken here.

This paper describes the work on BaO. The main conclusion offered is that a photon energy near 5 ev is required to raise an electron from the occupied energy band of BaO to the vacuum level. Various phenomena observed at lower photon energies are briefly mentioned.

2. EXPERIMENTAL TECHNIQUES

This report is based on observations of several hundred surfaces. They were of three general types, prepared in the following ways: (1) Evaporated films of Ba metal were oxidized in sealed-off phototubes. Heated silver tubes[2] admitted pure O_2 until BaO was formed; excess O_2 was removed with getters (usually W or Ta wires flashed at high temperatures). (2) BaO formed by pyrolysis of $BaCO_3$ was evaporated from pure Pt ribbons.[3] (3) BaO surfaces were formed directly by pyrolysis of $BaCO_3$ on various substrates.

The phototubes were of several different varieties, most of which have been described before:[4] (a) Spherical collectors with interchangeable emitters permitted simultaneous measurements of contact potentials and photoelectron energy distributions at 300°K as well as at somewhat higher temperatures; (b) Cylindrical diodes with central emitters were used to determine spectral distributions of photoelectric yields at 300°K and at slightly higher temperatures; (c) Diodes like those used in alkali halide work[1] furnished spectral distributions at 300°K and at ~85°K.

Other experimental details have been given previously.[4]

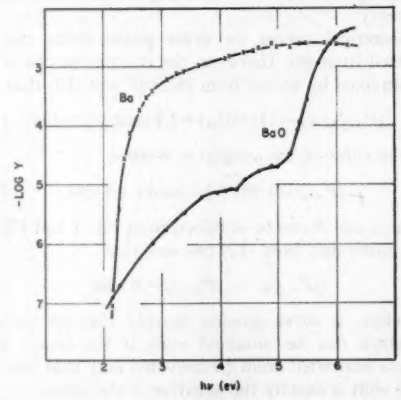

FIG. 1. Spectral distribution of the photoelectric yield Y (in electrons/quantum) for metallic Ba and for BaO formed by oxidizing this same sample.

3. SPECTRAL DISTRIBUTION OF THE PHOTOELECTRIC YIELD

Perhaps the most interesting way to observe the frequency variation of the photoelectric emission from BaO is to measure a Ba metal film and then to oxidize it (method 1, Section 2). Data obtained in this way with a phototube of type (a) in Section 2 are shown in Fig. 1. The threshold of the Ba metal is near 2.3 ev, and the yield follows the usual trend for a metal of this sort. When the metal is converted to BaO (at ~600°K), drastic changes occur in the photoemission. For $h\nu$ between 3 and 5 ev, the yield drops by a factor of 100 or more, depending on the completeness of the oxidation. For $h\nu$ between 1 and 2 ev (i.e., in a region where no emission is observable from pure Ba metal), a very small yield may appear. A rise in this yield may occur near 3.8 ev, the absorption edge of BaO.[5] (In Fig. 1

* Preliminary reports on this work have been given at American Physical Society meetings in Cambridge, Massachusetts, June, 1949 and in New York, January, 1950.

[1] L. Apker and E. Taft, Phys. Rev. **79**, 964 (1950); **81**, 698 (1951).

[2] J. B. Taylor, Rev. Sci. Instr. **6**, 243 (1935).

[3] We are grateful to George E. Moore of the Bell Telephone Laboratories for the pure Pt used here. (See Phys. Rev. **77**, 247 (1950).) The $BaCO_3$ was Mallinckrodt Ultra Pure.

[4] See reference 1. Also: Apker, Taft, and Dickey, Phys. Rev. **74**, 1462 (1948); **73**, 46 (1948). A diagram of one type of tube is given in a review by J. A. Becker, Elec. Eng. **68**, 937 (1950).

[5] W. W. Tyler, Phys. Rev. **83**, 548 (1951); E. Taft and J. Dickey, Phys. Rev. **78**, 625 (1950). This rise in the yield from BaO

this effect is not clear-cut, but a slight rise is nevertheless evident just above 4 ev.) As $h\nu$ increases above 5 ev, the yield rises abruptly to values near 10^{-2} electron/quantum, considerably higher than the maximum yield of Ba metal.

Examples of this same general behavior are shown in Fig. 2 for BaO specimens made in other ways. The abrupt rise at 5 ev has been characteristic of all our samples, regardless of the method used to make them. In contrast, the behavior for $h\nu<5$ ev depends on the way in which the sample was made and may also depend on irradiation history.[6]

We have interpreted these results as follows: The rise at 5 ev we believe to be due to photoelectrons ejected from the occupied band of BaO. Thus, the top of this band lies about 5 ev below the vacuum level.

The small yield for $h\nu<5$ ev we attribute to photoelectric emission from impurities and imperfections, probably of several kinds. Permanent centers (presumably electrons in vacancies) may be associated either with excess Ba or with foreign atoms in the material. Metastable centers may be produced during irradiation, particularly for $h\nu>3.8$ ev;[6] these may be due to traps either normally in BaO or associated with foreign atoms. If the time required for metastable centers to form or to decay is long enough, the effect may be isolated easily and treated independently. We have observed times as short as three seconds, however, in certain evaporated films. In such cases, separate treatment of metastable centers was not convenient in our work.

The rise in the yield at $h\nu\sim3.8$ ev we believe to be caused by exciton-induced photoelectric emission from the centers mentioned above. In some samples, metastable centers which formed rapidly during the measurement also contributed to the effect. Other structure near this edge may arise because of the onset of opacity in the film and because of frequency-dependent optical reflection at the surface.[1] The important point here is that this feature in the yield is not a primary effect. It may not be considered as due to occupied energy levels beginning 3.8 ev below the vacuum level. It is indicative only of the onset of optical absorption and related processes.

Since a small yield in many samples is observable for $h\nu\sim1.5$ ev, we conclude that occupied impurity levels may lie only a little more than 1 ev below the vacuum level. As Herring[7] has emphasized, the Franck-Condon principle must be kept in mind in considerations like these. We remember, therefore, that the photoelectric thresholds of these BaO samples may not be correlated in any simple way with thermionic work functions or with contact potentials. Further, conditions in the material may deviate from equilibrium. In similar work on RbI,[8] discrepancies with these origins amounted to more than 1 ev. In BaO, they appear to be less.

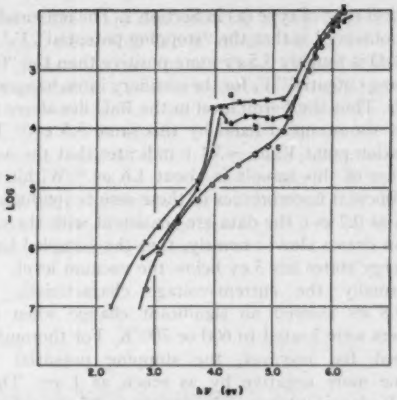

FIG. 2. Spectral distributions for BaO made as follows: (a) by pyrolysis of $BaCO_3$; (b) by oxidation of Ba metal; (c) by evaporation of BaO from a Pt ribbon. The thickness of the last sample was of the order of 10^{-6} cm. The structure near the absorption edge at 3.8 ev frequently does not appear for such thin samples, perhaps because of exciton destruction at surfaces.

The form of the spectral distribution in this region ($h\nu<3.8$ ev) varied considerably in our work. It was evident that the impurities were not always the same and that their concentration varied markedly. (It should be noted here that we are not considering impurity densities comparable with those in activated BaO cathodes.)

When the temperature is reduced to ~85°K, the yield for $h\nu<5$ ev sometimes increases when rapidly-formed metastable centers attain a higher concentration during the measurement. The rise in the spectral distribution at $h\nu\sim3.8$ ev retains its location, however, to within 0.1 ev. This agrees with the temperature independence of the optical absorption as measured by Tyler.[5] While there is an indication that the abrupt rise in the yield near 5 ev becomes slightly steeper,[9] this feature shifts by less than 0.1 ev also.

4. ENERGY DISTRIBUTION OF THE PHOTOELECTRONS

Figure 3 shows current-voltage characteristics for a typical BaO sample made by oxidizing Ba metal in a

was noticed previously by H. B. DeVore and John W. Dewdney, Phys. Rev. **83**, 805 (1951), to whom we are indebted for discussions of this subject. Tyler's data show another increase in the optical absorption coefficient just above 5 ev. As pointed out below, the photoemission rises abruptly near this same point. At the present stage of our knowledge, we see no connection between these two effects, and the agreement is interpreted here as coincidental.

[6] J. Dickey and E. Taft, Phys. Rev. **80**, 308 (1950). Extensive measurements have been made on activated samples by B. D. McNary, Phys. Rev. **81**, 631 (1951), to whom we are indebted for an advance copy of his manuscript. If the sample is pure, this effect is large only in the region of fundamental optical absorption, $h\nu>3.8$ ev. A less prominent effect may be obtained for smaller $h\nu$ if there is optical absorption outside the fundamental range.

[7] C. Herring, private communication; Phys. Rev. **73**, 1238 (T) (1948).

[8] L. Apker and E. Taft, Phys. Rev. **82**, 814 (1951).

[9] Such an effect could be due to the phenomena discussed by H. B. Callen, Phys. Rev. **79**, 533 (1950).

spherical tube of type (a) in Section 2. The outstanding effect observed is that the "stopping potential" V_0' for the BaO is roughly 3.5 ev more positive than the "0°K stopping potential" V_0 for the auxiliary interchangeable metals. Thus the Fermi level in the BaO lies above the top of the occupied band by this same 3.5 ev.[10] The saturation point V_s at ~3.1 v indicates that the work function of this sample is about 1.6 ev.[11] Within the experimental uncertainties in these results (perhaps as much as 0.2 ev), the data are consistent with the conclusion drawn above: namely, that the occupied band of energy states lies 5 ev below the vacuum level.

Normally the current-voltage characteristic for $h\nu=5.8$ ev showed no significant change when the emitters were heated to 600 or 700°K. For thoroughly oxidized Ba, however, the stopping potential V_0' became more negative by as much as 1 ev. Thus, $V_0'-V_0$ decreased from 3.5 ev to about 2.5 ev as shown in Fig. 3. This result would be expected if the Fermi

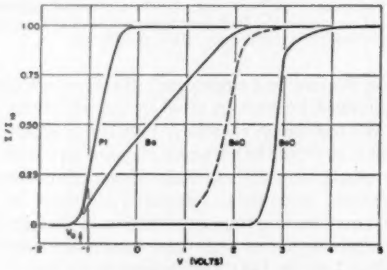

FIG. 3. Current-voltage characteristics for BaO and two typical metals; $h\nu=5.80$ ev, $T=300$°K. The dotted curve shows data on a vigorously oxidized sample at $T\sim650$°K. The point $V_0=-1.16$ volts corresponds to the Fermi level.

level dropped toward the occupied band when the temperature increased. This is a well-known characteristic of an N-type semiconductor with a very small concentration of donors. The data given here are consistent with this view, since the shift occurs only fothoroughly oxidized samples in which donor levels would be expected to exist only in greatly reduced concentration.

The spectral distribution of the yield for the BaO of Fig. 3 was practically the same as in Fig. 1. At 5.8 ev, therefore, all but about 1 percent of the yield arose in the occupied band of energy states. The rest came, of course, from the occupied impurity levels, some of which were as much as 3 ev higher in energy. The contribution of this latter component is not visible on the scale of Fig. 3. It is best seen on a logarithmic plot (of the type used to determine V_0', for example).[10] In such a case, it is still clearly distinguishable from the current arising in the occupied band, since this larger component rises abruptly out of the background. While the impurity yield tends to shift V_0' toward negative voltages, the resulting error is only 0.1 or 0.2 ev and of little consequence here.

Current-voltage characteristics for the impurity component rose to measurable values only when V was several tenths of 1 ev above V_0. (This is quite different from the behavior for a metallic emitter, of course, but is consistent with the Franck-Condon effect mentioned earlier.) They then increased in slope in a more or less regular manner, roughly along an exponential, at a rate near one decade per 1.3 v. This is much like the behavior of the so-called s-group of photoelectrons ejected from F-centers in RbI by exciton stimulation.[8] Since a similar process is possible in BaO for $h\nu>3.8$ ev, this resemblance is not surprising.

If the impurities were all identical, one would expect photoelectrons ejected by direct ionization ($h\nu<3.8$ ev) to emerge in a band of energies like the f-group observed for RbI.[8] We have not been able to reproduce such an effect with BaO (although some indications of it appeared in rare cases). There are probably several reasons for this: First, the data of Fig. 1 are not characteristic of a uniform material containing impurities of a single kind. Second, scattering of excited electrons may obliterate the effect if the impurity concentration increases with depth in the sample.[12] Third, patch fields may distort this kind of distribution to such a degree that the accelerating field technique[11] cannot remedy it. Finally, the range of $h\nu$ available between the photoelectric threshold and the optical absorption edge is rather small for convenient work on this effect.

5. CONCLUDING REMARKS

The salient result presented above is the abrupt rise in the photoelectric yield from BaO when $h\nu$ reaches 5 ev. A simple interpretation attributes this effect to emission from an occupied band of electron energy

[10] The symbols used here are the same as in Phys. Rev. **74**, 1462 (1948). See also H. B. Huntington and L. Apker, Phys. Rev. **81**, 321(A) (1951). We assume that equilibrium concepts are meaningful in this case. Thus, we avoid discussing complications like those mentioned in reference 8.

[11] In many cases, samples were non-uniform, and saturation points were not clear-cut. This was a common difficulty also in previous work on alkali halides (reference 8). Since the effect was difficult to eliminate in the case of BaO, the following procedure was sometimes adopted: The metal sleeves which covered the hairpin-shaped emitter support were held several volts more positive than the emitter. (Normally they are held at a potential which just eliminates the stray fields due to the uncontrolled contact potentials.) Under these conditions, retarding-potential measurements may be made in the usual way, but an accelerating field is maintained at the emitter surface. Although a small fraction of the current is diverted to the sleeves, tests with uniform surfaces showed that characteristics were not seriously distorted near the saturation point by this procedure [see, for example, Phys. Rev. **73**, 46 (1948)]. In this case of non-uniform surfaces, the saturation points became more sharp and reproducible. The stray fields due to the relatively large-scale patches then had only a small effect in the presence of the accelerating field at the emitter surface. Patch fields were most troublesome with samples made by methods (1) and (3) of Sec. 3. Evaporated films were much more uniform.

[12] Malcolm Hebb, private communication (to be published); Phys. Rev. **81**, 702 (1951).

states with an upper edge 5 ev below the vacuum level. Energy distribution data are consistent with this picture. Krumhansl has arrived at a more complete energy structure by combining this result with the optical data obtained at Cornell.[13]

Photoelectric data for $h\nu<5$ ev are treated only briefly. They are not believed to represent intrinsic emission from BaO. Yields in this region are variable and are ascribed to imperfections, some of which may be metastable; a more complete interpretation has not been attempted. Such yields are complicated further by Franck-Condon effects, by rapid changes in optical properties, and by an effect like the exciton-enhanced photoelectric emission observed in alkali halides.

We are indebted to Harvey Brooks, J. A. Burton, Malcolm Hebb, Conyers Herring, and A. W. Hull for stimulating conversations.

[13] J. Krumhansl, Phys. Rev. 82, 575 (1951) (T). Calculations by D. A. Wright, Proc. Phys. Soc. (London) 60, 13 (1948), place the edge and center of the occupied band 2.6 and 6.6 ev, respectively, below the vacuum level. This location of the band center is consistent with our result; the empirical value of the band width used by Wright in locating the edge was probably too large.

PHYSICAL REVIEW VOLUME 84, NUMBER 3 NOVEMBER 1, 1951

Statistical Theory of Properties of Solid Solutions

R. SMOLUCHOWSKI
Carnegie Institute of Technology, Pittsburgh, Pennsylvania
(Received July 3, 1951)

Properties of binary solid solutions are considered from the point of view of the fluctuation of local composition in the crystalline lattice. These variations influence the properties of the alloys by varying the corresponding local concentration of electrons. A simple general statistical method is given for calculating properties of random and ordered solid solutions. The theory is applied to saturation magnetization, temperature coefficient of electrical resistivity, thermoelectric power, and to other properties in various alloys. A satisfactory agreement with experiment is obtained.

1. INTRODUCTION

THE studies of properties and of behavior of solid solutions are very important for understanding of metals. The change of composition makes possible, in favorable cases, the distinction between the influence of various factors and the estimate of the validity of the inevitable theoretical approximations. Many of the properties are closely related to the behavior of "free" electrons and in particular to their concentration. Typical examples here are saturation magnetization, magnetic susceptibility, electronic specific heat, Hall effect, electrical resistance, optical properties, etc. In the conventional theoretical approach to these phenomena, in accord with the band theory point of view, the metal is treated as a whole and the particular property is related to the average electronic concentration.

This strict band approach is justified when the electrons in question are very nearly free and their wavelength large compared to the atomic size. For more tightly bound electrons, as for instance in transition metals, the local electronic configuration of an atom and of its nearest surroundings should be taken into account. Such theories, if exact, are very complicated and therefore a simpler, approximate procedure is desired. The present paper describes such a method which incorporates the main features of the band theory and of the "local" point of view.

Since the average electronic concentration does not depend upon the state of order in a crystal lattice, it is clear that a statistical treatment of local electronic configuration is particularly important in a consideration of the influence of order[1] on the properties and phenomena mentioned above. A first attempt in this direction was made[2] in a theory of the influence of order on magnetostriction of iron-cobalt alloys. It appeared later that the procedure there employed, although satisfactory for the specific purpose, led to a wrong dependence of the saturation magnetization on composition. The new method here presented is a simple general tool, it explains various experimental facts (including the relation between order and magnetostriction), and it applies to many alloy systems.

2. THE STATISTICAL METHOD

The basic procedure in the theory is to calculate first the fluctuations of the local electronic configuration, then to estimate their individual contributions to the particular property and finally to sum the contributions of the various fluctuations. The first question is thus the choice of the proper size n of the group of atoms within which the electronic fluctuation has a significant meaning for the particular property. A natural assumption is to consider as a basic unit an atom and its nearest neighborhood. In a close-packed lattice, either

[1] R. Smoluchowski, Intern. Conf. on Magnetism, Grenoble, 1950; J. phys. radium 12, 389 (1951); Phys. Rev. 78, 638 (1950).
[2] R. Smoluchowski and J. E. Goldman, Phys. Rev. 75, 140 (1949).

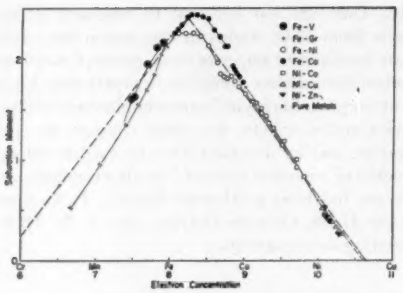

FIG. 1. Saturation magnetization in alloys.

cubic or hexagonal, an atom has twelve nearest neighbors and so, together with the central atom, there are thirteen atoms in the basic group. In a body-centered lattice, the six second nearest neighbors are only about 15 percent further out than the eight nearest and so a group of fifteen atoms, an atom and its fourteen neighbors, seems to be a proper choice (the third nearest neighbors are already over 40 percent further away). For a perfectly random binary alloy of A and B, in which the concentration of atoms A is p and the concentration of atoms B is $q=1-p$, one calculates the probability of having r atoms B among the n atoms in the group from the usual formula,

$$P_{n,r}=\binom{n}{r}p^{n-r}q^{r}. \tag{1}$$

Knowing the number of free electrons in both kinds of atoms, one obtains the probability of the occurrence of a particular local electronic concentration. The next step, the calculation of the contributions of the various local fluctuations to the particular property depends much upon the state of the theory of the property, upon whether the contributions are additive or not, and will in general differ from case to case.

3. SATURATION MAGNETIZATION

Saturation magnetization of alloys is usually correlated with electron concentration in an essentially

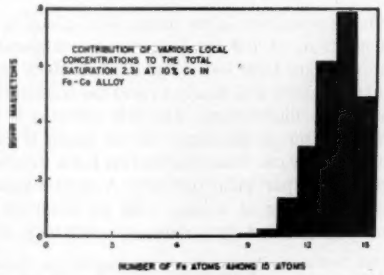
CONTRIBUTION OF VARIOUS LOCAL CONCENTRATIONS TO THE TOTAL SATURATION 2.31 AT 10% Co IN Fe-Co ALLOY
BOHR MAGNETONS
NUMBER OF Fe ATOMS AMONG 15 ATOMS

FIG. 2. Contribution of various fluctuations to the saturation moment of a random Fe-Co alloy.

semi-empirical manner, using the assumption that the $3d$-band is divided into two parts of appropriately chosen size. This theory leads, in the well-known manner, to a saturation moment which decreases linearly, at a rate of one Bohr magneton per electron, from its maximum value of about 2.56 at 8.35 electrons per atom as indicated in Fig. 1. A criticism of this point of view and an alternate explanation of the behavior was proposed elsewhere.[1] We assume that an ideally linear behavior of the saturation magnetization on both sides of the maximum is understood.

a. Iron-Cobalt Alloys

We shall apply now the method outlined above to the body-centered iron-cobalt alloys. For several reasons, this is a particularly simple and interesting case: the maximum saturation occurs at a 35 percent Co composition, the body-centered phase of that system extends up to 70 percent Co, and the lattice constant, the α-γ transformation temperature, the melting point, etc.,

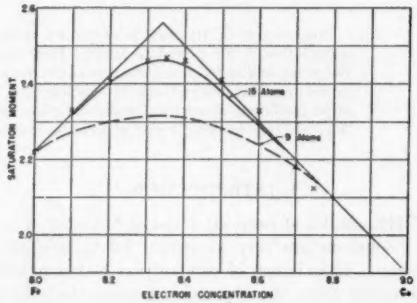

FIG. 3. Local and statistically averaged saturation moments for Fe-Co alloys.

vary only a little in that whole range. This is in contrast with the iron-nickel system considered later.

The saturation moment of pure iron is 2.22, that of body-centered cobalt is not known and so we have to obtain it by extrapolating the data for cobalt-rich alloys in the body-centered phase. The result is 1.90 as compared with 1.71 for hexagonal cobalt. On the basis of these values, the saturation magnetization reaches the maximum value of 2.56 at an electron concentration 8.34.

The linear relationship shown in Fig. 1 makes it possible to assign to each fluctuation of electron concentration a contribution to the saturation moment. These contributions, multiplied by the proper probability factors (1) for the occurrence of various ratios of atoms Fe and Co in the group of 15 atoms, are shown in Fig. 2 for an alloy containing 10 percent Co. The total moment in that case is 2.31. The results for the whole range of composition, together with the experimental points are shown in Fig. 3. The agreement is within 1½ percent which is satisfactory in view of the approximate

character of the theory. It may be noted here that had we assumed that the basic group in a body-centered lattice consists only of the eight nearest neighbors and the central atom, then the theoretical curve would fall much too low as shown in Fig. 3.

As indicated in the foregoing, the statistical treatment of local concentrations is particularly suitable for considering the influence of order since the degree of order does not influence the average electron concentration. The calculation of the saturation moment in a perfectly ordered 50:50 iron-cobalt alloy, on the basis of our theory, is as follows. In the ordered alloy there are only two alternatives in composition of the 15-atom group, either seven iron atoms and eight cobalt atoms or vice versa. The two electron concentrations are 8.467 and 8.533 giving for the saturation moments 2.43 and 2.37 with the average value 2.40. The theory indicates thus an increase of the saturation moment of about one percent on ordering. Experiment gives an increase of about four percent, which is not too satisfactory an agreement, although the sign and the order of magnitude are correct.

An interesting check of this theory can be obtained from neutron diffraction experiments. The presence of the small difference of only three percent between the moments 2.43 and 2.37 should be easily distinguished from the presence of the large difference of about 25 percent between the normal saturation moments of pure iron and pure cobalt as required by the usual theory. Preliminary, though not conclusive, results[3] seem to be in agreement with the existence of a small rather than large difference between the magnetic moments associated with the Fe and Co sites.

b. Iron-Nickel Alloys

A similar calculation has been made for the body-centered iron-nickel alloys using a 15-atom group. The difficulty in this case is due to the short range of composition within which the alloys are body-centered cubic and the highly irregular behavior of the lattice constant, which is presumably related to the complicated conditions in the two-phase region. The results are in fair agreement with experiment as shown in Fig. 4. In view of the uncertainty of extrapolation of the body-centered data to pure nickel, the usual value 0.6 was assumed for the saturation moment of nickel.

An interesting case in this alloy system is the face-centered cubic $FeNi_3$ composition in which an ordered lattice has a six percent higher saturation moment than the random lattice. It is natural to suppose that, since the face-centered iron is nonmagnetic, the iron atoms which are nearest neighbors in a random $FeNi_3$ lattice will not contribute to the saturation moment. This conclusion follows also from consideration of the known relationship between magnetic interaction, interatomic distance, and the size of the *d*-shell. The calculation of

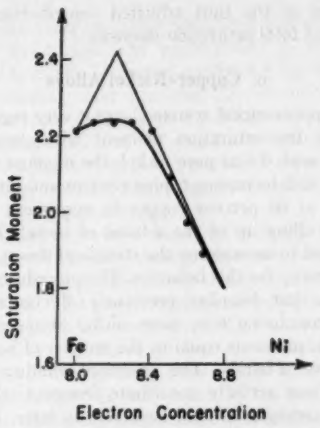

FIG. 4. Local and statistically averaged saturation moments for Fe-Ni alloys.

the saturation moment for the random $FeNi_3$ proceeds thus in the usual manner using a 13-atom group, but the contribution from each fluctuation is decreased in proportion to the iron-iron pairs. The result is 1.02 Bohr magnetons. In the ordered lattice we have again only two types of groups, a Ni atom surrounded by 8 Ni and 4 Fe atoms and a Fe atom surrounded by 12 Ni atoms. The average saturation moment corresponding to the two types of neighborhoods taken in proper ratio is 1.10. This corresponds to an increase of the saturation moment by eight percent in a rather good agreement with the experimental value of six percent. The absolute value of both calculated saturation moments is somewhat too low.

The procedure followed for the $FeNi_3$ alloy is applicable to other alloys[1] and can be briefly summarized as follows: In calculating contributions of the various concentration fluctuations account has to be taken of the variability of the magnetic interaction with distance between atoms as given, for instance, by the Néel curve.[1] Particular pairs of atoms in a fluctuation may lead to vanishing (or even negative) moments.

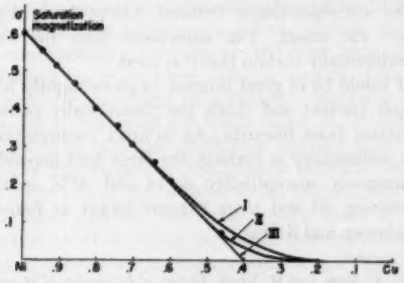

FIG. 5. Local and statistically averaged saturation moments for Cu-Ni alloys.

[3] C. G. Shull, private communication.

The sum of the thus adjusted contributions is the calculated total saturation moment.

c. Copper-Nickel Alloys

The copper-nickel system shows a very regular variation of the saturation moment with composition: starting with 0.6 at pure nickel, the moment decreases linearly with increasing copper content and extrapolates to zero at 60 percent copper in agreement with the gradual filling up of the d-band of nickel. It is thus important to see whether the statistical theory accounts satisfactorily for this behavior. The procedure is identical with that described previously: fluctuations of 13 atoms containing 6 or more nickel atoms contribute magnetic moments equal to the number of holes in the respective d-bands. The question whether all such fluctuations actually contribute irrespectively of the atomic arrangement will be taken up later. By multiplying the moments by the corresponding probability and summing the results, one obtains the curve I shown in Fig. 5. It appears that up to about 40 percent copper the behavior is linear and in agreement with experiment. At 54 percent copper, however, there is a definite discrepancy. This seems to be connected with the implicitly made assumption that as long as a fluctuation has less than 60 percent copper, it will contribute to the magnetic moment. We know that only three-dimensional arrays of atoms can be ferromagnetic and thus not all configurations of nickel atoms in a fluctuation will contribute to magnetism, although the fluctuation may have less than 60 percent copper. It seems natural to expect a configuration to be ferromagnetic if the nickel atoms form a cluster which extends across the 13-atomic group. A convenient way to express this condition is to require that in at least two neighboring close-packed directions, i.e., [110], all the neighbors of the central atom be nickel atoms. This condition is satisfied for all fluctuations having 8 and more nickel atoms. The probability that the condition is satisfied in other fluctuations is easily computed and for fluctuations containing seven and six nickel atoms it is 0.43 and 0.23 respectively. Thus the contributions of these fluctuations to the total magnetic moment have to be correspondingly reduced. Curve II in Fig. 5 shows the result. The agreement with the lowest experimentally certain point[4] is good.

It would be of great interest to go to slightly higher copper content and check the theoretically predicted deviation from linearity. An indirect confirmation of this nonlinearity is perhaps the large field dependence of magnetic susceptibility at 14 and 20°K in alloys containing 30 and more percent nickel as found by Kaufmann and Starr.[5]

[4] N. F. Mott and H. Jones, *Theory of Properties of Metals and Alloys* (Oxford University Press, London, 1936).
[5] A. R. Kaufmann and C. Starr, Phys. Rev. **63**, 445 (1943).

4. TEMPERATURE COEFFICIENT OF RESISTANCE

Transition metals show an abnormally high electrical resistance and, as shown by Mott,[6] the effect is satisfactorily explained by scattering of the conducting s-electrons into the unfilled states in the d-band. If the d-band is almost full, as it is in nickel, palladium, etc., the density of states $n(E)$ varies as

$$(E_0-E)^{\frac{1}{2}} \tag{2}$$

where E_0 corresponds to the top of the d-band. In that case, the probability of $s\rightarrow d$ scattering decreases with increasing temperature because of the temperature spread (of the order kT) of the Fermi distribution and the resulting change in the density of d-states into which the conducting s-electrons, at each E, can be scattered. Mott has calculated ϕ, the ratio of the relaxation time of conduction electrons with and without temperature spread of the Fermi distribution for various T/T_0 where T_0 is defined by $kT_0=E_0-E'$ and E' is the energy at Fermi surface. Multiplying the resistance calculated on the basis of the usual Gruneisen function by ϕ good agreement is obtained for palladium with $T_0=3450$. The change of $n(E)$ is greatest near the top of the band, and thus the effect of temperature on $s\rightarrow d$ scattering should be most pronounced for small T_0, and may lead to a vanishing or even negative temperature coefficient. The temperature-dependent resistance of nontransition, "normal," metals at not too low temperature, is proportional to T. For transition metals, it is thus proportional to $T\phi$ and

$$(d\rho/dT)(T/\rho)=1+(T/\phi)(d\phi/dT) \tag{3}$$

where ϕ depends upon T/T_0 and $d\phi/dT<0$. This temperature effect is, of course, independent of any ferromagnetic effects which also affect the $s\rightarrow d$ scattering and which are not being considered here.

The importance of $s\rightarrow d$ scattering indicates that in an alloy in proximity of a composition which corresponds to the boundary between an open and a filled d-band, the fluctuations of electron concentration should play an important role in determining the temperature coefficient of resistance. This is particularly well illustrated by the variation of the temperature coefficient of resistance in copper-nickel and silver-palladium alloys. In all such binary alloys, between Ni, Pd, Pt and Cu, Ag, Au, it is usually assumed that the 0.6 empty states in the unfilled d-band of the transition metal are gradually filled up by the excess of the s-electrons in the noble metal over the 0.6 electron in the s-band of the transition metal. The filling up would be completed at 60 percent of the noble metal. It would appear thus that the temperature dependence of resistance should be normal up to 40 percent of transition metal and from then on it may be abnormally low or abnormally high depending upon the importance

[6] N. F. Mott, Proc. Roy. Soc. (London) **153**, 699 (1936); **156**, 368 (1936); Proc. Phys. Soc. (London) **47**, 571 (1935).

of $s \rightarrow d$ scattering, ferromagnetic effects, etc. This conclusion is clearly not in agreement with experiment which shows that an anomalous influence of temperature is observed for as low contents of transition metals as 20 percent. It will be shown that the statistical theory of the local concentration fluctuations explains quantitatively the experimental facts.

a. Copper-Nickel Alloys

In a previous section, it was shown that the statistical method is in agreement with experimental data on the saturation moment in copper-nickel alloys. As is well known, the evidence indicates, with considerable certainty, that in these alloys, containing less than 40 percent copper, the 3*d*-band is full. At higher nickel content, the 3*d*-band is progressively less filled and finally the material becomes magnetic (at 400°K near 77 percent nickel). Figure 6 shows that the quantity $(d\rho/dT)(T/\rho)$ is not only low near 40 percent nickel, but it is abnormally low down to a nickel content of only 15 percent where, according to the band theory, there should be no $s \rightarrow d$ scattering. (As "normal" behavior a constant $(d\rho/dT)(T/\rho)$ is considered; this is not unreasonable in view of the difference of only 10 percent between the Debye characteristic temperatures of copper and nickel.)

In order to interpret this irregular behavior as due to the presence of local concentration fluctuations, we consider groups of 13 atoms, each having i transition atoms, a characteristic electron concentration c_i, resistivity ρ_i, probability of occurrence p_i, and a T_0 which we shall denote T_i. For each fluctuation an equation of type (3) is satisfied with the appropriate ρ_i and $\phi_i = \phi(T/T_i)$. Resistivities, in general, are of course not additive and so, in order to calculate the total $(d\bar{\rho}/dT)(T/\bar{\rho})$ resulting from the randomly distributed fluctuations in a given volume of metals, we use the formula,

$$\bar{\rho} = \prod_{i=0}^{13} \rho_i^{p_i}, \tag{4}$$

which gives

$$\frac{d\bar{\rho}}{dT}\frac{T}{\bar{\rho}} = 1 + \sum_{i=0}^{13} \frac{T}{T_i}\frac{p_i}{\phi_i}\frac{d\phi_i}{d(T/T_i)}. \tag{5}$$

This expression is further simplified by observing that Mott's numerically calculated ϕ can be approximated by $\exp[a(T/T_i)^2]$ with $a = 2.4$. We have then

$$\frac{d\bar{\rho}}{dT}\frac{T}{\bar{\rho}} = 1 - 2a\sum_{i=0}^{13} p_i \left(\frac{T}{T_i}\right)^2. \tag{6}$$

The critical concentration of 40 percent nickel corresponds to 7.8 Cu and 5.2 Ni atoms in the basic group. Thus for all fluctuations containing more than 8 Cu atoms $\phi = 1$ or $a = 0$. For other fluctuations, one obtains $T_i = T_0(n_i/0.6)^{\frac{1}{2}}$ from the known concentration n_i of empty d states in a particular fluctuation and the known $T_0 = 2200$ for nickel. The probabilities p_i are again calculated from the binominal coefficients applicable to perfectly random solid solutions. T_8 was put equal to T_7, since in these fluctuations the d-band is either just filled or almost full and the small uncertainty in the value 0.6 for the critical concentration of copper would make a clearcut distinction rather artificial. This point will be discussed again later.

The theoretical curve is compared with experimental points and with the best average experimental curve in Fig. 6. The data were taken from the work of Svensson[7] for $T = 400$°K. The comparison is made only for alloys containing less than 70 percent nickel, because at higher nickel content the alloys become ferromagnetic and there different effects play a role. The agreement is striking particularly in the position of the two concentrations at which the temperature coefficient of resistance vanishes. One of them, near 50:50, is the well-known constantan alloy. The good agreement in the

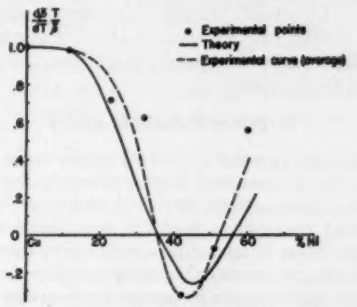

FIG. 6. Temperature variation of electrical resistance of Cu-Ni alloys.

absolute value of the minimum is rather fortuitous since, as mentioned before, and as follows from Eq. (4), most of the negative contributions are due to these fluctuations for which T_i is small and the latter is extremely sensitive to the critical concentration c_e at which the d-band is considered full. This sensitivity may be the reason why the unusually low temperature coefficients are relatively rare and are so much affected by minor soluble impurities. On the other hand, if the statistical treatment here used is correct, then the temperature coefficient of resistance can serve as a sensitive indicator of the exact value of the critical concentration. On the whole, one can say that, as a result of the presence of only discrete values of electron concentrations c_i encountered in the fluctuations, only these alloy systems will show a very small or even negative $d\bar{\rho}/dT$ in which the critical concentration c_e is close to one of the c_i's. The corresponding T/T_i is then very high. Thus a small change in c_e effects strongly

[7] B. Svensson, Ann. Physik (5) **25**, 263 (1936).

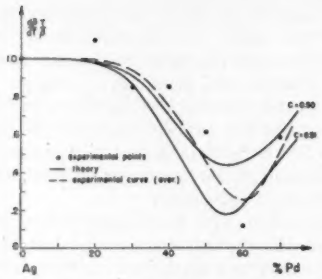

FIG. 7. Temperature variation of electrical resistance of Ag-Pd alloys.

the absolute value of $d\bar{\rho}/dT$ near the minimum, while the position of the minimum itself is always in proximity of c_e. In connection with the above, it should be kept in mind that in the calculation it was assumed that Mott's function ϕ, and its exponential approximation, is directly applicable to the copper-nickel alloys. This may not be actually the case in a more detailed treatment, although the uncertainty affects ϕ primarily for high T/T_i values which, as discussed above, are not too critical for the theory.

b. Silver-Palladium Alloys

These alloys present a case very similar to the copper-nickel alloys considered above. However, due to the lack of ferromagnetism there is no sensitive clue as to the exact composition at which the d-band is filled. Measurements of magnetic susceptibility, thermoelectric power, etc., permit the conclusion[4] that the d-band becomes filled up near 50 percent silver rather than at 60 percent as in the copper-nickel alloys. In his discussion of resistivity of palladium, Mott concluded that $T_0=3450°$K. Repeating the previous calculation with palladium concentrations, $c_e=0.50$ and $c_e=0.51$, one obtains the two curves shown in Fig. 7. The agreement is satisfactory. The curves illustrate also the previously discussed sensitivity of the absolute value of the minimum to a small variation in the critical concentration. The concentration $c_e=0.51$ seems to fit better.

On the basis of the above results, the conclusion might be drawn that palladium metal has about 0.5 electron in the s-band and 0.5 hole in the d-band. However, the relationship between the number of holes in the d-band of a pure metal and the concentration of an added element at which the band is full is perhaps not so simple as it is usually supposed. In other words, the difference between c_e for nickel-copper and for palladium-silver alloys may not be due simply to a difference in the number of holes c_h in the d-bands of the pure transition metals. The usual assumption in relating c_e to c_h is that at low concentration of the monovalent metal the number of electrons in the s-band is the same as in the pure transition metal, thus less than one, and that it does not change until the d-band is filled. This is not necessarily correct: the availability of electrons contributed by the noble metal will depend not only on the number of electrons but also on such factors as the ionization potential and differences in energy of the possible electronic states. It has been pointed out elsewhere[8] that these factors play an important role for instance in the anomalous influence of manganese on the α-γ transformation in iron, etc.

TABLE I. Ionization potentials.

	I	II		I	II
Cu	7.68	20.18	Ni	7.61	18.4
Ag	7.54	21.9	Pd	8.3	19.8
Au	9.19	20.0	Pt	8.9	18.47

A comparison of the first and second ionization potentials[9] for several elements shows clearly, Table I, the unusually loose binding of the valence s-electron in silver and the equally striking strong binding of the d-shell in silver and in palladium. It is very likely that these differences have an important effect on the electronic structure in alloys. For instance, it would be natural to expect in palladium alloys a stronger tendency to fill up the d-band than in nickel or platinum alloys. An example here is the disappearance of paramagnetic susceptibility in Au-Pd and Au-Pt alloys at 50 and at 65 percent gold respectively. Similarly, silver alloys would show a stronger tendency to fill up the d-band than copper or gold alloys. An example here is provided by the Pd-Ag and Pd-Au alloys, in which the minima of the thermoelectric power and of the temperature coefficient of electrical resistivity occur near 38 and 48 atomic percent of the noble metal respectively. Thus there are differences in the critical compositions without necessarily implying different numbers of holes in the d-bands in pure metals. The great similarity in the relative magnitude of the first and second ionization potentials of nickel and palladium makes it plausible to conclude that both metals have 0.6 hole in the d-bands. This agrees well with the final equilibrium concentration of hydrogen in palladium, which corresponds to 0.6 hydrogen atom per one atom of palladium.[10] It seems thus that as silver is added to palladium, the original number of 0.6 hole in the d-band is filled up in such a manner that at 50:50 there are no holes in the d-band (in the absence of fluctuations) and there are 0.5 electron in the s-band. This decrease in the number of s-electrons from 0.6 at pure Pd to 0.5 at the Ag-Pd composition is quite compatible with the simultaneous lowering of the average ionization potential of the s-electrons from 8.3 to $7.92=\frac{1}{2}(8.3+7.54)$ and raising of the corresponding quantity for the d-electrons from 19.8 to $20.35=\frac{1}{2}(19.8+21.9)$.

[8] R. Smoluchowski, Metal Progress **41**, 363 (1942); Phys. Rev. **61**, 390 (1942); R. Smoluchowski and J. S. Koehler, Ann. Rev. Phys. Chem. (1951).
[9] W. F. Meggers, J. Opt. Soc. Am. **31**, 39, 605 (1941).
[10] A. Sieverts and G. Zapf, Z. physik. Chem. **172**, 314 (1935).

5. THERMOELECTRIC POWER

As shown by Mott,[6] thermoelectric power of transition metals is closely related to the density of states near the top of the filled d-band; whenever the latter varies as the square root of the energy, the absolute thermoelectric power in a solid solution of a transition and a nontransition metal is given by:

$$S=\text{const}T(c-c_e)^{-1}\left\{\alpha+\left(\frac{c-c_e}{1-c_e}\right)^{\frac{1}{2}}\right\}^{-1};\quad c>c_e \quad (7)$$

where $\alpha=0.25$, c is the concentration of the transition metal and c_e is the critical concentration at which the d-band is filled. Similarly to the temperature coefficient of electrical resistance, the thermoelectric power reaches extreme value near the critical composition.

a. Palladium-Silver Alloys

As concluded previously, the d-band in palladium-silver alloys is filled up near the 50:50 composition. The thermoelectric power S obtained from (7) is shown in Fig. 8 as curve I, which represents the local thermoelectric power characteristic of individual fluctuations. The constant of proportionality was chosen to give agreement with experiment[11] for pure palladium at 900°C. The statistical procedure based again on a 13-atomic group gives the average thermoelectric power as indicated by curve II. Formula (7) assumes that neither s-electrons of palladium or of silver contribute to S. This is not strictly correct since, for instance, the thermoelectric power of silver, which is all due to s-electrons, though small, is not negligible. In view of this approximation, the agreement between calculation and theory is quite good.

b. Palladium-Gold Alloys

The calculations follow the same pattern as for palladium-silver alloys. As indicated previously, gold fills up the d-band in palladium at a slower rate than silver and thus it was first assumed that, as in the nickel-copper system, $c_e=0.40$. The result is shown in Fig. 9 by curve II which does not agree too well with experiment.[11] Putting $c_e=0.32$, a better fit, especially in the position of the minimum, is obtained, curve III. The corresponding local thermoelectric power is shown by curve I.

6. PARAMAGNETIC SUSCEPTIBILITY

The high paramagnetic susceptibility of transition metals is also related to the unfilled d-band and, in alloys with nontransition metals, it disappears at a concentration corresponding to a filled d-band. The theory[4] requires that the susceptibility be proportional to the density of states at the top of the band. However, the relative rate of decrease of the susceptibility with

[11] W. Geibel, Z. anorg. u. allgem. Chem. **69**, 38 (1910); **70**, 240 (1911).

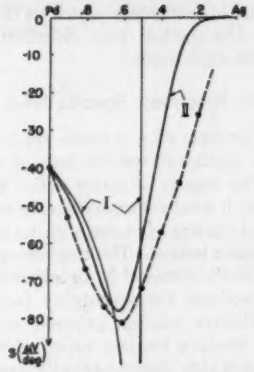

FIG. 8. Thermoelectric power of Ag-Pd alloys.

increasing content of the nontransition element as observed, for instance, in palladium-gold alloys is much too rapid for such a simple relation. The statistical method does not seem to improve the situation except for explaining the persistence of weak paramagnetism beyond the critical concentration. It seems thus that a change in the theory of paramagnetism of transition metals is necessary before a statistical method can be applied.

A similar conclusion follows from consideration of susceptibility of copper-nickel alloys below 40 percent nickel.[5] The variation of susceptibility with composition and temperature in that system is hard to reconcile with present theoretical explanations based on band theory. Some light on this problem may have been shed by the results of the statistical treatment of saturation magnetization in these alloys as discussed earlier.

7. OTHER PHENOMENA

a. Magnetostriction

Consideration of the influence of order on magnetostriction is based on the calculation of the change of the

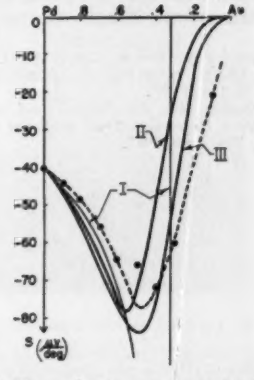

FIG. 9. Thermoelectric power of Au-Pd alloys.

effective magnetic moments[9] situated on the interacting lattice sites. The method here described gives good agreement with experiment.[1]

b. Electronic Specific Heat

A typical example of a possible application of the theory is the electronic specific heat of alloys which depends on the density of states $n(E_F)$ at the Fermi surface. To each local concentration fluctuation corresponds a local density of states with its characteristic electronic specific heat C_e. The total electronic specific heat is then easily obtained in an additive manner by taking into account the probability factor (1). The actual quantitative relation between $n(E_F)$ and C_e involves the effective electron mass, which is usually unknown and which may vary with local electronic density. Thus the validity of a strict comparison with experiment may be questionable. In certain cases simplifying assumptions are permissible and on that basis Goldman,[12] using the method here described, obtained an interpretation of the behavior of electronic specific heat and resistance in copper-nickel alloys.

Another important application of the statistical method to electronic specific heat may arise when there is a tendency to cluster[13] or to form short-range order. Both these tendencies should show up in the temperature dependence of electronic specific heat or rather in the influence of heat treatment on the electronic specific heat as measured at low temperatures. In that case, instead of the random probability, the corresponding expressions for nonrandom solutions[14] should be used. Typical systems in which the effect may be found are Au-Ni, Au-Mn, Cu-Pd, etc.

c. Crystal Structure and Lattice Constant

The role of electron concentration in determining crystal structure is well known and here the role of fluctuations of electronic concentration is particularly striking. For instance, the transformation between the body-centered and face-centered phases in iron and its alloys is extremely sensitive to changes in electron concentration[8] and small variations in composition affect the equilibrium range of existence of the two phases. It follows thus that fluctuations of the local electron concentration play a decisive role in the formation of potential nuclei (embryos) of a new phase. They determine the balance of free energy and thus the rate of nucleation. The fluctuations will be strongly affected by small alloy additions or by deviations from randomness and in this way the unusually strong dependence of nucleation rates in iron alloys on these two factors can be understood. Other examples could be here cited.

The lattice constant is often strongly dependent on the number of electrons which overlap from one Brillouin zone to the next. This is the basis of the explanation[15] of the anomalously large lattice constant of aluminum and of the anomalies of the c/a ratio in several magnesium alloys. In particular, the concentration corresponding to the onset of such an overlap shows up often as a sharp break in the lattice constant *vs* composition curve. It is thus to be expected that when the average electronic concentration has reached this critical value, then the fluctuations of the local electron concentration will produce local fluctuations in lattice parameters. The presence of such parameter fluctuations would affect electrical conductivity, various magnetic properties and such mechanical properties as critical shear strength, hardness, etc. Not enough data are available to check these conclusions for alloys mentioned above. However, several of the well-known anomalous properties of iron-silicon alloys may be interpreted in that way.[16]

8. CONCLUSIONS

A survey of the various applications of the statistical theory of properties of solid solutions indicates that numerous experimental facts can be explained in a quantitative manner. The statistical method provides in certain instances a sensitive indicator of the concentration at which d-bands in alloys of transition metals are filled up. It may be mentioned that the choice of the basic group, an atom and its neighbors, cannot be altered appreciably without destroying the agreement with experiment.

This work was supported by an AEC contract.

[12] J. E. Goldman, Phys. Rev. **82**, 339(A) (1951).
[13] R. Smoluchowski, Intern. Conf. on Metals, Amsterdam, 1948; Physica **15**, 179 (1949).
[14] R. Smoluchowski, Nat. Res. Council Conf. on *Phase Transformations*, Cornell University, 1948, published by John Wiley and Sons, Inc., New York, 1951.
[15] W. Hume-Rothery, *Atomic Theory for Students of Metallurgy* (Institute of Metals, London, 1946).
[16] R. Smoluchowski (to be published).

Electron Density Distribution in a High Frequency Discharge in the Presence of Plasma Resonance*

W. P. Allis and Sanborn C. Brown
Massachusetts Institute of Technology, Cambridge, Massachusetts

and

Edgar Everhart
University of Connecticut, Storrs, Connecticut

(Received July 20, 1951)

In a high frequency discharge plasma resonance maximizes the electric field, thus producing a high ionization rate in the regions near resonance. The effect of this on the distribution of electrons and of ionization in a parallel plane discharge is calculated and compared with the observation that the light from such a discharge often is a minimum at the center.

I. INTRODUCTION

It was pointed out by Schumann[1] that when a high frequency field is applied to an ionized gas of high electron concentration, the field tends to concentrate in those parts of the discharge where the plasma is near resonance.[2] The admittance of a high frequency discharge under such conditions was discussed in a recent paper.[3] The appearance of a microwave discharge at high current is shown in Fig. 1 in which the discharge is taking place between parallel plates at the right and left of the bright glow, and it is noted that the light intensity is greatest near the electrodes. It may be inferred that the field is greatest here, and this corresponds, according to Schumann, to regions where the plasma is in resonance and is shielding the central part of the discharge. It is the purpose of this paper to calculate the electron density throughout the discharge under such conditions, and to show that the ionization has sharp maxima in the resonance regions.

II. THE IONIZATION FUNCTION

For a given applied field of radian frequency, ω, plasma resonance occurs at an electron density,[2]

$$n=m\omega^2\epsilon_0/e^2, \tag{1}$$

where e and m are the charge and mass of an electron, and ϵ_0 is the electric permittivity of free space. It is convenient to measure electron concentration in terms of this by the variable,

$$r=ne^2/m\omega^2\epsilon_0, \tag{2}$$

which is unity when the plasma is in resonance. A damping constant for the plasma is given by

$$\beta=\nu_c/\omega, \tag{3}$$

where ν_c is the average frequency of collision of an electron with the molecules of the gas. The formula for the total current density, including both electron current and displacement current is given by Eqs. (5) and (9) of reference 3. In terms of the parameters defined above it is

$$J=[ne^2/m(\nu_c+j\omega)+j\omega\epsilon_0]E$$
$$=[r(\beta-j)/(\beta^2+1)+j]\omega\epsilon_0E, \tag{4}$$

from which the magnitude of the resistivity is

$$|E/J|=(1/\omega\epsilon_0)(\beta^2+1)^{\frac{1}{2}}[(r-1)^2+\beta^2]^{-\frac{1}{2}}. \tag{5}$$

This quantity has a maximum at resonance where $r=1$.

The ionization frequency per electron ν_i depends on the applied field, and over a limited range about a central value E_0 we shall assume, following Herlin and Brown,[4] that it varies as a power 2α of the field:

$$\nu_i/\nu_0=|E/E_0|^{2\alpha}. \tag{6}$$

Fig. 1. Appearance of the high frequency discharge.

* This work has been supported in part by the Signal Corps, the Air Materiel Command, and ONR.

[1] W. O. Schumann, Z. Physik **7**, 121 (1942).

[2] L. Tonks and I. Langmuir, Phys. Rev. **33**, 195 and 990 (1929).

[3] E. Everhart and S. C. Brown, Phys. Rev. **76**, 839 (1949).

[4] M. A. Herlin and S. C. Brown, Phys. Rev. **74**, 291 (1948) and Phys. Rev. **74**, 910 (1948). Our α is $\beta/2$ in their notation.

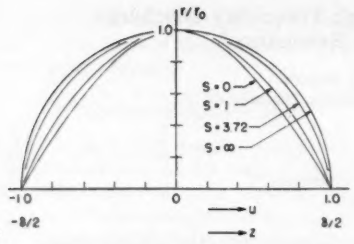

FIG. 2. Variation of electron density r across a discharge for which $\alpha=2$ in the limit of high pressures for various ratios $s=r_0(\beta^2+1)^{-\frac{1}{2}}$.

With the value of E from Eq. (5) this is

$$\nu_i=\nu_0|J/\omega\epsilon_0E_0|^{2\alpha}(\beta^2+1)^{\alpha}[(r-1)^2+\beta^2]^{-\alpha}. \quad (7)$$

The ionization rate is thus a function of the electron density with a maximum at $r=1$.

III. THE DIFFUSION EQUATION

The distribution of electrons in the discharge is determined by the production rate $n\nu_i$ in the gas and diffusion to the walls, and it will be assumed that the electron density is such that ambipolar diffusion exists. Limiting ourselves to the case of extended plane parallel plates perpendicular to the z-axis, the diffusion equation is[3]

$$d^2n/dz^2+n\nu_i/D_a=0 \quad (8)$$

where D_a is the ambipolar diffusion coefficient. It is convenient to normalize distance by the variable $u=2z/\delta$, where z is measured from the mid-plane and δ is the plate separation.

After substituting from Eq. (7) we then express Eq. (8) in terms of r and u:

$$d^2r/du^2+k^2r/(r^2-2r+1+\beta^2)^{\alpha}=0, \quad (9)$$

where

$$k^2=[\delta^2\nu_0(1+\beta^2)^{\alpha}/4D_a]|J/\omega\epsilon_0E_0|^{2\alpha}, \quad (10)$$

is a constant. It is determined as a characteristic value for Eq. (9) with the boundary conditions:

$$\begin{aligned} &r=r_0, \quad dr/du=0, \quad \text{at} \quad u=0 \\ &r=0, \quad \text{at} \quad u=\pm1. \end{aligned} \quad (11)$$

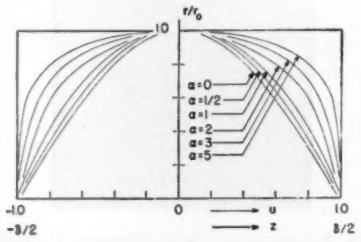

FIG. 3. Variation of electron density r across a discharge. Limiting form at very high electron concentrations $s\gg1$ for various values of α.

Equation (9) integrates once to give

$$\left(\frac{dr}{du}\right)^2=k^2\int_r^{r_0}\frac{2rdr}{(r^2-2r+1+\beta^2)^{\alpha}}=k^2L^2. \quad (12)$$

The function L introduced here is proportional to the electron density gradient and, therefore, also to the electron diffusion current. A second integration gives the electron density as an implicit function of position

$$ku=\int_r^{r_0}dr/L. \quad (13)$$

The characteristic value of k is then given by setting the lower limit $r=0$ with $u=1$.

IV. INTEGRATION

The integration in (12) is readily performed for any integral or half-integral value of α but the integration (13) causes trouble. We shall carry it out with four different approximations applicable to different discharges or to different parts of the same discharge.

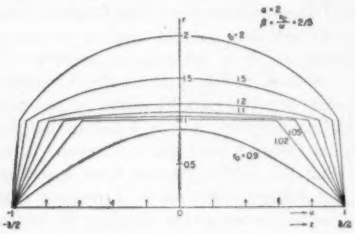

FIG. 4. Variation of electron density across a discharge at low pressures.

From these the general form of the solution may be readily visualized. The four approximations will be:

$$\text{A:} \quad 2r\ll r^2+1+\beta^2.$$

By neglecting the only negative term in the denominator of (12) all resonance effects on the electron distribution are eliminated. This approximation is always good at high pressures $\beta^2\gg1$ and also at any pressure for electron concentrations not near resonance. The next two approximations are sub-groups of A.

$$\text{B:} \quad r^2-2r\ll1+\beta^2.$$

This amounts to neglecting the ac electron current relative to the displacement current or to assuming a uniform field. It is good only for electron concentrations well below resonance or for sufficiently high pressures.

$$\text{C:} \quad \beta^2+1\ll r^2.$$

This approximation neglects the displacement current. It is good only at electron concentrations above resonance and therefore never good near the walls.

$$\text{D:} \quad \beta\ll1.$$

This neglects the resistive current and is the low

pressure limit. The effects of resonance dominate this approximation.

A: Neglecting the term $2r$ in the denominator of (12) the integration yields, for $\alpha \neq 1$,

$$L^2=[(r^2+1+\beta^2)^{1-\alpha}-(r_0^2+1+\beta^2)^{1-\alpha}]/(\alpha-1). \quad (14)$$

Substitution in (13) then leads to incomplete elliptic integrals[5] for all integral values of α. Substituting

$$\kappa=r_0(r_0^2+1+\beta^2)^{-1} \quad \text{and} \quad \cos\phi=r/r_0 \quad (15)$$

we find for $\alpha=2$

$$ku=(r_0^2+1+\beta^2)E(\kappa, \phi) \quad (16)$$

and for $\alpha=3$

$$ku=(r_0^2+1+\beta^2)^{\frac{1}{2}}[2E(\kappa/\sqrt{2}, \phi)-F(\kappa/\sqrt{2}, \phi)]. \quad (17)$$

Curves of r/r_0 *vs* u for $\alpha=2$ and various values of $r_0(\beta^2+1)^{-\frac{1}{2}}=s$ are shown in Fig. 2. The two limiting curves in this case ($\alpha=2$) are a cosine and a circle, the effect of increasing electron concentration being always to increase the concentration near the walls relative to that in the center.

B: Neglecting r^2-2r in the denominator of (12) leads to elementary integrations,

$$L^2=(r_0^2-r^2)/(1+\beta^2)^\alpha \quad (18)$$

$$r=r_0\cos[ku/(1+\beta^2)^{\alpha/2}]=r_0\cos(\pi u/2) \quad (19)$$

$$k=(1+\beta^2)^{\alpha/2}\pi/2. \quad (20)$$

This is the solution of the simple diffusion equation and substitution of this last expression into (10) and (7) leads to the usual equilibrium condition

$$\nu_i=\pi^2 D_a/\delta^2. \quad (21)$$

The field and ionization rate per electron are, in this case, uniform throughout the discharge.

C: The neglect of all but r^2 in the denominator of (12) leads to the integral

$$ku=(\alpha-1)^{\frac{1}{2}}r_0^{\alpha-1}\int_r^{r_0} r^{\alpha-1}(r_0^{2\alpha-2}-r^{2\alpha-2})^{-\frac{1}{2}}dr. \quad (22)$$

This integration has been performed for a number of values of α and the results are shown in Fig. 3. For $\alpha=0$ the curve is a cosine, for $\alpha=2$ it is a circle, and as $\alpha\to\infty$ it approaches a rectangular box.

D: The integrand of (12) has singularities at $r=1\pm j\beta$ but the approximations made in A, B, and C put these singularities back on the imaginary axis so that the path of integration did not go between them. At low pressures these singularities lie close to, and on either side of, the real axis and the integration (12) must pass between them if $r_0>1$. The major part of the integral then comes, for small β, from the saddle-point region near $r=1$. dr/du changes rapidly in this region and there is a bend in the plot of r *vs* u. In order to obtain the value L_0 of L at the boundary we may set $r=1$ in the numerator of (12) and integrate from zero to infinity without appreciable error.

$$L_0^2=\int_0^{r_0}\frac{2rdr}{[(r-1)^2+\beta^2]^\alpha}=\int_{-\infty}^{+\infty}\frac{2dr}{[(r-1)^2+\beta^2]^\alpha}$$

$$=\frac{2\sqrt{\pi}}{\beta^{2\alpha-1}}\frac{\Gamma(\alpha-1/2)}{\Gamma(\alpha)}. \quad (23)$$

In the central part of the discharge not near resonance approximation C holds, so that at the resonance point u_1

$$ku_1=(\alpha-1)^{\frac{1}{2}}r_0^{\alpha-1}\int_1^{r_0} r^{\alpha-1}(r_0^{2\alpha-2}-r^{2\alpha-2})^{-\frac{1}{2}}dr. \quad (24)$$

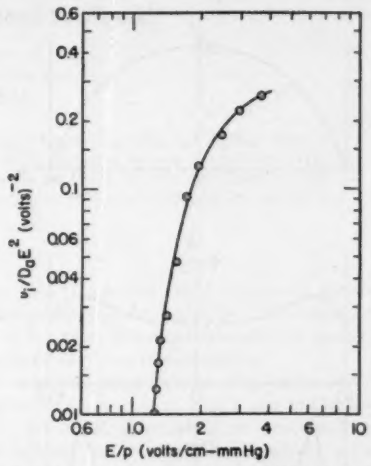

FIG. 5. Variation of ν_i/D_0E^2 with E/p in helium for large β.

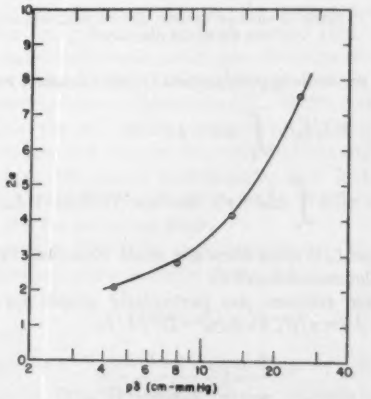

FIG. 6. Variation of α with $p\delta$ in helium for large β.

[5] E. Jahnke and F. Emde, *Tables of Functions* (Dover Publications, New York, 1943), pp. 52–72.

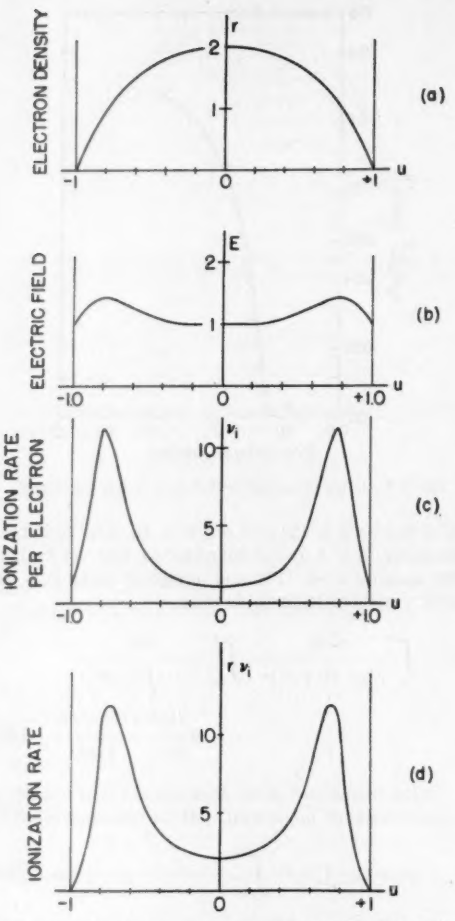

FIG. 7. Variation of electron density, electric field, and ionization rate across the discharge.

Near the walls approximation B holds because $r \ll 1$.

$$L^2 = L_0^2 - \int_0^r 2r\,dr = L_0^2 - r^2, \tag{25}$$

$$k(1-u_1) = \int_0^1 (L_0^2 - r^2)^{-\frac{1}{2}} dr = \sin^{-1}(1/L_0) \approx 1/L_0, \tag{26}$$

because L_0 is large when β is small. Equations (24) and (26) determine k and u_1.

These relations are particularly simple for $\alpha = 2$. Then $L_0^2 = \pi/\beta^2$, $k = r_0(r_0^2-1)^{\frac{1}{2}} + 1/L_0$,

$$\frac{1}{u_1} = 1 + \frac{1}{L_0 r_0 (r^2-1)^{\frac{1}{2}}}.$$

Curves for this case are shown in Fig. 4. These curves have sharp bends at the resonance points because of the approximations made. The lowest curve does not reach resonance and is a cosine.

V. DETERMINATION OF α

One method of determining α experimentally will be described to show that at a given frequency there is a relationship between α and β. The values of α can be obtained from measurements of the operating field E at various pressures p when the electron concentration is kept below resonance but not so small that ambipolar diffusion does not prevail. Under these conditions E is constant at a given pressure independent of both discharge current and position. Therefore ν_i/D_a will also be constant—equal, in fact, to π^2/δ^2 as is given by (21). Data are thus obtained for making a plot of $\nu_i/D_a E^2$ *vs* E/p which are the proper variables for the problem as Herlin and Brown[4] have shown. The slope of this curve on logarithmic paper is $2\alpha - 2$, from Eq. (6), and thus α is determined at various electric fields and pressures.

The procedure outlined above is essentially similar to that of Herlin and Brown who treated the breakdown condition instead of the steady-state discharge studied here. They point out further that there is a curve of $\nu_i/D_a E^2$ *vs* E/p for each value of $p\lambda$, where λ is the free space wavelength of the exciting field, and $\beta = 0.013 p\lambda$ (cm-mm Hg) for helium.

Data for the limiting case of large β have been obtained for helium and plotted in Fig. 5. The corresponding values of α *vs* $p\delta$ obtained from the slope of this curve are plotted in Fig. 6.

VI. DISTRIBUTION OF IONIZATION

The electric field and ionization distribution will be computed in detail for a particular discharge in helium. For a value of $p\delta$ of 23 we find from Fig. 6 that $\alpha = 7/2$. Also if $p\lambda = 77$ we find that $\beta = 1$. We further choose the electron density at the center of the discharge to be such that $n\lambda^2 = 2.2 \times 10^{13}$/cm so that $r_0 = 2$. The curve of electron density *vs* position for these values is shown in Fig. 7(a). The variation of electric field across the discharge is computed from Eq. (5) and shown in Fig. 7(b). Equation (6) can then be used to compute Fig. 7(c) which shows the variation of the ionization rate per electron at various positions across the discharge. The ionization rate will be the product of the ionization rate per electron by the electron concentration and is thus the product of the curve of Fig. 7(c) with that of Fig. 7(a). This is shown in Fig. 7(d). Assuming that the excitation at each point is proportional to the ionization at that point this should also correspond to the light intensity emitted by various portions of the discharge.

Elastic Scattering of Photons by Nuclei*

J. S. LEVINGER†
Cornell University, Ithaca, New York
(Received July 25, 1951)

The cross section for nuclear resonance scattering is estimated for the case when the photon energy is far from resonance with the excitation energy for any level of the scattering nucleus. For photon energy much less than 15 Mev we find that the cross section depends on the fourth power of the photon energy, and is very much smaller than the nuclear Thomson cross section for photon scattering by the nucleus as a whole.

I. INTRODUCTION

WILSON[1] has measured the elastic scattering of photons of 1.33 Mev (from Co^{60}) and 2.62 Mev (from ThC″). The purpose of his experiment is to find the Delbruck, or potential scattering, caused by the virtual production and annihilation of pairs in the coulomb field of the nucleus. The Delbruck scattering combines coherently with three other elastic scattering processes: Rayleigh scattering from the atomic electrons, Thomson scattering by the nucleus, and resonance scattering by the nucleus. It is necessary to know the amplitudes for the last three processes in order to interpret the experiments and find the value of the Delbruck scattering. The purpose of this note is to estimate the amplitude for nuclear resonance scattering.

II. NUCLEAR RESONANCE SCATTERING

There are two very different cases for nuclear resonance scattering of monoenergetic photons: (a) the photon energy is near a nuclear resonance energy, or (b) the photon energy is far from resonance. (By "far," we mean far enough from resonance so that the contribution of the nearest nuclear level is small compared to the contribution from all the other levels. 20 ev is about far enough.)

The first case, for nuclear resonance scattering by some particular level, has been studied by Guth,[2] and recently by Moon.[3] They find that the cross section for nuclear resonance scattering is of the order of 1 barn, if the photon energy is near resonance. At the moderate excitation energies used by Wilson the nuclear energy levels are widely spaced compared to 20 ev, so that it is unlikely that the photon energy is near a resonance. Further, nuclear resonance scattering would vary by several orders of magnitude, depending on whether a level of the scattering nucleus corresponded to the photon energy used. The other sources of scattering are smooth functions of atomic number and photon energy. Wilson has measured elastic scattering for several nuclei of similar atomic number (82 Pb, 83 Bi, 79 Au, 78 Pt), and has found only small variations of the scattering cross section with Z. This shows that in none of the cases measured is resonance scattering by some particular level of significance.

We therefore consider case (b), where the photon energy is far from resonance with any of the low-lying nuclear levels. Measurements[4] on photonuclear reactions indicate that nuclear levels which have large matrix elements for combination with the ground state lie mostly at an excitation energy of 15–20 Mev. (We are concerned in this note with nuclei of atomic number of at least 50, since these are the nuclei measured by Wilson.) The nuclear resonance scattering of a low energy gamma (such as 1.33 or 2.62 Mev) is mainly due to the "tails" of the resonance curves of the nuclear levels at 15 to 20 Mev.

The elastic scattering of photons by the charges bound in nuclei can be treated by the Kramers-Heisenberg dispersion formula.[5] The differential cross section is

$$d\sigma/d\Omega=(2\pi e\nu/c)^4\{\textstyle\sum_n[(r_\sigma)_{0n}^*(r_\rho)_{n0}/(W-E_n) - (r_\rho)_{0n}^*(r_\sigma)_{n0}/(W+E_n)]\}^2. \quad (1)$$

Equation (1) applies to the special case of elastic scattering by dipole transitions to intermediate states. We have neglected the damping term in the resonance denominator since the photon energy is far from resonance. ν is the frequency of the photon and W its energy; $(r_\sigma)_{0n}^*$ and $(r_\rho)_{n0}$ are the matrix elements between the ground (0) and nth excited state of the coordinate components along the directions of polarization of the incident and scattered photon. (σ and ρ represent the two polarizations.) E_n is the excitation energy of the nth nuclear energy level. The scattering must be summed over the final polarizations and averaged over the initial polarizations; this gives the characteristic factor for dipole scattering of $\frac{1}{2}(1+\cos^2\theta)$, where θ is the scattering angle.

We rewrite Eq. (1) by combining the two fractions and introducing the oscillator strength as

$$f_{0n}=(2ME_n/\hbar^2)z_{0n}^*z_{n0}. \quad (2)$$

* Part of this work was done while the author was a research associate under an ONR contract.
† Now at Louisiana State University, Baton Rouge, Louisiana.
[1] R. R. Wilson, Phys. Rev. **82**, 295 (A) (1951).
[2] E. P. Guth, Phys. Rev. **59**, 325 (1941).
[3] P. B. Moon, Proc. Phys. Soc. (London) **A64**, 76 (1951).
[4] Johns, Katz, Douglas, and Haslam, Phys. Rev. **80**, 1062 (1950).
[5] P. A. M. Dirac, *Principles of Quantum Mechanics* (Oxford University Press, London, 1947), Sec. 64.

We obtain

$$d\sigma/d\Omega = R_0^2 W^4 [\sum_n f_{0n}/(E_n^2 - W^2)]^2 \tfrac{1}{2}(1+\cos^2\theta). \quad (3)$$

Here z is the component of displacement of the charge, M is the proton mass, and $R_0 = e^2/Mc^2$ is the classical proton radius.

We can estimate the value of this expression by writing for the denominator an appropriately weighted average value E_a of the nuclear excitation energy for dipole transitions. Present measurements[4] suggest that $E_a = 15$ Mev might be an appropriate guess. The summed oscillator strength for dipole transitions for a nucleus with Z protons and N neutrons, with an exchange potential providing a fraction x of the attractive neutron-proton potential has been calculated[6] as

$$\sum_n f_{0n} = (NZ/A)(1+0.8x). \quad (4)$$

This calculation is in reasonable agreement with experimental measurements of the integrated photonuclear cross section. Using these expressions for the denominator and numerator we find the differential cross section for nuclear resonance scattering as

$$d\sigma/d\Omega = R_0^2 (W/E_a)^4 [(NZ/A)(1+0.8x)]^2 \tfrac{1}{2}(1+\cos^2\theta). \quad (5)$$

We note that this has the same W^4 dependence on photon energy as that for the Rayleigh scattering of visible light. In both cases the photon energy is far below the energies of the significant intermediate states.

It is of interest to compare the cross section for nuclear resonance scattering with that for nuclear Thomson scattering, which is given by

$$(d\sigma/d\Omega)_{\mathrm{Th}} = (Z^2 e^2/AMc^2)^2 \tfrac{1}{2}(1+\cos^2\theta) = R_0^2 (Z^2/A)^2 \tfrac{1}{2}(1+\cos^2\theta). \quad (6)$$

This expression is analogous to the well-known formula $(1/2)r_0^2(1+\cos^2\theta)$ for Thomson scattering by free electrons. The electron charge e is replaced by Ze, and the electron mass m by the nuclear mass AM. The form factor for the nucleus is taken as unity since for the photon energies considered the photon wavelength is much greater than the nuclear radius.

The ratio of the cross section for nuclear resonance scattering to that for nuclear Thomson scattering is then

$$(d\sigma/d\Omega)/(d\sigma/d\Omega)_{\mathrm{Th}} = (W/E_a)^4 [(N/Z)(1+0.8x)]^2. \quad (7)$$

The cross section for nuclear resonance scattering is negligible for the photon energies used by Wilson (1.33 Mev and 2.62 Mev) for which the ratio $(W/E_a)^4$ is extremely small. However, since the amplitudes for nuclear resonance scattering and nuclear Thomson scattering combine coherently, we should rather compare their amplitudes (a_{NR} and a_{Th}). If we consider the hypothetical case where these are the only scattering processes (most nearly valid for large scattering angles), the scattering by the nucleus is proportional to

$$a^2 = (a_{\mathrm{NR}} + a_{\mathrm{Th}})^2 \cong a_{\mathrm{Th}}^2 [1 - 2(W/E_a)^2 (N/Z)(1+0.8x)]. \quad (8)$$

(The amplitude for nuclear resonance scattering has a sign opposite to that for nuclear Thomson scattering since for the former the charged particles are tightly bound, and for the latter they are free.) We have used $a_{\mathrm{NR}}/a_{\mathrm{Th}} \ll 1$. Using photon energy $W = 2.62$ Mev, nuclear excitation energy $E_a = 15$ Mev, fraction of exchange force $x = \frac{1}{2}$, and values of N and Z for lead we find

$$a^2 = a_{\mathrm{Th}}^2 (1 - 0.12) = 0.88 a_{\mathrm{Th}}^2. \quad (9)$$

The effect of nuclear resonance scattering is seen to be barely appreciable in Wilson's experiments at 2.62 Mev, and is negligible at 1.33-Mev photon energy.

The author is grateful to R. R. Wilson, and H. A. Bethe for discussions concerning this problem.

[6] J. S. Levinger and H. A. Bethe, Phys. Rev. **78**, 115 (1950).

Boundary Conditions and Time-Dependent States

MARCOS MOSHINSKY
Institutos de Física y de Geofísica, Universidad de México, México, D.F., México

(Received July 11, 1951)

In a previous paper, a phenomenological description of nuclear reactions by means of boundary conditions was introduced. These boundary conditions that connect the several stages of the reaction (initial particles, compound nucleus, etc.) apply to time-dependent, as well as to stationary states. It is possible to discuss then the time development of any state specified initially. In the present paper a time-dependent description is obtained for the single-level S-wave scattering of two spinless particles, and for the process of disintegration of a compound particle. The only parameters on which this time-dependent description depends are the poles of the scattering matrix. The connection between the position of the poles of the scattering matrix in the complex plane, and the time-dependent behavior of the scattering and disintegration processes, is discussed. The form of the transient scattered current is also obtained. The generalized Hankel transforms on which the present developments are based, will be shown in a following paper to be a consequence of the expansion theorems for states in Fock space.

I. INTRODUCTION

IN a previous article[1] a phenomenological description of nuclear reactions was introduced, in which the several stages of the nuclear reaction were described in an appropriate Fock space.[2] It was shown there that the boundary conditions imposed on the components of the Fock wave function lead, for stationary states, to the same dependence of the cross sections on energy as would be obtained from any of the usual formulations of resonance reaction theory.[3]

An advantage of this description is that the boundary conditions obtained hold for time dependent states, as well as for stationary states. We can then deal, not only with such problems as the dependence of the cross sections on energy, which are of an essentially stationary nature, but also with problems such as the time development of a state specified at a given initial time.

We propose to discuss in this paper, the description in time of a scattering process, and the process of disintegration of a compound particle. We shall show the dependence of this description on the position of the poles of the scattering matrix.[4] The present developments will have then, a bearing on the connection of causality with the position of the poles of the scattering matrix, recently discussed by Schützer and Tiomno.[5]

With the help of the time-dependent state for a scattering process, we will also obtain the transient scattered current that appears before stationary conditions are established.

Our aim in the present paper is to obtain a set of basic time-dependent wave functions, with the help of which we shall discuss, in a following publication, the description of interactions through boundary conditions in Fock space, from a general quantum-mechanical standpoint. We shall show there that a time dependent matrix $\mathbf{U}(t)$ can be introduced, which provides all the information concerning our states and the observables associated with them that is of relevance in quantum mechanics. The interactions through boundary conditions in Fock space will be seen then to give as complete a description of the interaction process between particles as could be obtained if they interacted through a potential.

While the present discussion is nonrelativistic, it is hoped that the restriction of the interactions to the point of coincidence[1] of the colliding particles, will permit a comparatively simple extension to the relativistic range.

In the previous note, boundary conditions were obtained for several types of scattering and reaction problems, but in order to keep mathematical complications to a minimum, we shall restrict the discussion in this, and the following paper, to the interactions between two spinless particles leading to single-level S-wave scattering. The extension to other, more complex, types of interactions will be presented in a later publication.

According to what was said in the previous note, the state representing a single-level scattering process could be found in two stages. In the first stage, two particles of masses m_1, m_2 are present, while in the second, there is only a single compound particle of mass M. If we choose the center-of-mass frame of reference, the first stage is represented by the wave function $\psi_1(\mathbf{r}, t)$ where $\mathbf{r}$ is the relative position vector of the two particles, while the second stage is represented by the wave function $\psi_2(t)$. The Fock wave function for the state is then

$$\Psi(t)=\begin{bmatrix}\psi_1(\mathbf{r}, t)\\ \psi_2(t)\end{bmatrix}. \tag{1}$$

[1] M. Moshinsky, Phys. Rev. **81**, 347 (1951). This paper will be referred to as "previous note."
[2] V. Fock, Z. Physik **75**, 622 (1932).
[3] E. P. Wigner and L. Eisenbud, Phys. Rev. **72**, 29 (1947); G. Breit, Phys. Rev. **69**, 472 (1946); Feshbach, Peaslee, and Weisskopf, Phys. Rev. **71**, 145 (1947).
[4] J. A. Wheeler, Phys. Rev. **52**, 1107 (1937); W. Heisenberg, Z. Physik **120**, 513, 673 (1943); E. P. Wigner, Phys. Rev. **70**, 15 (1946).
[5] W. Schützer and J. Tiomno, Phys. Rev. **83**, 249 (1951). I am indebted to Drs. Schützer and Tiomno for a copy of their paper prior to publication.

To simplify the notation,[6] we now choose our units so that $\hbar=1$, $c=1$ and the reduced mass

$$\mu=(m_1m_2)(m_1+m_2)^{-1}=1.$$

We have from the previous note, that for $\mathbf{r}\neq 0$, $\psi_1(\mathbf{r}, t)$ satisfies the free particle Schrödinger equation:

$$-i(\partial\psi_1/\partial t)=\tfrac{1}{2}\nabla^2\psi_1 \tag{2}$$

and that the boundary conditions that determine the interaction are:[7]

$$-i(\partial\psi_2/\partial t)+E_0\psi_2=2\pi C'(\partial r\psi_1/\partial r)_{r=0}, \tag{3}$$

$$C'\psi_2=(r\psi_1)_{r=0}. \tag{4}$$

In (3), $E_0=[M-(m_1+m_2)]$ stands for the binding energy of the compound particle, and C' is a coupling constant whose physical significance will be given below.

We could eliminate ψ_2 between (3) and (4) and obtain a boundary condition in terms of ψ_1 alone, having the form:

$$-i(\partial r\psi_1/\partial t)_{r=0}+E_0(r\psi_1)_{r=0}=2\pi C'^2(\partial r\psi_1/\partial r)_{r=0}. \tag{5}$$

For a stationary wave function

$$\psi_1(\mathbf{r}, t)=\psi(\mathbf{r})\exp(-iE''t)$$

the boundary condition reduces to the familiar form:[8]

$$(r\psi)_{r=0}=C^2(k_0^2-k''^2)^{-1}(\partial r\psi/\partial r)_{r=0}, \tag{6}$$

where[9] $C=(4\pi)^{\frac{1}{2}}|C'|$, $E''=\frac{1}{2}k''^2$, $E_0=\frac{1}{2}k_0^2$. This condition determines completely the scattering problem, as the stationary ψ must be given by a plane plus a scattered wave, and the scattered wave must be an S-wave since otherwise $r\psi$ would be singular at $r=0$. The coefficent of the scattered wave is determined by (6) and so $\psi(\mathbf{r})$ takes the form:

$$\psi(\mathbf{r})=\exp(i\mathbf{k}''\cdot\mathbf{r})+C^2(k_0^2-k''^2-ik''C^2)^{-1}r^{-1}\exp(ikr). \tag{7}$$

The total cross section is then given by the usual single level formula:

$$\sigma=(4\pi/k''^2)\Gamma^2[(E_0-E'')^2+\Gamma^2]^{-1}, \tag{8}$$

where $\Gamma=\Gamma_0(k''/k_0)$ and $\Gamma_0=\frac{1}{2}C^2k_0$. This correlates the magnitude of the coupling constant C' with the width of the energy level at resonance Γ_0 and, as will be shown later, with the probability of decay of the compound system.

At first sight, one would be inclined to think that the generalization of the boundary condition (6) for stationary states, to time-dependent states, could be achieved in terms of a single wave function $\psi_1(\mathbf{r}, t)$ satisfying (2) and (5). The discussion of the many-level scattering process in the previous note, as well as the form of similar vibration problems,[10] show though, that the generalization should be made in terms of the formulation (1)–(4) in Fock space.

Having now the information concerning stationary states that our interactions through boundary conditions can provide, we want to investigate the behavior of time-dependent states. We shall discuss, in the present paper, two time-dependent states. The first one will be the state which initially is found in the form of two particles with relative momentum $\mathbf{k}''$, so that its development in time will provide a causal description of a resonance scattering process. The second, will be a state which initially is found in the form of a single compound particle, so that its development in time will provide a causal description of a disintegration process. The Fock wave functions corresponding to these two states, will be designated by Ψ_1, Ψ_2, where:

$$\Psi_1(\mathbf{k}'', t)=\begin{bmatrix}\psi_{11}(\mathbf{r}, \mathbf{k}'', t)\\ \psi_{21}(\mathbf{k}'', t)\end{bmatrix}, \quad \Psi_2(t)=\begin{bmatrix}\psi_{12}(\mathbf{r}, t)\\ \psi_{22}(t)\end{bmatrix}, \tag{9a, b}$$

and according to what was said above, we have that for $t=0$:

$$\Psi_1(\mathbf{k}'', 0)=(2\pi)^{-\frac{1}{2}}\begin{bmatrix}\exp(i\mathbf{k}''\cdot\mathbf{r})\\ 0\end{bmatrix}, \quad \Psi_2(0)=\begin{bmatrix}0\\ 1\end{bmatrix}. \tag{10a, b}$$

We will show in what follows, that the Eq. (2) and the boundary conditions (3, 4), satisfied by the components of the time-dependent Fock wave functions, determine these wave functions completely, once the initial form of them is given. In the next section, we will discuss a mathematical preliminary which is necessary for this determination.

II. GENERALIZED HANKEL TRANSFORMS

Any wave function $\psi_1(\mathbf{r}, t)$ representing that stage of our state in which two particles are present, can be developed in spherical waves according to well known rules.[11] As the boundary conditions (3, 4) allow only S-wave scattering, it is clear that we can restrict our discussion of time-dependent wave functions to the first term in the spherical wave development, i.e., to $l=0$. The terms in the development of $\psi_1(\mathbf{r}, t)$ corresponding to relative angular momentum higher than 0, will behave as free particle wave functions.

[6] The units for time, length, and mass are then $\hbar(\mu c^2)^{-1}$, $\hbar(\mu c)^{-1}$, and μ, respectively. All quantities that appear in the following developments are therefore dimensionless.

[7] In this article we consider that $i\partial/\partial t$ is the operator for the kinetic energy alone, i.e., we have eliminated a phase factor $\exp[-i(m_1+m_2)t]$ from the formulation of the previous note. The coupling constant C_{12} of the previous note will be assumed real and denoted by C', while C_{11} will be taken as zero, so that there is no direct coupling between the two particles in the first stage.

[8] E. P. Wigner, Phys. Rev. **73**, 1002 (1948).

[9] We shall designate by E'' the relative kinetic energy, and by $\mathbf{k}''$ the corresponding momentum of the two particles, as this would be appropriate in the bra and ket notation, to be introduced in the following article.

[10] A. G. Webster, *Partial Differential Equations in Mathematical Physics* (G. E. Stechert & Company, New York, 1933), second edition, pp. 124–129.

[11] N. F. Mott and H. S. W. Massey, *The Theory of Atomic Collisions* (Clarendon Press, Oxford, 1949), second edition, p. 22.

Before we attempt to obtain the explicit form of the time-dependent Fock states, let us look at the well-known procedure one follows in the case of two non-interacting particles. Let us assume that in the center-of-mass reference frame, we have two noninteracting particles with zero relative angular momentum, represented at $t=0$ by the wave packet $\psi(r)$. The Hankel transform corresponding to this wave packet is:

$$F(k)=(2/\pi)^{\frac{1}{2}}\int_0^\infty \psi(\rho)(k\rho)^{-1}\sin k\rho\ \rho^2 d\rho, \quad (11a)$$

$$\psi(r)=(2/\pi)^{\frac{1}{2}}\int_0^\infty F(k)(kr)^{-1}\sin kr\ k^2 dk. \quad (11b)$$

With the help of (11), the time dependent wave function can then be explicitly obtained in the form:

$$\psi(r,t)=(2/\pi)^{\frac{1}{2}}\int_0^\infty F(k)(kr)^{-1}\sin kr\exp(-i\tfrac{1}{2}k^2t)k^2dk. \quad (12)$$

The relations (11) are, of course, connected with the expressions in transformation theory, that take us from the configuration to the energy-angular momentum representation of the state. The transform $F(k)$ can also be expressed as an integral over all of configuration space, in the form:

$$F(k)=(2\pi)^{-\frac{1}{2}}\int (kr)^{-1}\sin kr\ \psi(r)\,d\tau, \quad (11c)$$

i.e., as $(2\pi)^{-\frac{1}{2}}$ times the scalar product of the two wave functions in the integrand.

From the above, we see that the explicit form for time-dependent Fock states could be found, if we had an appropriate generalization of the Hankel transforms (11). For this, we introduce a stationary Fock wave function corresponding to zero relative angular momentum for the two particles of the form:

$$\Phi(k)=\begin{bmatrix}\phi_1(k,r)\\ \phi_2(k)\end{bmatrix}. \quad (13)$$

The component $\phi_1(k,r)$ of (13) is defined so as to satisfy $\nabla^2\phi_1+k^2\phi_1=0$ and the boundary condition (6), and to reduce in the absence of interaction (i.e., $C=0$) to $(kr)^{-1}\sin kr$. For $\phi_1(k,r)$ we have then:

$$\phi_1(k,r)=(-2ikr)^{-1}[\exp(-ikr)-S(k)\exp(ikr)] \quad (14)$$

where $S(k)$, the single component of the scattering matrix,[4] is determined by the boundary condition (6), so that it becomes:

$$S(k)=(k_0^2-k^2-ikC^2)^{-1}(k_0^2-k^2+ikC^2). \quad (15)$$

The component $\phi_2(k)$ of (13) is determined by the boundary condition (4), so that $\Phi(k)$ takes finally the form:

$$\Phi(k)=\begin{bmatrix}\dfrac{kC^2}{k_0^2-k^2-ikC^2}\left(\dfrac{\cos kr}{kr}+\dfrac{k_0^2-k^2}{kC^2}\dfrac{\sin kr}{kr}\right)\\ 4\pi C'(k_0^2-k^2-ikC^2)^{-1}\end{bmatrix}. \quad (16)$$

Let us now designate by Ψ any other Fock state in which in the first stage, the two particles have zero relative angular momentum, so that at $t=0$, Ψ has the form:

$$\Psi=\begin{bmatrix}\psi_1(r)\\ \psi_2\end{bmatrix}. \quad (17)$$

The scalar product (Φ,Ψ) of the two Fock states is, according to the previous note, given by:

$$(\Phi,\Psi)=\int \phi_1^*\psi_1 d\tau+\phi_2^*\psi_2. \quad (18)$$

We can now give a formal generalization of the Hankel transforms (11), in terms of the relations:

$$F(k)=(2\pi)^{-1}(\Phi,\Psi)=(2/\pi)^{\frac{1}{2}}\int_0^\infty \phi_1^*(k,\rho)\psi_1(\rho)\rho^2 d\rho + (2\pi)^{-1}\phi_2^*(k)\psi_2, \quad (19a)$$

$$\Psi=\begin{bmatrix}\psi_1(r)\\ \psi_2\end{bmatrix}=(2/\pi)^{\frac{1}{2}}\int_0^\infty F(k)\begin{bmatrix}\phi_1(k,r)\\ \phi_2(k)\end{bmatrix}k^2dk. \quad (19b)$$

In the absence of interactions, i.e., when $C=0$ the relation (19) reduces to (11). A justification of the relation (19) from a quantum-mechanical standpoint, will be given in a following paper in which the $\Phi(k)$'s are shown to be the eigen Fock states of a complete set of commutaing observables, including an appropriately defined hamiltonian, as well as the relative angular momentum operator. The relation (19) indicates that a Fock state Ψ corresponding to the same relative angular momentum eigenvalue $l=0$ than $\Phi(k)$ does, can be expanded[12] in terms of the basic eigenstates $\Phi(k)$ corresponding to eigenvalues $E=\frac{1}{2}k^2$ of the hamiltonian. A rigorous mathematical derivation of (19) can also be given with the help of the functional methods developed by Kneser,[13] Hilb and others, and it will be presented elsewhere.

With the help of (19), we obtain the explicit form of the time dependent Fock state $\Psi(t)$ corresponding to the initial value (17), which is given by:

$$\Psi(t)\equiv\begin{bmatrix}\psi_1(r,t)\\ \psi_2(t)\end{bmatrix}=(2/\pi)^{\frac{1}{2}}\int_0^\infty F(k)\begin{bmatrix}\phi_1(k,r)\\ \phi_2(k)\end{bmatrix} \times\exp(-i\tfrac{1}{2}k^2t)k^2dk, \quad (20)$$

where $F(k)$ is defined by (19a).

[12] P. A. M. Dirac, *Quantum Mechanics* (Clarendon Press, Oxford, 1947), third edition, Chap. III, p. 64.

[13] A. Kneser, *Die Integralgleichungen und ihre Anwendung in der mathematischen Physik* (Vieweg, Braunschweig, Germany, 1922), second edition, Chapter VI, p. 236.

From (20) we see that the components of $\Psi(t)$ satisfy the boundary condition (4), as $[r\phi_1(k,r)]_{r=0}=C'\phi_2(k)$ from definition. Furthermore, we see from the form (16) of $\Phi(k)$, that the components of $\Psi(t)$ will satisfy the Schrödinger equation (2) and the boundary condition (3), in case we can interchange the differentiation procedures involved with the integral sign in (20).

III. TIME DEPENDENT STATES FOR SCATTERING AND DISINTEGRATION

We shall first determine the time-dependent state $\Psi_1(\mathbf{k}'',t)$ which gives a causal description of the resonance scattering process. Its initial form is given by (10a), which may be written as:

$$(2\pi)^{\frac{1}{2}}\Psi_1(\mathbf{k}'',0)=\begin{bmatrix}(k''r)^{-1}\sin k''r\\0\end{bmatrix}+\begin{bmatrix}\exp(i\mathbf{k}''\cdot\mathbf{r})-(k''r)^{-1}\sin k''r\\0\end{bmatrix}. \quad (21)$$

The second summand, when expanded in spherical waves,[11] represents a superposition of states for which the relative angular momentum $l>0$. According to the remarks of the previous section, we see that the second summand represents a noninteracting system of two particles, and the corresponding time-dependent behavior is obtained by multiplication with $\exp(-iE''t)$.

The time-dependent state represented initially by the first summand of (21), can be obtained with the help of (19a, 20), and if we designate the first component of this time-dependent state by $\psi_1(r,k'',t)$, we can write:

$$(2\pi)^{\frac{1}{2}}\psi_{11}(\mathbf{r},\mathbf{k}'',t)=[\psi_1(r,k'',t)-(k''r)^{-1}\sin(k''r)\exp(-i\tfrac{1}{2}k''^2t)]+\exp i[\mathbf{k}''\cdot\mathbf{r}-\tfrac{1}{2}k''^2t], \quad (22a)$$

$$(2\pi)^{\frac{1}{2}}\psi_{21}(\mathbf{k}'',t)=(1/C')[r\psi_1(r,k'',t)]_{r=0}. \quad (22b)$$

The last relation coming from the first, when we apply the boundary condition (4).

The time dependent state $\Psi_1(\mathbf{k}'',t)$ is completely determined once $\psi_1(r,k'',t)$ is known, and this, in turn, is given by (19, 20) of the previous section, if we introduce there, for the initial state, the form $\psi_1(r)=(k''r)^{-1}\sin k''r$, $\psi_2=0$. The calculations are carried in Appendix 1, and with the help of the results obtained there, we can write the first component of $\Psi_1(\mathbf{k}'',t)$ in the form:

$$(2\pi)^{\frac{1}{2}}\psi_{11}(\mathbf{r},\mathbf{k}'',t)=\exp i[\mathbf{k}''\cdot\mathbf{r}-\tfrac{1}{2}k''^2t]-\frac{C^2}{r}\left\{\frac{k_1\chi(r,k_1,t)}{(k_1^2-k''^2)(k_1-k_2)}+\frac{k_2\chi(r,k_2,t)}{(k_2^2-k''^2)(k_2-k_1)}-\frac{\chi(r,k'',t)}{2(k_0^2-k''^2-ik''C^2)}-\frac{\chi(r,-k'',t)}{2(k_0^2-k''^2+ik''C^2)}\right\}, \quad (23)$$

where for any complex k, we have:

$$\chi(r,k,t)=\exp i(kr-\tfrac{1}{2}k^2t)\times\operatorname{erfc}[(1-i)(4t)^{-\frac{1}{2}}(r-kt)], \quad (24)$$

and erfc(z) stands for the error integral function defined by:[14]

$$\operatorname{erfc}(z)=2\pi^{-\frac{1}{2}}\int_z^\infty\exp(-z^2)dz=1-\operatorname{erf}(z). \quad (25)$$

The only parameters that appear in the wave function (23) are k_1, k_2, which correspond to the values of k at the poles of the scattering matrix (15). Accordingly, k_1, k_2 are the roots of the equation:

$$k_0^2-k^2-ikC^2=0 \quad (26a)$$

and so, take the values:

$$\left.\begin{matrix}k_1\\k_2\end{matrix}\right\}=k_0\{\pm[1-(C^2/2k_0)^2]^{\frac{1}{2}}-i(C^2/2k_0)\}. \quad (26b)$$

The second component of $\Psi_1(\mathbf{k}'',t)$ can be obtained from (23) with the help of the boundary condition (4), so that we have:

$$(2\pi)^{\frac{1}{2}}\psi_{21}(\mathbf{k}'',t)=-4\pi C'\{\ \}_{r=0}, \quad (23a)$$

where the terms in the bracket are those inside the curly bracket of (23) evaluated at $r=0$.

The time-dependent state $\Psi_2(t)$, which gives a causal description of the disintegration process, is given initially by (10b), so its explicit form can be obtained from (19, 20) if we put there $\psi_1(r)=0$, $\psi_2=1$. For the calculations we again refer to Appendix 1, and we have, for the first component of $\Psi_2(t)$ the form:

$$\psi_{12}(\mathbf{r},t)=C'r^{-1}(k_1-k_2)^{-1}[k_1\chi(r,k_1,t)-k_2\chi(r,k_2,t)]. \quad (27a)$$

For the second component of $\Psi_2(t)$ we use the boundary condition (4), and we have:

$$\psi_{22}(t)=(k_1-k_2)^{-1}[k_1\chi(0,k_1,t)-k_2\chi(0,k_2,t)]. \quad (27b)$$

We have obtained in this section the explicit form of the time-dependent states $\Psi_1(\mathbf{k}'',t)$, $\Psi_2(t)$, representing the causal description of the process of resonance elastic scattering, and disintegration, respectively. In the following section, we will show that the components of these states satisfy Eq. (2) and the boundary conditions (3), (4), as well as the initial conditions (10a, b). We shall also discuss the asymptotic behavior of these time-dependent states when $t\to\infty$, as well as its dependence on the position of the poles of the scattering matrix, which are the only parameters present.

[14] E. T. Whittaker and G. N. Watson, *Modern Analysis* (Cambridge University Press, New York, 1943), American edition, pp. 341–343.

IV. PROPERTIES OF THE TIME-DEPENDENT STATES

Using the definition (24) of $\chi(r, k, t)$ we can easily check by direct substitution that:

$$\tfrac{1}{2}(\partial^2\chi/\partial r^2) = -i(\partial\chi/\partial t). \tag{28a}$$

It is clear therefore, that $r^{-1}\chi(r, k, t)$ satisfies Eq. (2) for any complex k. We see from the forms (23) (27a) of the first components of $\Psi_1(\mathbf{k}'', t)$, $\Psi_2(t)$, that they satisfy the time dependent Schrödinger equation (2) for $\mathbf{r}\neq 0$.

The components of $\Psi_1(\mathbf{k}'', t)$, $\Psi_2(t)$ must satisfy the boundary conditions (3, 4), and since (4) is always valid, as seen in (20), we can reduce the boundary condition (3) to the form (5) in which only the first component of the Fock state appears. Again, we need a property of the $\chi(r, k, t)$ which from its definition (24), is seen to satisfy the relation:

$$-i(\partial\chi/\partial t)_{r=0} + \tfrac{1}{2}k_0^2(\chi)_{r=0} - \tfrac{1}{2}C^2(\partial\chi/\partial r)_{r=0}$$
$$= \tfrac{1}{2}(k_0^2 - k^2 - ikC^2)(\chi)_{r=0} + (4\pi t)^{-\frac{1}{2}}(1-i)(C^2 - ik). \tag{28b}$$

Making use of (28b), which is valid for any complex k, and of the fact that k_1, k_2 are the roots of Eq. (26a), we can prove by direct substitution that $\psi_{11}(\mathbf{r}, \mathbf{k}'', t)$ and $\psi_{12}(\mathbf{r}, t)$ satisfy (5).

Finally, we want to show that $\Psi_1(\mathbf{k}'', t)$, $\Psi_2(t)$ reduce at $t=0$ to the initial values (10a, b). This is achieved with the help of the properties of $\chi(r, k, t)$. First, if $r\neq 0$ and $t\to 0$, $\chi(r, k, t)\to 0$, because the factor,

$$\operatorname{erfc}[(1-i)(4t)^{-\frac{1}{2}}(r-kt)] \to \operatorname{erfc}[(1-i)\infty] \to 0,$$

as seen in Appendix 2. From this we see immediately that for $t\to 0$, $\psi_{11}(\mathbf{r}, \mathbf{k}'', t)\to(2\pi)^{-\frac{1}{2}}\exp i\mathbf{k}''\cdot\mathbf{r}$ and $\psi_{12}(\mathbf{r}, t)$ $\to 0$. Now, if $r=0$, then

$$\chi(0, k, t) = \exp(-i\tfrac{1}{2}k^2t)\operatorname{erfc}[-(1-i)k(t/4)^{\frac{1}{2}}],$$

which from the definition (25) of $\operatorname{erfc}(z)$ takes for $t=0$ the value $\chi(0, k, 0)=1$. Accordingly, $\psi_{21}(\mathbf{k}'', t)$ reduces to the sum of the coefficients of the χ's contained in the curly bracket of (23), which is seen to be zero, so that $\psi_{21}(\mathbf{k}'', 0)=0$. From (27b) we see also that $\psi_{22}(0)=1$, so that the initial conditions (10a, b) hold.

The above analysis is seen to be independent of the position of k_1, k_2 in the complex k-plane, so long as k_1, k_2 are roots of Eq. (26a).

V. ASYMPTOTIC BEHAVIOR

We are interested now in the asymptotic form of our time-dependent states $\Psi_1(\mathbf{k}'', t)$, $\Psi_2(t)$ when $t\to\infty$, as this form should be the one corresponding to stationary states for scattering and disintegration, respectively. As the only parameters that appear in the explicit expressions of these states, are the poles of the scattering matrix, we see that these asymptotic forms will depend on the position of k_1, k_2 in the complex k-plane.

As k_1, k_2 are roots of (26a), we see that their values depend on those of the binding energy $E_0=\frac{1}{2}k_0^2$ and the coupling constant C^2. From the previous note, we see that C^2 must be real and positive if conservation of probability holds. The binding energy E_0 must be real, but it can be positive or negative. We see from (26b) that if $C^2>0$, $E_0>0$ and $(C^2/2k_0)<1$, then k_1, k_2 are in the lower half of the complex k-plane symmetrically situated with respect to the imaginary axis. If $(C^2/2k_0)$ $\geqslant 1$ then they are both on the negative imaginary axis. In case $E_0<0$, *i.e.*, $k_0=i\kappa_0$ where κ_0 is real >0, then k_1 is on the upper and k_2 on the lower imaginary axis. For any physically significant case, the poles of the scattering matrix are then, either in the lower half of the k-plane, or on the imaginary axis, and the general character of this result has been shown by Schützer and Tiomno.[5] We shall also investigate the possibility that the poles of the scattering matrix are on the upper half of the k-plane, to see how the causal description is affected.

To obtain the asymptotic behavior of our states, we need to know the asymptotic form of $\chi(r, k, t)$ for a given r and complex k, when $t\to\infty$. In Appendix 2 we show that when $t\to\infty$ we have:

$$\chi(r, k, t)\to 2\exp[i(kr - \tfrac{1}{2}k^2t)] \text{ when } -\tfrac{1}{4}\pi < \arg k < \tfrac{3}{4}\pi, \tag{29a}$$

$$\chi(r, k, t)\to 0, \text{ when } \tfrac{3}{4}\pi < \arg k < (7\pi/4). \tag{29b}$$

These relations hold also for $r=0$.

(a) Binding Energy $E_0>0$

We saw that in this case k_1, k_2 are in the lower half of the k-plane. Now we consider two separate possibilities, (i) $-\frac{1}{4}\pi\leqslant\arg k_1\leqslant 0$, (ii) $-\frac{1}{2}\pi\leqslant\arg k_1<-\frac{1}{4}\pi$. In the second case (ii), we have that $-k''$, k_2, k_1 are in the range indicated in (29b) so that the corresponding χ's$\to 0$, and in (23) we are left only with $\chi(r, k'', t)$, whose asymptotic form is given by (29a), so that finally:

$$(2\pi)^{\frac{1}{2}}\psi_{11}(\mathbf{r}, \mathbf{k}'', t)\to\left[\exp i\mathbf{k}''\cdot\mathbf{r} + \frac{C^2}{k_0^2 - k''^2 - ik''C^2}\times\frac{\exp ik''r}{r}\right]\exp(-i\tfrac{1}{2}k''^2t). \tag{30a}$$

The same result is obtained in the first case (i) because though $\chi(r, k_1, t)$ has then the asymptotic form (29a), the imaginary part of k_1^2 is negative and $\exp(-i\frac{1}{2}k_1^2t)\to 0$ when $t\to\infty$.

For binding energy $E_0>0$, the Fock state $\Psi_1(\mathbf{k}'', t)$ tends asymptotically to the stationary state (7) corresponding to the resonance scattering process.

It is of interest to consider the asymptotic form of the Fock state for disintegration $\Psi_2(t)$, in the physically important case, when the width of energy levels at resonance is much smaller than the separation of the levels, which in this case means $(\Gamma_0/E_0)\ll 1$. From (8) we have that $(C^2/k_0)=(\Gamma_0/E_0)\ll 1$, and from (26b) we see that case (i) holds. From the expression (27b) for $\psi_{22}(t)$ we see that its asymptotic form is:

$$2k_1(k_1-k_2)^{-1}\exp(-i\tfrac{1}{2}k_1^2t). \tag{30b}$$

According to the interpretation given to the components of a Fock state in the previous note, we see that $\psi_{22}^*(t)\psi_{22}(t)$ represents the probability of observing a state originally in the form of a single particle, still in that form at time t. From (30b), and the fact that $k_1^2 \simeq k_0^2 - iC^2k_0$, we see that this probability is given by:

$$\text{const}\exp(-C^2k_0t) \tag{30c}$$

and so, the width $\Gamma_0=\frac{1}{2}C^2k_0$ is related with the probability of disintegration of the compound particle, as one should expect.[15]

(b) Binding Energy $E_0<0$

In this case, k_1 is on the upper and k_2 on the lower imaginary axis, and therefore, $-k''$, k_2 have their arguments in the range (29b), so that the corresponding χ's$\to 0$, while the χ's corresponding to k'', k_1 have the asymptotic form (29a). It is clear then, that the asymptotic form of $(2\pi)^{\frac{1}{2}}\psi_{11}(\mathbf{r}, \mathbf{k}'', t)$ is given by (30a) plus the term:

$$2C^2\kappa_1(\kappa_1^2+k''^2)^{-1}(\kappa_1+\kappa_2)^{-1} \times[r^{-1}\exp(-\kappa_1 r)\exp(i\tfrac{1}{2}\kappa_1^2 t)], \tag{31}$$

where $k_1=i\kappa_1$, $k_2=-i\kappa_2$, and κ_1, κ_2 real >0.

The term in the square bracket of (31) is seen to satisfy Eq. (2) and the boundary condition (5), and it goes exponentially to zero when $r\to\infty$. It represents then a bound state corresponding to the negative energy $E_1=-\frac{1}{2}\kappa_1^2$, and its appearance in the stationary state for scattering just tells us that for $E_0<0$, i.e., $M<(m_1+m_2)$, a stable bound state can be formed as a result of the collision. Because of its behavior when $r\to\infty$ this bound state does not change the dependence of the cross section on energy, which continues to be given by (8).

From (27a) we see that when $t\to\infty$, $\psi_{12}(\mathbf{r}, t)$ tends, except for a constant factor, to the form (31). The Fock state $\Psi_2(t)$ tends then asymptotically to the above bound state of negative energy E_1.

(c) Poles of the Scattering Matrix in the Upper Half-Plane

As the poles of the scattering matrix k_1, k_2 are roots of Eq. (26a), they can be in the upper half-plane (excluding the imaginary axis), only if we abandon the restriction that C^2, E_0 are real and that $C^2>0$. We cannot though give arbitrary complex values to E_0, C^2 as the fundamental properties[16] of the S-matrix for real k:

$$S(k)S(-k)=1, \quad S^*(k)S(k)=1$$

must be preserved. To satisfy this restriction, we see that E_0, C^2 in (15) must remain real and we have only the freedom of taking $C^2<0$. In this case the poles k_1, k_2 when outside the imaginary axis, will be situated in the upper half-plane symmetrically with respect to this axis.

[15] E. Fermi, *Nuclear Physics* (University of Chicago Press, Chicago, 1950), revised edition, p. 154.
[16] Ning Hu, Phys. Rev. **74**, 132 (1948).

We indicate by k_1 the pole in the first quadrant, and by k_2 the pole in the second. Now, if $(3\pi/4)<\arg k_2<\pi$ the corresponding χ goes to zero, while in case $(\pi/2)<\arg k_2\leqslant(3\pi/4)$ the χ has the asymptotic form (29a) but this, in turn, goes to zero when $t\to\infty$ because k_2^2 has a negative imaginary part. We need to concern ourselves only with the χ's in (23) corresponding to k'', k_1. The asymptotic form for $\chi(r, k_1, t)$ is given by (29a), *and it goes to* ∞ when $t\to\infty$ because the imaginary part of k_1^2 is positive. The wave function $\psi_{11}(\mathbf{r}, \mathbf{k}'', t)$ will go then to ∞ when $t\to\infty$.

For poles in the upper half-plane (excluding the imaginary axis), it is not possible to give a causal description of the scattering process in terms of a wave function $\psi_{11}(\mathbf{r}, \mathbf{k}'', t)$, connecting the initial plane wave with a final plane plus scattered waves. This is in line with the general results of Schützer and Tiomno.[5]

VI. THE TRANSIENT SCATTERED CURRENT

In a scattering process, our main interest lies in the determination of the scattered current, which is directly connected with the cross section. As in the present analysis we have obtained a time dependent state $\psi_{11}(\mathbf{r}, \mathbf{k}'', t)$ for the description of the scattering process, we see that we are in a position to determine, not only the stationary scattered current that is established when $t\to\infty$, but also the transient scattered current that appears between the initiation of the phenomenon and the establishment of stationary conditions.

From (23) we see that $(2\pi)^{\frac{1}{2}}\psi_{11}(\mathbf{r}, \mathbf{k}'', t)$ is given by a plane plus a scattered S-wave, which we shall designate by $\psi_S(r, k'', t)$, and whose form is:

$$\psi_S(r, k'', t)=-C^2r^{-1}\sum_{i=1}^{4}A_i\chi(r, k_i, t), \tag{32}$$

where k_1, k_2 are, as before, the poles of the scattering matrix, $k_3=k''$, $k_4=-k''$ and the A_i's are the coefficients of the corresponding χ's in (23).

The scattered current $\mathbf{j}$ is expressed in the usual form in terms of the ψ_S, and the flux through an element of area dS, subtending a solid angle $d\omega$ at a relative distance R, is given by:

$$\begin{aligned}F(R, k'', t)d\omega &\equiv (r^{-1}\mathbf{r}\cdot\mathbf{j})_{r=R}dS \\ &= (2i)^{-1}[(r\psi_S)^*(\partial r\psi_S/\partial r) \\ &\quad -(r\psi_S)(\partial r\psi_S/\partial r)^*]_{r=R}d\omega. \end{aligned}\tag{33}$$

From the definition (24) of the functions $\chi(r, k, t)$ it is easily seen that the flux per unit solid angle at a relative distance R, becomes:

$$F(R, k'', t)=\mathrm{Re}C^4\left\{\left[\sum_{i=1}^{4}A_i\chi(R, k_i, t)\right]^* \times\left[\sum_{i=1}^{4}A_ik_i\chi(R, k_i, t)\right]\right\}, \tag{34}$$

where Re stands for real part of the expression (34).

From the properties of the χ's given in Secs. IV, V, we see that at $t=0$, $F(R, k'', 0)=0$, while when $t\to\infty$, the flux F tends to:

$$F(R, k'', t)\to C^4k''[(k_0^2-k''^2)^2+C^4k''^2]^{-1}, \quad (35)$$

so that the total cross section for the stationary state is given by (8).

The expression (34) for the transient scattered flux simplifies somewhat, in case the relative distance is large, i.e., if $R\gg|k''|^{-1}$, $|k_2|^{-1}$. In this case, it is seen that for any positive time $t>0$, $\chi(R, k_2, t)$, $\chi(R, -k'', t)\simeq 0$, so that the summation involved in (34) can be restricted to the values $i=1, 3$ of the indices.

It is a pleasure to acknowledge the support given to the present research by the Instituto Nacional de la Investigación Científica.

APPENDIX 1

In this appendix we shall obtain with the help of (19, 20) the time-dependent wave functions corresponding to the initial states:

$$\begin{bmatrix}(k''r)^{-1}\sin k''r\\ 0\end{bmatrix} \text{ and } \begin{bmatrix}0\\ 1\end{bmatrix}. \quad (36)$$

For the first of the above states, we have that the components of (17) are $\psi_1(r)=(k''r)^{-1}\sin k''r$ and $\psi_2=0$, so that the corresponding transform $F(k)$, given by (19a), is:

$$F(k)=\frac{kC^2}{k_0^2-k^2+ikC^2}\left\{(2/\pi)^{\frac{1}{2}}\int_0^\infty\left(\frac{\cos kr}{kr}+\frac{k_0^2-k^2}{kC^2}\frac{\sin kr}{kr}\right)\frac{\sin k''r}{k''r}r^2dr\right\}. \quad (37)$$

The part of (37) inside the curly bracket is clearly the ordinary Hankel transform (11) of that part of the integrand inside the round brackets. To evaluate (37), we just need the Hankel transforms of $(kr)^{-1}\sin kr$ and $(kr)^{-1}\cos kr$. We assert that these Hankel transforms are $(2\pi)^{\frac{1}{2}}k^{-1}\delta(k''^2-k^2)$ and $-(2\pi)^{\frac{1}{2}}[\pi k(k^2-k''^2)]^{-1}$ respectively, and because of the reciprocal relation (11b) that holds for Hankel transforms, our assertion will be valid if we can prove that:

$$(2/\pi)^{\frac{1}{2}}\int_0^\infty[(2\pi)^{\frac{1}{2}}k^{-1}\delta(k''^2-k^2)](k''r)^{-1}\times\sin(k''r)k''^2dk''=(kr)^{-1}\sin kr,$$

$$(2/\pi)^{\frac{1}{2}}\int_0^\infty(2\pi)^{\frac{1}{2}}[\pi k(k''^2-k^2)]^{-1}(k''r)^{-1}\times\sin(k''r)k''^2dk''=(kr)^{-1}\cos kr.$$

The first equation is obviously true, and the second will be valid if we interpret the integral in the sense of Cauchy's principal value,[17] as it can be written in the form:

$$(\pi ikr)^{-1}\int_{-\infty}^{\infty}(k''^2-k^2)^{-1}\exp(ik''r)k''dk'',$$

and the principal value of this integral, which is πi times the sum of its residues at the poles $k''=-k$, $k''=k$, is just $(kr)^{-1}\cos kr$. We have then for $F(k)$ the form:

$$F(k)=\frac{kC^2}{k_0^2-k^2+ikC^2}\frac{(2\pi)^{\frac{1}{2}}}{k}\times\left[-\frac{1}{\pi(k^2-k''^2)}+\frac{k_0^2-k^2}{kC^2}\delta(k''^2-k^2)\right]. \quad (38)$$

Introducing this $F(k)$ in (20) we obtain the first component of the time dependent function:

$$\psi_1(r, k'', t)=\frac{k''C^2(k_0^2-k''^2)}{(k_0^2-k''^2)^2+k''^2C^4}\left[\frac{\cos k''r}{k''r}+\frac{k_0^2-k''^2}{k''C^2}\frac{\sin k''r}{k''r}\right]\times\exp(-i\tfrac{1}{2}k''^2t)-\int_0^\infty\frac{2k^2C^4\exp(-i\frac{1}{2}k^2t)}{(k_0^2-k^2)^2+k^2C^4}\times\left[\frac{\cos kr}{kr}+\frac{k_0^2-k^2}{kC^2}\frac{\sin kr}{kr}\right]\frac{kdk}{\pi(k^2-k''^2)}, \quad (39)$$

where the integral must be interpreted in the sense of Cauchy's principal value.[17]

To evaluate the integral in (39), we first simplify it by using exponential functions and extending the range of integration from $-\infty$ to ∞, so that it becomes:

$$C^2(\pi ir)^{-1}\mathrm{P}\int_{-\infty}^{\infty}k\left[\prod_{j=1}^{4}(k-k_j)\right]^{-1}\exp i(kr-\tfrac{1}{2}k^2t)dk, \quad (40)$$

where P stands for principal value of the integral, and k_j, $j=1, 2, 3, 4$ have the same meaning than in Sec. VI. We shall furthermore assume that the binding energy $E_0>0$ and that the coupling constant C^2 is small enough so that k_1, k_2 are in the lower half of the k-complex plane, and k_3 is inside the wedge as in Fig. 1. This restriction is just for the purpose of simplifying the calculation, as the final results are shown in Sec. IV, to be valid independently of the position of the poles of the scattering matrix.

We now consider the path in the complex k-plane shown in Fig. 1. As on the arcs of circle represented by dotted lines in Fig. 1, k^2 has a negative imaginary part, we see that the integrand vanishes exponentially for large values of $|k|$ on them. Also inside the contour, (which includes the circle around k_3) the integrand is a

[17] See reference 14, p. 117.

analytic function of k, so using Cauchy's theorem we obtain:

$$\mathrm{P}\int_{-\infty}^{\infty} = \pi i\,\mathrm{Res}(k=-k'') - \pi i\,\mathrm{Res}(k=k'') - 2\pi i\,\mathrm{Res}(k=k_1) + \int_{-(1-i)\infty}^{(1-i)\infty}, \quad (41)$$

where $\mathrm{Res}(k=-k'')$, etc. stand for the residues of the integrand at those values of k.

In the integral on the right of (41) we decompose the rational part of the integrand into partial fractions, so we have:

$$k\left[\prod_{i=1}^{4}(k-k_i)\right]^{-1} = \sum_{i=1}^{4} A_i(k-k_i)^{-1} \quad (42)$$

where $A_1 = k_1[(k_1-k_2)(k_1-k_3)(k_1-k_4)]^{-1}$, etc. Furthermore, we introduce a change of variable $z = k\exp(i\pi/4)$

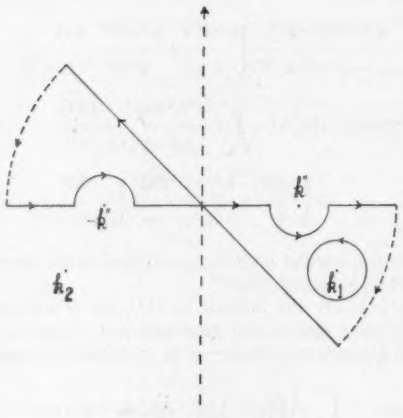

FIG. 1. Integration contour.

and we have for this integral:

$$\int_{-(1-i)\infty}^{(1-i)\infty} = \sum_{j=1}^{4} A_j \int_{-\infty}^{\infty} (z-z_j)^{-1}\exp(\lambda z - \nu z^2)dz \equiv \sum_{j=1}^{4} A_j F(\nu, \lambda, z_j), \quad (43)$$

where $\lambda = r\exp(i\pi/4)$, $\nu = (t/2)$, $z_j = k_j\exp(i\pi/4)$. Now, the functions $F(\nu, \lambda, z_j)$ defined by the integrals in (43) can be easily evaluated, either by differentiating them with respect to λ and solving the differential equation that appears, or with the help of a table of Fourier transforms.[13] The function $F(\nu, \lambda, z_j)$ takes then the form:

$$F(\nu, \lambda, z_j) = \exp(\lambda z_j - \nu z_j^2)\pi i \times\{\mathrm{erf}[(2i\nu^{\frac{1}{2}})^{-1}(\lambda - 2\nu z_j)]\pm 1\}, \quad (44)$$

where the + sign is used when the imaginary part of $z_j > 0$ and the − sign when it is <0. The function $\mathrm{erf}(z)$ is the error integral of (25).

With the help of (44) we can evaluate (43) using the + sign in (44) for the poles k'', k_1, and the − sign for $-k''$, k_2. From (43) and the values of the residues of the integrand in (41), we obtain finally:

$$\psi_1(r, k'', t) = (k''r)^{-1}\sin k''r\exp(-it\tfrac{1}{2}k''^2t) - C^2r^{-1}\sum_{i=1}^{4} A_i\chi(r, k_i, t), \quad (45)$$

where $\chi(r, k_i, t)$ is the function defined by (24). Introducing this value in (22a), we obtain the expression for the first component of $\Psi(\mathbf{k}'', t)$ given by (23).

If we now consider the second state in (36), we see that for this state the components of (17) are $\psi_1(r) = 0$, $\psi_2 = 1$ so that the corresponding transform $F(k)$ is by (19a) just:

$$F(k) = (2/\pi)^{\frac{1}{2}}C'(k_0^2 - k^2 + ikC^2)^{-1}. \quad (46)$$

The first component of the corresponding time dependent function, which is now $\psi_{12}(\mathbf{r}, t)$, is obtained by introducing (46) in (20), and we have:

$$\psi_{12}(r, t) = (2\pi^2C')^{-1}\int_0^{\infty} \frac{k^3C^4\exp(-it\tfrac{1}{2}k^2t)}{(k_0^2-k^2)^2+k^2C^4} \times\left[\frac{\cos kr}{kr} + \frac{k_0^2-k^2}{kC^2}\frac{\sin kr}{kr}\right]kdk. \quad (47)$$

This integral has a form similar to the one that appears in (39), except that the factor $(k^2-k''^2)^{-1}$ is not present, so that there are no poles at $k = \pm k''$. The evaluation of (47) can be made along similar lines than in the preceeding case, and we only need to eliminate the indentations of the contour at $k = \pm k''$, as there is no need to consider principal values here. The result of the integration is given in (27a).

APPENDIX 2

We shall summarize here some of the asymptotic properties of the error integral function $\mathrm{erfc}(z)$, and derive from them the asymptotic behavior of $\chi(r, k, t)$ defined by (24), when $t \to 0$ and $t \to \infty$.

It is known[14] that the error integral can be expressed in terms of confluent hypergeometric functions in the form:

$$\mathrm{erfc}(z) = (\pi z)^{-\frac{1}{2}}\exp(-\tfrac{1}{2}z^2)W_{-\frac{1}{2},\,\frac{1}{2}}(z^2) \quad (48)$$

and from the asymptotic behavior of these functions[14] we can obtain directly that for $|z| \to \infty$,

$$\mathrm{erfc}(z) \to \pi^{-\frac{1}{2}}z^{-1}\exp(-z^2), \text{ if } -\pi/2 < \arg z < \pi/2. \quad (49)$$

[13] G. E. Campbell and R. M. Foster, *Fourier Integrals for Practical Applications* (D. Van Nostrand Company, Inc., New York, 1948), Formula 728.5.

For $|\arg z|>\pi/2$ we use the relation:

$$\operatorname{erfc}(z)=1-2\pi^{-\frac{1}{2}}\int_0^z \exp(-z^2)dz$$

$$=1+2\pi^{-\frac{1}{2}}\int_0^{-z}\exp(-z^2)dz=2-\operatorname{erfc}(-z), \quad (50)$$

so if z is outside the range of (49), $-z$ whose argument is $\pi-\arg z$ will be inside the range, and we have for $|z|\to\infty$ that:

$$\operatorname{erfc}(z)\to 2+\pi^{-\frac{1}{2}}z^{-1}\exp(-z^2), \text{ if } \pi/2<\arg z<3\pi/2. \quad (51)$$

Thus the asymptotic behavior of erfc(z) is defined in the whole complex plane.

Now the function $\chi(r, k, t)$ can be written as:

$$\chi(r, k, t)=\exp i(r^2/2t)\exp z^2\operatorname{erfc}(z), \quad (52)$$

where $z=(2t)^{-\frac{1}{2}}(r-kt)\exp(-i\pi/4)$. When $r\neq 0$ and $t\to 0$, we see that $|z|\to(2t)^{-\frac{1}{2}}r\to\infty$ and $\arg z\to-\pi/4$. Applying then (49) we see that for $t\to 0$,

$$\chi(r, k, t)\to\exp i(r^2/2t)\exp(i\pi/4)\pi^{-\frac{1}{2}}r^{-1}(2t)^{\frac{1}{2}}\to 0 \quad (53)$$

for any complex k.

When $t\to\infty$ we have that $|z|\to|k|(t/2)^{\frac{1}{2}}\to\infty$ and $\arg z\to\frac{1}{4}\pi+\arg k$. From (49, 51), and using the fact that the exponential and erfc(z) are single-valued functions, we have that for $t\to\infty$:

$$\chi(r, k, t)\to-(\pi k^2t/2)^{-1}\exp(i\pi/4)\exp i(r^2/2t)\to 0$$
$$\text{if } 3\pi/4<\arg k<7\pi/4,$$
$$\chi(r, k, t)\to 2\exp i(kr-\tfrac{1}{2}k^2t) \quad (54)$$
$$-(\tfrac{1}{2}\pi k^2t)^{-\frac{1}{2}}\exp(i\pi/4)\exp i(r^2/2t)$$
$$\to 2\exp i(kr-\tfrac{1}{2}k^2t) \text{ if } -\pi/4<\arg k<3\pi/4.$$

This result is valid also for $r=0$.

PHYSICAL REVIEW VOLUME 84, NUMBER 3 NOVEMBER 1, 1951

Quantum Mechanics in Fock Space

MARCOS MOSHINSKY
Instilos de Fisica y de Geofisica, Universidad de México, México, D.F., México

(Received July 11, 1951)

In the present paper we propose to develop a quantum-mechanical scheme in Fock space that would describe interactions that take place through the formation of a compound particle. The discussion will be restricted to a dynamical system representing a single-level scattering process. The state of this dynamical system can be found in two stages: initial particles and compound nucleus. The dynamical behavior of this state will be given in terms of a hamiltonian (that has no classical analog) which will be derived from the boundary conditions satisfied by the state. The representation of the dynamical variables, associated with the two stages of the state, will be discussed, and a complete set of constants of motion of our dynamical system will be given. The expansion of an arbitrary Fock state in terms of the simultaneous eigenstates of this complete set of constants of motion, leads to the generalized Hankel transforms, used in a preceding article for the determination of the time dependent states for scattering and disintegration. In a representation in which the constants of motion are diagonal, the operator representing the relative kinetic energy of the two initial particles will be nondiagonal, particularly in the neighborhood of the resonance energy. The unitary matrix connecting any initial Fock state with the corresponding state at time t will be obtained, and with its help the time-dependent behavior of the Heisenberg dynamical variables of our dynamical system can be derived.

I. INTRODUCTION AND SUMMARY

IN preceding articles[1,2] a reformulation of the phenomenological picture of nuclear resonance reactions was achieved in terms of a description in Fock space,[3] in which interactions took place through appropriate boundary conditions. This reformulation was shown to be useful for the description of time dependent states and, in particular, the time dependent description of a nuclear scattering process was discussed in detail in (I).

In the present paper we propose to elaborate a quantum-mechanical scheme in Fock space, that would describe interactions that take place through the formation of a compound particle. For reasons of space, as well as of mathematical simplicity, this scheme will be developed in connection with the problem of scattering of spinless particles whose discussion was initiated in (I). It will be shown though, that the extension of the scheme to the other types of interaction discussed in (II) will not present any essential difficulty.

A scattering process taking place through the formation of a compound particle could be indicated schematically as:

$$A+a\rightleftarrows C, \quad (1)$$

where A represents the initial nucleus, a the incident

[1] M. Moshinsky, Phys. Rev. **84**, 525 (1951). This paper will be referred to as (I).
[2] M. Moshinsky, Phys. Rev. **81**, 347 (1951). This paper will be referred to as (II).
[3] V. Fock, Z. Physik **75**, 622 (1932).

particle, and C the compound nucleus, all of which will be assumed spinless. The description of the scattering process will not be given in the configuration space of the nucleons present, but in the configuration space of the particles present,[2] which will be considered as elementary particles. The scattering process (1) gives then rise to a dynamical system whose states can be found in two stages: The first one, in which two particles A, a are present, the second, where we have a single compound particle C.

The bra and ket notation of Dirac[4] will be used for the states describing the scattering process (1), and representations of these bras and kets can be obtained with the help of an observable that indicates the stages of the states. The connection between the different representations of these Fock states, i.e., transformation theory, will be developed, as well as the representation of linear operators in Fock space.

The dynamical behavior of the state, describing the scattering process (1), was determined in (I) by boundary conditions, obtained from considerations of conservation of probability, connecting the two stages of the state. In quantum mechanics, the dynamical behavior of a state should be determined by the hamiltonian, and in the present paper we shall introduce the hamiltonian for the dynamical system (1), as that linear operator in Fock space that transforms any time dependent Fock state $|Qt\rangle$ into the state $i(d|Qt\rangle/dt)$. With the help of the boundary conditions, an explicit form for this hamiltonian, in any representation, will be obtained.

Besides the hamiltonian there are other observables of the dynamical system (1) such as the relative angular momentum, relative momentum, etc., of the two particles in the first stage. We shall show how to represent these observables in terms of linear hermitian operators in Fock space. As usual, those operators that commute with the hamiltonian will correspond to the constants of motion of the dynamical system (1).

We will obtain the eigen Fock states corresponding to a complete set of constants of motion of the dynamical system (1). The expansion of an arbitrary Fock state in terms of these eigenstates, will lead us to the generalized Hankel transforms (19I), which were used in (I) for the determination of the time-dependent Fock states.

Finally, we shall proceed to determine the time dependent linear operator $\mathbf{U}(t)$ in Fock space, that transforms any initial Fock state $|Q\rangle$ of the dynamical system (1), into the corresponding state $|Qt\rangle$ at time t. The linear operator $\mathbf{U}(t)$ will be given by a unitary matrix which satisfies, as usual,[5] the equation:[6]

$$i(d\mathbf{U}/dt)=\mathbf{H}\mathbf{U}, \tag{2}$$

where $\mathbf{H}$ is the hamiltonian of the dynamical system (1). The unitary matrix $\mathbf{U}(t)$ determines, from a quantum-mechanical standpoint, the dynamical system (1) completely, i.e., it determines the time dependent behavior of all the Heisenberg dynamical variables[5] associated with this dynamical system.

II. TRANSFORMATION THEORY IN FOCK SPACE

We have shown in (I), that interactions between two spinless particles leading to single-level S-wave scattering, can be described in terms of a Fock state of the form:[7]

$$\Psi=\begin{bmatrix}\psi_1(\mathbf{r})\\ \psi_2\end{bmatrix}. \tag{3}$$

The two components of the Fock state describe the fact that it may be found, either in the form of the two particles A, a, represented in their relative configuration space by $\psi_1(\mathbf{r})$, or in the form of a single compound particle C represented by ψ_2.

It is convenient to represent states of the type (3) in the bra and ket notation of Dirac,[4] which greatly simplifies the following analysis. For this purpose we introduce an observable which is restricted to take the values 1 and 2 only, so as to indicate the stage of our state, i.e., if the observable has the value 1 we have the first stage where two particles are present, while for 2 we have the stage in which a single compound particle is present. States of the form (1) would then be denoted by a ket $|\ \rangle$, whose representation would be given by the vector:

$$|\ \rangle=\begin{bmatrix}\langle 1\mathbf{r}|\ \rangle\\ \langle 2|\ \rangle\end{bmatrix}. \tag{4}$$

The appearance of $\mathbf{r}$ in the component $\langle 1\mathbf{r}|\ \rangle$ of (4), indicates that the first stage of our state is represented in the relative configuration representation.

The bra state $\langle\ |$ corresponding to (4), will be represented[4] by the vector:

$$\langle\ |=[\langle\ |1\mathbf{r}\rangle\langle\ |2\rangle]. \tag{5}$$

The scalar product of two states $\langle P|$, $|Q\rangle$ will be defined by:

$$\langle P|Q\rangle=\langle P|1\mathbf{r}\rangle\langle 1\mathbf{r}|Q\rangle+\langle P|2\rangle\langle 2|Q\rangle, \tag{6}$$

where

$$\langle P|1\mathbf{r}\rangle\langle 1\mathbf{r}|Q\rangle\equiv\int\langle P|1\mathbf{r}\rangle d\mathbf{r}\langle 1\mathbf{r}|Q\rangle.$$

In the present paper the convention of summation of repeated indices, will be extended to variables that can

[4] P. A. M. Dirac, *Quantum Mechanics* (Clarendon Press, Oxford, 1947), third edition, Chapter III.

[5] W. Pauli, *Handbuch der Physik*, 2 Auf. Band 24, pp. 138–142; see reference 4, Chapter V, pp. 108–118.

[6] Same units will be used as in (I), i.e., $\hbar=c=\mu=1$.

[7] The Fock state is represented in the center-of-mass reference frame, and this restriction to states of zero total momentum, should be kept in mind. It will be removed at the conclusion of this article.

take a continuous range of values, thus:

$$\langle\,|\mathbf{r}\rangle\langle\mathbf{r}|\,\rangle \equiv \int \langle\,|\mathbf{r}\rangle d\mathbf{r}\langle\mathbf{r}|\,\rangle;$$
$$\langle\,|\mathbf{k}\rangle\langle\mathbf{k}|\,\rangle \equiv \int \langle\,|\mathbf{k}\rangle d\mathbf{k}\langle\mathbf{k}|\,\rangle. \tag{7}$$

The transformation of the first stage $\langle 1\mathbf{r}|\,\rangle$ of the ket (4), to the momentum representation $\langle 1\mathbf{k}|\,\rangle$, can be achieved with the help of the usual[8] transformation function:

$$\langle\mathbf{k}|\mathbf{r}\rangle = \langle\mathbf{r}|\mathbf{k}\rangle^* = (2\pi)^{-\frac{1}{2}} \exp(-i\mathbf{k}\cdot\mathbf{r}). \tag{8}$$

The second stage $\langle 2|\,\rangle$ of the ket (4) represents a single compound particle, and it should remain unaffected by a change of representation for the system of two particles in the first stage. The transformation matrices $\mathbf{T}$, $\mathbf{T}^{-1}$ which take the ket (4) from the relative configuration to the relative momentum representation, and *vice versa*, should have the form:

$$\mathbf{T} = \begin{bmatrix} \langle\mathbf{k}|\mathbf{r}\rangle & 0 \\ 0 & 1 \end{bmatrix}; \quad \mathbf{T}^{-1} = \begin{bmatrix} \langle\mathbf{r}|\mathbf{k}\rangle & 0 \\ 0 & 1 \end{bmatrix}. \tag{9}$$

Thus, the ket (4) in the momentum representation, is given by:

$$\begin{bmatrix} \langle 1\mathbf{k}|\,\rangle \\ \langle 2|\,\rangle \end{bmatrix} = \mathbf{T}|\,\rangle = \begin{bmatrix} \langle\mathbf{k}|\mathbf{r}\rangle\langle 1\mathbf{r}|\,\rangle \\ \langle 2|\,\rangle \end{bmatrix}. \tag{10}$$

Any linear operator $\mathbf{F}$ which acts on a Fock state (10) could be given in the momentum representation by the matrix:

$$\mathbf{F} = \begin{bmatrix} \langle 1\mathbf{k}'|F|\mathbf{k}''1\rangle & \langle 1\mathbf{k}'|F|2\rangle \\ \langle 2|F|\mathbf{k}''1\rangle & \langle 2|F|2\rangle \end{bmatrix}. \tag{11}$$

The action of the operator $\mathbf{F}$ on any ket state, should be interpreted in the sense of a matrix operation on a vector with respect to indices 1, 2 *and* $\mathbf{k}''$. The appearance of a repeated index $\mathbf{k}''$ will imply an integration, in accordance with the convention (7). A similar remark applies to operations on bra states, and for products of linear operators.

We shall now introduce the basic ket $|\mathbf{k}''1\rangle$ to represent a state in which two particles are present with relative momentum $\mathbf{k}''$, and the basic ket $|2\rangle$ to represent the state corresponding to a single compound particle. The vectors corresponding to these kets in the momentum representation are:

$$|\mathbf{k}''1\rangle = \begin{bmatrix} \delta(\mathbf{k}'-\mathbf{k}'') \\ 0 \end{bmatrix}, \quad |2\rangle = \begin{bmatrix} 0 \\ 1 \end{bmatrix}. \tag{12}$$

The basic bras $\langle 1\mathbf{k}'|$, $\langle 2|$ are given by the transposed conjugates of the vectors (12). The configuration representation of the kets (12) is obtained with the help of $\mathbf{T}^{-1}$, so we need only to replace $\delta(\mathbf{k}'-\mathbf{k}'')$ by $\langle\mathbf{r}'|\mathbf{k}''\rangle$ in (12) to have the corresponding vectors.

The unit operator in Fock space $\mathbf{I}$, can be defined in terms of the basic kets, and in the momentum representation it is given by:

$$\mathbf{I} = \|\,|\mathbf{k}''1\rangle|2\rangle\,\| = \begin{bmatrix} \delta(\mathbf{k}'-\mathbf{k}'') & 0 \\ 0 & 1 \end{bmatrix}. \tag{13}$$

In what follows we shall indicate by $\langle P|$, $|Q\rangle$; etc., the constant states, and by $\langle Pt|$, $|Qt\rangle$, etc., the corresponding time dependent states, i.e., those time dependent Fock states which at $t=0$ reduce to $\langle P|$, $|Q\rangle$, etc.

III. THE HAMILTONIAN

We showed in (I) that the time-dependent behavior of the Fock state, representing a single-level scattering process, was determined by the Schrödinger equation (2I) and the boundary conditions (3, 4I). In the notation developed in the previous section, these equation and boundary conditions, applied to a time-dependent ket $|Qt\rangle$, become:

$$-i(\partial\langle 1\mathbf{r}|Qt\rangle/\partial t) = \tfrac{1}{2}\nabla^2\langle 1\mathbf{r}|Qt\rangle, \text{ for } \mathbf{r}\neq 0, \tag{14a}$$
$$-i(\partial\langle 2|Qt\rangle/\partial t) + E_0\langle 2|Qt\rangle = 2\pi C'(\partial r\langle 1\mathbf{r}|Qt\rangle/\partial r)_{r=0}, \tag{14b}$$
$$C'\langle 2|Qt\rangle = (r\langle 1\mathbf{r}|Qt\rangle)_{r=0} \tag{14c}$$

The ket $|Qt\rangle$ is determined completely by the relations (14) once its initial value $|Q\rangle$ is specified

We can now define the hamiltonian of our dynamical system (1), as the linear operator in Fock space $\mathbf{H}$ that transforms the ket $|Qt\rangle$ into $i(d|Qt\rangle/dt)$. To obtain the explicit form of this linear operator, let us consider the time derivative of the scalar product $\langle P|Qt\rangle$ of the form (6), in which $\langle P|$ is an arbitrary constant bra whose component $\langle P|\mathbf{r}1\rangle$ is bounded at $\mathbf{r}=0$, and vanishes appropriately at $\mathbf{r}\to\infty$. We have then:

$$i\frac{d}{dt}\langle P|Qt\rangle = \int \langle P|\mathbf{r}1\rangle i\frac{\partial}{\partial t}\langle 1\mathbf{r}|Qt\rangle d\mathbf{r} + \langle P|2\rangle i\frac{\partial}{\partial t}\langle 2|Qt\rangle. \tag{15a}$$

The "component $\langle 1\mathbf{r}|Qt\rangle$ satisfies the Schrödinger equation (14a) for $\mathbf{r}\neq 0$, so that surrounding the origin by a sphere of radius r_0, we can transform the integral in (15a) into:

$$\lim_{r_0\to 0} \tfrac{1}{2}\int_0^{\pi}\int_0^{2\pi} [r\langle P|\mathbf{r}1\rangle(\partial r\langle 1\mathbf{r}|Qt\rangle/\partial r) - (\partial r\langle P|\mathbf{r}1\rangle/\partial r)r\langle 1\mathbf{r}|Qt\rangle]_{r=r_0} \sin\theta d\varphi d\theta$$
$$-\tfrac{1}{2}\int (\nabla^2\langle P|\mathbf{r}1\rangle)\langle 1\mathbf{r}|Qt\rangle d\mathbf{r}. \tag{15b}$$

[8] See reference 4, p. 97.

Since $\langle P|\mathbf{r}1\rangle$ is bounded at the origin, and $\langle 1\mathbf{r}|Q t\rangle$ has a singularity at $\mathbf{r}=0$ only for the S-wave component (as shown in (I)), the first term in (15b) reduces to:

$$-2\pi(\partial r\langle P|\mathbf{r}1\rangle/\partial r)_{r=0}(r\langle 1\mathbf{r}|Q t\rangle)_{r=0}. \tag{15c}$$

Using now the boundary conditions (14b, c) we can write finally:

$$\begin{aligned} i(d\langle P|Qt\rangle/dt)=&\int \tfrac{1}{2}k^2\langle P|\mathbf{k}1\rangle\langle 1\mathbf{k}|Qt\rangle d\mathbf{k}\\ &-2\pi C'[(\partial r\langle P|\mathbf{r}1\rangle/\partial r)_{r=0}\langle 2|Qt\rangle\\ &+\langle P|2\rangle(\partial r\langle 1\mathbf{r}|Qt\rangle/\partial r)_{r=0}]\\ &+\langle P|2\rangle\tfrac{1}{2}k_0^2\langle 2|Qt\rangle\equiv\langle P|H|Qt\rangle, \end{aligned} \tag{16}$$

where the integral stands for the second term in (15b) expressed in the momentum representation.

For $t=0$, (16) defines the matrix element of the hamiltonian $\mathbf{H}$, corresponding to two arbitrary Fock states $\langle P|$, $|Q\rangle$. As the representative of a bra is the complex conjugate of the representative for a ket,[4] we see from (16) that $\langle P|H|Q\rangle^*=\langle Q|H|P\rangle$, and the linear operator $\mathbf{H}$ is hermitian. An hermitian matrix for the hamiltonian $\mathbf{H}$ can then be obtained in any given representation.

The hamiltonian $\mathbf{H}$ defined by (16), has clearly no classical analog, as interactions between particles in terms of boundary conditions cannot be formulated in classical mechanics.

IV. PROJECTION OPERATORS AND OBSERVABLES

When our dynamical system (1) is in the first stage, i.e., when the two initial particles are present, there are dynamical variables such as the relative angular momentum, position, momentum, etc., of the two particles, whose expectation values can be obtained from measurements. We expect that these dynamical variables can be represented by linear operators in Fock space of the form (11), which are furthermore hermitian. Before giving their explicit form though, we need to discuss the two basic dynamical variables whose expectation values give the probability of finding a state in the first or in the second stage.

Let us introduce the two hermitian linear operators in Fock space $\mathbf{I}_1$, $\mathbf{I}_2$, defined in the momentum representation by:

$$\mathbf{I}_1=\begin{bmatrix}\delta(\mathbf{k}'-\mathbf{k}'') & 0\\ 0 & 0\end{bmatrix};\quad \mathbf{I}_2=\begin{bmatrix}0 & 0\\ 0 & 1\end{bmatrix}. \tag{17}$$

The operators $\mathbf{I}_1$, $\mathbf{I}_2$ are projection operators, as they reduce any ket of the form (10) to the first or the second stage. Furthermore, $\mathbf{I}_1+\mathbf{I}_2=\mathbf{I}$ where $\mathbf{I}$ is the unit operator (13).

The expectation values of $\mathbf{I}_1$, $\mathbf{I}_2$ for a state $|Q\rangle$ are $\langle Q|\mathbf{k}1\rangle\langle 1\mathbf{k}|Q\rangle$ and $\langle Q|2\rangle\langle 2|Q\rangle$, respectively. The operators $\mathbf{I}_1$, $\mathbf{I}_2$ are therefore, the ones associated with the first and second stage of the Fock state, as their expectation values give the probability[5] of finding the state in the form of two particles, or in the form of a single compound particle respectively.

With the help of $\mathbf{I}_1$ it now becomes clear what would be the representation of any dynamical variable associated with the relative motion of the two particles in the first stage. We just multiply the ordinary representation of the dynamical variable by $\mathbf{I}_1$ and have its representation in Fock space. Thus for example, for the ith component of the relative angular momentum $\mathbf{L}_i$, we have in the momentum representation a matrix of the form:

$$\begin{aligned}\mathbf{L}_i=&-i\epsilon_{ijl}k_j'\partial/\partial k_l'\mathbf{I}_1\\ \equiv&\begin{bmatrix}-i\epsilon_{ijl}k_j'\partial/\partial k_l'\delta(\mathbf{k}'-\mathbf{k}'') & 0\\ 0 & 0\end{bmatrix},\end{aligned} \tag{18}$$

in which ϵ_{ijl} is the usual antisymmetric symbol which is $\neq 0$ only if ijl are even or odd permutations of 1, 2, 3, when it equals $+1$ or -1 respectively.

The linear operators for the components of the relative position $\mathbf{X}_i$ and momentum $\mathbf{P}_j$ are given in the momentum representation by the matrices:

$$\mathbf{X}_i=i\partial/\partial k_i'\mathbf{I}_1,\quad \mathbf{P}_j=k_j'\mathbf{I}_1. \tag{19}$$

The components $\mathbf{L}_i$ of the vector of relative angular momentum, are constants of motion of the dynamical system (1), as we shall show that they commute with the hamiltonian.

Designating by $\langle P'|$, $|Q'\rangle$ two arbitrary states, and defining $\langle P'|$, $|Q'\rangle$ by:

$$\langle P'|=\langle P|\mathbf{L}_i,\ |Q'\rangle=\mathbf{L}_i|Q\rangle \tag{20}$$

we see from (16) that:

$$\begin{aligned}\langle P|HL_i-L_iH|Q\rangle=&\langle P|H|Q'\rangle-\langle P'|H|Q\rangle\\ =&-2\pi C'[\langle P|2\rangle(\partial r\langle 1\mathbf{r}|Q'\rangle/\partial r)_{r=0}\\ &-(\partial r\langle P'|\mathbf{r}1\rangle/\partial r)_{r=0}\langle 2|Q\rangle],\end{aligned} \tag{21}$$

where use was made of the hermiticity of $\mathbf{L}_i$ and of the fact that from (18) and (20) we have $\langle 2|Q'\rangle=\langle P'|2\rangle=0$. The term $\langle 1\mathbf{r}|Q'\rangle$ could be expanded in spherical waves in which the S-wave would be missing from the definition (20). As we showed in (I) that there is interaction between the initial particles only in the S-wave, we conclude that $\langle 1\mathbf{r}|Q'\rangle$ is regular at $r=0$ and therefore:

$$(\partial r\langle 1\mathbf{r}|Q'\rangle/\partial r)_{r=0}=0.$$

A similar analysis holds for $\langle P'|\mathbf{r}1\rangle$ so that we obtain:

$$\langle P|HL_i-L_iH|Q\rangle=0, \tag{22}$$

and as $\langle P|$, $|Q\rangle$ are arbitary, we see that $\mathbf{L}_i$ commutes with $\mathbf{H}$.

The total angular momentum

$$\mathbf{L}^2=\sum_{i=1}^{3}\mathbf{L}_i^2$$

is clearly also a constant of motion, and $\mathbf{H}$, $\mathbf{L}^2$, $\mathbf{L}_3$ will form a set of commuting constants of motion.

V. EIGENSTATES AND EXPANSION THEOREMS

We proceed to obtain the simultaneous eigenstates of commuting set of constants of motion:

$$\mathbf{H},\ \mathbf{L}^2,\ \mathbf{L}_3. \tag{23}$$

We shall show that this set of constants of motion is a complete set of commuting observables,[4] and that therefore, an arbitrary Fock state can be expanded in terms of the simultaneous eigenstates of this set.

We first notice that if in (16), $\langle P|$ is put equal to the basic bra $\langle 1\mathbf{r}|$ defined by:

$$\langle 1\mathbf{r}| = [\delta(\mathbf{r}-\mathbf{r}')\ \ 0]$$

we obtain

$$\langle 1\mathbf{r}|H|Q\rangle = -\tfrac{1}{2}\nabla^2\langle 1\mathbf{r}|Q\rangle - 2\pi C'[\partial r'\delta(\mathbf{r}-\mathbf{r}')/\partial r']_{r'=0}\langle 2|Q\rangle. \tag{24}$$

The term inside the square bracket can be written as:

$$\delta(\mathbf{r}-\mathbf{r}') - \mathbf{r}'\cdot\nabla\delta(\mathbf{r}-\mathbf{r}'),$$

which when $\mathbf{r}'\to 0$ clearly reduces to $\delta(\mathbf{r})$. In Eq. (24) we can thus replace the square bracket by $\delta(\mathbf{r})$.

We now designate by $|Elm\rangle$ the ket which is an eigenstate of $\mathbf{H}$, $\mathbf{L}^2$, $\mathbf{L}_3$ corresponding to the eigenvalues E, $l(l+1)$ and m, respectively.[9] From (16, 18) the eigenket $|Elm\rangle$ in the configuration representation satisfies the equations:

$$-\tfrac{1}{2}\nabla^2\langle 1\mathbf{r}|Elm\rangle - 2\pi C'\delta(\mathbf{r})\langle 2|Elm\rangle = E\langle 1\mathbf{r}|Elm\rangle, \tag{25a}$$

$$-2\pi C'(\partial r\langle 1\mathbf{r}|Elm\rangle/\partial r)_{r=0} + \tfrac{1}{2}k_0^2\langle 2|Elm\rangle = E\langle 2|Elm\rangle, \tag{25b}$$

$$L^2\langle 1\mathbf{r}|Elm\rangle = l(l+1)\langle 1\mathbf{r}|Elm\rangle, \tag{26a}$$

$$L_3\langle 1\mathbf{r}|Elm\rangle = m\langle 1\mathbf{r}|Elm\rangle. \tag{26b}$$

In (26) L^2, L_3 stand for the usual differential operators for the total angular momentum and its projection.

From Eqs. (25a), (26) we see that for $\mathbf{r}\neq 0$, $\langle 1\mathbf{r}|Elm\rangle$ must have the form:

$$\langle 1\mathbf{r}|Elm\rangle = [a_{lm}j_l(kr) + b_{lm}n_l(kr)]P_l^m(\cos\theta)e^{im\varphi}, \tag{27}$$

where a_{lm}, b_{lm} are numerical factors that depend on $k=(2E)^{\frac{1}{2}}$, and as $\mathbf{r}=0$ is excluded, the irregular spherical Bessel function[10] $n_l(kr)$ also appears in (27).

If $b_{lm}\neq 0$ we have that $\langle 1\mathbf{r}|Elm\rangle$ has a singularity[10] of the order $r^{-(l+1)}$ when $r\to 0$. The singularity in $\langle 1\mathbf{r}|Elm\rangle$ for $l\neq 0$ would be too high to satisfy (25), as we know that[11]

$$\nabla^2 r^{-1} = -4\pi\delta(\mathbf{r}). \tag{28}$$

It is clear, therefore, that for $l\neq 0$ the only possible solution of the system of Eqs. (25), (26) is:

$$\langle 1\mathbf{r}|Elm\rangle = a_{lm}j_l(kr)P_l^m(\cos\theta)e^{im\varphi},\ \langle 2|Elm\rangle = 0. \tag{29}$$

We see that the two particles in the first stage of our dynamical system do not interact if their relative angular momentum is larger than zero.

The first component of the eigenket $|E00\rangle$ is given by (27) when $l, m=0$, and it has a singularity of the order r^{-1} when $r\to 0$. Substituting this value of $\langle 1\mathbf{r}|E00\rangle$ into Eq. (25a) and making use of (28) we obtain:

$$2\pi[r\langle 1\mathbf{r}|E00\rangle - C'\langle 2|E00\rangle]\delta(\mathbf{r}) = 0. \tag{30}$$

This equation implies that the square bracket must vanish for $\mathbf{r}=0$, so that we obtain the boundary condition:

$$(r\langle 1\mathbf{r}|E00\rangle)_{r=0} = C'\langle 2|E00\rangle. \tag{31}$$

From (31) and Eq. (25b) corresponding to the ket $|E00\rangle$, we obtain:

$$(r\langle 1\mathbf{r}|E00\rangle)_{r=0} = 4\pi C'^2(k_0^2-k^2)^{-1}(\partial r\langle 1\mathbf{r}|E00\rangle/\partial r)_{r=0} \tag{32}$$

which is precisely the boundary condition for stationary states given in (6I).

Equations (31), (32) determine the eigenket $|E00\rangle$ up to a factor, and its components are given by:

$$\langle 1\mathbf{r}|E00\rangle = a_{00}(k)[j_0(kr) - 4\pi C'^2k(k_0^2-k^2)^{-1}n_0(kr)], \tag{33a}$$

$$\langle 2|E00\rangle = a_{00}(k)4\pi C'(k_0^2-k^2)^{-1}. \tag{33b}$$

The set of commuting constants of motion of our dynamical system is a complete set,[4] as the eigenkets common to them are determined up to a factor. This factor should be determined by the normalization condition, so as to make the scalar product of two eigenstates $|E'l'm'\rangle$, $|E''l''m''\rangle$ equal to:

$$\langle E'l'm'|E''l''m''\rangle = \delta(E'-E'')\delta_{l'l''}\delta_{m'm''}. \tag{34}$$

We see from (29) and (33) that eigenkets corresponding to different l or m are orthogonal. The eigenkets corresponding to the same l, m in which $l>0$, form an orthonormal set, if the a_{lm} are taken essentially as the normalization coefficients for spherical harmonics. It remains to show that for a convenient value of $a_{00}(k)$ the eigenkets $|E00\rangle$ form an orthonormal set.

In the configuration representation, the scalar product of the two eigenkets $|E'00\rangle$, $|E''00\rangle$ is given by

$$\langle E'00|E''00\rangle = 4\pi\int_0^\infty \langle 1\mathbf{r}|E'00\rangle^*\langle 1\mathbf{r}|E''00\rangle r^2dr + \langle 2|E'00\rangle^*\langle 2|E''00\rangle. \tag{35}$$

Introducing the explicit form (33) of the component of

[9] We restrict ourselves to a dynamical system (1) for which the binding energy (see reference 1) $E_0>0$. In this case, we showed in (I) that the eigenvalues E are restricted to real positive values.

[10] J. A. Stratton, *Electromagnetic Theory* (McGraw-Hill Book Company, Inc., New York, 1941), pp. 404–405.

[11] See reference 4, p. 156.

these kets, and making use of the relation:[12]

$$(2\pi)^{-1}\int_0^\infty \exp(ikr)dr=\delta_+(k)=\tfrac{1}{2}[\delta(k)+i(\pi k)^{-1}]$$

we obtain straightforwardly that:

$$\langle E'00|E''00\rangle=a_{00}^*(k')a_{00}(k'')2\pi^2k'^{-1}(k_0^2-k'^2)^{-2}\times[(k_0^2-k'^2)^2+C^4k'^2]\delta(E'-E''). \quad (36)$$

The ket $|E00\rangle$ would be normalized if we give to the corresponding factor[13] $a_{00}(k)$ the value:

$$a_{00}(k)=(2\pi^2)^{-1}k^{\frac{1}{2}}(k_0^2-k^2)(k_0^2-k^2-ikC^2)^{-1}. \quad (37)$$

With the coefficients determined as above, the eigenkets $|Elm\rangle$ form a complete orthonormalized set,[4] so that an arbitrary ket $|Q\rangle$ can be expanded in terms of them in the usual way:

$$|Q\rangle=\int_0^\infty\sum_{l=0}^\infty\sum_{m=-l}^{l}|Elm\rangle\langle Elm|Q\rangle dE. \quad (38)$$

If the ket $|Q\rangle$ corresponds to zero angular momentum, i.e., $\mathbf{L}^2|Q\rangle=0$, then $\langle Elm|Q\rangle=0$ if $l\neq0$, and in the configuration representation the expansion theorem becomes

$$\begin{bmatrix}\langle 1\mathbf{r}|Q\rangle\\ \langle 2|Q\rangle\end{bmatrix}=\int_0^\infty\begin{bmatrix}\langle 1\mathbf{r}|E00\rangle\\ \langle 2|E00\rangle\end{bmatrix}\langle E00|Q\rangle dE, \quad (39a)$$

$$\langle E00|Q\rangle=4\pi\int_0^\infty\langle 1\mathbf{r}|E00\rangle^*\langle 1\mathbf{r}|Q\rangle r^2dr+\langle 2|E00\rangle^*\langle 2|Q\rangle. \quad (39b)$$

If we introduce the values of $\langle 1\mathbf{r}|E00\rangle$, $\langle 2|E00\rangle$ given by (33), (37), and put $E=\frac{1}{2}k^2$, we see that (39) becomes identical with the generalized Hankel transforms (19I). We have therefore justified, from a general quantum-mechanical standpoint, the mathematical developments introduced in (I), which were used for the time dependent description of the scattering and disintegration processes.

With the help of the eigenstates $|Elm\rangle$, given by (29), (33), any observable $\mathbf{F}$ could be expressed in the hamiltonian-angular momentum representation, i.e., we could find the matrix elements:

$$\langle E'l'm'|F|E''l''m''\rangle. \quad (40)$$

The operators $\mathbf{H}$, $\mathbf{L}^2$, $\mathbf{L}_3$ are, of course, diagonal in this representation, and it is interesting to obtain the representation of the relative kinetic energy operator

$$\tfrac{1}{2}\mathbf{P}^2=\tfrac{1}{2}\sum_{i=1}^3\mathbf{P}_i^2.$$

From (19) we see that

$$\langle E'l'm'|\tfrac{1}{2}P^2|E''l''m''\rangle=\int\tfrac{1}{2}k^2\langle E'l'm'|\mathbf{k}1\rangle\langle 1\mathbf{k}|E''l''m''\rangle d\mathbf{k}. \quad (41)$$

Making use of (16) in which we put $\langle P|=\langle E'l'm'|$, $|Q\rangle=|E''l''m''\rangle$, and of the diagonal form of $\mathbf{H}$, we obtain straightforwardly that

$$\langle E'l'm'|\tfrac{1}{2}P^2|E''l''m''\rangle=E'\delta(E'-E'')\delta_{l'l''}\delta_{m'm''}, \quad (42a)$$

if $l'\neq0$, or $l''\neq0$, or both l', $l''\neq0$; and that

$$\langle E'00|\tfrac{1}{2}P^2|E''00\rangle=E'\delta(E'-E'')+\frac{4C'^2(k_0^2-k'^2-k''^2)(k''k')^{\frac{1}{2}}}{(k_0^2-k''^2-ik''C^2)(k_0^2-k'^2+ik'C^2)}, \quad (42b)$$

where $E'=\frac{1}{2}k'^2$, $E''=\frac{1}{2}k''^2$.

In the hamiltonian-angular momentum representation, the relative kinetic energy of the two particles in the first stage, is a nondiagonal matrix. From (42) we see that the nondiagonal terms become particularly prominent in the neighborhood of the resonance energy $E_0=\frac{1}{2}k_0^2$.

VI. THE UNITARY MATRIX U(t)

We want now to obtain a linear time dependent operator in Fock space $\mathbf{U}(t)$, that transforms any initial Fock state into the corresponding state at time t. For any ket $|Q\rangle$ we have then:

$$|Qt\rangle=\mathbf{U}(t)|Q\rangle. \quad (43)$$

Introducing this relation into (16), we obtain immediately that:

$$i\langle d\langle P|U|Q\rangle/dt\rangle=\langle P|HU|Q\rangle \quad (44)$$

for any two arbitrary Fock states $\langle P|$, $|Q\rangle$, so that $\mathbf{U}(t)$ satisfies (2).

The simplest way of obtaining $\mathbf{U}(t)$, is to solve (44) in the hamiltonian-angular momentum representation, in which $\mathbf{H}$ is diagonal, so that $\mathbf{U}(t)$ in this representation, which at $t=0$ reduces to the unit matrix, becomes

$$\langle E'l'm'|U|E''l''m''\rangle=\exp(-iE't)\delta(E'-E'')\delta_{l'l''}\delta_{m'm''}. \quad (45)$$

The matrix $\mathbf{U}(t)$ is unitary in this representation, a property which is clearly maintained in any other representation as well.[5]

Using (45), any time dependent state could be expressed in the form,

$$|Qt\rangle=\mathbf{U}(t)|Q\rangle=\int_0^\infty\sum_{l=0}^\infty\sum_{m=-l}^{l}|Elm\rangle\exp(-iEt)\langle Elm|Q\rangle dE. \quad (46)$$

[12] W. Heisenberg, Z. Physik **120**, 519 (1943).

[13] The normalization condition (36) determines $a_{00}(k)$ only up to an arbitrary phase factor, but this phase factor does not affect the form of the expansion theorem (38).

If we express the $|Q t\rangle$ and the scalar product $\langle E l m|Q\rangle$ in the configuration representation, we obtain precisely the procedure followed in Secs. II, III of (I) for the determination of any time dependent state. When we equate $|Q\rangle$ to the basic kets $|\mathbf{k}''1\rangle, |2\rangle$ of (12), we obtain, respectively, the time dependent states for scattering and disintegration $\Psi_1(\mathbf{k}'', t)$, $\Psi_2(t)$, given by (23, 27I). In the configuration representation we have, therefore,

$$\begin{aligned}&\langle 1\mathbf{r}|U|\mathbf{k}''1\rangle=\psi_{11}(\mathbf{r},\mathbf{k}'',t), \quad \langle 1\mathbf{r}|U|2\rangle=\psi_{12}(\mathbf{r},t),\\ &\langle 2|U|\mathbf{k}''1\rangle=\psi_{21}(\mathbf{k}'',t), \quad \langle 2|U|2\rangle=\psi_{22}(t).\end{aligned} \tag{47}$$

If we want to express $\mathbf{U}(t)$ in a pure momentum representation, i.e., to have it in the form of the operator (11), we apply the transformation matrix $\mathbf{T}$ to (47) and obtain

$$\begin{aligned}\langle 1\mathbf{k}'|U|\mathbf{k}''1\rangle&=\langle\mathbf{k}'|\mathbf{r}\rangle\langle 1\mathbf{r}|U|\mathbf{k}''1\rangle,\\ \langle 1\mathbf{k}'|U|2\rangle&=\langle\mathbf{k}'|\mathbf{r}\rangle\langle 1\mathbf{r}|U|2\rangle,\end{aligned} \tag{48}$$

while $\langle 2|U|\mathbf{k}''1\rangle$, $\langle 2|U|2\rangle$ remain unaffected.

In the appendix we evaluate the Fourier transform of the function $r^{-1}\chi(r,k,t)$ which appears in ψ_{11}, ψ_{12}. Using this result, we can evaluate the Fourier transforms (48), and obtain the following explicit form of $\mathbf{U}(t)$ in the momentum representation

$$\langle 1\mathbf{k}'|U|\mathbf{k}''1\rangle=\delta(\mathbf{k}'-\mathbf{k}'')\exp(-i\tfrac{1}{2}k''^2t)$$
$$+(C^2/2\pi^2)\sum_{i=1}^{6}\left\{k_i\left[\prod_{j=1}^{6}{}'(k_i-k_j)\right]^{-1}\chi_0(k_i,t)\right\}, \tag{49a}$$

$$\langle 1\mathbf{k}''|U|2\rangle=-C'(2/\pi)^{\frac{1}{2}}$$
$$\times\sum_{i=1}^{4}\left\{k_i\left[\prod_{j=1}^{4}{}'(k_i-k_j)\right]^{-1}\chi_0(k_i,t)\right\}$$
$$=\psi_{21}(\mathbf{k}'',t)=\langle 2|U|\mathbf{k}''1\rangle, \tag{49b}$$

$$\langle 2|U|2\rangle=\psi_{22}(t)$$
$$=(k_1-k_2)^{-1}[k_1\chi_0(k_1,t)-k_2\chi_0(k_2,t)]. \tag{49c}$$

In (49), k_1, k_2 stand for the poles of the scattering matrix $S(k)$ of (15I), while $k_3=k''$, $k_4=-k''$, and $k_5=k'$, $k_6=-k'$. The terms

$$\prod_{j=1}^{6}{}'(k_i-k_j), \quad \prod_{j=1}^{4}{}'(k_i-k_j)$$

mean products in which the factor $j=i$ has been omitted. The function $\chi_0(k,t)=\chi(0,k,t)$, so that for any complex k it is given by:

$$\chi_0(k,t)=\exp(-i\tfrac{1}{2}k^2t)\operatorname{erfc}[-(1-i)k(t/4)^{\frac{1}{2}}], \tag{50}$$

where $\operatorname{erfc}(z)$ is the error integral function of (25I).

The component $\langle 1\mathbf{k}'|U|\mathbf{k}''1\rangle$ is symmetric with respect to $\mathbf{k}'$, $\mathbf{k}''$ as can be seen from (49a) by writing out explicitly the coefficients of the χ_0's. Furthermore, from (49b) we see that $\langle 1\mathbf{k}''|U|2\rangle=\langle 2|U|\mathbf{k}''1\rangle$, so that we conclude that the unitary matrix $\mathbf{U}(t)$ is symmetric[14] in the momentum representation, i.e., $\mathbf{U}'(t)=\mathbf{U}(t)$.

With the help of $\mathbf{U}(t)$ the Schrödinger dynamical variables given in the momentum representation in Sec. IV, could be transformed into the corresponding Heisenberg dynamical variables, in terms of the usual[5] relation:

$$\mathbf{F}(t)=\mathbf{U}^{*\prime}(t)\mathbf{F}\mathbf{U}(t), \tag{51}$$

where $\mathbf{U}^{*\prime}(t)$ stands for the conjugate transposed[14] of $\mathbf{U}(t)$, and the matrix product should be interpreted in the sense of (11). In principle, the time dependence of all Heisenberg dynamical variables associated with the dynamical system (1) can be determined.

An interesting application of (51) is that the commutator of the relative momentum and position of the two initial particles is not a constant of motion. In fact, from (19, 51) we have:

$$\mathbf{X}_i(t)\mathbf{P}_j(t)-\mathbf{P}_j(t)\mathbf{X}_i(t)=i\delta_{ij}\mathbf{I}_1(t)=i\delta_{ij}[\mathbf{I}-\mathbf{I}_2(t)], \tag{52}$$

where in the momentum representation $\mathbf{I}_2(t)$ is given by:

$$\mathbf{I}_2(t)=\begin{bmatrix}\langle 1\mathbf{k}'|U|2\rangle^*\langle 2|U|\mathbf{k}''1\rangle & \langle 1\mathbf{k}'|U|2\rangle^*\langle 2|U|2\rangle\\ \langle 2|U|2\rangle^*\langle 2|U|\mathbf{k}''1\rangle & \langle 2|U|2\rangle^*\langle 2|U|2\rangle\end{bmatrix}. \tag{53}$$

VII. CONCLUSION

We have assumed in all the preceding developments that the dynamical system (1) was described in the center-of-mass frame of reference. It is clear that in arbitrary frame of reference, our states $|Q\rangle$ would be characterized also by the total momentum $\boldsymbol{\kappa}$ of the system. The unitary matrix $\mathbf{U}(t)$ of the previous section, would just have to be multiplied by the factor:[15]

$$\delta(\boldsymbol{\kappa}'-\boldsymbol{\kappa}'')\exp(-i\kappa''^2t/2m) \tag{54}$$

to apply to states in an arbitrary frame of reference.

The developments of the present paper were restricted to the dynamical system (1) representing a single-level S-wave scattering process. We have obtained in (I') boundary conditions for the description of the many-level elastic scattering process, as well as for two-particle nuclear reactions, which could be indicated schematically as:

$$A+a\rightleftarrows\begin{Bmatrix}C_1\\ \vdots\\ C_n\end{Bmatrix}, \tag{55a}$$

and

$$A+a\rightleftarrows C\rightleftarrows B+b, \tag{55b}$$

respectively. The procedure followed in the present paper suggests how to formulate the states of the dynamical systems (55) in Fock space, and also how to obtain the corresponding hamiltonians from the bound-

[14] In the present notation, $\mathbf{F}'$ means that we take the transposed of the 2×2 matrix (11), and also interchange $\mathbf{k}'$, $\mathbf{k}''$.

[15] m stands for the sum of the masses of the two particles in the first stage, in units of the reduced mass.

ary conditions. We expect, therefore, no essential difficulty in the generalization of the present developments to the dynamical systems (55).

This work was made possible by the generous support of the Instituto Nacional de la Investigación Científica.

APPENDIX

We shall evaluate here the Fourier transform of the function:

$$r^{-1}\chi(r,k,t)=r^{-1}\exp i(kr-\tfrac{1}{2}k^2t)\,\mathrm{erfc}(u), \qquad (56)$$

where

$$\mathrm{erfc}(u)=2\pi^{-\frac{1}{2}}\int_u^\infty \exp(-z^2)dz, \quad u=(1-i)(4t)^{-\frac{1}{2}}(r-kt),$$

and k is an arbitrary complex number.

As χ depends only on the magnitude of the position vector, we have:

$$I(k,k',t)=(2\pi)^{-\frac{1}{2}}\int \exp(-i\mathbf{k}'\cdot\mathbf{r})r^{-1}\chi(r,k,t)d\mathbf{r}$$

$$=(2/\pi)^{\frac{1}{2}}k'^{-1}\int_0^\infty \chi(r,k,t)\sin k'r\,dr$$

$$=(2/\pi)^{\frac{1}{2}}(2ik')^{-1}\exp(-i\tfrac{1}{2}k^2t)$$

$$\times[I_+(k,k',t)-I_-(k,k',t)], \qquad (57)$$

where

$$I_\pm(k,k',t)=\int_0^\infty \exp[i(k\pm k')r]\,\mathrm{erfc}(u)dr.$$

Integrating by parts we obtain:

$$I_\pm(k,k',t)=[-i(k\pm k')^{-1}\exp[i(k\pm k')r]\,\mathrm{erfc}(u)]_0^\infty$$

$$-i(k\pm k')^{-1}\int_0^\infty \exp[i(k\pm k')r]$$

$$\times\exp(-u^2)[2\pi^{-\frac{1}{2}}(1-i)(4t)^{-\frac{1}{2}}]dr. \qquad (58)$$

When $r\to\infty$, $\mathrm{erfc}(u)\to 0$ as shown in Appendix 2 of (I), so that the first parenthesis reduces to its value at $r=0$. Denoting by $u_\pm'$ the expression:

$$u_\pm'=(1-i)(r\pm k't)(4t)^{-\frac{1}{2}} \qquad (59)$$

we can reduce $I_\pm(k,k',t)$ to the form:

$$I_\pm(k,k',t)=i(k\pm k')^{-1}\,\mathrm{erfc}[-(1-i)k(t/4)^{\frac{1}{2}}]$$

$$-i(k\pm k')^{-1}\exp[i(k^2-k'^2)(t/2)]$$

$$\times\left\{2\pi^{-\frac{1}{2}}\int_0^\infty \exp(-u_\pm'^2)(1-i)(4t)^{-\frac{1}{2}}dr\right\}. \qquad (60)$$

The term in the curly bracket can be written as:

$$2\pi^{-\frac{1}{2}}\int_{V_\pm}^\infty \exp(-u'^2)du'=\mathrm{erfc}(V_\pm), \qquad (61)$$

where $V_\pm=\pm(1-i)k'(t/4)^{\frac{1}{2}}$.

Using (57, 60, 61), we can write finally:

$$I(k,k',t)=-(2/\pi)^{\frac{1}{2}}(k^2-k'^2)^{-1}\chi_0(k,t)$$

$$+(2/\pi)^{\frac{1}{2}}(2k')^{-1}(k-k')^{-1}\chi_0(k',t)$$

$$-(2/\pi)^{\frac{1}{2}}(2k')^{-1}(k+k')^{-1}\chi_0(-k',t), \qquad (62)$$

where $\chi_0(k,t)$ is given by (50).

Gauge-Independent Quantum Electrodynamics*

FREDERIK J. BELINFANTE AND JOHN S. LOMONT†
Department of Physics, Purdue University, Lafayette, Indiana
(Received May 21, 1951)

We discuss a *covariant*, but not manifestly covariant, form of quantum electrodynamics. No gauge-dependent potentials are introduced as independent (canonical) variables. Only the transverse electromagnetic field is quantized as a photon field. We formulate the theory first in interaction representation, although only flat space-like surfaces σ are considered. The interaction operator given by Eq. (10) is then used for describing Lorentz transformations (rotations of σ) as well as time dependence (parallel progress of σ). The integrability of the generalized Schrödinger equation is then proved. As we transform to Heisenberg representation the electron wave function ψ loses its spinor character and the transverse photon field $\mathfrak{E}$, $\mathfrak{B}$ its tensor character, but by adding the coulomb field $\mathbf{E}_{\parallel}$ to $\mathfrak{E}$ we restore the tensor character of the electromagnetic field. The gauge-independent quantum electrodynamics of Pauli's *Handbuch* article is a special form of the result thus obtained for the particular case that the number of electrons is known and finite. Our theory has a more general form allowing use of positon (hole) theory.

INTRODUCTION

QUANTUM electrodynamics in its conventional form is gauge-invariant, that is, physical results calculated by it are invariant under a change of the gauge of the longitudinal and scalar potentials used as some of the canonical variables in that theory. It is, however, slightly unsatisfactory that these physically meaningless gauge-dependent variables enter the theory at all. The interesting fact that gauge-invariance is in some way linked up with the fact of conservation of charge is not very essential[1] and certainly does not outweigh the bothersome facts that (1) quantization of these gauge-dependent variables necessitates discussion of such unphysical features as longitudinal and even "scalar" photons, the latter of negative energy;[2] (2) consequently, the redundant degrees of freedom of the electromagnetic field thus introduced have to be undone again by "auxiliary conditions," which render the state vector unnormalizable and are a source of much nuisance and ambiguity if not mathematical inconsistency in various problems.[3]

In his article in the *Handbuch der Physik*, Pauli[3] has developed long ago a different type of quantum electrodynamics, in which the gauge-dependent variables did not occur, so that auxiliary conditions could be avoided. This theory was relativistically covariant in its essence although not in its external form. It was given in Heisenberg representation, which made the proof of its invariance somewhat cumbersome. The fact that Pauli did not use the method of second quantization, and thus made his theory formally not applicable to positon theory, is of little importance, as his theory is easily generalized in this regard.[4] The theory developed below might have been derived from Pauli's theory in this generalized form by transforming it to interaction representation by methods similar to the ones used for nonscalar interactions.[5,6] For the validity of such derivation, use would have to be made of the Lorentz-invariance of the generalized Pauli theory. It seemed, however, more appropriate, in particular with a view to certain future applications, to prove the invariance of our theory directly in interaction representation, and then reversely derive the invariance of Pauli's theory from that of our theory.

1. THE FIELD VARIABLES IN INTERACTION REPRESENTATION

The variables describing the electron field in interaction representation are the undors (Dirac spinors) ${}^{\circ}\psi$ and ${}^{\circ}\psi^{\dagger}$ satisfying the free electron Dirac equation and the usual covariant four-dimensional anticommutation relations.

The photon field is described by a tensor field ${}^{\circ}\mathfrak{F}_{\mu\nu}({}^{\circ}\mathfrak{E}, {}^{\circ}\mathfrak{B})$ satisfying in interaction representation the vacuum maxwell equations (charges omitted), so that by $\operatorname{div}{}^{\circ}\mathfrak{E}=\operatorname{div}{}^{\circ}\mathfrak{B}=0$ the field is purely transverse. The four-dimensional commutation relations for ${}^{\circ}\mathfrak{F}_{\mu\nu}$ are the usual ones:[7]

$$[{}^{\circ}\mathfrak{F}_{\lambda\mu}(x); {}^{\circ}\mathfrak{F}_{\rho\sigma}(x')]=4\pi i\hbar c\{g_{\mu\sigma}\partial_{\lambda}\partial_{\rho}+g_{\lambda\rho}\partial_{\mu}\partial_{\sigma} -g_{\mu\rho}\partial_{\lambda}\partial_{\sigma}-g_{\lambda\sigma}\partial_{\mu}\partial_{\rho}\}D(x-x'), \quad (1)$$

with $D(x)$ given by Eqs. (12)–(15) of reference 5. For

* Based, in part, on chapter II-B of a thesis presented by one of us (J.S.L.) in partial fulfillment of the requirements for a degree of Doctor of Philosophy at Purdue University, June, 1951.

† Now at North American Aviation, Inc., A.E.R. Div., 12214 Lakewood Blvd., Downey, California.

[1] See the remark below Eq. (23) of F. J. Belinfante, Physica **7**, 449 (1940).

[2] F. J. Belinfante, Phys. Rev. **76**, 226 (1949).

[3] W. Pauli, Kapitel 2, B.8, p. 269 of Geiger and Scheel's *Handbuch der Physik* (Springer, Berlin, 1933), second edition, Vol. **24/1**.

[4] F. J. Belinfante, Phys. Rev. **75**, 1633(A) (1949).

[5] F. J. Belinfante, Phys. Rev. **76**, 66 (1949).

[6] F. J. Belinfante and J. S. Lomont, Phys. Rev. **77**, 757(A) (1950).

[7] *Notation:* $\mathbf{x}$ is the spatial part (with components x_k) of x (with components x^{μ}); italic indices run from 1 to 3 and Greek indices run from 0 to 3; $x^0=-x_0=ct$; $\mathbf{r}'=\mathbf{x}'-\mathbf{x}=-\mathbf{r}$, $r=|\mathbf{r}|$; $\partial_{\mu}=\partial/\partial x^{\mu}$; $\nabla_k=\partial/\partial x_k$, $\nabla_k'=\partial/\partial x_k'$; $\Delta=\nabla\cdot\nabla$. Often we write F for $F(\mathbf{x})$ and F' for $F(\mathbf{x}')$, $f'=\int d^3\mathbf{x}$ and $f'=\int d^3\mathbf{x}'$. $[A;B]=AB-BA$. δ_{kn} = Kronecker symbol. Superscript ° denotes interaction representation, $^{\text{II}}$ denotes Heisenberg representation. $a=(ihc)^{-1}$.

$t=t'$ this yields the usual commutation relations for $\mathfrak{E}$ and $\mathfrak{B}$:

$$[\mathfrak{E}_k(\mathbf{x});\ \mathfrak{E}_l(\mathbf{x}')]=[\mathfrak{B}_{kl}(\mathbf{x});\ \mathfrak{B}_{mn}(\mathbf{x}')]=0,$$
$$[\mathfrak{B}_{kl}(\mathbf{x});\ \mathfrak{E}_m(\mathbf{x}')]=4\pi i\hbar c\{\delta_{km}\nabla_l-\delta_{lm}\nabla_k\}\delta^{(3)}(\mathbf{r}'). \quad (2)$$

We shall introduce the following functional of $\mathfrak{B}$:

$$\mathfrak{A}(\mathbf{x},t)\equiv\int d^3\mathbf{x}'\ \mathrm{curl}'\mathfrak{B}(\mathbf{x}',t)/4\pi r, \quad (3)$$

so that

$$\mathrm{div}\mathfrak{A}=0,\quad \mathrm{curl}\mathfrak{A}=\mathfrak{B}. \quad (4)$$

Then

$$[\mathfrak{A}_l(\mathbf{x},t);\ \mathfrak{E}_m(\mathbf{x}',t)]=i\hbar c\{\delta_{lm}\Delta'-\nabla_l'\nabla_m'\}(1/r)$$
$$=-4\pi i\hbar c\{\delta_{lm}\delta^{(3)}(\mathbf{r}')-\delta_{lm}{}^{\mathrm{long}}(\mathbf{r}')\}$$
$$=-4\pi i\hbar c\delta_{lm}{}^{\mathrm{tr}}(\mathbf{r}'). \quad (5)$$

Here, $\delta_{lm}{}^{\mathrm{long}}(\mathbf{x})$ and $\delta_{lm}{}^{\mathrm{tr}}(\mathbf{x})$ are the longitudinal and transverse delta-functions defined earlier by one of the authors.[8] In fact, the commutation relation (5) is identical with the commutation relation between the transverse parts of the fields $\mathbf{E}$ and $\mathbf{A}$ in conventional quantum electrodynamics. In the present theory, we

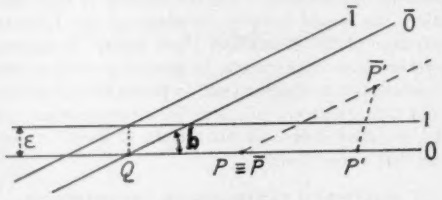

FIG. 1. Possible displacements $\epsilon(\xi,\eta,\zeta)$ of the flat surface 0. The displacement $0\to\bar{0}$ represents a rotation; $0\to1$ represents a parallel displacement.

are not going to define any longitudinal counterpart to $\mathfrak{A}$. In fact, our solenoidal $\mathfrak{A}$ is a most natural description of the potential field in interaction representation.[9]

We shall also introduce a longitudinal field

$$\mathbf{E}_{\mathrm{II}}(\mathbf{x},t)\equiv-\nabla V(\mathbf{x},t), \quad (6)$$

$$V(\mathbf{x},t)\equiv\int d^3\mathbf{x}'\rho(\mathbf{x}',t)/r. \quad (7)$$

Here, for electrons,

$$\rho\equiv e{:}\psi^\dagger\psi{:},\quad \mathbf{j}\equiv e{:}\psi^\dagger\alpha\psi{:}, \quad (8)$$

where : : is Wick's notation for subtraction of the vacuum charge density.[10] In (6), we used a letter $\mathbf{E}$ instead of $\mathfrak{E}$, because V and $\mathbf{E}_{\mathrm{II}}$ are derived from the field of charged matter, and not from the electromagnetic field.

2. THE GENERALIZED SCHRÖDINGER EQUATION

Let $\Psi_0[\sigma]$ be the state vector on a space-like surface σ; let $d\sigma_0=d\xi d\eta d\zeta$ be the projection of a surface element on the plane $\tau=$ constant of some Lorentz frame $\xi\eta\zeta\tau$. Let $\sigma+\delta\sigma$ denote a new surface obtained from σ by infinitesimal displacement $\delta(c\tau)=\epsilon(\xi,\eta,\zeta)$ of its points. Then, with $a=(i\hbar c)^{-1}$, the generalized Schrödinger equation is

$$\Psi_0[\sigma+\delta\sigma]-\Psi_0[\sigma]$$
$$=a\int d\sigma_0\,\epsilon(\xi,\eta,\zeta)\,{}^\circ W(\xi,\eta,\zeta;\sigma)\,\Psi_0[\sigma]. \quad (9)$$

Here, ${}^\circ W$ is a function of the point ξ,η,ζ as well as a functional of the field variables in all points of the surface σ. We shall define the value of this functional of σ for flat surfaces σ only. Therefore we restrict the displacement $\epsilon(\xi,\eta,\zeta)$ in (9) to either a rotation like $0\to\bar{0}$ in Fig. 1, or a parallel displacement like $0\to1$.

It is then convenient to express ${}^\circ W(\xi,\sigma)$ in terms of the field components calculated in a Lorentz frame $(xyzt)$, in which σ is a plane $t=$ constant. In such special frame of reference we put[11]

$$W=(\mathbf{E}_{\mathrm{II}}{}^2/8\pi)+(\mathfrak{E}\cdot\mathbf{E}_{\mathrm{II}}/4\pi)-\mathfrak{A}\cdot\mathbf{j}. \quad (10)$$

Note that (10) by Eqs. (3), (6)–(7) is expressed completely in terms of gauge-independent variables $\mathfrak{E}$, $\mathfrak{B}$, ρ, and $\mathbf{j}$ without introduction of redundant variables. Although, by $\mathrm{div}\mathfrak{E}=0$, the middle term in the right hand member of (10) will drop out in Eq. (9) for parallel displacements $\delta c\tau=\epsilon=$ constant, we yet need this term for rotations of σ, which are then accompanied by a Lorentz transformation of the frame of reference used in defining W by (10).

3. PROOF OF LORENTZ INVARIANCE OF THE THEORY

The Lorentz invariance of the field equations and commutation relations for the tensor $\{{}^\circ\mathfrak{E},{}^\circ\mathfrak{B}\}$ and the undors ${}^\circ\psi$ and ${}^\circ\psi^\dagger$ is obvious. What we have to show is merely the covariance of the Schrödinger equation, which means that (9) with (10) should (in Fig. 1) give the same change $\Psi_0[1]-\Psi_0[0]$ of the state vector with time when calculated directly $(0\to1)$ as when calculated in a different Lorentz frame $(0\to\bar{0}\to\bar{1}\to1)$. In other words, we must prove the integrability of (9).

We follow almost exactly the method used in Chapter 2 of reference (5) for the Proca field. As explained there, it is sufficient to show the equality, up to terms bilinear

[8] F. J. Belinfante, Physica 12, 1 (1946). Note that these longitudinal and transverse delta-functions are different from zero for large as well as for small values of their space-like arguments.

[9] If in interaction representation the potentials A^μ are resolved into Fourier components $A^\mu(k)\exp(ik_\nu x^\nu)$, the component of $A^\mu(k)$ outside the plane tangent along k^μ to the light cone has no physical meaning due to the Lorentz condition $k_\mu A^\mu(k)=0$. Furthermore, in this plane, components of $A^\mu(k)$ parallel to k^μ are physically meaningless as they do not contribute to the field strengths. All four-vectors connecting any pair of points on two lines parallel to k^μ describe therefore from a physical point of view the same field. In particular we may choose $A^\mu(k)$ in the intersection of the plane tangent along k^μ to the light cone, with the plane $t=$ constant. Doing so, we find a potential without time component and with solenoidal spatial component $\mathfrak{A}$ as used in our theory. The fact that in a different Lorentz frame $\mathfrak{A}$ then represents a different four-vector does not matter, as we have seen that such different "arrows in space-time" connecting points of the same pair of parallel lines $\parallel k^\mu$ are physically equivalent (different by a gauge transformation only).

[10] G. S. Wick, Phys. Rev. 80, 268 (1950).

[11] Compare Eq. (49) of F. J. Belinfante, Physica 12, 17 (1946).

in the infinitesimal displacements ϵ = constant for $\bar{0}\to 1$ and $\bar{0}\to\bar{1}$, and [12] $\varphi(\mathbf{x}')=\mathbf{b}\cdot(\mathbf{x}'-\mathbf{x}_Q)$ for $0\to\bar{0}$ and $1\to\bar{1}$, of

$$\Psi_0[\bar{1}]=[1+a\int'\mathbf{b}\cdot(\mathbf{x}'-\mathbf{x}_Q)\{{}^\circ W'+\epsilon\partial_0\,{}^\circ W'\}]\Psi_0[1]$$

and

$$\Psi_0[\bar{1}]=[1+a\epsilon\int\{{}^\circ W+\mathbf{b}\cdot(\mathbf{x}-\mathbf{x}_Q)\partial_0\,{}^\circ W+\delta\,{}^\circ W\}]\Psi_0[\bar{0}],$$

where

$$\Psi_0[1]=[1+a\epsilon\int{}^\circ W]\Psi_0[0],$$

$$\Psi_0[\bar{0}]=[1+a\int'\mathbf{b}\cdot(\mathbf{x}'-\mathbf{x}_Q)\,{}^\circ W']\Psi_0[0].$$

For this purpose we need only show that[7]

$$a\int\int'\mathbf{b}\cdot(\mathbf{x}'-\mathbf{x}_Q)[{}^\circ W';\,{}^\circ W]=\int\delta\,{}^\circ W. \tag{11}$$

Here, $\delta\,{}^\circ W$ is the variation ${}^\circ\overline{W}(P)-{}^\circ W(P)$ of (10) under the infinitesimal Lorentz transformation $0\to\bar{0}$ in the point $P(\mathbf{x})$.

As, for $t'=t$, $\rho(\mathbf{x}')$ commutes with $\rho(\mathbf{x})$ and with $\mathbf{j}(\mathbf{x})$, also $\mathbf{E}_{11}(\mathbf{x}')$ and $\mathbf{E}_{11}(\mathbf{x})$ defined by (6)–(7) will commute with each other and with $\mathbf{j}(\mathbf{x})$ and $\mathbf{j}(\mathbf{x}')$ in the commutator $[W';W]$ with W from (10). Naturally they also commute with the photon field $\mathfrak{E},\mathfrak{B},\mathfrak{A}$. The only contribution to the left-hand member of (11) therefore arises from Eq. (5). This yields

$$\int\int'\mathbf{b}\cdot(\mathbf{x}'-\mathbf{x}_Q)\textstyle\sum_{l,m}({}^\circ j_l'\,{}^\circ E_{11m}-{}^\circ E_{11l}'\,{}^\circ j_m)\delta_{lm}{}^{\mathrm{tr}}(\mathbf{r}).$$

Integration over $\mathbf{x}$ gives by Eq. (22) of reference (8)

$$\int'\mathbf{b}\cdot(\mathbf{x}'-\mathbf{x}_Q)\{{}^\circ\mathbf{j}'\cdot({}^\circ\mathbf{E}_{11}')_\perp-{}^\circ\mathbf{E}_{11}'\cdot{}^\circ\mathbf{j}_\perp'\}.$$

The first term apparently vanishes. In the second term substitute (6) and integrate by parts. Since $\mathrm{div}\mathbf{j}_\perp=0$, this yields

$$-\int\mathbf{b}\cdot{}^\circ\mathbf{j}_\perp\,{}^\circ V \tag{12}$$

for the left-hand member of (11).

For calculating the right-hand member of (11) we first note that ${}^\circ W(P)$ is invariant under (finite) translation of the origin, so that it is allowed to consider the co-ordinates $\mathbf{x}$, t of the point P invariant. (P is the point where we calculate $\delta\,{}^\circ W$ in the integrand of (11).) Then, for the point $P(x)$ and for a different point $P'(x')$ the infinitesimal Lorentz transformation from the x-frame to the $\bar{x}$-frame gives

$$\left.\begin{aligned}\delta\mathbf{x}'&\equiv\bar{\mathbf{x}}(P')-\mathbf{x}(P')=-\mathbf{b}(ct'-ct);\quad \delta\mathbf{x}=0;\\ \delta ct'&\equiv c\bar{t}(P')-ct(P')=-\mathbf{b}\cdot(\mathbf{x}'-\mathbf{x});\quad \delta ct=0.\end{aligned}\right\} \tag{13}$$

Under this transformation, we have (with $\delta f\equiv\bar{f}-f$):

$$\left.\begin{aligned}\delta\,{}^\circ\mathfrak{E}&=\mathbf{b}\times{}^\circ\mathfrak{B}, & \delta\,{}^\circ\mathfrak{B}&=-\mathbf{b}\times{}^\circ\mathfrak{E};\\ \delta\,{}^\circ\rho&=-\mathbf{b}\cdot{}^\circ\mathbf{j}, & \delta\,{}^\circ\mathbf{j}&=-\mathbf{b}\,{}^\circ\rho;\\ \delta\,{}^\circ\psi^\dagger&=-\tfrac{1}{2}\,{}^\circ\psi^\dagger\boldsymbol{\alpha}\cdot\mathbf{b}, & \delta\,{}^\circ\psi&=-\tfrac{1}{2}\mathbf{b}\cdot\boldsymbol{\alpha}\,{}^\circ\psi;\end{aligned}\right\} \tag{14}$$

$$\delta\nabla'=\mathbf{b}\partial/c\partial t'\,(=\mathbf{b}\partial/c\partial t,\ \text{when } t'=t). \tag{15}$$

Let a new point $\bar{P}'$ be defined by $\bar{x}(\bar{P}')=x(P')\equiv x'$, (see Fig. 1), so that, for $F(\mathbf{x},t)\equiv\int d^3\mathbf{x}'f(\mathbf{x}',t)/r$, we find

$$\delta F(x)=\int_{t'=t}d^3\mathbf{x}'\frac{\bar{f}(\bar{P}')-f(P')}{r}$$

$$=\int d^3\mathbf{x}'\frac{\delta f(x')+f(\bar{P}')-f(P')}{r}, \tag{16}$$

where $r\equiv|\mathbf{x}'-\mathbf{x}|=|\bar{\mathbf{x}}(\bar{P}')-\bar{\mathbf{x}}(\bar{P})|$, while $\bar{t}(\bar{P}')=\bar{t}(\bar{P})$ as $t'=t$. Now, by (13) with $t'=t$, the vector $P'\bar{P}'$ has components

$$\left.\begin{aligned}\bar{\mathbf{x}}(\bar{P}')-\bar{\mathbf{x}}(P')&=\mathbf{x}(P')-\bar{\mathbf{x}}(P')=-\delta\mathbf{x}'=0,\\ c\bar{t}(\bar{P}')-c\bar{t}(P')&=ct(P')-c\bar{t}(P')=-\delta ct'=\mathbf{b}\cdot\mathbf{r}'.\end{aligned}\right\} \tag{17}$$

Thence, (16) gives

$$\delta(\int'f'/r)=\int'\{\delta f'+(\mathbf{b}\cdot\mathbf{r}')(\partial f'/c\partial t)\}/r. \tag{18}$$

This may be used for calculating $\delta\,{}^\circ\mathfrak{A}$ and $\delta\,{}^\circ V$. By (3), (18), (15), and the maxwell equation $\partial\,{}^\circ\mathfrak{B}/c\partial t=-\nabla\times{}^\circ\mathfrak{E}$, we find

$$\begin{aligned}\delta\,{}^\circ\mathfrak{A}(\mathbf{x})&=\int'(4\pi r)^{-1}\cdot[(\delta\nabla')\times{}^\circ\mathfrak{B}'+\nabla'\times\delta\,{}^\circ\mathfrak{B}'\\ &\qquad+(\mathbf{b}\cdot\mathbf{r}')\nabla'\times\partial\,{}^\circ\mathfrak{B}'/c\partial t]\\ &=-\int'(4\pi r)^{-1}\cdot[\mathbf{b}\times(\nabla'\times{}^\circ\mathfrak{E}')\\ &\qquad+\nabla'\times(\mathbf{b}\times{}^\circ\mathfrak{E}')+(\mathbf{b}\cdot\mathbf{r}')\nabla'\times(\nabla'\times{}^\circ\mathfrak{E}')]\\ &=\int'(4\pi r)^{-1}\cdot[2(\mathbf{b}\cdot\nabla')\,{}^\circ\mathfrak{E}'-\nabla'({}^\circ\mathfrak{E}'\cdot\mathbf{b})-\mathbf{b}(\nabla'\cdot{}^\circ\mathfrak{E}')\\ &\qquad+(\mathbf{b}\cdot\mathbf{r}')\{\Delta'\,{}^\circ\mathfrak{E}'-\nabla'(\nabla'\cdot{}^\circ\mathfrak{E}')\}].\end{aligned} \tag{19}$$

Integrating by parts wherever ∇' acts on ${}^\circ\mathfrak{E}'$, we obtain, by

$$\mathbf{r}'\Delta'(1/4\pi r)=-\mathbf{r}'\delta^{(3)}(\mathbf{r}')=0, \tag{20}$$

$$\delta\,{}^\circ\mathfrak{A}(\mathbf{x})=-\int'(\mathbf{b}\cdot\mathbf{r}')({}^\circ\mathfrak{E}'\cdot\nabla')\nabla'(1/4\pi r). \tag{21}$$

Similarly, by (7), (18) and $\partial\,{}^\circ\rho/c\partial t=-\mathrm{div}\,{}^\circ\mathbf{j}$:

$$\begin{aligned}\delta\,{}^\circ V(\mathbf{x})&=\int'\{-(\mathbf{b}\cdot{}^\circ\mathbf{j}')-(\mathbf{b}\cdot\mathbf{r}')(\nabla'\cdot{}^\circ\mathbf{j}')\}/r\\ &=\int'(\mathbf{b}\cdot\mathbf{r}')({}^\circ\mathbf{j}'\cdot\nabla')(1/r),\end{aligned} \tag{22}$$

and by (6), (15), and (22)

$$\begin{aligned}\delta\,{}^\circ\mathbf{E}_{11}(\mathbf{x})&=-\nabla(\delta\,{}^\circ V)-\int'(\mathbf{b}/r)\partial\,{}^\circ\rho'/c\partial t\\ &=\int'[-(\mathbf{b}\cdot\mathbf{r}')({}^\circ\mathbf{j}'\cdot\nabla')\nabla(1/r)\\ &\qquad+\mathbf{b}({}^\circ\mathbf{j}'\cdot\nabla')(1/r)+\mathbf{b}(\nabla'\cdot{}^\circ\mathbf{j}')/r]\\ &=\int'(\mathbf{b}\cdot\mathbf{r}')({}^\circ\mathbf{j}'\cdot\nabla')\nabla'(1/r).\end{aligned} \tag{23}$$

From (21) and (23) we find

$$\int\{({}^\circ\mathfrak{E}\cdot\delta\,{}^\circ\mathbf{E}_{11}/4\pi)-{}^\circ\mathbf{j}\cdot\delta\,{}^\circ\mathfrak{A}\}=0. \tag{24}$$

Further, from (6)–(7), (14), and (3),

$$\begin{aligned}&\int\{({}^\circ\mathbf{E}_{11}\cdot\delta\,{}^\circ\mathfrak{E}/4\pi)-{}^\circ\mathfrak{A}\cdot\delta\,{}^\circ\mathbf{j}\}\\ &=-\int(\mathbf{b}\times{}^\circ\mathfrak{B})\cdot\nabla\int'\,{}^\circ\rho'/4\pi r\\ &\qquad+\int{}^\circ\rho\mathbf{b}\cdot\int'(\nabla'\times{}^\circ\mathfrak{B}')/4\pi r\\ &\qquad=\int'\,{}^\circ\rho'\mathbf{b}\cdot\int\nabla\times({}^\circ\mathfrak{B}/4\pi r)=0.\end{aligned} \tag{25}$$

Adding (24) and (25) we find

$$\int\delta\{({}^\circ\mathfrak{E}\cdot{}^\circ\mathbf{E}_{11}/4\pi)-{}^\circ\mathfrak{A}\cdot{}^\circ\mathbf{j}\}=0, \tag{26}$$

[12] Notation as in reference (5), except $\mathbf{b}$ here for $\bar{\mathbf{b}}$ there. Also we use here the $xyzl$-frame tangent to (and coincident with) the surface 0 for the $\xi\eta\zeta\tau$-system of reference 5.

so, by (10), (6), and (23),

$$\int \delta\,{}^{\circ}W = -\int\int'(\mathbf{b}\cdot\mathbf{r}')({}^{\circ}\mathbf{j}'\cdot\nabla')\nabla'(1/4\pi r)\cdot\nabla\ {}^{\circ}V. \quad (27)$$

By Eqs. (13), (22), and (1) of reference 8 this gives

$$\begin{aligned}\int \delta\,{}^{\circ}W &= \int\int'(\mathbf{b}\cdot\mathbf{r}')\textstyle\sum_{m,n}{}^{\circ}j'_m(\nabla_n\,{}^{\circ}V)\delta_{mn}{}^{\text{long}}(\mathbf{r}')\\ &= \int'(\mathbf{b}\cdot\mathbf{x}')^{\circ}\mathbf{j}'\cdot(\nabla'\,{}^{\circ}V')_{\text{II}} - \int(\mathbf{b}\cdot\mathbf{x})^{\circ}\mathbf{j}_{\text{II}}\cdot\nabla\,{}^{\circ}V\\ &= \int(\mathbf{b}\cdot\mathbf{x})^{\circ}\mathbf{j}_{\perp}\cdot\nabla\ {}^{\circ}V = -\int {}^{\circ}V\,{}^{\circ}\mathbf{j}_{\perp}\cdot\mathbf{b}. \quad (28)\end{aligned}$$

Comparing (28) with (12) we see that we have proved (11) and by this the integrability of the generalized Schrödinger equation (9) with (10) and the Lorentz-invariance of our theory.

4. HEISENBERG FORM OF FIELD EQUATIONS IN INTERACTION REPRESENTATION

Obviously the field equations of motion

$$\left.\begin{aligned}\partial\,{}^{\circ}\mathfrak{E}/c\partial t = \text{curl}\,{}^{\circ}\mathfrak{B},\quad \partial\,{}^{\circ}\mathfrak{B}/c\partial t = -\text{curl}\,{}^{\circ}\mathfrak{E},\\ i\hbar\partial\,{}^{\circ}\psi/\partial t = (mc^2\beta - i\hbar c\boldsymbol{\alpha}\cdot\nabla)^{\circ}\psi,\end{aligned}\right\} \quad (29)$$

and all derived equations such as

$$\left.\begin{aligned}\partial\,{}^{\circ}\mathfrak{A}/c\partial t = -{}^{\circ}\mathfrak{E},\quad \partial\,{}^{\circ}V/c\partial t = -\text{div}\int'\,{}^{\circ}\mathbf{j}'/r,\\ \partial\,{}^{\circ}\mathbf{E}_{\text{II}}/c\partial t = -4\pi\,{}^{\circ}\mathbf{j}_{\text{II}},\end{aligned}\right\} \quad (29a)$$

can be summarized by

$$i\hbar\partial\,{}^{\circ}q(t)/\partial t = {}^{\circ}q(t)\,{}^{\circ}\mathcal{K}_0(t) - {}^{\circ}\mathcal{K}_0(t)\,{}^{\circ}q(t), \quad (30)$$

where

$$\mathcal{K}_0 \equiv \int\{{}^{\circ}\mathfrak{E}^2+{}^{\circ}\mathfrak{B}^2\}/8\pi + \int\psi^{\dagger}(mc^2\beta - i\hbar c\boldsymbol{\alpha}\cdot\nabla)\psi - \mathcal{K}_{\text{vac}}. \quad (31)$$

The subtraction of the c-number $\mathcal{K}_{\text{vac}}$ is most easily performed by splitting up the field variables into positive and negative frequency parts and then rearranging factors, which could be indicated by Wick's[10] symbol $:\cdots:$. Omitting vanishing integrals such as $\int\{{}^{\circ}\mathfrak{E}^{(+)}\cdot{}^{\circ}\mathfrak{E}^{(+)}+{}^{\circ}\mathfrak{B}^{(+)}\cdot{}^{\circ}\mathfrak{B}^{(+)}\}$ or $\int{}^{\circ}\overline{\psi^{(+)}}(\cdots)^{\circ}\psi^{(-)}$, we may also write

$$\begin{aligned}{}^{\circ}\mathcal{K}_0 = \int\{&{}^{\circ}\mathfrak{E}^{(-)}\cdot{}^{\circ}\mathfrak{E}^{(+)}+{}^{\circ}\mathfrak{B}^{(-)}\cdot{}^{\circ}\mathfrak{B}^{(+)}\}/4\pi\\ &+\int{}^{\circ}\overline{\psi^{(+)}}(mc^2+\hbar c\boldsymbol{\gamma}\cdot\nabla)\,{}^{\circ}\psi^{(+)}\\ &-\int{}^{\circ}\psi^{(-)}(mc^2-\hbar c\boldsymbol{\gamma}^{\mathrm{T}}\cdot\nabla)\,{}^{\circ}\overline{\psi^{(-)}}. \quad (32)\end{aligned}$$

Here we put $\bar{\psi}=\psi^{\dagger}\beta$, and $\boldsymbol{\gamma}=-i\beta\boldsymbol{\alpha}$.

5. TRANSFORMATION TO HEISENBERG REPRESENTATION

In Eq. (9) replace $\Psi_0[\sigma]$ by an operator $U[\sigma]$, and solve this equation with [13]

$$U(-\infty)=1 \quad (33)$$

as boundary condition for U on σ at $t=-\infty$. If we write t instead of σ for surfaces $t=$constant, Dyson's solution for U is then the infinite series[14]

$$\begin{aligned}U(t) = 1 &+ (i\hbar)^{-1}\int_{-\infty}^{t} dt_1\,{}^{\circ}\mathcal{W}_1\\ &+ (i\hbar)^{-2}\int_{-\infty}^{t}dt_1\int_{-\infty}^{t_1}dt_2\,{}^{\circ}\mathcal{W}_1\,{}^{\circ}\mathcal{W}_2+\cdots. \quad (34)\end{aligned}$$

where $\mathcal{W}_n=\mathcal{W}(t_n)=\int d^3\mathbf{x}W(\mathbf{x},t_n)$. The inverse of U is seen to be

$$\begin{aligned}U(t)^{-1} = 1 &- (i\hbar)^{-1}\int_{-\infty}^{t} dt_1\,{}^{\circ}\mathcal{W}_1\\ &+ (i\hbar)^{-2}\int_{-\infty}^{t}dt_1\int_{-\infty}^{t_1}dt_2\,{}^{\circ}\mathcal{W}_2\,{}^{\circ}W_1-\cdots = U(t)^{\dagger}, \quad (35)\end{aligned}$$

so that U is unitary. Apparently

$$i\hbar dU(t)^{-1}/dt = -U(t)^{-1}\,{}^{\circ}\mathcal{W}(t) = -{}^{\text{H}}\mathcal{W}(t)U(t)^{-1}, \quad (36)$$

where the superscript prefix $^{\text{H}}$ is defined by

$${}^{\text{H}}Q(t) = U(t)^{-1}\,{}^{\circ}Q(t)\,U(t). \quad (37)$$

We also put

$$U(t)^{-1}\Psi_0(t)=\Phi. \quad (38)$$

Then, by (36), and by (9) or $i\hbar d\Psi_0(t)/dt = {}^{\circ}\mathcal{W}(t)\Psi_0(t)$, one easily finds $d\Phi/dt=0$, so that Φ is a time-independent state vector. From (37) and (38) and the unitariness (35) of U, we find for matrix elements of $Q(t)$ between states a and b:

$$(\Psi_{0a}(t)^{\dagger},\,{}^{\circ}Q(t)\Psi_{0b}(t)) = (\Phi_a{}^{\dagger},\,{}^{\text{H}}Q(t)\Phi_b). \quad (39)$$

We thus have performed a transformation from interaction representation to Heisenberg representation.

6. LORENTZ COVARIANCE OF FIELD VARIABLES IN HEISENBERG REPRESENTATION

Since $^{\circ}W$ was no scalar, we should expect the variables in Heisenberg representation to satisfy Lorentz transformations different from those for the variables in interaction representation,[6,15] but we might try to find new variables, which form tensors in Heisenberg representation. From (37), and from Eq. (9) with U for Ψ_0, with $\mathbf{x}'$ for ξ and with $\mathbf{b}\cdot\mathbf{r}'$ for ϵ, we find

$$\begin{aligned}\delta^{\text{H}}q(\mathbf{x}) &= U^{-1}(\delta^{\circ}q)U + U^{-1}\,{}^{\circ}q(\delta U) - U^{-1}(\delta U)U^{-1}\,{}^{\circ}qU\\ &= U^{-1}(\delta^{\circ}q)U + a\int'(\mathbf{b}\cdot\mathbf{r}')U^{-1}[{}^{\circ}q;\,{}^{\circ}W']U; \quad (40)\end{aligned}$$

so, if $\delta^{\circ}q={}^{\circ}f(q)$, then

$$\delta^{\text{H}}q = {}^{\text{H}}f(q) + a\int'(\mathbf{b}\cdot\mathbf{r}')^{\text{H}}[q;\,W']. \quad (41)$$

It is easily seen that $\delta\rho$, δV, $\delta\mathbf{E}_{\text{II}}$ and $\delta\mathbf{j}$ are not affected but for labels $^{\text{H}}$ replacing $^{\circ}$ in Eqs. (14), (22), (23). (In the case of $\delta^{\text{H}}\mathbf{j}$, the delta-functions from $[\mathbf{j};\,W']$ are cancelled by the factor $\mathbf{r}'$ in (41).)

However, we find, by (41), (14), (10), (5), (20), (23),

[13] Assuming this in every Lorentz frame we tacitly assume that in some way $W(-\infty)=0$ in Eq. (9) when used for a change of slope of σ at $t=-\infty$.

[14] F. J. Dyson, Phys. Rev. 75, 486 (1949).

[15] See chapter 3 of reference 5.

and (2):

$$\delta\,{}^{\mathrm{H}}\mathfrak{E}(\mathbf{x})=(\mathbf{b}\times{}^{\mathrm{H}}\mathfrak{B})+f'(\mathbf{b}\cdot\mathbf{r}')\{{}^{\mathrm{H}}\mathbf{j}'\triangle-({}^{\mathrm{H}}\mathbf{j}'\cdot\nabla)\nabla\}(1/r)$$
$$=(\mathbf{b}\times{}^{\mathrm{H}}\mathfrak{B})-\delta\,{}^{\mathrm{H}}\mathbf{E}_{\mathrm{II}}(\mathbf{x}); \tag{42}$$
$$\partial\,{}^{\mathrm{H}}\mathfrak{B}(\mathbf{x})=-(\mathbf{b}\times{}^{\mathrm{H}}\mathfrak{E})+f'(\mathbf{b}\cdot\mathbf{r}')({}^{\mathrm{H}}\mathbf{E}_{\mathrm{II}}'\times\nabla)\delta(\mathbf{r}')$$
$$=-\mathbf{b}\times({}^{\mathrm{H}}\mathfrak{E}+{}^{\mathrm{H}}\mathbf{E}_{\mathrm{II}}). \tag{43}$$

These equations suggest the introduction of a new variable

$$\mathbf{E}=\mathfrak{E}+\mathbf{E}_{\mathrm{II}}, \tag{44}$$

so that from (42)–(43) we find the infinitesimal tensor transformation

$$\delta\,{}^{\mathrm{H}}\mathbf{E}=\mathbf{b}\times{}^{\mathrm{H}}\mathfrak{B},\quad \delta\,{}^{\mathrm{H}}\mathfrak{B}=-\mathbf{b}\times{}^{\mathrm{H}}\mathbf{E}. \tag{45}$$

Since $\mathfrak{E}$ is transverse (in either representation), the notation (44) is consistent as far as $\mathbf{E}_{\mathrm{II}}$ can now be regarded as the longitudinal part of $\mathbf{E}$, while apparently

$$\mathbf{E}_{\perp}=\mathfrak{E}. \tag{46}$$

Thus the electromagnetic tensor ${}^{\mathrm{H}}\mathbf{E}$, ${}^{\mathrm{H}}\mathfrak{B}$ in Heisenberg representation has a longitudinal electric part which by (6)–(7) is just the coulomb field derived from the field of charged matter, while only the transverse part of the electromagnetic field is quantized as a photon field.

In a similar way it is easily shown by (41), (21), (10), (5), (20), and (44), that

$$\delta\,{}^{\mathrm{H}}\mathfrak{A}(\mathbf{x})=-f'(\mathbf{b}\cdot\mathbf{r}')({}^{\mathrm{H}}\mathbf{E}'\cdot\nabla')\nabla'(1/4\pi r), \tag{47}$$

which differs from (21) by the occurrence of $\mathbf{E}$ instead of $\mathfrak{E}$.

Finally we find from (41), (14), (10), from

$$\left.\begin{aligned}[\psi;\rho']&=e\psi'\delta(\mathbf{r}'),\quad [\psi;\mathbf{j}']=e\boldsymbol{\alpha}\psi'\delta(\mathbf{r}'),\\ [\psi;V']&=e\psi/r,\quad [\psi;\mathbf{E}_{\mathrm{II}}']=-e\psi\nabla'(1/r),\end{aligned}\right\} \tag{48}$$

and from (44), that

$$\delta\,{}^{\mathrm{H}}\psi=-\tfrac{1}{2}\mathbf{b}\cdot\boldsymbol{\alpha}\,{}^{\mathrm{H}}\psi-(e/i\hbar c)f'(\mathbf{b}\cdot\mathbf{r}')\{{}^{\mathrm{H}}\psi\,{}^{\mathrm{H}}\mathbf{E}'$$
$$+{}^{\mathrm{H}}\mathbf{E}'\,{}^{\mathrm{H}}\psi\}\cdot\nabla'(1/8\pi r)$$
$$=-\tfrac{1}{2}\mathbf{b}\cdot\boldsymbol{\alpha}\,{}^{\mathrm{H}}\psi+(e/4\pi i\hbar c)f'\mathbf{b}\cdot{}^{\mathrm{H}}\mathbf{E}'\,{}^{\mathrm{H}}\psi/r$$
$$+(e/i\hbar c)f'(\mathbf{b}\cdot\mathbf{r}')\,{}^{\mathrm{H}}\rho'\,{}^{\mathrm{H}}\psi/r. \tag{49}$$

In the last term we used $\mathrm{div}\mathbf{E}=\mathrm{div}\mathbf{E}_{\mathrm{II}}=4\pi\rho$ (by (44), (6), (7)), and we used (20). In the one but last term, the special ordering of factors was superfluous according to (48).

We conclude that ${}^{\mathrm{H}}\psi$ is no undor under Lorentz transformations, although ${}^{\mathrm{H}}\rho$ and ${}^{\mathrm{H}}\mathbf{j}$ defined by (8) form a four-vector.[16]

In order to eliminate $\mathbf{E}_{\mathrm{II}}$ from (49) we use

$$\tfrac{1}{2}f'(\mathbf{b}\cdot\mathbf{r}')\,{}^{\mathrm{H}}\rho'/r=-f'(\mathbf{b}\cdot\mathbf{r}'/8\pi r)\triangle'\,{}^{\mathrm{H}}V'$$
$$=\text{(integrating by parts and using (20))}$$
$$=-f'\,{}^{\mathrm{H}}V'(\mathbf{b}\cdot\nabla')(1/4\pi r)=-f'\,{}^{\mathrm{H}}\mathbf{E}_{\mathrm{II}}'\cdot\mathbf{b}/4\pi r$$

so that

$$\delta\,{}^{\mathrm{H}}\psi=\{-\tfrac{1}{2}\mathbf{b}\cdot\boldsymbol{\alpha}+(e/i\hbar c)\mathbf{b}\cdot f'\,{}^{\mathrm{H}}\mathfrak{E}'/4\pi r$$
$$+(e/2i\hbar c)f'(\mathbf{b}\cdot\mathbf{r}')\,{}^{\mathrm{H}}\rho'/r\}\,{}^{\mathrm{H}}\psi. \tag{50}$$

We shall need all these equations, when we want to investigate the covariance of the energy density tensor.

7. HEISENBERG FIELD EQUATIONS OF MOTION

The equations of motion for ${}^{\circ}q(t)$ or for any function of the ${}^{\circ}q(t)$ can be written in the form (30). In particular the ${}^{\mathrm{H}}q(t)$ are such functions, so that

$$i\hbar\partial\,{}^{\mathrm{H}}q(t)/\partial t={}^{\mathrm{H}}q(t)\,{}^{\circ}\mathfrak{K}_0(t)-{}^{\circ}\mathfrak{K}_0(t)\,{}^{\mathrm{H}}q(t). \tag{30a}$$

However, we can also write, by (37), (36), and (9),

$$i\hbar\partial\,{}^{\mathrm{H}}q(t)/\partial t=U(t)^{-1}\{i\hbar\partial\,{}^{\circ}q(t)/\partial t$$
$$+{}^{\circ}q(t)\,{}^{\circ}\mathfrak{W}(t)-{}^{\circ}\mathfrak{W}(t)\,{}^{\circ}q(t)\}U(t). \tag{51}$$

Putting

$$\mathfrak{K}_0+\mathfrak{W}=\mathfrak{K} \tag{52}$$

we find from (51) and (30)

$$i\hbar\partial\,{}^{\mathrm{H}}q(t)/\partial t={}^{\mathrm{H}}q(t)\,{}^{\mathrm{H}}\mathfrak{K}(t)-{}^{\mathrm{H}}\mathfrak{K}(t)\,{}^{\mathrm{H}}q(t). \tag{53}$$

In fact,

$${}^{\mathrm{H}}\mathfrak{K}(t)={}^{\circ}\mathfrak{K}_0(t) \tag{54}$$

follows directly from (52), (37), (34)–(35), and (30).

From (10) and (44) we derive

$$W=(\mathbf{E}^2-\mathfrak{E}^2)/8\pi-\mathfrak{A}\cdot\mathbf{j}, \tag{55}$$

so that, by (31) and (52),

$$\mathfrak{K}=\int\{\mathbf{E}^2+\mathfrak{B}^2\}/8\pi-\int\mathfrak{A}\cdot\mathbf{j}$$
$$+\int\psi^{\dagger}(mc^2\beta-i\hbar c\boldsymbol{\alpha}\cdot\nabla)\psi-\mathfrak{K}_{\mathrm{vac}}. \tag{56}$$

From (53), (31), (52), (10), (48), (5), (44), (6)–(7), (2) we find the field equations of motion in Heisenberg representation, while the identities are the same as before:

$$i\hbar\partial\,{}^{\mathrm{H}}\psi/\partial t=(mc^2\beta-i\hbar c\boldsymbol{\alpha}\cdot\nabla-e\boldsymbol{\alpha}\cdot{}^{\mathrm{H}}\mathfrak{A})\,{}^{\mathrm{H}}\psi$$
$$+\tfrac{1}{2}e({}^{\mathrm{H}}V\,{}^{\mathrm{H}}\psi+{}^{\mathrm{H}}\psi\,{}^{\mathrm{H}}V), \tag{57}$$
$$\partial\,{}^{\mathrm{H}}\rho/c\partial t=-\mathrm{div}\,{}^{\mathrm{H}}\mathbf{j}, \tag{58}$$
$$\partial\,{}^{\mathrm{H}}\mathfrak{A}/c\partial t=-{}^{\mathrm{H}}\mathfrak{E},\ \text{so that}\ {}^{\mathrm{H}}\mathbf{E}=-\nabla\,{}^{\mathrm{H}}V-\partial\,{}^{\mathrm{H}}\mathfrak{A}/c\partial t, \tag{59}$$
$$\mathrm{div}\,{}^{\mathrm{H}}\mathfrak{A}=0,\quad \mathrm{curl}\,{}^{\mathrm{H}}\mathfrak{A}={}^{\mathrm{H}}\mathfrak{B}, \tag{60}$$
$$\partial\,{}^{\mathrm{H}}V/c\partial t=-\mathrm{div}\int d^3\mathbf{x}'\,{}^{\mathrm{H}}\mathbf{j}(\mathbf{x}')/r, \tag{61}$$
$$\partial\,{}^{\mathrm{H}}\mathbf{E}_{\mathrm{II}}/c\partial t=-4\pi\,{}^{\mathrm{H}}\mathbf{j}_{\mathrm{II}}, \tag{62}$$
$$\partial\,{}^{\mathrm{H}}\mathfrak{E}/c\partial t=\mathrm{curl}\,{}^{\mathrm{H}}\mathfrak{B}-4\pi\,{}^{\mathrm{H}}\mathbf{j}_{\perp}, \tag{63}$$
$$\partial\,{}^{\mathrm{H}}\mathbf{E}/c\partial t=\mathrm{curl}\,{}^{\mathrm{H}}\mathfrak{B}-4\pi\,{}^{\mathrm{H}}\mathbf{j}, \tag{64}$$
$$\mathrm{div}\,{}^{\mathrm{H}}\mathfrak{E}=0,\quad \mathrm{div}\,{}^{\mathrm{H}}\mathbf{E}_{\mathrm{II}}=\mathrm{div}\,{}^{\mathrm{H}}\mathbf{E}=4\pi\,{}^{\mathrm{H}}\rho,$$
$$\mathrm{div}\,{}^{\mathrm{H}}\mathfrak{B}=0, \tag{65}$$
$$\partial\,{}^{\mathrm{H}}\mathfrak{B}/c\partial t=-\mathrm{curl}\,{}^{\mathrm{H}}\mathfrak{E}=-\mathrm{curl}\,{}^{\mathrm{H}}\mathbf{E}. \tag{66}$$

Our Eqs. (44), (6)–(7), (56), (57), and (64)–(66) are equivalent to or are field-theoretical generalizations of

[16] A transformation like (49) but with $\mathrm{div}\,{}^{\mathrm{H}}\mathbf{E}/4\pi$ replacing ${}^{\mathrm{H}}\rho$ is obtained in manifestly covariant (conventional) quantum electrodynamics for the quantity $\psi'=\exp(ieL/\hbar c)\psi$, where $-\nabla L=\mathbf{A}_{\mathrm{II}}$. This ψ' there replaced ψ as $\mathbf{E}$ is replaced by $\mathbf{E}-(1/\mathrm{div})(4\pi\rho)$ when the coulomb interaction is separated and the longitudinal photon field is eliminated by introduction of a new set of canonical variables. See reference 8.

Eqs. (184), (186), (187) or (175), (169), and (172)–(173), of Pauli's *Handbuch* article,[3] so that essentially we have given a new proof of the intrinsic Lorentz covariance of Pauli's theory (confirming that $\mathbf{E}_{11}$ should not be quantized as a photon field). At the same time, we have shown how Pauli's theory can be extended to electron fields quantized according to the exclusion principle, and also how it can be formulated in interaction representation, making possible some unique covariant kind of distinction between positon and negaton states.

In some following papers we shall formulate a covariant auxiliary condition stating that all photons present can be regarded as at some time having been emitted by a source,[17] we shall discuss the energy density tensor in gauge independent quantum electrodynamics, and we shall show how our proof of the integrability of the generalized Schrödinger equation lends itself to interesting speculations on how a covariant quantum electrodynamics freed from self-interactions might be formulated.[18]

Grateful acknowledgment is made to the Purdue Research Foundation for a research fellowship awarded one of us to make possible this investigation.

[17] Compare also F. J. Belinfante, Phys. Rev. **81**, 307(A) (1951).
[18] F. J. Belinfante and J. S. Lomont, Phys. Rev. **83**, 225(A) (1951). See also F. J. Belinfante, Prog. Theor. Phys. **6**, 202 (1951), and Phys. Rev. **82**, 767(A) (1951).

PHYSICAL REVIEW VOLUME 84, NUMBER 3 NOVEMBER 1, 1951

A Variational Principle for Gauge-Independent Electrodynamics

FREDERIK J. BELINFANTE
Department of Physics, Purdue University, Lafayette, Indiana
(Received July 2, 1951)

A new lagrangian for the maxwell field is defined, expressed completely in terms of gauge-independent transverse field-strengths ($\mathfrak{E}$, $\mathfrak{B}$) and matter variables ($\mathbf{x}_i$, $\mathbf{v}_i$, and $\mathbf{p}_i$ in the classical theory; ψ and $\psi^\dagger$ in the wave-mechanical theory). The coulomb field is defined in terms of matter variables, and a (solenoidal) vector potential is defined in terms of the magnetic field strength $\mathfrak{B}$. The variational principle gives the usual equations of motion and field equations. Quantization leads automatically to the formulas of gauge-independent quantum electrodynamics.

1. CLASSICAL THEORY

THE usual lagrangian of electrodynamics has the disadvantage of being expressed in terms of the potentials, which are not uniquely determined and have no direct physical meaning. However, it is possible to derive the maxwell equations for the field and the relativistic equations of motion for charged particles in the field from a variational principle, in which only physically meaningful quantities are to be varied. For instance, in classical electrodynamics we may put, for charged particles (point charges) moving in the microscopic maxwell field with transverse (solenoidal) part $\mathfrak{E}$, $\mathfrak{B}$,

$$\mathfrak{L}=\mathfrak{L}_m+\int[\mathfrak{A}\cdot\mathfrak{E}^\cdot/4\pi c-(\mathfrak{E}^2+\mathfrak{B}^2)/8\pi+\mathfrak{A}\cdot\mathbf{j}-\tfrac{1}{2}\rho V], \quad (1)$$

with[1]

$$\mathfrak{L}_m=\textstyle\sum_i \mathbf{p}_i\cdot(\mathbf{x}^\cdot_i-\mathbf{v}_i)-m_ic^2(1-\mathbf{v}_i^2/c^2)^{\frac{1}{2}}, \quad (2)$$

where $^\cdot$ denotes time differentiation ($\mathfrak{E}^\cdot=\partial\mathfrak{E}/\partial t$, $\mathbf{x}^\cdot_i=d\mathbf{x}_i/dt$); and then vary the functions $\mathbf{x}_i(t)$, $\mathbf{p}_i(t)$, $\mathbf{v}_i(t)$, and the transverse fields $\mathfrak{E}(\mathbf{x},t)$ and $\mathfrak{B}(\mathbf{x},t)$ independently in

$$\delta\int\mathfrak{L}dt=0, \quad (3)$$

keeping the variations zero at the limits of integration. In Eq. (1), ρ, $\mathbf{j}$, V, $\mathfrak{A}$, and $\int'$ are abbreviations for

$$\rho(\mathbf{x},t)=\textstyle\sum_i e_i\delta(\mathbf{x}-\mathbf{x}_i(t)), \quad (4a)$$

$$\mathbf{j}(\mathbf{x},t)=\textstyle\sum_i(e_i/c)\mathbf{v}_i\delta(\mathbf{x}-\mathbf{x}_i(t)), \quad (4b)$$

$$V(\mathbf{x},t)=\int'\rho(\mathbf{x}',t)/r, \quad (5a)$$

$$\mathfrak{A}(\mathbf{x},t)=\int'[\mathrm{curl}'\mathfrak{B}(\mathbf{x}',t)]/4\pi r, \quad (5b)$$

$$\int'=\int d^3\mathbf{x}, \quad \int'=\int d^3\mathbf{x}', \quad r=|\mathbf{x}-\mathbf{x}'|. \quad (6)$$

From the definition of the electromagnetic radiation field $\mathfrak{E}$, $\mathfrak{B}$ as being a transverse field it follows that

$$\mathrm{div}\mathfrak{B}=0, \quad \mathrm{div}\mathfrak{E}=0. \quad (7a\text{-}b)$$

From (7a) and the definition (5b) we deduce the identities

$$\mathrm{curl}\mathfrak{A}=\mathfrak{B}, \quad \mathrm{div}\mathfrak{A}=0. \quad (8a\text{-}b)$$

We shall further define another vector field

$$\mathbf{E}=-\nabla V-\mathfrak{A}^\cdot/c. \quad (9)$$

On account of (8b), the second term is transverse, while the first term is obviously longitudinal (irrotational), so that we may write

$$\mathbf{E}_{11}=-\nabla V, \quad \mathbf{E}_\perp=-\mathfrak{A}^\cdot/c, \quad \mathbf{E}=\mathbf{E}_{11}+\mathbf{E}_\perp. \quad (10a\text{-}b\text{-}c)$$

[1] For a discussion of this form for $\mathfrak{L}_m$ see F. J. Belinfante, Phys. Rev. **74**, 779 (1948).

The field $\mathbf{E}_{\parallel}$ defined by (10a) with (5a) is what one calls the coulomb field. From (9)–(10) and (5a) we find the identity

$$\operatorname{div}\mathbf{E}=\operatorname{div}\mathbf{E}_{\parallel}=4\pi\rho. \tag{11}$$

Thus, the *identities* among the maxwell equations (Eqs. (7a) and (11)) are a consequence of the definitions of the field. (Compare also the alternative definition of $\mathbf{E}$ by Eq. (14).) The *field equations of motion* for the electromagnetic radiation field will now follow by variation of the transverse fields $\mathfrak{F}(\mathbf{x}, t)$ and $\mathfrak{B}(\mathbf{x}, t)$ in (3) with (1). Properly speaking, one should keep these fields transverse while they are varied. This can easily be done by equating these fields temporarily to the curl of other vector fields and then varying the latter. The results thus obtained turn out to be identical with the results Eqs. (12) and (15) obtained by direct arbitrary variation of $\mathfrak{F}$ and $\mathfrak{B}$ themselves. This is due to the fact that the members of the latter equations appear to have no longitudinal parts anyhow, on account of Eqs. (7)–(8).

We thus obtain, by variation of $\mathfrak{F}$,

$$\mathfrak{F}=-\mathfrak{A}^{\cdot}/c. \tag{12}$$

By the definition (5b), this relates $\mathfrak{F}$ to $\mathfrak{B}^{\cdot}$. By (8) and (10) this relation can also be written as

$$\operatorname{curl}\mathbf{E}=\operatorname{curl}\mathfrak{F}=-\partial\mathfrak{B}/c\partial t. \tag{13}$$

Moreover, (12) yields a new interpretation of (9)–(10) as

$$\mathbf{E}=-\nabla V+\mathfrak{F}, \quad \mathbf{E}_{\perp}=\mathfrak{F}, \tag{14}$$

so that $\mathbf{E}$ is the sum of the coulomb field $\mathbf{E}_{\parallel}$ and the electric radiation field $\mathfrak{F}$. Therefore we call $\mathbf{E}$ the *total* electric field strength. (We also could have started with (14) as a definition, and then have derived (9)–(10) by means of (12).)

Variation of $\mathfrak{B}$ in (3) with (1) alters also $\mathfrak{A}$ in (1) according to the definition (5b), so that this variation yields

$$-\frac{\mathfrak{B}}{4\pi}+\operatorname{curl}\int d^3x'\frac{\mathbf{j}(\mathbf{x}')+\mathfrak{F}^{\cdot}(\mathbf{x}')/4\pi c}{4\pi r}=0; \tag{15}$$

thence

$$\operatorname{curl}\mathfrak{B}=4\pi\mathbf{j}_{\perp}+\mathfrak{F}^{\cdot}/c, \tag{16}$$

where $\mathbf{j}_{\perp}(\mathbf{x})=\operatorname{curl}\operatorname{curl}\int'\mathbf{j}(\mathbf{x}')/4\pi r$ is the solenoidal part[2] of $\mathbf{j}$.

We now turn to the equations of motion for the matter variables. Variation of $\mathbf{x}_i$ yields

$$-\mathbf{p}_i^{\cdot}+(e_i/c)\nabla_i\mathfrak{A}(\mathbf{x}_i)\cdot\mathbf{v}_i-e_i\nabla_i V(\mathbf{x}_i)=0, \tag{17}$$

where we used the dependence of $\mathbf{j}$ and ρ and thence of V by the definitions (4) and (5a) on the function $\mathbf{x}_i(t)$ being varied.

[2] This follows from $\mathbf{j}=(\operatorname{curl}\operatorname{curl}-\nabla\operatorname{div})\int'\mathbf{j}(\mathbf{x}')/4\pi r=\mathbf{j}_{\perp}+\mathbf{j}_{\parallel}$ with $\operatorname{div}\mathbf{j}_{\perp}=\operatorname{curl}\mathbf{j}_{\parallel}=0$.

Variation of $\mathbf{p}_i$ yields

$$\mathbf{x}_i^{\cdot}=\mathbf{v}_i. \tag{18}$$

Independent variation of $\mathbf{v}_i$ yields[3]

$$-\mathbf{p}_i+m_i\mathbf{v}_i(1-\mathbf{v}_i^2/c^2)^{-\frac{1}{2}}+(e_i/c)\mathfrak{A}(\mathbf{x}_i)=0. \tag{19}$$

Substitution of $\mathbf{p}_i$ from (19) in Eq. (17) gives the equation of motion

$$(d/dt)\{m_i\mathbf{v}_i(1-\mathbf{v}_i^2/c^2)^{-\frac{1}{2}}\}=e_i\mathbf{E}(\mathbf{x}_i)+(e_i/c)\mathbf{v}_i\times\mathfrak{B}(\mathbf{x}_i), \tag{20}$$

where we used the equality

$$d\mathfrak{A}(\mathbf{x}_i(t), t)/dt=\partial\mathfrak{A}(\mathbf{x}_i, t)/\partial t+\mathbf{x}_i^{\cdot}\cdot\nabla_i\mathfrak{A}(\mathbf{x}_i, t), \tag{21}$$

the equation (18), the identity (8a) and the definition (9).

From Eqs. (4) we find

$$\rho^{\cdot}/c+\operatorname{div}\mathbf{j}=\textstyle\sum_i(e_i/c)\{-\mathbf{x}_i^{\cdot}+\mathbf{v}_i\}\cdot\nabla\,\delta(\mathbf{x}-\mathbf{x}_i(t))=0, \tag{22}$$

where we finally used Eq. (18). From (5a) and (22) follows

$$V^{\cdot}/c=-\int'\operatorname{div}'\mathbf{j}(\mathbf{x}')/r=-\operatorname{div}\int'\mathbf{j}(\mathbf{x}')/r, \tag{23}$$

so that, by (10a) and footnote 2,

$$\mathbf{E}_{\parallel}^{\cdot}/c=-\nabla V^{\cdot}/c=\nabla\operatorname{div}\int'\mathbf{j}(\mathbf{x}')/r=-4\pi\mathbf{j}_{\parallel}^{\cdot}. \tag{24}$$

Adding (24) finally to (16), we find by (10c) with (14)

$$\operatorname{curl}\mathfrak{B}=4\pi\mathbf{j}+\partial\mathbf{E}/c\partial t. \tag{25}$$

By (7a), (11), (13), (25), and (20) we have derived Maxwell's equations and the relativistic equation of motion of point charges in the electromagnetic field, both featuring $\mathbf{E}$ according to (14) composed of the coulomb field and the electric radiation field, only the latter being considered as an independent variable in the variational principle (3). We obtained these results without introducing potentials as independent variables, and the only potentials introduced by Eqs. (5) as mathematical abbreviations have by their definition a uniquely determined gauge depending only on the Lorentz frame, in which we work.

2. QUANTUM THEORY

In relativistic quantum electrodynamics, we replace the matter terms (2) in the lagrangian (1) by the analogous terms of the Dirac theory,

$$\mathfrak{L}_m=\int\psi^{\dagger}(i\hbar\partial/\partial t-c\boldsymbol{\alpha}\cdot\mathbf{p}_{\mathrm{op}}-mc^2\beta)\psi, \tag{26}$$

where $\mathbf{p}_{\mathrm{op}}=-i\hbar\nabla$, while the definitions (4) are now replaced by

$$\rho=e:\psi^{\dagger}\psi:, \quad \mathbf{j}=e:\psi^{\dagger}\boldsymbol{\alpha}\psi:. \tag{27}$$

Here, : : is Wick's notation for omission of the vacuum current and density.[4]

[3] This equation defines the derived variables $\mathbf{v}_i$ in terms of the canonical variables $\mathbf{p}_i$, $\mathbf{x}_i$, and $\mathfrak{B}(\mathbf{x})$. Compare page 781 of reference 1.

[4] G. S. Wick, Phys. Rev. **80**, 268 (1950).

Variation of $\psi^\dagger$ and of ψ now yields

$$i\hbar\partial\psi/\partial t=\{mc^2\beta+c\boldsymbol{\alpha}\cdot\mathbf{p}_{op}-e\mathfrak{A}\cdot\boldsymbol{\alpha}\}\psi+\tfrac{1}{2}e(V\psi+\psi V) \quad (28)$$

and hermitian conjugate equation. This is Dirac's equation, including self-interaction as V is given by (5a) and ψ is quantized according to the exclusion principle. Equations (17) and (18) are now replaced by the results of application of the generalized theorem of Ehrenfest, which gives the time-derivatives of $\int\psi^\dagger\mathbf{p}_{op}\psi$ and of $\int\psi^\dagger\mathbf{x}\psi$, as calculated from (28) and conjugate equation.

From (27) and (28) and the commutativity of ρ and V one also easily finds again the continuity equation $\rho^4/c+\mathrm{div}\mathbf{j}=0$ (Eq. (22)), which we used in deriving Eq. (25) from Eq. (16). There are no other alterations in the derivation of the maxwell equations from (3) with (1) and (26) in quantum theory.

We remark that $\mathfrak{L}$ is linear in time-derivatives. The pairs of canonical conjugates are $\mathbf{x}_i$ with $\mathbf{p}_i$ in the classical theory ($\mathbf{v}_i$ being derived variables, see footnote 3), or ψ with $i\hbar\psi^\dagger$ in wave mechanics; and $\mathfrak{E}(\mathbf{x})$ with $\mathfrak{A}(\mathbf{x})/4\pi c$ in both cases. The hamiltonian is obtained from $-\mathfrak{L}$ by omission of the terms $-pq^4$ from it, and gives for the total energy the usual expression,

$$\mathfrak{IC}=\int\{\psi^\dagger(mc^2\beta-i\hbar c\boldsymbol{\alpha}\cdot\nabla)\psi+\tfrac{1}{2}\rho V-\mathbf{j}\cdot\mathfrak{A}+(\mathfrak{E}^2+\mathfrak{B}^2)/8\pi\}. \quad (29)$$

Expanding the transverse fields $\mathfrak{E}$ and $\mathfrak{A}/4\pi c$ in fourier components, and quantizing these in the usual way as canonically conjugate variables, one finds, after recombination of the fourier components to transverse fields, that the commutator of $\mathfrak{E}$ and $\mathfrak{A}/4\pi c$ is $i\hbar\times$ the so-called *transverse delta-function*,[5] or

$$[\mathfrak{E}_k(\mathbf{x},t);\mathfrak{A}_l(\mathbf{x}',t)]=4\pi i\hbar c\delta_{kl}{}^{tr}(\mathbf{x}-\mathbf{x}')\equiv i\hbar c\{\nabla_k\nabla_l-\delta_{kl}\nabla\cdot\nabla\}(1/r). \quad (30)$$

The commutation relations of the coulomb field $\mathbf{E}_{II}$, on the other hand, simply follow from those of the matter field, by (10a) with (5a). These are just the commutation relations of the gauge-independent quantum electrodynamics recently proposed by the author in collaboration with J. S. Lomont.[6]

[5] F. J. Belinfante, Physica **12**, 1 (1946).
[6] F. J. Belinfante and J. S. Lomont, Phys. Rev. **83**, 225(A) (1951) and Phys. Rev. **84**, 541 (1951).

PHYSICAL REVIEW VOLUME 84, NUMBER 3 NOVEMBER 1, 1951

Size and Thermal Conductivity Effects in Paramagnetic Relaxation*

JULIAN EISENSTEIN
University of Wisconsin, Madison, Wisconsin
(Received July 25, 1951)

The Casimir-du Pré thermodynamic theory of paramagnetic relaxation is generalized by taking account of the thermal conductivity of the paramagnetic salt. The case of a spherical specimen in a constant temperature bath is considered. One finds that infinitely many times are required to characterize the relaxation when a magnetic field is suddenly applied. The alternating current susceptibility is calculated and is shown to contain terms depending on the size and thermal conductivity of the specimen. A limited comparison of the theory with experimental data is made.

IN 1938 Casimir and du Pré[1] developed a simple thermodynamic interpretation of the frequency dependence of the complex paramagnetic susceptibility. They considered the system of all ionic spins to be an entity separate from the crystalline lattice and assumed that the spin system was always in thermodynamic equilibrium with an oscillatory magnetic field. Energy is transferred from the field to the spin system which rises in temperature and transfers heat to the lattice. If isothermal conditions are maintained, there is a further transfer of heat from the lattice to the constant temperature bath. The mathematical development of these ideas leads to Debye-type curves for the susceptibility.

The Casimir-du Pré theory is in fairly good agreement with experiment.[2] However recent measurements by Kramers, Bijl, and Gorter[3] and by Benzie and Cooke[4] have revealed discrepancies. These authors have suggested that a suitable distribution of spin-lattice relaxation times could account for the experimental results. An alternative suggestion—that the thermal conductivity of the specimen alters the theoretical susceptibility curves—is considered here.

We shall consider a spherical specimen of a paramagnetic salt immersed in a constant temperature bath since no new results are obtained for an adiabatically isolated specimen. The differential equation for the

* This work was done under contract with the AEC.
[1] H. B. G. Casimir and F. K. du Pré, Physica **5**, 507 (1938).
[2] For an extensive survey of experimental results see C. J. Gorter, *Paramagnetic Relaxation* (Elsevier Publishing Company, Inc., Amsterdam, 1947).
[3] Kramers, Bijl, and Gorter, Physica **16**, 65 (1950).
[4] R. J. Benzie and A. H. Cooke, Proc. Phys. Soc. (London) **A63**, 20 (1950).

conduction of heat in an isotropic solid is

$$\rho c\partial T/\partial t = K\nabla^2 T + Q(x, y, z, t). \quad (1)$$

In this equation ρ is the density, c the specific heat, T the temperature, K the thermal conductivity, and $Q(x, y, z, t)$ the heat input per unit time per unit volume. In the present application ρ is the density of the salt; c is taken to be c_L, the specific heat of the lattice; and T is taken to be T_L, the lattice temperature. We shall assume Q to be proportional to the local temperature difference of the lattice and spin systems,

$$Q(x, y, z, t) = \alpha(T_S - T_L) = \alpha\theta. \quad (2)$$

By virtue of the first law of thermodynamics the amount of heat transferred per unit volume from the spin system to the lattice in time dt can be written as

$$\delta Q = dU - HdM = -\alpha\theta dt, \quad (3)$$

which can easily be transformed into

$$\left[\left(\frac{\partial U}{\partial T_S}\right)_H - H\left(\frac{\partial M}{\partial T_S}\right)_H\right]dT_S + \left[\left(\frac{\partial U}{\partial H}\right)_{T_S} - H\left(\frac{\partial M}{\partial H}\right)_{T_S}\right]dH = -\alpha\theta dt. \quad (4)$$

The variation of the bracketed quantities with t will be neglected. This approximation also occurs in the work of Casimir and du Pré.

We shall set

$$\begin{aligned} H &= H_0 \qquad (t<0), \\ H &= H_0 + h_0 e^{i\omega t} \quad (t\geq 0). \end{aligned} \quad (5)$$

By combining (1), (2), (4), and (5) one obtains

$$\rho c_L \partial T_L/\partial t = K\nabla^2 T_L + \alpha\theta \quad (6)$$

$$\begin{aligned} A\partial\theta/\partial t + A\partial T_L/\partial t + \alpha\theta &= 0 \qquad (t<0) \\ &= -Ci\omega h_0 e^{i\omega t} \quad (t\geq 0), \end{aligned} \quad (7)$$

where

$$A = (\partial U/\partial T_S)_H - H(\partial M/\partial T_S)_H, \quad (8)$$

$$\begin{aligned} C &= (\partial U/\partial H)_{T_S} - H(\partial M/\partial H)_{T_S} \\ &= \rho(c_H - c_M)(\partial M/\partial H)_{T_S}/(\partial M/\partial T_S)_H. \end{aligned} \quad (9)$$

It follows immediately from (4) that A is equal to ρc_H, c_H being the specific heat of the spin system at constant H. The second expression for C in (9) can be derived fairly easily. c_M is the specific heat of the spin system at constant magnetization.

For $t<0$ (6) and (7) have the trivial solutions $T_L = T_0$, the temperature of the bath, and $\theta = 0$. Consequently only the case $t\geq 0$ will be considered henceforth. (6) and (7) can be solved by a laplace transform method. To determine T_L uniquely it is necessary to impose the physical requirement that it remain finite as $r\to 0$. The following abbreviations are introduced to facilitate writing the solution:

$$\begin{aligned} &B = \alpha + \alpha A/\rho c_L = \alpha(1 + c_H/c_L), \\ &\kappa = K/\rho c_L, \\ &\lambda = (i\omega/\kappa)^{\frac{1}{2}}(Ai\omega + B)^{\frac{1}{2}}(Ai\omega + \alpha)^{-\frac{1}{2}}. \end{aligned}$$

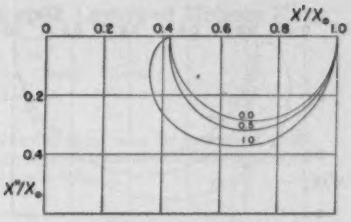

FIG. 1. Theoretical susceptibility curves for $(c_H - c_M)/c_H = 0.571$ and various values of T/τ.

We shall also denote by $p_n^{\pm}$ the two roots of

$$p^2 + [(B/A) + (n^2\pi^2\kappa/r_0^2)]p + n^2\pi^2\kappa\alpha/r_0^2 A = 0, \quad (n = 1, 2, 3, \cdots) \quad (10)$$

r_0 is the radius of the specimen. One then has

$$\begin{aligned} T_L = T_0 &+ \alpha C h_0 e^{i\omega t}[\rho c_L(B + Ai\omega)]^{-1} \\ &\times\{(r_0 \sinh\lambda r)(r \sinh\lambda r_0)^{-1} - 1\} \\ &+ (2\alpha C i\omega h_0\kappa/\rho c_L r r_0)\sum_{\substack{n=1 \\ \pm}}^{\infty} \exp(p_n^{\pm} t) \\ &\times (B + Ap_n^{\pm})^{-1}(p_n^{\pm} - i\omega)^{-1}(p_n^{\pm})^{-1} \\ &\times (Ap_n^{\pm} + \alpha)^2(A^2 p_n^{\pm 2} + 2Ap_n^{\pm}\alpha + \alpha B)^{-1} \\ &\times (-1)^n \sin(n\pi r/r_0)(in\pi). \end{aligned} \quad (11)$$

θ can readily be calculated from (6) by substituting (11). An inspection of the roots of (10) reveals that $p_n^{\pm}$ always contains a real part which is less than zero. The establishment of equilibrium when a magnetic field is suddenly applied therefore proceeds with the infinitely many relaxation times $\mathrm{Re}(1/p_n^{\pm})$.

In calculating the susceptibility it is not necessary to retain the exponentially decreasing terms since they will be negligible a certain time after turning on the oscillatory field. They will therefore be omitted from future consideration.

It follows from

$$dM/dH = (\partial M/\partial H)_{T_S} + (\partial M/\partial T_S)_H dT_S/dH,$$

the expression given for C in (9), and the definition of θ that

$$dM/dH = (\partial M/\partial H)_{T_S}\{1 + \rho C^{-1}(c_H - c_M) \times (d\theta/dH + dT_L/dH)\}. \quad (12)$$

$\chi_0 = (\partial M/\partial H)_{T_S}$ is the static or isothermal value of the susceptibility while dM/dH is the quantity determined experimentally. From (12), (11), and the solution of (6) for θ, one finds

$$\begin{aligned} dM/dH = \chi_0\{1 &+ \rho(c_H - c_M)[-(B + Ai\omega)^{-1} \\ &\times (\alpha/\rho c_L + i\omega) + (\alpha^2/\rho c_L)(B + Ai\omega)^{-1} \\ &\times (\alpha + Ai\omega)^{-1}(r_0 \sinh\lambda r) \\ &\times (r \sinh\lambda r_0)^{-1}]\}. \end{aligned} \quad (13)$$

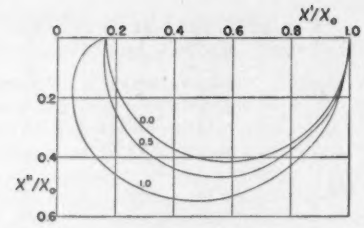

FIG. 2. Theoretical susceptibility curves for $(c_H-c_M)/c_H=0.842$ and various values of T/τ.

Equation (13) is an expression for what we might call the local value of the susceptibility. The susceptibility of the specimen as a whole can be obtained by averaging (13) over its volume. The result is

$$(dM/dH)_{total}=\chi_0\{1+\rho(c_H-c_M)[-(B+Ai\omega)^{-1}\times(\alpha/\rho c_L+i\omega)+(3\alpha^2\kappa/r_0^3\rho c_L i\omega)(Ai\omega+B)^{-2}\times[\lambda r_0\coth\lambda r_0-1]]\}. \quad (14)$$

Equation (14) can be evaluated readily in the limiting cases of 0 and ∞ frequency. For $\omega=0$ one finds

$$dM/dH=\chi_0.$$

As the frequency goes to zero, the measured value of the susceptibility approaches the isothermal value and the temperature of the specimen remains constant. For $\omega=\infty$ one obtains

$$dM/dH=\chi_0 c_M/c_H,$$

which is the well-known formula of Debye for the adiabatic susceptibility.

If only the first few terms in the series expansion of the hyperbolic cotangent are retained the following expressions for the real and imaginary parts of the susceptibility are obtained:

$$\chi'/\chi_0=1-c_H^{-1}(c_H-c_M)[\omega^2\tau^2(1+\omega^2\tau^2)^{-1}+(T/\tau)(2\omega^2\tau^2)(1+\omega^2\tau^2)^{-2}+\cdots], \quad (15)$$

$$\chi''/\chi_0=c_H^{-1}(c_H-c_M)[\omega\tau(1+\omega^2\tau^2)^{-1}+(T/\tau)(\omega\tau-\omega^3\tau^3)(1+\omega^2\tau^2)^{-2}+\cdots]. \quad (16)$$

In these expressions,

$$\tau=(A/B)(1+c_H/c_L), \quad T=\rho c_H r_0^2/15K.$$

Theoretical curves for the susceptibility calculated by using (15) and (16) are given in Figs. 1 and 2 for two values of $(c_H-c_M)/c_H$ and for three values of the ratio T/τ. It is clear from the curves that size and thermal conductivity effects alter their shape. Because of the scarcity of experimental data in the low temperature region it is difficult to say whether or not the terms involving T/τ in the foregoing expansions are actually important. The substance on which the most work has been done is probably potassium chrome alum. Bijl[5] has measured the specific heat resistance, which is the reciprocal of the thermal conductivity, in the liquid helium temperature region. He found that this quantity depended on the way the salt was cooled. At 2°K, K has a value somewhere between 0.03 and 0.12 watt cm^{-1} deg^{-1}. We shall take K to be 0.08 watt cm^{-1} deg^{-1} as an average value. c_H-c_M is equal to CH^2T^{-2} and c_H is equal to $(b+CH^2)T^{-2}$. Here C is the constant in the curie law and according to data cited by Burton, Grayson Smith, and Wilhelm[6] has a value of 0.0033 deg g^{-1} at 2°K. Kramers, Bijl, and Gorter[3] assign the value 0.75×10^6 oersted[2] to b/C. The density of potassium chrome alum is 1.83 g cm^{-3}. Casimir, Bijl, and du Pré[7] in measurements on a powder specimen immersed in liquid helium at 2.04°K found that the relaxation time τ was about 3.1×10^{-3} sec in a field of 1000 oersted and about 5.2×10^{-3} sec in a field of 2000 oersted. The values of T/τ computed from these data for a specimen of 1-cm radius are 0.07 at 1000 oersted and 0.12 at 2000 oersted. It therefore appears that at 2.04°K the size and thermal conductivity do not affect the relaxation in potassium chrome alum in an important way. At lower temperatures the decrease of the thermal conductivity may necessitate consideration of the additional terms in (15) and (16). The increase of c_H at lower temperatures should be nearly compensated by the increase of τ.

I am indebted to Dr. F. Rodgers for suggesting to me that the thermal conductivity might influence the theoretical curves for the susceptibility. I should also like to thank Dr. Rodgers for several discussions of the problem.

[5] D. Bijl, Physica 14, 684 (1948–49).
[6] Burton, Grayson Smith, and Wilhelm, *Phenomena at the Temperature of Liquid Helium* (Reinhold Publishing Corporation, New York, 1940).
[7] Casimir, Bijl, and du Pré, Physica 8, 449 (1941).

On the Thermomechanical Effect in Adsorbed Layers of Helium II

LOTHAR MEYER AND EARL LONG
Institute for the Study of Metals, University of Chicago, Chicago, Illinois
(Received July 16, 1951)

An expression is derived for the thermomechanical effect in adsorbed films, using the methods of quasi-thermodynamics. The results are discussed in comparison with the fountain effect in bulk liquid helium II, and with the existing qualitative measurements on adsorbed helium II films.

PHENOMENA have been reported recently[1] which indicate that thermomechanical effects occur in adsorbed layers of helium below the λ-temperature, in the absence of bulk liquid. It seemed therefore desirable to derive the equations which should govern these phenomena in surface layers.

In the thermomechanical effects, i.e., the pressure differences due to temperature differences, irreversible processes such as heat flow cannot be separated from the reversible heat engine producing the pressure differences. A suitable method of treating such a phenomenon is due to Onsager,[2] and has been used by de Groot[3] to derive the so-called fountain pressure relation for bulk liquid helium.

Let us assume that the system consists of two chambers *I* and *II*, filled with adsorbent, and connected by an opening such as a slit or a diaphragm, so narrow that the flow of vapor due to small pressure differences is negligible, and only a transfer of mass due to superfluid motion of the helium film matters. The pressure P in these chambers is smaller than the vapor pressure P_0 of the bulk liquid at this temperature, so that only an adsorbed film on the surface of the adsorbent—but no bulk liquid—is present. Deviation from equilibrium between the two chambers will produce the flow of mass and energy. Following de Groot[3] (Eqs. (6) and (7), see reference 3) we may write

$$\dot{M}=-\alpha_{11}\Delta(\mu/T)+\alpha_{12}\Delta(1/T), \tag{1}$$

$$\dot{U}=-\alpha_{21}\Delta(\mu/T)+\alpha_{22}\Delta(1/T), \tag{2}$$

where M is the mass, U the energy, μ the chemical potential of the adsorbed film, and T the temperature.

The condition for steady state is: no net mass flow, $\dot{M}=0$. This yields

$$\Delta(\mu/T)=(\alpha_{12}/\alpha_{11})\Delta(1/T). \tag{3}$$

Using Onsager's reciprocity relation,

$$\alpha_{12}=\alpha_{21}, \tag{4}$$

and the fact that at constant temperature, by dividing (2) by (1),

$$\dot{U}/\dot{M}=\alpha_{21}/\alpha_{11}=\alpha_{12}/\alpha_{11}=Q_T, \tag{5}$$

the amount of energy transferred by the unit of mass, we get from (3)

$$\Delta(\mu/T)=Q_T\Delta(1/T). \tag{6}$$

For a surface phase

$$\Delta(\mu/T)=T^{-2}\{TV_n\Delta P-TA_n\Delta\gamma-H_n\Delta T\}. \tag{7}$$

The subscript n designates the quantity per gram of adsorbate, V is the volume, A the surface area, H the heat function: $H=G+TS=U+PV$, and γ the surface tension.[4] Combining (6) and (7) we get

$$V_n\Delta P-A_n\Delta\gamma=[(H_n-Q_T)/T]\Delta T=(Q_p/T)\Delta T, \tag{8}$$

where Q_p is the difference of the energy transported in ordinary flow (H) and the energy (Q_T) transported by the special form of flow (in this case "film"-flow); Q_T produces the thermomechanical effects. Q_p is the amount of heat produced where the "film" flow starts, and absorbed where it ends, corresponding to the Peltier heat in thermoelectricity. For thin surface layers the first term on the left-hand side of (8) is small compared with the second and can be neglected.

The physical significance of (8) can be readily seen by transformation into an expression which involves only experimentally measurable quantities.

The surface tension γ is a function of pressure P and temperature T, which uniquely define the amount adsorbed per unit area of the surface, is therefore not an independent variable, and can be replaced by the independent variables P and T. The necessary relation is provided by the Gibbs-Duhem equation, which reads for surface layers of one component[5]

$$V_n\Delta P-A_n\Delta\gamma=S_n\Delta T+\Delta\mu. \tag{9}$$

Using (9) in (8) we get

$$\Delta\mu=\{(Q_p/T)+S_n\}\Delta T. \tag{10}$$

The surface layer is in equilibrium with its vapor; therefore,

$$\Delta\mu=\Delta\mu_g, \tag{11}$$

where the suffix g designates the gas phase. Inserting the well-known relation,

$$\Delta\mu_g=-S_g\Delta T+V_g\Delta T \tag{12}$$

[1] E. Long and L. Meyer, Phys. Rev. **79**, 1031 (1950).
[2] L. Onsager, Phys. Rev. **37**, 405 (1931); **38**, 2265 (1931).
[3] S. R. de Groot, Physica **XIII**, 555 (1947).
[4] Equation (7) follows, e.g., from Eqs. 1,54.10 and 1,54.11 in Guggenheim, *Thermodynamics* (Interscience Publishers, Inc., New York, New York, 1949).
[5] See reference 4, Eq. 1,55.2.

into (10) we get

$$\Delta P/\Delta T=\{(Q_p/T)+(S_g-S_n)\}/V_g. \qquad (13)^6$$

If it is assumed, as in the bulk liquid case, that the thermomechanical heat $Q_p=TS_n$, then (13) reduces to

$$\Delta P/\Delta T=S_g/V_g. \qquad (13\text{-a})$$

Under the same assumption, the fountain pressure relation for bulk liquid helium is

$$\Delta P/\Delta T=S_l/V_l, \qquad (14)$$

where the suffix l denotes the liquid phase.

However, the pressure terms of Eqs. (13-a) and (14) have entirely different meanings; the ΔP of (13-a) refers to the pressure of the gas phase in equilibrium with the film, whereas the ΔP of (14) describes the sum of the vapor pressure plus a hydrostatic pressure head, measured inside the liquid at the entrance of the slit.

Thus in the film case (13-a) the entropy and volume of the gas phase appear, instead of those for the liquid phase which apply to the bulk liquid case (14). In bulk liquid helium the fountain effect is about ten times greater than the pressure difference due to the change of vapor pressure with temperature. A comparison of (13) with the Clapeyron equation,

$$\Delta P/\Delta T=(S_g-S_n)/(V_g-V_n), \qquad (15)$$

shows that the thermomechanical effect in adsorbed layers produces only a deviation of about 10–20 percent from the vapor pressure curve. The physical reason for this difference between bulk liquid and adsorbed layers is as follows: in the bulk liquid, the forces produced by the thermomechanical effect are compensated by the hydrostatic pressure of the liquid, which is measured directly. In the case of adsorbed layers the forces produced thermomechanically are of the same order of magnitude. They are, however, compensated by surface tension forces (see Eq. (8)) which cannot be measured directly. Only their secondary influence on the total pressure P is subject to measurement,[7] which reduces the effect in the ratio specific volume of vapor to specific volume of the condensed phase.

Equations (13) and (13-a) are derived under the tacit assumption of negligible dead space, i.e., A_n and eventually V_n are essentially not changed by changes of the pressure in the gas phase. In actual experimental arrangements, however, changes of the pressure and therefore the amount of material in the gas phase go at the expense of the adsorbed layers. This effect produces deviations from a pure vapor pressure curve which easily might exceed the deviations derived above due to thermomechanical effects.

The rather strong pressure fluctuations observed by producing transient temperature gradients across a super-leak[1] are not necessarily in contradiction to Eq. (13), which is valid only for the steady state without net mass flow. In the experiments quoted the temperature gradients are changed continuously, which probably produced a much greater transfer of mass from one chamber to the other than would be necessary merely to obtain quasi-equilibrium. It is known that non-equilibrium thermomechanical forces are able to produce bubbles in liquid He II,[8] and it seems quite possible that the thermomechanical forces under non-equilibrium conditions are much stronger than calculated for the steady-state case.[9]

Thanks are due to J. W. Stout for helpful criticism.

[6] Professor J. W. Stout observed that Eq. (13) can be obtained directly from Eq. (6) in the form $\Delta\mu T-\mu\Delta T=-Q_T\Delta T$, with $\mu=H_n-TS_n$ and using (11) and (12).

[7] The factor by which the influence of the total pressure on an equilibrium pressure, such as partial pressure, is expressed, is likewise the well-known ratio of specific gas volume to specific volume of the condensed phase.

[8] L. Meyer and J. H. Mellink, Physica **XIII**, 214 (1947).

[9] Compare R. Bowers and K. Mendelssohn, Proc. Phys. Soc. (London), A., 4 **XIII**, 178 (1950).

The Temperature Variation of the Compressibility of Molten Sodium*

T. E. POCHAPSKY
Columbia University, New York, New York
(Received June 12, 1951)

The present method for the determination of the adiabatic compressibility of molten sodium depends in the first instance upon the measurement of the velocity of propagation of a short train of ultra-high frequency compressional acoustic waves in the material. This figure is then combined with the best available value of the density to yield the compressibility, on the assumption that the rigidity of the liquid is zero.

The wave trains are produced and detected by a piezoelectric transducer, and the resultant signal is exhibited on the screen of an oscilloscope whose sweep circuit is time-calibrated to permit the measurement of the transit time of a train over a known path length in the medium. A novel acoustic interferometer is employed, with which small changes in velocity can be measured with high precision.

The velocity of compressional waves in molten sodium at the freezing point, 97.6°C, is 252,600±500 cm/sec, and its temperature coefficient remains constant at the value −52.4±0.3 cm/sec °C at least to 545°C. The adiabatic compressibility is 16.85×10^{-12} cgs at 97.6°C, and its temperature coefficient increases from 0.012×10^{-12} cgs at this temperature to 0.013×10^{-12} cgs at 545°C. The relations between these quantities and other elastic and thermal properties of solid and liquid sodium are discussed.

I. INTRODUCTION

CONSIDERABLE information is available concerning the elastic and thermal properties of sodium in the solid state. Thus the principal adiabatic and isothermal elastic constants at zero pressure have been measured between 79°K and 210°K,[1] and the isothermal compressibility at high pressures between 273°K and the melting point, 371°K.[2] The thermal expansion of the material between 79°K and 371°K is known,[3] as is the specific heat at constant pressure over various temperature intervals up to 371°K.[4]

Progress toward an understanding of the process of melting in sodium demands a knowledge of the changes which the aforementioned properties undergo when the substance passes into the liquid state. The thermal expansion[5] and the specific heat at constant pressure[6] of liquid sodium have been measured, as has the change in specific volume on melting,[7] but inherent experimental difficulties have prevented a direct determination of the compressibility of the molten metal.

The present paper describes a series of measurements of the variation of the velocity of sound in liquid sodium with temperature between 371°K and 545°K. The adiabatic compressibility, κ_S, of the material is given in terms of this quantity by the expression,

$$\kappa_S=(\rho V^2)^{-1}, \tag{1}$$

in which V denotes the velocity of a compressional sound wave in the material and ρ the density, and it is assumed that the rigidity modulus is zero. The adiabatic compressibility is related to the isothermal compressibility, κ_T, by the formula,

$$\kappa_T-\kappa_S=T\beta^2/\rho c_p, \tag{2}$$

in which T denotes the absolute temperature, β the volume coefficient of expansion, and c_p the specific heat at constant pressure. The specific heat at constant volume, c_v, may be computed with the formula,

$$\kappa_T/\kappa_S=c_p/c_v. \tag{3}$$

II. EXPERIMENTAL METHOD

Electronic Equipment

The experimental method consists in the measurement of the time of transit of a short train of high frequency compressional acoustic waves over a predetermined path length in the specimen material. The wave trains are excited by a piezoelectric quartz crystal and, after reflection from a plane surface in the medium, are detected by the same crystal. The initial and reflected signals are exhibited on the screen of a cathode-ray oscilloscope, separated by a time-calibrated sweep.

The method has been extensively employed to measure the velocity of acoustic waves in various solids and liquids.[8] Those applications, like the present one, rely in large measure upon special electronic equipment developed by the Massachusetts Institute of Technology Radiation Laboratory for the production and utilization of short high frequency signals. Appropriate references to the published literature of the Laboratory are given here, and detailed description is limited to certain novel features designed to enhance the pre-

* Publication assisted by the Ernest Kempton Adams Fund.
[1] S. L. Quimby and Sidney Siegel, Phys. Rev. **54**, 293 (1938).
[2] P. W. Bridgman, (*a*) Proc. Am. Acad. Arts Sci. **70**, 71 (1935); (*b*) Proc. Am. Acad. Arts Sci. **58**, 166 (1923).
[3] Sidney Siegel and S. L. Quimby, Phys. Rev. **54**, 76 (1938); E. Hagen, Wied. Ann. **19**, 436 (1883); E. A. Griffiths and E. Griffiths, Proc. Phys. Soc. (London) **27**, 477 (1915).
[4] G. L. Pickard and F. E. Simon, Proc. Phys. Soc. (London) **61**, 1 (1948); K. K. Kelley, U. S. Dept. Commerce, Bur. Mines Bull. **371** (1934); Ezer Griffiths, Proc. Roy. Soc. (London) **89**, 561 (1914); E. Rengade, Compt. rend. **156**, 1879 (1913).
[5] E. Hagen, see reference 3.
[6] The available data are reviewed by K. K. Kelley, reference 4.
[7] E. A. Griffiths and E. Griffiths, see reference 3.
[8] H. B. Huntington, Phys. Rev. **72**, 321 (1947); J. K. Galt, Massachusetts Institute of Technology, Research Laboratory of Electronics, Tech. Report No. 45, (Sept. 17, 1947); D. Lazarus, Phys. Rev. **76**, 545 (1949); O. J. Kleppa, J. Chem. Phys. **18**, 1331 (1950).

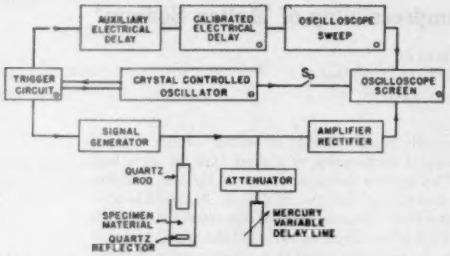

FIG. 1. Functional diagram of electro-acoustic apparatus.

cision of the method and extend its range to high temperatures.

Figure 1 is a functional diagram of the electro-acoustic apparatus. The trigger circuit supplies a 100-volt pulse of one microsecond duration at intervals of approximately one millisecond. Each pulse initiates the following events: (1) the signal generator supplies a sinusoidally varying potential difference of 12.2 megacycle frequency for a period of approximately 3 microseconds; (2) after a measurable time interval, the oscilloscope beam sweeps across the screen; (3) if the switch S is closed, a crystal controlled oscillator of 100 kilocycle frequency registers time markers on the oscilloscope sweep.

The output of the signal generator is impressed on an X-cut quartz crystal cemented to the upper end of a cylindrical rod of optical grade fused quartz, the lower end of which is immersed in the specimen material. The resulting acoustic wave train travels down the quartz rod and into the specimen, with partial reflections at the interface and at a quartz reflector accurately positioned beneath. Both reflected trains are detected by the quartz crystal, amplified, rectified and exhibited as pulses on the oscilloscope screen. The fronts of the two pulses are brought consecutively to the initial point on the sweep by manipulation of the oscilloscope sweep delay, and the associated difference in delay time is then the transit time of the disturbance in the medium. The scale of the sweep delay is calibrated with the time markers on the sweep.

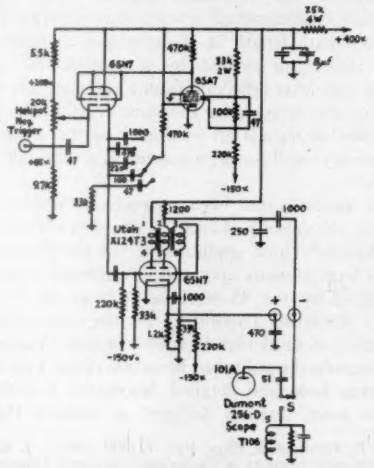

FIG. 2. The auxiliary electrical delay circuit and method for coupling it to the Dumont type 256-D oscilloscope. (After R. M. Walker.)

The transit time is approximately 40 microseconds, and the accuracy with which this can be measured is roughly the wave period, i.e., 0.1 microsecond or 0.2 percent. The consequent percent uncertainty in the measurement of the velocity is the same, but that of the temperature coefficient of the velocity is of the order 10 percent, since the total change in transit time over the temperature range here studied is only 1 microsecond. Therefore the change in the velocity with temperature is measured in the following manner.

The output of the signal generator is impressed on a second quartz crystal mounted at the bottom of a vertical column of mercury which contains a polished steel reflector. The reflector is affixed to the lower end of a spring-loaded piston, the upper end of which is in contact with a fine screw. Thus the position of the reflector, and hence the effective height of the mercury column, can be varied at will and the amount of the variation observed with precision. The length of the mercury column is first so adjusted that the second reflected wave train annuls the train received from the quartz-specimen interface. Next, this adjustment is varied until the third reflected wave train annuls that received from the reflector in the specimen. If, now, the temperature of the specimen is altered, then both these adjustments are likewise altered, the first in consequence of the change in wave velocity in the quartz rod and the second in consequence of the change in the wave velocities in both the specimen and the quartz rod. The change in transit time in the specimen, Δt, is given by the expression $\Delta t = (6\Delta L_2 - 4\Delta L_1)/V_m$, where ΔL_1 is the variation in the length of the mercury column required to annul the wave train reflected from the interface, ΔL_2 that required to annul the wave train from the reflector in the specimen, and V_m is the velocity of sound in mercury. The estimated uncertainty in the values of Δt thus obtained is 0.005 microsecond.[9]

The basic electronic equipment is the Dumont 256-D oscilloscope, in which the items marked with an O in Fig. 1 are incorporated. This instrument permits a choice of either of two values of the full scale range of the calibrated electrical delay, *viz.*, 100 microseconds or 1000 microseconds. The over-all transit time of the disturbance in the quartz rod and specimen is approximately 140 microseconds; therefore, an increase by a factor 10 in the precision of measurement is obtained

[9] This interferometric method may be contrasted with that devised by Arenberg, Massachusetts Institute of Technology Radiation Laboratory, Report No. 932.

if a fixed electrical delay of suitable magnitude is inserted in series with the calibrated electrical delay. Figure 2 is a diagram of this circuit, which was devised for the writer by Mr. Robert M. Walker of the Watson Scientific Computing Laboratory, and of the method for coupling it to the oscilloscope.

The signal generator and amplifier are essentially those described by Beers and Durand[10] and Galt,[11] respectively. Two 807 tubes are added to the signal generator to increase the output and to obtain cathode-follower coupling to the 100-ohm output cable. This unit yields the peak voltage amplitude in the first quarter cycle; the rise time of the amplifier is 0.1 microsecond.

The variable mercury delay line is mounted in a thermally insulated enclosure, the temperature of which is maintained at 40.7 ± 0.1°C. The uncertainty in temperature corresponds to an uncertainty of 0.001 microsecond in Δt.

The Vacuum Furnace

Figure 3 shows a cross section of the vacuum furnace and associated apparatus. The specimen material is contained in a thin-walled nickel crucible of 200-cc capacity, which is supported by three invar legs on the upper end of a vertical, hollow, stainless steel cylinder. This cylinder floats on a column of mercury contained in a concentric cylindrical well, and the crucible can be raised or lowered at will by altering appropriately the amount of mercury in the well.

The heating element of the furnace is a winding of No. 15 nichrome wire spaced 7 turns per inch on a cylindrical copper tube $2\frac{5}{16}$ in. i.d., $3\frac{1}{2}$ in. o.d., and 10 in. long. The winding is electrically insulated from the tube with a double layer of 5-mil mica sheets, and the turns are held in place with a thin layer of Alundum cement. The element is mounted on three legs of invar and Lavite; these rest on a platform which supports, in addition, two radiation shields, the inner of nickel and the outer of brass.

The quartz rod passes downward through a hole in the top of the brass radiation shield, at which point it is fastened to the shield with a clamp. The quartz reflector is held in position beneath the quartz rod by three clear quartz fingers 3 mm in diameter, which are fused at their upper extremities to the rod and at the lower to the reflector. The latter, constructed by fusing a quartz disk to a half-inch of tubing of the same diameter, has the shape of an inverted cup, and is surrounded by a truncated cone of thin sheet nickel with its vertex down. The cone is open at the bottom so that, as the crucible of molten sodium is raised, the unavoidable surface layer of oxide is guided into the cup and there trapped, and a fresh, clean surface of pure metal is let to form the interface between the quartz rod and the medium. (The cone is not shown in Fig. 3.)

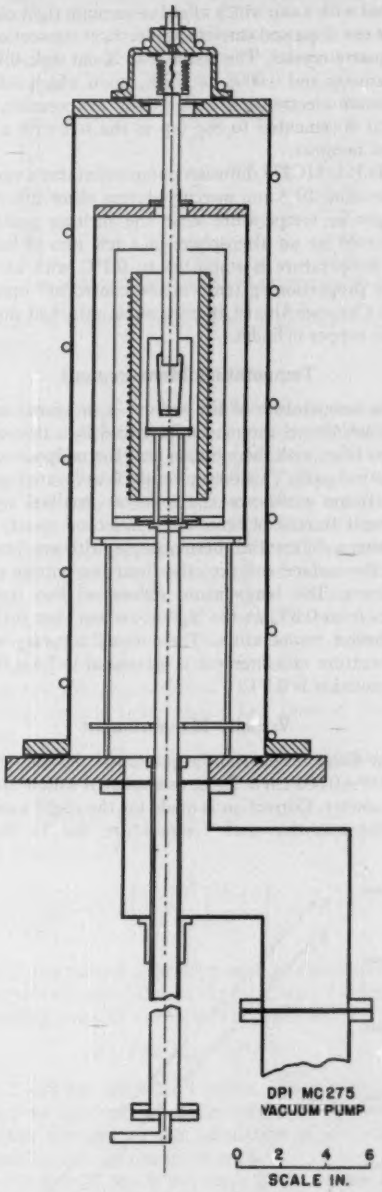

FIG. 3. The vacuum furnace.

The upper end of the quartz rod emerges from the furnace envelope through a hole in the top. The hole is

[10] Massachusetts Institute of Technology, Radiation Laboratory Series, *Vacuum Tube Amplifiers* 18, Ch. 8, Edited by G. E. Valley, Jr., and H. Wallman (McGraw-Hill Book Company, Inc., New York, 1948).

[11] J. K. Galt, see reference 8.

covered with a cap which affords a vacuum tight closure of the envelope and carries the electrical connections to the quartz crystal. The latter is an X-cut disk, 0.75 in. in diameter and 0.0098 in. thick, upon which suitable aluminum electrodes are placed by evaporation. The crystal is cemented to the top of the rod with a thin film of beeswax.

A D.P.I. MC275 diffusion pump maintains a vacuum of the order 10^{-5} mm mercury during observation, but changes in temperature near the melting point are facilitated by an atmosphere of a few mm of helium. The temperature is stabilized to 0.1°C with an electronic proportioning temperature controller[12] operated by a Chromel-Alumel thermocouple attached directly to the copper cylinder.

Temperature Measurement

The temperature of the sodium is measured with a Chromel-Alumel thermocouple placed in a thin-walled quartz tube, with the junction near the midpoint of the acoustical path. This thermocouple is calibrated against a platinum resistance thermometer certified by the National Bureau of Standards. A second quartz tube contains a differential thermocouple, with one junction near the surface and the other near the bottom of the specimen. The temperature difference thus revealed varies from 0.2°C at the highest to less than 0.1°C at the lowest temperature. The over-all accuracy of the temperature measurement is estimated to be ±0.5°C; the precision is 0.1°C.

Velocity Measurement

The distance between the quartz rod and the reflector is 5.169±0.002 cm at 25°C, as measured with a Starrett micrometer. Correction is made for the slight variation of this quantity with temperature due to thermal expansion of the quartz supporting fingers. The frequency of the crystal-controlled tuning oscillator is 100,000±40 cycles/sec, as revealed by comparison with the standard frequency broadcast by station WWV. The uncertainties in the measured values of the velocity and its temperature coefficient are estimated to be 0.2 percent and 0.5 percent, respectively.

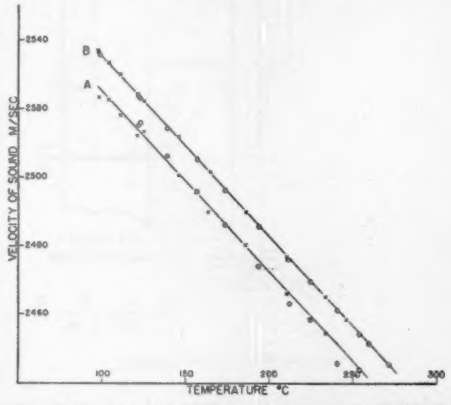

FIG. 4. Curve *A*, the velocity of sound in molten sodium at various temperatures. Curve *B*; the temperature variation of the velocity of sound; only the slope of this curve is significant.

[12] D. Lazarus and A. W. Lawson, Rev. Sci. Instr. **18**, 730 (1947).

III. SPECIMEN MATERIAL

The specimen material is Mallinckrodt analytical reagent grade sodium triply distilled in vacuum, with the rejection of the first and last quarters of the distillate in the first distillation. The still is constructed of nickel, and the final distillation leaves the material in the crucible in which the measurements are made. A lid is clamped on the crucible in an atmosphere of helium, by manipulations made outside the still, and the closed crucible is transferred to the vacuum furnace. The furnace envelope, slightly raised to permit access, is filled with helium maintained is continuous flow; the crucible lid is quickly removed in this atmosphere and the furnace is immediately closed and sealed.

Spectroscopic analysis of the material made after completion of the measurements reveals no nickel or copper, a few thousandths of one percent silicon, and a few hundredths of one percent aluminum and calcium. The analysis of a singly distilled specimen is the same, except for the presence of a few hundredths percent copper. Measurements of the velocity of sound made upon the singly distilled specimen are indistiguishable from those made upon the triply distilled specimen.

IV. RESULTS

The present experimental method yields a precise determination of the freezing point of sodium at zero pressure. The thermal insulation provided by the vacuum in such that the temperature and the velocity of sound in the molten material remain constant for half an hour while solidification proceeds from the outside toward the axis of the crucible. Toward the end of this period the disturbance reflected in the medium disappears quickly. The freezing point of sodium at zero pressure is found to be 97.6°C, with an accuracy which is probably better than 0.1°C because this temperature is proximal to the thermocouple calibration point at the steam temperature.

The observed values of the velocity of sound at various temperatures are plotted on Curve *A* of Fig. 4. Curve *B* shows the temperature variation of this quantity, as measured with the interferometer. The ordinates of this curve are displaced by an arbitrary constant amount with respect to those of Curve *A*; only the *slope* of the curve is significant. Circles indicate measurements made on heating the specimen, and crosses measurements made on subsequent cooling. It will be noted (Curve *B*) that, over the interval here investigated, the velocity of sound varies linearly with the

temperature. The value of the temperature coefficient is -52.4 ± 0.3 cm/sec °C.

Curve A is the straight line which has the same slope as the line B and which, subject to this condition, best represents the plotted points. Observations at lower temperatures are given greater weight than those at higher temperatures in the placement of this line, because the front of the reflected pulse loses its sharpness somewhat as the material is heated. The ordinate of the line A at the temperature 97.6°C is the value of the velocity of sound at the freezing point, *viz.*, 252,600 $\pm$500 cm/sec.

A careful review of the work of numerous investigators indicates that the following are the best available values of the remaining physical constants of liquid sodium which appear in the formulas (1) and (2) above: density at the melting point = 0.930 g/cc;[13] coefficient of volume expansion $=2.78\times10^{-4}$/°C;[14] specific heat at constant pressure = 7.5 cal/mole °C, with an accuracy of about 2 percent between 98°C and 178°C.[6] Corresponding values of the adiabatic and isothermal compressibilities of liquid sodium at various temperatures are given in Table I.

It is significant that no change in the temperature coefficient of velocity is detected in the neighborhood of the freezing point. The velocity of a compressional wave in an isotropic medium is given by the expression,

$$V^2=\left(\frac{1}{\kappa}+\frac{4}{3}\mu\right)\Big/\rho,$$

in which μ is the rigidity modulus of the medium. Accordingly, the constancy of the temperature coefficient of V implies that either μ is zero in the liquid at the melting point and above, or the temperature coefficient of μ/ρ is constant over the temperature range here investigated. The former conclusion is the more plausible. It is supported by the concordance, noted below, of data which relate the change of compressibility on freezing to other measurable quantities, and further by the initial results of a detailed study, now in progress, of the rigidity of both solid and liquid sodium in the immediate neighborhood of the freezing point.

O. J. Kleppa measured the velocity of sound in liquid sodium at the melting point by an acoustical method similar in principle to that here described.[8] He obtained the value 2395 m/sec, which is to be compared with the figure 2526 m/sec given above. A possible source of the discrepancy is the lack of purity of Kleppa's specimen material. The latter contained over one percent solid impurity by chemical analysis, and a considerable volume of occluded gas as well. It was not predistilled and the measurements were made with the specimen, protected by a layer of mineral oil, in an atmosphere of nitrogen.

TABLE I. The adiabatic and isothermal compressibilities of liquid sodium. The number of significant figures does not indicate the accuracy of the absolute value.

Temperature, C	$\kappa_S\times10^{12}$ cgs	$\kappa_T\times10^{12}$ cgs
97.6	16.85	19.11
100	16.88	19.16
120	17.11	19.49
140	17.35	19.85
160	17.59	20.19
180	17.84	20.55
200	18.09	20.89
220	18.34	21.26
240	18.60	21.61
260	18.86	21.98
272	19.02	22.19

V. DISCUSSION

The present experimental method cannot be used to measure the compressibility of polycrystalline solid sodium because, first, sodium crystals are highly anisotropic, and second, it is not possible to prepare a specimen in which the linear dimensions of the crystals are small compared with the 0.3 mm acoustic wavelength. Thus, all attempts to transmit a train of compressional waves through as little as $\frac{1}{2}$ inch of polycrystalline material have been unsuccessful. The alternative is to compute the results of acoustic measurements on large single crystals. This work is now in progress. Pending a successful outcome, the compressibility of the solid and its temperature coefficient can be evaluated with the foregoing and other elastic and thermal data as follows.

Let p denote the pressure, v the specific volume, and T the temperature; then

$$dv/dp=[\partial v/\partial T]_p dT/dp+[\partial v/\partial p]_T,$$

and it follows that[15]

$$\frac{d}{dp}(v'-v'')=\left[\frac{\beta'}{\rho'}-\frac{\beta''}{\rho''}\right]\frac{dT_m}{dp}-\left[\frac{\kappa'}{\rho'}-\frac{\kappa''}{\rho''}\right], \qquad (4)$$

in which the primed quantities refer to the liquid, the double primed quantities to the solid, and T_m denotes the melting point of the solid. Furthermore,

$$dT_m/dp=T_m(v'-v'')/L, \qquad (5)$$

where L denotes the heat of fusion. The following are adopted as the best available values of the several quantities essential to the calculation of κ''; all are expressed in the cgs system of units.

$L=114.3\times10^7$; this is the mean of the values 113.7×10^7 obtained by Rengade[4] and 115.0×10^7 by E. Griffiths.[4] $(v'-v'')=0.02640$.[3] $\beta''=2.34\times10^{-4}$; this is the mean of the values 2.46×10^{-4} given by Hagen[3] and 2.22×10^{-4} by the Griffiths.[3] (It may be noted that

[13] E. A. and E. Griffiths, and E. Hagen, reference 3. See also, however, Hackspill, Compt. rend. 152, 259 (1911), who reported the value 0.9385 but who found the freezing point of his material to be 96.5°C.

[14] Reference 13 and E. Rinck, Ann. chim. et Phys. 18, 395 (1932).

[15] P. W. Bridgman, Phys. Rev. 6, 32 (1915).

Hagen's expansion curve between 273°K and 360°K is a smooth continuation of that between 80°K and 290°K published by Siegel and Quimby.)[3] $\rho''=0.954$.[16] $d(v'-v'')/dp=-2.58\times10^{-12}$; this is the slope at zero pressure of a cubic curve which represents at pressures 1, 1000, 2000, 3000 kg/cm² the values of $(v'-v'')$ observed by Bridgman.[15] The corresponding value of the isothermal compressibility of solid sodium at the melting point is 16.68×10^{-12} cgs.

The isothermal compressibility of polycrystalline sodium at 298°K in the pressure range 100 to 500 kg/cm² has been measured directly by Richards, Hall, and Mair,[17] who observed no significant variation of compressibility with pressure in this interval and obtained the value $\kappa_T=15.6\times10^{-12}$ cgs. Now there is good reason to believe that the temperature coefficient of the isothermal compressibility of sodium does not depend upon the temperature. Thus Quimby and Siegel[1] noted that κ_T at zero pressure varies linearly with the temperature between 80°K and 210°K, and Bridgman[18] observed that, within the uncertainty of his measurements, the same is true of κ_T at 5000 kg/cm² pressure between 273°K and the melting point. In accordance with this assumption and aforementioned values of κ_T at 371°K and 298°K, the temperature coefficient of the isothermal compressibility at zero pressure is 0.015×10^{-12} cgs.

Bridgman's observations at high pressures, cited in the preceding paragraph, can be extrapolated to yield the compressibility at zero pressure provided the coefficient of thermal expansion at zero pressure is known. The temperature coefficient of compressibility obtained in this manner is likewise 0.015×10^{-12} cgs when the mean value of β at zero pressure over the temperature range is assumed to be 2.21×10^{-4}, the value reported by Hagen[3] and the Griffiths.[3,19] The temperature coefficient given by Quimby and Siegel[1] is 0.017×10^{-12} cgs. Since that of the liquid is 0.017×10^{-12} cgs, it thus appears that the temperature coefficient of the isothermal compressibility of sodium is almost constant over the temperature range 80°K to 545°K.

The value of the adiabatic compressibility of the solid at the melting point, computed with Eq. (2) and the value $c_p=1.27\times10^7$ cgs,[20] is 15.01×10^{-12} cgs. The specific heats at constant volume computed (Eq. (3)) with the foregoing values of c_p and the compressibilities are c_v(solid) = 6.30 cal/mole°C and c_v(liquid) = 6.61 cal/mole °C.

The compressibility of a solid or liquid may be regarded as composed of a part which depends simply upon the average intermolecular distance and a part which depends upon any existing regularity in the molecular configuration.[21] It can be argued on the basis of the foregoing data that in sodium the first of these contributions is preponderant. Bridgman's observations[18] yield the pressure-volume curve of the solid material at the melting point, and the slope of this curve the compressibility. The curve may be extrapolated into the region of negative pressure to the point at which the specific volume of the solid, and hence the average interatomic distance, is the same as that of the liquid at the same temperature. If, now, the compressibility is determined principally by the interatomic distance, then the compressibility of the solid computed from the slope of the curve at this point must be nearly the same as the observed compressibility of the liquid. The former is, in fact, 18.9×10^{-12} cgs, while the latter is 19.1×10^{-12} cgs. The closeness of the agreement must be regarded as fortuitous, since the accuracy of the extrapolation does not warrant it.[19]

In conclusion, the writer gratefully acknowledges his indebtedness to Mr. A. W. Costello, of the Columbia University Radiation Laboratory, for his assistance in calibrating the oscilloscope crystal; to Mr. R. M. Walker, of the Watson Scientific Computing Laboratory, for the delay circuit shown in Fig. 2; to Dr. T. I. Taylor, of the Chemistry Department at Columbia University, for the spectroscopic analysis of the sodium; and to Dr. S. L. Quimby, who suggested the research and followed its progress with helpful counsel and encouragement.

[16] Both Hagen and the Griffiths obtained this figure. See reference 3.

[17] Richards, Hall, and Mair, J. Am. Chem. Soc. **50**, 3304 (1928).

[18] See reference 2a.

[19] The compressibility at 25°C and zero pressure obtained by this extrapolation is 16.5×10^{-12} cgs, which is to be compared with the measured value, 15.6×10^{-12} cgs.

[20] K. K. Kelley, reference 4.

[21] J. Frenkel, *Kinetic Theory of Liquids* (Oxford University Press, London, 1946), p. 171.

Microwave Determination of the Probability of Collision of Slow Electrons in Gases*

ARTHUR V. PHELPS, O. T. FUNDINGSLAND,† AND SANBORN C. BROWN
Research Laboratory of Electronics, Massachusetts Institute of Technology, Cambridge, Massachusetts

(Received July 23, 1951)

A microwave method is given for determining the collision probability for momentum transfer for electrons in thermal equilibrium with a gas. An integral equation is developed which gives the ratio of the resistive and reactive components of the microwave conductivity in terms of the collision frequency for electrons with the gas atoms. Two approximate solutions are given for the collision frequency as a function of electron energy. An experimental procedure is described in which the conductivity ratio is determined from the shift in the resonant frequency and the change in conductance of a resonant cavity. Measurements are made during the decay of a pulsed discharge after the electrons have cooled to the gas temperature. Preliminary results are given for several gases.

I. INTRODUCTION

EXPERIMENTAL determinations of the probability of elastic collision between electrons and gas atoms obtained by electron beam methods show wide discrepancies for electron energies below about one electron volt. Recently several attempts have been made to obtain a better understanding of the low energy region. Huxley and Zaazou[1] used measurements of the average energy and drift velocity of electrons in a dc field to calculate the electron mean free path for average energies down to about one-third of an electron volt. They carried out their calculations for the assumption of a constant collision probability, using both a Maxwell and a Druyvesteyn electron energy distribution function. Margenau and Adler[2] have used microwave measurements of the high frequency conductivity of the positive column in a mercury discharge to evaluate the mean free path for average electron energies between about 0.6 and 1.1 volts. These authors restricted their discussion to a maxwellian electron energy distribution function but treated both the cases of constant collision probability and of constant collision frequency. In this paper a microwave method is described for determining the probability of collision by measuring the conductivity of a decaying plasma after the electrons reach thermal equilibrium with the gas.

II. THEORY OF THE METHOD

Margenau[3] has given a general theory for the behavior of electrons in a gas under the action of a high frequency electric field when only elastic collisions need be considered. From his results we may write for the complex conductivity, σ_c:

$$\sigma_c=\sigma_r+j\sigma_i=\frac{J}{E}=-\frac{4\pi}{3}\frac{ne^2}{m\omega}\int_0^\infty\frac{[(\nu_c/\omega)-j]}{1+(\nu_c/\omega)^2}v^3\frac{\partial f_0}{\partial v}dv. \quad (1)$$

Here n is the electron density, e and m are the electronic charge and mass, ω is the radian frequency of the applied field, f_0 is the first term in the spherical harmonic expansion of the normalized electron velocity distribution function and ν_c is the collision frequency for momentum transfer for electrons of velocity v colliding with neutral atoms. The "probability of collision for momentum transfer," P_c, is related to the collision frequency by $\nu_c=v/l=vp_0P_c$, where l is the mean free path and p_0 is the pressure normalized to zero degrees centigrade. The momentum transfer collision probability[4] takes into account the fact that the effectiveness of collisions in resisting current flow increases as the scattering angle increases. The electron beam type of experiment determines a "total" collision probability,[5] since electrons are lost to the beam if they suffer any angular deflection greater than the angular aperture of the detector. The values of P_c calculated from measurements of the distribution in angle of the scattered electrons usually differ from the "total" collision probabilities by a few percent.

When the electron velocity distribution function is known, the collision frequency can be determined from the ratio of the real to the imaginary part of the conductivity. Thus

$$\frac{\sigma_r}{\sigma_i}=-\int_0^\infty\frac{(\nu_c/\omega)v^3df_0}{1+(\nu_c/\omega)^2}\Big/\int_0^\infty\frac{v^3df_0}{1+(\nu_c/\omega)^2}, \quad (2)$$

is an equation in which the conductivity ratio, σ_r/σ_i, is a function of the parameters describing f_0 and ν_c/ω and is to be solved for ν_c as a function of the electron velocity. Note that by expressing the theory in terms of the conductivity ratio we have eliminated the necessity for knowing the electron density.

Margenau[3] showed that the steady-state distribution function for electrons in an atomic gas in the absence of inelastic collisions and large diffusion loss could be

* This work has been supported in part by the Signal Corps, Air Materiel Command, and ONR.

† On leave from the Geophysical Research Directorate, Air Force Cambridge Research Laboratories, Cambridge, Massachusetts.

[1] L. G. H. Huxley and A. A. Zaazou, Proc. Roy. Soc. (London), A196, 402 (1949).

[2] H. Margenau and F. P. Adler, Phys. Rev. 79, 970 (1950).

[3] H. Margenau, Phys. Rev. 69, 508 (1946).

[4] E. H. Kennard, *Kinetic Theory of Gases* (McGraw-Hill Book Company, Inc., New York, 1942), Chapters III and IV.

[5] R. B. Brode, Revs. Modern Phys. 5, 257 (1933).

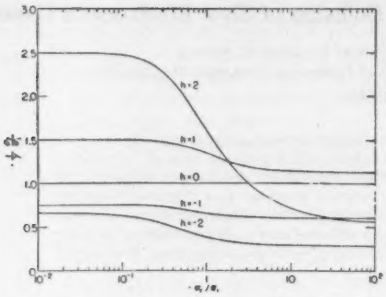

FIG. 1. Theoretical curves of $\sigma_r/\gamma\sigma_i$ as a function of σ_r/σ_i.

given as

$$\ln f_0 = -\int_0^u \{kT_g/e + MeE^2/(3m^2\omega^2[1+(\nu_c/\omega)^2])\}^{-1}du. \tag{3}$$

Here u is the electron energy expressed in volts, T_g is the temperature of the gas atoms of mass M, and E is the rms value of the applied electric field. For low pressures ($\nu_c^2 \ll \omega^2$) the distribution is nearly maxwellian with an energy $\langle u\rangle = (kT_g/e + MeE^2/3m^2\omega^2)$. At low fields $\langle u\rangle = kT_g/e$. Writing the maxwellian energy distribution as $f_0 = A\exp(-u/\langle u\rangle)$, Eq. (2) becomes

$$\frac{\sigma_r}{\sigma_i} = -\int_0^\infty \frac{(\nu_c/\omega)u^{1.5}\exp(-u/\langle u\rangle)du}{(\nu_c/\omega)^2+1} \Bigg/ \int_0^\infty \frac{u^{1.5}\exp(-u/\langle u\rangle)du}{(\nu_c/\omega)^2+1}, \tag{4}$$

We will present two approximate solutions of Eq. (4) for the collision frequency, ν_c. A low field approximation, restricted to electrons in thermal equilibrium with the gas and to a simple velocity dependence for ν_c, is valid over the whole range of ν_c/ω. A low pressure approximation is given in which the only restriction placed on ν_c is that $(\nu_c/\omega)^2 \ll 1$.

Low Field Approximation

To obtain $\nu_c(u)$ one can assume that ν_c is proportional to some power of the electron velocity and evaluate the proportionality constant and exponent by fitting experimental measurements of σ_r/σ_i to the theoretical curves calculated from Eq. (4). Thus if $\nu_c = ap_0v^h$, $P_c = av^{h-1}$ and Eq. (4) becomes

$$\frac{\sigma_r}{\sigma_i}(\gamma, h) = -\gamma\int_0^\infty \frac{y^{0.5H+1.5}\exp(-y)dy}{y^h+\gamma^{-2}} \Bigg/ \int_0^\infty \frac{y^{1.5}\exp(-y)dy}{y^h+\gamma^{-2}}, \tag{5}$$

where $\gamma = (2e\langle u\rangle/m)^{0.5h}ap_0/\omega = (2kT_g/m)^{0.5h}ap_0/\omega$ is the number of collisions per radian of the electric field for electrons having a velocity equal to the most probable velocity of the distribution function, and $y = (u/\langle u\rangle)$.

For the case of constant collision frequency, $h=0$ and Eq. (5) reduces to $\sigma_r/\sigma_i = -\nu_c/\omega$. The constant mean free path case, for which $h=+1$, has been evaluated by Margenau[3] in terms of error functions and exponential integrals. We have evaluated the integrals for $h=+2$ in terms of Lommel functions and for $h=-1$ and -2 in terms of the solutions for $h=+1$ and $+2$. Figure 1 shows the results of these calculations in the form of $\sigma_r/\gamma\sigma_i$ as a function of σ_r/σ_i for various values of "h".

There are two experimentally convenient means for determining the two parameters "h" and "a" for this approximation. In one procedure the gas pressure p_0 is varied at constant frequency and temperature to obtain a curve of $\sigma_r/p_0\sigma_i$ *versus* σ_r/σ_i covering a range of values of σ_r/σ_i near unity. The value of γ/p_0 is adjusted to give the best fit between the experimental points and the theoretical curve for some value of "h". When ambiguity exists in the sign of "h", the gas temperature or the electric field can be used to raise the average electron energy and to determine whether σ_r/σ_i, and, therefore γ, increases or decreases. Another procedure is to make measurements of σ_r/σ_i as a function of pressure at two different gas temperatures. The pressure and temperature readings which give the same value of σ_r/σ_i, and therefore γ, fix a value of "h". The coefficient "a" can then be determined from the theoretical curves of σ_r/σ_i *versus* γ. The disadvantage of this approximation is that a single set of values for "a" and "h" may not fit the experimental data over a wide range of electron energies.

Low Pressure Approximation

Another means of determining $\nu_c(u)$ is to measure σ_r/σ_i at low enough pressures so that $(\nu_c/\omega)^2 \ll 1$ over the velocity range in which the distribution function, f_0, is significant. Equation (4) then reduces to

$$\sigma_r(\langle u\rangle)/\sigma_i = -[4/(3\pi^{\frac{1}{2}}\langle u\rangle^{2.5})] \times \int_0^\infty (\nu_c/\omega)u^{1.5}\exp(-u/\langle u\rangle)du. \tag{6}$$

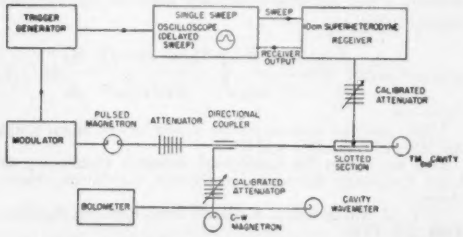

FIG. 2. Block diagram of apparatus used to measure the conductivity ratio.

This integral equation of the first kind can be solved approximately[6] by representing the experimental data for σ_r/σ_i by a polynomial of the form,

$$\sigma_r(\langle u\rangle)/\sigma_i = -\sum_{i\geq -3}^{l} a_i(\langle u\rangle^{0.5})^i p_0. \tag{7}$$

Multiplying Eqs. (6) and (7) by $\langle u\rangle^{2.5}$, and performing an inverse laplace transformation, we get

$$\nu_c(u)/p_0\omega = \sum_{i\geq -3}^{l} \frac{a_i(u^{0.5})^i}{[(j+3)/2]!}(3/2)! \tag{8}$$

and

$$P_c = \omega(m/2e)^{\frac{1}{2}} \sum_{i\geq -3}^{l} \frac{a_i(u^{0.5})^{i-1}}{[(j+3)/2]!}(3/2)!. \tag{9}$$

Thus the a_i's determined from the experimental curve of $\sigma_r/\sigma_i p_0$ can be used in Eqs. (8) and (9) to give curves of ν_c/p_0 and P_c as functions of electron energy.

III. EXPERIMENT

The normalized input impedance of a microwave resonant cavity can be written as[7,8]

$$z = z_s + \frac{1/\beta}{1/Q_a + j(\omega/\omega_a - \omega_a/\omega) + (1/\epsilon_0\omega)\int_V \mathbf{J}\cdot\mathbf{E}_a dv \Big/ \int_V \mathbf{E}\cdot\mathbf{E}_a dv}. \tag{10}$$

Here z_s is a series impedance including the losses in the coupling loops and the effects of resonant modes other than the dominant one. The coefficient β describes the degree of coupling between the transmission line and the fields of the dominant mode of the resonant cavity.

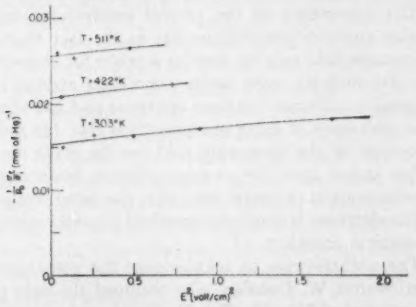

FIG. 3. Measured values of $\langle\sigma_r\rangle/p_0\langle\sigma_i\rangle$ as a function of the square of the electric field at three different gas temperatures for electrons in nitrogen.

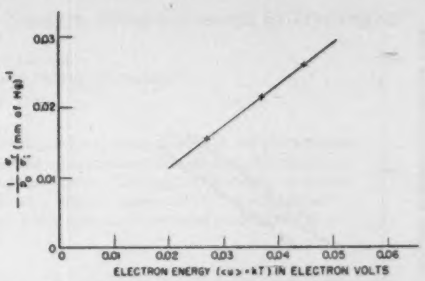

FIG. 4. Zero field value of the conductivity ratio, σ_r/σ_i, as a function of the electron energy.

Q_a and ω_a are the Q and resonant frequency of the cavity, ϵ_0 the permittivity of free space, $\mathbf{J}$ and $\mathbf{E}$ are the electron current and perturbed electric field in the cavity, and $\mathbf{E}_a$ is the electric field associated with the dominant mode. The magnitude of the electron current, J, is assumed small compared to the magnitude of the displacement current, $\omega\epsilon_0 E$, so that the electric field, $\mathbf{E}$, is very nearly equal to that of the dominant mode, $\mathbf{E}_a$.

Equation (10) shows that the effect of an electron current can be determined by measuring the change in resonant frequency and the change in conductance of a cavity at resonance. Substituting in Eq. (10) the definition of $\mathbf{J}=(\sigma_r+j\sigma_i)\mathbf{E}$, the change in resonant frequency is given by

$$\frac{2\Delta\omega}{\omega_a} = -\frac{1}{\epsilon_0\omega}\int_V \sigma_i E^2 dv \Big/ \int_V E^2 dv.$$

The change in cavity conductance from that of the empty cavity is given by

$$\Delta g \equiv \Delta(\beta/Q_a) = (\beta/\epsilon_0\omega)\int_V \sigma_r E^2 dv \Big/ \int_V E^2 dv,$$

so that we may write

$$\omega\Delta g/2\beta\Delta\omega = \int_V \sigma_r E^2 dv \Big/ \int_V \sigma_i E^2 dv = \langle\sigma_r\rangle/\langle\sigma_i\rangle. \tag{11}$$

In general σ_r and σ_i are functions of the electric field. Complications in the solution arising from non-uniformity in the electric field of the cavity are avoided by restricting the discussion to the zero-field values of σ_r/σ_i. These are obtained in practice by extrapolating the measured values of $\langle\sigma_r\rangle/\langle\sigma_i\rangle$ to zero electric field.

Measurement of the change in cavity conductance rather than the width of the resonance curve avoids the problem of changes in the electric field and in conductivity ratio occurring as the cavity impedance changes with the frequency. The electric field is determined in essentially the same manner as for breakdown measurements.[8] The coupling coefficient β is measured on the empty cavity.

[6] R. D. Crout, J. Math. Phys. **19**, 34 (1940).
[7] J. C. Slater, *Microwave Electronics* (D. Van Nostrand Company, New York, 1950), Chapter V.
[8] S. C. Brown *et al.*, "Methods of measuring properties of ionized gases at microwave frequencies," Technical Report No. 66, Research Laboratory of Electronics, Massachusetts Institute of Technology, Cambridge, Massachusetts.

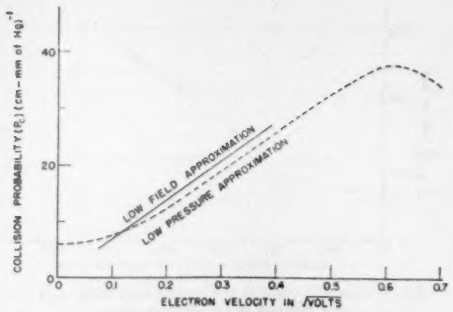

FIG. 5. Calculated values of the probability of collision for themal electrons in nitrogen.

The time required for the electrons to cool from the high average energies during the discharge to the temperature of the gas by loss of energy through elastic collisions can be estimated from average electron considerations. The rate of this energy loss is equal to the product of the fractional energy loss per collision, which is assumed to be $2m/M$ for monatomic gases; the average excess energy, $u-kT_g/e$; and the collision frequency,

$$du/dt=-(2m/M)(u-kT_g/e)\nu_c. \tag{12}$$

If the collision frequency is independent of the electron velocity, the time constant for the energy decay is $M/2m\nu_c$. As an example of the times involved, the time required for electrons in helium to cool to within 10 percent of thermal energies is about $90/p_0$ microseconds. Conductivity measurements were made at post-discharge times varying from about 0.2 millisecond in H_2 to 10 milliseconds in He.

A block diagram of the apparatus used to measure the conductivity ratio is shown in Fig. 2. A 10-cm pulsed magnetron is used to break down the gas periodically and provide a plasma of electrons whose conductivity is measured. The gas is contained in a resonant cavity operating in the TM_{010} mode. The change in the cavity impedance due to the electrons is measured by using a continuous wave tunable magnetron and a standing wave detector which is sensitive only for a period of a few microseconds during the afterglow. The transient standing wave detector[8] consists of a calibrated wave guide-beyond-cut-off attenuator followed by a superheterodyne receiver whose local oscillator frequency is controlled by a delayed sweep from a single sweep oscilloscope. The output of the receiver is observed on the single sweep oscilloscope and the standing wave ratio is determined by adjusting the calibrated attenuator to maintain constant amplitude at the output of the receiver. The delay circuit for the single sweep oscilloscope and the modulator for the pulsed magnetron are synchronized by a trigger generator operating at 60 cps. The output of the continuous wave magnetron is monitored with a cavity wavemeter and a bolometer. The power incident on the cavity is controlled by a calibrated variable attenuator.

IV. CONCLUSION

To illustrate the methods already discussed, we give preliminary results obtained from the microwave measurements of the conductivity of thermal electrons in nitrogen. Figure 3 shows measured values of $\langle\sigma_r\rangle/p_0\langle\sigma_i\rangle$ as a function of the square of the electric field in a cavity at three different gas temperatures. The zero field values of $\sigma_r/p_0\sigma_i$ from Fig. 3 are plotted as a function of the electron energy, $\langle u\rangle$, in Fig. 4. Since the conductivity ratios for these data were of the order of -0.1, $(\nu_c/\omega)^2\sim 0.01$ and the data may be analyzed using either the low pressure approximation or the low field approximation. The experimental points lie on a straight line through the origin and, over the range of velocities in which the distribution function is significant, both solutions give the same values of P_c to within the experimental error. These results are shown in Fig. 5 where the low field approximation gives $h=2$ and $P_c=70\sqrt{u}$. The low pressure approximation gives $P_c=6.0+160u-220u^2$ for $j=1$, 3, and 5.

Preliminary microwave measurements of the collision probability for electrons having a mean energy of 0.039 ev yield the following results for P_c at 1 mm of Hg pressure in units of cm^2/cm^3: He, 19; Ne, 3.3; A, 2.1; Kr, 54; Xe, 180; H_2, 46; and N_2, 15. The P_c values obtained for He, Ne and A are in good agreement with the theoretical calculations by Allis and Morse.[9]

The importance of the present method for determining collision probabilities lies in the fact that the microwave field may be used as a probe for measuring the conductivity ratio under conditions approaching thermal equilibrium between electrons and gas atoms. The advantage of using microwaves is that the radian frequency of the measuring field can be made appreciably larger than the average collision frequency of the electrons at pressures such that the mean free path of the electrons is small compared to the dimensions of a practical container.

The authors wish to acknowledge the assistance of Mrs. Norma W. Donelan, who obtained the data presented, and of Miss Hsi-Teh Hsieh, who calculated the conductivity integrals.

[9] W. P. Allis and P. M. Morse, Z. Physik **70**, 567 (1931).

Electron Recombination and Collision Cross-Section Measurements in Hydrogen*

LAWRENCE J. VARNERIN, JR.
Sylvania Electric Products, Incorporated, Boston, Massachusetts
(Received July 23, 1951)

Electron densities and mean collision cross sections are deduced from measurements of the propagation constant for microwaves in a plasma. From the electron collision cross-section measurements, inferences are drawn concerning the slope of the cross-section electron velocity curve. The measurements are compared with those made by electron beam techniques. From the electron density measurements the recombination coefficient of hydrogen as a function of pressure is obtained. These data are interpreted on the basis of dissociative and ion-ion recombination.

I. INTRODUCTION

THE measurement of the decay of electron density in a plasma has been made possible by the use of microwave techniques. Biondi and Brown[1,2] were able to identify both recombination and diffusion modes of decay. Their method was based on a measurement of the shift in resonant frequency of a microwave cavity containing a decaying plasma. This method, which initially determined only the inductive loading of the cavity by electrons and not the resistive component, has been extended by Phelps, Fundingsland, and Brown[3] in the preceding paper to measure the resistive component. The resistive component is of primary importance in determining the collision cross section of electrons with gas molecules. These methods employed resonant devices. The method to be discussed here involves no resonant structures and depends on the propagation constant of microwaves in a section of rectangular wave guide containing the plasma.

II. METHOD

A plasma is established by a one-microsecond rf magnetron pulse in a section of 10-cm band wave guide as shown in Fig. 1. The discharge tube is electrically one-half wavelength long with a quarter wavelength block of quartz against the shorted end of the wave guide. The gas is confined in a quarter wavelength section of guide. The quartz block is used to prevent ionization in that section of the tube. In a tube without a quartz block, relatively little ionization occurs in the $\lambda_g/4$ section nearest the shorted end of the wave guide because the voltage standing wave is low there. The vacuum seal is made with a glass window sealed to a Kovar frame. The metal parts of the tube are made of silver-plated Kovar joined by means of high temperature brazing alloys.

During the decay period, the plasma will rapidly tend to uniformity if the dominant electron loss mechanism is that of recombination. This results from the fact that the rate of electron loss is proportional to the square of the density, so that local high concentrations are more rapidly recombined.

A glass three-stage oil diffusion pump was used with the vacuum system. Only metal stopcocks were used. A mercury manometer and McLeod gauge were used to measure pressure. The tube was isolated from the mercury by a single liquid air trap during bakeout and by a second trap during measurement. Hydrogen obtained through a palladium leak was used for study.

Measurements are made during the plasma decay period after the electrons have come to thermal equilibrium with the gas. By means of a weak rf probing signal, measurements of voltage standing wave ratio and phase are made in the line as a function of time. The method of transient standing wave measurements is essentially the same as that of reference 3. With these measurements, the transmission line equations can be used to determine the characteristic impedance of the gas tube at the gas-glass window boundary looking into the tube.

The impedance of the measuring tube normalized with respect to the empty guide impedance at the gas-glass window boundary is given by

$$z = j(2\pi/k\lambda_g)\,\mathrm{ctnh}(k\lambda_g/4), \tag{1}$$

where k is the propagation coefficient of the gas section and λ_g is the guided wavelength of the empty guide. k is given by

$$k = (2\pi/\lambda_g)[-1 + j(\sigma_c/\omega\epsilon_0)(\lambda_g/\lambda_0)^2]^{\frac{1}{2}}, \tag{2}$$

where σ_c is the complex conductivity of the plasma, ω the radian frequency of the electric field, and ϵ_0 the permittivity of free space.

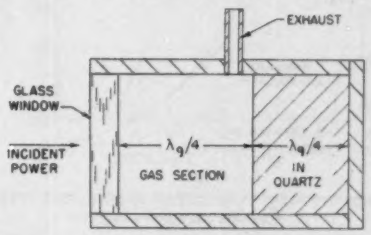

FIG. 1. Measuring tube.

* This research was sponsored by the Signal Corps Engineering Laboratories, Fort Monmouth, New Jersey.

[1] M. A. Biondi and S. C. Brown, Phys. Rev. **75**, 1700 (1949).
[2] M. A. Biondi and S. C. Brown, Phys. Rev. **76**, 1697 (1949).
[3] Phelps, Fundingsland, and Brown, Phys. Rev. **84**, 559 (1951).

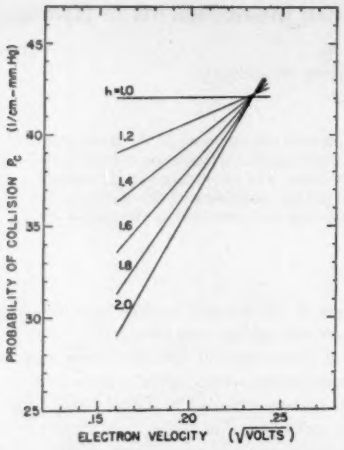

FIG. 2. Probability of collision as a function of electron velocity.

The complex conductivity, σ_c, can be determined experimentally as a function of time from the type of experiment described above and the use of Eqs. (1) and (2). Basically the absolute magnitude of σ_c and the ratio of real to imaginary parts σ_r/σ_i are determined.

III. ANALYSIS OF COLLISION CROSS-SECTION DATA

Measurements of σ_r/σ_i as a function of pressure were made for different pressures in the range 1.5 to 50 mm Hg. From the theory of reference 3, P_c can be represented by

$$P_c = av^{h-1}. \tag{3}$$

If a value of h is assumed, a value of a can be calculated for which the theory best represents the data. In Fig. 2, a tentative set of curves for $P_c(v)$ is obtained. It is noted that all curves agree in the neighborhood of 0.233 (volt)$^{\frac{1}{2}}$, and it is therefore believed that the experiments give the value of $P_c=42$ at 0.233 (volt)$^{\frac{1}{2}}$ with an accuracy of about 5 percent.

Phelps, Fundingsland, and Brown calculate the quantity

$$(ap_0/\omega)(\sigma_i/\sigma_r)(2kT/m)^{h/2},$$

as a function of σ_r/σ_i, on the assumption embodied in Eq. (3). Multiplying the foregoing by experimental values of $\sigma_r/p_0\sigma_i$, one should obtain a quantity,

$$(a/\omega)(2kT/m)^{h/2},$$

which is independent of σ_r/σ_i if the correct function for $P_c(v)$ has been assumed. Choosing the value of h which renders the product most nearly constant will give the best representation of P_c as a power of electron velocity. This yields a value of $h=1.6$.

The scatter in experimental data introduces an uncertainty of about 0.2 in h, while a pressure dependent systematic error might contribute again as much uncertainty. It is reasonably well established that $h>1.0$. This means that the P_c *versus* electron velocity curve has a positive slope.

Experimental values of P_c are plotted as a function of electron velocity in Fig. 3. The data of Normand,[4] Brüche,[5] and Ramsauer and Kollath[6] are shown. At velocities less than 1 (volt)$^{\frac{1}{2}}$, Normand's results differ markedly from those of the other investigators. Brüche and Ramsauer and Kollath are in substantial agreement.

Part of the information obtained by the present technique is given as a point established at 0.233 (volt)$^{\frac{1}{2}}$. While the slope of the curve passing through this point is not definitely established, a positive slope is fairly certain. Thus, the present measurement lends support to Ramsauer and Kollath. The nearly perfect agreement in magnitude is somewhat illusory in view of the slightly different nature of the cross section measured.[3]

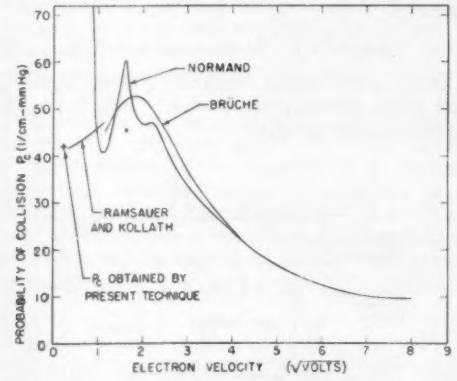

FIG. 3. Comparison of probability of collision as a function of electron velocity with data of other workers.

IV. RECOMBINATION MEASUREMENTS IN HYDROGEN

The present technique has been used to study recombination phenomena in hydrogen. After the electrons have had sufficient time to come to thermal equilibrium with the gas, Biondi and Brown[2] found that the only mode of electron density decay that could explain the experimental results was that of recombination. This is recognized by the fact that a reciprocal density plot as a function of time is a straight line.

Data obtained by the present technique for hydrogen at room temperature are given in Fig. 4. The range of electron densities varied from 1×10^9 to 2×10^{10} electrons/cm^3. The theory of reference 3 for $h=1.0$ was used in calculating densities. The density so determined is relatively insensitive to the choice of h. Previous data by Biondi and Brown[2] are shown in the low pressure range. The low pressure part of the curve is extremely

[4] C. E. Normand, Phys. Rev. **35**, 1217 (1930).
[5] E. Brüche, Ann. Physik **82**, 912 (1927).
[6] C. Ramsauer and R. Kollath, Ann. Physik **4**, 91 (1929).

sensitive to minute traces of impurities. Repeated bakeouts succeeded in lowering the curve somewhat with each bakeout. The tube and vacuum system were baked for one week at 330°C before taking data. After this a bakeout for four days at 340°C effected no change in the general form of the curve. Biondi and Brown used spectroscopically pure hydrogen while palladium purified hydrogen has been used in the present investigation. It is possible that the different results can be explained on this basis. Richardson and Holt[7] reported a value of α of 2×10^{-6} cm³/electron-sec from 1 to 3 mm Hg, rising to 6.2×10^{-6} cm³/electron-sec at 7 mm Hg, remaining essentially constant to a pressure of 19.8 mm Hg. While the general type of curve they obtained resembles that of the present investigation, the absolute values are considerably different.

The shape of the curve of Fig. 4 suggests that the recombination coefficient has a pressure independent component α_0 and a pressure dependent component $\alpha(p_0)$. The measured coefficient α_m is then

$$\alpha_m=\alpha_0+\alpha(p_0). \tag{4}$$

If α_0 is taken as 0.34×10^{-6} cm³/electron-sec, $\alpha(p_0)$ can be plotted as in Fig. 5 on a log plot. Within experimental error $\alpha(p_0)$ is proportional to p_0^2 for pressures up to 25 mm Hg. The range of data at higher pressures is insufficient to establish any clear-cut dependence on a power of pressure. $\alpha(p_0)$ is given approximately by

$$\alpha(p_0)=0.0026p_0^2 \text{ for } p_0<25 \text{ mm}.$$

Bates and Massey[8] proposed a mechanism by which a measured recombination coefficient could represent the combined effects of a direct electron-positive ion recombination α_e plus a negative ion-positive ion recombination α_i controlled by a quasi-equilibrium between the electron and negative ion densities. In such a case the measured recombination coefficient is given by

$$\alpha_m=\alpha_e+\lambda\alpha_i, \tag{5}$$

where λ is a constant given by

$$\lambda=n_-/n_e, \tag{6}$$

and by the mass action law is proportional to p_0 if the density of neutral atom or molecule to which the electron attaches is proportional to p_0. This mechanism might very well explain the present measurements. In the low pressure range, α_i, according to the Thomson theory,[9] is proportional to p_0, while at higher pressures it becomes independent of p_0. Thus, $\lambda\alpha_i$ is proportional to p_0^2 at low pressures and to p_0 at high pressures. The p_0^2 dependence at low pressures is verified, while the

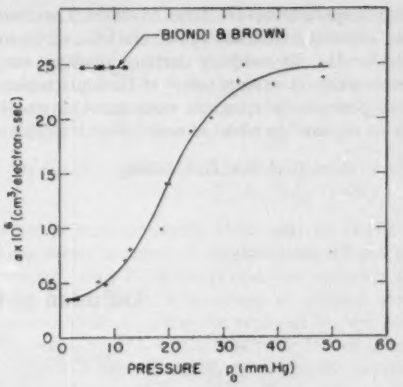

FIG. 4. Recombination coefficient in hydrogen as a function of pressure.

data at higher pressures are inconclusive in establishing the expected p_0 dependence.

The possibility that either H_1^- or H_2^- may have been present has been considered. For the case of either ion and its recombination to H_1^+ or H_2^+, α_i can be calculated from the Thomson[9] theory of recombination. In the case of H_2^-, λ can be inferred from the measured $\alpha(p_0)$ and the calculated α_i. From the statistical mechanical equation[10] relating n_- and n_0, one can determine the electron affinity. The electron affinity so obtained is 0.14 ev. Eyring, Hirshfelder, and Taylor[11] calculated the electron affinity as -2.4 ev. For this

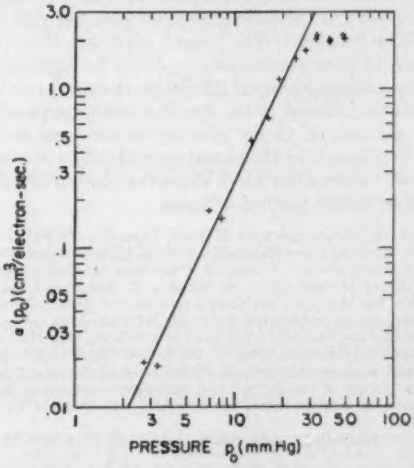

FIG. 5. Pressure dependent component of hydrogen recombination coefficient.

[7] J. M. Richardson and R. B. Holt, Phys. Rev. **81**, 153 (1951).
[8] D. R. Bates and H. S. W. Massey, Proc. Roy. Soc. (London) **A187**, 261 (1946).
[9] J. J. Thomson, Phil. Mag. **47**, 337 (1924).
[10] R. H. Fowler, *Statistical Mechanics* (Cambridge University Press, London, 1929), first edition, p. 281.
[11] Eyring, Hirshfelder, and Taylor, J. Chem. Phys. **4**, 479 (1936).

reason, it appears that H_2^- is not involved. The existence of H_1^- remains a possibility. Calculations, such as were made for H_2^- to compare electron affinities, are not possible since the concentration of H_1 is unknown.

The pressure independent component is much too large to explain[12] in terms of a radiative recombination process. Dissociative recombination, as suggested by Bates,[13] can very well account for the observed data.

The author wishes to express his gratitude to Professor S. C. Brown and to Professor W. P. Allis of Massachusetts Institute of Technology for stimulating discussions and to Mr. K. W. Rau for expert assistance.

[12] D. R. Bates, Phys. Rev. **77**, 718 (1950).

[13] D. R. Bates, Phys. Rev. **78**, 492 (1950).

PHYSICAL REVIEW VOLUME 84, NUMBER 3 NOVEMBER 1, 1951

Diffusion as Hydrodynamic Motion

M. H. JOHNSON
Naval Research Laboratory, Washington, D. C.
(Received July 16, 1951)

A phenomenological definition of diffusion in a binary mixture suggests a description of the motion by a hydrodynamic equation which contains a frictional force proportional to the relative diffusion velocity. Plausible assumptions give a set of hydrodynamic equations for any gaseous mixture, which may include charged molecules in a magnetic field. The equations determine the diffusion velocities in terms of the applied forces, the pressure gradients, and the binary diffusion coefficients. The same equations are also derived from kinetic theory in the first diffusion approximation. In higher approximations where thermal diffusion first appears, the equations are no longer valid.

IN a previous paper[1] the motion of electrons and ions through a neutral gas in a magnetic field was analyzed with hydrodynamic equations in which frictional forces represented the retarding action of the gas. A phenomenological definition of diffusion suggested the frictional force, and its dependence on both diffusion velocity and diffusion coefficient.[2] Thus diffusion velocities could be related to the forces acting on each type of ion without the difficult ideas of mean free path and collision frequency. The present paper has three purposes: to state assumptions necessary for applications of the phenomenological definition; to extend previous equations, limited to ion densities small compared to the gas density, to any gaseous mixture;[3] and to test the conclusions by the second approximation of kinetic theory,[4] a procedure which shows that there is no simple way to include thermal diffusion.

Let p_r, ρ_r, and n_r be the pressure, mass density, and number density of the rth species of molecules in a mixture of N species. Each gas is assumed to obey the ideal gas law, $p_r=n_rkT$. To define the diffusion coefficient D_{rs}, suppose the mixture consists of the two species r and s at a uniform temperature and uniform total pressure, $p=p_r+p_s$. Let the mean molecular velocities $\langle \mathbf{c}_r\rangle_M$ and $\langle \mathbf{c}_s\rangle_M$ at a point $\mathbf{r}$, t be measured in a reference frame such that $n_r\langle \mathbf{c}_r\rangle_M+n_s\langle \mathbf{c}_s\rangle_M=0$. We assert as an experimental fact that the diffusion current is then given by

$$n_r\langle \mathbf{c}_r\rangle_M=-D_{rs}\partial n_r/\partial \mathbf{r}. \tag{1}$$

For the coefficients so defined, $D_{rs}=D_{sr}$, which can be seen by applying the definition to the species s. To remove the restriction to a special reference frame it is only necessary to express $\langle \mathbf{c}_r\rangle_M$ in terms of the velocity difference $\langle \mathbf{c}_r\rangle_M-\langle \mathbf{c}_s\rangle_M$; $\langle \mathbf{c}_r\rangle_M=n_s(n_r+n_s)^{-1}(\langle \mathbf{c}_r\rangle_M-\langle \mathbf{c}_s\rangle_M)$. If, at the same time, n_r is replaced by p_r through the ideal gas law, Eq. (1) may be written

$$-\partial p_r/\partial \mathbf{r}=\theta_{rs}(\langle \mathbf{c}_r\rangle_M-\langle \mathbf{c}_s\rangle_M), \tag{2a}$$

$$\theta_{rs}\equiv kTn_rn_s(n_r+n_s)^{-1}(D_{rs})^{-1}. \tag{2b}$$

Equation (2), which is equivalent to Eq. (1), may be applied in any reference frame for both terms are invariant to Galilean transformations.

The form of Eq. (2) suggests an equilibrium of hydrodynamic forces since the negative pressure gradient is the force exerted on a fluid in a unit volume by the fluid outside that volume. The right-hand member has the appearance of a frictional force, for it is proportional to and oppositely directed to the relative velocity of the

[1] M. H. Johnson and E. O. Hulburt, Phys. Rev. **79**, 802 (1950).

[2] A. Einstein introduced such a force in his well-known theory of Brownian motion. Thereafter it has been repeatedly used in the theory of electrolytes. A. Schlüter, Z. Naturforsch. **5a**, 72 (1950); **6a**, 73 (1951), has based a treatment of gaseous diffusion on the concept of frictional forces. He introduced the forces and evaluated the frictional coefficients in a different way than that followed in reference 1 and in the present paper. The hydrodynamic equations he obtained, explicitly given in his second paper for a mixture of two ionized and one neutral component in the presence of external fields, are essentially the same as Eq. (6) above.

[3] For a preliminary report, see M. H. Johnson, Phys. Rev. **82**, 298 (1951).

[4] S. Chapman and G. T. Cowling *The Mathematical Theory of Non-uniform Gases*, Cambridge University Press, Cambridge, England (1939), Chaps. 7, 8, 9, and 18. We shall use the notation and units of this book. For symbols we have sometimes incompletely defined, the list of symbols at the beginning of the book should be consulted, where page references to all definitions will be found.

two fluids. Moreover, with this interpretation the force exerted by species r on species s is equal in magnitude and opposite in direction to that exerted by s on r, which can be seen by writing Eq. (2) for species s. Hence we assume that Eq. (2) represents an equilibrium of hydrodynamic forces; the left side is the self-force of molecules r and the right side is the force exerted by molecules s on molecules r.

Our final assumption may now be stated: if a force between two groups of molecules is specified by physical parameters of the two groups, it is not altered by the presence of molecules foreign to both groups. For example, by applying this hypothesis to the force between molecules of species r inside and outside a unit volume, the self-force is $-\partial p_r/\partial \mathbf{r}$ whatever may be the mixture containing the species r. Likewise, the frictional force exerted by molecules of species s on molecules of species r is $\theta_{rs}(\langle \mathbf{c}_r\rangle_M - \langle \mathbf{c}_s\rangle_M)$, where θ_{rs} is given by Eq. (2b), whatever gases comprise the mixture.

The last hypothesis determines the dependence of D_{rs} on the number densities. In the foregoing binary mixture (r, s), arbitrarily divide molecules r into two groups of number densities n_r' and n_r'', with $n_r'+n_r''=n_r$. Considering the mixture as one of three components, we have

$$-\partial p_s/\partial \mathbf{r} = \theta_{sr}'(\langle \mathbf{c}_s\rangle_M - \langle \mathbf{c}_r'\rangle_M) + \theta_{sr}''(\langle \mathbf{c}_r''\rangle_M - \langle \mathbf{c}_r''\rangle_M), \quad (3a)$$

$$-\partial p_r'/\partial \mathbf{r} = \theta_{rs}'(\langle \mathbf{c}_r'\rangle_M - \langle \mathbf{c}_s\rangle_M) + \theta_{rr}(\langle \mathbf{c}_r'\rangle_M - \langle \mathbf{c}_r''\rangle_M), \quad (3b)$$

$$-\partial p_r''/\partial \mathbf{r} = \theta_{rs}''(\langle \mathbf{c}_r''\rangle_M - \langle \mathbf{c}_s\rangle_M) + \theta_{rr}(\langle \mathbf{c}_r''\rangle_M - \langle \mathbf{c}_r'\rangle_M). \quad (3c)$$

Adding the last two equations,

$$-\partial p_r/\partial \mathbf{r} = \theta_{rs}'(\langle \mathbf{c}_r'\rangle_M - \langle \mathbf{c}_s\rangle_M) + \theta_{rs}''(\langle \mathbf{c}_r''\rangle_M - \langle \mathbf{c}_s\rangle_M). \quad (4)$$

But Eq. (3a) and Eq. (4) must be identical with the force equilibrium for the binary mixture (r, s). That requires

$$(\theta_{sr}' - n_r'\theta_{sr}/n_r)\langle \mathbf{c}_r'\rangle_M + (\theta_{sr}'' - n_r''\theta_{sr}/n_r)\langle \mathbf{c}_r''\rangle_M = 0 \quad (5)$$

for arbitrary values of $\langle \mathbf{c}_r'\rangle_M$ and $\langle \mathbf{c}_r''\rangle_M$ since, with n, n_r' and n_r'' fixed, two of the velocities $\langle \mathbf{c}_s\rangle_M$, $\langle \mathbf{c}_r'\rangle_M$ and $\langle \mathbf{c}_r''\rangle_M$ can be made to assume any preassigned value by adjusting the three pressure gradients. Equation (5) can be satisfied if, and only if, θ_{sr}/n_r does not depend on n_r. A similar division of species s shows θ_{sr}/n_s cannot depend on n_s. Hence $\theta_{rs}/n_r n_s$ cannot depend on the number densities or, by Eq. (2b), $D_{rs}(n_r+n_s)$ cannot depend on the number density of either species.

Consider a mixture of N components in which molecules r have a charge e_r and mass m_r. The various forces in the dynamical equilibrium for molecules r are: the self-force, $-\partial p_r/\partial \mathbf{r}$; a frictional force, $\theta_{rs}(\langle \mathbf{c}_r\rangle_M - \langle \mathbf{c}_s\rangle_M)$, for each species $s (s\neq r)$; an external force, $\rho_r \mathbf{F}_r$, which may be partly gravitational and partly electrical in origin; the ampere force $n_r e_r \langle \mathbf{c}_r\rangle_M \times \mathbf{H}$ on the electric current, produced by the motion of the charges, in a magnetic field $\mathbf{H}$; and finally the force of inertial reaction, $-\rho_r \mathbf{a}$, which must be included according to d'Alembert's principle if the gas as a whole has an acceleration $\mathbf{a}$. Collecting all terms, the hydrodynamic equations for the equilibrium of forces become

$$-\partial p_r/\partial \mathbf{r} + \rho_r(\mathbf{F}_r - \mathbf{a}) + n_r e_r \langle \mathbf{c}_r\rangle_M \times \mathbf{H} = \sum_s \theta_{rs}(\langle \mathbf{c}_r\rangle_M - \langle \mathbf{c}_s\rangle_M). \quad (6)$$

There are N such equations which may be solved for the N velocities in terms of the pressure gradients and the external forces. Equation (6) may be applied in any reference frame for it is invariant to galilean transformations. Thus $\langle \mathbf{c}_r\rangle_M$ may be replaced by the mean peculiar velocity, $\langle \mathbf{C}_r\rangle_M = \langle \mathbf{c}_r\rangle_M - \mathbf{c}_0$, provided we use the electromagnetic field, $\mathbf{E}$ and $\mathbf{H}$, proper to the reference frame in which $\mathbf{c}_0 = \rho^{-1}\sum_s \rho_s \langle \mathbf{c}_s\rangle_M = 0$.

The hydrodynamic equations solve a variety of problems. For example, to obtain conductivities of an ionic mixture, the terms on the left side of Eq. (6) which do not contain $\mathbf{E}$ or $\mathbf{H}$ may be omitted. If the equations are then solved for the velocities, the total electric current, $\mathbf{j} = \sum_s n_s e_s \langle \mathbf{c}_s\rangle_M$, is obtained as a linear vector function of $\mathbf{E}$. The coefficient of $\mathbf{E}$ is the conductivity dyadic.

We now turn to kinetic theory. The second approximation to the distribution function[5] is $f_r^{(0)}(1+\phi_r)$ where $f_r^{(0)}$ is the maxwell function,

$$f_r^{(0)} = n_r(m_r/2\pi kT)^{\frac{1}{2}} \exp(-m_r C_r^2/2kT), \quad (7)$$

and ϕ_r satisfies the equation,

$$\frac{D_0 f_r^{(0)}}{Dt} + \mathbf{C}_r \cdot \frac{\partial f_r^{(0)}}{\partial \mathbf{r}} + \left(\mathbf{F}_r - \frac{D_0 \mathbf{c}_0}{Dt}\right)\cdot \frac{\partial f_r^{(0)}}{\partial \mathbf{C}_r} + \frac{e_r}{m_r} f_r^{(0)}(\mathbf{C}_r \times \mathbf{H})\cdot \frac{\partial \phi_r}{\partial \mathbf{C}_r} = -\sum_s I_{rs}(\phi_r + \phi_s), \quad (8a)$$

$$I_{rs}(\phi_r+\phi_s) \equiv \int\int f_r^{(0)} f_s^{(0)} (\phi_r + \phi_s - \phi_r' - \phi_s') k_{rs}\, d\mathbf{k}\, d\mathbf{c}_s. \quad (8b)$$

The solution of Eq. (8) has the form,

$$\phi_r = \mathbf{D}_r \cdot \mathbf{C}_r, \quad (9)$$

where $\mathbf{D}_r$ is a linear vector function of the pressure gradients, the forces $\mathbf{F}_s$ and the temperature gradient; the coefficients depend on $\mathbf{H}$ and on the magnitude of $\mathbf{C}_r$. With Eq. (9), the diffusion currents become

$$n_r \langle \mathbf{C}_r\rangle_M = \int f_r^{(0)} \mathbf{C}_r \phi_r\, d\mathbf{c}_r = \tfrac{1}{3}\int f_r^{(0)} C_r^2 \mathbf{D}_r\, d\mathbf{c}_r. \quad (10)$$

The solution of the integral equations for $\mathbf{D}_r$, which

[5] T. G. Cowling, Proc. Roy. Soc. (London), A 183, 453 (1945); see reference 4, Chap. 18.

present a formidable mathematical problem, have been given by Cowling[4] when $\mathbf{D}_r$ does not depend on the velocity, i.e., in the first diffusion approximation. To this order, terms containing the temperature gradient drop out and there is no thermal diffusion.

The hydrodynamic equations may be regarded as a momentum balance. Similar relations are obtained from kinetic theory by multiplying Eq. (8) by $m_r\mathbf{C}_r d\mathbf{c}_r$ and integrating over $d\mathbf{c}_r$. The first term vanishes because it contains $\mathbf{C}_r$ only as a scalar. The second term becomes $(\partial/\partial\mathbf{r})\cdot\langle\mathbf{CC}\rangle_{kr}=(\partial/\partial\mathbf{r})\cdot\mathbf{p}^{(0)}=\partial p_r/\partial\mathbf{r}$. The third and fourth can be integrated by parts so that the whole equation becomes

$$-\frac{\partial p_r}{\partial\mathbf{r}}+\rho_r\left(\mathbf{F}_r-\frac{D_0\mathbf{c}_0}{Dt}\right)+n_r e_r\langle\mathbf{C}_r\rangle_{kr}\times\mathbf{H}$$

$$=\sum_s\Delta_{rs}^{(1)}(m_r\mathbf{C}_r), \quad (11a)$$

with

$$\Delta_{rs}^{(1)}(m_r\mathbf{C}_r)\equiv\int m_r\mathbf{C}_r I_{rs}(\phi_r+\phi_s)d\mathbf{c}_r. \quad (11b)$$

The integral $\Delta_{rs}^{(1)}(m_r\mathbf{C}_r)$ is the momentum per unit volume transferred by collisions from molecules r to molecules s. Identifying $D_0\mathbf{c}_0/Dt$ with $\mathbf{a}$, the left side of Eq. (11a) is the same as the left side of Eq. (6). Hence the second approximation to kinetic theory leads to the same expressions for the hydrodynamic forces even in the case that the thermal gradient is not zero.

When $\mathbf{D}_r$ does not depend on C_r Eq. (10) becomes

$$\langle\mathbf{C}_r\rangle_{kr}=(kT/m_r)\mathbf{D}_r. \quad (12)$$

There is then a simple connection between $\Delta_{rs}^{(1)}(m_r\mathbf{C}_r)$ and the velocities, for we have

$$\Delta_{rs}^{(1)}(m_r\mathbf{C}_r)$$

$$=\int\int\int f_r^{(0)}f_s^{(0)}m_r\mathbf{C}_r[\mathbf{D}_r\cdot(\mathbf{C}_r-\mathbf{C}_r')+\mathbf{D}_s\cdot(\mathbf{C}_s-\mathbf{C}_s')]k_{rs}dwd\mathbf{c}_r d\mathbf{c}_s$$

$$=\int\int\int f_r^{(0)}f_r^{(0)}m_r\mathbf{C}_r(\mathbf{C}_r-\mathbf{C}_r')dwd\mathbf{c}_r d\mathbf{c}_s\cdot(\mathbf{D}_r-m_r\mathbf{D}_s/m_s)$$

$$=\int\int\int f_r^{(0)}f_s^{(0)}m_r\mathbf{C}_r(\mathbf{C}_r-\mathbf{C}_r')dwd\mathbf{c}_r d\mathbf{c}_s\cdot(\langle\mathbf{C}_r\rangle_{kr}-\langle\mathbf{C}_s\rangle_{kr})(m_r/kT). \quad (13)$$

As $\Delta_{rs}^{(1)}(m_r\mathbf{C}_r)$ is a linear vector function of $\langle\mathbf{C}_r\rangle_{kr}-\langle\mathbf{C}_s\rangle_{kr}$ which does not depend on $\mathbf{D}_r$ or $\mathbf{D}_s$, all reference to species other than r or s has disappeared from Eq. (13). The momentum transferred from molecules r to molecules s is independent of the mixture, in accord with the final hypothesis made in deriving Eq. (8). Moreover the right side of Eq. (13) must have the known value for a binary mixture, that is

$$\Delta_{rs}^{(1)}(m_r\mathbf{C}_r)=(kT(n_r+n_s)^{-1}n_r n_s/[D_{rs}]_1)(\langle\mathbf{C}_r\rangle_{kr}-\langle\mathbf{C}_s\rangle_{kr}), \quad (14)$$

where $[D_{rs}]_1$ is the first approximation to the binary diffusion coefficient. Inserting Eq. (4) into Eq. (11a) we obtain Eq. (8) if it is understood that $[D_{rs}]_1$ be used in Eq. (2b). The hydrodynamic equations are therefore equivalent to the first diffusion approximation.[6]

If $\mathbf{D}_r$ depends on C_r, $\Delta_{rs}^{(1)}(m_r\mathbf{C}_r)$ becomes a linear vector function of all the velocities and of the temperature gradient; each coefficient is a complicated integral which depends on all the components in the mixture. Consequently the right side of Eq. (11a) cannot be resolved into a sum of terms, each of which refers to an isolated binary mixture, so that it no longer has the same form as the right side of Eq. (6). In higher diffusion approximations the simple connection between momentum transfer and diffusion velocities, Eq. (14), is lost and the hypothesis underlying the right side of Eq. (6) is not valid. Since thermal diffusion appears only if $\mathbf{D}_r$ depends on C_r, it is not possible to describe thermal diffusion by adding a sum of binary terms proportional to the temperature gradient to right side of Eq. (6).

[6] I am indebted to Professor Cowling for the observation that Eq. (6) may be derived from Eq. (37) of his 1945 paper (see reference 5) by multiplying the latter equation by $\mathbf{d}_s$ and summing over s, thus establishing the equivalence.

Magnetic Susceptibility of Manganese Selenide*

ROBERT LINDSAY
Rice Institute, Houston, Texas
(Received July 13, 1951)

The susceptibility-temperature relation for the antiferromagnetic compound MnSe was measured over a range of temperatures between 70°C and −196°C. Evidence was found of a large thermal hysteresis and a dependence of susceptibility on field strength. A tentative theory is advanced to explain the thermal hysteresis in terms of three phases which possess different susceptibilities.

I. INTRODUCTION

THE susceptibility of a typical antiferromagnetic substance decreases with decreasing temperature below a certain critical temperature, and for most substances this suceptibility *vs* temperature relation is a reversible one. However, MnSe has been found by Squire,[1] Bizette and Tsai,[2] and by Haraldsen and Klemm[3] to have several anomalies. Squire, who used a field strength of 700 gauss, obtained a larger maximum susceptibility and a higher indicated critical temperature than Bizette and Tsai, who made their measurements at a field strength of 30,000 gauss. Squire noted small magnetic hysteresis effects in the vicinity of the critical temperature when fields of the order of 10 gauss were applied. Bizette and Tsai observed a temperature hysteresis when the sample was cooled to −196°C and held at that temperature for a period of 12 hours or more and allowed to warm up. Some of the data of Haraldsen and Klemm showed a dependency of susceptibility on field strength. The experiments described below were made with the object of investigating some of these anomalies further.

II. EXPERIMENTAL

The apparatus was patterned after the ring balance devised by Sucksmith.[4] A diagram of this system is shown in Fig. 1. The balance case was a rectangular brass box (*A*) mounted on a vibration damping frame (*B*). The ring (*C*), 6.0 cm in diameter, was made from a strip of phosphor-bronze 0.17 mm thick and 3.0 mm wide. The sylphon bellows (*D*) permitted vertical movement of the entire ring and suspended sample. A loop of copper wire (*E*), soldered to the ring at (*F*) and immersed in an annular oil bath (*G*) provided damping of vibrations. Two mirrors (*M*) were mounted on the ring so that the radius to each made an angle of 49 degrees with the horizontal. A beam of light from a fine horizontal wire filament (*H*), focused by an achromatic converging lens, was successively reflected by the two mirrors and then emerged from the box. The image of the filament was viewed through a traveling microscope (*I*). When a vertical downward force acted upon the ring, this image was displaced upward because the slight distortion of the ring moved the mirrors.

The specimen container was a pharmaceutical gelatine capsule 11.04 mm long and 4.93 mm in diameter. It was suspended by a quartz fiber in the non-uniform part of the field of a Weiss electromagnet (*P*−*P*). Sidewise motion towards either pole-piece when the field was set up was prevented by a spiral spring (*J*) of fine copper wire cemented to a quartz rod (*K*). The plane of the spring was perpendicular to the quartz fiber.

The sensitivity of the system was 0.149 mm dyne and was found to be independent of temperature within the limits of the desired accuracy. A specimen of mass m, and susceptibility χ_m, when placed in a magnetic field of strength H and vertical gradient dH/dx experiences a force given by $F=\chi_m m H dH/dx$. The quantity HdH/dx was determined by measurements on the standard paramagnetic salt $FeSO_4\cdot(NH_4)_2SO_4\cdot 6H_2O$.[5]

Surrounding the lower portion of the Pyrex tube enclosing the suspension was a copper tube (*L*) of thickness $\frac{1}{8}$ in. with a bottom 1 in. thick. A small window was cut in the side to permit a view of the sample. This copper jacket provided uniform temperature over the specimen. After the balance chamber had been filled with dry helium at a pressure of one atmosphere, step-wise cooling was accomplished in the following fashion. Liquid nitrogen was forced into the surrounding Dewar flask a little at a time and allowed to evaporate. After a sufficiently low temperature had been reached, the necessary readings were quickly taken. The high thermal capacity of the copper tube and the good thermal insulation kept the temperature fairly constant. On the warming part of the cycle readings were taken as the temperature slowly increased after all the liquid nitrogen had evaporated. By injecting more liquid nitrogen into the flask at points along the warming cycle a closer approximation to equilibrium conditions could be obtained. For the attainment of temperatures above 25°C, a heating coil wrapped around the copper tube was used. All temperature measurements were made

* Part of a thesis submitted to the Rice Institute, Houston, Texas, in partial fulfillment of the requirements for the degree of Doctor of Philosophy.

[1] C. F. Squire, Phys. Rev. **56**, 922 (1939).

[2] H. Bizette and B. Tsai, Compt. rend. **212**, 75 (1941).

[3] H. Haraldsen and W. Klemm, Zeits. anorg. u. allgem. Chem. **220**, 183 (1934).

[4] W. Sucksmith, Phil. Mag. **8**, 158 (1929).

[5] L. C. Jackson, Trans. Roy. Soc. (London) (A) **224**, 1 (1924).

with a copper-constantan thermocouple, the junction being located close to the specimen.

The powder samples of MnSe came from a batch prepared by Kelley.[6] The compound had been obtained by heating manganese and selenium in their proper combining ratio to a temperature at which the chemical reaction would take place and then the excess selenium was driven off.

III. RESULTS

The graph in Fig. 2 represents a typical run (although there were some runs with significant deviations from this pattern). In all cases the cooling curve appeared to be influenced in some way by the previous temperature history of the sample, while the warming curve was a function of the length of time which the sample was held at low temperatures. For the data plotted in Fig. 2, the sample had previously been cooled to −196°C and then allowed to warm up to 28°C. The cooling curve (*A*) from 28°C to −55°C was almost linear. Between −55°C and −90°C there was a noticeable increase in slope followed by a gradual levelling off beyond −90°C. The curve showed a rather broad maximum at −120°C and started dropping off quite steeply beyond −135°C. At −196°C it required 20 hours for final equilibrium to be reached.

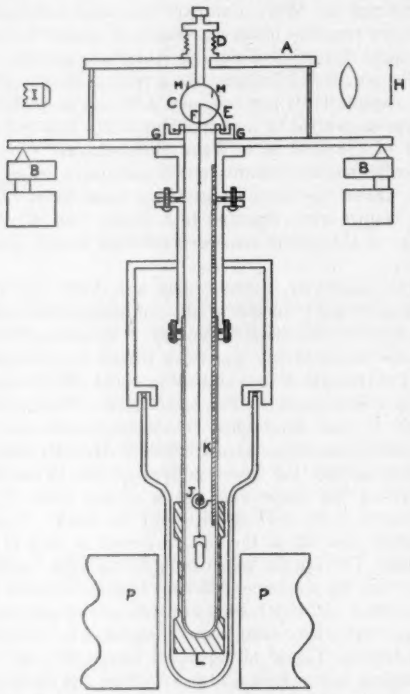

FIG. 1. Schematic diagram of susceptibility measuring apparatus.

When the sample was warmed to 70°C before cooling was started, the subsequent cooling curve showed a much smaller slope between 70°C and −60°C, while the maximum value of the susceptibility occurred at −135°C with a lower absolute value than in the case shown in Fig. 2. If held at −196°C sufficiently long, all samples, regardless of previous history, approached the equilibrium value shown in Fig. 2.

Curve (*B*) in Fig. 2 was obtained after the sample was held at −196°C for 20 hours and had then been allowed to warm up to 30°C. A period of 8 hours was required for this warming process. Curve (*B*) was reversible up to −25°C. A maximum in the vicinity of −100°C was noted. Above −25°C the curve ceased to be reversible. There was a slight rise up to a maximum at 10°C, during which the original cooling curve (*A*) was crossed and then the susceptibility decreased to approximately its original value at 28°C. Other runs indicated that the slope of the warming curve above 28°C was continuous with the slope of the prior cooling curve below that temperature. On one run, the warming was stopped at 13°C and the subsequent cooling curve was that shown in curve (*C*).

Figure 3 shows cooling curves taken on the same run for two different field strengths. The cooling was started at 25°C on a sample which had previously been cooled to −196°C. The higher values of susceptibility occurred with the lower value of the field strength. The maximum value of the susceptibility for 4300 gauss was higher than that in Fig. 2. The points at −196°C were taken after the sample had only been one hour at that temperature. The same sample was used in Fig. 3 as in Fig. 2.

IV. DISCUSSION

The cooling and warming cycle shown in Fig. 2 will be considered as representing typical behavior with the qualifications noted in the previous section. A tentative theory is advanced which considers the possibility of phase changes with temperature. The existence of three different phases is postulated which shall hereafter be referred to as I, II, and III. It is assumed that phase I predominates at room temperature. From room temperature to −55°C, the susceptibility is representative of phase I. The change in slope below −55°C is explained by saying that phase II starts to come in and has a relatively higher susceptibility than phase I. Below −135°C, phase III starts to form. The levelling off of the cooling curve between −115°C and −125°C represents antiferromagnetic behavior in phases I and II. The long time required for attaining equilibrium at −196°C suggests that the complete transformation of the other two phases into phase III is taking place. The warming curve taken after equilibrium has been reached is considered as being almost completely repre-

[6] K. K. Kelley, J. Am. Chem. Soc. **61**, 203 (1939).

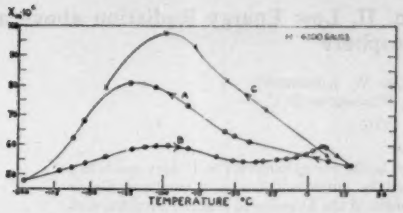

FIG. 2. (*A*) and (*B*): Cooling and warming curves showing thermal hysteresis. (*C*): Cooling curve obtained after warming of previously cooled sample is stopped at 13°C.

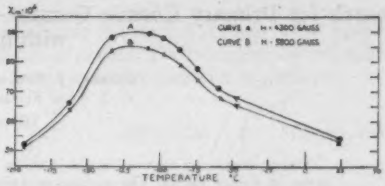

FIG. 3. Cooling curves showing dependence of susceptibility on field strength.

sentative of phase III. The hump in the vicinity of −100°C indicates that phase III is antiferromagnetic with a critical temperature at about that point. Above −25°C phase III starts going back into phase II. This is evidenced by the gradual rise in the susceptibility up to 10°C and by the cessation of reversibility. At 10°C phase II is in preponderance. If curve (*C*), which was obtained when cooling was started at 13°C, can be taken as representative of phase II, then the data indicate that phase II has a higher maximum susceptibility than phase I and the critical temperature is higher than for phase I. When warming is continued above 10°C along curve (*B*), most of phase II passes back into phase I.

Modifications in crystal structure might be responsible for the changes in phase suggested above. The antiferromagnetic compounds MnO, FeO, NiO, and CoO[7] have been shown to have, like MnSe, a NaCl type structure above the critical temperature. Below their critical temperatures, MnO, FeO, and NiO undergo deformations to rhombohedral symmetry while CoO deforms to tetragonal symmetry. It is possible that similar changes take place in MnSe. The crystal structure of MnSe at room temperature has been studied by Baroni,[8] who found three distinct structures depending on the method of preparation. MnSeα was a stable NaCl type while MnSeβ and MnSeγ were unstable zincblende and wurtzite types, respectively, which both eventually passed back into the α-type. It is possible that these varying structures might be associated with the phase changes suggested above.

It is possible to correlate Kelley's measurements of the specific heat of MnSe[6] with these magnetic measurements. Kelley measured the specific heat of a sample while it was slowly warming up from −196°C to room temperature. A very sharp peak was found in the vicinity of −25°C. On the warming curve for susceptibility it is noted that this is approximately the same temperature at which phase III is postulated as passing over into phase II. When specific heat measurements were made on a sample which had been cooled only to −45°C, no sharp peak was noted. This lack of anomaly would indicate no phase change, a fact which is consistent with the magnetic measurements in this range.

The author wishes to thank Professor C. W. Heaps for suggesting the problem and for his invaluable aid and advice during the course of the research. Appreciation is also expressed to Dr. K. K. Kelley of the Bureau of Mines and to Professor C. F. Squire for furnishing the samples.

[7] J. S. Smart and S. Greenwald, Phys. Rev. **82**, 113 (1951).

[8] A. Baroni, Z. Krist. **99**, 336 (1938).

A Search for Primary Cosmic Gamma-Radiation. II. Low Energy Radiation above and within the Atmosphere

GILBERT J. PERLOW AND CHARLES W. KISSINGER*
U. S. Naval Research Laboratory, Washington, D. C.
(Received July 23, 1951)

Measurements are reported on the intensity of gamma-rays in the energy range 0.1 to 15 Mev, made in a series of rocket flights. The gamma-radiation was detected by anticoincidence in a bundle of Geiger counters. Registration of coincidences permitted a measurement of the intensity of charged particles, with the same geometry. The two quantities displayed a simultaneous maximum during flight, the counting rate of charged particles being ten times that of γ-rays at the maximum. A diurnal effect was looked for and not found. A theoretical treatment is given of the origin of the γ-radiation at the maximum. It is shown to be accountable for by bremsstrahlung of the electronic component and subsequent multiple Compton scattering. An estimate is given of the radiation due to annihilation of positrons followed by Compton scattering. This is shown to be only a few percent of the bremsstrahlung effect.

After all corrections are applied a weak residual γ-radiation is found above the atmosphere. Arguments are given for identifying this as an albedo. Two types of albedo are considered, the first and more important is associated with back-scattering and is not calculated, while the second is due to the curvature of the earth. A calculation shows the latter to give 25 percent of the observed counting rate at 82 km.

In conjunction with the conclusions of paper I of this series and with other evidence at higher energies, it is concluded that primary cosmic gamma-radiation contributes at most a very small fraction to the incoming cosmic-ray energy flux.

I. INTRODUCTION

IN a previous paper[1] we reported on a rocket measurement of the primary cosmic gamma-ray energy flow into the atmosphere for the energy range 3.4 to 90 Mev. Our measurement indicated a possible energy flux, in the range investigated, of one part in 1300 of the total incoming energy given by the ionization integrals of Millikan and co-workers. The difficulty of assessing all corrections made a null result admissible however. It was pointed out that gamma-rays in the Bev range apparently are ruled out by other evidence. The experiment reported here is an investigation of lower energies, with some overlapping of the previous work. The detector was sensitive to gamma-rays from 0.1 Mev to 15 Mev with maximum efficiency at about 7 Mev. It was felt that if a null or very small flux were obtained, one would be justified in assuming a similar result for the spectral regions as yet unexplored.[2] This conclusion would have certain cosmological implications.

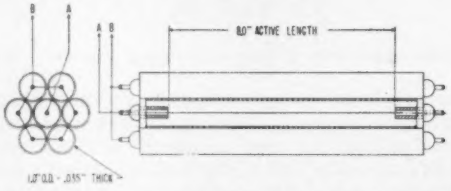

FIG. 1. The apparatus. Anticoincidences A–B detected low energy γ-rays in A. Coincidences AB detected charged particles in A.

The present experiment was performed three times, first in the V-2 rocket of the previous paper, and later in two Aerobee rockets. One of the latter flights was made at night in order to detect any diurnal effect. The flights were made at White Sands, New Mexico, geomagnetic latitude 41°. Additional measurements with a scaled-down version of the detector were made by Bergstralh and Schroeder[3] using Skyhook balloons at Camp Ripley, Minnesota. They looked for a diurnal effect and found none as large as their statistical probable error (about 3 percent).

Section II describes the experimental method and the results. In Sec. III a theoretical treatment is given of the radiation encountered in the atmospheric portion of the flight. Section IV treats the radiation observed above the atmosphere. The analysis shows that the atmospheric radiation can reasonably be accounted for by bremsstrahlung and multiple Compton scattering in the electronic component, and that some of the radiation found above the atmosphere, possibly all of it, is secondary to processes lower down.

II. EXPERIMENTAL METHOD

Figure 1 illustrates the apparatus. It consisted of a tightly packed bundle of seven Geiger counters, each having 0.035-in. Cu wall thickness and a nominal active length of 8 in. The six counters in the outer ring were connected in parallel to form set B. The center counter, labelled A, was separate. The data registered consisted of coincidences AB and anticoincidences A–B. The

* Present address: National Bureau of Standards, Washington, D. C.

[1] G. J. Perlow and C. W. Kissinger, Phys. Rev. **81**, 552 (1951).

[2] T. R. Burnight, Phys. Rev. **76**, 165(A) (1949) has described rocket measurements of soft x-rays above the atmosphere. The intensity was enough to visibly blacken a photographic plate behind a very thin aluminum window in a few minutes. It appears reasonably clear however, that this phenomenon has an origin different from that of cosmic radiation. See also: Tousey, Watanabe, and Purcell, Phys. Rev. **83**, 792 (1951), and Friedman, Lichtman, and Byram, Phys. Rev. **83**, 1025 (1951).

[3] T. A. Bergstralh and C. A. Schroeder, Phys. Rev. **81**, 244 (1951).

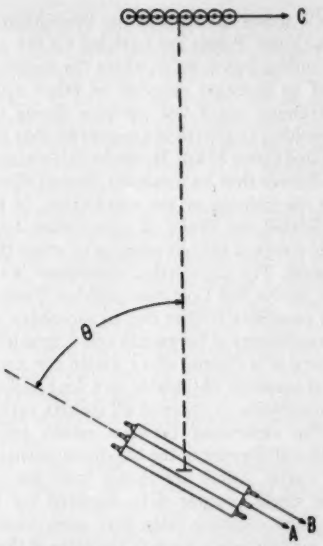

FIG. 2. Measurement of leakage. By taking data at various angles θ to the vertical, the inefficiency of the B ring may be calculated for isotropic radiation.

former events were due to ionizing particles traversing counter A and tripping one or more counters of the surrounding ring B. The anticoincidences $A-B$ represented the effect of a radiation which produced ionizing particles in the walls immediately surrounding the active volume of A, which particles, however, were not sufficiently energetic to penetrate the walls a second time and trip a B counter. AB thus measures charged particles, energetic γ-rays, and energetic neutrons, but is very much more effective for the charged particles. $A-B$ measures low energy γ-rays and low energy neutron-produced radiation. It is much more effective for the γ-rays, however.

The energy range of γ-rays which will produce anticoincidences $A-B$ is determined at the lower limit by absorption in the walls and at the upper by the energy of the secondaries. For the lower limit we may conveniently take an energy such that the intensity is reduced by a factor $1/e$ at the inner wall of counter A. This corresponds to a γ-ray energy of 100 kev. The upper limit is considerably less sharp because there is no minimum energy transfer which may occur in a Compton collision. The matter is discussed under "efficiency" in Sec. III.

There were two causes of error inherent in the apparatus which permitted some ionizing rays to count as anticoincidences. In both cases corrections could be applied. One was the lack of perfect shielding efficiency of the B ring for ionizing radiation which penetrated counter A. This was measured by the arrangement shown in Fig. 2. A bank of counters C was placed above the bundle and the rates N_{AC-B} and N_{AC} measured as a function of angle θ. The inefficiency η (=1-efficiency) in an isotropic field of radiation is given by

$$\eta=\int_0^{\pi/2} N_{AC-B}(\theta)\sin\theta d\theta \Big/ \int_0^{\pi/2} N_{AC}(\theta)\sin\theta d\theta.$$

The integrations were done graphically using measured values of the rates. For the various bundles used η was 2.3–2.5 percent. The dependence of the ratio N_{AC-B}/N_{AC} on θ showed that all but a negligible part of the inefficiency at sea level counting rate was geometrical in origin.

A second cause of error was double-pulsing in the A counter. That is, a certain fraction of the A counts are followed by a spurious discharge in a time less than $\sim 10^{-3}$ sec. The latter register as an event $A-B$. It is known that spurious pulses of this type are associated with the plateau slope in a Geiger counter. For this reason all the counters chosen had usable plateaus of at least 500 volts (threshold = 1000v) and plateau slopes of less than 0.04 percent/volt at 1220 v, the flight value. The circuit used to test the counters had a recovery time (~ 25 μsec) sufficiently short to be sensitive to double pulsing. In addition, a direct measurement of double pulsing was made by stretching to 4200 μsec the output pulse which signaled a coincidence AB, and placing this in turn in coincidence with the output pulse from the $A-B$ circuit. The latter had a width of 5 μsec. The effect is shown as a function of counter voltage for two typical bundles in Fig. 3. After subtraction of the predicted accidental rate, the effect re-

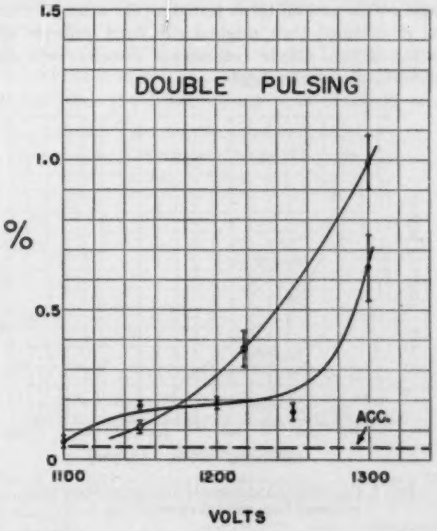

FIG. 3. The ordinate gives the relative number of times that counter A was followed by a spurious pulse.

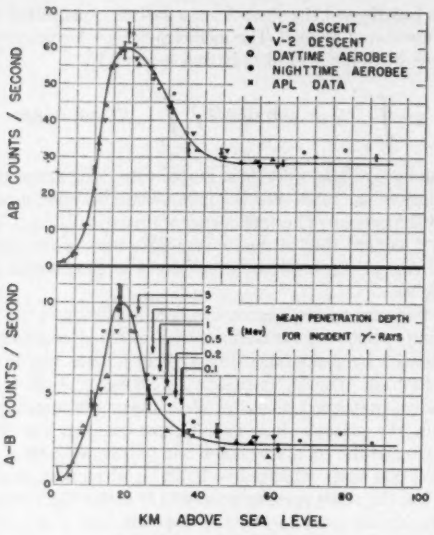

FIG. 4. Data of three flights.

maining was about 0.3 percent of the AB rate at 1220 volts.

In all cases the bundle was mounted in the nose of the rocket and the surrounding material kept to a minimum. The rocket skin thickness was 0.125-in. Al for the V-2 and 0.050-in. Al for the Aerobee. The bundle and the rocket were co-axial. All counters were of the ether-argon type, manufactured commercially in a single batch, and all those tested a year after purchase had maintained their original threshold voltages and plateau slopes. Diode coincidence circuits were employed in the electronics.[4]

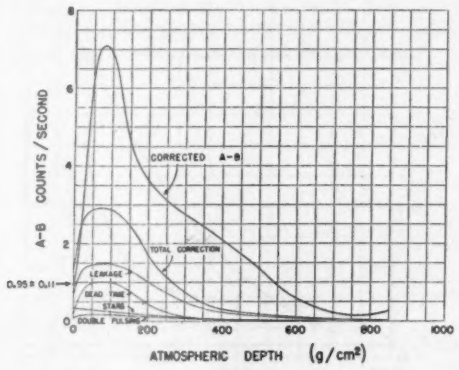

FIG. 5. Corrections and corrected anticoincidence rate obtained from smooth curve of Fig. 4.

[4] Howland, Schroeder, and Shipman, Jr., Rev. Sci. Instr. 18, 551 (1947).

Figure 4 shows the data of the three flights plotted against altitude. Points are included for the ascending and descending legs down to where the rocket nose was blown off to facilitate recovery of other equipment.[5] The instrument space lost pressure during the night flight, resulting in electrical arc-over so that data were not obtained above 37 km. However, this was sufficiently high to observe that no measured diurnal effect existed in either the ionizing or the γ-radiation. In Fig. 4 we have indicated the depth of penetration for vertical incoming γ-rays of various energies to which the bundle can respond. The penetration considered is the mean free path to the first Compton collision. Vertical radiation will penetrate further due to successive collisions. The measurements of Bergstralh and Schroeder[6] confirm the absence of a diurnal effect within the much better statistical accuracy obtainable in a long balloon flight.

The orientation in space of all rockets varied during flight. The agreement between ascent and descent shows the indifference of the bundle to orientation. For the AB curve, points are shown from the composite curve of single counter data reported by the APL group.[6] Their counting rates have been normalized to ours by multiplication by 8/6, the ratio of the nominal active lengths of the counters. The agreement is seen to be good. The increase in the $A-B$ counting rate at very low altitudes is a real effect due to ground radioactivity.

Figure 5 has been obtained from Fig. 4 by correcting the smooth curve and replotting against atmospheric depth. The corrections and the corrected curve are shown. In addition to the shielding and double pulsing effects discussed before, there is a correction for electronic and counter dead-time and one for neutron-induced stars. For the latter we have proceeded in much the same way as in the previous paper.[1] The starting point is the emulsion measurement of Yagoda *et al.* made in a V-2 and their observation that the prong distribution is characteristic of the stars produced by secondaries. The mountain altitude data of the Bristol group[7] is used to obtain the distributions. The stars which affect the $A-B$ rate are of type "0n" with no "grey" prongs, since the range of the latter is adequate to produce an AB. The probability P of a star-generated event is taken as

$$P=Q\sum_N C_N D_N \exp\{-g(N)\}.$$

Here Q is the probability that a star is produced within the range of a 10-Mev proton (typical "black" track) from the active volume of counter A. C_N is the probability that the star contains N prongs (grey or black). D_N is the probability that one of the black particles enters the active volume. It is greater than 0.9 for $N>3$. The factor $\exp\{-g(N)\}$ is the probability (based

[5] G. J. Perlow, Sci. Monthly 69, 382 (1949).
[6] Gangnes, Jenkins, Jr., and Van Allen, Phys. Rev. 75, 57 (1949).
[7] Brown, Camerini, Fowler, Heitler, King, and Powell, Phil. Mag. 40, 862 (1949).

on a poisson distribution) that an N prong star with an expected number of grey tracks $g(N)$ actually contains none. The variation of P with height is contained in Q. We have used the data of Lord[8] for the slope of the variation and of Yagoda and others[9] for normalization to the free-space point. The star correction amounts to 15 percent above the atmosphere and is unimportant at depths greater than 40 g/cm². It is probably overestimated at all depths.

Table I is a summary of the data above the atmosphere. The V-2 data cover the region 51 to 60 km, or 90 seconds, and the daytime Aerobee 46 to 80 km, or 50 seconds. The choice of altitude ranges is governed by such factors as absence of noise on the telemetering record, uprightness of the rocket, etc. There is a small difference between the counting rates in the two rockets. Skin thickness, difference in dimension, and true intensity difference probably all enter in. The difference in $A-B$ rates after correction is just outside of statistical probable error.

In order to get some idea of the energy above the atmosphere despite our ignorance of its spectral distribution, we assume for the moment that all we measure are photons below ~7 Mev. For these, the efficiency is approximately proportional to energy and we may assign an energy flux without knowledge of the spectrum, as in reference 1. In this way we obtain ~0.3 Mev/cm² sec sterad for the unidirectional energy intensity and ~0.9 Mev/cm² sec for the flow across 1 horizontal cm². This is seen to be comparable to the quantity reported in reference 1 for the energy range $3.4 \leq E \leq 90$ Mev and ~2000 times smaller than the total incoming energy which goes into atmospheric ionization.

We have applied the pertinent (and small) corrections to obtain a corrected AB rate and a value of the unidirectional charged particle intensity assuming isotropic radiation from the upper hemisphere. This result is in agreement with the single counter measurements of the APL group.[6] The vertical intensity at this latitude is considerably lower[10] than the figure so obtained. The difference is presumably due to albedo, i.e. to secondaries from the atmosphere.

TABLE I. The radiation above the atmosphere.

	V-2	Aerobee
AB	28.3±0.4	30.6±0.5/sec
$A-B$	2.3±0.1	2.7±0.2
Corrections to $A-B$		
Leakage	0.71	0.77
Double-pulsing	0.07	0.08
Dead-time	0.21	0.25
Stars	0.33	0.33
Total corrections	1.3	1.4
Corrected $A-B$	1.0±0.1	1.3±0.2
"Vertical" γ-ray energy flow	0.3 Mev/cm² sec sterad	
γ-ray enery flow across 1 horizontal cm² assumed to come from one hemisphere	0.9 Mev/cm² sec	
Corresponding quantity from previous measurement, $3.4 \leq E \leq 90$ Mev	1.4 Mev/cm² sec	
Total primary energy flow (Millikan *et al.*)	1800 Mev/cm² sec	
Corrected AB (V-2)	29.2±0.4/sec	
Charged particle intensity (hemispherical isotropy assumed)	0.12/cm² sec sterad	
APL single counter[a]	0.13/cm² sec sterad	

[a] See reference 6.

III. THE ATMOSPHERIC RADIATION

A. Calculation of the Spectrum

We may note first that the atmospheric gamma-radiation is quite intense. At the intensity maximum its counting rate is about one-tenth that of the ionizing radiation, but the detection efficiency for much of it is only a few tenths of one percent. Thus its intensity is in the order of 100 times greater than that of the charged particles. This factor may be understood by an analysis of the origin of the radiation.

We expect the following sources of the low energy gamma-rays: 1. The bremsstrahlung of electrons. 2. The annihilation of positrons. 3. The direct production of low energy quanta by neutral meson decay. In addition there is present the secondary radiation arising from multiple Compton scattering of these three. Further sources which may contribute to a small extent are nuclear gamma-rays and the x-rays associated with capture of negative mesons into atomic orbits. These are not treated.

We have calculated the effect of item 1 in some detail and have made estimates of items 2 and 3. Considering the last item, the Bristol group[11] has obtained γ-ray

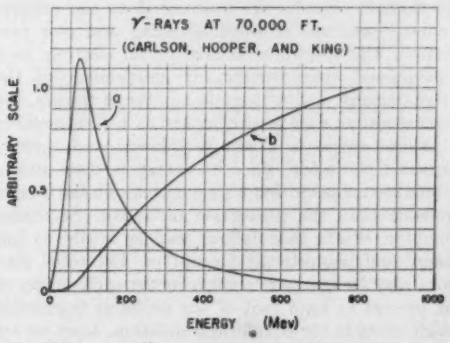

FIG. 6. Intensity of γ-rays from π^0 meson decay. Curve a, differential number spectrum $n(E)$. Curve b, integral energy spectrum $\int_E^\infty En(E)dE$.

[8] J. J. Lord, Phys. Rev. **81**, 901 (1951).
[9] Yagoda, de Carvalho, and Kaplan, Phys. Rev. **78**, 765 (1950).
[10] J. A. Van Allen and S. F. Singer, Phys. Rev. **78**, 819 (1950). Winkler, Stix, Dwight, and Sabin, Phys. Rev. **79**, 656 (1950). Perlow, Bergstralh, Johnson, and Shipman, Jr., Phys. Rev. **80**, 133(A) (1950).
[11] Carlson, Hooper, and King, Phil. Mag. **41**, 701 (1950).

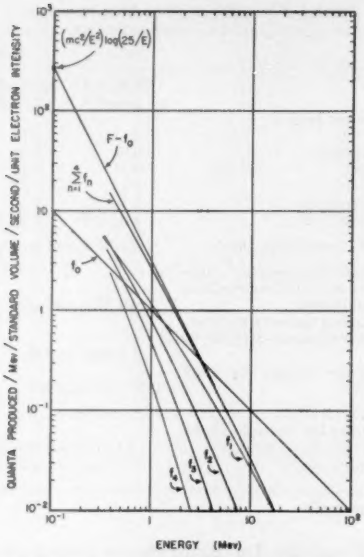

FIG. 7. Production spectrum of the various components of the γ-radiation. f_0 is the parent bremsstrahlung spectrum; $f_1 \cdots f_4$ the successive generations of scattering. Σf_n is the sum of 4 scattered generations; $F-f_0$ is the complete scattering spectrum determined by joining Σf_n to the indicated point at 0.1 Mev.

spectra at 70,000 ft altitude which they show to be due to π^0 decay. Their differential number distribution $n(E)$ is shown in Fig. 6 as curve a. Curve b is a plot of $\int_0^E En(E)dE$ the energy contributed by all photons having quantum energy $<E$. The great preponderance (>90 percent) of the energy originates as energetic quanta ($E>100$ Mev) which therefore produce the electronic cascades and item 1. We are thus justified in neglecting item 3.

The calculation of item 1 proceeds from the following: the electron cascades are maintained by the complementary processes of bremsstrahlung and pair production. The spectrum radiated by an electron, to a conventional approximation, is independent of the latter's energy, and as regards number of quanta, the lower quantum energies are favored as $1/E$. Sometimes a photon suffers a Compton collision and thereby escapes the cascade, since its energy is then usually reduced to the point that a second such collision is more probable than the production of a pair. Successive Compton effects then follow, leading finally to low energy and photoelectric absorption. The recoil electrons may be energetic enough in the early stages of the process to form part of the radiating population which exists in the equilibrium situation. Since we are interested only in the ratio of photons to electrons, the origin of the latter is of no concern. In the median case an electron requires an energy of $\sim$7.5 Mev to be observed by the bundle, while γ-rays of $<$15 Mev may count. Electrons of energy between these values are a special case. However, we shall assume them to radiate the same spectrum as those above 15 Mev. We also assume that those below 7.5 Mev do not radiate at all. The errors in these assumptions are compensatory and small in any case.

The γ-ray intensity depends on values of the electron intensity within distances of a few mean free paths from the point of measurement. If the electron intensity is uniform over this region, the details of the cascade are irrelevant and the calculation becomes much simpler.[12] This is the case we treat. It should be correct at the intensity maximum, while giving too high an intensity of γ-rays above this altitude and too low below.

The electron intensity is assumed to be isotropic over a sphere as a computational convenience. Isotropy over a hemisphere gives the same results, and even large deviations from isotropy have only a slight effect since the bundle is not very sensitive to orientation.

We calculate below the production spectrum of bremsstrahlung, the production spectrum of the scattered radiation, from these the intensities, and by means of an efficiency factor relate the latter to the counting rates of electrons and γ-rays.

An intensity of 1 electron/cm^2 sec sterad corresponds to a total length of track 4π cm/sec in one cm^3 of volume. In the approximation we use there are dE/E photons of energy E, dE radiated per radiation length (X_0 cm) of path. Hence, if we choose as a standard, a volume of numerical magnitude $X_0/4\pi$ cm^3, the differential production spectrum of bremsstrahlung may be written:

$$f_0(E)dE=dE/E, \tag{1}$$

where $f_0(E)dE$ is the number of quanta of energy E, dE produced per standard volume per second by unit electron intensity.

The production spectrum of scattered radiation may be calculated by taking $f_0(E)$ as the progenitor of a next generation $f_1(E)$. In similar fashion $f_1(E)$ produces a next generation $f_2(E)$ and so on.

$$\begin{aligned} f_1(E)dE&=dE\int_E^\infty f_0(E')P(E',E)dE',\\ &\vdots\\ f_n(E)dE&=dE\int_E^\infty f_{n-1}(E')P(E',E)dE' \end{aligned} \tag{2}$$

where $P(E',E)dE$ is the probability that a photon of energy E' will produce one of E in dE by means of a Compton collision. The complete production spectrum

[12] The closely allied problem of the radiation intensity in a medium containing a uniformly distributed radioactive source has been treated by W. R. Faust and M. H. Johnson, Phys. Rev. **75**, 467 (1949) and by P. R. Karr and J. C. Lamkin, Phys. Rev. **76**, 1843 (1949). Our treatment of the scattering is somewhat similar to the latter.

is the sum:

$$F(E)dE=dE\sum_{n=0}^{\infty} f_n(E). \tag{3}$$

$P(E', E)$ takes into account that the photon E' may produce a pair instead of scattering, thus:

$$P(E', E)=\{Z\varphi_c(E')/[Z\varphi_c(E')+\varphi_{pr}(E')]\}\cdot d\varphi_c(E', E)/\varphi_c(E'). \tag{4}$$

where φ_c and φ_{pr} are the total cross sections for Compton effect and pair production per electron and atom respectively.[13] The quantity $d\varphi_c$ is the differential Klein-Nishina cross section and may be written:

$$d\varphi_C(E', E)=\frac{\pi e^4}{mc^2}\cdot\frac{1}{E'^2}\left[\frac{E'}{E}+\frac{E}{E'}-1+\left\{\frac{mc^2}{E'}-\frac{mc^2}{E}+1\right\}^2\right]dE \tag{5}$$

whenever $E'\geq E\geq E'/(1+2E'/mc^2)$ from the Compton formula. Otherwise $d\varphi_c=0$.

Mr. H. Caulk has evaluated $F(E)$ to $n=4$ by numerical means. The infinite upper limit of Eq. (2) was replaced by 100 Mev. For the region below $\sim mc^2$, the convergence is no longer rapid and a separate treatment is required. Asymptotically the mean wavelength change in scattering approaches the Compton wavelength $\lambda_0\equiv h/mc$ for $\lambda\gg\lambda_0$. After many scatterings, the quanta "forget" their remote ancestry and we may write for the number of low energy quanta produced by one ancestor:

$$q(\lambda)d\lambda=d\lambda/\lambda_0 \tag{6}$$

independent of the original energy, or

$$q(E)dE=mc^2dE/E^2, \quad E\ll mc^2, \tag{7}$$

whence

$$F-f_0\rightarrow q(E)\int_0^{E_u} f_0(E')dE'. \tag{8}$$

Pair production is taken care of in the choice of E_u. For $E>E_u$ materialization is assumed invariably, while $E<E_u$ produces scattering only. A simple numerical calculation using the total cross sections for pair production and Compton scattering gives $E_u\sim 25$ Mev. The result is not very sensitive to this value. Inserting (1) and (7) in (8) and integrating, we obtain

$$F(E)-f_0(E)=(mc^2/E^2)\log(25/E), \quad E\ll mc^2. \tag{9}$$

This joins well with the values obtained above mc^2.

Figure 7 is a graph of the various spectra. The $F-f_0$ curve is made to go through the point given by Eq. (9) at $E=0.1$ Mev.

The spectrum of scattered radiation is fitted quite well by

$$F(E)-f_0(E)=3.0E^{-2.0} \tag{10}$$

over the range $0.1\leq E\leq 15$ Mev. Therefore,

$$F(E)=1/E+3/E^2. \tag{11}$$

The simplicity of the final result is fortuitous. The intensity spectrum $I_\gamma(E)$ of the γ-radiation is related to the production spectrum by

$$I_\gamma(E)=I_eF(E)/\mu(E)X_0 \text{ (Mev cm}^2\text{ sec sterad)}^{-1}. \tag{12}$$

I_e is the electron intensity, and $\mu(E)$ is the linear absorption coefficient. Introducing the air density ρ, the mass absorption coefficient μ/ρ, and the radiation thickness $\rho X_0=43$ g/cm^2, we have

$$\frac{I_\gamma}{I_e}=\frac{1}{43\mu(E)/\rho}\cdot\left\{\frac{1}{E}+\frac{3}{E^2}\right\}. \tag{13}$$

I_γ/I_e is plotted *vs* E in Fig. 8.

B. The Efficiency

A considerable literature[14] exists on the efficiency of a single Geiger counter for γ-radiation incident normal to the axis ("broadside" radiation). Our problem differs in three respects: a. The radiation is isotropic rather than broadside. b. The efficiency decreases above a certain energy due to penetration of the outer ring B by conversion products. c. The disposition of material about the counting volume is more complicated. We define an efficiency function $B(E)$ for isotropic radiation. If N_γ is the γ-ray counting rate of the device,

$$N_\gamma=\int_E B(E)I_\gamma(E)dE. \tag{14}$$

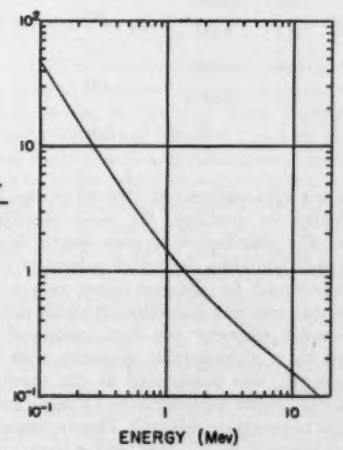

FIG. 8. Calculated relative intensity of γ-rays to electrons as a function of the γ-ray energy. The electrons have energy $>\sim 10^7$ ev.

[13] Values of the quantities appearing in this section have been taken wherever possible from W. Heitler, *The Quantum Theory of Radiation* (Oxford University Press, London, 1944), second edition.

[14] A bibliography may be found in M. Healea, Nucleonics 1, 68 (1947).

The function $B(E)$ has been determined at $E=1.2$ Mev by use of a standard Co^{60} source having a strength of 10 rutherfords ($2\times10^7\gamma$'s/sec).[15] The counting rate was determined as a function of the angle θ between the bundle axis and the line of length R joining bundle and source. It may be shown that:

$$B(1.2)=(8\pi^2R^2/2\times10^7)\int_0^{\pi}N_\gamma\sin\theta d\theta. \quad (15)$$

We assume that B varies with energy in the same manner as does the efficiency for broadside radiation. The data for copper counters of Renard[16] and the calculations of Marty[17] are used for the energy dependence and our value at 1.2 Mev for normalization. This applies up to an energy E_p at which the secondaries can begin

TABLE II. Values of the quantities used in calculating the atmospheric radiation.

E(Mev)	$B(E)$	$\mu(E)/\rho$	$\int_{\Delta E}\frac{B(E)}{E\mu(E)/\rho}dE$	$\int_{\Delta E}\frac{3B(E)}{E^2\mu(E)/\rho}dE$
0.1	1.14	0.15		
			3	82
0.15	0.89	0.13		
			2	36
0.2	0.84	0.12		
			3	41
0.3	1.04	0.11		
			7	52
0.5	1.58	0.087		
			22	90
1.0	3.21	0.063		
			62	122
2.0	6.4	0.044		
			82	100
3.0	9.9	0.036		
			213	165
5.0	16.6	0.028		
			292	146
7.2	24.3	0.023		
			311	117
10.0	15.5	0.020		
			194	58
15.0	0.0	0.0176		
Sum			1191	1009

to produce coincidences. At this stage the geometry complicates the problem. We have simplified it as follows. The distribution in path length through the copper wall bounding the active volume of counter A was determined by drawing-board techniques. The median thickness was determined from the distribution. The complex geometry was next considered as being replaced by a plane-parallel geometry with this wall thickness. E_p was determined as the energy of the gamma-ray, whose secondaries had a mean energy just adequate to penetrate this wall. This corresponds to an electron energy[18] of 4.7 Mev and a γ-ray energy of 7.2 Mev. As the γ-ray energy is increased, there is less and less wall available for the conversion, and the efficiency decreases nearly linearly until the electron range is 2 wall thicknesses. At this point the efficiency vanishes. This occurs at an electron energy of 10.8 Mev corresponding to γ-rays of 15 Mev.

This picture is necessarily rough. We do not think it introduces too large an uncertainty into the results however. The counting rate contributed by γ-rays in the region of decreasing efficiency is calculated to be ~30 percent of the total.

The counting rate of electrons is given by

$$\begin{aligned}N_e&=\pi I_e\times\text{surface area}\\&=480I_e/\text{sec}.\end{aligned} \quad (16)$$

Using this, and Eqs. (13) and (14), we have

$$\frac{N_\gamma}{N_e}=\frac{1}{480\times43}\int_{0.1}^{15}\frac{B(E)}{\mu(E)/\rho}\left\{\frac{1}{E}+\frac{3}{E^2}\right\}dE. \quad (17)$$

Values of the various quantities are given in Table II. We have, finally,

$$N_\gamma/N_e=0.11. \quad (18)$$

The ratio of measured (and corrected) counting rates in the neighborhood of the intensity maximum is given by

$$N_{A-B}/N_{AB}=0.12. \quad (19)$$

We do not know exactly how much of N_{AB} to ascribe to electrons and how much to other charged components. We may make an estimate based on Rossi's analysis[19] at the maximum for vertical radiation. He obtains ~65 percent for the fraction of electrons of $>10^7$ ev to the total charged vertical component. If we assume this ratio at our maximum (radiation from all directions), we obtain

$$N_{A-B}/(N_{AB})_{\text{electrons}}\sim0.18. \quad (20)$$

Our calculation accounts for ~60 percent of the measurement. The annihilation radiation of positrons is estimated below.

Annihilation of Positrons

We require the number of positrons which annihilate per unit time in a given volume. An upper limit to the intensity I_+ of positrons is $I_+\sim I_e/2$, neglecting collision electrons and Compton recoils, and the path length traversed per cm^3 and second is $4\pi I_+$.

Dividing this by the average range of the atmospheric positrons gives the number of stopping per cm^3 and second. We may estimate the range as the radiation length X_0. Thus, for example, Heitler[20] gives the mean range of a 50-Mev electron as $\sim X_0/2$ and a 500-Mev electron as $\sim2X_0$, the range increasing only logarith-

[15] We are indebted to the National Bureau of Standards for this source and its standardization.
[16] G. Renard, J. phys. et radium **9**, 212 (1948).
[17] N. Marty, J. phys. et radium **8**, 29 (1947).
[18] F. L. Hereford and C. P. Swann, Phys. Rev. **78**, 727 (1950).
[19] B. Rossi, Revs. Modern Phys. **20**, 537 (1948).
[20] See reference 11, p. 223.

mically with energy. Then in the standard volume ($X_0/4\pi$ cm^3) we have for $I_e=1$, as production spectrum of parent quanta,

$$f_{0+}(E)=\delta(E-mc^2) \tag{1'}$$

for this energy region Eq. (7) is a reasonable approximation for the scattered spectrum. The calculation then procedes analogously,

$$F_+(E)=mc^2/E^2+\delta(E-mc^2), \tag{11'}$$

$$I_{\gamma+}(E)=F_+(E)I_e/\mu(E)X_0 \tag{12' and 13'}$$

$$=\frac{I_e}{43\mu(E)/\rho}\left\{\frac{mc^2}{E^2}+\delta(E-mc^2)\right\},$$

$$N_{\gamma+}/N_e=\frac{1}{480\times 43}\left\{\int_{0.1}^{0.51}\frac{mc^2}{E^2}\frac{B(E)}{\mu(E)/\rho}dE+\frac{B(mc^2)}{\mu(mc^2)/\rho}\right\}. \tag{17'}$$

The integral, which represents the effect of scattering, is evaluated from the data in Table II as before. It has the value 36, compared to 18 for the second term which represents the annihilation quanta. Then

$$N_{\gamma+}/N_e=0.0026. \tag{18'}$$

This is negligible compared to the bremsstrahlung, (Eq. (18)).

We may conclude this section with the observation that, all approximations considered, the explanation given of the sources of the atmospheric radiation accounts for the measurements and that there is not room for any important additional source.

IV. THE RADIATION ABOVE THE ATMOSPHERE

After all corrections, the γ-ray counting rate per second above the atmosphere (Table I) remains at 1.0 ± 0.1 for the V-2 and 1.3 ± 0.2 for the daytime Aerobee. The probable errors shown are the statistical ones. The difference between the two flights may be taken, if one chooses, as due to an unknown systematic correction rather than a true effect. We have no choice, however, but to acknowledge the existence of a gamma-ray flux above the atmosphere. For the Aerobee flight it is possible to ascertain whether there was any significant change in counting rate above 50 km. None was observed. We do not believe however that the radiation is primary. Some, if not all, of it certainly originates in the atmosphere below the rocket and escapes out. We shall show below how a part of this has been calculated.

We consider two cases. In the first the earth is assumed flat and the radiation leaving the atmosphere is due to diffusion upward. A calculation of this is similar to that of determining the back scattering of γ-rays incident on an absorber[21] but is made more difficult by the fact that the γ-rays themselves are secondaries and are produced at various depths in the absorber. We have attempted a rough solution of the problem by analogy to the random walk, but we have not obtained a trustworthy result other than that the phenomenon exists and must produce some "albedo."

The second case depends on the curvature of the earth and is amenable to calculation. Primaries at grazing incidence, whose extended paths would reemerge from the atmosphere, produce low energy γ-rays by intermediate processes. These leave the atmosphere and form part of the albedo. Although the solid angle subtended at the rocket for such an effect is small, the multiplication along the relatively long air paths makes it significant. Figure 9 shows the process. The rocket is at height h. A primary ray under consideration has a path which passes a perpendicular height p from the earth. According to the rocket measurements of R. Havens,[22] the atmospheric thickness above p is given by $t_p=a\exp(-h/H)$, where the "scale height" H has the value 8.2 km and $a=420$ g/cm^2. This holds within seasonal variation at $p=40$–60 km where the effect

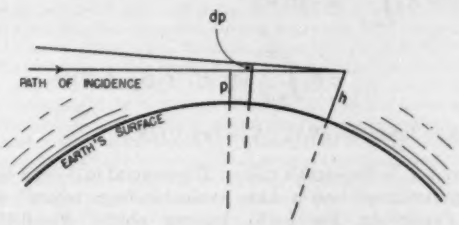

FIG. 9. Production of γ-ray albedo due to curvature of the earth.

mainly occurs. The atmospheric thickness t_i traversed along the path of incidence has a nearly constant proportionality $t_i=63t_p$ in this same range, according to calculations of Newell and Pressly[22] based on Havens' atmosphere.

We have to consider the spread of the radiation about the direction of incidence. Examination of the calculation of the previous section shows that the counting rate would be diminished by only 15 percent if the detector responded only to energies above 1 Mev. For such energies the angular spread is relatively small. If it is taken as zero and calculation made for various h, and if the result does not vary much with h, we shall be justified in assuming that the scattering of rays away from the direction of incidence is approximately balanced by the scattering of others toward it. A trial calculation shows this to be the case. We have therefore neglected the angular spread.

In order to obtain the γ-ray intensity along the path

[21] L. L. Foldy, Phys. Rev. **82**, 927 (1951). L. V. Spencer and F. Jenkins, Phys. Rev. **76**, 1885 (1949).
[22] Private communication.

of incidence, a Gross transformation has been made of the corrected altitude counting rate curve. This gives approximately the vertical intensity in units of γ-ray counts/sec sterad per bundle. By virtue of the isotropy of the primaries, the intensity along the path of incidence has the same variation with thickness traversed. The intensity and composition of the primary radiation need not be considered. The transformed function may be approximated, for our purpose, by straight lines:

$$I(t_i)=\begin{cases} t_i/60, & 0\leq t_i\leq 130 \text{ g/cm}^2 \\ 4.3-t_i/60, & 130\leq t_i\leq 220 \text{ g/cm}^2. \end{cases} \quad (21)$$

The calculation is not taken to greater thickness. The greatest vertical depth considered is $t_p=3.5$ g/cm^2 corresponding to 39.3 km. The lines intersect at $p=43.6$ km. With the aid of a little geometry we may show that the counting rate of albedo is $N=N_1+N_2$, where approximately

$$N_1=K_1\int_{43.6}^{h}(h-p)^{-\frac{1}{2}}\exp(-p/H)dp,$$

$$N_2=K_2\int_{39.3}^{43.6}(h-p)^{-\frac{1}{2}}dp \quad (22)$$

$$-K_1\int_{39.3}^{43.6}(h-p)^{-\frac{1}{2}}\exp(-p/H)dp,$$

$$K_1=2\pi 63a/60(2R_e)^{\frac{1}{2}},\quad K_2=2\pi 4.3/(2R_e)^{\frac{1}{2}},$$

and R_e is the earth's radius. The integral in N_1 can be transformed into a form evaluable from tables[23] of $\int\exp(x^2)dx$. For $h=82$ km we obtain $N_1=0.17$, $N_2=0.07$, whence $N=0.24$ count/sec.

This is one-fourth of the corrected rate above the atmosphere. It is likely that the remaining three-fourths would be explained by a treatment of the "flat-earth" or diffusion albedo.

It should be noted that a similar treatment may be accorded the various other secondary radiations. One expects, for example, an albedo of electrons, protons, and neutrons. Calculation of the former two is complicated by the earth's magnetic field.

If the albedo explanation of the observed flux is correct, then our measurements taken along with those at high energy indicate at most a very small primary gamma-ray component. An immediate implication is support for the contention that magnetic fields exist over large regions of space. As is well known, the fields increase the path length, hence the intensity, of charged particles and not that of photons.

The authors are grateful for the continued interest and encouragement of Dr. H. E. Newell, Jr., in their work. We wish to acknowledge the aid of other colleagues in the Rocket Sonde Branch, chiefly; Mr. H. M. Caulk for numerical evaluation of the scattering integrals; Messrs. J. Siry and H. Spitz and Miss E. Pressly for other mathematical work at various times; Messrs. J. T. Mengel, D. Mazur, and N. R. Best for telemetering of data from the rockets; Mr. C. P. Smith, Mr. V. Goblirsch, and the late Mr. R. Chamberlain for the engineering details associated with the rocket installations. Mr. C. A. Schroeder helped in the electronic design and Mr. P. R. McCray in the construction. In addition we are grateful for help in telemetering from the personnel of the New Mexico College of Agriculture and Mechanical Arts, chiefly Messrs. C. Ricketts and H. A. Ware. We were aided by military and civilian personnel of the White Sands Proving Ground and wish especially to thank Maj. N. Pozinsky, USMC, Mr. H. Karsch and Mr. L. D. White.

We have had fruitful conversations during the course of this investigation with Dr. M. H. Johnson and Professor J. A. Wheeler.

[23] H. M. Terrill and L. Sweeney, J. Franklin Inst. 237, 495 (1944).

Letters to the Editor

PUBLICATION of brief reports of important discoveries in physics may be secured by addressing them to this department. The closing date for this department is five weeks prior to the date of issue. No proof will be sent to the authors. The Board of Editors does not hold itself responsible for the opinions expressed by the correspondents. Communications should not exceed 600 words in length.

The Absorption of Pions by Deuterons*

R. DURBIN, H. LOAR, AND J. STEINBERGER
Columbia University, New York, New York
(Received September 17, 1951)

THE study of the absorption of positive pions by deuterons, which, together with its inverse, has been used to determine the spin of the meson,[1,2] has been extended. We present here results on the energy dependence of the angular distribution and of the total cross section, in the hope that they will prove useful in the attempt to understand the pion-nucleon interaction.

The reaction is $\pi^+ + d \rightarrow p + p$. The reaction rate is determined by the rate of recoil proton pairs in coincidence with incoming mesons, incident successively on water and heavy water targets. The experimental technique has already been described.[1] The water cells are 1" thick along the beam direction. The energy dispersion due to target thickness and meson beam inhomogeneity is approximately ± 7 Mev. The angular dispersion is approximately $\pm 14°$. Despite this poor resolution the coincidence rate of recoil protons is only $\sim$1/minute in the Nevis meson beam of $\sim$500/sec. The uncertainties in the result are almost entirely statistical; the geometrical factors have been calculated with greater accuracy, and the combined uncertainties in counting efficiency and beam composition are less than 10 percent.

The results are given in Table I. All parameters as well as differential cross sections are in the center of mass system. The recoil angles listed are averaged over the angular dispersion. This affects only the angles near 90°, since, because of the symmetry, 90° is the extreme angle, and larger angles are recorded as smaller angles. When the proton counter axes are set at 90° relative to the meson beam, the average detection angle is 83°.

It is possible to represent the angular dependence as $\alpha + \beta \cos^2\theta$, since meson angular momenta with respect to the deuteron of more than two Planck units should not contribute appreciably at these energies. The best fits to such a distribution are given in Table II, together with absolute cross sections.

In Table II we have also included the results of Cartwright, Richman, Wilcox, and Whitehead.[3] The angular distribution found at Berkeley and our results are only in fair agreement.

There is no large change in the angular distribution in the energy range 25–53 Mev for the incident meson in the center of mass system. The total cross section increases by a factor 2.25 ± 0.32.

To see the implication of this result on the meson nucleon interaction, it is necessary to separate the effects of the nuclear binding in initial and final states as well as the kinematical factors. The effects of the binding on the angular distribution are complicated, and are discussed in the following note.[4] The kinematical factors are

TABLE I. Differential cross sections for the absorption of pions by deuterons in the center of mass system. Rms statistical errors are given.

$E_\pi = 25$ Mev		$E_\pi = 40$ Mev		$E_\pi = 53$ Mev	
θ_{cm}	$d\sigma/d\Omega$ cm²/sterad	θ_{cm}	$d\sigma/d\Omega$	θ_{cm}	$d\sigma/d\Omega$
29°	$8.5 \pm 1.1 \times 10^{-28}$	30°	$17.4 \pm 2.6 \times 10^{-28}$	30°	$20.1 \pm 4 \times 10^{-28}$
35°	7.3 ± 1.6	50°	9.2 ± 1.5	60°	5.7 ± 1.8
45°	7.5 ± 2.2	70°	8.4 ± 2.4	83°	5.5 ± 2.1
50°	7.1 ± 0.9	83°	4.0 ± 1.7	...	...
82°	1.7 ± 0.6	...	...	...	...

TABLE II. Total cross sections and best fit angular distributions for the data in Table I.

E_π	Angular distribution	Total cross section
21.5 Mev[a]	$10.7\ (\cos^2\theta + 0.07) \times 10^{-28}$ sterad/cm²	$2.8 \pm 0.8 \times 10^{-27}$ cm²
25 Mev	$9\ (\cos^2\theta + 0.22) \times 10^{-28}$ sterad/cm²	$3.1 \pm 0.3 \times 10^{-27}$ cm²
40 Mev	$18\ (\cos^2\theta + 0.2) \times 10^{-28}$ sterad/cm²	$6.1 \pm 0.6 \times 10^{-27}$ cm²
53 Mev	$21.5\ (\cos^2\theta + 0.18) \times 10^{-28}$ sterad/cm²	$7.0 \pm 0.7 \times 10^{-27}$ cm²

[a] We include the result of the Berkeley group on the inverse reaction, inverted on the basis of the law of detailed balance and zero spin for the pion.

K = momentum space/(relative velocity of incoming nucleons $\times$ total meson energy).

The factor 1/total meson energy is not strictly a kinematical factor; it is due to the normalization of the meson wave and is included because it is omitted in the theoretical analysis which follows this letter.

$$k_{53}/k_{25} = 0.71.$$

The average square of the matrix element for the process therefore increases by the factor $2.3/0.71 = 3.25 \pm 45$ in the energy range 25–53 Mev. This is a considerable increase, especially since the effects of binding also decrease the cross section at higher relative to lower meson energy. This effect is approximately

$$|f(k/k_{53})/f(k/k_{25})|^2,$$

where $f(k/k_{53})$ is the fourier amplitude of the deuteron or the diproton wave function for the momentum of one of the recoil protons resulting in the absorption of a 53-Mev meson. These fourier amplitudes decrease at least as $1/k^2$ and probably more nearly as $1/k^3$ for such large momenta. If this factor is also taken into account, then the meson-nucleon interaction must increase by a factor $\sqrt{4.5} - \sqrt{6}$ in the meson energy interval 25–53 Mev. The meson momentum increases by the factor 1.53 in this interval so that the meson nucleon interaction must increase approximately as the square of the momentum of the meson. This is of course a stronger momentum dependence than the linear dependence predicted in pseudoscalar theory with pseudovector coupling. Other theories predict an even weaker dependence and are also in conflict with other experiments. The steep energy dependence is probably of the same origin as the steep excitation function in neutral photomeson production[5,6] and may be due to some resonance effect, as has already been suggested in connection with the photomeson experiments.[7,8]

We wish to thank the operating crew of the Nevis cyclotron, under the direction of J. Spiro, for the bombardments.

* Research sponsored by a joint program of the ONR and AEC.
[1] Durbin, Loar, and Steinberger, Phys. Rev. **83**, 646 (1951).
[2] Clark, Roberts, and Wilson, Phys. Rev. **83**, 649 (1951).
[3] M. Whitehead and C. Richman, Phys. Rev. **83**, 855 (1951).
[4] Chew, Goldberger, Steinberger, and Yang, Phys. Rev. **84**, 581 (1951).
[5] A. Silverman and M. Stearns, Phys. Rev. **83**, 853 (1951).
[6] Panofsky, Steinberger, and Steller (to be published).
[7] K. Brueckner and K. Case, Phys. Rev. **83**, 1141 (1951).
[8] Y. Fujimoto and H. Miyazawa (to be published).

A Theoretical Analysis of the Process $\pi^+ + d \rightleftarrows p + p$

GEOFFREY F. CHEW, *Brookhaven National Laboratory, Upton, New York*
M. L. GOLDBERGER, *Institute for Nuclear Studies, University of Chicago, Chicago, Illinois*
J. M. STEINBERGER, *Columbia University, New York City, New York*
AND
C. N. YANG, *Institute for Advanced Study, Princeton, New Jersey*
(Received September 17, 1951)

THE experiment described in the preceeding letter[1] as well as those on the inverse reaction, the production of mesons in the collision of two protons, may be analyzed in the spirit of

the impulse approximation.[2] It will be shown that the predominantly $\cos^2\theta$ angular distribution can be understood without great difficulty, and that the reaction may be used to obtain information on the high momentum components of the $n-p$ and $p-p$ interaction.

The matrix element for the transition is to be written

$$(\psi_f, T\psi_i), \tag{1}$$

where ψ_i is the internal wave function of the deuteron in its ground state and ψ_f the continuum wave function of a diproton with relative momentum, k_f. The operator T must have the form,

$$t_1 \exp(\tfrac{1}{2}i\mathbf{q}\cdot\mathbf{r})+t_2 \exp(-\tfrac{1}{2}i\mathbf{q}\cdot\mathbf{r}),$$

where $\mathbf{q}$ is the meson momentum, $\mathbf{r}$ is the relative nucleon coordinate and, if the meson is pseudoscalar, t_i must be some pseudoscalar operator. We assume that t_i is of the form,

$$t_i=\boldsymbol{\sigma}_i\cdot[a\boldsymbol{\nabla}_r+b\mathbf{q}]\tau_i^+, \tag{2}$$

where $\boldsymbol{\sigma}_i$ and τ_i are the nucleon spin and isotopic spin operators and a and b may be arbitrary scalar functions of q. The restricted form of the dependence of (2) on nucleon variables is motivated by meson theory.[3] Otherwise the formulation here is completely phenomenological.

The experiment to be analyzed involves sufficiently small meson energies that one may replace $\exp(\frac{1}{2}i\mathbf{q}\cdot\mathbf{r})$ by unity. The error incurred thereby is of the order $q^3/k_f^3\approx 0.1$. In this approximation the term in (2) proportional to a can lead only to final states of odd parity (triplet) and obviously yields an isotropic angular distribution.

The term proportional to b gives a contribution to the cross section which may be anisotropic if the deuteron is partly a D state. The final nucleon states here must be of even parity (singlet), and do not interfere with the $\boldsymbol{\sigma}\cdot\boldsymbol{\nabla}$ terms. The contribution to the square of the matrix element, appropriately summed and averaged, is

$$\tfrac{1}{4}|b|^2\, q^3\{F_0^2+2^{\frac{1}{2}}\cos(\delta_0-\delta_2)\cdot\tfrac{1}{2}F_0F_2(3\cos^2\theta-1) +\tfrac{1}{2}F_2^2(3\cos^2\theta+1)\}, \tag{3}$$

where

$$F_0=\int_0^\infty u_f(r)u_i(r)dr, \quad F_2=\int_0^\infty w_f(r)w_i(r)dr,$$

if u_i and w_i are the radial parts of the deuteron S and D functions as defined by Rarita and Schwinger,[4] and u_f and w_f are the S and D radial functions for the continuum diproton system, normalized asymptotically to $\sin(kr+\delta_0)$ and $\sin(kr+\delta_2-\pi)$, respectively. The angle between the incident meson and one of the outgoing protons in the center-of-mass system is θ.

At very low meson energies the triplet transitions induced by the $\boldsymbol{\sigma}\cdot\boldsymbol{\nabla}$ term in (2) dominate, but the experimental evidence shows that between 20 and 50 Mev the singlet transitions are more important. In the first place, the very small cross section for the reaction, $p+p\rightarrow\pi^0+2p$,[5] compared to that for $p+p\rightarrow\pi^++d$,[6] is easily explained[7] only if the $\boldsymbol{\sigma}\cdot\mathbf{q}$ term is dominant. Confirmation is given by the observed constancy of the angular distribution in the meson energy.[1] This constancy is not possible if singlet and triplet transitions are of comparable probability, since they have different energy dependences. It is therefore inconsistent with the experimental accuracy attained up to now in the energy region above 20 Mev to include the terms proportional to a in the analysis. They are omitted in the following.

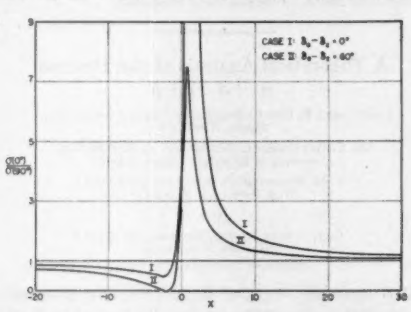

FIG. 1. Theoretical ratio of the cross section at 0° to that at 90° as a function of x.

Considering first the question of angular dependence, formula (3) may be written $\alpha+\beta\cos^2\theta$, where

$$\frac{\alpha+\beta}{\alpha}=\frac{\sigma(0°)}{\sigma(90°)}=\frac{x^2+4x\cos(\delta_0-\delta_2)+4}{x^2-2x\cos(\delta_0-\delta_2)+1}, \tag{4}$$

if $x=\sqrt{2}F_0/F_2$. The function (4) is plotted in Fig. 1 for two values of $\delta_0-\delta_2$. An attempted theoretical estimate of the constants F_0 and F_2, together with a discussion of terms of higher order in q^2/k_f^2, will be given later in a more complete report. It should be stated at once, however, that ignorance of the nuclear wave functions at short distances makes definite conclusions impossible. If the central part of the triplet $n-p$ force is equal to the singlet $p-p$ force, as suggested by the work of Pease and Feshbach,[8] then F_0 and x very nearly vanish. (The functions u_i and u_f are "almost" orthogonal.) Then $\sigma(0°)/\sigma(90°)=4$. On the other hand, nuclear force models designed only to fit scattering data have a sufficient number of free parameters that the sign and magnitude of x can be made almost anything. To fit the experimental value of $\sigma(0°)/\sigma(90°)=6$, x must be either 0 or 2-3, as seen from Fig. 1.

It will be shown in the more complete report that as the meson energy increases, the integrals F_0 and F_2 must decrease at least as fast as $1/k_f^2$ and probably as $1/k_f^4$. The observed increase in the absorption cross section then requires the parameter b in (2) to be an increasing function of meson energy. This is in definite disagreement with the weak coupling meson theory, indicating that the meson wave function is strongly perturbed in the region near the nucleon.

The authors wish to acknowledge great benefit from conversations with R. Serber. For comparison with other published phenomenological treatments of this problem, the following points of difference should be noted: Cheston,[9] Fujimoto and Yamaguchi,[10] and Brueckner[11] either omit or inadequately approximate both the diproton wave function and the deuteron D-state. Watson and Brueckner do not attempt to separate the meson-nucleon interaction from the interaction between the two nucleons and therefore their article is not an analysis in the sense of this work.

[1] Durbin, Loar, and Steinberger, Phys. Rev. **84**, 581 (1951).
[2] G. F. Chew and G. C. Wick (to be published).
[3] In pseudoscalar theory with pseudovector coupling, the operator t has the form $(g/\mu c)[\boldsymbol{\sigma}\cdot\mathbf{q}+i\hbar(E_q/Mc)\boldsymbol{\sigma}\cdot\boldsymbol{\nabla}]$.
[4] W. Rarita and J. Schwinger, Phys. Rev. **59**, 436 (1941).
[5] Moyer, Madey, Hildegrand, Knable, and Hales, Phys. Rev. **83**, 206 (1951).
[6] M. Whitehead and C. Richman, Phys. Rev. **83**, 855 (1951).
[7] K. M. Watson and K. A. Brueckner, Phys. Rev. **83**, 1 (1951).
[8] R. L. Pease and H. Feshbach, Phys. Rev. **81**, 142 (1951).
[9] W. B. Cheston (to be published).
[10] Y. Fujimoto and Y. Yamaguchi, Prog. Theor. Phys. **6**, 166 (1951).
[11] K. Brueckner, Phys. Rev. **82**, 598 (1951).

Penetrating Showers Produced in Beryllium at Sea Level

W. Y. CHANG, G. DEL CASTILLO,* AND LEON GRODZINS
Physics Department, Purdue University, Lafayette, Indiana
(Received August 6, 1951)

THE cloud-chamber equipment, previously reported,[1] has been set up at Purdue to investigate penetrating showers produced in Be, C, and Pb. Figure 1 shows the arrangement. All the counters have a diameter of one inch. The lengths of trays A, B, C and D (fivefold coincidence) are respectively 6, 3.5, 12, and 14 inches. Tray C counters are connected for shower detection of at least two particles. The chamber expands, when a shower is produced (by a charged primary particle, presumably a high energy proton) in the 10-inch C block above (later replaced by

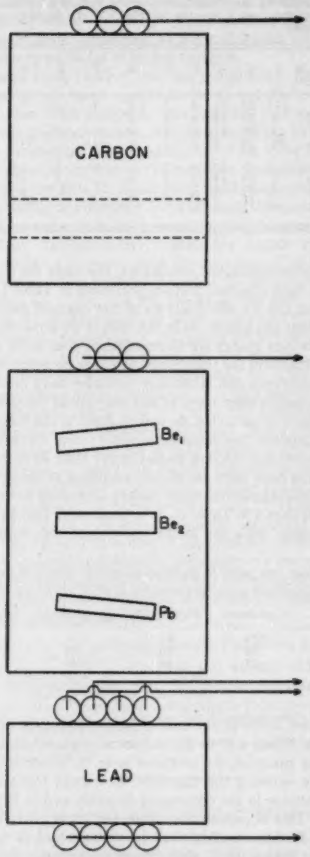

FIG. 1. Arrangement for shower equipments.

same amount of Pb, i.e., 43 g/cm², or in the Be_1 or Be_2 plate (4.8 g/cm²) inside, and has at least two particles to discharge two neighboring tray C counters, one of them being energetic enough to pass through the Pb block (110 g/cm²) below and then discharge a tray D counter. The Pb plate (17 g/cm²) inside the chamber serves to infer the nature of the particles passing through it. The illuminated depth of the chamber was greater on both sides than the depth (4 inches) of the Be or Pb plate, so that particles which pass in front of the plates can easily be seen. Only those showers have been selected, which have their axes near to the central portion of the plates and appear to have all of their particles falling within the surface of the plates. Most of the small and medium showers have entered the chamber in this manner due to counter disposition. In this way we shall be more certain about the multiplicity and penetrating power of the shower particles. In all the experiments stereoscopic pictures have been taken.

The results for beryllium will be reported here, while those for carbon and lead will be discussed in another note, because the experimental conditions for C and Pb are the same. The total experimental period for Be was about 11 months; for the first 6 months carbon was above the chamber, for the remainder, lead.

A particle is defined as penetrating if it passes through the bottom Pb plate (17 g/cm²) inside the chamber without multiplication or multiple scattering greater than 20 degrees.[3] In the case of Be, a penetrating shower is defined as follows: Two or more tracks, as seen in the gas space immediately below their origin, must appear from the same point within a Be plate. (1) When only two particles are seen, both of them must be penetrating particles as defined above; for, if only one of them is penetrating, the stopped one may be just a knock-on electron. We have observed 36 cases of this latter type, which were therefore discarded, though some may be real consequences of nucleon-nucleon collisions. (2) When 3 or more are seen in the space below the origin, at least one of them must be penetrating. The chance is considerably smaller for two knock-on electrons to be ejected from about the same point by a single penetrating particle. Only 3 such cases (three or more particles seen and only one penetrating) have been found and are included in our statistics. A single penetrating particle can discharge two neighboring tray C counters if it has one knock-on electron in this direction, and discharge one tray D counter if it is energetic enough to penetrate the 110 g/cm² Pb block. Therefore, we are concerned here with showers, each of which has at least one particle having a range in Pb of at least about 130 g/cm².

TABLE I. Multiplicity distribution for beryllium. Working period—11 months. N is the number of charged particles per shower.

Absorber	Gas space \ N	1	2	3	4	5	6
	2nd		27	9	1		1
Be_1	3rd		30	7		1	
4.8 g/cm²	4th	3	32	2		1	
Be_2	3rd		18	3	2	1	1
4.8 g/cm²	4th		20	2	2	1	

Under the above conditions the showers produced in the two Be plates have been selected and tabulated in Table I, which shows the multiplicity distribution of the charged particles as seen in the different gas spaces (in descending order) inside the chamber. The particles counted in the third or fourth gas space are those which appear to be a continuation of the tracks in the preceding space. Secondaries are not included. In this way we may learn more about the behavior of the shower particles with respect to their penetrating power in the Be and Pb plates. Most of the stopped particles are simply absorbed by the plates without producing any observable effect, some produce secondaries, and a few are scattered at angles greater than 20 degrees. From the total numbers of the shower particles in the different gas spaces, we have estimated the mean free paths of the particles respectively in Be_2 and Pb plates, using the relation $n=n_0e^{-x/L}$. For Be_1 showers, $L_{Be_2}=85$ g/cm² and $L_{Pb}=180$ g/cm². This may indicate that initially the showers might have more low energy particles which are easily absorbed by the Be_2 plate, while after the Be_2 plate relatively more penetrating particles remained which would then have a larger mean free path in Pb. Also, the effect of atomic number tends to decrease the mean free path in Be. The above figures are only approximate because of low statistics and difficulty in tracing the tracks, and so the conclusions are merely tentative. For Be_2 showers $L_{Pb}=200$ g/cm², comparable with L_{Pb} for Be_1 showers.

The average multiplicity per shower in the space immediately below the origin of production is about 2.5 from the data of both Be_1 and Be_2. This figure is smaller than that for C and Pb showers, both having 2.8 in the first gas space. This difference must not be

TABLE II. Angular distribution for beryllium. N_1 is the number of particles in the space just below the origin making the projected angle θ with the primary particles.

θ, deg	N_1	θ, deg	N_1	θ, deg	N_1
0–2	95	6.1–8	4	20–22	3
2.1–4	18	8.1–10	2	30–32	1
4.1–6	11	12 –14	3	34–36	1

over-emphasized because of poor statistics. Besides, exact comparison is not justified, for the experimental conditions and conditions for selecting showers are somewhat different for Be and for C and Pb. However, in general, one may say that Be, C, and Pb have similar multiplicity and angular distributions, which may indicate a mechanism of multiple production. This point will be discussed in more details in the note for C and Pb. It is to be noted that our multiplicity for Be seems to be smaller than that obtained recently by Fretter[3] from 13 cases for Li above a chamber at sea level. The projected angles with the primary were measured of the shower particles in the space just below the origin. The distribution is shown in Table II, indicating that the shower particles are emitted with an extremely strong preference for the direction of the primary.

We are thankful to Princeton University for the apparatus used in this work, which one of us (W.Y.C.) and his co-workers built at Princeton, and to our Colleagues at Purdue for their interest and support in these experiments.

* Supported in part by Purdue Research Foundation and Mexican Research Commission C.I.C.I.C.

[1] W. Y. Chang and J. R. Winckler, Rev. Sci. Instr. **20**, 276 (1949).
[2] Rochester, Proc. Roy. Soc. (London) **A187**, 464 (1946).
[3] W. B. Fretter, Phys. Rev. **80**, 921 (1950).

Penetrating Showers Produced in Carbon and Lead at Sea Level

W. Y. Chang and G. del Castillo*
Physics Department, Purdue University, Lafayette, Indiana
(Received August 6, 1951)

THE experimental arrangement and general conditions for recording the showers have been briefly described in the preceding note for the Be showers.[1] The first 6 months were spent studying the showers produced in the 10-inch C block above the chamber, while the next 5 months were for the showers from a Pb block of the same thickness, 43 g/cm², which replaced the C block (counter disposition kept the same); the Be plates remained inside the chamber for all the 11 months. Since the C and Pb blocks used had the same amount of material in g/cm², the absorption of shower particles with a given energy distribution would be approximately the same in the two elements. The Pb block was placed about 1.5 inches below the middle of the replaced 10-inch C block, so that the scattered (more in Pb) shower particles would have a larger chance to enter the chamber. The Be and Pb plates, respectively 4.8 and 17 g/cm², inside the chamber serve to study the particles of the C and Pb showers. There are altogether 63, 84, and 73 showers selected, respectively, from Be, C, and Pb. The statistics are compatible with the three different working periods and amounts in g/cm² of the three elements used.

As with Be, a penetrating particle is defined as one passing through the Pb plate (17 g/cm²) inside the chamber without multiplication or scattering larger than 20 degrees. A penetrating shower is here defined as one which has at least two tracks seen in the first gas space and at least one of them a penetrating particle (the stopped one must show no appreciable scattering). They must, of course, appear to come from the same origin within the C or Pb block as examined in both the direct and stereoscopic pictures. Single isolated penetrating particles are discarded, for most of them are presumably mu-mesons. A few of them may be penetrating showers with only one penetrating particle entering the chamber and the rest absorbed by the material above the chamber. Here we are concerned with showers, each of which has at least one penetrating particle having a minimum range lying between 140 g/cm² Pb and 140 g/cm² Pb plus 43 g/cm² Pb or C (see Be note). In both experiments for C and Pb, quite a few large mixed showers with total number of particles around 10 or larger have been observed. They have not been included in our statistics because of uncertainty in their origins because of some particles being badly scattered in random directions.

TABLE I. Multiplicity distribution for carbon and lead. Working period —6 months for carbon and 5 months for Pb. N is the number of charged particles per shower.

Absorber	Gas space \ N	1	2	3	4	5	6	7	8	9	10	15
Carbon 43 g/cm²	1st	···	52	21	3	5	1	1	···	···	···	1
	2nd	1	55	18	3	4	2	···	···	···	···	1
	3rd	4	60	11	4	2	2	···	···	···	···	1
	4th	40	33	8	1	1	1	···	···	···	···	···
Lead 43 g/cm²	1st	···	47	15	3	2	2	1	1	1	1	···
	2nd	1	49	13	3	2	3	···	1	1	···	···
	3rd	5	51	9	3	2	2	···	···	1	···	···
	4th	40	27	5	1	···	···	···	···	···	···	···

Under the aforementioned conditions, the data for C and Pb showers have been obtained and are presented in Table I, according to the multiplicity distributions of the charged particles observed in the four gas spaces. As in the case of Be showers, the particles in the various spaces are those which appear to be a continuation of the tracks in the preceding space (see Be note for manner of recording showers), and secondary particles have not been included. One hopes to learn more in this way about the penetrating power of the shower particles. As before, most of the stopped particles do not produce any observable effect, some have secondaries, and a few are scattered at angles larger than 20 degrees. The mean free paths have been estimated, assuming as before that the shower particles are absorbed exponentially according to $n = n_0 e^{-x/L}$. The values are shown in Table II. It is to be noted that here we are concerned mostly with the latter sections of the range of the

TABLE II. Mean free paths in g/cm² at successive points of the range.

	C showers	Pb showers	Be_1 showers	Be_2 showers
L_{Be1}	120	85	···	···
L_{Be2}	70	50	85	···
L_{Pb}	45	40	180	200

shower particles, while in the case of Be we are in the early parts of their range. When a C or Pb shower is produced in the upper portion of the material, its particles have to traverse the lower portion before entering the chamber. The mean free path in Be appears to decrease in the downward direction and in Pb becomes still smaller. This is conceivable from the energy consideration. The effect of atomic number must be remembered in comparing L_{Be} and L_{Pb}. Values for C showers are consistently larger than the corresponding values for Pb showers. However, as before, these figures must not be emphasized too much, because of low statistics and difficulty in tracing a track in the different spaces.

The average multiplicity per shower has been estimated for the charged particles as observed in the first gas space. Both C and Pb showers have the same value of 2.8. The average multiplicity at the origin may be higher because some low energy shower particles may have been absorbed by the material between the origin and the chamber. Reference to the Be results seems to indicate that the initial absorption is not too serious and hence the increase in multiplicity may not be high. The multiplicity of all ionizing particles as obtained recently by Fretter[3] and Green[5] for Pb and C,

TABLE III. Angular distribution—carbon and lead. N_1 is the number of particles in the first gas space making the projected angle θ with the shower axis.*

θ, deg	N_1(C)	N_1(Pb)	θ, deg	N_1(C)	N_1(Pb)
0–2	140	98	14–16	3	3
2.1–4	41	36	16.1–18	···	4
4.1–6	22	27	18.1–20	4	···
6.1–8	9	17	23–25	1	2
8.1–10	8	12	···	···	···
10.1–12	···	6	42–44	···	1

* See reference 5.

respectively, are higher than ours. This may be due, in addition to the foregoing reason (probably a minor one), to the fact that their experiments were performed at high altitudes where there are more primary particles of higher energies.

It is seen from Table I that the multiplicity distributions obtained under the same conditions for C and Pb are very similar to each other. This similarity may indicate that mesons are produced from nucleon-nucleon collisions according to the process of multiple production. The distribution for Be, C, or Pb is generally compatible with the theory[4] of multiple production for primary energies of a few Bev. If, on the other hand, successive interactions, each producing one meson,[5] occurred fairly frequently within the same nucleus of carbon, they would be very frequently within the Pb nucleus. Consequently, appreciably higher multiplicity of mesons would be expected from Pb than from C or Be. According to the mechanism of plural production, in order to have the same multiplicity for C, Be, and Pb, the mean free path, in the nuclear matter, of the primary particles must be so small that the primary particle could dissipate all of its energy within even the C or Be nucleus and certainly then within the Pb nucleus. However, this condition does not seem to be supported by other observations, such as successive events produced by a high energy particle from the first shower, which may be either the primary proton or a knock-on proton (see Fretter[6] and Green[7]). Moreover, the criterion of smaller mean free path as already defined would probably lead to the emission of more low energy charged particles from the same nucleus and hence to a larger angular spread. The angular distributions of shower particles for C and Pb as shown in Table III,[8] and for Be as given before, all show extremely strong preference for the forward direction of the primary particles.

We are thankful to Princeton University for the apparatus used in this work, which one of us (W.Y.C.) and his co-workers built at Princeton, and to our colleagues at Purdue for their interest and support in these experiments.

* Supported in part by Purdue Research Foundation and Mexican Research Commission C.I.C.I.C.

[1] Chang, del Castillo, Grodzins, Phys. Rev. **84**, 582 (1951).
[2] W. B. Fretter, Phys. Rev. **76**, 511 (1949).
[3] F. R. Green, Phys. Rev. **80**, 832 (1950).
[4] E. Fermi, Prog. Theor. Phys. **5**, 570 (1950); Phys. Rev. **81**, 863 (1951).
[5] Heitler and Janossy, Proc. Phys. Soc. (London) **A62**, 364, 669 (1949); Helv. Phys. Acta **23**, 417 (1950).
[6] The shower axis is determined by the average angle with the vertical of the penetrating particles.

Gamma-Coincident Beta-Spectra of I^{131}

B. H. Ketelle, H. Zeldes, A. R. Brosi, and R. A. Dandl
Chemistry Division, Oak Ridge National Laboratory, Oak Ridge, Tennessee*

(Received September 4, 1951)

In a study of I^{131} decay the beta-energy distributions coincident with particular gamma-rays were measured. This was done by mounting an essentially weightless iodine source on a Be disk in a thin magnetic lens spectrometer. The NaI—Tl crystal of a scintillation spectrometer was mounted immediately behind the beryllium disk. Coincidences between pulses in the proportional counter detector and pulses from the scintillation spectrometer corresponding to a definite gamma-ray energy were measured. A delay in the differential discriminator of the scintillation spectrometer was matched by a 1 μsec delay line between the proportional counter and the coincidence circuit. A resolving time of about 0.3 μsec was used in the coincidence circuit.

The pulse-height distribution from the scintillation counter is shown in Fig. 1C. It can be seen that pulses arising from the individual 720-kev, 635-kev, and 364-kev gamma-rays can be counted without including more than a few percent of pulses arising from a second gamma-ray. In the case of the 284-kev gamma-ray of the order of 10 percent of the pulses will be contributed by the 364-kev gamma-ray.

Only the 284-kev gamma-ray is definitely coincident with the *K*-conversion electrons of the 80-kev gamma-ray. The K-conversion peak of the 80-kev gamma-ray is shown in curve B of Fig. 1.

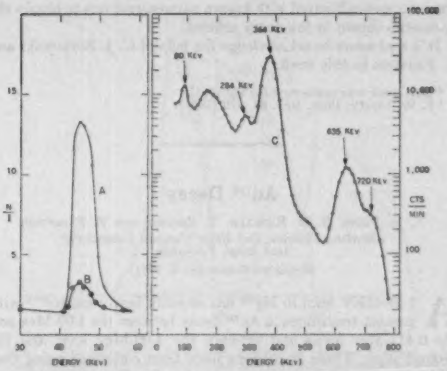

Fig. 1. Curve A. *K*-conversion electron peak of 80-kev gamma-ray coincident with the 284-kev gamma-ray; Curve B. *K*-conversion electron peak of 80-kev gamma-ray; Curve C. Scintillation spectrometer pulse-height distribution of I^{131} gamma-radiation.

Curve A of Fig. 1 shows the energy distribution of electrons coincident with the 284-kev gamma-ray. The two curves are normalized to have the underlying beta-distributions at the same level. Because of statistical fluctuations in the coincidence counting rates it cannot be stated that the 364-, 635-, or 720-kev gamma-rays are in no case coincident with conversion electrons of the 80-kev gamma-ray. The data do indicate that not more than 15 percent of the transitions of these gamma-rays are coincident with the 80-kev gamma-ray.

Kurie plots of the coincident electron energy distributions in Fig. 2 show that the 720-, 635-, and 364-kev gammas are in coincidence with beta-groups with maximum energies of 250, 335, and 606 kev, respectively. The 284-kev gamma-ray also is coincident with a 606-kev maximum energy beta-group. The excess of low energy electrons in the 606-kev beta-curve was shown to be the result of back scattering from the beryllium source mount. Energy distribution curves of several well-known beta-emitters mounted on beryllium indicate that the energy at which scattering becomes important is a function of the maximum energy of the beta-emitter. In the case of the 250-kev and 335-kev beta-groups this scattering becomes important only at energies lower than those plotted in Fig. 2.

These data support the decay scheme for I^{131} shown in Fig. 2. This scheme shows beta-transitions to both a 635-kev and a 720-kev level in Xe^{131} as postulated by Emery.[1] The scintillation spec-

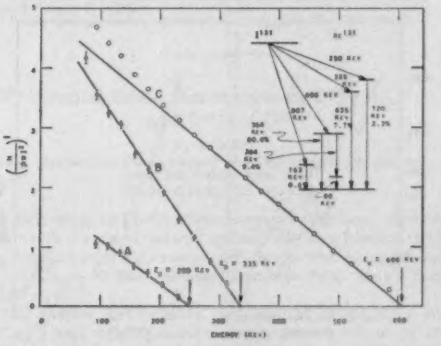

Fig. 2. Kurie plot of I^{131} beta-energy distribution. Curve A. Coincident with 720-kev gamma-rays; Curve B. Coincident with 635-kev gamma-rays; Curve C. Coincident with either 364-kev or 284-kev gamma-rays.

trometer was calibrated with known gamma-emitters to obtain the intensities shown in the decay scheme.

It is a pleasure to acknowledge the help of C. J. Borkowski and E. Fairstein in this work.

* This work was performed for the AEC.
[1] E. W. Emery, Phys. Rev. **83**, 679 (1951).

Au^{198} Decay

A. R. Brosi, B. H. Ketelle, H. Zeldes, and E. Fairstein
Chemistry Division, Oak Ridge National Laboratory, Oak Ridge, Tennessee*
(Received September 4, 1951)

A 1.09-MEV level in Hg^{198} has recently been reported[1-3] with gamma-transitions in Au^{198} decay between the 1.09-Mev and the 0.411-Mev levels and between the 1.09-Mev level and the ground state. These transitions have been confirmed using Oak Ridge National Laboratory reactor bombarded gold which was purified after bombardment by the method given by Noyes and Bray.[4] The NaI—Tl scintillation spectrometer pulse distribution in Fig. 1A shows the presence of the recently reported 1.09-Mev and 0.680-Mev gamma-rays in addition to the well-known 0.411-Mev gamma-ray. The shoulder on the curve corresponding to a gamma-ray energy of 0.820 Mev was shown to be the result of random coincidences between two 0.411-Mev gamma-rays.

Further evidence that the 0.680-Mev gamma-transition is part of the Au^{198} decay scheme was obtained by measuring the electron energy distribution coincident with it. This was done by mounting an essentially weightless source in a thin magnetic lens spectrometer on a beryllium disk thick enough to absorb the 0.97-Mev beta-group. A 13 g/cm² platinum absorber was placed between the beryllium disk and a NaI—Tl counter to reduce the counting rate of the 0.411-Mev gamma-ray relative to that of the 0.680-Mev gamma-ray by a factor of 25. With this reduction in intensity the random coincidences of the 0.411-Mev gamma-ray were essentially eliminated.

Coincidences were recorded between pulses from the detector on the thin lens spectrometer and the pulses produced by the 0.680-Mev gamma-ray in the NaI—Tl scintillation spectrometer. The energy distribution of the coincident electron pulses is shown as an N/I vs E plot in Fig. 1B. These data show that the 0.680-Mev gamma-ray is coincident with both a low energy beta-group and the K-conversion electron peak of the 0.411-Mev gamma-ray. The Kurie plot of the beta-energy distribution shown in Fig. 2 indicates a maximum energy of 290±15 kev for the coincident beta-group. These results are consistent with the coincidence absorption measurements of Cavanagh[2] and the decay scheme

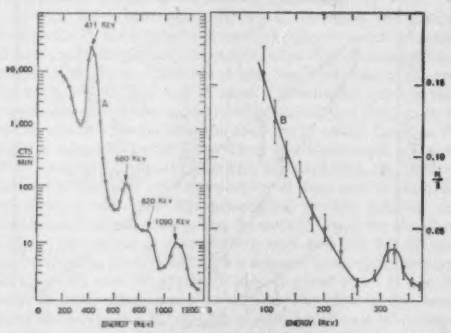

FIG. 1. Curve A: Scintillation spectrometer pulse-height distribution of Au^{198} gamma-radiation; curve B: electron energy distribution coincident with 680-kev gamma-radiation.

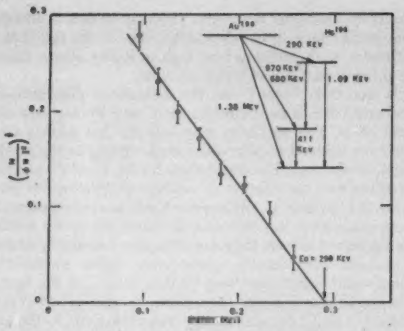

FIG. 2. Kurie plot of Au^{198} beta-energy distribution coincident with 680-kev gamma-radiation.

shown in Fig. 2. No attempt was made to confirm the low intensity beta-transition to the ground state reported by Elliott and Wolfson.[3]

Approximate measurements indicate that about 1 percent of the disintegrations are through the 0.680-Mev gamma-ray and about 0.2 percent are through the 1.09-Mev gamma-ray.

It is a pleasure to acknowledge the help of C. J. Borkowski and R. A. Dandl in this work.

* This work was performed for the AEC.
[1] Cavanaugh, Turner, Booker, and Dunster, Proc. Phys. Soc. (London) **A64**, 13 (1951).
[2] P. E. Cavanagh, Phys. Rev. **82**, 791 (1951).
[3] L. G. Elliott and J. L. Wolfson, Phys. Rev. **82**, 333 (1951).
[4] A. A. Noyes and W. C. Bray, *A System of Qualitative Analysis for the Rare Elements* (The Macmillan Company, New York, 1943).

Computation of Photonuclear Resonance Curves from Relative Activity Curves Monitored by Induced Radioactivity

R. Sagane*
Institute for Atomic Research and Department of Physics, Iowa State College, Ames, Iowa
(Received September 10, 1951)

In preference to the "total spectrum method," Katz and Cameron[1] have recently presented their "photon difference method" for obtaining photonuclear cross sections from observed bremsstrahlung activation curves. It is the purpose of the present note to point out that it is possible to obtain results of equal or better accuracy in the energy region of 20 to 100 Mev by monitoring with induced radioactivity. This latter method is relatively simple and may be extended to energies as low as 10–12 Mev if suitable monitor activities, characterized by low energy resonances, are used. To obtain good accuracy the activation curves must, of course, be measured carefully and it is preferable to employ two or three different radioactive monitors simultaneously.

The radioactivity induced in a monitor sample is proportional to the integral, over the resonance, of $\sigma_M \times N_{k,\gamma}$ (cross section times number of quanta). The character of the resonance curves for various suitable monitors is known with some accuracy and the relative number of bremsstrahlung quanta has been given by a number of authors.[2-4] The use of a monitor radioactivity in effect serves to normalize the bremsstrahlung spectra in terms of the area under the $\sigma_M \times N_{k,\gamma}$ curves. Schiff curves corresponding to $E_{max} > 20$ Mev and normalized in this way on the basis of the reported resonance curves[5] for Ta are shown in Fig. 1, which turned out to be substantially equivalent to normalization at 13.5 Mev.

When an activation curve is determined with the use of a radioactivity monitor, the change of relative activity ΔI attendant upon

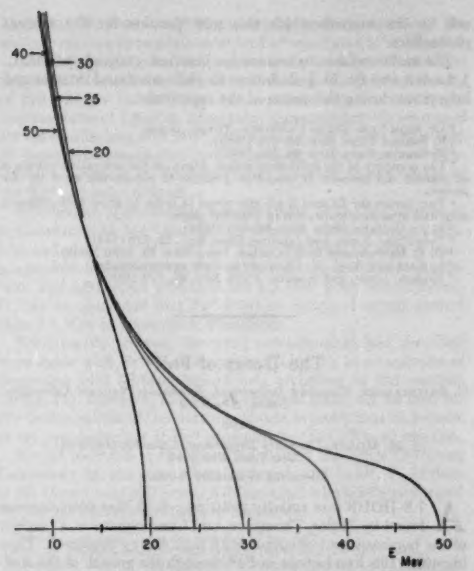

FIG. 1. Relative number of quanta, corresponding to several E_{max} settings, calculated by Schiff's formula ($C=111$) and normalized for constant activity of tantalum monitor. The resonance curve for Ta assumed to be as reported (see reference 5).

a change of E_{max} is proportional to the integral of σ times the difference between the appropriate normalized spectra. The character of this second factor is illustrated by the curve bounding the shaded area in Fig. 2. The desired cross section first may be roughly estimated by differentiation of the activation curve and then revised, by successive trials, so that the incremental relative yield ΔI is closely proportional to the integral of $\sigma \times \Delta n_{\Delta\nu}$. This procedure is illustrated graphically in Fig. 2 for the reaction $C^{12}(\gamma, n)C^{11}$, monitored by the radioactivity induced in copper. It is estimated that if the accuracy of the activation curve is of the order of 1 or 2 percent, the shape of the resonance curves may be computed in this way with an accuracy of 3 to 5 percent. Subsequent recomputation in the light of new data can be readily performed.

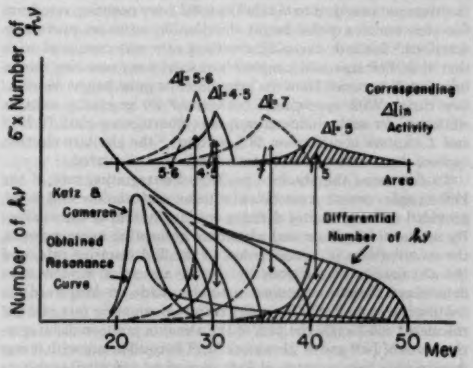

FIG. 2. Examples of procedure on how to adjust the area for

$$\int_{E_m}^{E_m+\Delta} \sigma \times N_{\Delta\nu} dE \propto \Delta I.$$

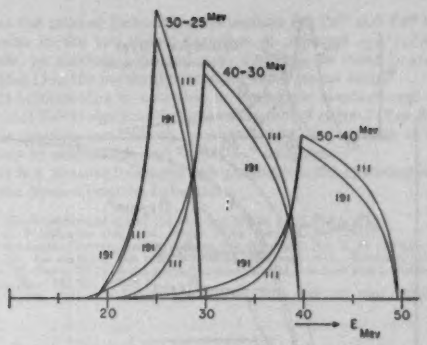

FIG. 3. Comparison of differential number of photons between Schiff curves corresponding to $C=191$ and $C=111$. Normalization was made with C^{11} activity.

The foregoing method is quite insensitive to the assumed shapes of the bremsstrahlung spectra and of the monitor resonance, if no prominent high energy "tail" is present. In Fig. 3 are given differential numbers of photons between Schiff's curves for constant activation of Cu corresponding to constant $C=191$ and $C=111$. The effects due to the difference of assumed value for the constant C are not very large. The necessity for detailed computations of ion-chamber response, differential absorption in the donut wall (because the monitor samples are usually insensitive to low energy quanta), and similar somewhat complicated phenomena is, of course, avoided. Special care should be taken in the use of monitor substances which are particularly sensitive to neutrons or to scattered x-rays. Errors from spurious induced activities may be kept to less than 5 percent, and commonly less than 2 percent, if suitable precautions are taken and the effects of geometrical changes (sample location, relative position, and thickness) are explored, enabling one to obtain a little better accuracy than with the usual Victoreen chamber.

The author wishes to express his heartiest gratitude to Dr. L. J. Laslett and Dr. D. J. Zaffarano for their continuous interest and help given during the course of the experiment. Thanks are also due Mr. D. V. Steward for the help given in numerical calculations.

* On leave from Tokyo University, Tokyo, Japan.
[1] L. Katz and A. G. W. Cameron (private communication).
[2] L. I. Schiff, Phys. Rev. **83**, 252 (1951).
[3] B. Rossi and K. Greisen, Revs. Modern Phys. **13**, 252 (1941).
[4] W. Heitler, *The Quantum Theory of Radiation* (Oxford University Press, Oxford, England, 1944).
[5] Johns, Katz, Douglas, and Haslam, Phys. Rev. **80**, 1062 (1950).

Unusual Broad Resonances in $C^{12}(\gamma,n)C^{11}$ and $O^{16}(\gamma,n)O^{15}$

R. SAGANE*
Institute for Atomic Research, and Department of Physics, Iowa State College, Ames, Iowa
(Received September 10, 1951)

THE study of photonuclear resonances has been continued with the use of induced radioactivity as a monitor.[1,2] Use has been made of high energy x-radiation, with an upper limit adjustable to 70 Mev, obtained from the Iowa State College synchrotron.

The samples and monitors used were all of the same area ($\frac{1}{2}'' \times \frac{1}{4}''$) and with thicknesses usually from 1 mil to 10 mil. Lucite was used as a sample for carbon and oxygen. The targets were irradiated at fixed positions, either 10" or 20" from the x-ray source, and were so oriented that the beam struck a stack of

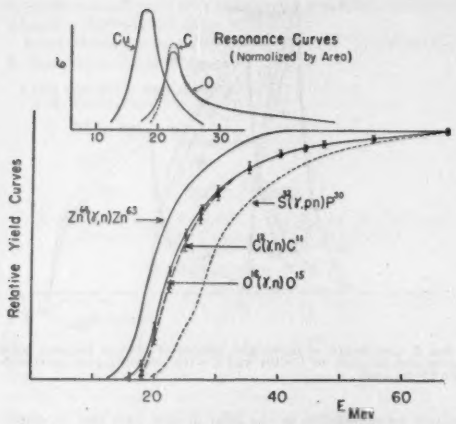

FIG. 1. Relative yield curves for C^{12} and O^{16}. Curves for S^{32} and Zn^{64} are also given for comparison.

several samples and monitors at normal incidence. The relative activity induced in the samples was thus independent of the dependence of geometrical beam-width upon energy.

The relative yield curves[2] for C^{11} and O^{15}, with C^{12} as a monitor, are given in Fig. 1. (In constructing these curves a correction has been made for the appreciable cross section possessed by copper at energies as high as the carbon and oxygen thresholds.)[4] The corresponding cross-section curves, computed by the method previously reported,[2] are also shown in Fig. 1. It is noteworthy that these resonances are quite similar, each being markedly asymmetrical and exhibiting a prominent high energy "tail" which extends to over 60 Mev. The carbon and oxygen resonances may be contrasted with the more common type illustrated by the copper curve reproduced in Fig. 1.

The high energy cross sections for carbon and oxygen are roughly proportional to E^{-4}, which suggests that this portion of the curve may be interpreted in terms of the nuclear photoeffect.[5] Additional evidence for this process is found in the reported[6] 90° excess of neutrons from carbon. Similar high energy tails have been found and are now under further investigation for the reactions $S(\gamma, pn)$, $Pb(\gamma, p$ or $\gamma, pn)$, $Al(\gamma, 2p)$, $Zn(\gamma, n)$, $Mg(\gamma, p$ or $\gamma, pn)$, and $Fe(\gamma, n)$.

The resonance curves for the reaction $C^{12}(\gamma, n)C^{11}$ as determined in the present work and as reported by other workers,[7-9] may be compared in Fig. 2. The main peak of the resonance found here agrees well with that given in the recent report of Katz and Cameron[7] if the energy scale of the synchrotron is adjusted to an 18.8-Mev C^{12} threshold. The author wishes, however, to draw attention to the existence of the long tail appearing at high energies

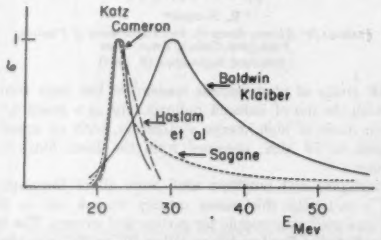

FIG. 2. Comparison of the resonance curves for $C^{12}(\gamma, n)C^{11}$ reported by different workers.

and to the support which this may provide for the nuclear photoeffect.

The author wishes to express his heartiest gratitude to Dr. L. J. Laslett and Dr. D. J. Zaffarano for their continued interest and help given during the course of the experiment.

* On leave from Tokyo University, Tokyo, Japan.
[1] R. Sagane, Phys. Rev. **83**, 174 (1951).
[2] R. Sagane, Phys. Rev. **84**, 586 (1951).
[3] The accuracy of the individual points shown on the activation curves is at present ±3 percent. It would be possible to reduce the error to ±1 percent.
[4] Two curves for Zn and S are also given in order to show how different activities approach saturation in different ways.
[5] E. D. Courant, Phys. Rev. **82**, 703 (1951).
[6] Terwilliger, Jones, and Jarmine, Phys. Rev. **82**, 820 (1951).
[7] G. C. Baldwin and G. S. Klaiber, Phys. Rev. **73**, 1156 (1948).
[8] L. Katz and A. G. W. Cameron (private communication).
[9] Haslam, Jones, and Horsley, Phys. Rev. **82**, 270 (1951).

The Decay of Fe^{52}*

G. FRIEDLANDER, *Chemistry Department, Brookhaven National Laboratory, Upton, New York*
AND
J. M. MILLER, *Chemistry Department, Columbia University, New York, New York*

(Received September 7, 1951)

A 7.8-HOUR iron activity emitting ~0.55 Mev positrons was found by Miller, Thompson, and Cunningham[1] as a product of the bombardment of copper with high energy deuterons. They identified this iron isotope as Fe^{52} through the growth of the well-known 21-minute Mn^{52}.

In order to measure yields of Fe^{52} in various spallation reactions, it is necessary to know what fraction of the Fe^{52} decays occur by electron capture. A search for manganese K x-rays resulting from electron capture in Fe^{52} was therefore undertaken by means of a proportional counter and pulse height analyzer.[2] Samples of Fe^{52} were prepared by bombardment of copper with 370-Mev protons in the circulating beam of the Columbia University Cyclotron at Nevis. The iron activity, with a fraction of a milligram of carrier, was purified by a procedure which involved carrying on $Al(OH)_3$, isopropyl ether extractions, and a separation from gallium by $Fe(OH)_3$ precipitation in 3M NaOH. The final samples were precipitated as $Fe(OH)_3$ from neutral solution on 0.1 mg/cm² Nylon.

Manganese K x-rays were found with a pulse height analyzer in conjunction with a proportional counter filled to one atmosphere with argon and methane. The decay of these x-rays could be analyzed into an 8-hour half-life and a very long-lived component, presumably due to Fe^{55}. The samples were rather weak and it was therefore not practical to obtain the total x-ray counting rate from the area under a pulse height distribution curve as previously described.[2] Instead, the peak counting rate was compared with that of an Fe^{55} standard sample whose total x-ray counting rate in turn was determined from the area under its pulse height distribution curve. With appropriate corrections[3] for geometry, counter efficiency, air and window absorption, fluorescence yield (0.27),[4] and L capture contribution (8.5 percent),[5] the absolute electron capture decay rate of Fe^{52} in the sample was calculated.

To determine the absolute positron disintegration rate of the Fe^{52} sample, counts were taken with an end-window GM tube, provided with a geometry-defining opening in front of the window. By means of beryllium and aluminum absorption measurements, the contributions of x- and γ-rays to the GM counting rate, and the attenuation of positrons by the air and mica window were determined. Small corrections were also made for long-lived activities (Fe^{59} and Fe^{55}). From the corrected counting rate and the calculated solid angle the sum of the absolute positron disintegration rates of Fe^{52} and of 21-minute Mn^{52} in equilibrium with it was determined. Decay curves of Fe^{52} showed no tail attributable to 5.8-day Mn^{52}. It was thus established that at least 95 percent of the Fe^{52} decays go to the 21-minute Mn^{52} isomer. From the electron capture and positron decay rates of the sample and the fact that

21-minute Mn^{52} decays 99.95 percent by positron emission,[1] the electron capture to positron ratio for Fe^{52} was found to be 1.6±0.4.

The Fe^{52} decay undoubtedly proceeds by an allowed transition ($\log ft \sim 4$). One can therefore deduce[7] a maximum positron energy of 640±40 kev for Fe^{52} from the measured electron capture to positron ratio of 1.6±0.4. Absorption measurements on sources of Fe^{52} in equilibrium with Mn^{52} gave an end point for the low energy β^+ component compatible with this energy. The presence of the 2.7-Mev positrons of Mn^{52} makes an accurate determination of the Fe^{52} end point difficult.

Scintillation spectrometer measurements of an Fe^{52} sample in equilibrium with Mn^{52} showed the presence of annihilation radiation and of a γ-ray of about 1.5 Mev. Immediately after a manganese-iron separation, the Fe^{52} exhibited only annihilation radiation. The subsequent growth of the 1.5-Mev γ-ray was observed. It may be concluded that Fe^{52} emits no γ-rays of energy greater than 0.5 Mev in appreciable abundance.

For intensity reasons, the γ-ray measurements just described were made with Fe^{52} samples produced by the bombardment of chromium with 30-Mev helium ions according to the reaction $Cr^{50}(\alpha, 2n)$. However, the Fe^{52} so obtained could not be used for the determination of the electron capture to positron ratio because of the preponderance of Fe^{55} produced by the $Cr^{53}(\alpha, n)$ reaction.

We are indebted to the operating staff of the Nevis Cyclotron Laboratory for the proton bombardment, and to Dr. P. Abelson of the Department of Terrestrial Magnetism who kindly performed the helium ion bombardment of chromium.

* Work performed under the auspices of the AEC.
[1] Miller, Thompson, and Cunningham, Phys. Rev. 74, 347 (1948).
[2] Bernstein, Brewer, and Rubinson, Nucleonics 6, No. 2, 39 (1950).
[3] Friedlander, Perlman, Alburger, and Sunyar, Phys. Rev. 80, 30 (1950).
[4] A. H. Compton and S. K. Allison, *X-Rays in Theory and Experiment* (D. Van Nostrand Company, Inc., New York, 1935).
[5] M. E. Rose and J. L. Jackson, Phys. Rev. 76, 1540 (1949).
[6] R. K. Osborne and M. Deutsch, Phys. Rev. 71, 467 (1947).
[7] E. Feenberg and G. Trigg, Revs. Modern Phys. 22, 399 (1950).

Yields of Iron Isotopes in High Energy Nuclear Reactions*

J. M. Miller
Chemistry Department, Columbia University, New York, New York
AND
G. Friedlander
Chemistry Department, Brookhaven National Laboratory, Upton, New York
(Received September 7, 1951)

THE determination[1] of the electron capture to positron ratio in Fe^{52} has made it possible to obtain directly the relative disintegration rates of Fe^{52} and Fe^{55} in a sample by comparison of the 8-hour and long-lived Mn x-ray activities as measured with a proportional counter and pulse-height analyzer.[2] Such measurements have been carried out on iron samples separated from cobalt and copper targets bombarded with 370-Mev protons in the circulating beam of the Columbia University cyclotron at Nevis. With thin targets (~5-Mev energy loss) the ratios of formation cross sections (σ_{55}/σ_{52}) were 136±20 and 168±25 for cobalt and copper targets, respectively. With a thick copper target (energy loss ~60 Mev) a ratio of 206±30 for (σ_{55}/σ_{52}) was obtained. Although it is not certain that the difference between the results for the thick and thin copper targets is real, it is in the expected direction since the energy loss of the protons in the thick target would tend to reduce the Fe^{52} yield more than the Fe^{55} yield.[3]

The rather high cross section for the formation of Fe^{55} relative to that for Fe^{52} is of interest in connection with the results of Bartell *et al.*[4] They reported alternating high and low yields for successive atomic numbers among the products of the bombardment of copper with 190-Mev deuterons. Since they did not investigate the Fe^{55} yield, their observation that the yield of iron was low compared with that of manganese would be modified if the relative yields of Fe^{55} and Fe^{52} in their bombardment were similar to those found here. That this may be so is indicated by the fact that the ratio of formation cross sections for Fe^{55} and Fe^{52} was similar in the two cases; Bartell *et al.* reported (σ_{55}/σ_{52})=20 while, by absolute beta- and x-ray counting, we found (σ_{55}/σ_{52}) =45±15 in the bombardment of the thick copper target.

It is interesting to note that in our copper bombardment the yield of Fe^{55} is significantly higher than that of either Fe^{52} or Fe^{59}. This result is qualitatively consistent with the emission of nucleons by evaporation and "knock-on" processes.

It is a pleasure to express our gratitude to the operating staff of the Nevis Cyclotron Laboratory.

* Work performed under the auspices of the AEC.
[1] G. Friedlander and J. M. Miller, Phys. Rev. 84, 588 (1951).
[2] Bernstein, Brewer, and Rubinson, Nucleonics 6, No. 2, 39 (1950).
[3] See, for example, the proton-induced star work of L. Germain, Phys. Rev. 82, 596 (1951) and the spallation results of M. Lindner and I. Perlman, Phys. Rev. 78, 505 (1950).
[4] Bartell, Helmholz, Softky, and Stewart, Phys. Rev. 80, 1006 (1950).

Coupling among Nuclear Magnetic Dipoles in Molecules*

H. S. Gutowsky, D. W. McCall, and C. P. Slichter
University of Illinois, Urbana, Illinois
(Received September 10, 1951)

MULTIPLE nuclear magnetic resonance lines have been reported in several liquids, such as the Sb resonances[1] in aqueous $NaSbF_6$, and the P^{31} and F^{19} resonances[2] in $POCl_2F$, $POClF_2$, and CH_3OPF_2. Suggested interpretations of these effects include hindrance to molecular rotation[1-3] and second-order magnetic dipolar interactions.[4] We feel that new measurements of ours, together with the previously published results,[2] exclude both of the above suggestions, in general, and we would like to propose the hypothesis that the splittings come from a second-order interaction between the nuclear magnetic moments and some magnetic field internal to the molecule.

Significant experimental facts seem to be as follows. (1) The splitting is associated with the nuclear magnetic moments since $\delta H_A/\delta H_B = \mu_B/\mu_A$, where δH is the multiplet separation.[2] (2) Nuclei of the same species do not interact when they are in chemically equivalent positions in a molecule.[2] As an additional example, in HPF_2 we observe that P splits the F-resonance into two components and the F split the P into seven components, but there is no observable splitting of the F-resonances by the fluorines acting among themselves. (3) The relative intensities and number of components of a line A are determined by the statistical weights and the number of possible spin states of the B which cause the splitting.[2] Note that B have been in chemically equivalent positions in the twelve compounds we have observed thus far. (4) Our recent experiments show the splittings are independent of temperature and the strength of the static field H_0. The splittings remain the same in CH_3OPF_2 and $POCl_2F$ from room temperature until the narrow components diminish in intensity and are lost in a broadening background line at about −80°C. (5) Although the splittings are several tenths of a gauss, we have found in almost all cases that the components are at least as narrow as the 0.01-gauss magnet inhomogeneity over the sample. (6) The P^{31}-resonances in PF_3 and PH_3 are quadruple with splittings of 0.82 and 0.10 gauss, respectively. The ratio of these splittings is 8.2 while the calculated ratio of the magnetic dipolar fields (μ/r^3) is about 0.7.

On the basis of these facts, we feel there are the following crucial objections to:

Rotational hindrance: In this case identical nuclei should interact, counter to observations. It is difficult also to reconcile any restriction of molecular tumbling with the observed narrow line widths or with the observed temperature independence of the splittings. Moreover, in the case of HPF_2, the phosphorus resonance has seven components, not nine as predicted by Andrew's analysis.[3] The evidence concerning $NaSBF_6$[1] is not conclusive al-

though the breadth of the Sb resonance lines tends to support Andrew's hypothesis for this particular compound.

Second-order magnetic dipole interaction: The second-order splitting is of order $(\mu^2/r^6)/H_0$ gauss, where r is the internuclear distance. Predicted splittings are several milligauss, contrasting with observed H^1, F^{19}, and P^{31} splittings in the range from 0.10 to 0.75 gauss. We find experimentally that the splittings are independent of field, disagreeing with the above estimate. Also, the observed ratio of the P^{31} splittings in PF_3 and PH_3 disagrees with the predicted ratio by a factor of ten. Lastly, the objections concerning chemically equivalent fluorines not interacting apply also to the second-order interaction.

In view of the arguments and data cited, both the rotational hindrance and direct second-order dipolar interaction mechanisms have serious flaws, and instead we wish to propose that the splittings arise from a second-order interaction between the nuclear magnetic moments and some magnetic field internal to the molecule. It seems to us that the most likely coupling is via the electrons by a mechanism analogous to the chemical shift. This view is supported to some extent by correlations found between observed values for the nuclear magnetic shielding and the splittings. Expressions similar to Ramsey's equations[5] have been derived, but the detailed calculations, as with Ramsey's equations, require a knowledge of molecular electronic wave functions. The expressions are similar also to Foley's equations[6] for the pseudo-quadrupole effect, except in our case we are concerned with coupling of different nuclei, rather than of a nucleus with itself. The order of magnitude in favorable cases appears to be similar to the fluorine effective field on itself; from Foley's paper one can calculate this field to be several tenths of a gauss.

The interaction that we propose is of the form $A\mathbf{\mu}_1\cdot\mathbf{\mu}_2$, where A is a constant independent of temperature and H_0. Such a form can actually be obtained from arguments of rotational invariance alone, and thus would result from any form of coupling through molecular magnetic fields. In a private communication, E. L. Hahn has called our attention to the fact that, as a result of a selection rule, pairs of chemically equivalent nuclei will not give a split resonance from an interaction of the form we propose, whereas chemically nonequivalent nuclei will have a fine structure splitting in agreement with our observations. We have generalized Hahn's remark about pairs to the case of an arbitrary number of spins, and find the correct number, spacing, and intensities of lines. If the spin-spin interaction were proportional merely to the product of components of magnetic moment along H_0, there would be a splitting from interactions with chemically equivalent pairs. A more detailed account will appear in another journal.

We thank Dr. D. L. Dexter and Dr. W. R. Heller for several helpful discussions, and T. R. Carver and R. E. McClure for their assistance with several measurements. Equipment used in some of the experiments was provided by a grant from Research Corporation.

* Supported in part by the ONR.

[1] W. G. Proctor and F. C. Yu, Phys. Rev. **81**, 20 (1951).
[2] H. S. Gutowsky and D. W. McCall, Phys. Rev. **82**, 748 (1951).
[3] E. R. Andrew, Phys. Rev. **82**, 443 (1951).
[4] A proposal made by E. M. Purcell during discussions at the Am. Phys. Soc. meeting in Washington, D. C., April, 1951, to account for milligauss proton splittings in ethanol reported by Arnold, Dharmatti, and Packard, Phys. Rev. **83**, 210 (1951).
[5] N. F. Ramsey, Phys. Rev. **78**, 699 (1950).
[6] H. M. Foley, Phys. Rev. **72**, 504 (1947).
[7] G. C. Wick, Phys. Rev. **73**, 51 (1948).

Asymptotic Behavior of Angular Correlation Functions

W. OPECHOWSKI
Department of Physics, University of British Columbia, Vancouver, Canada
(Received September 10, 1951)

IN the standard theory of angular correlation,[1] one considers a "cascade process" consisting of a quick successive emission of two particles by a quantum-mechanical system at rest (e.g., an atomic nucleus emitting first an alpha-particle and, immediately after, a photon). If the direction of emission of, for example, the first emitted particle is chosen as the axis of quantization, then the relative probability $W(\theta)$, henceforth called "the correlation function," for the second particle to be emitted at an angle θ with respect to this axis is given, according to the theory, by an expression of the form:

$$W(\theta)=\Sigma_{m_1}F_{J_1{}^{m_1}}\Sigma_m(J'm'|J_1m_1Jm)^2\Phi_m(\theta). \quad (1)$$

The symbols in Eq. (1) have the following meaning: J', m' and J, m are the total angular momentum quantum numbers of the system before and after the emission of the first particle whose total angular quantum numbers are J_1, m_1. The (real) transformation coefficient for the vector addition of these angular momenta is denoted by $(J'm'|J_1m_1Jm)$. The $F_{J_1{}^{m_1}}$'s are numbers which depend on the nature and properties of the first particle as well as on J_1, m_1. The $\Phi_m(\theta)$'s are functions of θ, which depend solely on the characteristics of the second of the two transitions constituting the cascade process, i.e., on the angular momenta involved, and on the nature and properties of the second particle.

Let us now consider two cascade processes which are identical except for the nature and properties of the particle emitted in the first transition. In other words, all total angular momenta involved and the $\Phi_m(\theta)$'s are, respectively, equal in the two processes, but the set of the $F_{J_1{}^{m_1}}$'s for one process is different from that for the other. In general, the correlation functions for such two processes will, of course, be quite different. However, it will be shown below that, asymptotically, for $J'\to\infty$ and $J_1\to\infty$, they become identical. In other words: For large total angular momenta of the initial state of the system, and of the particle emitted in the first transition, the correlation function is always the same, no matter what the nature and properties of the particle are, provided all other characteristics of the cascade process are the same.[2]

In order to prove this proposition, it is sufficient to look into the asymptotic behavior of the transformation coefficients in Eq. (1). Starting from the well-known explicit expression for these coefficients (e.g., in the convenient form given by Van der Waerden[3]), one finds, by a simple calculation, the asymptotic equation:

$$(J'm'|J_1m_1Jm)\sim J_1{}^JL(\lambda_1Jm), \quad (2a)$$

where

$$L(\lambda_1Jm)=[(J+m)!(J-m)!]^{-\frac{1}{2}}\Sigma_\alpha(-1)^\alpha\binom{J+m}{\lambda_1-\alpha}\binom{J-m}{\alpha}. \quad (2b)$$

The parameter λ_1 is defined by the equation $J'=J_1+J-\lambda_1$. In the derivation of Eqs. (2), J_1, m_1, J, m, and λ_1 are kept constant, only J_1 (and, hence, J' too) being allowed to increase indefinitely. Combining Eqs. (1) and (2), one obtains

$$W(\theta)\sim J_1{}^{2J}\{\Sigma_{m_1}F_{J_1{}^{m_1}}\}\{\Sigma_m[L(\lambda_1Jm)]^2\Phi_m(\theta)\}. \quad (3)$$

Now, the correlation function being a relative probability, a θ-independent factor does not change its physical meaning, and may be disregarded. One may thus drop both θ-independent factors in Eq. (3). Hence, finally,

$$W(\theta)\sim\Sigma_m[L(\lambda_1Jm)]^2\Phi_m(\theta). \quad (4)$$

This completes the proof of the proposition stated, for $W(\theta)$, as given by Eq. (4), is free from any reference to the nature and properties of the first particle.

Although the asymptotic form (4) of the correlation function does not depend on the total angular momentum quantum numbers of the initial state of the system and of the first particle, it does still depend, classically speaking, on the angle between the two angular momenta. For this is what the dependence of $W(\theta)$ on λ_1 in Eq. (4) means physically. The dependence on λ_1 can be shown to disappear only if $J\to\infty$ too. Of course, this mathematically possible case is very remote from any physically realizable situation. As an example, we may consider the case in which the particle emitted in the second transition is a photon whose total angular momentum (quantum number J_2) is parallel to the total

angular momentum (quantum number J'') of the final state of the system, so that $J=J''+J_2$. In the simplest case, when $J_2=1$, one finds, from (2b) and (4), using the expression for the $\Phi_m(\theta)$'s which can be obtained from Falkoff and Uhlenbeck's paper,[1]

$$\left.\begin{aligned} W(\theta)&\sim 1-\tfrac{1}{3}\cos^2\theta \quad \text{if} \quad \lambda_1=0,\\ W(\theta)&\sim 1-[(J''-2)/(3J''+2)]\cos^2\theta \quad \text{if} \quad \lambda_1=1.\end{aligned}\right\} \tag{5}$$

The two Eqs. (5) become identical for $J''\to\infty$, i.e., for $J\to\infty$.

The actual computation of the asymptotic form of correlation functions from Eqs. (2b) and (4) is, of course, much simpler than the computation of these functions for finite values of J_1. From the practical point of view, this is not, however, of much help because the asymptotic form is being approached, in general, rather slowly as J_1 increases.

[1] D. L. Falkoff and G. E. Uhlenbeck, Phys. Rev. 79, 323 (1950); D. S. Ling, Jr., and D. L. Falkoff, Phys. Rev. 76, 1639 (1949).
[2] The assumption that only one particle is emitted in each transition is not essential and has been made solely to simplify the language. The proposition holds as well for the case when more than one particle is emitted in each transition if the direction of emission of only one particle is observed in each transition (e.g., the case of beta-gamma angular correlation).
[3] B. L. Van der Waerden, *Die gruppentheoretische Methode in der Quantenmechanik* (Springer, Berlin, 1931), p. 69, Eq. (18.2).

The Decay of Neutrons into Neutral Hydrogen Atoms

S. G. Cohen
Hebrew University, Jerusalem, Israel
(Received September 10, 1951)

THE possibility of radioactive decay by "bound electron creation," i.e., decay such that the electron emitted from the nucleus falls into one of the bound states of the product atom instead of being emitted into the continuum of free states, has been discussed by Daudel, Benoist, Jacques, Jean, and Lecoin.[1-3] Such a process can only have an appreciable probability if the creation can take place in the K-shell, where the value of the wave function of the electron at the boundary of the nucleus is appreciably large. In general, the K-shell of the product nucleus would be already full—and then K-creation would be impossible. The case of the radioactive decay of tritium into He^3, however, is an exception, since two electrons are required to complete the K-shell in helium. Sherk[4] has calculated the ratio of the probabilities of K-creation to the normal disintegration to be 0.0065 for atomic tritium and 0.0035 for molecular tritium.

The purpose of this note is to point out that the possibility of K-creation also exists in the case of the decay of the neutron, as the electron can clearly fall into one of the K-states of the hydrogen atom; i.e., there should be a finite probability that a neutron should decay directly into a neutral hydrogen atom. Using the general formula quoted by Sherk[4], it is easy to calculate the ratio of the probabilities of K-creation to the normal β-decay for the neutron. Assuming the energy of disintegration to be 760 kev, one obtains the value 6×10^{-4} for this ratio. This ratio is much smaller than the corresponding ratio for tritium, since the ratio is proportional to E_β^{-4} where E_β is the maximum energy of the β-spectrum.

The process of the decay of the neutron into a neutral hydrogen atom also provides an interesting example of recoil of the product nucleus after β-decay, on the neutrino hypothesis. In the case of K-electron creation, as in the inverse process of K-capture, the neutrino must carry off a unique energy almost equal to the energy of disintegration, and thus the product atom must recoil with a unique momentum, equal and opposite to the momentum of the neutrino. In the case of the decay of the neutron by K-creation, one may therefore calculate the unique energy of recoil of the neutral hydrogen atoms from the known energy of disintegration and one obtains a recoil energy of 283 ev. For the decay of atomic tritium by K-creation the recoil energy of the He^3 neutral atom would be about 0.05 ev and for molecular tritium the recoil energy of the resultant hydrogen-helium complex would be half this value (assuming the maximum energy of the β-spectrum of tritium to be about 17 kev).

[1] Daudel, Benoist, Jacques, and Jean, Compt. rend. 224, 1427 (1947).
[2] Daudel, Jean, and Lecoin, Compt. rend. 225, 290 (1947).
[3] Daudel, Jean, and Lecoin, J. phys. radium 8, 238 (1947).
[4] R. M. Sherk, Phys. Rev. 75, 789 (1949).

The Dissociation of Ethyl-Acetate in a Geiger-Müller Counter

Stephen S. Friedland and Henry S. Katzenstein
Department of Physics, University of Connecticut, Storrs, Connecticut
(Received September 4, 1951)

IN an earlier paper,[1] it was shown that when a Geiger-Müller counter was filled with ethyl-acetate and argon and run till it no longer acted as a self-quenching counter, a mass spectroscopic analysis of the contents showed a large increase in mass 44 and a decrease in masses characteristic of the cracking pattern of ethyl-acetate. At the time it was stated that mass 44 was CO_2, a dissociation fragment of ethyl-acetate, and this increase in CO_2 and decrease of ethyl-acetate was in agreement with the Korff-Present theory.

Despite the excellent agreement described there remained the possibility that the CO_2 was in reality being driven out of the walls of the counter by the heat of the discharge in the tube and the ethyl-acetate was being absorbed into the metal portions. To determine which concept was correct the following experiment has been performed.

A counter, similar to the one used in the earlier experiments, was filled with just argon. The counter was run as a non-selfquenching counter for at least 10^{10} counts. The contents of the counter were then studied with the mass spectrometer. The only peak present was mass 40 for argon. No detectable CO_2 peak was observed.

It is now believed that this evidence establishes that the mass 44 increase observed earlier was definitely a dissociation product of the ethyl-acetate.

We wish to acknowledge the assistance of the AEC and the Research Corporation for their support of this work.

[1] S. S. Friedland, Phys. Rev. 74, 898 (1948).

The Sea-Level Latitude Variation of Fast Cosmic-Ray Neutrons

P. S. Gill and L. F. Curtiss
Aligarh University, Aligarh, India
(Received August 24, 1951)

USING BF_3 proportional counters, containing boron enriched in B^{10}, imbedded in a paraffin block 15×15×17 inches as a moderator of fast neutrons, the intensity of such neutrons generated in the atmosphere by cosmic rays has been measured in India as a function of latitude. The arrangement of the apparatus used will be given elsewhere.[1] The observation stations were chosen within the narrow range of longitudes 78°E to 81°E, extending from near the geomagnetic equator to about 20°N geomagnetic latitude.

In Table I are given the geomagnetic latitude, barometric pressure, and neutron counts per minute for each of the three stations, Aligarh, Nagpur, and Madras. The barometric pressure

Table I. Latitude variation of fast neutrons.

Observation station	Geomagnetic latitude	Barometric pressure (inches)	Neutron counts per minute
Aligarh	18°12′	29.27	2.08 ±0.03
Nagpur	11° 9′	29.07	1.49 ±0.02
Madras	3° 4′	30.13	1.57 ±0.04

is an average of hourly values for the duration for which the data were collected. The data at Aligarh give an accuracy of one percent while the limitations of time made it difficult to achieve the same accuracy at the other two stations. This, however, does not change the general conclusion.

Since fast neutrons in the atmosphere are presumably created by nuclear disintegrations caused by the interaction of cosmic radiation and atomic nuclei, it was thought worthwhile to study the latitude variation of cosmic-ray particles which produce disintegrations in nuclei of air atoms. These measurements indicate a very large latitude effect amounting to about twenty-five percent between Aligarh (18°12'N) and the geomagnetic equator. The value of the neutron intensity at Madras should be slightly less than that at Nagpur, keeping in view the fact that the general latitude curve for radiation passing through 12 cm of lead is fairly flat from the equator to around 10°N. On the other hand, the change is very rapid in the intermediate latitudes of 15° to 30°. The time of observation at these two stations at our disposal made it impossible to increase the accuracy of measurements. Such a large latitude effect would mean that cosmic-ray particles responsible for the production of up to 10 Mev neutrons in the atmosphere are highly field-sensitive. This effect is of the same order of magnitude as that on large cosmic-ray bursts shown by Jesse and Gill.[3] Perhaps the burst-producing radiation is the same which generates fast cosmic-ray neutrons in the atmosphere. These observations suggest that more extensive measurements of this nature covering larger range of latitudes should be taken.

The authors acknowledge the support of the Fulbright program which made it possible for one of us (L.F.C.) to come to India.

* National Bureau of Standards, Washington, D. C. Fulbright research scholar at Aligarh University.
[1] L. F. Curtiss and P. S. Gill (to be published).
[2] W. P. Jesse and P. S. Gill, Phys. Rev. 55, 414 (1939).

Rotational Structure of the ν_3 Raman Band of Methane

B. P. Stoicheff,* C. Cumming,† G. E. St. John,* and H. L. Welsh
McLennan Laboratory, University of Toronto, Toronto, Canada
(Received September 10, 1951)

ACCORDING to Teller's[1] theory of the Coriolis interaction in tetrahedral molecules the ν_3 Raman band of methane consists of fifteen sub-branches; only three of these are active in infrared absorption. In the early work of Dickinson, Dillon, and Rasetti[2] fourteen Raman lines were observed, corresponding to an unresolved Q branch and higher members of the intense S^+ and O^- branches. In the present investigation a multiple reflection Raman tube[3] and a quartz spectrograph with a dispersion of 27 cm^{-1}/mm at 2537A were used to obtain greater detail of the band. Sixty-eight lines were resolved, and evidence was found for all but one (O^+) of the fifteen sub-branches. The results of an analysis of these Raman data, combined with the infrared measurements of Nielsen and Nielsen,[4] are reported here.

A preliminary study showed that forty-two of the Raman lines were unblended and could be measured with sufficient accuracy for use in the analysis. By means of combination sum relations the following constants were derived:

$$\left.\begin{aligned}\nu_0&=3018.7\ \text{cm}^{-1}\\ B_0-B_1&=0.050\ \text{cm}^{-1}\end{aligned}\right\}\text{from } S^0 \text{ and } O^0 \text{ lines},$$

$$\left.\begin{aligned}\nu_0&=3018.1\ \text{cm}^{-1}\\ B_0-B_1&=0.035\ \text{cm}^{-1}\end{aligned}\right\}\text{from infrared } R^- \text{ and } P^+ \text{ lines},$$

$$\left.\begin{aligned}\nu_0+3B_1\zeta_1&=3019.6\ \text{cm}^{-1}\\ B_0-B_1&=0.036\ \text{cm}^{-1}\end{aligned}\right\}\text{from } S^+ \text{ and } O^- \text{ lines}.$$

The value $B_1\zeta_1=0.29$ was determined from the relation

$$S^+(J-1)+O^-(J)-R^-(J)-P^+(J-1)=12B_1\zeta_1.$$

The two values of ν_0 indicate a systematic difference between the Raman and infrared frequencies; to obtain consistency the infrared frequencies (reduced to cm^{-1} in vacuo) were raised by 0.6 cm^{-1}. The marked difference between the convergence factors B_0-B_1 for branches involving F_1^0 states and those involving F_1^+ and F_1^- states shows a departure from the simple theory. The rotational constants, B and D, were therefore determined from combination differences of lines of the same type (e.g., S^+ and P^+ lines). A least-squares analysis gave the following values:

$$\left.\begin{aligned}B_0&=5.253,\ D_0=1.9\times10^{-4}\\ B_1&=5.200,\ D_1=1.0\times10^{-4}\end{aligned}\right\}\text{from } S^0 \text{ and } O^0 \text{ lines},$$

$$\left.\begin{aligned}B_0&=5.232,\ D_0=1.5\times10^{-4}\\ B_1&=5.202,\ D_1=1.0\times10^{-4}\end{aligned}\right\}\text{from } S^+ \text{ and infrared } P^+ \text{ lines},$$

$$\left.\begin{aligned}B_0&=5.233,\ D_0=1.0\times10^{-4}\\ B_1&=5.197,\ D_1=0.8\times10^{-4}\end{aligned}\right\}\text{from } O^- \text{ and infrared } R^- \text{ lines}.$$

The perturbation in the ground state, manifested by the different values of B_0, is not understandable from the theoretical viewpoint. It is therefore concluded that the tacit assumption of identical upper states in the combination differences is not valid for some of the relations used.

A more acceptable analysis was obtained by assuming that the ground state is unperturbed, and has rotational constants $B_0=5.253$ and $D_0=1.9\times10^{-4}$, as found from combination differences of S^0 and O^0 lines. The upper rotational states, $F_1(J)$, for the various branches were then calculated from the observed frequencies, and these values of $F_1(J)$ were used to derive constants, B_1 and D_1, for each branch. The results are given in Table I. This

TABLE I. Rotational constants of the upper state of the ν_3 band of CH_4 assuming $B_0=5.253$ cm^{-1} and $D_0=1.9\times10^{-4}$ cm^{-1}.

Branch	B_1 (cm^{-1})	D_1 (cm$^{-1}\times10^4$)
O^- (R. E.)	5.235	3.8
R^+, P^- (R. E.)	5.235	3.1
R^0, P^0 (R. E.)	5.217	1.8
R^-, P^+ (I. R. and R. E.)	5.217	1.8
S^+ (R. E.)	5.206	1.0
S^0, O^0 (R. E.)	5.202	1.8

array of rotational constants for the $v=1$ vibrational state gives a consistent analysis of the Raman and infrared bands; the observed frequencies are reproduced with an average discrepancy of about 0.1 cm^{-1}, and the values of B_0-B_1 are in agreement with those calculated from combination sums. However, the reason for the multiplicity of B_1 values is not immediately apparent from the theory. A perturbation of ν_3 due to Coriolis interaction with the E part of $2\nu_2$ does not explain the results satisfactorily. It is probable that second-order perturbations due to centrifugal distortion and anharmonicities, such as those considered by Shaffer, Nielsen, and Thomas,[5] are of the same order of magnitude as the perturbation by $2\nu_2$ and must also be taken into account.

Although the individual lines of the Q branch were not resolved, the contour at high dispersion is striking: there is a sharp maximum of intensity at $\Delta\nu=3021.5$ cm^{-1}, a broad maximum at about $\Delta\nu=3017$ cm^{-1}, and a gradual decrease in intensity towards smaller frequency shifts. This intensity distribution is readily explained by the convergence and Coriolis terms in the frequency formulas for the Q sub-branches. The Q^0 and Q^- sub-branches are degraded towards lower frequency shifts; the Q^+ sub-branch forms a band head at $\Delta\nu=3021.5$ cm^{-1}, on the side of the band origin towards higher frequency shifts. At low dispersion this band head is the most prominent feature of the Q branch and has been measured by the earlier workers as ν_3.

* Holder of a Garnet W. McKee-Lachlan Gilchrist Scholarship, School of Graduate Studies, University of Toronto, 1950–51.
† Holder of a scholarship under the Research Council of Ontario, 1950–51.
[1] E. Teller, Hand-und Jahrb. d. Chem. Phys. 9, II, 43 (1934).
[2] Dickinson, Dillon, and Rasetti, Phys. Rev. 34, 582 (1929).
[3] Welsh, Cumming, and Stansbury, J. Opt. Soc. Am. (to be published).
[4] A. H. Nielsen and H. H. Nielsen, Phys. Rev. 48, 864 (1935).
[5] Shaffer, Nielsen, and Thomas, Phys. Rev. 56, 895 (1939).

Paramagnetic Resonance in Trivalent Molybdenum

S. RAMASESHAN AND G. SURYAN
Physics Department, Indian Institute of Science, Bangalore, India
(Received September 18, 1951)

IT is well known that molybdenum in its lower valencies exhibits paramagnetism. Bose[1] has measured the susceptibilities of trivalent molybdenum compounds such as $K_3MoCl_6 \cdot 12H_2O$ and $Mo(SCN)_6(NH_3)_4 \cdot 4H_2O$ and found that the effective Bohr magneton number is near the spin-only value. As the study of paramagnetic resonance absorption spectra affords a very reliable method for the determination of the ionic g values, experiments have been undertaken on compounds of Mo^{+++}. A double salt of Mo^{+++} was prepared by the reduction of a solution of molybdic acid in concentrated HCl by potassium amalgam. The green crystals so obtained are unstable in air but are easily preserved in paraffin wax. The salt is believed to be K_2MoCl_5 which is known to exist in two isomeric forms, one green and the other red.[2] Paramagnetic resonance experiments in this compound have been performed with the familiar experimental set-up at 3 cm. A sharp resonance was obtained. The experimental g value is 1.76 ± 0.02 and the half-breadth $2\Delta H_{\frac{1}{2}} = 190$ oersteds. g values calculated from susceptibility data for Mo^{+++} in $K_3MoCl_6 \cdot 12H_2O$ and $Mo(SCN)_6(NH_3)_4 \cdot 4H_2O$ are, respectively, 1.86 and 1.92. It is interesting to note that Mo^{+++} shows a sharp resonance spectrum even in the polycrystalline state similar to those in Cr^{+++} and V^{++} compounds. All these three ions are in the same electronic state $^4F_{\frac{3}{2}}$.

Similar sharp resonances occur in Cu^{++} salts, and the sharpness has been attributed to exchange interaction. It is probable that the same explanation may hold in the case of Mo^{+++}. Further investigations are in progress.

The authors are grateful to Professor R. S. Krishnan for the kind interest he took in this work.

[1] D. M. Bose and H. G. Bhar, Z. Physik **48**, 716 (1928).
[2] J. W. Mellor, *Treatise on Inorganic Chemistry* (Longmans, Green and Company, London, 1931), Vol. XI.

Multiple Events Produced in Hydrogen by Very High Energy Cosmic-Ray Particles at an Altitude of 90,000 Feet*

M. L. VIDALE AND MARCEL SCHEIN
Department of Physics, University of Chicago, Chicago, Illinois
(Received August 30, 1951)

A COUNTER experiment has been performed in order to study the production of mesons in the interactions of cosmic-ray particles with hydrogen nuclei. The apparatus used was flown from Chicago on September 6, 1950, by means of a General Mills constant level balloon. The balloon reached an altitude of 90,000 feet and floated at that height for 4½ hours. The proton target consisted of a spherical metal Dewar, 30 cm in diameter, filled with hydrogen. The experimental arrangement is shown in Fig. 1. Four crossed counter trays (A, B, E, and F) determined the direction of the incoming particle; two counter trays (T and $H-G$) detected multiple events. A master pulse was triggered by the coincidence $ABCD$ or $EFGH$. The pulses from each counter were in coincidence with the master pulse and were registered individually on a moving photographic film (hodoscope). Towards the middle of the flight the hydrogen was ejected from the Dewar. The remaining time at altitude was used as a control experiment without hydrogen.

Of all the coincidences recorded by the equipment, only those will be discussed in which not more than one counter was activated in any one of the four trays A, B, E, or F (see Fig. 1). Coincidences of this type are assumed to be due to a single incident particle interacting in the liquid hydrogen or in the walls of the Dewar. Table I gives the frequency of events obtained during 130 minutes of flight at 90,000 feet with an average of 1.4 g/cm² of liquid hydrogen interposed between the counter trays, and during 110

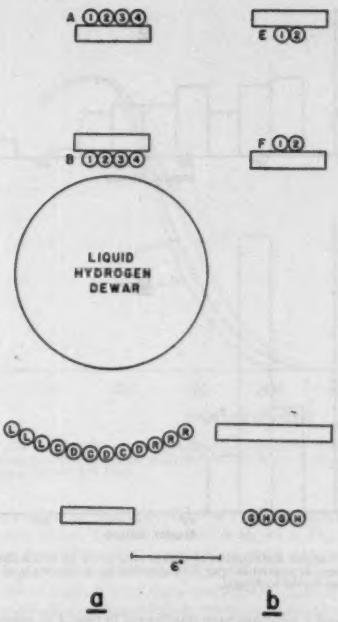

FIG. 1. Schematic diagram of apparatus used for the study of multiple events originating in liquid hydrogen. a, front view; b, side view.

minutes after the ejection of the hydrogen. The frequency of events in which 2 or 3 counters were activated in tray T decreases noticeably after the ejection of the hydrogen.

A selection of those coincidences in which at least three counters were activated in tray T eliminates the possibility that some of the events recorded may have been the result of knock-on electrons, the break-up of α-particles, elastic collisions, and other interactions giving rise to events consisting of two secondary particles only. Figures 2a and b are histograms of the frequency of events in which 3 or more counters were activated in tray T, originating in the walls of the Dewar and of the liquid hydrogen, respectively, plotted as a function of their total angular width. This width is assumed to correspond to the angular separation, as seen from the geometrical center of the Dewar, of the two farthest counters activated in tray T. Figure 2a shows that events originating in the walls of the Dewar are distributed almost isotropically over the area of these counters. The absence of events of an angular width of less than 4° results from the requirement that three counters be discharged in counter tray T. The finite size of the counters places a lower limit on the minimum angular separation observed. Figure 2b shows that events originating in hydrogen have a spread of only 15°, indicating that low energy interactions cannot have contributed significantly to the counting rate. This is in agreement with the fact that real stars cannot be produced in proton-proton collisions. The fact that the number of events in

TABLE I. Frequency of multiple events observed with the hydrogen equipment.

Number of counters activated in tray T	Frequency of events with hydrogen (counts/hr)	Frequency of events without hydrogen (counts/hr)
≥ 2	43	33
≥ 3	24	12

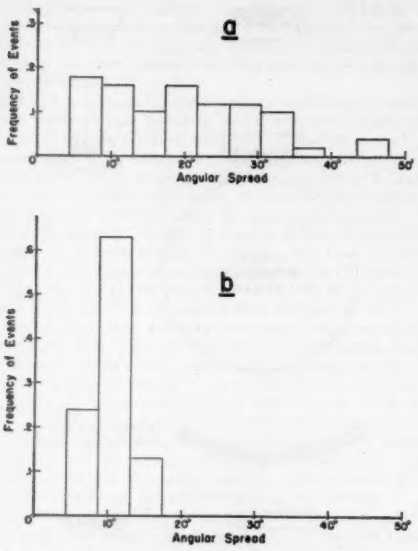

FIG. 2. Angular distribution of events of type 1a in which three or more counters were activated in tray T originating in: a, the walls of the Dewar flask; b, the liquid hydrogen.

which 2 and 3 counters were discharged in tray T is approximately equal (see Table I) indicates that the multiplicity of events observed to originate in liquid hydrogen is high. From geometrical considerations it follows that in case three or more counters were activated, the shower must have consisted of 6 or more particles. Taking this fact into account, due to the low flux of α-particles present in the cosmic radiation (~15 percent) and to their relatively low average energy per nucleon (compared to the corresponding energy for primary protons), it can be estimated that not more than 10 to 20 percent of the observed counting rate is due to the interaction of α-particles and heavier nuclei with the target protons. The remaining 80 percent to 90 percent has to be attributed to multiple meson production in proton-proton collisions.

Table II gives the flux of primary protons required to explain the observed counting rate corresponding to the following values of the collision cross section: (a) cross-sectional area of a single proton πr_0^2, where $r_0 = 1.4 \times 10^{-13}$ cm; (b) two times πr_0^2; and (c) four times πr_0^2. From the known flux of primary protons, the minimum proton energy corresponding to each value of the collision cross section was calculated. The results are listed in Table II.

It is concluded that primary protons of an energy of 50 to 100 Bev do interact in hydrogen with a cross section equal to 1 to 2 times the geometrical cross section of a single proton, producing on the average 4 or more charged mesons. These results are in satisfactory agreement with the predictions of Fermi's theory of high energy nucleon-nucleon interactions.[1] Since primary protons of energy lower than 10 Bev are about 10 times more numerous in the cosmic radiation above Chicago than those between 50 and 100 Bev, it is evident that multiple meson production in hydrogen must have a very low probability for nucleon energies $E < 10$ Bev.

TABLE II. Proton flux which would yield the observed counting rate of collimated showers under hydrogen for various assumed collision cross sections. The third column gives the minimum proton energy necessary to produce such a shower as estimated from the flux and the known energy spectrum.

Collision cross sections (in units of πr_0^2 6.15×10^{-26} cm^2)	Proton flux (per cm^2 sterad sec)	Minimum proton energy (Bev)
1	0.01	50
2	0.0055	130
4	0.0028	250

The authors would like to thank Professor Earl Long of the Institute for the Study of Metals of the University of Chicago for his valuable assistance in the design of the Dewar container and for making the liquid hydrogen available. The cooperation of the ONR and of the staff of the General Mills Company in arranging this balloon flight is deeply appreciated.

* Assisted by the joint program of the ONR and AEC.
[1] E. Fermi, Prog. Theor. Phys. 5, 570 (1950); Phys. Rev. 81, 683 (1951).

Radiative Corrections to the Hyperfine Structure and the Fine Structure Constant

NORMAN M. KROLL AND FRANKLIN POLLOCK
Columbia University, New York, New York
(Received September 6, 1951)

RECENT determinations of the fine structure constant, α, have rested almost entirely upon the precision measurement[1] of the hyperfine structure of hydrogen together with the corrected Fermi formula.[2] Omitted from the formula are all radiative corrections and meson field corrections other than those which can be described as anomalous magnetic moments.[3] We shall describe here a calculation of the second order radiative corrections. While these are fully described to order α by the anomalous moment as computed by Schwinger, it has long been known that a more precise evaluation of the second order energy would yield smaller corrections, the most important of which would be of order $\alpha^2 z$ rather than α. Our evaluation has been confined to that part of the energy which is of order $\alpha^2 z$ relative to the Fermi formula. In units of mc^2 then, the energy of interest is of order $\alpha^2 z^2 g_P(m/M)$, g_P being the nuclear magnetic moment in nuclear magnetons.

The second order electromagnetic self-energy of a particle moving in a prescribed static external field can be written as

$$\Delta E = \Delta E_P + \Delta E_F, \text{ with}$$

$$\Delta E_P = -(ie/cT)\int \bar{\psi}_a(x)\gamma_\mu A_\mu^{(P)}(x)\psi_a(x)d_4x$$

$$\Delta E_F = (i\hbar\alpha/cT)\int \bar{\psi}_a(x_2)\gamma_\mu S_F^a(x_2, x_1)\gamma_\mu \psi_a(x_1) D_F(x_2 - x_1) d_4x_2 d_4x_1.$$

Here $\psi_a(x)$ is a particular stationary state of a Dirac particle in the external field, $A_\mu^{(P)}(x)$ is the polarization potential induced in the vacuum, and $S_F^a(x_2, x_1)$ is, apart from a constant factor, a Greens function for the Dirac particle. S_F^a reduces to $S_F(x_2 - x_1)$ for a vanishing external potential. All integrals are from $-\infty$ to $+\infty$ with the understanding that the final timelike integration is really a time average over an extended interval; this being indicated by the factors $1/cT$. Henceforth, the potential will be taken to be that of a point magnetic dipole superposed upon a point charge.

Evaluation of the polarization energy, ΔE_P, is straightforward because of the availability of a convenient expression for $A_\mu^P(x)$.[4] As only the order α^2 corrections are desired, certain approximations can be made which facilitate the calculation. One contribution is obtained by taking the polarization potential of the nuclear dipole field with the wave functions of the coulomb field, while a second equal contribution arises from the polarization potential of the coulomb field in conjunction with the modification in the wave functions, ψ_a, produced by the nuclear dipole field. The total energy in units of the uncorrected hyperfine structure energy for the state ψ_a is $\frac{1}{2}\alpha^2 z \delta_{l0}$.

The calculation of the fluctuation energy, ΔE_F, is complicated by the fact that it contains the infinite mass correction, and by the fact that a convenient expression for S_F^a is not available. We proceed by first transforming to momentum space and then

separating ΔE_F into two terms, $\Delta E_F'$ and $\Delta E_F''$ in a manner originated by Feynman.[5] $\Delta E_F'$ contains explicit functions of the momenta and involves the potential at most linearly. Apart from renormalizations, which we ignore, it yields an order α correction to the hyperfine structure arising only from the anomalous electron moment. There are no order α^2 corrections. $\Delta E_F''$ contains the potential quadratically only and also contains S_F[6]. Its evaluation to order α^2 is enormously simplified by neglecting the space parts of the momenta $\hat{p}_1$ and $\hat{p}_2$ associated with the state ψ_a everywhere except in $\psi_a(P_1)$ and $\bar{\psi}_a(P_2)$, and by replacing S_F by its zero field approximation.[6] The corrections to the hyperfine structure appear as cross terms between the coulomb and dipole potentials. The validity of the approximation used depends upon the reduced weight of low momentum transfers associated with the dipole field and with the Feynman separation.

The evaluation of $\Delta E_F''$ yields an energy $-[(13/4)-\ln 2]\alpha^2\pi'\delta_{10}$, again in units of the Fermi energy. The total correction from ΔE_F and ΔE_F is thus $-[(5/2)-\ln 2]\alpha^2\pi \approx -1.81\alpha^2\pi$,[7] which is more than twelve times as large as the Bethe-Longmire estimate. Inclusion of this correction reduces the value of α^{-1} obtained from the hyperfine structure from 137.043 to 137.036. Recent measurements of the $2P_{\frac{1}{2}}-2P_{\frac{3}{2}}$ separation in deuterium indicate that a reduction in α^{-1} is indeed required, and these measurements are not inconsistent with the corrected value given here.[8]

Inclusion of meson field effects may be expected to decrease further α^{-1}. In fact, an accurate determination of α^{-1} by a method independent of mesonic effects would be a useful means of experimentally determining their magnitude.

* Work supported in part by the Signal Corps and ONR.
[1] Kusch and Prodell, Phys. Rev. 79, 1009 (1950).
[2] Dumond and Cohen, least-squares adjustment of the atomic constants as of December 1950, (report to the national research council), p. 30.
[3] Estimates of a part of these omitted effects have been given by Bethe and Longmire (Phys. Rev. 75, 306 (1949)), where they are described as arising from a spatial extension of the anomalous moments.
[4] See Karplus and Kroll, Phys. Rev. 77, (1950) for explicit definitions of D_F, S_F and $A_F{}^P(x)$. There $A_F{}^P$ is denoted by $(\alpha/2\pi)\bar{A}_F{}^{(1)}$ (Eq. 14).
[5] Private communication. The separation is described in detail in the dissertation of M. Baranger, *Relativistic Corrections to the Lamb Shift* (Cornell University, New York, 1951).
[6] The authors are indebted to H. A. Bethe for pointing out to them the possibility of these approximations, and to M. Baranger for a copy of his thesis, in which their application to another problem is illustrated.
[7] A similar result, using a different method, has been obtained by R. Karplus and A. Klein. We wish to thank these authors for discussing their results with us.
[8] W. E. Lamb (private communication).

Continuous γ-Spectrum Accompanying Electron Capture

D. Maeder and P. Preiswerk
Swiss Federal Institute of Technology, Zürich, Switzerland
(Received September 20, 1951)

IT is well known that the emission of electrons from a radioactive nucleus is accompanied by a low intensity continuous spectrum of γ-radiation (bremsstrahlung). An analogous effect occurs when a nucleus captures an electron of the atomic shell. The theory of this radiative K-capture has been given by Morrison and Schiff.[1] An experimental evidence of this γ-radiation has been found in the study of the disintegration of Fe^{55}.[2] With the new technique using scintillations from NaI crystals for detecting γ-rays and measuring their energies, we were able to study the shape of the spectrum of the low intensity γ-radiation emitted by a Fe^{55} sample.

Figure 1 shows the pulse distribution of the scintillations excited by the Fe^{55} γ-radiation. To determine the upper limit of the γ-spectrum of Fe^{55} we proceed in the following way: From measurements of the pulse distribution for several monochromatic γ-rays of different energies, we are able to construct the pulse distribution which should result from the shape of the continuous γ-ray spectrum theoretically predicted by Morrison and Schiff, assuming different upper limits of the spectrum. As an example of

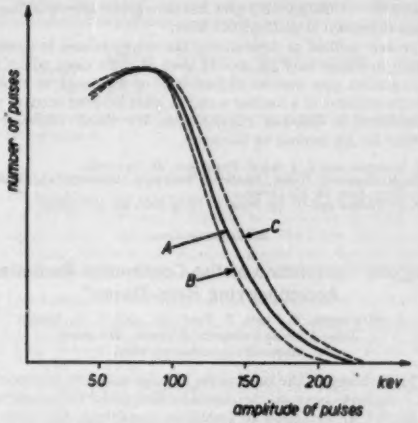

FIG. 1. Pulse distribution of the γ-radiation from Fe^{55}: A = observed curve; B = constructed curve with $E_{max}(h\nu)$ = 0.200 Mev; C = constructed curve with $E_{max}(h\nu)$ = 0.210 Mev.

the calibration, the pulse distribution for the nonconverted part of the isomeric 88-kev transition in Ag^{109} is shown in Fig. 2. (The $Ag-K\alpha$-line has been partly absorbed.) A good agreement between the experimental pulse distribution and the calculated one is obtained for an upper limit of the γ-spectrum at $E_{max}(h\nu) = 0.205$ Mev. The qualitative agreement of the curves supports the correctness of the assumed spectrum.

In the electron capture process, the whole energy available most frequently goes off with the neutrino, but may be shared between the neutrino and a γ-quantum. The upper limit of the γ-spectrum corresponds to the case when the whole disintegration energy is taken away by the γ-quantum. From the upper limit the mass difference of the parent and the daughter atoms can therefore be obtained directly; in our case it is:

$$M(Fe^{55}) - M(Mn^{55}) = E_{max}(h\nu) + E_K = (0.212 \pm 0.010) \text{ Mev}.$$

This value is in good agreement with the recent determination from the threshold of the $Mn^{55}(p, n)Fe^{55}$ reaction, for which a

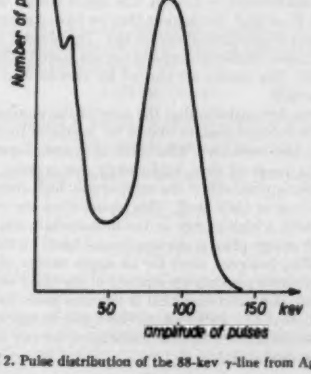

FIG. 2. Pulse distribution of the 88-kev γ-line from Ag^{109}.

Q-value of $-(1.006\pm0.010)$ Mev has been given[3] corresponding to a mass difference of (0.22 ± 0.01) Mev.

The new method of determining the energy-release in electron capture processes may be applied even in some cases where the disintegration goes over an excited level of the daughter nucleus with the emission of a nuclear γ-ray. A more detailed account will be published in *Helvetica Physica Acta*. We thank Professor P. Scherrer for his interest in this work.

[1] P. Morrison and L. I. Schiff, Phys. Rev. **58**, 24 (1940).
[2] Bradt, Gugelot, Huber, Medicus, Preiswerk, Scherrer, and Steffen, Helv. Phys. Acta **19**, 222 (1946).
[3] P. H. Stelson and W. M. Preston, Phys. Rev. **83**, 469 (1951).

Angular Correlation of the Continuous Radiation Accompanying Beta-Decay*

L. Madansky, F. Lipps, P. Bolgiano, and T. H. Berlin
Johns Hopkins University, Baltimore, Maryland
(Received September 18, 1951)

THE theory of the continuous gamma-radiation accompanying beta-decay was developed by Knipp and Uhlenbeck[1] and by Bloch.[2] An extension to forbidden transitions was made by Chang and Falkoff,[3] especially for the scalar interaction. This radiation has been found by several investigators,[4] and recently it has been possible to measure the shape of the gamma-ray continuum at low energies (50 kev–300 kev).[5] Theoretical predictions show that for low energies the shapes of the gamma-continua are almost identical for allowed and first-forbidden transitions for any interaction. This point has been verified experimentally (to be published).

We thought it might be of interest to calculate the angular correlation between the beta-particle and its associated gamma-quantum and to see if one could distinguish between allowed and forbidden transitions. We calculated the correlation for allowed and first-forbidden transitions, making use of the tensor interaction and neglecting charge dependence. We obtained the following expressions for the allowed and first-forbidden correlation functions $W(\theta)$. The first-forbidden formula is for the special selection rule ($\Delta J=2$; yes). Allowed correlation function

$$W_A(\theta)=\frac{[W_0-(W+k)]^2}{k}\sin\theta p\frac{(W+k)}{q^2}\left(\frac{(W+k)^2+W^2}{W+k}q-q^2-1\right),$$

first-forbidden correlation function, tensor interaction ($\Delta J=2$; yes)

$$W_F(\theta)=CW_A(\theta)\{[(W_0-(W+k)]^2+(W+k)^2-1-2kq\},$$

where W=final energy of beta-ray, $q=W-p\cos\theta$, $p=(W^2-1)^{\frac{1}{2}}$, k=photon energy in relativistic units, and C=a constant for equalization at 90° (see below).

We have plotted a correlation for the following experimental situation. The beta-transition is taken as first-forbidden tensor for the special case ($\Delta J=2$; yes). The upper energy of the beta-spectrum is $W_0=4mc^2$. We assume that we have a gamma-counter which accepts all gammas above 50 kev. The angular correlations for allowed cases are also plotted and are equalized to the forbidden curves at 90°. The results are plotted for various final energies of the beta-particle.

The curves demonstrate that the ratio of the number of coincidences at the forward peak to that at 90° is greater for the allowed than for the first forbidden. The ratio, of course, depends on the value of the range of final beta-energy one accepts. This ratio becomes quite appreciable if one accepts only high energy gamma-rays in the counter ($h\nu>2mc^2$). This occurs when one beta-particle is created with a high energy in the intermediate state and then emits a high energy photon. An experiment based on this condition is not feasible, however, since for an upper energy of $W_0=4mc^2$, only 10^{-5}-gammas per beta are emitted in the range above 1 Mev.

The calculations also show that it becomes easier to distinguish between allowed and forbidden as the upper energy of the beta-spectrum is increased. From the calculation we can conclude the following results:

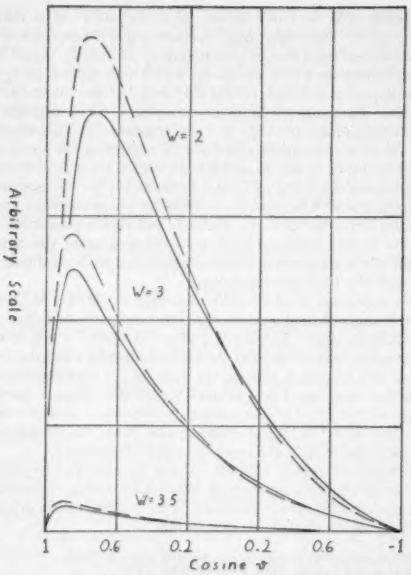

FIG. 1. The angular correlation $W(\theta)$ as a function of $\cos\theta$ for final beta-energies of 2, 3, and 3.5 mc^2. Dotted curves are for allowed transitions, solid curves for first-forbidden transitions—tensor interaction ($\Delta J=2$, yes). The curves for equalized at 90° for each final beta-energy.

1° The correlation for allowed transitions is independent of the form of the interaction;

2° The nuclear matrix elements for first-forbidden transitions are identical with the ones obtained in the ordinary beta-decay. Hence the shape of the beta-ray spectrum uniquely determines the angular correlation.

Although the internal bremsstrahlung does not provide any new information on the form of beta-decay interaction, it does provide a secondary means of studying beta-decay.

* This work was supported in part by the AEC.
[1] J. K. Knipp and G. E. Uhlenbeck, Physica **3**, 425 (1936).
[2] F. Bloch, Phys. Rev. **50**, 272 (1936).
[3] C. S. Wang Chang and D. L. Falkoff, Phys. Rev. **76**, 365 (1949).
[4] C. S. Wu, Phys. Rev. **59**, 481 (1941), also including references to earlier work.
[5] L. Madansky and F. Rasetti, Phys. Rev. **83**, 187 (1951).

Additional Data on the Radioactive Isotopes of Tin and Tellurium*

J. M. Cork, A. E. Stoddard, C. E. Branyan, W. J. Childs, D. W. Martin, and J. M. LeBlanc
Department of Physics, University of Michigan, Ann Arbor, Michigan
(Received September 10, 1951)

THE existence of many stable isotopes in tin together with the small cross section for neutron capture displayed by most of them, has made difficult the correct assignment of the observed radioactivities. Spectrometric studies of specimens enriched in masses 112 (72.5 percent), 116 (89.6 percent), 122 (45.8 percent), and 124 (83.1 percent) and irradiated in the pile for two months, yield results differing from those previously reported[1,2] for certain of the isotopes.

Tin-113. This isotope is produced by neutron capture in Sn-112 with the largest cross section of any of the isotopes, and gives in the spectrometer several electron lines. Three low energy lines are interpretable as of Auger origin accompanying indium x-rays. Three strong lines are the K, L, and M electron groups for the known transition in indium-113 (112 min) whose energy is here

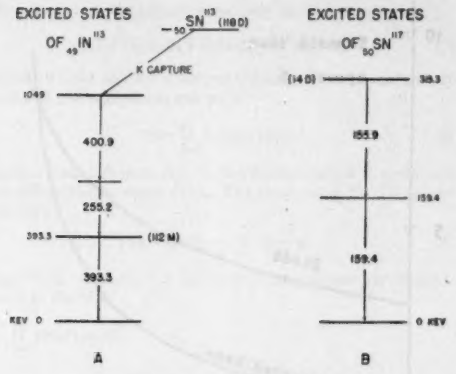

FIG. 1. Decay schemes for Sn^{113} and Sn^{117}.

found to be 393.3 kev. Two weaker electron lines with energies of 227.2 and 373.0 kev are present and appear by their half-life to be associated with the same activity and hence represent gamma-transitions in indium with energies of 255.2 and 400.9 kev. No evidence could be found either spectrometrically or by absorption for a gamma-ray of energy around 90 kev, as reported, nor could any positrons be observed coming from the specimen. The half-life of the enriched specimen as observed for 8 months appears to be 118±2 days, a value higher than those previously reported, which ranged from 70 to 112 days. A possible decay scheme is presented in Fig. 1(A).

Tin-117. An excited state of tin-117, whose half-life has been variously reported as from 13.0 to 14.5 days, was produced by neutron capture in tin-116. This specimen yielded 4 electron conversion lines at energies of 126.7, 129.3, 151.5, and 155.0 kev in addition to lines due to indium-113 and one other of Auger origin. This indicates the existence of two gamma-rays of energy 155.9 and 159.4 kev. The former is highly converted with a K/L ratio of about 7. Only the weak K line is observed for the latter. No evidence is found for the existence of a 174-kev gamma-ray as reported.[2] The half-life is noted to be 14.0±0.5 days. A nuclear level scheme is proposed in Fig. 1(B).

Tin-123. Neutron capture in enriched tin-122 yields a beta-active emitter whose half-life has been reported[3] as from 130 to 136 days. The maximum beta-energy has been given as 1.42 Mev with a converted gamma-ray of 394 kev. It now appears highly probable that this gamma-ray when observed in any isotopic enrichment is due to traces of tin-113, and is the highly converted indium gamma-radiation. No gamma-radiation appears to be associated with tin-123. The half-life observed in this investigation, following the decay of the enriched specimen for 18 months and allowing for the presence of some 2.5-year antimony-125 radiation, appears to be slightly less than that previously reported, namely 125±3 days. No further information of a conflicting nature applying to the other known radioactivities in tin has so far been found.

Tellurium. Using isotopes of tellurium enriched in masses 120 (22.3 percent), 122 (86.2 percent), 126 (95.4 percent), and 128 (90 percent), some information has been obtained of a revisory nature to that previously reported.[4] It is believed that the energies of the internally converted gamma-rays as now determined photographically are accurate to ±0.2 percent. The radioactive decay of the various specimens has been followed for over 300 days leading to half-lives somewhat different than are in the literature.

All of the gamma-rays found in this investigation to be associated with the enriched isotopes represent isomeric transitions in Te with the probable exception that a 575-kev gamma occurs in Sb-121 following K capture from Te-121. The evidence for this

TABLE I. Summary of half-lives and gamma-energies in tellurium.

Mass	121	123	125	127	129
Half-life	140-day	121-day	58-day[a]	115-day	33.5-day
Gamma energy (kev)	81.8 213 6 575(Z=51)	88.7 159.2	109.6 35.3	88.7	106.0

[a] See reference 5.

575-kev gamma is a single electron line at 544.7 kev in the enriched Te-121 specimen. No evidence could be found for a gamma-ray of energy 615 kev following K capture in Te-121 as reported, indicating the above interpretation of the 544.7-kev electron line. The revised values of the gamma-energies and the half-lines as here determined are shown collectively in Table I.[5]

[*] This investigation was aided by the joint support of the AEC and ONR.

[1] J. Livingood and G. Seaborg, Phys. Rev. 55, 667 (1939); J. Mihelich and R. Hill, Phys. Rev. 77, 743 and 79, 781 (1950); C. Nelson and G. Boyd, Oak Ridge National Laboratory Report 499 (1949); and S. Barnes, Phys. Rev. 56, 414 (1939).

[2] E. Mallary and M. Pool, Phys. Rev. 77, 743 (1950).

[3] W. Grummitt and G. Wilkinson, Nature 158, 163 (1946); J. Lee and M. Pool, Phys. Rev. 76, 606 (1948); and Ketelle, Nelson, and Boyd, Phys. Rev. 79, 242 (1950).

[4] Katz, Hill, and Goldhaber, Phys. Rev. 78, 9 (1950); K. Siegbahn and W. Forsling, Arkiv Fysik 1, 505 (1950); R. D. Hill, Phys. Rev. 76, 186, 333 (1949); and J. Edwards and M. Pool, Phys. Rev. 69, 140 (1946).

[5] R. D. Hill, Phys. Rev. 76, 186, 333 (1949).

Electrodynamic Displacement of Atomic Energy Levels

ROBERT KARPLUS, ABRAHAM KLEIN, AND JULIAN SCHWINGER
Harvard University, Cambridge, Massachusetts
(Received September 10, 1951)

THE modifications in the fine structure and hyperfine structure of hydrogenic atoms, produced by electrodynamic effects, have thus far been computed essentially only to the order $\alpha=1/$"137". In view of the high accuracy of recent measurements we have extended the theory to include effects of order $Z\alpha^2$. In contrast with corrections of order α^2, these terms arise from a more precise treatment of the nuclear coulomb field in the relativistic domain, rather than from higher order electrodynamic phenomena.

For the hyperfine structure of S levels, we find the following fractional correction of order $Z\alpha^2$,

$$-(5/2-\log 2)Z\alpha^2. \tag{1}$$

In conjunction with the known α^2 contribution to the electron moment,[1] we have, as the total electrodynamic correction factor

$$1+\alpha/2\pi-(2.97/\pi^2)\alpha^2-(5/2-\log 2)Z\alpha^2 = 1.001145-0.963\cdot 10^{-4}Z = 1.001049,\ Z=1. \tag{2}$$

In a recent survey of atomic constants, Dumond and Cohen[2] have provided tables of constants based upon an adjustable correction factor, which was arbitrarily written

$$1.001147/(1+\Gamma). \tag{3}$$

Thus the reciprocal of the fine structure constant is stated as

$$1/\alpha=(137.0429\pm 0.0009)(1-0.486\Gamma). \tag{4}$$

The electrodynamic correction embodied in (2) would, in itself, imply

$$\Gamma=0.98\cdot 10^{-4}, \tag{5}$$

whence

$$1/\alpha=137.0364. \tag{6}$$

However, this ignores the contribution to Γ associated with the spatially distributed nature of the proton magnetic moment.

An indication of the magnitude of this effect can be obtained from the ratio of the hyperfine structures in hydrogen and deuterium. If the residual discrepancy in this quantity[3] is ascribed to

the spatial distribution of the nucleon moments, we should have

$$\Gamma_{\text{nucl}}=0.26\cdot 10^{-4}, \tag{7}$$

which, incorporated in Γ, gives

$$1/\alpha=137.0346. \tag{8}$$

The effects under consideration produce the following contribution to the displacement of an nS level,

$$\frac{8Z^4\alpha^3}{n^3}\frac{3}{3\pi}\left[3\pi Z\alpha\left(1+\frac{11}{128}-\frac{1}{2}\log 2+\frac{5}{192}\right)\right]\text{Ry}. \tag{9}$$

For the $n=2$ level of hydrogen this amounts to 7.08 Mc/sec.[4] If the previous computation[5] of the $2S-2P_{\frac{1}{2}}$ displacement is corrected slightly for the new value of α, and 0.94 Mc/sec subtracted to account for the α^3 contribution to the magnetic moment, the addition of (9) yields

$$1057.75 \text{ Mc/sec} \tag{10}$$

for the improved theoretical value of the "Lamb shift" in hydrogen. This may be compared with the published experimental value[6] of 1062±5 Mc/sec. Still not included in the theoretical value are α^3 effects other than in the magnetic moment, and the possible influence of nucleon structure and mass.[7]

We are indebted to N. M. Kroll for numerous enlightening discussions.

[1] R. Karplus and N. M. Kroll, Phys. Rev. **77**, 536 (1950).
[2] J. W. M. Dumond and E. R. Cohen, National Research Council Report, December, 1950, Phys. Rev. **82**, 555 (1951).
[3] F. E. Low and E. E. Salpeter, Phys. Rev. **83**, 478 (1951).
[4] Essentially the same result has also been obtained by M. Baranger, Ph.D. thesis, Cornell (1951). We are grateful to H. A. Bethe for informing us of this calculation, and to Dr. Baranger for supplying us with a copy of his thesis.
[5] Bethe, Brown, and Stehn, Phys. Rev. **77**, 370 (1950).
[6] R. C. Retherford and W. E. Lamb, Phys. Rev. **75**, 1325 (1949).
[7] Apart from the simple mass correction employed in reference 5. Note that if the reduced mass is not substituted for the electron mass in the logarithm, the "Lamb shift" (10) becomes 1057.82 Mc/sec.

Influence of Initial Velocities on Electron Transit Times in Diodes

J. T. WALLMARK
Royal Institute of Technology, Stockholm, Sweden
(Received August 27, 1951)

IN a recent letter[1] and a more detailed article[2] Barut has given a method to calculate the transit time of electrons with initial velocities in diodes with partial space charge, assuming a homogeneous initial velocity distribution. In practical cases calculations for a nonhomogeneous velocity distribution are of more interest. The author has undertaken such calculations by means of a first-order perturbation method.

Assume a parallel plane diode with a homogeneous flow of electrons. The electric field, potential, etc., may be calculated from published data on partial space charge.[3-5] Consider, then, a small number of electrons with a velocity that differs from the main velocity by the amount Δ. If the number is small enough its influence on the space charge conditions may be neglected, corresponding to a first-order approximation.

The transit time for these electrons is

$$\tau=\int_0^d dx/v.$$

By substituting the values

$$v=[(2e/m)(V\pm\Delta)]^{\frac{1}{2}}$$

$$dx=\frac{dV}{[(16/9)E^2\eta(V/V_a)^{\frac{1}{2}}+E_0^2]^{\frac{1}{2}}},$$

where E is the electric field strength without space charge, E_0 is the electric field strength at the cathode, $\eta=I/I_s$ is the relative current compared to space charge saturated current, and V_a is the anode voltage we obtain the elliptic integral

$$\tau=\left(\frac{m}{2e}\right)^{\frac{1}{2}}\int_0^{V_a}\frac{dV}{[\{(16/9)E^2\eta(V/V_a)^{\frac{1}{2}}+E_0^2\}(V\pm D)]^{\frac{1}{2}}}.$$

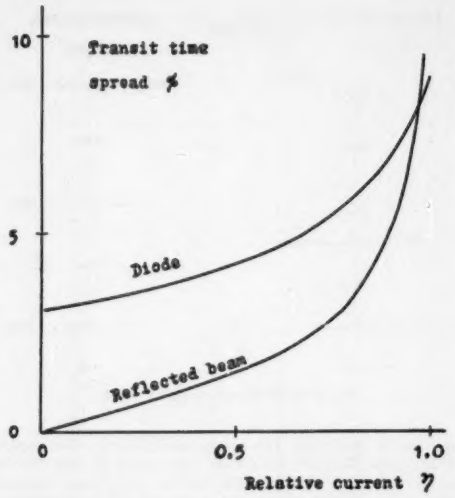

FIG. 1.

The integral may be solved by standard methods. The results will be shown applied to two practical cases, first on ordinary diode with an anode voltage of 100 volts and an anode–cathode distance of 5 mm. Figure 1 shows the spread in transit time as a function of current density in the diode for a difference in initial velocity of 0.1 volt (roughly corresponding to conditions for an oxide cathode at 1100°K).

Figure 1 also shows the spread in transit time for a reflected beam under the same circumstances. In that case the difference in transit time is much reduced as a result of the influence of different path lengths.

A complete report is in preparation.

[1] A. O. Barut, Phys. Rev. **81**, 274 (1951); **82**, 554 (1951).
[2] A. O. Barut, Z. angew. Math. Phys. **II**: 1, 35 (1951).
[3] J. T. Wallmark, Proc. Inst. Radio Engrs., to be published.
[4] H. F. Ivey, Phys. Rev. **76**, 554 (1949).
[5] R. Cockburn, Proc. Phys. Soc. (London) **47**, 810 (1935).

Group Uniqueness in the Irreducible Volume Character of Events

B. T. DARLING AND M. LEICHTER
Department of Physics and Astronomy, Ohio State University, Columbus, Ohio
(Received May 16, 1951)

THE derivation of the mass quantization condition on the basis of the irreducible volume character of events[1] involved, for purposes of relativistic invariance, an averaging of the difference equation (corresponding to Dirac's equation) over the four-dimensional rotation group. This led of necessity to complex values for the space-time variables. In view of this complex character of space one should consider averaging over more general bounded subgroups of the linear group than just the rotation group. (The Lorentz group cannot be used because it is not compact.) Every bounded subgroup of the full linear group is, however, equivalent to a unitary group.[2] It will now be shown that the integration (averaging) of the difference equation over the complete four-dimensional unitary group annihilates the dynamical equation.

The difference equation corresponding to Dirac's equation is

$$[\gamma_\lambda\Delta_\lambda\nabla_\lambda+\kappa\nabla]\psi=0. \tag{1}$$

(For the definition of the operators Δ_λ, ∇_λ, and ∇ see reference 1).

Its average over the unitary group may be written as

$$\int[\gamma_\lambda\Delta_\lambda\nabla_\lambda+\kappa\nabla]dR\psi\Big/\int dR=0, \tag{2}$$

where dR is the element of volume of the four dimensional unitary group. If ψ is analytic we can write[1]

$$\nabla\psi=\prod_{\lambda=1}^{4}(\cos\omega\gamma_\lambda u_\rho)\psi, \tag{3}$$

where ω is the difference step, $\gamma_{\lambda\rho}$ are the elements of R, and u_ρ are the differential operators $\partial/\partial x_\rho$. The first term of Eq. (2) can be written as[1]

$$\gamma_\lambda\Delta_\lambda\nabla_\lambda\psi=-\frac{1}{\omega^2}\sum_{\sigma=1}^{4}\gamma_\sigma\frac{\partial\nabla}{\partial u_\sigma}\psi. \tag{4}$$

Expanding $\cos\omega\gamma_\lambda u_\rho$ in a power series and integrating we get a result of the form

$$\int\prod_{\lambda=1}^{4}\cos\omega\gamma_\lambda u_\rho dR$$

$$=\sum_{k=0}^{\infty}\Big[\sum_{i_1+i_2+i_3+i_4=k}c_{i_1i_2i_3i_4}u_1^{i_1}u_2^{i_2}u_3^{i_3}u_4^{i_4}\Big]. \tag{5}$$

Inasmuch as the element of group volume is invariant under, say, right translations we have

$$\int f(Ru)dR=\int f(RTu)d(RT)=\int f(Ru')dR, \tag{6}$$

where T is unitary and $u'=Tu$. Hence

$$\sum_{k=0}^{\infty}\Big[\sum_{i_1+i_2+i_3+i_4=k}c_{i_1i_2i_3i_4}u_1^{i_1}u_2^{i_2}u_3^{i_3}u_4^{i_4}\Big]$$

$$=\sum_{k=0}^{\infty}\Big[\sum_{i_1+i_2+i_3+i_4=k}c_{i_1i_2i_3i_4}(u_1')^{i_1}(u_2')^{i_2}(u_3')^{i_3}(u_4')^{i_4}\Big]. \tag{7}$$

Equation (7) is an identity in u and implies that the homogeneous polynomials

$$\sum_{i_1+i_2+i_3+i_4=k}c_{i_1i_2i_3i_4}u_1^{i_1}u_2^{i_2}u_3^{i_3}u_4^{i_4} \tag{8}$$

are invariant under a unitary transformation. But the only invariant of a unitary transformation is the unitary scalar product (and functions of it). Hence the polynomials (8) cannot be invariant. It now follows from the validity of Eq. (7) that

$$c_{i_1i_2i_3i_4}=0 \tag{9}$$

except for $i_1=i_2=i_3=i_4=0$. Thus

$$\int\nabla dR\psi=\text{const }\psi \tag{10}$$

and consequently from Eq. (4) it follows that

$$\int\gamma_\lambda\Delta_\lambda\nabla_\lambda dR\psi=0. \tag{11}$$

Combining Eqs. (2), (10), and (11) we get finally

$$\kappa\,(\text{constant }\psi)=0 \tag{12}$$

or

$$\psi=0. \tag{13}$$

We may now conclude that the rotation group is the only compact group we can use to obtain relativistic invariance.

[1] B. T. Darling, Phys. Rev. **80**, 460 (1950).
[2] F. D. Murnaghan, *The Theory of Group Representations* (Johns Hopkins Press, Baltimore, Maryland, 1938), p. 57.

Actual Path Length of Electrons in Foils

C. N. YANG*
Department of Physics, University of Illinois, Urbana, Illinois
(Received September 10, 1951)

THE angular and spatial distribution due to multiple scattering of a beam of charged particles after passing through a foil has been extensively studied by many authors. We wish to discuss in this note a related problem: the distribution with respect to the actual path length of the particles.

Let $l+\Delta$ be the actual path length of a particle after passing through a foil of thickness l.[1] Under the small angle approximation

$$\Delta=\Delta_y+\Delta_z,\quad \Delta y=\tfrac{1}{2}\Sigma_i t_i\theta_{yi}^2,\quad \Delta z=\tfrac{1}{2}\Sigma_i t_i\theta_{zi}^2, \tag{1}$$

where t_i, $t_i\tan\theta_{yi}$, and $t_i\tan_{zi}$ are the projections along the t, y, and z axes of the displacement of the particle between the $(i-1)$- and i-th scatterings. The approximation made in (1) in neglecting terms of order θ^4 amounts to a correction on Δ of less than 3 percent for θ as large as $\sim 20°$.

We want to calculate the probability $P(l;\, y,\, \theta_y,\, \Delta_y;\, z,\, \theta_z,\, \Delta_z)$ $\times dyd\theta_y d\Delta_y dzd\theta_z d\Delta_z$ that a particle at the thickness l has lateral displacements, direction of motion, and increment of path length in the specified ranges. Under the usual gaussian approximation (as in reference 1) we can write down the following diffusion equation for P:

$$\frac{\partial P}{\partial t}=-\theta_y\frac{\partial P}{\partial y}-\theta_z\frac{\partial P}{\partial z}+\frac{1}{w^2}\frac{\partial^2 P}{\partial\theta_y^2}+\frac{1}{w^2}\frac{\partial^2 P}{\partial\theta_z^2}-\frac{1}{2}\theta_y^2\frac{\partial P}{\partial\Delta_y}-\frac{1}{2}\theta_z^2\frac{\partial P}{\partial\Delta_z}. \tag{2}$$

This is separable into a product of distribution in $(t-y)$ and $(t-z)$ planes:

$$P=F(t;\, y,\, \theta_y,\, \Delta_y)F(t;\, z,\, \theta_z,\, \Delta_z), \tag{3}$$

where F satisfies

$$\frac{\partial F}{\partial t}=-\theta\frac{\partial F}{\partial y}+\frac{1}{w^2}\frac{\partial F}{\partial\theta}-\frac{1}{2}\theta^2\frac{\partial F}{\partial\Delta}. \tag{4}$$

The initial condition is

$$F(0;\, y,\, \theta,\, \Delta)=\delta(y)\delta(\theta)\delta(\Delta). \tag{5}$$

Equation (4) can be solved by first taking the fourier transform with respect to Δ and y:

$$F=\int\int_{-\infty}dpdq\psi(t;\, p,\, q,\, \theta)\exp(ipy+iq\Delta), \tag{6}$$

$$\partial\psi/\partial t=[(1/w^2)(\partial^2/\partial\theta^2)-\tfrac{1}{2}iq\theta^2-ip\theta]\psi. \tag{7}$$

This is easily reducible to a form identical with the Schrödinger equation for a harmonic oscillator. The only difference is that the "frequency" is here complex. Expanding ψ into normalized eigenfunctions ϕ of the harmonic oscillator one could solve for the t-dependence of the coefficients. One then uses the initial condition (5) to determine the constants of integration. The solution obtained this way is

$$\psi=\frac{1}{4\pi^2}\sum_{n=0}^{\infty}\phi_n\Big(\frac{w\rho}{q}\Big)\phi_n\Big(w\theta+\frac{w\rho}{q}\Big)\exp\Big\{t\Big(\frac{i\rho^2}{2q}-[2n+1]\omega\Big)\Big\}, \tag{8}$$

where

$$\phi_n(x)=(\pi^{\frac{1}{2}}2^n n!)^{-\frac{1}{2}}\omega^{\frac{1}{2}}H_n(\omega^{\frac{1}{2}}x)\exp(-\tfrac{1}{2}\omega x^2), \tag{9}$$

$$\omega^2=iq/2w^2, \tag{10}$$

and $H_n(x)$ are the hermite polynomials.[2] The real parts of ω, $\omega^{\frac{1}{2}}$, $\omega^{\frac{1}{2}}$ are chosen positive. The distribution function P can be computed from (8), (6), and (3).

The general solution given above can be used to compute the probability $A(\Delta)d\Delta$ (for any given geometry) that the charge particle has in a foil of thickness t a path length between $t+\Delta$ and $t+\Delta+d\Delta$. The final result for two common cases is given below:

Case I. All particles are detected irrespective of their position and angle of emergence.

$$\text{probability}=A(\Delta)d\Delta=B_I(v)dv, \tag{11}$$

$$v=2w^2\Delta/t^2, \tag{12}$$

$$B_I(v)=2\pi^{-\frac{1}{2}}v^{-\frac{1}{2}}(u-3u^9+5u^{25}-7u^{49}+\cdots), \tag{13}$$

$$u=\exp(-1/v).$$

The following asymptotic approximations of B_I are good to within 1 percent in the ranges indicated:

$$B_I(v)=2\pi^{-\frac{1}{2}}v^{-\frac{1}{2}}(e^{-1/v}-3e^{-9/v}) \quad \text{for } v\leqq 2.0,$$

$$B_I(v)=\tfrac{1}{4}\pi\exp(-\pi^2v/16) \quad \text{for } v\geqq 2.0.$$

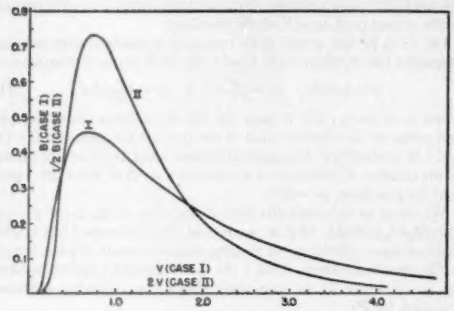

FIG. 1. Distribution function with respect to path length. $v=$(actual path length$-$thickness of foil) $\times 2w^2/t^2$ $Bdv=$probability.

Case II. Only those particles with $\theta_y=\theta_z=0$ at emergence are detected. The position of emergence is arbitrary. In this case

$$B_{II}(v)=4\pi^{-\frac{1}{2}}v^{-5/2}\left[(u+9u^9+25u^{25}+\cdots)-\frac{v}{2}(u+u^9+u^{25}+\cdots)\right].$$

The following asymptotic approximations of B_{II} are good to within 1 percent in the ranges indicated:

$$B_{II}(v)=4\pi^{-\frac{1}{2}}v^{-5/2}\left(1-\frac{v}{2}\right)e^{-1/v} \quad \text{for} \quad v\leqq 1.0,$$

$$B_{II}(v)=\tfrac{1}{2}\pi^2\exp(-\pi^2 v/4) \quad \text{for} \quad v\geqq 1.0.$$

The distribution function B_I and B_{II} are plotted in Fig. 1. The average value $\langle\Delta\rangle_{Av}$ of Δ for any case can be easily computed by the following method without first solving for the complete distribution with respect to Δ:

Equation (1) can be written

$$\Delta=\tfrac{1}{2}\int_0^t(\theta_y^2+\theta_z^2)dt'.$$

Hence

$$\langle\Delta\rangle_{Av}=\tfrac{1}{2}\int_0^t\langle(\theta_y^2+\theta_z^2)_{Av}\rangle dt'. \qquad (14)$$

For case I the probability for a particle to have the angle θ_y at thickness t' is given by $G(t',\theta_y)d\theta_y$ where G is defined in reference 1, Eq. (1.63). From this we find

$$\langle\theta_y^2\rangle_{Av}=\langle\theta_z^2\rangle_{Av}=2t'/w^2.$$

Hence by (14)

$$\langle\Delta\rangle_{Av}=t^2/w^2.$$

For case II suppose N is the number of incoming particles. The number of particles at thickness t' having angles $\cong\theta_y$ and θ_z is

$$NG(t',\theta_y')G(t',\theta_z')d\theta_y'd\theta_z'. \qquad (15)$$

The probability for these particles to come out with angles of emergence $d\theta_y\geqq\theta_y\geqq 0$, $d\theta_z\geqq\theta_z\geqq 0$ is

$$G(t-t',-\theta_y')d\theta_y G(t-t',-\theta_z')d\theta_z. \qquad (16)$$

The product of (15) and (16) therefore gives the number of particles with the specified angle of emergence that had the angles $\cong\theta_y'$ and θ_z' at t'. Hence the probability for a detected particle to have the angles θ_y' and θ_z' at t' is

$$[G(t,0)]^{-2}G(t',\theta_y')G(t',\theta_z')G(t-t',-\theta_y')G(t-t',-\theta_z')d\theta_y'd\theta_z'.$$

From this we can easily calculate the average $\langle\theta_y^2\rangle_{Av}$ at t'. Substitution of the result into (14) gives finally

$$\langle\Delta\rangle_{Av}=t^2/3w^2.$$

It is evident that this method of calculation of $\langle\Delta\rangle_{Av}$ can be applied whenever we know the angular and spatial distribution functions. One could, for example, dispense with the gaussian approximation and use the exact numerical solution of Snyder and Scott[2] to compute $\langle\theta_y^2\rangle_{Av}$ and $\langle\Delta\rangle_{Av}$.

The author is pleased to thank Drs. Goldwasser and Hanson and Mr. Modesitt for interesting discussions.

* Now back at the Institute for Advanced Study, Princeton, New Jersey.

[1] B. Rossi and K. Greisen, Revs. Modern Phys. 13, 240 (1941). We use these authors' notation in their Sec. 23.

[2] See, e.g., L. I. Schiff, *Quantum Mechanics* (McGraw-Hill Book Company, Inc., New York, 1949), Sec. 13.

[3] H. Snyder and W. T. Scott, Phys. Rev. 76, 220 (1949).

Alpha-Alpha Correlations in the Photodisintegration of C^{12} and the Resonant Absorption of Electromagnetic Radiation of Non-E.D. Character

VALENTINE L. TELEGDI
Institute for Nuclear Studies and Department of Physics, University of Chicago, Chicago, Illinois

(Received September 18, 1951)

THE photodisintegration of C^{12} leading, in the final state, to three alpha-particles, has been the subject of a number of recent investigations.[1-5] These established the following facts:

(a) The cross section for the reaction goes through a pronounced resonance, with a peak value of the order of 10^{-28} cm^2 at approximately $E_\gamma=18$ Mev and a half-width of roughly 3.5 Mev, and increases again after a minimum around $E_\gamma=21$ Mev.

(b) In the region of the first resonance, the reaction proceeds predominantly via the well-known 3-Mev level of Be^8, while some other mechanism(s) prevail in the region of re-increase.

(c) A small fraction of the disintegrations, increasing with E_γ, involves the ground state of Be^8.

A better understanding of these facts as well as some information on the spins of Be^{8*} and Be^8 can be gained by analyzing more deeply some anomalies encountered in the investigation of this reaction with the resonant gamma-radiation from Li^7+p.

Diagram *A* in Fig. 1 shows a histogram of the energy distribution of the alpha-particles from 483 stars produced by the 17.6-Mev line in nuclear emulsions. To permit an analysis after Bethe[6] the distributions to be expected for the first alpha-particle (W_1) and the alpha-particles from the break-up of Be^{8*}(W_{23}) in the 3-Mev state have been drawn in. For the calculation of W_{23} a level width Γ of 1.1 Mev and absence of correlation between the direction of flight of Be^{8*} and the velocities, in the C. G. system of Be^{8*}, of the alpha-particles resulting from the break-up have been assumed. The gamma-ray momentum has been neglected throughout.

While the general agreement of the theoretical distribution $W=W_{\alpha}+W_{23}$ warrants statement (b), the deviations for $E\leq 3.5$ Mev seem to be outside statistical fluctuations. A somewhat more satisfactory agreement can be obtained by assuming[2] that about 16 percent of the disintegrations proceed via an 8-Mev level of $\Gamma=0.75$ Mev in Be^8. This mechanism would explain the appearance of an extra maximum around $E\simeq 1.5$ Mev, but fails to produce the very noticeable minimum between 2.0 and 4.0 Mev. It is also discredited by the observation that at higher photon energies this level does not participate more strongly if at all.[5] Further, Nabholz *et al.*[7] have emphasized that similar discrepancies occur for $E_\gamma=14.6$ Mev, which is insufficient to excite the 8-Mev level.

We wish to show that the appearance of this minimum can be explained quite naturally on the assumption that the 3.0-Mev level in Be^8 has $J=2$. It might be noted that this is in contradiction with Wheeler's[8] conclusions. On the basis of the assignment $J=2$, the observed distribution may arise as a result of angular correlation effects. Electric quadrupole (E.Q.) absorption would not give correlation, because the alpha-particle emitted from the 2^+ state of carbon would be expected to be mainly an *s* wave. Magnetic dipole (M.D.) absorption, on the other hand, would lead to a 1^+ state in carbon (j_1), decaying by emission of an alpha-particle of two units of angular momentum (l_1) to the 3-Mev state of Be^8 ($j=2^+$) which breaks up with a *d* wave (l_2) with respect to its

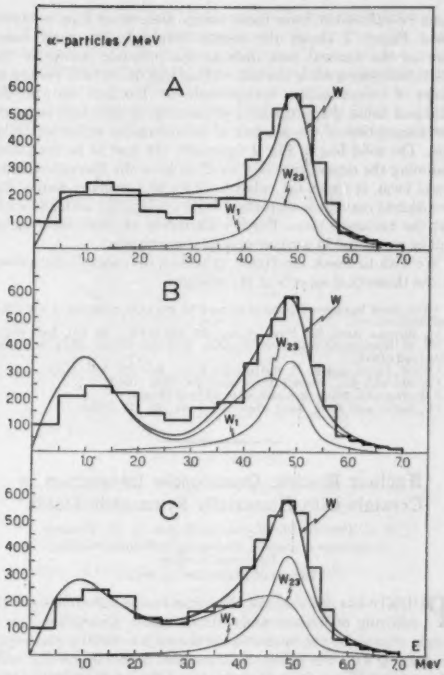

FIG. 1. The histograms in all three diagrams show the energy distribution observed experimentally in 483 photodisintegrations of C^{13} by 17.6-Mev gamma-rays. The curves W are the theoretical distributions, calculated (*A*) for pure E.Q. absorption, (*B*) for pure M.D. absorption, and (*C*) for equal M.D. and E.Q. absorption cross sections.

center of gravity ($j_3=0$). For this sequence, one obtains the correlation function

$$W(\vartheta)=(15/4)\sin^2\vartheta\cos^2\vartheta. \quad (1)$$

Equation (1) leads to the energy distribution

$$W_{23}(E)=(15/4)(2/E_1E^*)^4[(2/E_1E^*)(E_1/4+E^*/2-E)^3 -(2/E_1E^*)^2(E_1/4+E^*/2-E)^4], \quad (2)$$

in which E=energy of an alpha-particle from Be^{8*} break-up, E_1=energy of alpha emitted from carbon, E^*=excitation of Be^{8*}.

Diagram *B* shows the distribution Eq. (2), modified to take the finite width ($\Gamma=1.1$ Mev) of the Be^8 level into account. It is to be noted that W_{23} has a minimum which coincides with the minimum in the experimental histogram.

It has been estimated[9] that the absorption cross sections for M.D. and E.Q. in carbon in our energy region are comparable. In diagram *C* we give the alpha-particle distribution computed on the assumption that the M.D. and E.Q. cross sections are equal. This calculated distribution clearly reproduces all the features of the experimental histogram. Upon comparison of diagrams *A*, *B*, and *C* it is apparent that the experimental distribution may be understood provided that the M.D. and E.Q. (γ, α) cross sections are of about equal magnitude.

It might be asked whether a possible electric dipole (E.D.) contribution to the absorption would not impair the agreement displayed in diagram *C*. E.D. absorption should mainly induce the sequence $j_1=1^-$, $l_1=1$, $j=2^+$, $l_2=2$, $j_3=0^+$, which leads to a correlation derivable from Lloyd's tables,[10] *viz*:

$$W(\vartheta)=1+P_2(\cos\vartheta). \quad (3)$$

The corresponding $W_{23}(E)$ is an upwards parabola, with its minimum at 2.72 Mev for $E_\gamma=17.6$ Mev. A small admixture to the distribution shown in diagram *C* would rather improve the agreement.

Pending a more detailed experimental investigation of this reaction, especially at higher energies, the following picture is proposed:

(a) in the region of the first peak in the cross section, the absorption is due to M.D. and E.Q. effects;

(b) the correlation is evidence for Be^{8*} ($E^*=3.0$ Mev) having $J=2$, while the small participation of Be^8 in the ground state indicates that the latter has $J=0$. In fact, the 1^+ state in carbon to which M.D. absorption leads cannot decay by alpha-emission to $J=0^+$, while in the E.Q. absorption $l_1=0$ is favored with respect to $l_1=2$;

(c) the re-increase in the cross section is to be attributed to another absorption mechanism, probably to the low energy wing of the E.D. "resonance." It is to be noted that with E.D. absorption the direct disintegration into three alpha-particles becomes a more probable competitive reaction mechanism.

A study of the angular distribution of the reaction products would afford a stringent test of our assumptions. Such a study encounters considerable difficulties caused by the large width of the Be^{8*} level. The situation is more favorable in the analogous photodisintegration of O^{16}.

I am indebted to Drs. E. N. Adams, II, and M. L. Goldberger for discussions and to Dr. D. C. Peaslee for correspondence on this subject.

[1] Goward, Telegdi, and Wilkins, Proc. Phys. Soc. (London) (A)63, 402 (1950).
[2] V. L. Telegdi and W. Zünti, Helv. Phys. Acta 23, 751 (1950).
[3] V. L. Telegdi, Proc. Harwell Nuclear Physics Conference (1950), p. 62.
[4] J. J. Wilkins and F. K. Goward, Proc. Phys. Soc. (London) (A)64, 201 (1951).
[5] V. L. Telegdi and M. Eder, Helv. Phys. Acta, (to be published).
[6] H. A. Bethe, Revs. Modern Phys. 9, 218 (1937).
[7] Nabholz, Stoll, and Wäffler, Helv. Phys. Acta 23, 858 (1950). While some of the views expressed in this note have been subsequently revised, it is my understanding that this point has been maintained.
[8] J. A. Wheeler, Phys. Rev. 59, 27 (1941).
[9] J. Blatt and V. F. Weisskopf, Section 7.22 of Chapter XII of privately circulated notes of their book on nuclear physics. Order of magnitude agreement with the observed cross section in carbon at 17.6 Mev is obtained by inserting in these authors' formulas the observed level distance of C^{13} instead of their value $D_0=0.5$ Mev.
[10] S. P. Lloyd, Phys. Rev. 83, 776 (1951).

Short Range Interaction of Electrons and Fine Structure of Positronium*

MARTIN DEUTSCH AND EVERETT DULIT
Laboratory for Nuclear Science and Engineering and Department of Physics, Massachusetts Institute of Technology, Cambridge, Massachusetts
(Received September 11, 1951)

PIRENNE[1] and Berestetski[2] have published detailed theoretical analyses of the relativistic interaction of positron and negatron. Besides the well-known terms which characterize the interaction between charged particles, e.g., electron and proton, there appears a new, short-range term due to virtual annihilation and re-creation of the pair. Pirenne has shown that this spin dependent term which contributes only to the energy of ^3S states may be considered as an exchange interaction. In particular it contributes to the energy of the lowest bound $^3S_1$ state of the system (ortho-positronium). The energy of this state above the $^1S_0$ para-state is given by $E=E_1+E_2=8.5\times10^{-4}$ ev, where $E_1=(32/3)\pi\mu_e^2\psi^2(0)=4.8\times10^{-4}$ ev is the magnetic spin-spin interaction which gives rise to the hyperfine structure of hydrogen and $E_2=8\pi\mu_e^2\psi^2(0)=3.7\times10^{-4}$ ev is the new exchange term.

We have measured the separation E by observing the quenching in a magnetic field of the ortho-state which is metastable against annihilation, and find that $E=9.4\times10^{-4}$ ev$\pm$15 percent. This is in good agreement with the theoretical value and demonstrates clearly the spin-dependent close-range interaction. The principle of the experiment is very similar to the quenching of the metas-

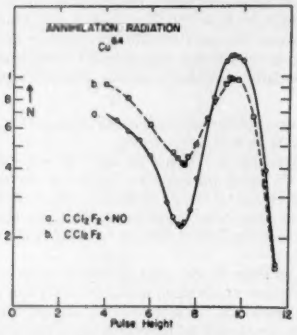

FIG. 1. Annihilation radiation spectra for $f=1$ and $f=0$.

table $2S$ state of hydrogen by an electric field.[3] In the case of positronium in a magnetic field the state with $S=1$, $M=0$ gets a small admixture of $S=0$ by virtue of the quadratic Zeeman effect. Linear Zeeman effect is absent in all states. To an accuracy more than sufficient for our purpose, the fraction of para-state admixed to the ortho state with $M=0$ is $a^2=(2\mu_0 H/E)^2$. Only the ortho-positronium atoms with $M=0$ are affected, since the probability of reorientation before annihilation is negligibly small. The pure ortho-state decays by three-photon emission at the rate $\lambda_0=7\times10^6$ sec^{-1},[4,5] while the para-state decays at the rate $\lambda_p=8\times10^9$ sec^{-1} by two-photon annihilation.[4] The effect of the admixture of para-state in a magnetic field H is therefore twofold: (1) The decay rate of one third of the ortho-positronium atoms is increased to $\lambda(H)=\lambda_0(1-a^2)+\lambda_p a^2$. (2) The probability that an ortho-positronium atom decay by three-photon annihilation, nearly unity in the absence of a field,[6] is reduced to $f(H)=\lambda_0(1-a^2)/(\lambda_0(1-a^2)+\lambda_p a^2)$. By measuring $f(H)$ *vs* H we have found a^2 and from this E. A large volume of uniform magnetic field was provided by a large electromagnet of the Research Laboratory of Electronics.[6] We are indebted to Prof. F. Bitter for the opportunity to use this magnet.

f was determined by observing in a scintillation spectrometer the annihilation radiation spectrum produced in freon. Experimental conditions were much improved over those in our earlier communications.[5] Figure 1 shows typical spectra obtained in the absence of a field in pure freon ($f\simeq1$) and freon with 3 percent nitric oxide ($f\simeq0$). Spectra obtained in pure freon with a magnetic field were intermediate between these two. In the actual experiments only points near the maximum and the minimum of a spectrum were measured with very good statistical accuracy.

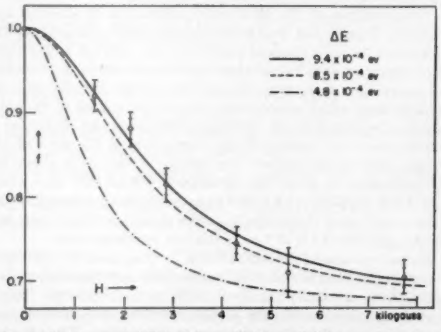

FIG. 2. Relative probability of three-photon annihilation as a function of magnetic field. Theoretical curves for different values of the fine structure of positronium.

f can be calculated from these points after some simple corrections. Figure 2 shows the results obtained. The short crossbars on the vertical bars indicate the probable scatter of the individual points while the full vertical lengths include the uncertainty of normalization, background, etc. The fact that, for the strongest fields, f approaches $\frac{1}{2}$ of its value at zero field supports our assumption of the absence of re-orientation before annihilation. The solid line in Fig. 2 represents the best fit to the points assuming the dependence of f on H to have the theoretical functional form. It yields the value $E=9.4\times10^{-4}$ ev given above. The two dashed curves are theoretical curves calculated with and without the exchange term. Further discussion of these experiments will be presented in a paper now in preparation.

We wish to thank Dr. Henry Primakoff for valuable discussions of the theoretical aspects of the problem.

* This work has been supported in part by the joint program of the ONR and AEC.

[1] J. Pirenne, Arch. Sci. Phys. et Nat. **28**, 233 (1946); **29**, 121, 207 (1947).
[2] V. B. Berestetskii and L. D. Landau, J. Exptl. Theor. Phys. SSSR **19**, 673, 1130 (1949).
[3] W. E. Lamb and R. C. Retherford, Phys. Rev. **79**, 549 (1950).
[4] A. Ore and J. L. Powell, Phys. Rev. **75**, 1696 (1949).
[5] M. Deutsch, Phys. Rev. **82**, 455; **83**, 866 (1951).
[6] F. Bitter and F. E. Reed, Rev. Sci. Instr. **22**, 171 (1951).

Nuclear Electric Quadrupole Interaction in Crystals with Nonaxially Symmetric Fields*

H. E. PETCH,† D. W. SMELLIE,‡ AND G. M. VOLKOFF
Department of Physics, University of British Columbia, Vancouver, Canada
(Received September 17, 1951)

POUND[1] has reported the theory and some experiments on the splitting of nuclear magnetic resonance absorption lines in single crystals by the interaction of the nuclear electric quadrupole moment Q with the electric field gradient at the site of the nuclei in question. His work on the influence of the crystal orientation on the line splitting is restricted primarily to the special case of crystals in which the field gradient tensor has an axis of symmetry. Becker and Kruger[2] report further experiments on rotating a crystal with an axially symmetric field. Schuster and Pake,[3] and Hatton, Rollin, and Seymour[4] report some additional work on crystals, but they do not discuss the dependence of the line splitting on the crystal orientation.

We have extended Pound's theory[1] to cover the dependence of the line splitting on the crystal orientation for the general case of crystals in which the traceless symmetric field gradient tensor does not necessarily have an axis of symmetry, but is given in terms of its principal axes by:

$$\partial E_x/\partial x=eq(1-\eta)/2\ \partial E_y/\partial y=eq(1+\eta/2\ \partial E_z/\partial z=-eq$$

with

$$eq=\Sigma_j e_j(3\cos^2\theta_j-1)r_j^{-3}\ \eta=\left(\frac{\partial E_x}{\partial x}-\frac{\partial E_y}{\partial y}\right)\Big/\frac{\partial E_z}{\partial z}$$

in the notation of Pound's paper.[1] (The z axis is here chosen as the one with the largest absolute value of the field gradient component, and x with the smallest, so that $0\leq\eta\leq1$). We have also experimentally verified this theory in the case of the Li^7 lines obtained from a single crystal of $LiAl(SiO_3)_2$ (spodumene).

We choose three mutually perpendicular right-handed axes in the crystal which are easily recognized externally, and label them X, Y, Z (in the monoclinic spodumene crystal the b axis was chosen as X, the c axis as Y, and the direction perpendicular to b and c as Z. The crystallographic a axis lies between our Y and $-Z$ axes.). Let X have the direction cosines λ_i, Y have μ_i, and Z have ν_i, with respect to the right-handed axes x, y, z in which the field gradient tensor is diagonal at the site of the nuclei in question. (Although in spodumene there are four Li atoms per unit cell the existence of known symmetry centers and of twofold screw axes in the b direction guarantees that the principal axes of the field gradient tensor have the same orientation at the four sites

with some one of the principal axes parallel to the b direction.) Let X, Y, Z in turn be made perpendicular to the uniform external magnetic field H_0, and in each case let the crystal be rotated about this axis normal to H_0. We have found that first-order perturbation theory gives for the frequency difference $2\Delta\nu$ between the two lines arising from the transitions between Zeeman levels m ($>\frac{1}{2}$) and $m-1$ and the levels $-(m-1)$ and $-m$, the expression:

$$2\Delta\nu = A + B\cos 2\theta + C\sin 2\theta, \tag{1}$$

where for the case of the rotation about the X axis

$$\begin{aligned} A_X &= 2k[\tfrac{1}{2} - \tfrac{1}{3}\lambda_3^2 + \tfrac{1}{3}\eta(\lambda_2^2 - \lambda_1^2)] \\ B_X &= 2k[\tfrac{1}{3}(\nu_3^2 - \nu_2^2) + \tfrac{1}{3}\eta(\mu_1^2 - \nu_1^2 - \mu_3^2 + \nu_2^2)] \\ C_X &= 2k[-3\mu_3\nu_3 + \eta(\mu_2\nu_2 - \mu_1\nu_1)] \\ k &= [e^2qQ/h][3(2m-1)/8I(2I-1)]. \end{aligned} \tag{2}$$

Here m is the largest magnetic quantum number of the four values involved in the two transitions. θ_X is measured from the position in which Y coincides with H_0. Expressions for the Y and Z rotations are obtained by cyclic permutation from the above. Pound's results[1] refer to the Y rotation in the special case $\eta=0$, $\lambda_1=\mu_2=\nu_3=1$, the other direction cosines being zero, so that $A_Y=k$, $B_Y=3k$, $C_Y=0$, and Eq. (1) reduces to

$$2\Delta\nu = 2k(3\cos^2\theta - 1).$$

It may be easily shown that of the nine constants A, B, C for the X, Y, Z rotations only five are independent, *viz.* the three C's and any one pair A, B, the other two pairs being related to the first one by the four identities:

$$A_X + A_Y + A_Z = 0, \quad A_Y - B_Y = A_Z + B_Z, \quad A_Z - B_Z = A_X + B_X,$$

$A_X - B_X = A_Y + B_Y$ (from which it also follows that $B_X + B_Y + B_Z = 0$). Thus by performing the three rotations one obtains experimental values for five independent quantities of the nine A, B, C. The five independent relations of the form (2) involving these five quantities, taken together with the six orthonormality conditions for the direction cosines, may be solved for the eleven unknowns consisting of $|k|$, η and the nine direction cosines. This gives an experimental determination of the orientation within the crystal of the principal axes of the field gradient tensor, of the asymmetry parameter η, and of the magnitude of the quadrupole coupling constant $|e^2qQ/h|$.

In some types of crystals it may be known from their symmetry properties that one of the principal axes of the field gradient tensor must be parallel to one of the crystallographic axes. (In the case of spodumene the b axis must be parallel to some one of the principal axis.) If, say, the X axis of rotation could be made to coincide exactly with this principal axis then the above algebra would be considerably simplified, for then $C_Y=C_Z=0$, and the X rotation alone would give the complete information.

The three rotations were performed for a natural single crystal of spodumene of approximate dimensions $10\times10\times8$ mm in a recording oscillating detector spectrometer designed and built by Collins[4] which is similar to the one described by Pound and Knight.[5] The frequency differences $2\Delta\nu$ between the two outer components ($m=I=\frac{3}{2}$) of the Li^7 line was measured in a magnetic field of approximately $H_0=7190$ gauss corresponding to the unperturbed resonance frequency $\nu_0=\mu H_0/Ih=11.90$ Mc/sec. (A spot check was made for one particular crystal orientation which gave a large $\Delta\nu$ to verify that in accordance with Eqs. (1) and (2) the observed $\Delta\nu$ is actually independent of H_0 which was varied from approximately 6500 to 8000 gauss.) Figure 1 is a reproduction of several examples of recorded absorption derivative curves. Figure 2 gives the $2\Delta\nu$ curve for the X rotation.

The other two rotations also gave similar curves of the general form of Eq. (1). The experimental values of the constants (in kilocycles/sec) are:

$A_X = 34.0$	$B_X = -4.7$	$C_X = 41.6$
$A_Y = -14.8$	$B_Y = 53.0$	$C_Y = 5.4$
$A_Z = -19.2$	$B_Z = -47.8$	$C_Z = 1.9$

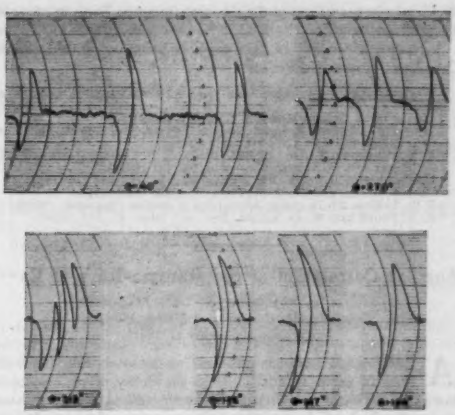

FIG. 1. Examples of recorded absorption derivative curves. The first three show selected splittings for the X rotation. The last three demonstrate the accuracy with which the position of zero splitting at $\theta_Y=147°$ was determined for the Y rotation. A change of θ_Y by $\pm1°$ produces a marked decrease in the maximum of the derivative curve. The sweep rate in all cases is 10 kc/sec per division.

The above deviations of C_Y and C_Z from zero correspond to errors of less than 3° in aligning the rotation axes. The relative signs for the above nine quantities are definitely given by the experiment, but not the absolute signs. The above experimental values lead to the following values computed from the general formulas:

$\eta = 0.793$	$\lvert k\rvert = 18.9$ kc/sec	$\lvert e^2qQ/h\rvert = 75.6$ kc/sec
$\lambda_1 = -0.074$	$\lambda_2 = 0.997$	$\lambda_3 = 0.020$
$\mu_1 = 0.746$	$\mu_2 = 0.042$	$\mu_3 = 0.665$
$\nu_1 = 0.662$	$\nu_2 = 0.065$	$\nu_3 = -0.747$

Only the relative signs of the above direction cosines are important. Since $\lambda_2\approx1$ it appears that the y principal axis is parallel to the b direction. The deviation of λ_2 from unity, and of λ_1, λ_3, μ_2, and ν_2 from zero is a measure of the accuracy of aligning the rotation axes.

Experiments on the frequency splitting of the Li^6 and Al^{27} lines in spodumene, and second-order perturbation calculations ap-

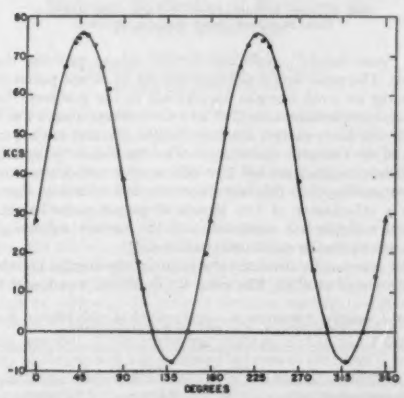

FIG. 2. Frequency difference between the two outer components of the Li^7 line for the X rotation about the b axis of spodumene. The circles are the experimental points. The solid curve represents $2\Delta\nu=33.95-41.85\cos^2(\theta_X+41°45')$. $\theta_X=0$ when the c axis of spodumene coincides with the magnetic field H_0.

plicable to larger values of e^2qQ/h in asymmetric fields are now in progress.

A complete account of this work is being submitted to the *Canadian Journal of Physics.*

* Work supported by grant from the National Research Council of Canada.
† Holder of an Ontario Research Council Scholarship.
‡ Holder of a National Research Council Bursary. Now with the Dominion Gulf Company, Box 281, Larder Lake, Ontario.
[1] R. V. Pound, Phys. Rev. **79**, 685 (1950).
[2] G. Becker and H. Kruger, Naturwiss. **38**, 121 (1951).
[3] N. A. Schuster and G. E. Pake, Phys. Rev. **81**, 157 and 886 (1951).
[4] Hatton, Rollin, and Seymour, Phys. Rev. **83**, 672 (1951).
[5] T. L. Collins, Ph.D. thesis, University of British Columbia, (1950).
[6] R. V. Pound and W. D. Knight, Rev. Sci. Instr. **21**, 219 (1950).

Angular Correlation of the Gamma-Rays of Cs^{134}*

BEROL L. ROBINSON† AND LEON MADANSKY
Johns Hopkins University, Baltimore, Maryland
(Received September 12, 1951)

A PROGRAM has been initiated for the study of the correlations of cascade radiations[1] in the decay of radioisotopes. We make use of the proportional properties of scintillation crystals and of the high efficiency of NaI(Tl) as a γ-ray detector. We reduce the accidental counting rates considerably by using fast amplifiers and a fast coincidence circuit for timing, and slower, linear amplifiers in parallel, pulse-height selection channels. There are no heavy metals in the vicinity of the detecting crystal and no collimation is used. We rely only upon pulse-height selection to eliminate false coincidences due to scattered radiation.

Each photomultiplier output goes to two parallel channels. One consists of a fast amplifier and leads to a "fast" coincidence circuit whose resolving time is 30 μsec. The other channel is a linear amplifier and single channel pulse-height selector and leads

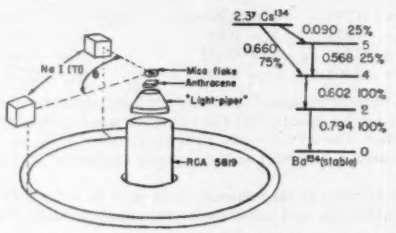

FIG. 1. Decay scheme of Cs^{134} and schematic sketch of detector system (β-ray detector exploded).

to a "pulse-height" coincidence circuit, whose resolving time is $\frac{3}{4}$ μsec. The pulse-height selectors are set to accept pulses corresponding to γ-ray energies appropriate to the problem. For instance, in experiments on Co^{60} and Cs^{134}, whose γ-rays are all of nearly the same energy, the pulse-height selectors are set to the peak of the Compton distribution. The "fast" and "pulse-height" coincidence signals are fed into still another coincidence circuit. An output signal in this last stage then indicates that there has been a coincidence of two signals of proper pulse height. All critical voltages are regulated, and the battery supplying the photomultipliers is monitored continuously.

The system was checked by measuring the angular correlation of the γ-rays of Co^{60}. The ratio $W(\pi)/W(\frac{1}{2}\pi)$ was found to be

TABLE I. Angular correlation of γ-rays coincident with 660-kev β-ray of Cs^{134}. Spins 4, 2, 0, and quadrupole radiations.

	$W(\pi/2)$	$W(3\pi/4)$	$W(\pi)$
Theoretical value	1	1.073	1.167
Theoretical value corrected for solid angle	1	1.063	1.139
Experimental value	1	1.085±0.03	1.109±0.03

TABLE II. Theoretical and experimental "over-all" correlation ratios for Cs^{134}.

Spin of 3rd state	Multipole character of 1st γ-ray	$W(\pi/2)$	$W(3\pi/4)$	$W(\pi)$
5	Dipole	1	1.036	1.074
5	Quadrupole	1	1.027	1.037
6	Quadrupole	1	1.063	1.139
Experimental values		1	1.046±0.01	1.106±0.01

1.17±0.05, in good agreement with the results of other experiments.[2]

With a slight modification of this system we have investigated the γ-ray cascade following the β-decay of the 2.3-year isomer of Cs^{134}. The decay scheme is shown in Fig. 1.[3] The source was deposited on a mica flake mounted upon a chip of anthracene (about 1 cm×1 cm×1.5 mm) as shown in Fig. 1. The output of the β-detector photomultiplier was amplified by one of the fast amplifiers and fed into the "fast" coincidence circuit. The 90-kev β-ray was entirely suppressed since it gave pulses too small to actuate the fast coincidence circuit. The anthracene was quite insensitive to γ-rays and the overall efficiency for the 660-kev β-ray was about $\frac{1}{3}$. Thus we required a coincidence of two γ-rays with the further condition that one of them be in coincidence with a 660-kev β-ray.

Some 4000 events were counted at each of three positions, (90°, 135°, 180°). The angular correlation of the γ-rays coincident with the 660-kev β-ray is in good agreement with the theoretical correlation function for transitions involving spins 4, 2, 0, and quadrupole radiations. The results are shown in Table I.

At the same time we measured the "over-all" correlation of all the γ-rays; that is, accepting any of the three γ-rays. The results are shown in Table II and are in agreement with the other observations.[2]

Assuming the spins 4, 2, 0, and quadrupole radiations, theoretical correlation functions were calculated[4] on the assumptions that the third excited state of Ba^{134} had spin 5 (dipole and quadrupole radiation) and spin 6 (quadrupole radiation.) Using the β-decay branching ratio of 3:1 and correcting for solid angle, we derive the results shown in Table II.

The spins of the excited states of Ba^{134} may then be assigned as indicated in Fig. 1. This assignment is in agreement with the character of the radiations as deduced from interval conversion coefficients.[5]

Work is in progress on other triple correlations.

We are indebted to Dr. M. E. Rose of the Oak Ridge National Laboratory for the calculation of the angular correlations of the first and third γ-rays with the second unobserved one.

* This work was supported by the AEC.
† AEC Predoctoral Fellow, 1950–1952.
[1] D. R. Hamilton, Phys. Rev. **58**, 122 (1940); G. Goertzel, Phys. Rev. **70**, 897 (1946); D. L. Falkoff, Phys. Rev. **73**, 518 (1948); D. R. Hamilton, Phys. Rev. **74**, 782 (1948).
[2] E. L. Brady and M. Deutsch, Phys. Rev. **78**, 558 (1950); J. R. Beyster and M. L. Wiedenbeck, Phys. Rev. **79**, 411 (1950).
[3] *Nuclear Data*, Nat. Bur. Standards Circular 499, p. 160, (1950).
[4] M. E. Rose (private communication). See also Biedenharn, Arfken, and Rose, Phys. Rev. **83**, 586 (1951).
[5] Charles L. Peacock and John L. Braud, Phys. Rev. **83**, 484 (1951).

Anomalous Resistance of Noble Metals Containing Paramagnetic Ions

A. N. GERRITSEN
Kamerlingh Onnes Laboratory, Leiden, Netherlands
AND
J. KORRINGA
Ohio State University, Columbus, Ohio
(Received August 16, 1951)

EXPERIMENTS performed by Gerritsen and Linde[1] on diluted alloys of Mn in Cu, Ag, and Au reveal anomalies which are similar but more pronounced than those observed in

samples of "pure" noble metals.[2,3] Typical results are shown in Figs. I, 4 and II, 3–7 of reference 1.

A theoretical account can be given if we assume that it is possible to construct wave packets, formed from distorted Bloch waves with energy near the surface of the Fermi-sea only, which correspond to a state of one electron localized in a volume equal to the volume per Mn ion, and which, for low concentration c, do not contribute to the conductivity.

The interaction between a Mn^{++} ion, which is in a ^6S state, and such an electron will remove the spin-degeneracy. The magnetic dipole interaction would give the energies $\pm E_1=\pm(8\pi/3)5\mu^2|\chi(0)|^2$ with respect to the Fermi level, $\chi(r)$ being the orbital part of the wave function of these packets. The exchange interaction is of opposite sign and probably larger. Such a splitting may very well be of the order of a few °K. As a result of overlap and finite lifetime these local states will form a band of width ΔE. Both ΔE and E_1 will increase with increasing c.

The conduction electrons with energy in the intervals $\pm[E_1\pm\Delta E/2]$ give, due to resonance scattering, a negligible contribution to the current in an applied field. Therefore the conductivity is:

$$\sigma=\sigma_0[1+(\partial f_0/\partial E_1)\Delta E], \tag{1}$$

where f_0 is the Fermi function without field and σ_0 is the conductivity in the absence of this resonance effect. Equation (1) can reproduce the $R-T$ curves for low c between $T=0$ and the minimum very well. Some experimental values of E_1 and ΔE as a function of c are shown in Fig. 1.

There will be, apart from resonance scattering and coulomb scattering, another process which we will call nonresonance scattering. This occurs for all electrons and consists of a second order transition with a "local" state as a virtual intermediate state. We calculated it as if all conduction electrons were at the Fermi level.

The contribution of the nonresonance scattering and the coulomb scattering to the total resistance will be of the same order of magnitude. If ψ_k is a Bloch wave normalized in the volume per Mn ion, the first is proportional to $|\int\psi_k^*V\chi d\tau|^4/E_1^2=V_{kk}^4/E_1^2$, the latter to $|\psi_k^*U\psi_k\cdot d\tau|^2$, where V is the effective field acting on the electron in the local state, and U is the effective perturbation in the lattice potential.

Calculating separately the contribution from Mn ions with one or both local states unoccupied, gives Eq. (2) with $H=0$.

In a magnetic field H the magnetic ions will be quantized according to $\cos\vartheta_m=m/j$, $m=-j,\cdots,j$ and distributed according to a Boltzmann law $\exp(-2m\mu H/kT)$. Moreover, the field will cause a perturbation of the local states:

$$E_m=\pm\lambda_m=\pm[\mu^2H^2+E_1^2+2\mu HE_1m/j]^{\frac{1}{2}}.$$

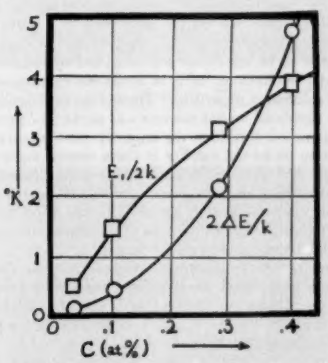

FIG. 1. Values of E_1 and ΔE as a function of c deduced from the experiments with the use of formula (1).

A calculation of the spin part of the perturbed wave functions and of the transition probabilities for ξ and η electrons separately leads to:

$$\begin{aligned}&-(\partial f_{\xi(\eta)}/\partial\mathcal{E})_{a.c.}=(f_{\xi(\eta)}-f_0)/\tau_{\xi(\eta)},\\ &1/\tau_{\xi(\eta)}=[N(\zeta_0)/4\pi^2\hbar]V_{kk}^2(P\pm Q);\\ &P=\Sigma_m(x^{2m}/\lambda_m^2)[1-f_0(-\lambda_m)f_0(\lambda_m)\\ &\qquad-\tfrac{1}{2}\{f_0(-\lambda_m)-f_0(\lambda_m)\}\{f_0(-2\lambda_m)-f_0(2\lambda_m)\}]/\Sigma x^{2m},\\ &Q=\Sigma_m(x^{2m}/2\lambda_m^2)(\mu H+E_1m/j)\{f_0(-\lambda_m)-f_0(\lambda_m)\}\\ &\qquad\times\{2-f_0(-2\lambda_m)-f_0(2\lambda_m)\}/\Sigma x^{2m}.\end{aligned} \tag{2}$$

$N(\zeta_0)$ is the density of states at the Fermi level, $x=\exp(-\mu H/kT)$. For $H=0$, $Q=0$, $x=1$, and $\lambda_m=E_1$.

From (2) we find:

$$\begin{aligned}&\sigma(H,T)=\tfrac{1}{2}(\sigma_\xi+\sigma_\eta)[1+\tfrac{1}{2}BH^2(\sigma_\xi^2+\sigma_\eta^2)]^{-1},\\ &\sigma_{\xi(\eta)}=(N_{eff}e^2/m_0)[1/\tau_{\xi(\eta)}+1/\tau_C+1/\tau_T]^{-1}.\end{aligned} \tag{3}$$

τ_C and τ_T are the effective collision times for coulomb and temperature scattering ($\tau_\xi\approx\tau_C\ll\tau_T$ at low temperatures). B is the coefficient determining the magnetoresistance of pure silver.

At low H we find $\Delta R/R\approx a(T,c)H^2$, with $a<0$ for low T and not too small c. At larger fieldstrength the $\Delta R/R$ *vs* H curves show saturation. The sudden increase of $\Delta R/R$ at low H for "large" c (see Fig. II, 5 of reference 1, $c=0.61$ atomic percent) will be due to the conductivity of the local states. It can be shown that this becomes important for this magnitude of c; in a magnetic field the energy of the local states differs at different Mn ions, the electrons can no longer make transitions from one ion to another, and the corresponding term in the conductivity will decrease rapidly in a magnetic field.

A further consequence of this model is an anomalous specific heat:

$$\rho c_V=\tfrac{1}{3}\pi^2k^2TN(\zeta_0)-nE_1(d/dT)\tanh(E_1/2kT),$$

where n is the number of Mn ions per unit volume. The local states could also lead to exchange interaction between the Mn ions; some of the irreproducible effects in the magnetoresistance, and the behavior of the susceptibility[4] seem to point to this direction.

A detailed account will be published in *Physica*.

[1] A. N. Gerritsen and J. O. Linde, Physica **17**, 573, 584 (1951).
[2] E. Mendoza and J. G. Thomas, Phil. Mag. (7) **42**, 291 (1951), where further literature may be found.
[3] D. K. C. MacDonald, Phil. Mag. (7) **42**, 756 (1951).
[4] *Le Magnétisme* (Institut International de Coopération Intellectuelle, Paris, 1940), Vol. III, pp. 306 ff.

Multiple Scattering of Electrons in Nuclear Emulsions*

DALE R. CORSON
Cornell University, Ithaca, New York
(Received September 10, 1951)

THE Fowler[1] method for deducing the momentum of a fast particle from its multiple coulomb scattering is highly useful in nuclear emulsion work and several preliminary calibration measurements have been reported.[2–4] Recently extensive calibration measurements have been reported,[5–7] among them an abstract[5] of the results recorded here.

The results are best presented in terms of multiple scattering theory, the Snyder and Scott[8] version being chosen as the most convenient here. Snyder and Scott give normalized distribution curves for the probability $W(\eta,s)$ that the particle will be scattered through an angle η (projected on a plane) in traveling a distance s. η is measured in terms of a unit angle η_0, which is a function of the atomic number of the scattering material and of the mass and energy of the particle. s is measured in terms of the mean free path for scattering λ which is a function of the atomic number of both the scatterer and the particle and of the particle's energy. Using Snyder and Scott's prescription for calculating these quantities, we find for singly-charged particles in Ilford G-5 emulsion that $\eta_0=1.39\,(m/\mu)(E^2-1)^{-\frac{1}{2}}$ degrees and $\lambda=0.160\,(E^2-1)/E^2$ mi-

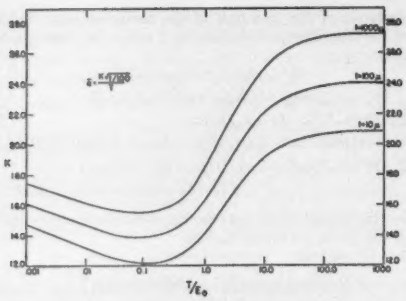

FIG. 1. The variation of the scattering constant K as a function of the ratio of kinetic energy to rest energy (T/E_0) for various cell lengths t.

crons where m and μ are masses of electron and scattered particle, respectively, and E is the ratio of the particle's kinetic energy to its total energy. To calculate mean scattering angles we must evaluate $\langle\eta\rangle_{Av}=\int\eta W(\eta)d\eta$. This must be done numerically, but Snyder and Scott give interpolation data which make the calculation particularly simple. We can write

$$\langle\eta\rangle_{Av}=z^{\frac{1}{2}}\int(\eta/z^{\frac{1}{2}})W(\eta)z^{\frac{1}{2}}(d\eta/z^{\frac{1}{2}})=z^{\frac{1}{2}}\int Rf(R)dR=z^{\frac{1}{2}}\langle R\rangle_{Av},$$

where $R=\eta/z^{\frac{1}{2}}$ and $f(R)=z^{\frac{1}{2}}W(\eta)$. We get $f(R)$ *vs* R for various z's directly from Snyder and Scott's data. $\langle R\rangle_{Av}$ increases from about 1.5 to 1.8 as z varies from 100 to 3000, so that $\langle\eta\rangle_{Av}$ increases somewhat more rapidly than $z^{\frac{1}{2}}$. $\langle R\rangle_{Av}$ is calculated using only values of R out to $4\langle R\rangle_{Av}$ and in the measurements all angles greater than four times the final mean are disregarded. With $\langle\eta\rangle_{Av}$ evaluated, we get mean angle in degrees from $\langle\theta\rangle_{Av}=\langle\eta\rangle_{Av}\eta_0$. This gives the mean projected angle between successive tangents to points on the track separated by a distance $x=z\lambda$. In the Fowler method we measure the mean angle $\langle\alpha\rangle_{Av}$ between successive chords. If the distribution of angles were gaussian the relationship would be $\langle\alpha\rangle_{Av}=(2/3)^{\frac{1}{2}}\langle\theta\rangle_{Av}$, and this is what is used in this discussion. The distribution is not quite gaussian, but out to angles of four times the mean, small error is introduced by this assumption. We have finally that

$$\langle\alpha\rangle_{Av}=(2/3)^{\frac{1}{2}}(x/\lambda)^{\frac{1}{2}}\langle R\rangle_{Av}\eta_0.$$

It is convenient to calculate $\langle\alpha\rangle_{Av}$ in terms of the particle's kinetic energy (T) and of the ratio (T/E_0) of its kinetic energy to its rest energy. When we do this, using the values of η_0 and λ appropriate to the G-5 emulsion we get

$$\langle\alpha\rangle_{Av}=1.46x^{\frac{1}{2}}\langle R\rangle_{Av}(1+T/E_0)/[T(2+T/E_0)],$$

where α is measured in degrees, x in microns, and T and E_0 in Mev. $\langle R\rangle_{Av}$ is a function of x/λ and therefore is a function of x and T/E_0, so that we can then write $\langle\alpha\rangle_{Av}=k(x, T/E_0)x^{\frac{1}{2}}/T=K(x, T/E_0)(x/100)^{\frac{1}{2}}/T$ where $K=10k$, since it is customary to refer all measurements to cell lengths of 100 microns. K *vs* T/E_0 for various x's is plotted in Fig. 1.

Measurements have been made on approximately 90 cm of electron and positron track produced by particles of well defined energy. The particles were produced in a thin radiator by synchrotron radiation and passed through $\frac{1}{16}$ in. of aluminum and about $\frac{1}{2}$ in. of air before striking the emulsion. Only the first 1000 microns of tracks which entered the emulsion at the air surface were used for measurement. The tracks were nearly parallel with the long edge of the plate (x-axis). The y-coordinate was read to 0.1μ (using an eyepiece scale for which the smallest division corresponded to 0.93μ) at intervals of 100μ. X-axis travel was produced by a micrometer screw drive on the microscope stage.

TABLE I.

Particle	Cm of track	$K(100)$
40 Mev positrons	13.4	24.6±1.0
113 Mev positrons	29.3	23.0±0.7
196 Mev positrons	21.9	25.0±0.8
196 Mev electrons	20.8	27.3±0.8
283 Mev positrons	6.5	25.0±1.5

The "noise" in the measurements has been eliminated by using a method similar to one previously outlined.[2] Examination of the curves in Fig. 1 shows that for cell lengths between 10 and 1000 mμ and for T/E_0's from 0.1 to 1000 the variation of the scattering constant with cell length can be well represented by $\langle\alpha(x)\rangle_{Av}=K(100, T/E_0)(X/100)^{0.56}T^{-1}=\langle\alpha(100)\rangle_{Av}(X/100)^{0.56}$. We can show that the second differences measured in the Fowler scheme are given by $\langle D_m(x)\rangle_{Av}^2=\langle\alpha_t(100)\rangle_{Av}^2X^{2.12}/100^{1.12}+6\langle\Delta y\rangle_{Av}^2$ where m is used to indicate measured values and t true values. $\langle\Delta y\rangle_{Av}$ is the mean uncertainty of the y coordinate readings. Thus a plot of $\langle D_m(x)\rangle_{Av}^2$ *vs* $X^{2.12}$ yields $\langle\alpha_t(100)\rangle_{Av}$ and thus $K(100, T/E_0)$. For large T/E_0 this is the number commonly referred to as the scattering constant.

The results of the measurements, using this noise elimination method, are shown in Table I. A weighted average of all the individual measurements gives a $K(100)=25.1\pm0.6$. (The use of the $X^{0.56}$ variation in the noise elimination gives a K somewhat lower than the one reported in the abstract.)

I am indebted to Mrs. Margaret R. Keck for most of the observations on which these measurements are based.

* This work was supported by the ONR.

[1] P. H. Fowler, Phil. Mag. **41**, 169 (1950).
[2] U. Camerini *et al.*, Phil. Mag. **41**, 701 (1950).
[3] D. R. Corson, Phys. Rev. **80**, 303 (1950).
[4] L. Voyvodic and E. Pickup, Phys. Rev. **81**, 471 (1951); **81**, 890 (1951).
[5] D. R. Corson, Phys. Rev. **83**, 217 (1951).
[6] K. Gottstein *et al.*, Phil. Mag. **42**, 708 (1951).
[7] L. Voyvodic and E. Pickup, Phys. Rev. (to be published).
[8] Berger, Lord, and Schein, Phys. Rev. **83**, 850 (1951).
[9] H. S. Snyder and W. T. Scott, Phys. Rev. **76**, 220 (1949).

Discharge Mechanism in Argon Counters

LAURA COLLI, UGO FACCHINI, AND EMILIO GATTI
C.I.S.E.—Piazza Cimitero Monumentale, Milano, Italy
(Received September 10, 1951)

A PREVIOUS paper[1] reported a study on the behavior of argon counters in proportional and Geiger regions.

By observing the shapes of the pulses obtained from α and β particles in the counter, it has been found that, in these regions, the mechanisms responsible for the discharge building-up are the photoelectric effect on the cathode and, as is known, the α-Townsend process on the wire.

The argon employed in the afore-mentioned experiments was 98 percent pure, purified on hot calcium later.

We endeavored to establish the validity of our observations, as dependent upon the purity of argon, in a later series of experiments.

The argon to be employed was analyzed by measurement of drift velocity of electrons, using an ionization chamber containing a beam of collimated α-particles.[2] These observations showed that the argon circulated on hot calcium was about 99.7 percent pure, containing carbon dioxide as the impurity most expected.

In order to prove the validity of these results, argon of purity better than 99.9 percent from different origins (spectral argon Lindemann, soldering argon, and commercial argon circulated on calcium magnesium alloy at 450°C[3]) was used, mixed with about 0.1 percent of carbon dioxide. This mixture behaved in the counters like argon purified as in reference 1.

The 99.9 percent pure argon (without carbon dioxide), as studied in a preliminary way, showed that other processes are acting in the discharge, together with the photoelectric effect; these processes are due to metastable excited states of argon atoms produced in the avalanche.

As is known metastable atoms generally produce secondary electrons by impact on impurities contained in the gas or at the

FIG. 1(a). β-pulse in Geiger zone; counter diameter—60 mm; pressure of argon plus 0.1 percent CO_2—760 mm Hg; Geiger threshold—3050 volts; RC—0.1 μsec; time between photopulse—4 μsec.

(b)

(c)

FIGS. 1(b) and 1(c). Burst at the starting and end points of unstable corona zone; counter diameter—20 mm; pressure—760 mm Hg; RC—10 μsec; markers—100 μsec. The photoelectric pulse groups appear like signal pulses.

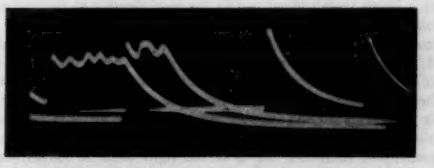

FIG. 1(d). Bursts in unstable corona zone; counter diameter—130 mm; pressure—760 mm Hg; RC—200 μsec; sweep time—30 msec.

(e)

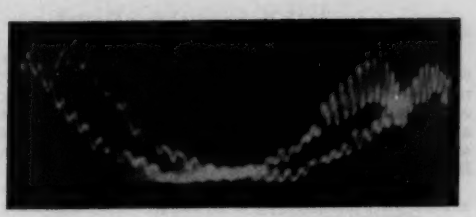

(f)

FIGS. 1(e) and 1(f). Details of bursts in unstable corona zone; data as in Fig. 1(a). The single photopulses in the bursts can be seen using the small RC value.

cathode by means of photons long after the avalanche (some tens of μsecs); therefore their behavior is strongly affected by some particular impurities (like mercury vapor acting at 10^{-4} percent concentration[4]) under these conditions no Geiger zone was found because these secondary electrons are too much delayed in respect to the motion of positive ions.

The action of the small percentage of carbon dioxide in the argon may be accounted for through fast decay of metastable atoms.

The objective of the present paper is to extend the results obtained, in the case of argon plus 0.1 percent carbon dioxide mixture, in both the unstable and the self-sustaining corona regions.

The experimental apparatus used is the same as described in reference 1. Counters used range in diameter from 2 to 13 cm and from 15 to 100 cm Hg pressure. All the counters have brass cathodes and tungsten wires 0.2 mm in diameter.

In the aforementioned paper, it has been shown that in the high proportional zone, the photoelectric process produces a convergent succession of pulses, and in the Geiger zone this series becomes divergent until the space charge on the wire lowers the field and restores the convergence. (The shape of these pulse groups is shown in Fig. 1(a).)

Under these conditions, the shape of the pulse group is almost independent of the primary ionizing β-particle, and the pulses spread completely along the wire, the counter acts as a Geiger counter. The length of this Geiger zone is very small (from one to a few tens of volts).

At slightly higher voltage value, there is an unstable corona zone. Here each pulse group of the kind of Fig. 1(a) is not quenched, but is followed by a number of pulse groups of similar shape, smaller in height than the first.

Figures 1(b), (c), and (d), taken at high RC values, show complete bursts from different counters. Photographs (e) and (f), taken at smaller RC values, show the detailed shapes of pulse groups of corona bursts.

The duration of a burst increases with increasing voltage and at some tens of volts above the Geiger zone the corona discharge becomes self-sustaining, giving a current of the order of some μa. These phenomena may be accounted for as follows:

Let us consider the first pulse group [Fig. 1(b)]; the bulk of positive ions generated at the first pulse group lowers the field on the wire below the threshold of divergence. Migration of these ions toward the cathode restores the field above its threshold value after a given time; if the photoelectric pulse succession is not quenched by this time, the following photoelectric pulses become divergent again; after which the whole process is repeated.

The second pulse group is smaller than the first because positive ions of the first group are still in the counter and lower the field; in fact the time between the top of two successive groups is smaller than an evaluated ion transit time across the counter.

We conclude that in this region space charge does not always succeed in quenching the pulse. Bursts are statistically quenched in a zone of some tens of volts, after which the corona is stable.

Counters as described in the foregoing behave like the so-called "slow counters."

Several accounts have been published on discharge mechanism of these counters.[4] It has been pointed out that the discharge spreading along the wire is due to photoelectrons from the cathode. According to Montgomery and Montgomery,[5] this process creates a space charge able to quench the pulse, and the discharge starts again by extraction of electrons from the cathode through positive ions impact.

Following our results on argon plus 0.1 percent carbon dioxide mixture, which probably apply to any counter where the spreading is caused by photoelectric effect, it must be pointed out that only the photoelectric process causes the restarting of the pulse, as the cathodic propagation of the discharge is slow enough in respect to positive ion drift velocity.

In our case, the ion-cathode process does not play an important role in the discharge; the fact that the pulse in the Geiger zone contains about 10^5 charges enables us to conclude that the probability for this process in the studied mixture is less than 10^{-6}.

We gladly thank Professor G. Bolla and Professor B. Ferretti for their helpful discussions.

[1] Colli, Facchini, and Gatti, Phys. Rev. **80**, 92 (1950).
[2] L. Colli and U. Facchini, (to be published).
[3] M. Druyvesteyn and F. Penning, Revs. Modern Phys. **12**, 87 (1940).
[4] J. D. Curran and S. C. Craggs, *Counting Tubes* (Butterworths' Scientific Publications, London, 1949).
[5] C. G. Montgomery and D. D. Montgomery, Phys. Rev. **57**, 1030 (1940).

Minimum Gamma-Gamma Cross Section in Gold

A. G. W. CAMERON AND L. KATZ
Department of Physics, University of Saskatchewan, Saskatoon, Saskatchewan, Canada

(Received September 17, 1951)

IN previous attempts[1-3] to observe scattered photons from (γ, γ) reactions initiated by high energy x-rays, two[1,2] gave negative results and one[3] detected only high energy photons attributed to a Goldhaber-Teller[4] resonance scattering process. The γ-ray decay of a compound nucleus formed by photonuclear excitation could be detected if some of the photon cascades could lead to an isomeric state. The 68-minute Pb^{204m} activity has been excited by x-rays,[5,6] but this could also result from the reaction $Pb^{206}(\gamma, 2n)Pb^{204m}$. We have measured the activation curve for the reaction $Au^{197}(\gamma, \gamma)Au^{197m}$. Since gold contains only one isotope, the 7.5-second isomer can be excited only by the above reaction.

A relative activation curve was obtained using a dropping apparatus described elsewhere.[7] Absolute activities resulted from normalization against the known $Cu^{63}(\gamma, n)Cu^{62}$ reaction,[8] and from correction for external and internal absorption of the three Au^{197m} conversion electrons.[9] Weakness of the 7.5-second activity prevented the activation shape from being determined as accurately as usual, but the accuracy was sufficient for a computation of the general shape of the cross-section curve by the photon difference method.[10] The cross-section curve is shown in Fig. 1. The absolute values are subject to uncertainties in the absorption corrections and in the conversion coefficients, but they should be correct to within a factor 2.

An additional 30-second activity was observed at the higher x-ray energies, which was produced to the same extent in gold samples of very high but different purities. No likely end product of a photonuclear reaction in gold is known to have this half-life. The activation curve suggests that a charged particle is emitted in the unknown reaction.

No observable short-lived activities in the gold were produced in irradiations with fast neutrons. The neutron contamination of the x-ray beam thus could not have contributed appreciably to the Au^{197m} yield due to inelastic scattering.

The (γ, γ') cross-section curve of Fig. 1 is similar in shape below 15 Mev to that for the $Ta^{181}(\gamma, n)Ta^{180}$ reaction,[5,10] the half-width of the latter is smaller, probably due to "cascade" competition

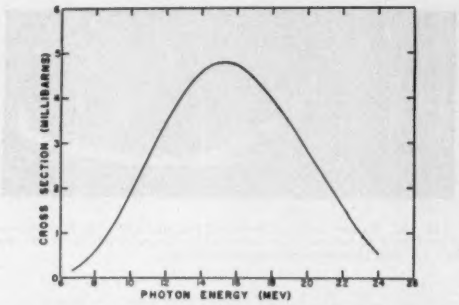

FIG. 1. Cross-section curve for the reaction $Au^{197}(\gamma, \gamma')Au^{197m}$. This is a minimum cross section; ground-state transitions and $(\gamma, \gamma' n)$ reactions are not detected. The peak value of 5 millibarns occurs at 15 Mev, the half-width is 10 Mev, and the integrated cross section is 0.05 Mev-barns.

with the $(\gamma, 2n)$ reaction. The reaction $Au^{197}(\gamma, n)Au^{196}$ is expected[11] to have a peak cross section of 500 millibarns near 15 Mev. The ratio of (γ, γ') to (γ, n) cross sections in gold thus has the unexpectedly large minimum value of 0.01.

The true (γ, γ') to (γ, n) cross-section ratio is probably much larger than this. If the nucleus is excited by photons in a dipole interaction,[4,12] there will be many more paths by which decay by photon cascades can lead to the ground state than to the isomeric state of considerably different spin. The product nuclei for (γ, n) reactions in Br^{81}, Zr^{90}, and Mo^{98} have isomeric states; measurements of these reactions in this laboratory show that the presumably smaller spin change between target and product nucleus is favored by factors from 3 to 5. It is therefore not unreasonable to guess that the total (γ, γ') cross section in Au^{197} has a peak value of the order of 25 millibarns.

The radiation width for electric radiation of multipole order l is given[13] as

$$\Gamma_\gamma^{(l)} = \frac{2(l+1)(2l+1)}{l[(2l+1)!!]^2}\frac{e^2}{\hbar c}\left(\frac{R}{\hbar c}\right)^{2l}\frac{1}{D_0} \times \int_0^E (\hbar\omega)^{2l+1}\frac{\omega_l(E-\hbar\omega)}{\omega_l(E)}d(\hbar\omega), \quad (1)$$

where E is the excitation energy, D_0 the spacing between low-lying levels ($\sim$0.5 Mev), $\omega_l(E)$ the level density at excitation E, and $(2l+1)!! = 1.3.5\cdots(2l+1)$. Magnetic radiation widths are smaller than electric ones of the same multipole order by a factor $(\hbar/McR)^2$. Radiation widths for dipole and quadrupole emission from Au^{197} with $E = 15$ Mev are listed in Table I. From statistical theory[14] we calculate the neutron emission width to be $\Gamma_n = 100$ electron volts for the same excitation. The large (γ, γ') to (γ, n) cross-section ratio cannot result from magnetic dipole and electric quadrupole radiation, but is of the right order of magnitude to result from electric dipole radiation. At low excitations electric dipole radiation widths are much less than calculated from Eq. (1), owing to very small nuclear electric dipole moments. Thus, the agreement obtained here may be taken as additional support for the electric dipole interaction theories[4,12] at higher excitations.

TABLE I. Radiation widths for decay of Au^{197} from 15-Mev excitation, computed from Eq. (1) with $\omega_l(E-\hbar\omega) = \text{const} \exp 2[0.5(E-\hbar\omega)]^{\frac{1}{2}}$. The second column gives the partial radiation width for emission of 7- to 15-Mev photons (which cannot be followed by neutron emission); the third column gives the total radiation width for emission of photons of any energy. Widths are in electron volts.

Type of radiation	Γ_γ for $7 \leq \hbar\omega \leq 15$	Γ_γ for $0 \leq \hbar\omega \leq 15$
Electric dipole	12	170
Magnetic dipole	2.4×10^{-3}	3.3×10^{-2}
Electric quadrupole	0.07	0.3
Magnetic quadrupole	1.4×10^{-3}	6×10^{-3}

The energy distribution of the initial photons given by the integrand of Eq. (1) is strongly peaked at low photon energies. Thus, at the end of several steps of a typical photon cascade, neutron emission will be possible, removing such nuclei from detectability in this experiment. We estimate that the decay of the gold nucleus can proceed by initial photon emission in as many as one-third of the photonuclear excitations.

[1] Keck, Stearns, and Wilson, Phys. Rev. **79**, 199 (1950).
[2] E. R. Gaerttner and M. L. Yeater, Phys. Rev. **76**, 363 (1949).
[3] Dressel, Goldhaber, and Hanson, Phys. Rev. **77**, 754 (1950).
[4] M. Goldhaber and E. Teller, Phys. Rev. **74**, 1046 (1948).
[5] G. C. Baldwin and G. S. Klaiber, Phys. Rev. **70**, 259 (1946).
[6] R. Sagane, Phys. Rev. **83**, 174 (1951).
[7] L. Katz and A. G. W. Cameron, Phys. Rev. **83**, 892 (1951), and to be published.
[8] Johns, Katz, Douglas, and Haslam, Phys. Rev. **80**, 1062 (1950).
[9] Huber, Humbel, Schneider, de Shalit, and Zunti, Helv. Phys. Acta **24**, 127 (1951).
[10] L. Katz and A. G. W. Cameron, Can. J. Phys., to be published.
[11] A. G. W. Cameron, Phys. Rev. **82**, 272 (1951).
[12] J. S. Levinger and H. A. Bethe, Phys. Rev. **78**, 115 (1950).
[13] J. M. Blatt and V. F. Weisskopf, privately circulated notes to appear as Chapter XII in their book, *Theoretical Nuclear Physics*.
[14] V. F. Weisskopf, in *Lecture Series in Nuclear Physics*, (U. S. Government Printing Office, Washington, D. C., 1947), MDDC 1175, p. 104.

Conductivity of the Sodium Tungsten Bronzes*

B. W. Brown and E. Banks
Polytechnic Institute of Brooklyn, Brooklyn, New York
(Received September 12, 1951)

RECENT work by Straumanis and Dravnieks[1] and Huibregtse, Barker, and Danielson[2] has shown that the cubic sodium tungsten bronzes (Na_xWO_3, where x varies between 0.95 and 0.3) have high electrical conductivity. These workers found a positive temperature coefficient of resistivity, but the conclusion that the conductivity was metallic in nature was not justified by their data, which did not show a linear dependence of resistivity upon temperature. This linear temperature dependence would be expected from the free electron model proposed by Stubbin and Mellor[3] and Kupka and Sienko[4] on the basis of magnetic susceptibility measurements. The magnitude of the conductivity reported previously appeared too low to fit in with a free electron picture, and gave a value for the mobility of electrons, as calculated by Huibregtse, *et al.*, which was smaller than that of metallic sodium by a factor of twenty-four.

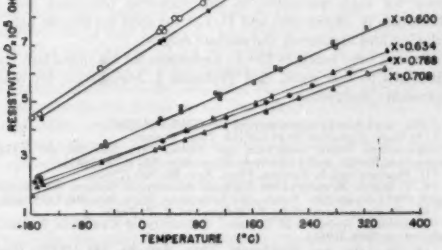

FIG. 1. Plot of resistivity *vs* temperature for six compositions of sodium tungsten bronze, Na_xWO_3.

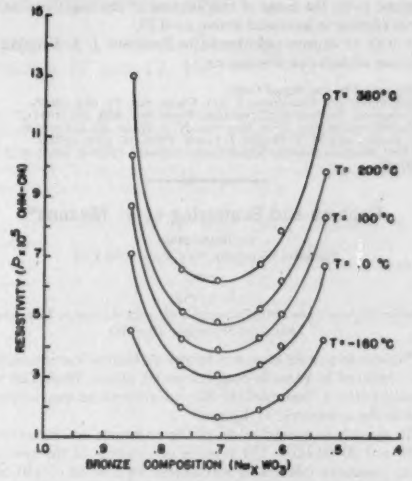

FIG. 2. Resistivity isotherms for various sodium tungsten bronzes.

The measurements reported here were made by a potential probe method (to eliminate contact effects) over a temperature range of $-160°$ to $+360°$C, for single crystals of six different compositions. The results, shown in Fig. 1, indicate a linear temperature dependence of resistivity over the entire temperature range studied. This is quantitative confirmation of the metallic nature of conduction in these materials. Using our value for the conductivity of $Na_{0.768}WO_3$ (3.0×10^4 ohm^{-1}-cm^{-1} at 25°C) and the value obtained by Huibregtse, *et al.* for the Hall coefficient of $Na_{0.633}WO_3$ (-5.3×10^{-4} cm^3/coulomb at 25°C), we obtain an electron mobility of 16 cm^2/volt-sec as compared with 2c m^2/volt-sec calculated by Huibregtse, *et al.* and 48 cm^2/volt-sec reported for metallic sodium. It appears that the mobility of electrons in these bronzes is approximately 35 percent of their mobility in metallic sodium.

In Fig. 2 a series of resistivity isotherms is shown as a function of bronze composition. The compositions were determined by x-ray analysis of powdered bronzes heated in contact with a single crystal until composition equilibrium was obtained. These compositions have lattice constants that fall on the linear portion of a lattice constant—composition curve of a previously prepared series of powdered bronzes.[5] These isotherm curves show a minimum in resistivity at approximately $x=0.70$. The temperature coefficients of resistivity behave in a similar manner (Table I).

We propose a tentative interpretation of this resistivity minimum in terms of equilibrium between undissociated sodium atoms and sodium ions plus free electrons. In the region below $x=0.70$ each sodium atom introduced contributes one free electron and one random scattering center (Na^+); while above $x=0.70$ the addition of undissociated sodium atoms contributes only additional scattering centers. These additional scattering centers are

TABLE I. Resistivity of sodium tungsten bronzes $-Na_xWO_3$.

Composition	Temp. (°C)	Resistivity $\rho\times10^5$	Temp. coef. of resist. ohm-cm per °C
$x=0.852$	26.5	7.50 ± 0.04	16.33×10^{-8}
$x=0.768$	27.5	3.65 ± 0.03	8.75×10^{-8}
$x=0.708$	29.0	3.34 ± 0.02	8.40×10^{-8}
$x=0.634$	27.0	3.67 ± 0.03	9.38×10^{-8}
$x=0.600$	26.0	4.50 ± 0.04	10.62×10^{-8}
$x=0.527$	31.0	7.18 ± 0.02	15.66×10^{-8}

presumed to be the cause of the increase of the resistivity as the sodium content is increased above $x=0.70$.

We wish to express our thanks to Professor J. J. Dropkin for numerous stimulating discussions.

* Supported by the Signal Corps.
[1] Straumanis and Dravnieks, J. Am. Chem. Soc. **71**, 683 (1949).
[2] Hulbregtse, Barker, and Danielson, Phys. Rev. **826**, 770 (1951).
[3] Stubbin and Mellor, Proc. Roy. Soc. N. S. Wales, **82**, 225 (1948).
[4] F. Kupka and M. J. Sienko, J. Chem. Phys. **18**, 1296 (1950).
[5] Third Progress Report, Signal Corps contract (July 6, 1951), p. 5 (unpublished).

Capture and Scattering of π^+ Mesons*

G. Bernardini
Columbia University, New York, New York
AND
F. Levy†
Palmer Physical Laboratory, Princeton University, Princeton, New Jersey
(Received September 17, 1951)

TO obtain a more complete survey on the nuclear interactions induced by pions in complex nuclei, plates (Ilford G5) were exposed to the π^+ beams of the Nevis Cyclotron as was previously done in the symmetric π^- beams.[1]

The spreads in energy values of the π^+ beams are, respectively, 35–50 and 70–80 Mev. The relative occurrences of the two competing processes (stars and scatterings) in a total of 150 interactions found scanning "along the track" are indicated in Table I. We did not find any "stops in flight."[1,2] In Table I, $\Sigma l'$ are total

Table I. Relative occurrence of stars and scattering.

Energy (in Mev)	$\Sigma l'$ (in cm)	Stars	Elastic scattering >40°	Inelastic scattering	λ (in cm)
35–50	3120±180	55	25	2	38 ±4.5
70–80	2250±100	63	16	9	25.5±3

lengths of tracks and λ the evaluated mean free paths.[1] The first are corrected for the estimated electron and μ meson impurities.[1] The scatterings include some probable, but doubtful cases due to very steep tracks.

As in the π^- case the capture process predominates over the scatterings at both energies, but now the energy dependence of catastrophic processes (stars and inelastic scatterings) is more evident since the cross sections for star production by π^+ are respectively 0.38 and 0.67 barn, and the corresponding figures for π^- are 0.62 and 0.76. The origin of this difference between π^+ and π^- is not clear, but taking into account the energy dependence of the capture cross section a difference between $\lambda\pi^+$ and $\lambda\pi^-$ is expected as a result of the coulomb barrier. Some evaluations are in progress to estimate this effect.

The coulomb field could also explain the lack of strongly inelastic scatterings (frequently found with π^- of 70–100 Mev[1]) in which the scattered π^+ meson has a very low energy ($E\lesssim 10$ Mev).

In Table II the frequencies of stars *versus* number of prongs are indicated. Because the features of these stars do not change ap-

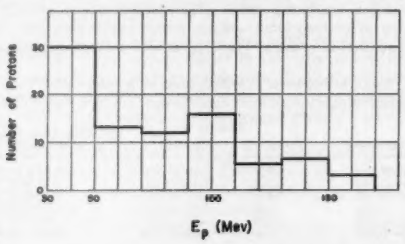

Fig. 1.

Table II. Frequencies of stars *vs* prongs.

No. prongs	0	1	2	3	4	5	6	7	Total
π^+	0	11(6)	32(20;6)	31(19;5)	18(11;2)	15(8;2)	6(3;2)	2(1;0)	115(68;17)
π^-	12	38(8)	27(8;0)	21(8;0)	4(0;0)	2(0;0)	0	0	104(24;0)

preciably between 50 and 100 Mev both energy ranges have been included in the table. The first figure enclosed by the parentheses are of those stars having one fast proton ($E\gtrsim 30$ Mev), the second figure, those having two fast protons. In a total of ~350 stars (including 150 stars found in "scanning per area") all induced by π^- mesons, only one star with 2 fast proton prongs was observed. On the contrary, stars with 2 fast proton prongs represent more than 10 percent of ~250 (155 found "scanning per area") π^+ captures. Table II also gives a simple explanation of the "stops in flight." They are captures associated with the emission of neutrons only. Therefore, as was pointed out,[2] they do not require the existence of a $\pi\to\pi^0$ scattering.

Considering the π^- capture as the mirror-image of the π^+ capture it is also possible to conclude that the charge-exchange scattering competes, if at all, only in a few percent in all π interactions. An energy-momentum balance of the π^+ stars allows as an upper limit for the $\pi\to\pi^0$ scattering a cross section not larger than $\frac{1}{10}$ of the total scattering cross section and $\simeq 0.02\sigma$ geom. Wilson and Perry[4] in a direct search for the scattered π^0 reach a similar conclusion in the light nuclei.

The frequencies of one and two fast proton stars give some support to the two-nucleon model recently discussed.[5] With this model the probability of a π capture in nuclear matter can be written

$$W_c(\pi)=\Gamma\sigma(\pi^+ + d\to 2p).$$

Using the known value of σ,[6] Γ turns out to be of the order of 10. A more definite estimate of Γ would involve a quite questionable definition of the mean free path of pions in nuclear matter (we find, for π^+ of ~50 Mev, $\lambda\simeq 3r_0$).

In some cases the two-nucleon absorption was evident because the two fast proton prongs show almost all the energy and momentum of the incoming π^+. Two of these cases could be easily interpreted with the reaction scheme

$$\pi^+ + {}_7N^{14}\to 3\alpha + 2p.$$

The energy and angular distribution of fast protons emitted in π captures are given in Fig. 1 and Table III. They are preliminary results but they could possibly be of some use in the discussion of further meson experiments.

Table III. Angular distribution of fast protons in π-captures.

$(\theta\pi p)$ in degrees	0–30	30–60	60–90	90–120	120–150	150–180
No. of fast protons	7	23	23	15	11	3

We are indebted to Messrs. J. Spiro, H. Edwards, and G. Rosenbaum for their assistance in the cyclotron operation and to Mesdames N. Bernardini and D. Lee for their invaluable help in scanning and measuring the nuclear events.

We owe very much to Dr. L. Lederman for his important contributions to this work, and Professor J. Steinberger for many interesting discussions.

* This work jointly sponsored by the ONR and AEC.
† On leave of absence from CNRS, Paris, France.
[1] Bernardini, Booth, Lederman, and Tinlot, Phys. Rev. **82**, 105 (1951); Bernardini, Booth, and Lederman, Phys. Rev. **83**, 1075 (1951).
[2] H. Bradner and B. Rankin, Phys. Rev. **80**, 916 (1950).
[3] E. T. Booth, Meeting of the National Academy of Science, Washington, April, 1951; Bernardini, Booth, and Lederman, Phys. Rev. **83**, 1975 (1951).
[4] Kindly communicated by R. Wilson and J. P. Perry.
[5] Brueckner, Serber, and Watson, University of California Radiation Laboratory, 1358 (1951).
[6] Durbin, Loar, and Steinberger, Phys. Rev. **83**, 646 (1951); Clark, Roberts, and Wilson, Phys. Rev. **83**, 649 (1951); Phys. Rev. (to be published); (kindly sent by the above authors).

Proceedings of the American Physical Society

MINUTES OF THE MEETING OF THE DIVISION OF FLUID DYNAMICS AT ITHACA, NEW YORK, SEPTEMBER 11 AND 12, 1951

THE Division of Fluid Dynamics of the American Physical Society held its fall meeting at Cornell University, Ithaca, New York, at a two-day session on September 11 and 12, 1951. The invited papers are listed below in the symposia program. There were twenty-four contributed papers, abstracts of which are contained below.

J. HOWARD MCMILLEN, *Secretary*
U. S. Naval Ordnance Laboratory
White Oak, Maryland

Symposium on Combustion and Detonation

(J. H. MCMILLEN presiding)

1. Spectroscopic Studies of Low Pressure Combustion Flames. S. S. PENNER, *California Institute of Technology.*

2. Combustion Aerodynamics. HOWARD W. EMMONS, *Harvard University.*

3. Mechanical Theory of Spinning Detonation. J. A. FAY, *Cornell University.*

Symposium on High Temperature Aerodynamics

(ARTHUR KANTROWITZ presiding)

1. Dynamics of Hypervelocity (8000 to 20,000 ft/sec) Pellets. JOHN S. RINEHART, *U. S. Naval Ordnance Test Station, Inyokern, California.*

2. Some Heat Transfer Problems in Astroballistics. FRED L. WHIPPLE, *Harvard College Observatory.*

3. Recent Strong Shock Experiments. E. L. RESLER, S. C. LIN, AND A. KANTROWITZ, *Cornell University.*

4. Departures from Thermodynamic Equilibrium in the Chromospheric Hydrodynamic Field. RICHARD N. THOMAS, *University of Utah.*

Invited Paper on Hydrodynamics

Thermodynamical Foundations of Hydrodynamics. S. R. DE GROOT, *Institute of Fluid Dynamics, University of Maryland.*

Contributed Papers

1. A Method for Calculating the Pressure in the Rarefaction Wave of a Spherical Blast. J. A. MCFADDEN, *U. S. Naval Ordnance Laboratory.*—A sphere containing an ideal gas at uniformly high pressure is allowed to expand into a surrounding medium of low pressure. The pressure in the rarefaction zone can be calculated by a combination of analytic and numerical methods in a convenient coordinate system. In the dynamical equations for isentropic flow, particle velocity and sound velocity are taken as the dependent variables, while the independent variables are the time t and a slope coordinate $(x-R)/t$, where x is the radial coordinate, and R is the radius of the original high pressure sphere. For short times after the beginning of the blast, analytic solutions may be obtained by a series development in powers of the time. In the case of the common gases, i.e., $\gamma=5/3$, $7/5$, the coefficients in these series are simple polynomials in the slope coordinate. For later times, finite-difference methods are applicable. Before the arrival of the wave front at the center of the sphere, the foregoing coordinate system is especially advantageous for numerical computations. The analytic solutions for small time are used in starting the numerical calculation; without these the initial time derivatives would be indeterminate.

2. Gas Dissociation at High Mach Numbers. R. N. SCHWARTZ AND J. ECKERMAN, *U. S. Naval Ordnance Laboratory.*—In order to study the effects of vibrational excitation and dissociation on missile flight at high Mach numbers, $\frac{1}{4}$-in. spheres are being fired through bromine gas at Mach numbers up to 13.[1] Spark shadowgraphs were made of spheres in cold air and in bromine gas at the same Mach numbers. A comparison of the shock configurations of the two cases show little difference despite the large differences in vibrational excitation and dissociation. The region of dissociation in the flow has been visualized by an optical absorption technique. The technique utilizes the strong absorption of molecular bromine of wavelengths around 4500A. Atomic bromine does not absorb these wavelengths. Initial results indicate that the dissociated gas streams far out into the wake, i.e., the reassociation distance is large compared to sphere diameter. The calculated magnitude of drag, assuming these large reassociation distances, is much different from that given by equilibrium theory. Incidentally, it was observed that the spheres luminesce in bromine at 6200 ft/sec.

[1] Z. I. Slawsky, Phys. Rev. 76, 882 (1949).

3. The Coronamicrophone.* D. WEIMER, *Princeton University.*—Professor S. G. A. Bergman of Sweden supplied us with a pressure measuring instrument for testing in the shock tube. It operates by measuring the corona current between the point of a wire and a coaxial ring. Seven such rings and wires are grouped together to increase its sensitivity; however, the entire gage is of small dimensions and offers little disturbance to the air flow behind the shock wave. With suitable calibrations we have found that the discharge from the wire is density sensitive, and for shock strengths in the range of $\xi=0.6$ to $\xi=0.96$ the response of the gage was found to be a unique function of the density rather than the pressure (ξ being the pressure ahead of the shock divided by the pressure behind the shock). The pressure of the undisturbed air ahead of the shock was varied from 500 mm to 760 mm. The rise time of the gage is less than 100 microseconds, and it operates between 3 and 5 kv with corona currents up to 600 microamperes. The signal level is high, as for example a shock of $\xi=0.7$ produces a 1.5-volt signal across a 10-k ohm driving-point resistance.

* Work supported by the ONR.

4. An Apparatus for the Production and Measurement of Transient One-Dimensional Flow.* R. J. EMRICH AND A. B. LAPONSKY, *Lehigh University.*—A piston accelerated into one end of a gas-filled tube produced a finite compression wave. The growth of a shock out of this compression wave as it progresses down the tube has not heretofore been experimentally studied in detail. An apparatus has been developed to carry out such a study. It is essentially a shock tube in which the bursting diaphragm is replaced by a relatively massive piston. To produce a shock within practical distances (7 meters), piston accelerations of the order of 10^4 m/sec^2 are required. Such accelerations have been attained by two methods: In one, the piston is held by a steel rod near its breaking strength when 250-psi pressure is introduced into the

chamber behind the piston; a chisel nicks the rod to release the piston. In the other, the whole chamber is itself an ordinary shock tube with aluminum foil diaphragm; the shock generated by this auxiliary tube reflects off the rear of the piston thus setting it into motion. Piston and shock positions are detected optically and recorded on a chronograph with microsecond accuracy.

* Partially supported by ONR

5. Measurements on Shocks Produced by the Motion of a Piston in a Tube.* A. B. LAPONSKY, *Lehigh University.*—Shocks forming at the head and in the interior of compression waves have been observed and their motions compared with those calculated from the measured piston motions. The calculation of shock motion is carried out using the method of characteristics. Knowing the velocity and position of the piston as a function of time, the characteristics of the compression wave are constructed in the x, t plane and the birth-point of the shock predicted. The subsequent shock path is obtained by a finite difference method employing the approximation[1,2] that the characteristics are straight lines throughout the entire flow field. The observed and calculated shock motions are in reasonably good agreement. A small but consistent deviation exists in that the observed shock is nearer to the piston than predicted. This deviation becomes greater as the shock strength increases, and is in the direction to be accounted for by interaction of the flow with the tube walls.

* Partially supported by ONR.
[1] S. Chandrasekahr, B.R.L. Report No. 423, Aberdeen Proving Ground (1943).
[2] K. O. Friedrichs, Communications on Appl. Math. 1, 211 (1948).

6. Dissipation of Air Shocks in a Rectangular Tube.* C. W. CURTIS AND R. J. EMRICH, *Lehigh University.*—A shock tube has been built to permit more accurate measurement[1] of losses in shock strength with travel in a tube. It combines (1) a small hydraulic radius (area to perimeter ratio of tube cross section) to accentuate the losses, (2) a large number of closely spaced detection stations to permit more detailed measurement of a single shock, and (3) heavy metal walls to reduce temperature variations along the tube. It has a rectangular cross section $\frac{1}{4}$ in. by 3 in., 12 detection stations spaced 50 cm apart and duralumin walls $\frac{3}{4}$ in. thick. The total length of tube is 7.4 meters. Losses have been measured for shocks ranging in strength $(P-P_0)/P_0$ from 0.2 to 1.2. Compared to values obtained for larger tubes of circular cross section,[1] the fractional losses in shock strength resulting from travel in the rectangular tube are larger by approximately the inverse ratio of the hydraulic radii. With this tube the accuracy is sufficient not only to measure the loss but to determine its change with distance. Results of the measurements will be discussed.

* Partially supported by ONR.
[1] C. W. Emrich and R. J. Curtis, Phys. Rev. 77, 573(A) (1950).

7. Pressure Drag in Trasonic Flow.* WAYLAND GRIFFITH, *Princeton University.*—The pressure distribution over a 15° wedge has been determined experimentally for Mach numbers between 0.86 and 1.30 using the shock tube. Such data have been unobtainable from wind tunnels so far because of wall interference. This difficulty was overcome by using a very small model (0.080-in. thickness) in the Princeton shock tube and measuring the density distribution optically rather than with pressure taps. A smoothly increasing drag curve is obtained in the sonic range, the drag coefficient being 0.0416 at $M=1$. The shock tube data agree with wind tunnel results of Liepmann and Bryson[1] on both ends of the sonic range and bear out the theoretical predictions of Cole[2] and of Guderley and Yoshihara.[3]

* Supported by an ONR contract.
[1] H. Liepmann and A. Bryson, Jr., J. Aeronant Sci. 17, 745 (1950).
[2] J. D. Cole, "Drag of a finite wedge at high subsonic speeds," GALCIT Report (1950).
[3] G. Guderley and H. Yoshihara, J. Aeronant Sci. 17, 723 (1950).

8. Growth of a Laminar Boundary Layer Behind a Shock Wave.* R. K. LOBB, *Institute for Fluid Dynamics and Applied Mathematics, University of Maryland.*—A theoretical and experimental investigation of the growth of the laminar boundary layer behind a transient step-shock wave is being carried out. Solutions have been obtained for an insulated flat plate and a plate at a constant temperature. A linear relationship between viscosity and temperature ratio has been assumed and variations of velocity in the stream direction neglected. The experimental results were obtained by means of a shock tube equipped with a Zehnder-Mach interferometer

* Research supported by the Office of Air Research.

9. Photoelastic Stress Analysis of a Shock Loaded Structure.* ROBERT G. JAHN, *Princeton Univeristy* (introduced by W. Bleakney).—To study the form and intensity of the stress distributions set up inside an object subjected to a shock wave, a solid model of photoelastic Bakelite was mounted in the shock tube and the stress progressions in it analyzed by means of a conventional circular polariscope. Using a shock of pressure ratio 6.9:1 it was necessary to employ a model 4-inches thick to observe significant fringe shifts, and this, in turn, introduced problems of initial stress patterns and light intensity. The rapid progression of the stress distributions precluded the application of the standard photoelastic analysis, via isoclinic patterns, etc., and forced the introduction of a somewhat more qualitative method of approach based exclusively on a series of $p-q$ (difference of principle stresses) patterns taken at 10–20-microsecond intervals starting at the time of impact. The results of this method can be checked theoretically for some cases where steady flow has been established around the block. Such study yields information not only about the development of impact stresses, but also about the propagation of waves and shocks in solids.

* Supported in part by ONR contract.

10. Experiments with Strong Shock Waves in a Low Density Shock Tube. GEORGE A. LUNDQUIST, *U. S. Naval Ordnance Laboratory* (introduced by P. P. Wegener).—The shock tube has found wide use for the production of relatively weak, low velocity shock waves and for the study of the various flow phenomena connected with these waves. Stronger waves require that extreme pressure ratios be set up across the shock tube diaphragm. In shock tubes of large dimensions these pressure ratios can be obtained practically only by evacuating the expansion chamber to very low pressures. A serious difficulty is then encountered in that conventional types of shock-speed timing and triggering devices fail to function at the low gas densities. A new type of shock-speed timing device utilizing the change in electric current through a glow discharge to indicate the passage of a shock wave has been used to time shocks reliably in air at a pressure of 0.3 mm of Hg and velocities up to 1300 meters per second. This device has been used to measure the velocity of strong shock waves at different distances from the diaphragm. The velocities measured near the diaphragm are appreciably slower than those predicted by shock-tube theory, while at increasing distances the measurements closely approach the theoretical values. This may be the result of the catching up of secondary shocks formed by erratic diaphragm breakage. Characteristics of the flow behind the shock wave may show similar effects.

11. Interferometric Studies of Two-Dimensional Turbulent Jet Mixing at $M1.7$.* DANIEL BERSHADER AND BOYD CARY, *Institute for Fluid Dynamics and Applied Mathematics, University of Maryland.*—Density distributions have been obtained in the turbulent mixing region of a small rectangular jet of Mach number 1.7 discharging into the atmosphere under full expansion. Following earlier interferometric applications, the nozzle, whose construction has been described previously,[1] was shortened considerably in order to present a minimum

boundary layer width at the orifice. The results are given in a nondimensional form,[1] allowing a comparison with theoretical work on jet mixing as applied to compressible flow by Pai.[2] In addition, the experiments have been extended to over-and-under expanded jets, although in these cases the problem of retaining two-dimensionality becomes more difficult. It is planned to extend these investigations to include other Mach numbers.

* Assisted by the Office of Air Research.

[1] D. Bershader, Rev. Sci. Instr. 20, 260–275 (1949).
[2] D. Bershader and S. I. Pai, J. Appl. Phys. 21, 616 (1950).
[3] S. I. Pai, J. Aeronaut Sci. 16, 463–469 (1949).

12. Effect of Dissociation on Laminar Boundary-Layer Characteristics. J. CONRAD CROWN, *U. S. Naval Ordnance Laboratory* (introduced by P. P. Wegener).—The laminar boundary-layer characteristics for a semi-infinite flat plate are calculated allowing for variable specific heats and dissociation of air, both on an equilibrium basis. Simple formulas are given for drag coefficient, recovery factor, and heat-transfer coefficient. The method used permits the easy calculation of these quantities for any viscosity law. The analysis corroborates the observation of Crocco that enthalpy is the more important parameter than temperature for calculating the aforementioned quantities and suggests the product of density and viscosity as a key parameter in terms of which the final formulas are expressed.

13. Solution of the General Two-Dimensional Subsonic Compressible Flow by a New Physical Transformation. ROBERT W. TRUITT, *North Carolina State College* (introduced by A. Kantrowitz).—The fundamental equation of motion is used to derive a new equation relating the local pressure coefficients in the corresponding subsonic compressible and incompressible flow fields, by using a point-to-point time- and space-unit transformation which is defined on the local velocity of sound. This new direct method of defining time- and space-units on the most critical physical process, the local velocity of sound, results in a differential or body-segment-to-segment solution which gives an integral nonlinear solution. This new fundamental derivation includes the effect of the specific heat ratio and does not necessitate the small perturbation assumption which inevitably leads to a linearized solution. The agreement of the new equation with experimental data is excellent and gives better agreement than does the Karman-Tsien relation.

14. On Supersonic Flow of Jet in Uniform Stream.* S. I. PAI, *Institute for Fluid Dynamics and Applied Maihematics, University of Maryland* (introduced by R. J. Seeger).—It is well known that a supersonic gas jet issuing from a reservoir into a medium at rest has a periodic structure, if the difference of pressure of the jet from the medium is not large. This paper investigates a similar situation when a supersonic gas jet is issuing into a uniform stream. It is found that, if the uniform stream is subsonic, the supersonic jet has *almost* periodic structure, and the approximate wavelength increases with the Mach number of the surrounding stream for a given Mach number of the jet. If the uniform stream is supersonic, the supersonic jet does not have periodic structure. The transmission and the reflection of small disturbance at the boundary of the jet, i.e., a vortex sheet are investigated. Factors of transmission and reflection of disturbances on the vortex sheet are found. They are functions of the Mach numbers of the jet and that of uniform stream. The reflection wave may be of the same sign or of opposite sign of the incident wave or zero according to the Mach numbers of the two streams.

* This work was carried out under Contract AF 33(038)–10481 sponsored by the Office of Air Research.

15. On Wave Radiation in Compressible Flow through an Axial Compressor. N. ROTT, *Cornell University* (introduced by A. Kantrowitz).—The two-dimensional flow pattern of cascades in a linearized supersonic stream will generally show periodic disturbances nondecaying at infinity. It is legitimate to define the wave energy contained in the nondecaying non-uniform part of the flow as "losses."[1] For three-dimensional investigation of wave energy losses in linearized approximation it is proposed to represent the non-uniform part of the flow by superposition of potentials, whose variation in circumferential direction is harmonic. Actually, these potentials are generalizations of earlier solutions of Ackeret and Meyer[2] to the compressible case. Discussion of these solutions shows that the first appearance of wave energy radiation will be found when the resultant Mach number of axial and circumferential velocity reaches unity. This would also be the conclusion from two-dimensional considerations; however, it is found that for low frequency harmonic components, especially for small hub, the limit is raised to slightly supersonic resultant Mach numbers. Typical three-dimensional effects may be discussed as consequence of this behavior.

[1] See A. Kantrowitz, NACA TR No. 974.
[2] Ackeret and Meyer, Mitt. Inst. Aerodynamik, Zurich, No. 11 (1946).

16. On Reflection of a Weak Shock Wave from a Laminar Boundary Layer. ALFRED RITTER, *Cornell University* (introduced by A. Kantrowitz).—The interaction between a plane, oblique shock wave and a laminar boundary layer along a flat plate is investigated. The problem is solved by dividing the flow field into a viscous layer near the wall and a supersonic potential outer flow with the direction of the stream line at the edge of the viscous layer as a boundary condition for the outer flow. By use of the boundary layer approximations, the deflection of the streamline can be determined, and hence the outer flow is also determined. It is found that: (a) The incident compression wave is reflected, locally as an expansion wave. (b) The pressure disturbance decays exponentially from a definite value at the point of incidence to zero far upstream of the point of incidence. Downstream of the point of incidence, the pressure rises to maximum and then drops off to the value corresponding to regular reflection. (c) For $M_\infty \doteq 2$ and $Re_\delta \doteq 1500$, the upstream influence is of the order of 30 boundary layer displacement thicknesses. (d) Boundary layer separation may occur upstream of the point of incidence. The separation point moves upstream with increasing shock strength, increasing Reynolds number, and decreasing Mach number.

17. Heat Transfer in Isotropic Turbulence. STANLEY CORRSIN, *The Johns Hopkins University*.—The postulated problem of heat transfer in a stationary isotropic turbulence under constant small temperature gradient is examined from both lagrangian and eulerian points of view. By combination of Taylor's "diffusion by continuous movements" and a new temperature fluctuation equation somewhat like the well-known turbulent energy equation, it is possible to obtain (1) an expression for the turbulent heat transfer coefficient which depends only on velocity field, and (2) an approximate expression for the corresponding correlation coefficient which depends only on velocity field and fluid physical properties.

18. A Study of Vibratory Flame Movement. Part I. Apparatus and Preliminary Experimental Results.* L. M. SOMERS AND G. H. MARKSTEIN, *Cornell Aeronautical Laboratory, Inc.*—Although the spontaneous excitation of organ-pipe oscillations by flames propagating in tubes has been studied frequently in the past,[1] the published results are mostly unsuitable for evaluating the effects of various parameters. The aim of the present study is to explore systematically the influence of combustible mixture composition, tube length, and other variables. Techniques employed include high speed shadowgraph and schlieren movies and recording of pressure and radiation transients. Preliminary results showed that the

vibratory phase of flame propagation was always accompanied by periodic appearance and disappearance of cellular flame structure.[2] The positions of the centers of cells appearing in any cycle coincided with intersections of cell boundaries in the preceding cycle. Cell size increased with amplitude of vibration. Low frequencies were excited over wide composition ranges. With increasing frequency, the excitation limits narrowed to regions within the range of spontaneous cellular flame structure.

* Sponsored by the ONR and the Office of Air Research through Project SQUID.
[1] E.g., Coward, Hartwell, and Georgeson, J. Chem. Soc., Pt. 2, 1482 (1937).
[2] G. H. Markstein, J. Aeronaut. Sci. **18**, 199 (1951).

19. A Study of Vibratory Flame Movement. Part II. Stability of a Plane Flame Front in Pulsating Flow.* W. SQUIRE AND G. H. MARKSTEIN, *Cornell Aeronautical Laboratory, Inc.*—Thermal excitation of organ-pipe oscillations occurs when heat is added periodically in phase with the pressure oscillation somewhere along the tube.[1] A flame burning in a tube may thus cause spontaneous oscillations if the burning rate is modulated by the oscillation under favorable phase relations. Burning rate being equal to burning velocity times flame surface area, modulation of either factor may contribute to excitation. Pressure (or temperature) effects on burning velocity have been assumed in previous work.[2] Experimental results (preceding abstract) suggest, however, that effects of oscillation on flame surface area may be important, possibly dominant. Generalization of theory of flame front stability[3] showed that alternating acceleration may cause parametric excitation of standing waves on flame front surface. Results of treatment will be discussed and compared with experimental data.

* Sponsored by the ONR and the Office of Air Research through Project SQUID.
[1] Lord Rayleigh, *Theory of Sound* (Dover Publications, New York, 1945), Vol. II, p. 226.
[2] G. Guderley, Z. Angew. Math. Mech. **18**, 285 (1938).
[3] G. H. Markstein, J. Aeronaut. Sci. **18**, 199, (1951); *ibid.*, 428 (1951).

20. The Effect of Pressure on the Detonation Velocity in Gases.* A. J. MOORADIAN† AND W. E. GORDON,‡ *University of Missouri.*—The detonation velocity in several gas mixtures (hydrogen and oxygen with different diluents) decreases with decreasing initial pressure. A straight line is obtained when the deviation from the theoretical value is plotted against the reciprocal of the pressure. On extrapolation to infinite pressure the velocity is always within one or two percent of the theoretical except for the most dilute mixtures at the detonation limit. The linear relationship may be explained by pressure-independent energy losses, the main contribution being from heat conduction to the walls of the tube. Large negative deviations from theory observed by previous workers[1,2] in low density mixtures, such as with helium diluent, have not been confirmed when the worst case so noted has been repeated in long smooth tube, and with adequate initiation. It is therefore concluded that the Chapman-Jouget theory, assuming complete reaction in the wave front, and allowing only for heat losses, is in excellent agreement with the observed facts.

* Work supported by the ONR.
† Now at the National Research Council, Chalk River, Ontario, Canada.
‡ Now at Arthur D. Little, Inc., Cambridge, Massachusetts.
[1] Lewis and Friauf, J. Am. Chem. Soc. **52**, 3905 (1930).
[2] Bereta, Greene, and Kistiakowsky, J. Am. Chem. Soc. **72**, 1080 (1950).

21. Detonation Limits in Hydrogen-Oxygen Mixtures.* A. J. MOORADIAN† AND W. E. GORDON,‡ *University of Missouri.*—The limits for stable detonation as functions of both pressure and composition have been investigated in hydrogen-oxygen with four diluent gases, air, hydrogen, argon, and helium. In a mixture below the detonation limit which is over-initiated, strong detonation (above the Chapman-Jouget point) occurs, but as the wave gradually loses strength and settles toward the *C-J* condition, it reaches a point where detonation ceases, and it abruptly falls in velocity and degenerates to a simple shock wave. The composition limit mixture with argon contains less than half as much hydrogen (5 to 6 percent) as with air diluent (14 to 15 percent). It is found, however, that the "initiation temperature," i.e., the temperature at the shock front is about the same for all mixtures near the composition limit. Also it is found that a very small amount of water vapor (less than 0.1 percent) inhibits detonation in 15 percent H_2—air. It is concluded that the detonation limits are similar to the ordinary explosion limits, and that a chain-branching explosive reaction is necessary for the detonation of gases in tubes. Some considerations concerning the prevention of detonation in practical situations are given.

* Work supported by the ONR.
† Now at the National Research Council, Chalk River, Ontario, Canada.
‡ Now at Arthur D. Little, Inc., Cambridge, Massachusetts.

22. Computation of Two-Dimensional Laminar Flames. GEORGE A. BALL, *Harvard University.*—Solutions have been computed for a flame in a two-dimensional channel. The flow is assumed laminar, incompressible, and inviscid. The flame is replaced by a discontinuity surface across which the density is discontinuous. The solutions have been obtained by numerical relaxation of the stream function. Two cases have been solved, one for uniform parallel flow far upstream of the flame and the other for an initial parabolic velocity distribution. The flame shapes obtained assuming a constant value of flame speed are in close agreement with the shapes observed experimentally. Other results are given in terms of the streamline patterns, the velocity distribution, the pressure distribution, and the distribution of rotation.

23. Radiation Produced by Strong Shock Waves. H. E. PETSCHEK, *Cornell University* (introduced by A. Kantrowitz).—Intense radiation may be expected from strong shock waves resulting from the high temperatures and large degrees of ionization obtained in the gas behind the shock wave. Shock waves in the Mach number range from 6 to 10 were obtained in argon in a glass tube by using high pressure hydrogen as a driver gas. Drum camera pictures of these shock waves moving down the tube revealed that, instead of a fairly uniform region of radiation between the shock wave and the gas interface, as might be expected, from gas dynamics, a thin highly luminous region existed at the shock front followed by virtually no radiation. A very much fainter luminous region of the same nature was also observed in air where the degree of ionization is much smaller. By setting a photomultiplier at an angle to the shock tube the radiation from the surface of the shock has been measured. It has also been determined with a high speed oscilloscope and a photomultiplier that the thickness of the luminous region of an $M=7$ shock going into argon at 2.5 cm of Hg pressure is no larger than 0.06 cm.

24. Photoelastic Stress Analysis of a Shock Loaded Structure. C. RIPARBELLI, H. HITCH, AND G. BOEHLER, *Cornell University* (introduced by A. Kantrowitz).—The analysis of impact stress propagation in solids of nonconstant section (i.e., not cylindrical bars) has occasioned the development of this technique, of which some of the first results are presented. High velocity moving pictures (4000 frames per second) were taken in the polariscope of specimens made out of gelatine. The specimens were struck by a hammer at various velocities between zero and 30 ft/sec. The propagation velocity of elastic waves in the specimens is about 15 ft/sec. Moving pictures of isocromatic patterns are presented, with emphasis on the boundary effects in plates of various shapes. A comparison with the static results is offered. Some of the pictures were taken by a mercury lamp, some others by flash bulbs.